LIPIDOME MODULATION IN ENVIRONMENTALLY-TRIGGERED AUTOIMMUNITY

By

Olivia Kristen Favor

A DISSERTATION

Submitted to
Michigan State University
in partial fulfillment of the requirements
for the degree of

Pharmacology and Toxicology – Environmental Toxicology – Doctor of Philosophy

ABSTRACT

Autoimmune diseases are chronic, uncured, life-altering illnesses caused by immune cells mistakenly attacking and damaging host tissues. While genetic predispositions play a vital role in the onset and development of autoimmune disease, exposure to environmental toxicants such as bacterial lipopolysaccharide (LPS) and respirable crystalline silica (cSiO₂) has also been etiologically implicated in autoimmune pathogenesis and progression. Current mainstay drugs for managing autoimmune disease symptoms (e.g., glucocorticoids, monoclonal antibodies) effectively reduce inflammation and associated tissue damage but also burden patients with adverse side effects and steep financial costs from long-term use. Intriguingly, preclinical and clinical studies suggest that two lipidome-modifying agents, dietary ω-3 polyunsaturated fatty acids (PUFAs) and small molecule inhibitors of soluble epoxide hydrolase (sEH), may improve disease status in systemic autoimmune diseases, including lupus. Previous studies conducted in our laboratory suggest that the ω-3 PUFA docosahexaenoic acid (DHA) abrogates cSiO₂-triggered autoimmune responses when given at realistic human equivalent doses to female lupus-prone NZBWF1 mice and suppresses LPS-induced expression of proinflammatory mediators at physiologically relevant concentrations in several macrophage models. In addition, the sEH inhibitor 1-trifluoromethoxyphenul-3-(1-propionylpiperidin-4-yl)urea (TPPU) delays the onset of genetically driven glomerulonephritis (GN) and prolongs lifespan in NZBWF1 mice with excellent pharmacokinetic properties. In this dissertation, I sought to build upon these findings by testing the overarching hypothesis that modulating the cellular lipidome delays initiation and progression of environmentally-triggered autoimmunity.

Three research aims were pursued to test my hypothesis. In the first aim, we utilized a previously reported *in vivo* model of LPS-accelerated (GN) in NZBWF1 mice to compare the

impacts of rough and smooth LPS chemotypes on GN onset and to subsequently evaluate the effects of DHA and/or sEH inhibition on disease development. Rough LPS elicited severe GN while smooth LPS did not. Additionally, DHA and sEH inhibition separately ameliorated LPSaccelerated GN, but therapeutic effects were diminished upon combining the treatments. In the second aim, we employed a novel in vitro alveolar macrophage surrogate model—the fetal liverderived alveolar macrophage (FLAM)—to query the impacts of LPS, cSiO₂, and DHA on a broad oxylipin panel consisting of 156 metabolites, as well as proinflammatory cytokine release, lysosomal membrane permeabilization (LMP), mitochondrial toxicity, and cell death. cSiO₂ evoked marked biosynthesis of ω-6 PUFA metabolites in vehicle-treated cells, while DHA significantly skewed the cellular lipidome toward ω-3 PUFA metabolites following cSiO₂ exposure. DHA also suppressed cSiO2-induced proinflammatory cytokine release but did not affect LMP, mitochondrial toxicity, or cell death. In the third aim, we used a novel in vivo model of acute cSiO₂-triggered lupus flaring in NZBWF1 mice to assess the impacts of sEH inhibition on lung inflammation and early autoimmunity. sEH inhibition reduced neutrophil and monocyte numbers in lung lavage fluid but did not improve cSiO2-induced centriacinar inflammation and fibrosis, perivascular ectopic lymphoid tissue neogenesis, T and B lymphocyte infiltration into the lung, secretion of antinuclear antibodies into lavage fluid and plasma, or gene expression and production of proinflammatory mediators in the lung.

Taken together, the studies presented in this dissertation provide valuable insight into how lipidome-modulating interventions (e.g., ω -3 PUFAs and sEH inhibitors) may impact the initiation and development of environmentally-triggered autoimmune diseases such as lupus. Furthermore, this dissertation highlights several novel preclinical models that can be used in future *in vitro* and *in vivo* screening of lipidome-modulating agents against environmentally-triggered autoimmunity.

This dissertation is dedicated to my Father in Heaven. Thank you for sustaining me throughout every step of this journey.

ACKNOWLEDGMENTS

During the early days of my PhD, I once read that pursuing a PhD is analogous to running a marathon. It is a journey marked by moments of success and moments of failure, interlaced with feelings of excitement, discouragement, confidence, uncertainty, fear, and curiosity. As I reflect on the past five years I have spent on this journey, I realize I never would have crossed the finish line without the support and encouragement of countless people—too many people to adequately name in this dissertation.

To my PhD research mentors, Dr. Kin Sing Stephen Lee and Dr. James Pestka: Thank you for giving me the opportunity of a lifetime to pursue my PhD in Pharmacology and Toxicology. You saw potential in me at times when it was difficult for me to see it in myself, and I am grateful for every word of encouragement, patience, and critique you have given to me over the past five years. I have grown not only as a scientist but also as a person because of you.

To my PhD committee members, Dr. Jack Harkema and Dr. Cheryl Rockwell: Thank you for providing valuable insight into my research project from start to finish. I have deeply enjoyed our conversations together and learned so much from you. I am also very grateful for all the letters of support you have written on my behalf for the grant applications I have submitted over the last several years.

To Dr. James Wagner, Ryan Lewandowski, Sarah Shareef, Ashleigh Tindle, Jenan Shareef, and Anna Skedel: Thank you for helping me carry out every planned and impromptu mouse necropsy and countless *in vivo* follow-up analyses for my research project. All of you have taught me the importance of staying organized—and having fun—as a scientist.

To Dr. Andrew Olive: Thank you for providing encouragement to me in the latter parts of my PhD. I am incredibly grateful for the opportunity to continue working on exciting science with you and Dr. Pestka as a postdoctoral researcher.

To Dr. Maris Cinelli, Dr. Fan Zhang, Dr. Morteza Sarparast, Devon Dattmore, Katayoon Maghami, Derek Vonarx, Keshav Pralahad, Elham Pourmand, Tommy Reason, Jennifer Hinman, Christopher Prill, Sara Ali, Sachini Kodippili Patabendige, Megha Singhal, Megan Shuck, and Angel Edwards: Thank you for providing your perspectives on organic and medicinal chemistry to my research project. All of you have helped me to look at my project through lenses I may have not otherwise considered. Thank you also for embracing me as part of the group, even though I conducted all my research in a separate building from you.

To Dr. Kathryn Wierenga, Dr. Preeti Chauhan, Dr. Lichchavi Rajasinghe, Dr. Lauren Heine, Elizabeth Ross, Augie Evered, Shamya Harris, Alexa Richardson, Adrianna Kirby, Riley Spalding, and Tony McKenzie: Thank you for advising me, encouraging me, commiserating with me, talking with me, and helping me with not only scientific tasks but also situations outside of the lab. You are like another family to me, and I wish all of you the very best in the journeys that are currently unfolding for each one of you.

To Dr. Anne Dorrance, Dr. Karen Liby, Dr. Richard Neubig, Dr. Bryan Copple, Dr. Norbert Kaminski, and Dr. John LaPres: Thank you for accepting me into the BioMolecular Sciences Gateway Program, Pharmacology and Toxicology Doctoral Program, Integrative Pharmacological Sciences Training Program, and Environmental and Integrative Toxicology Doctoral Program. All of you have been instrumental in the continued success of these outstanding programs, and I am grateful for all the learning opportunities I have received from each one. Thank you for investing in my growth as a scientist.

To Shelli Pfeiffer, Ashley Wallin, Tracie Carr, Beverly Dickinson, Patty Gregory, Meagan Kroll, Stephen Stofflet, Bradley Robinson, Heather Defeijer-Rupp, Jake Wier, Kasey Baldwin, Lauren St. John, Jessica Bennett, and Jessica Spitzley: Thank you for providing excellent administrative support during my PhD journey, whether if it was related to laboratory orders, enrolling for classes, managing grant funds, printing research posters, informing me of department events, or moving Dr. Pestka's lab from the Food Science Building to the Biomedical and Physical Sciences Building. All of you have played a significant role in my success as a predoctoral researcher at Michigan State University.

To Leslie Pittsley: Thank you for teaching me the foundational hands-on skills I needed for the *in vivo* components of my research project and for spending hours collecting blood samples from my mice. To the staff at MSU Campus Animal Resources: Thank you for taking care of my research animals on a daily basis.

To Dr. Babak Borhan and Dr. Hadi Gholami: Thank you for giving me the opportunity to conduct research with you when I was still an undergraduate student at Michigan State University. The experiences I had in the lab with you prompted me to pursue my PhD in the first place, and your confidence in me spurred me on when I lacked confidence.

The research presented in this dissertation would not have been possible without financial support from the National Institute of Environmental Health Sciences, the National Science Foundation, the Lupus Foundation of America, the Robert and Carol Deibel Family, the MSU Integrative Pharmacological Sciences Training Program, and the MSU Institute of Integrative Toxicology. Thank you for financially supporting not only my PhD research, but also the continued quest for scientific discovery at Michigan State University.

To Sarah Pelton, Kaitlyn Keliin, Tyler Buchanan, Hannah Kissling, Phil and Henrietta DuCap, Nick and Asia Richardson, Dennis Sutherby, Mike and Jackie McDonald, Marmalade McDonald, David McDonald, and all my friends, new and longstanding: Thank you for pouring words of encouragement into me when I felt discouraged enough to quit and words of excitement onto me when I celebrated victories along the way. I am humbled by your support and grateful for each and every one of you.

To my uncle Gary Joseph: Thank you for being a father figure to me. Thank you for letting me talk your ear off about nerdy science projects and for telling me how proud you are of me. I am proud to be your niece, and I look forward to sharing many more nerdy science stories with you in the future.

To my brother Andrew Favor: Thank you for every time you have provided a patient listening ear to me when I felt discouraged during my PhD. I am so grateful for all the memories we have created together over the past five years, both on Discord calls during weekends and inperson during my visits home. You are an excellent brother and friend, and I am grateful to be your younger sister.

To my mother Carol Favor: Thank you for encouraging me to keep moving toward the finish line every time I felt ready to quit. Thank you for reminding me that my worth is not in the work that I produce, but in who I am as a person. You have taught me so much about what it means to persevere through trials simply by modeling it to me through your actions. I am so grateful for our relationship and your unwavering support of me. Thank you for everything. I love you, and I am proud to be your daughter.

Finally, I would like to thank my best friend, advocate, and significant other Matthew McDonald for encouraging me to run the race set out for me with endurance and to keep my sight

set upon the grand prize. Thank you for reminding me to fix my eyes upon the gracious One who has made this journey possible and makes all things, including life itself, possible. I am so grateful I met you on this journey. Thank you for loving me just as I am, in all the highs and lows I have experienced by your side. I am proud to be your woman. I love you, I am in love with you, and I really like you!

TABLE OF CONTENTS

LIST OF ABBREVIATIONS xi
CHAPTER 1: INTRODUCTION1
CHAPTER 2: CENTRALITY OF MYELOID-LINEAGE PHAGOCYTES IN PARTICLE-TRIGGERED INFLAMMATION AND AUTOIMMUNITY
CHAPTER 3: LIPIDOME MODULATION BY DIETARY OMEGA-3 POLYUNSATURATED FATTY ACID SUPPLEMENTATION OR SELECTIVE SOLUBLE EPOXIDE HYDROLASE INHIBITION SUPPRESSES ROUGH LPS-ACCELERATED GLOMERULONEPHRITIS IN LUPUS-PRONE MICE54
CHAPTER 4: OMEGA-3 DOCOSAHEXAENOIC ACID SUPPRESSES SILICA-INDUCED PROINFLAMMATORY CYTOKINE RELEASE AND OXYLIPIN PRODUCTION IN NOVEL FETAL LIVER-DERIVED ALVEOLAR-LIKE MACROPHAGES
CHAPTER 5: SOLUBLE EPOXIDE HYDROLASE INHIBITOR TPPU SUPPRESSES PULMONARY INFLAMMATORY CELL INFILTRATION BUT DOES NOT PREVENT LUNG PATHOLOGY OR EARLY AUTOIMMUNITY IN LUPUS-PRONE MICE ACUTELY EXPOSED TO CRYSTALLINE SILICA
CHAPTER 6: CONCLUSIONS AND FUTURE DIRECTIONS
REFERENCES
APPENDIX A: CHAPTER 3 SUPPORTING FIGURES AND TABLES
APPENDIX B: CHAPTER 4 SUPPORTING FIGURES AND TABLES
APPENDIX C: CHAPTER 5 SUPPORTING FIGURES AND TABLES

LIST OF ABBREVIATIONS

AAb Autoantibody

AAg Autoantigen

AC Apoptotic cell

ALA Alpha-linolenic acid

Alum Aluminum-containing salts

AM Alveolar macrophage

ANOVA Analysis of variance

ARA Arachidonic acid

BALF Bronchoalveolar lavage fluid

BMDM Bone marrow-derived macrophage

BSA Bovine serum albumin

BW Body weight

CaOx Calcium oxalate

CaP Calcium phosphate

CC Cholesterol crystal

CNT Carbon nanotube

CON Control

COX Cyclooxygenase

cSiO₂ Crystalline silica

CYP450 cytochrome P450

C57 C57BL/6 mouse

d Day

DAMP Damage-associated molecular pattern

DGLA Dihomo-γ-linolenic acid

DHA Docosahexaenoic acid

DiHDoPE Dihydroxydocosapentaenoic acid

DiHETrE Dihydroxyeicosatrienoic acid

DiHFA Dihydroxy fatty acid

dsDNA Double-stranded DNA

ELT Ectopic lymphoid tissue

EPA Eicosapentaenoic acid

EpDPE Epoxydocosapentaenoic acid

EpETrE Epoxyeicosatrienoic acid

EpFA Epoxy fatty acid

FAME Fatty acid methyl ester

FBS Fetal bovine serum

FLAM Fetal liver-derived alveolar-like macrophage

g Gram

GC Gas chromatography

GC-MS Gas chromatography-mass spectrometry

GLC Gas-liquid chromatography

GM-CSF Granulocyte-macrophage colony-stimulating factor

GN Glomerulonephritis

HDoHE Hydroxydocosahexaenoic acid

HED Human equivalent dose

HEPE Hydroxyeicosapentaenoic acid

HETE Hydroxyeicosatetraenoic acid

HFA Hydroxy fatty acid

HUFA Highly unsaturated fatty acid

H&E Hematoxylin and eosin

h Hour

IFN Interferon

i.p. Intraperitoneal

LA Linoleic acid

LC-MS Liquid chromatography-mass spectrometry

LC-MS/MS Liquid chromatography-tandem mass spectrometry

LDH Lactate dehydrogenase

LMP Lysosomal membrane permeabilization

LOX Lipoxygenase

LPS Lipopolysaccharide

LTB4 Leukotriene B4

LTR LysoTracker Red

mg Milligram

min Minute

MK Maximum kill

MSU Monosodium urate; Michigan State University

MTR MitoTracker Red

MUFA Monounsaturated fatty acid

NF-κB Nuclear factor kappa B

NZBWF1 New Zealand Black/White F1 mouse

P/S Penicillin-streptomycin

PAMP Pattern-associated molecular pattern

PASH Periodic acid-Schiff hematoxylin

PBS Phosphate-buffered saline

PGE2 Prostaglandin E2

PLA2 Phospholipase A2

PUFA Polyunsaturated fatty acid

OA Oleic acid

RCN Relative copy number

R-LPS Rough variant lipopolysaccharide

ROS Reactive oxygen species

RPMI Roswell Park Memorial Institute

s Second

sEH Soluble epoxide hydrolase

SEM Standard error of the mean

SFA Saturated fatty acid

SG SYTOX Green

SPM Specialized pro-resolving lipid mediator

SiO₂ Silicon dioxide

SKC Silica-killed cell

S-LPS Smooth variant lipopolysaccharide

TGF-β Transforming growth factor beta

TiO₂ Titanium dioxide

TLR Toll-like receptor

TNF-α Tumor necrosis factor alpha

TPPU 1-(4-Trifluoro-methoxy-phenyl)-3-(1-propionylpiperidin-4-yl) urea

TXB2 Thromboxane B2

UPLC Ultra-performance liquid chromatography

VEH Vehicle

wk Week

CHAPTER 1: INTRODUCTION

INTRODUCTION

Autoimmune diseases comprise a distinct category of more than 100 chronic illnesses characterized by the immune system afflicting irreversible damage to host cells, tissues, and organs. Although genetic predisposition significantly contributes to the initiation and progression of autoimmunity, preclinical and epidemiological studies suggest that the exposome (i.e., lifetime exposure to environmental factors) plays an equally important role [1-3]. Environmental factors that have been etiologically linked to autoimmune pathogenesis include bacterial infections, exposure to toxicants, and lifestyle choices [4].

Roughly 5-9% of the world population and 50 million Americans live with one or more autoimmune diseases [5, 6]. However, the number of afflicted individuals may be higher than reported numbers because autoimmune diseases are often difficult to diagnose accurately, due to symptoms shared with non-autoimmune illnesses and heterogeneous clinical presentation between autoimmune patients [7, 8]. Signs and symptoms associated with many autoimmune diseases include but are not limited to increased plasma titers of autoantibodies (AAb), systemic inflammation, fatigue, pain, weight change, and fever [9].

To date, no autoimmune diseases have been cured, but a variety of drugs are currently used to manage symptoms and prolong lifespan including corticosteroids (e.g., prednisone), disease-modifying antirheumatic drugs (DMARDs) (e.g., methotrexate), non-steroidal anti-inflammatory drugs (NSAIDs) (e.g., ibuprofen), and monoclonal antibodies (e.g., etanercept) [10-12]. While these medications are highly efficacious at reducing inflammation and resultant tissue damage, they can lead to adverse side effects such as infection, bleeding, ulcers, and bone damage [13]. In addition, steep financial costs connected to long-term medical care and loss of work productivity can further burden patients and consequently decrease quality of life [14-17]. Taken together, there

is a critical need for safer, less expensive interventions to prevent both the initiation and progression of autoimmune disease.

One potential solution involves modifying the endogenous lipidome to reduce systemic inflammation, autoimmune responses, and subsequent tissue damage. The National Institute of Health (NIH) announced a ten-year strategic plan in 2020 for nutrition research, which involves using precision nutrition to "reduce the burden of disease in clinical settings" [18]. In line with this premise, previous investigations demonstrate that dietary ω -3 polyunsaturated fatty acids (PUFAs) and small molecule inhibitors of soluble epoxide hydrolase (sEH) attenuate toxic responses in mouse models of toxicant-triggered inflammation and autoimmunity [19-23]. Furthermore, clinical data suggest that dietary ω -3 PUFAs and sEH inhibition may improve disease outcomes in individuals afflicted with lupus [24], rheumatoid arthritis [25], diabetic neuropathic pain [26], and other inflammatory conditions [27].

The objective of this dissertation is to test the guiding hypothesis that modulation of the cellular lipidome delays initiation and progression of environmentally-triggered autoimmunity. Herein, two known environmental triggers of the prototypical autoimmune disease lupus—bacterial lipopolysaccharide (LPS) and respirable crystalline silica (cSiO₂)—were employed in a novel alveolar macrophage (AM) model *in vitro* and in female lupus-prone NZBWF1 mice *in vivo* to assess the efficacy of two lipidome-modulating treatments: 1) the ω-3 PUFA docosahexaenoic acid (DHA), which has been previously studied in Dr. Pestka's lab, and 2) the sEH inhibitor 1-(4-trifluoro-methoxy-phenyl)-3-(1-propionylpiperidin-4-yl) urea (TPPU), which has previously been studied in Dr. Lee's lab.

CHAPTER SUMMARIES

The current chapter, Chapter 1, addresses the scope of the research presented in this

dissertation, including pertinent background information, unanswered research questions in the field, and the overall guiding hypothesis and research aims for this dissertation. This chapter also provides succinct summaries of each chapter found herein.

Chapter 2 provides a comprehensive literature review of critical molecular mechanisms by which exogenous (i.e., silica, asbestos, carbon nanotubes, titanium dioxide, aluminum-containing salts) and endogenous (i.e., monosodium urate, cholesterol crystals, calcium-containing salts) particles promote unresolved inflammation and autoimmunity by inducing toxic responses in myeloid-lineage phagocytes, with emphases on inflammasome activation and necrotic and programmed cell death pathways. This chapter was published as a first-author manuscript in *Frontiers in Toxicology* in 2021 and can be accessed online (doi: 10.3389/ftox.2021.777768).

In Chapter 3, we conducted two studies in a previously described preclinical model of LPS-accelerated severe lupus nephritis (ASLN) [28-33] in female lupus-prone NZBWF1 mice. In Study 1, we compared the effects of rough LPS (R-LPS) and smooth LPS (S-LPS) on glomerulonephritis (GN) induction to clarify how the presence or absence of O antigen polysaccharide impacts this widely used preclinical model. The results indicated that repeated injection with R-LPS accelerated severe GN whereas repeated injection with S-LPS did not. In Study 2, we evaluated how dietary DHA supplementation and/or pharmacologic inhibition of sEH influence R-LPS-accelerated GN. We found that DHA consumption and sEH inhibition alone suppressed GN, but the ameliorative effects of these interventions were lessened upon combining the treatments. Additionally, we demonstrated for the first time that administration of TPPU in AIN-93G mouse diet is an effective method for reaching drug steady-state levels in the plasma, as well as stabilizing epoxy fatty acid metabolite levels in the plasma. This chapter was published as

a co-first author manuscript with my colleague Dr. Preeti Chauhan in *Frontiers in Immunology* in 2023 and can be accessed online (doi: 10.3389/fimmu.2023.1124910).

In Chapter 4, we investigated the effects of DHA on proinflammatory cytokine release, lysosomal membrane permeabilization, mitochondrial toxicity, cell death, and oxylipin production in fetal liver-derived alveolar macrophages (FLAMs), a novel self-renewing alveolar macrophage model previously published by Dr. Pestka's lab [34]. FLAMs derived from C57BL/6 mice were employed to test this hypothesis. Herein, we demonstrate for the first time in FLAMs that cSiO₂ induces production of ω-6 PUFA metabolites and that pre-treatment with DHA contributes to increased production of ω-3 PUFA metabolites at the expense of ω-6 PUFA metabolites. Contrastingly, we found that DHA does not delay the onset of LMP, mitochondrial depolarization, and subsequent cell death in cSiO₂-exposed FLAMs. Taken together, our results indicate that lipidomic modulation of AMs is a key mechanism of DHA in preventing initial onset and progression of cSiO₂-induced proinflammatory cytokine release, which can perpetuate local lung inflammation and systemic autoimmunity. This chapter is in preparation to be submitted to *Frontiers in Immunology* for publication.

In Chapter 5, we evaluated the effects of the sEH inhibitor TPPU on early cSiO₂-induced lung inflammation and autoimmunity in female lupus-prone NZBWF1 mice. Cohorts of mice were placed on either control diet or experimental diet supplemented with the sEH inhibitor TPPU (22.5 mg/kg diet) at 6 wk of age, given one intranasal instillation of 2.5 mg cSiO₂ or PBS vehicle at 8 wk of age, then sacrificed at either 7 d PI or 28 d PI. We found that TPPU significantly dampened cSiO₂-induced elevation of total and differential immune cell counts in the bronchoalveolar lavage fluid (BALF) at both 7 d PI and 28 d PI. On the other hand, TPPU did not significantly improve cSiO₂-triggered centriacinar histopathology in the lung; recruitment of CD206⁺ monocytes,

Ly6B.2⁺ neutrophils, CD3⁺ T lymphocytes, and CD45R⁺ B lymphocytes to the lung, expression of proinflammatory cytokines, chemokines, and type I IFN-regulated genes in the lung; production of proinflammatory mediator proteins in the lung; or secretion of antinuclear autoantibodies into the BALF and plasma. This chapter is in preparation to be submitted to *Scientific Reports* for publication.

The final chapter, **Chapter 6**, summarizes and discusses the conclusions drawn from the research presented in Chapters 3-5, and proposes future research directions to build upon the findings of this dissertation. Proposed research directions include 1) comparing cSiO₂-induced oxylipin profiles in NZBWF1 FLAMs treated with DHA, ARA, TPPU, or vehicle, 2) evaluating paracrine effects of DHA-, ARA-, and TPPU-derived oxylipins on cSiO₂-induced proinflammatory cytokine release in NZBWF1 FLAMs, 3) identifying fatty acid receptors that mediate lipid metabolite protective effects against cSiO₂-induced proinflammatory cytokine release in NZBWF1 FLAMs, 4) comparing effects of control, DHA-supplemented, and TPPU-enriched diets on the kinetics of LPS- and cSiO₂-induced changes in pulmonary, renal, and plasma oxylipin profiles, and 5) investigating the impacts of direct lipid metabolite administration on LPS- and cSiO₂-triggered autoimmunity in female lupus-prone NZBWF1 mice.

CHAPTER 2: CENTRALITY OF MYELOID-LINEAGE PHAGOCYTES IN PARTICLE-TRIGGERED INFLAMMATION AND AUTOIMMUNITY

PUBLICATION NOTICE

The following chapter has been published by Frontiers in Toxicology and is available through the Frontiers of Toxicology website at "Favor OK, Pestka JJ, Bates MA, Lee KSS. Centrality of Myeloid-Lineage Phagocytes in Particle-Triggered Inflammation and Autoimmunity. Front Toxicol. 2021 Nov 4;3:777768. doi: 10.3389/ftox.2021.777768. PMID: 35295146; PMCID: PMC8915915."

ABSTRACT

Exposure to exogenous particles found as airborne contaminants or endogenous particles that form by crystallization of certain nutrients can activate inflammatory pathways and potentially accelerate autoimmunity onset and progression in genetically predisposed individuals. The first line of innate immunological defense against particles are myeloid-lineage phagocytes, namely macrophages and neutrophils, which recognize/internalize the particle, release inflammatory mediators, undergo programmed/unprogrammed death, and recruit/activate other leukocytes to clear the particles and resolve inflammation. However, immunogenic cell death and release of damage-associated molecules, collectively referred to as "danger signals", coupled with failure to efficiently clear dead/dying cells, can elicit unresolved inflammation, accumulation of selfantigens, and adaptive leukocyte recruitment/activation. Collectively, these events can promote loss of immunological self-tolerance and onset/progression of autoimmunity. This review discusses critical molecular mechanisms by which exogenous (i.e., silica, asbestos, carbon nanotubes, titanium dioxide, aluminum-containing salts) and endogenous (i.e., monosodium urate, cholesterol crystals, calcium-containing salts) particles may promote unresolved inflammation and autoimmunity by inducing toxic responses in myeloid-lineage phagocytes with emphases on inflammasome activation and necrotic and programmed cell death pathways. A prototypical example is occupational exposure to respirable crystalline silica, which is etiologically linked to systemic lupus erythematosus (SLE) and other human autoimmune diseases. Importantly, airway instillation of SLE-prone mice with crystalline silica elicits severe pulmonary pathology involving accumulation of particle-laden alveolar macrophages, dying and dead cells, nuclear and cytoplasmic debris, and neutrophilic inflammation that drive cytokine, chemokine, and interferonregulated gene expression. Silica-induced immunogenic cell death and danger signal release

triggers accumulation T and B cells, along with IgG-secreting plasma cells, indicative of ectopic lymphoid tissue (ELT) neogenesis, and broad-spectrum autoantibody production in the lung. These events drive early autoimmunity onset and accelerate end-stage autoimmune glomerulonephritis. Intriguingly, dietary supplementation with ω -3 fatty acids has been demonstrated to be an intervention against silica-triggered murine autoimmunity. Taken together, further insight into how particles drive immunogenic cell death and danger signaling in myeloid-lineage phagocytes and how these responses are influenced by the genome will be essential for identification of novel interventions for preventing and treating inflammatory and autoimmune diseases associated with these agents.

INTRODUCTION

Exogenous and endogenous particles have profound effects on human health. The concept of particle toxicology was first introduced in the 15th century when occupational exposure to dust was etiologically linked to lung disease (reviewed in Donaldson and Seaton [35]). Paracelsus, the toxicologist who famously quoted "The dose makes the poison", documented in a 1567 book his observations of lung disease symptoms in smelters and miners. In 1700, these observations were expanded upon by Bernardino Ramazzini, also known as the father of occupational medicine, who recognized that human disease could be triggered by environmental factors in his work *Diseases of Workers*. Industrialization in the 19th century elicited a rise in occupationally related diseases such as silicosis, asbestosis, lung cancer, and pulmonary fibrosis, leading to a significant increase in both *in vitro* and *in vivo* particle toxicology studies in the 20th century [36].

Over the past 50 years, the field of particle toxicology has expanded to encompass not only pathological impacts of environmental particles but also of endogenously formed crystals, hereafter referred to as endogenous particles [35]. Growing interest in endogenous particles is

largely attributed to increased worldwide prevalence of genetic hyperuricemia and familial hypercholesterolemia, which are predispositions for crystallization of monosodium urate (MSU) and cholesterol, respectively [37, 38]. Hyperuricemia is a risk factor for gout, coronary heart disease, and neurodegenerative disorders [39, 40], and hypercholesterolemia is a risk factor for coronary heart disease [41], atherosclerosis [42], non-alcoholic steatohepatitis (NASH) [43], and cholesterol gallstone disease [44]. The observed pathological outcomes associated with MSU and cholesterol crystals have spurred ongoing *in vitro* and *in vivo* studies to determine the mechanisms by which these endogenous particles, as well as other types of endogenous particles (e.g., calcium-containing salts) elicit toxicity.

In parallel with the growing interest in particle toxicology, immunologist Polly Matzinger and her colleagues introduced the 'danger model' to explain the development of autoimmune disease, which contrasts the classic 'self/non-self model' [45-47]. While the self/non-self model posits that autoreactivity occurs when the adaptive immunity mistakenly recognizes host 'self' tissues as foreign 'non-self' tissues, the danger model suggests that accumulation of dead cell corpses and released danger signals (e.g. cytokines, chemokines, alarmins, nucleic acids) contribute to heightened proinflammatory responses in innate immune cells, activation of antigen-presenting cells, and differentiation of autoreactive T and B cells, leading to loss of immunological self-tolerance and autoimmunity [48]. In the context of particle toxicology, Matzinger's danger model provides a useful framework for understanding the mechanisms by which exogenous and endogenous particles induce inflammation and autoimmunity.

The purpose of this literature review is to provide an overview of critical molecular mechanisms by which exogenous (i.e., silica, asbestos, carbon nanotubes, titanium dioxide, aluminum-containing salts) and endogenous (i.e., MSU, cholesterol crystals, calcium-containing

salts) particles promote unresolved inflammation and autoimmunity by inducing toxic responses in myeloid-lineage phagocytes with emphases on inflammasome activation and necrotic and programmed cell death pathways. Autoimmune diseases are defined by uncontrolled innate immunity leading to hyperactivation of adaptive immunity, the latter of which drives tissue damage and disease pathogenesis [49]. The review will focus specifically on myeloid-lineage phagocytes (i.e., macrophages, neutrophils), as these cells comprise the first line of immunological defense against particles [50].

Exogenous and endogenous particles and their sources

Exogenous particles are defined here as any particles originating from environmental or synthetic sources. These include silicon dioxide (SiO₂), asbestos, carbon nanotubes (CNTs), titanium dioxide (TiO₂), and aluminum-containing salts (alum). SiO₂ is one of the most abundant compounds in the Earth's crust [51] and is classified based on its level of crystallinity, with crystalline SiO₂ (cSiO₂) demonstrating a periodic order of atoms and amorphous SiO₂ (aSiO₂) having either an anarchic order of atoms or crystalline structures [52]. Asbestos refers to a broad group of fibrous, chain-like silicate minerals that have high tensile strength, large surface area, and resistance to abrasion and chemical corrosion—all characteristics that made it ideal for construction, mining, and other industrial applications such as pipefitting, shipyard work, insulation manufacturing, and textile production in the 20th century [53, 54]. Like asbestos, CNTs are fibrous, carbon-containing materials that have high tensile strength and large surface area [55], rendering them useful in construction and electronics [56, 57]. TiO₂ can exist as either nanospheres or nanobelts [58], giving them versatile use in construction, agriculture, food additives, cosmetics, and biomedicine [59-61]. Alum was serendipitously discovered as a vaccine adjuvant nearly 100 years ago [62] and is now the most utilized adjuvant in the world [63]. Another highly relevant exogenous particle is particulate matter (PM), which may consist of carbon, sulfate, nitrate, silicon, ammonium, and sodium emissions from both manmade and organic sources [64]. Due to the complex and heterogenous composition of PM, its toxic mechanisms are much more difficult to characterize than the previously mentioned particles. A detailed discussion of PM toxicity falls outside the scope of this review, but the reader is referred to several excellent reviews on this topic [65-70].

Exposure to exogenous particles can occur by inhalation, ingestion, or injection. SiO₂ was first identified as an inhalation hazard in the 1920s when it was etiologically linked to silicosis in miners [71, 72]. Today, SiO₂ remains an occupational inhalation hazard in construction, mining, ceramic manufacturing, dental mold production, and jewelry production [73-75]. Asbestos exposure primarily occurs by inhalation [76], and despite decreased industrial use in the United States and Europe, industrial asbestos use is being deferred to Asian and Latin-American countries [77]. CNTs can either pose as respirable toxicants similar to asbestos fibers in industrial settings [78] or function as carrier systems in targeted drug, vaccine, cancer, and gene therapies [79, 80]. TiO₂ exposure can occur by inhalation in industrial environments or ingestion of commercial products, and it exhibits toxicity in the lungs, digestive tract, brain, and cardiovascular system [61]. Exposure to alum occurs primarily by injection as a vaccine adjuvant [81] but can also occur by inhalation in foundry work and related occupations [82, 83]. While the National Institute for Occupational Safety and Health (NIOSH) recommends using respirators in occupations with high, prolonged particle exposure [84], low compliance with such guidelines is associated with respirator discomfort, lack of training on health hazards, self-employment, and breathing problems that would be aggravated by respirator use [85].

Endogenous particles are defined as any particle that forms within biological systems. From an environmental perspective, many of these are formed by crystallization of nutrients, typically in individuals with corresponding genetic predispositions. Endogenous particles include MSU, cholesterol crystals (CCs), and calcium salts such as calcium phosphate (CaP) and calcium oxalate (CaOx). MSU originates from crystallized uric acid, a byproduct of purine nucleic acid catabolism released by dying cells [86]. Cholesterol is derived from dietary sources and biosynthesis in the liver [87]. Dysregulated cholesterol metabolism can contribute to deposition of low-density lipoproteins (LDLs) and high-density lipoproteins (HDLs) in tissues, engulfment of LDLs and HDLs by recruited macrophages and DCs, and intracellular CC formation [88-90]. Like cholesterol, calcium occurs both in dietary and body sources, and it can crystallize as CaP and CaOx salts within renal tubules and blood vessels [91, 92]. While biomolecules and minerals found in endogenous particles can originate from diet and/or metabolism, crystal formation itself occurs in myeloid phagocytes and along tubular structures within the body.

Endogenous particles are thought to form by crystallization resulting from supersaturation of biological molecules (e.g., cholesterol, uric acid) and minerals (e.g., calcium) in the joints, arteries, and urinary tract [52]. Although the precise mechanisms for crystal formation have yet to be elucidated, genome-wide associated studies have identified loci that contribute to overproduction and insufficient metabolism of uric acid, LDL, HDL, and calcium-containing salts [93-97]. Overabundance of these biomolecules in synovial fluid, serum, or urine creates conditions for supersaturation, increasing the likelihood of crystallization and disease development (**Table 2.1**).

Recognition of exogenous and endogenous particles by myeloid-lineage phagocytes

Particles can stimulate multiple types of surface receptors to promote incorporation into phagosomes, an intracellular vesicle that transports phagocytosed particles. Macrophages, neutrophils, DCs can recognize particles through a diverse repertoire of surface receptors (**Figure 2.1**). For instance, SiO₂ and TiO₂ both bind to members of the class A scavenger receptor family including SR-A1 and macrophage receptor with collagenous structure (MARCO). However, SiO₂ also binds the class B scavenger receptors SR-B1 and CD36/SR-B2, whereas TiO₂ does not [98-100]. In macrophages, stimulation of class A and class B scavenger receptors by their respective ligands has been associated with p38 MAPK and JNK activation and enhanced particle endocytosis [101]. Alternatively, CNTs, which are more fibrous than SiO₂ and TiO₂ particles, are recognized by the phosphatidylserine receptor T cell immunoglobulin mucin 4 (Tim4) [102].

Contrary to exogenous particles, endogenous particles are recognized by a more diverse set of surface receptors and elicit different intracellular signaling pathways. For example, MSU crystals interact with C-type lectin (Clec)-12a on macrophages and DCs [103, 104] and FcγRIII/CD16 on neutrophils [105]. FcγRIII is also expressed in murine macrophages and DCs [106]. On human macrophages, neutrophils, and DCs, CCs can bind to Clec4e to potentiate proinflammatory immune responses [107]. FcγRIII stimulation by MSU and Clec4e stimulation by CCs trigger downstream spleen tyrosine kinase (Syk) signaling [108, 109]. Alternatively, both MSU and alum can directly interact with membrane cholesterol moieties and induce Syk signaling in DCs, potentially by lipid membrane sorting [110, 111].

Surface receptors for asbestos, CaP, and CaOx have not yet been identified, but it is possible that phagocytes recognize these particles directly by membrane lipid binding or indirectly through complement receptor signaling. Accordingly, complement C5 binding to the C5a receptor

(C5aR) can amplify MSU-driven toxicity [112]. In addition, activation of C5aR by C5 and complement receptor 3 (CR3) by complement factor iC3b can augment CC-induced toxic responses [113].

Differential expression of particle-sensing receptors in myeloid-lineage phagocytes

Not only is it important to consider the types of surface receptors that can be stimulated by particles, but it is also crucial to further emphasize which myeloid-lineage phagocytes express which receptors, because different particles might activate different subsets of myeloid cells. For instance, SR-A1 is expressed by macrophages, monocytes, and DCs, while MARCO is primarily expressed by macrophages and DCs [114, 115]. CD36 is expressed by many cell types including macrophages, monocytes, DCs, and non-hematopoietic cells, whereas SR-B1 is predominantly expressed by macrophages and hepatocytes [116, 117]. Macrophages and DCs have been shown to express Tim4, but data pertaining to Tim4 expression in neutrophils is currently lacking [118, 119]. On the other hand, macrophages, neutrophils, and DCs express Clec12a [103, 104, 120], FcγRIII [105, 106], and Clec4e (in humans only) [107]. Collectively, these observations suggest that myeloid-lineage phagocytes might be better prepared to respond to endogenous particles compared to exogenous particles. Nevertheless, additional research is required to confirm or reject such a hypothesis.

Several studies published over the past decade have shed additional light on differential expression patterns of particle-sensing receptors in tissue-resident macrophages that commonly interact with particles, including bone marrow-derived macrophages (BMDMs), alveolar macrophages (AMs), and hepatic Kupffer cells (KCs). A comprehensive gene expression review across different tissue-resident macrophage types found that SR-A1 expression is high in BMDMs and low in both AMs and KCs, whereas MARCO expression is low in BMDMs and high in both

AMs and KCs [121]. In the same analysis, notable observations were made in relation to the other receptors mentioned in the present review: 1) SR-B1 expression is higher in AMs and KCs compared to BMDMs; 2) CD36 expression is high in BMDMs but lower in AMs and KCs; 3) Tim4 expression is low in BMDMs and AMs but high in KCs; 4) Clec12a is highly expressed in BMDMs but not in AMs or KCs; 5) Clec4e expression is high in BMDMs and AMs but low in KCs; 6) FcγRIII is highly expressed in BMDMs, AMs, and KCs; and 7) C5aR expression is high only in BMDMs [121]. In two different studies, MARCO and Tim4 expression were found to be lower in BMDMs compared to KCs [122, 123]. Two other studies also showed that Clec4e expression increases in macrophages localized to the kidneys during acute renal inflammation, suggesting Clec4e perpetuates proinflammatory cytokine signaling and cell death in the kidney [124, 125].

Not only do tissue-resident macrophages demonstrate differential expression patterns for many particle-sensing surface receptors, but similar patterns can be detected in blood-derived monocytes. A single-cell gene expression analysis with human monocytes found that expression levels for SR-A1, MARCO, CD36, and Clec4e significantly differed between classical monocytes (CD14++CD16-), intermediate monocytes (CD14++CD16+), and non-classical monocytes (CD14+CD16+) [126]. A different study comparing FcγRIII expression in classical and non-classical monocytes found that expression was higher in classical monocytes than non-classical monocytes in mice, but expression was lower in classical monocytes than non-classical monocytes in humans [127]. Furthermore, FcγRIII expression in murine classical monocytes was similar to that in neutrophils, while expression in human neutrophils was remarkably higher than both classical and non-classical monocytes [127]. Although surface receptor expression patterns were not compared between monocytes and macrophages in either of these studies, such distinctions

might require a case-by-case basis approach. For instance, monocytes and BMDMs express similar levels of Clec12a [128], but CD36 expression increases in monocytes differentiating into BMDMs [129]. Accordingly, future research in this area would provide valuable insight into specific myeloid-lineage phagocyte subsets that respond to different types of exogenous and endogenous particles. Future therapies for particle-induced inflammatory and autoimmune disease may potentially include antagonists that prevent particle-receptor interactions and downstream toxicity. *Inflammasome activation: a central mechanism of particle-induced toxicity and proinflammatory immune responses*

Following phagocytosis, one central mechanism of toxicity initiated by exogenous and endogenous particles alike is inflammasome activation [130-136]. Inflammasomes are cytosolic multiprotein complexes that assemble upon sensing diverse stimuli—including microbial moieties, endogenous danger signals, and particles—to promote proinflammatory signaling [137, 138]. Because of their importance in orchestrating innate immune responses, inflammasomes are primarily studied in innate immune cells, most notably macrophages; however, other investigators are beginning to investigate their roles in adaptive immune cells and nonhematopoietic cells [139]. Pattern recognition receptors (PRRs) from the nucleotide-binding oligomerization domain (NOD) leucine-rich region-containing receptor (NLR) family, including NLRP1, NLRP3, and NLRC4, as well as absent-in-melanoma 2 (AIM2) and pyrin, form well-defined inflammasome complexes [140-144]. In addition, the NLRs NLRP2, NLRP6, NLRP7, NLRP12, and NLRC5, as well as interferon-inducible protein 16 (IFI16), also form inflammasome complexes, albeit less well-characterized or atypical complexes [145-149].

The NLRP3 inflammasome is the most studied inflammasome due to its putative roles in various pathologies including rheumatic disease [150], Alzheimer's disease [151], acute

myocardial infarction [152], kidney disease [153], type 2 diabetes [154], obesity [155], cancer [156], and COVID-19, which is caused by severe acute respiratory syndrome coronavirus 2 (SARS-CoV-2) infection [157]. This inflammasome also plays a pertinent role in particle-driven diseases such as pulmonary fibrosis, asthma, chronic obstructive pulmonary disease (COPD), malignant mesothelioma, and other lung cancers [138]. NLRP3 inflammasome oligomers consist of the NOD-like receptor NLRP3, the adapter protein apoptosis-associated speck-like protein containing a caspase recruitment domain (ASC), and pro-caspase-1 as an effector [158]. Three distinct pathways are implicated for NLRP3 inflammasome activation: 1) the canonical pathway, 2) the alternative pathway, and 3) the noncanonical pathway [159]. The alternative and noncanonical pathways fall beyond the scope of this review, though readers are directed to other excellent discussions of these topics for further information [160, 161].

Step 1: Priming

Canonical inflammasome activation occurs in a two-step process that first requires a priming signal to promote transcriptional upregulation of inflammasome-related proteins and a subsequent activating signal to trigger inflammasome oligomerization and caspase-1 activation [162]. Priming can be accomplished upon recognition of damage-associated molecular patterns (DAMPs), pathogen-associated molecular patterns (PAMPs), or cytokines by specific surface receptors. For example, the bacterial PAMP lipopolysaccharide (LPS) activates toll-like receptor (TLR)-4, the endogenous DAMP high group mobility group box 1 (HMGB1) activates TLR2/4/9, and tumor necrosis factor (TNF)-α and interleukin (IL)-1α activate the TNF and IL-1 receptors, respectively [163-165]. These binding events contribute to phosphorylation of the inhibitor of nuclear factor kappa-B kinase (IKK)-β subunit within the cytosolic IKK2 complex. IKKβ then phosphorylates IκBα and targets it for K48-ubiquitination and proteasomal degradation.

Degradation of IκBα liberates the dimeric transcription factor nuclear factor-kappa B (NF-κB), allowing its translocation into the nucleus where it upregulates the inflammasome subunits NLRP3, ASC, and pro-caspase-1 as well as pro-IL-1β and pro-IL-18 [166] (**Figure 2.2**). Under homeostatic conditions, DAMPs and proinflammatory cytokines are typically contained inside phagocytes; however, these danger signals can be released into the extracellular environment following particle-induced cell death [167, 168]. If clearance of extracellular particles, DAMPs, and cytokines is hindered, perpetual stimulation of DAMP/cytokine receptors and particle-sensing receptors may ensue, leading to aberrant inflammasome priming and activation.

Step 2: Activation

Following the priming signal, a separate activating signal triggers inflammasome assembly and caspase-1 maturation. Contrary to the priming step, which is initiated by a select set of ligands, the activating step can be triggered by many different stimuli including ATP [169], mitochondrial reactive oxygen species (mtROS) [170], mitochondrial DNA (mtDNA) [171], ceramide [172], bacterial toxins [173], and particles [138]. The diverse nature of these stimuli suggests they do not directly act upon inflammasome subunits but rather induce a few common intracellular events that lead to inflammasome oligomerization. Lawlor and Vince propose that these signals may converge on lysosomal rupture, mitochondrial dysfunction, and endoplasmic reticulum (ER) stress [174] (Figure 2.3).

Lysosomal membrane permeabilization

Once particles or other stimuli are incorporated into a phagosome, the phagosome fuses with a lysosome to form an intracellular phagolysosome [175]. The role of the phagolysosome is to digest internalized materials; however, many crystalline particles such as cSiO₂, cholesterol, alum, and MSU disrupt the phagolysosomal membrane in a process called lysosomal membrane

permeabilization (LMP) [131, 176]. LMP describes any process by which the lysosomal membrane is disrupted and lysosomal enzymes (such as cathepsins) are released into the cytosol [177]. Although the precise mechanisms by which particles induce LMP remain unknown, one critical study recently found that a subfamily of silanols, termed "nearly free silanols," on the surface of cSiO₂ and aSiO₂ particles promote membranolysis by direct membrane interaction [178]. Once cathepsins are released from ruptured phagolysosomes, some cathepsins may directly activate the inflammasome [179-181] or elicit dysfunction of other intracellular organelles, including the mitochondria and ER, that can indirectly activate the inflammasome. Accordingly, exogenous and endogenous particles that are engulfed by phagocytes can directly elicit LMP and indirectly promote mitochondrial and ER stress.

Mitochondrial dysfunction

As mentioned in the previous section, cathepsins released by particle-triggered LMP may promote downstream mitochondrial dysfunction [182, 183]. Mitochondrial dysfunction has been linked to inflammasome activation specifically by the release of mitochondrial DAMPs (mtDAMPs) such as ATP, oxidized mtDNA, and mtROS [170, 184]. A large body of evidence suggests ATP can trigger inflammasome assembly and caspase-1 activation in macrophages, specifically by promoting K⁺ ion efflux through either the P2X7 surface receptor or the TWIK2 K⁺ channel [169, 185, 186]. In phagocytes, particle exposure also can trigger apoptosis, a process that can begin in the mitochondria [187-192]. It is possible that opening of the mitochondrial permeability transition pore (MPTP) during apoptosis allows oxidized mtDNA and mtROS to exit depolarized mitochondria and activate the inflammasome, but this requires additional investigation. Once in the cytosol, oxidized mtDNA can directly bind NLRP3 to promote caspase-1 activation and resultant IL-1β maturation [171, 193].

Conversely, the requirement of mtROS in inflammasome activation is debatable, with some investigators arguing that mtROS are indispensable for inflammasome activation and others suggesting that mtROS only partially contribute to inflammasome activity [173, 194, 195]. Of interest, activation of the transcription factor nuclear factor erythroid 2-related factor 2 (Nrf2), which mediates transcription of antioxidant genes, has been shown to inhibit inflammasomedriven IL-1\beta maturation, supporting a clear role for total cellular ROS in promoting inflammasome assembly [28, 29, 196]. It is currently unclear how much of this response is driven by mtROS specifically; however, it is reasonable to expect mtROS play a fairly large role because mitochondria are major drivers of ROS production [197]. Evidence suggests mtROS can further disrupt lysosomal compartments [198]. On the other hand, lysosomal leakage has been previously shown to occur upstream from perturbations in mitochondrial membrane potential following cSiO₂ exposure in AMs [182, 183]. Taken together, these findings suggest that lysosomal and mitochondrial dysfunction might reciprocally influence one another in the context of particleinduced toxicity. Such a notion requires additional study, as the mechanisms driving cyclical lysosomal and mitochondrial dysfunction remain unclear.

Endoplasmic reticulum stress

Similar to mitochondrial dysfunction, ER stress has also been linked to inflammasome activation. Extracellular ATP, a mtDAMP released from dying cells, stimulates the transcription factor CCAAT enhancer binding protein homologous protein (CHOP) in LPS-primed BMDMs to induce Ca²⁺ signaling, which promotes Ca²⁺ efflux from the ER, downstream mitochondrial damage, and resultant caspase-1 activation [199]. Additionally, ER stress promotes NF-κB-dependent transcription of pro-IL-1β and activation of the oxidative protein folding pathway to induce ROS production [200]. Elevated ROS levels initiate the dissociation of thioredoxin-

interacting protein (TXNIP) from thioredoxin (TXN) and its subsequent association with the LRR of NLRP3, which promotes inflammasome oligomerization and caspase-1 activation [200]. Furthermore, ER stress can activate inositol-requiring enzyme 1 alpha (IRE1α), which promotes translocation of TXNIP to the mitochondria and the release of mtDAMPs including mtROS and mtDNA [201]. In previous studies, it has been demonstrated in macrophages that SiO₂ upregulates CHOP [202], asbestos increases CHOP expression and cytosolic Ca²⁺ [203], and MWCNTs promotes intracellular lipid accumulation, CHOP phosphorylation, and CD36 expression [204]. Additional research is needed to determine the specific steps that occur between particle phagocytosis and downstream ER stress.

Taken together, inflammasome-activating exogenous (**Table 2.2**) and endogenous (**Table 2.3**) particles have multifaceted impacts on intracellular lysosomal, mitochondrial, and ER-related functionality, and these pathways can feed into each other to mount robust inflammatory responses that drive rheumatic and autoimmune disease.

Particle-induced cell death pathways that contribute to innate and adaptive immune responses

Consistent with Matzinger's danger model [47], exposure to exogenous (**Table 2.2**) and endogenous (**Table 2.3**) particles can trigger inflammasome-dependent and -independent cell death pathways in phagocytes, resulting in the release of DAMPs and autoantigens that can activate innate and adaptive immunity. Of note for the present review are necrosis, pyroptosis, apoptosis, necroptosis, and NETosis. In addition, we provide a brief perspective on PANoptosis, a recently proposed unified cell death pathway involving pyroptosis, apoptosis, and necroptosis.

<u>Necrosis</u>

Necrosis is an unprogrammed cell death pathway characterized by organellar disorganization, cellular swelling, plasma membrane rupture, and DAMP release [205]. No

specific signaling pathway is associated with necrosis, but it is usually preceded by lysosomal rupture, mitochondrial swelling, and ROS production [206, 207]. Necrosis in generally considered a proinflammatory mode of cell death, as DAMPs released from dying cells provoke inflammatory gene expression and signaling in neighboring innate and adaptive immune cells [208] (Figure 2.4A). Both exogenous and endogenous particles have been shown to provoke necrotic cell death in a variety of cell types including AMs, fibroblasts, mesothelial cells, and kidney epithelial cells. Primary mechanisms by which particles induce necrosis include upstream LMP, mitochondrial depolarization, and ROS production [183, 209, 210], though it might also be possible that particles directly disrupt the plasma membrane [178, 211] or promote necrosis through other unelucidated mechanisms. Infectious agents, mechanical stress, hypoxia, and chemical and radiation exposure can also compromise the integrity of the cell membrane, leading to necrosis [212]. When particles induce necrosis, the dying cell releases particles and DAMPs, which can perpetuate unresolved inflammation if not efficiently cleared.

Pyroptosis

Pyroptosis is a programmed lytic cell death pathway that is dependent on inflammasome activation [213, 214]. As previously discussed, many different types of exogenous and endogenous particles can activate the inflammasome [130-136]. When the NLRP3 inflammasome assembles and activates caspase-1 following particle exposure, caspase-1 not only converts pro-IL-1β and pro-IL-18 to their mature forms but also cleaves the N-terminal pore-forming domain (PFD) of gasdermin D (GSDMD). PFD monomers oligomerize and insert into the plasma membrane, which destabilizes plasma membrane potential and leads to an osmotic movement of water into the cell that mediates cellular swelling and lysis [215] (**Figure 2.4B**). Like necrosis, pyroptosis is considered a proinflammatory cell death pathway because the GSDMD pore and resultant lysis

caused by its insertion into the plasma membrane allows passage of DAMPs from intracellular to extracellular environments [208].

Apoptosis

Exposure to exogenous and exogenous particles such as SiO₂, asbestos, CCs, MSU, and CaP can induce apoptosis in macrophages [183, 192, 216-218]. Unlike necrosis, apoptosis is morphologically defined by nuclear DNA cleavage, cytoskeletal rearrangement, cellular shrinkage, and plasma membrane blebbing [205] (Figure 2.4C). In apoptosis, the plasma membrane does not rupture but rather invaginates organelles and DAMPs in apoptotic bodies that are engulfed by phagocytes [219]. Accordingly, apoptosis is a quiescent mode of cell death; however, if apoptotic bodies are insufficiently removed, they undergo secondary necrosis, which releases DAMPs into the extracellular space [220]. Apoptosis can be induced by death receptor (DR) signaling (extrinsic pathway), mitochondrial signaling (intrinsic pathway), or perforin/granzyme signaling [212, 221]. The perforin/granzyme pathway falls outside the scope of the present review, but readers are encouraged to consult other excellent reviews on this topic [222-224]. While particles have not been shown to bind DRs and particle-sensing receptors are not known to activate signaling components downstream from DRs [187, 188], an overview of extrinsic apoptosis is warranted because particle exposure can induce expression and secretion of DR ligands such as TNF- α [134, 225-229]. In the context of particle-triggered apoptosis, however, the intrinsic pathway is most relevant because particles can indirectly elicit mitochondrial stress [183, 187, 188].

In the extrinsic pathway, the initiation phase is triggered by activation of a DR in the TNF receptor superfamily (e.g., TNF receptor [TNFR]-1 or Fas receptor [FasR]) by its corresponding ligand (e.g., TNF-α or Fas ligand [FasL]), which triggers association of an adapter protein to the

intracellular domain of the DR [212]. The recruited adapter protein differs depending on the DR activated: FasL recruits Fas-associated protein with death domain (FADD) to FasR, and TNF-α recruits TNFR1-associated death domain protein (TRADD) to TNFR1 [221]. Specific to TNFR1, TNF receptor associated factor (TRAF)-2/5, receptor-interacting serine/threonine-protein kinase (RIPK)-1, and cellular inhibitor of apoptosis protein (cIAP)-1/2 are subsequently recruited to the intracellular receptor domain of TNFR1 and associate with TRADD (i.e., Complex I). Cylindromatosis tumor suppressor protein (CYLD) then deubiquitylates RIPK1 which allows this protein to leave Complex I and leads to association of FADD and RIPK3 (i.e., Complex II). Following these events, FADD associates with multiple pro-caspase-8 proteins to form a deathinducing signaling complex (DISC) that cleaves pro-caspase-8 to caspase-8 [230]. Caspase-8 then proteolytically activates caspase-3 and -7 and triggers the execution phase of apoptosis [221]. During the execution phase, mature caspases-3 and -7 cleave nuclear DNA and intracellular proteins, which are encapsulated in apoptotic bodies [231]. Apoptotic cells express phosphatidylserine (PS) in the outer leaflet of the plasma membrane, which serves as an "eat me" signal for phagocytes to engulf the dying cells, a process termed efferocytosis that functions to remove apoptotic bodies, thus preventing secondary necrosis and DAMP release [232].

In the intrinsic pathway, particle-driven organellar dysfunction leads to MPTP opening, as described in the previous section. This releases cytochrome c (cyt c) into the cytosol, where it binds with apoptotic protease activating factor 1 (Apaf-1) and pro-caspase-9 to form a multiprotein apoptosome complex that is structurally and functionally analogous to the inflammasome. During this process, mitochondrial second mitochondria-derived activator of caspases (SMAC) and high temperature requirement protein A2 (HtrA2) block the activity of inhibitors of apoptosis proteins (IAPs) to promote apoptosis [233]. Pro-caspase-9 molecules proteolytically activate each other

within the apoptosome in a manner that resembles caspase-1 activation in the inflammasome. Activated caspase-9 then activates caspase-3, which activates caspase-activated DNase (CAD). Subsequently, caspase-3 cleaves nuclear DNA, triggers cytoskeletal rearrangement, and induces formation of apoptotic bodies, which are cleared by phagocytes under normal conditions [221]. However, phagocytotic capacity might be exhausted under conditions of persistent particle exposure, which raises the likelihood of secondary necrosis, DAMP release, and ongoing inflammatory signaling.

Necroptosis

Exogenous particles (e.g., SiO₂, TiO₂) and endogenous particles (e.g., CCs, MSU, CaP, CaOx) have been demonstrated to induce necroptosis in neutrophils, with less well-defined effects in macrophages [234, 235]. Necroptosis is a programmed cell death pathway that morphologically resembles necrosis but shares cellular machinery with the extrinsic apoptotic pathway. Accordingly, the early steps of necroptosis involve DR activation and recruitment of signaling proteins to the intracellular domain of the DR (e.g., TNFR1) to form Complex I as previously described [236]. TNFR1 endocytosis, cIAP1/2 inhibition, and RIPK1 deubiquitylation by CYLD triggers formation of cytosolic Complex II, which involves dissociation of TRAF2/5 and cIAP1/2 and association of FADD and pro-caspase-8 as previously described [237, 238]. Under normal conditions, Complex II can induce extrinsic apoptosis. However, impairment of pro-caspase-8 activity allows formation of a RIPK1 and RIPK3-containing complex called the necrosome [239]. The necrosome facilitates activation of the pseudokinase mixed lineage kinase domain-like (MLKL) via phosphorylation, and MLKL monomers forms oligomers at phosphatidylinositol 3phosphate sites on the inner leaflet of the plasma membrane. Consequently, the MLKL oligomers elicit plasma membrane permeabilization by currently undefined mechanisms, leading to

destabilization of membrane potential and cell lysis (**Figure 2.4D**). As with necrosis and pyroptosis, necroptosis allows DAMP release from the cell, and these DAMPs can induce downstream inflammatory responses [237]. While the exact mechanisms of particle-induced necroptosis have yet to be fully elucidated, it is possible that cathepsins released from disrupted phagolysosomes promote assembly of the RIPK1-RIPK3 necrosome, which promotes MLKL polymerization [235]. Another possibility is that TNF-α released from dying cells interacts with TNFR1 on viable nearby cells, promoting either extrinsic apoptosis or necroptosis depending on pro-caspase-8 activity.

PANoptosis

PANoptosis is a recently coined term that unifies inflammatory cell death involving simultaneous activation of pyroptosis, apoptosis, and necroptosis [240]. Currently, two hypotheses have been proposed for PANoptosis-induced cell death. In the first scenario, an inflammatory stimulus simultaneously activates the inflammasome, apoptosome, and necrosome, which execute their respective forms of cell death. In the second model, PANoptosis is induced through inflammatory stimuli that trigger formation of a multiprotein complex called the PANoptosome, which triggers pyroptosis, apoptosis, and necroptosis at the same time. In myeloid-lineage phagocytes (e.g., neutrophils and macrophages exposed to LPS, caspase-8 (apoptosis), FADD (apoptosis and necroptosis), RIPK1 (necroptosis), NLRP3 (pyroptosis), ASC (pyroptosis), and caspase-1 (pyroptosis) can assemble into the PANoptosome. Accordingly, the PANoptosome can trigger apoptosis by caspase-8-dependent activation of caspase-3/7, pyroptosis by caspase-1-dependent cleavage of GSDMD, and necroptosis by RIPK3-dependent phosphorylation of MLKL [241] (Figure 2.5). The result is a detrimental cell death pathway that permits release of inflammatory DAMPs into the extracellular space. While it is still unclear which factors dictate

execution of PANoptosis versus individual activation of pyroptosis, apoptosis, or necroptosis, inhibition of TGF-β-activated kinase 1 (TAK1) has previously been associated with PANoptosome formation in macrophages [242].

Currently, there is no evidence linking particle exposure to PANoptosis in myeloid-lineage phagocytes, yet the current evidence supports such a possibility. Multiple particles have been previously reported to induce pyroptosis, apoptosis, and necroptosis in phagocytes (summarized by Mulay, Herrmann [243]), but whether these multiple forms of cell death occur simultaneously in the same model is yet to be determined. Intriguingly, components of these three pathways can regulate one another. Not only can caspase-8 promote pyroptosis by cleaving GSDMD, but it can also prevent necroptosis by degrading RIPK. Necroptotic MLKL pore formation also can trigger NLRP3 inflammasome activity by K⁺ efflux [244].

NETosis

In addition to pyroptosis, apoptosis, and necroptosis, exogenous particles (e.g., SiO₂, alum) and endogenous particles (e.g., MSU, CCs, CaP) can induce NETosis (reviewed by [245] and [246]). NETosis describes the process by which neutrophil extracellular traps (NETs) are formed within and released from neutrophils [247]. NETs are web-like structures composed of decondensed chromatin decorated with cytosolic myeloperoxidase (MPO) and neutrophil elastase (NE) [248]. NETs can be released from neutrophils by two mutually exclusive pathways: 1) suicidal NETosis and 2) vital NETosis [249] (**Figure 2.6**).

In suicidal NETosis, phagocytosis of particles elicits Ca²⁺ efflux from ER, which triggers activation of protein kinase C (PKC). PKC activates the MEK/ERK pathway, ERK phosphorylates the gp91phox subunit of NADPH oxidase to induce ROS production, and increased cytosolic ROS activate peptidyl arginine deiminase 4 (PAD4). Together with MPO and NE, which translocate to

the nucleus, PAD4 promotes chromatin decondensation and nuclear membrane disruption. Consequently, NETs are released from the nucleus into the cytosol, where they are further decorated with cytosolic proteins, and ultimately released into the extracellular environment upon cell lysis [250, 251]. Unlike suicidal NETosis, in vital NETosis, NETs are packaged into vesicles and released by exocytosis, and thus, the neutrophil remains viable. Stimulation of TLR2/4 or CR3 by Gram-positive bacteria (e.g., *S. aureus*) or Gram-negative bacteria (e.g., *E. coli*) activates PAD4, which partners with nuclear MPO and NE to induce nuclear membrane disruption and chromatin decondensation. [250, 251]. While released NETs can immobilize bacteria and viruses, they can also potentiate inflammation [248]. This raises a few questions pertaining to NETosis and particle toxicology. First, can released NETs capture extracellular particles and prevent their interactions with other phagocytes? Second, can NETs in particle-exposed neutrophils be decorated with particles prior to their release? Answering these questions could provide further insight into the protective and/or pathologic roles of NETs in particle-driven diseases.

Physicochemical attributes that influence particle-induced toxicity and proinflammatory responses

Although many published studies suggest that different particles elicit similar toxic mechanisms in myeloid-lineage phagocytes, these responses depend greatly on the physicochemical attributes of the particle. Such attributes may include, but are not limited to, particle length [252-254], size [255-257], shape [258-260], surface area [261, 262], and surface charge [178, 263-265]. An in-depth discussion of these attributes goes beyond the scope of this review, but the reader is encouraged to consult other previously published reviews on this topic [168, 266-268]. While current research has focused on characterizing relationships between

particle attributes and toxic responses exhibited by exogenous particles, these relationships have not yet been characterized in relation to endogenous particles.

From particle exposure to loss of immunological self-tolerance

As discussed in previous sections, inflammasome activity and cell death induced by exogenous particles (Table 2.2) and endogenous particles (Table 2.3) permit DAMP release into the extracellular environment, where they can stimulate innate and adaptive immune cells. Released DAMPs include proinflammatory cytokines, nucleic acids, uric acid, cholesterol, heat shock proteins, HMGB1, type I interferons (IFNs), NETs, and mtDAMPs including mtDNA, ATP, cardiolipin, and cyt c (reviewed by Gallo and Gallucci [86] and Grazioli and Pugin [269]). DCs, which are commonly referenced as bridges between innate and adaptive immunity [270], may also be bridges between particle exposure and loss of immunological self-tolerance because they interact with both particles and released DAMPs [86]. For example, DCs secrete cytokines involved in Th1 and Th17 differentiation (i.e., IL-1α, IL-1β, IL-2, IL-6, IL-17, IL-23) in response to MSU [271], CCs [272], or alum [273]. SiO₂ and TiO₂ induce caspase-1-dependent IL-1β maturation and apoptotic cell death in DCs [274], and extracellular IL-1β plays critical roles in promoting Th17 polarization [275]. In addition, HMGB1, ATP, TNF- α , and NETs can stimulate DC maturation, proinflammatory cytokine production (i.e., IL-6, CXCL8, IL-12, TNF-α), and subsequent T cell activation [276-278]. Furthermore, specific DC subsets secrete type I IFN and B-cell activating factor (BAFF), which regulate B cell differentiation into antibody-secreting plasma cells [279]. Intriguingly, DCs also can promote and maintain immunological tolerance by inducing regulatory T cell (Treg) differentiation through cell-to-cell contact or secreted cytokines such as TGF-β and IL-10 [280, 281]. Consequently, activated Tregs can suppress differentiation of naïve T cells into effector T cells, as well as the functions of activated CD4⁺ and CD8⁺ T cells,

B cells, macrophages, and DCs. Treg depletion has been associated with exacerbated immune responses to self- and non-self antigens and development of autoimmunity [282, 283]. Nonetheless, the impacts of Treg function on particle-driven inflammation remain unclear. For instance, imbalances in the Treg/Th17 ratio significantly aggravate SiO₂- and MSU-induced inflammation in the lungs and joints of mice, respectively [284, 285], but inhaled SiO₂ and asbestos elicit recruitment of Tregs to the lungs, which secrete TGF-β and IL-10 and contribute to resultant development of pulmonary fibrosis [286-288]. Accordingly, DCs play crucial roles in regulating T cell differentiation, interacting with proximal particles and DAMPs, and maintaining immunological self-tolerance. Dysregulated DC activation by particles and DAMPs, on the other hand, represents one major bridge connecting particle-induced innate immunity to irregular adaptive immunity.

Cells undergoing particle-induced death not only release DAMPs into the extracellular space, but also autoantigens that can be recognized by T and B cells and consequently trigger autoimmunity. Autoantigens are self-proteins that are erroneously recognized as foreign proteins by the host's immune system [289]. When presented by DCs or other APCs, autoantigens promote activation of autoreactive T cells, which evade elimination in individuals with genetic predispositions to autoimmune disease and specifically target the presented self-proteins [290]. In addition, autoreactive T cells promote differentiation of autoreactive B cells into plasma cells, which secrete autoantibodies specific to the presented self-proteins [291]. Autoantigens involved in systemic autoimmune diseases such as systemic lupus erythematosus (SLE) include dsDNA, small nuclear ribonucleoprotein (snRNP), cardiolipin, and histone proteins (i.e., H2B, H3, H4) [292, 293]. In some cases, autoantigens with post-translational modifications (PTMs), but not native self-proteins, are recognized by autoreactive T and B cells [293]. These PTMs include

phosphorylation/dephosphorylation [294, 295], methylation [296], acetylation [297], citrullination [298], oxidation [299], and isomerization [300]. Since cytotoxic processes can contribute to modification of autoantigen structure and immunogenicity, it is tempting to speculate that intracellular mechanisms involved in inflammasome activation may also contribute to formation of PTM autoantigens and novel autoantigens. For example, cathepsins released from particle-containing phagolysosomes may non-specifically cleave mitochondrial and cytosolic proteins to create novel self-proteins that elicit immunological autoreactivity when released from dying cells. Caspase-1 may cleave mitochondrial and cytosolic proteins other than its identified substrates (i.e., pro-IL-1β, pro-IL-18, GSDMD) at specific sites, though this possibility seems less likely.

In addition to the roles that released DAMPs, autoantigens, and other danger signals play in aberrant activation of the immune system, genetics constitute a major determinant in the loss of immunological self-tolerance and resultant development of autoimmunity. Although some autoimmune diseases are monogenic, the majority are polygenic by nature [49]. Genetic polymorphisms leading to increased expression and activation of inflammasome proteins (e.g., NLRP3), TLRs (e.g., TLR7, TLR9), transcription factors (e.g., STAT4), and IFN signaling proteins (e.g., IRF5) have been associated with increased susceptibility and severity of several autoimmune diseases including SLE, rheumatoid arthritis (RA), and multiple sclerosis [301, 302]. In addition, loss-of-function mutations in efferocytosis receptors (e.g., MerTK), which leads to decreased engulfment of cytotoxic cell debris, have been associated with systemic autoimmunity [303]. Unique to autoimmune diseases are genetic polymorphisms in the major histocompatibility complex (MHC), or human leukocyte antigen (HLA) region in humans [304], which is crucial for presenting antigens to CD4⁺ helper T cells [305]. Taken together, these genetic aberrations set the stage for increased inflammasome priming and activation, elevated proinflammatory cytokine and

IFN production, and hindered cell debris clearance contributing to inflammatory tissue damage. In individuals susceptible to autoimmunity, these genetic variants may also contribute to enhanced autoantigen presentation to T and B cells, tissue damage by autoreactive T cells, and autoantibody production by autoreactive plasma cells, leading to development of autoimmunity.

Particle-triggered autoinflammatory and autoimmune diseases

Consistent with evoking inflammatory responses and cell death in phagocytes, exogenous and endogenous particles can trigger development of both chronic inflammatory and autoimmune diseases [52, 306]. Workplace inhalation of asbestos fibers has a long-recorded history of potentiating asbestosis and malignant mesothelioma [307-309]. In rodents, CNT inhalation has been associated with proinflammatory AM polarization and pulmonary fibrosis [310], [311]. TiO₂ exposure has been connected to malabsorption, neuroinflammation, and cardiopulmonary inflammation in rodents and humans [61, 312, 313]. MSU deposition in joints and blood vessels can promote gouty arthritis [39], coronary heart disease, and neurodegeneration [40]. CCs can contribute to coronary heart disease [41], atherosclerosis [42], non-alcoholic steatohepatitis (NASH) [43], and cholesterol gallstone disease [44] if deposited in blood vessels, liver, or gallbladder, respectively. Furthermore, CaP and CaOx deposition can lead to pseudogout, nephropathy, and atherosclerosis [314-316]. Although different particles share similar mechanisms of promoting persistent inflammation, they elicit different pathologies depending on their routes of exposure and distribution in the body.

In addition to genetic predispositions, other factors that may modulate autoimmune susceptibility include particle exposure level, aging, and biological sex. Dose-response impacts of particle exposure on autoimmune pathogenesis remain largely uninvestigated. However, according to Paracelsus's paradigm statement "The dose makes the poison," it can be assumed that chronic

exposures to many particles are more likely to induce aberrant inflammation and autoimmunity compared to acute exposures to few particles [317]. This trend has been noted with respirable cSiO₂ exposure in both mice [318, 319] and humans [320, 321]. Conversely, aging seems to have unclear impacts on the development of autoimmune disease. Older adults (>60 years) have higher prevalence of non-organ-specific autoantibodies than younger adults (20-60 years), but older adults are less likely than younger adults to develop autoimmune disease [322]. Accordingly, aging contributes to restructuring of the immune system, leading to impaired immune responses, increased inflammation and oxidative stress, and increased autoantibody production [323]. This suggests that the immune system is much more sensitive and reactive to autoantigens in younger adults compared to older adults, as many systemic autoimmune diseases manifest between 30-50 years of age [324]. A third factor that influences autoimmunity yet remains an enigma is biological sex. In general, autoimmune disease is more prevalent in women compared to men [325]. Postulated reasons for this observation include pregnancy and hormonal changes during puberty and menopause [326]. While particle-induced inflammation and autoimmunity might be more biased toward men working in dusty occupations, more women are beginning to enter similar occupations, with emphases on making dental molds and using scouring powders in custodial work [327, 328].

While exposure to exogenous and endogenous particles has been linked to inflammatory and autoimmune diseases, much less is known about their roles in initiating and exacerbating autoinflammatory disease. Briefly, autoinflammatory diseases are defined by uncontrolled innate immunity contributing to direct tissue damage and disease pathogenesis, whereas autoimmune diseases are potentiated by unresolved innate immunity leading to hyperactivation of adaptive immunity, the latter of which primarily drives tissue damage and disease pathogenesis [49]. Most

autoinflammatory diseases are caused by genetic mutations contributing to aberrant inflammasome activity, IL-1β activation, protein folding, IFN signaling, complement activation, and proinflammatory cytokine signaling [329]. Considering these mechanisms, it is not unreasonable to speculate that particles can worsen, or even trigger, autoinflammatory disease, beginning with myeloid-lineage phagocytes. Research in this area is crucial for verifying an etiological link between particle exposure and autoinflammatory disease and would provide additional rationale for regulating workplace particle exposure and fine-tuning dietary constituents for individuals predisposed to either autoinflammatory or autoimmune disease.

<u>Linking particle-induced inflammation to autoimmune diseases—crystalline silica as a</u> prototypical example

Both preclinical and clinical studies have established that exposure to respirable cSiO₂ contributes to SLE and other human autoimmune diseases [330-332]. Patients with SLE typically have recurrent cycles of flaring and remission that eventually can over time cause cumulative damage to kidney, lung, heart, skin, and/or brain [333]. Intriguingly, both autoimmune flaring and disease progression can be induced by instilling SiO₂ to airways of mouse models of SLE [20, 318, 334-338]. This is perhaps best exemplified in SLE-prone female New Zealand Black White (F1) (NZBWF1) mice which show autoantibody-driven glomerulonephritis with proteinuria by age 34 weeks resulting in death by age 52 weeks [339]. Our laboratory has demonstrated in this model that four weekly intranasal cSiO₂ instillations of 1 mg triggers glomerulonephritis 12 wk earlier than the conventional genome-driven model [20, 318]. Before glomerulonephritis onset in these mice, cSiO₂ elicits severe pulmonary pathology involving continual accumulation of particle-laden AMs, dying and dead cells resulting from PANoptosis, nuclear and cytoplasmic debris, and neutrophilic inflammation. Furthermore, there is buildup of large numbers of T and B cells, along

with IgG-secreting plasma cells, suggestive of ectopic lymphoid tissue (ELT). Consistent with prolonged particle-induced pulmonary inflammation and ELT formation, lung fluid and blood from cSiO₂-instilled mice have elevated proinflammatory cytokines, chemokines, and autoantibodies. As illustrated in **Figure 2.7**, these observations support the lung playing an essential role as the nexus for cSiO₂-induced systemic autoimmune flaring and glomerulonephritis in the NZBWF1 mouse.

A potential promising intervention against cSiO₂-induced chronic lung inflammation and resultant autoimmunity is increasing dietary intake of the marine polyunsaturated fatty acids (PUFAs) docosahexaenoic acid (C22:6 ω-3; DHA) and eicosapentaenoic acid (C20:5 ω-3; EPA) [340]. Modes of action for ω-3 PUFAs' ameliorative effects include 1) moderating membrane and lipid raft function, 2) up- and down-regulating gene expression, 3) competition with ω-6 PUFAs and their downstream proinflammatory eicosanoids, and 4) pro-resolving actions of their downstream metabolites (reviewed by Akbar, Yang [341], Calder [342], Ferreira, Pereira [343], and Wierenga, Strakovsky [344]). Preclinical [345-347] and clinical investigations [341, 348-350] indicate that ω-3 PUFAs can counter onset and progression of lupus symptoms, including nephritis. We have found that dietary DHA supplementation reflecting realistic human consumption (i.e., 2 and 5 g/d) can be employed as a prophylactic approach against cSiO₂-triggered autoimmune flaring in NZBWF1 mice [20]. DHA consumption specifically inhibited cSiO₂triggered pulmonary accumulation of B and T cells, follicular dendritic cells, and IgG+ plasma cells. Importantly, DHA dose-dependently inhibited cSiO₂-triggered lung mRNA signatures indicative of inflammation-, chemokine-, and interferon (IFN)-related gene pathways [351]. Additionally, DHA supplementation suppresses both cSiO₂-induced autoantibody responses against a large number of SLE-associated autoantigens [352] and cSiO₂-triggered

glomerulonephritis [20]. Lastly, we have recently demonstrated that DHA supplementation has value as a therapeutic intervention in this model [353]. The demonstration that DHA acts at many stages of $cSiO_2$ -induced autoimmunity (**Figure 2.7**) raises the possibility that ω -3 PUFA supplementation could be used as an intervention against other diseases associated with particle-triggered inflammation and autoimmunity.

CONCLUSIONS AND FUTURE DIRECTIONS

Particle toxicology is a longstanding research field with origins in the 16th century. While this field primarily focused on toxic impacts of inhaled particles in the lung and their connections to occupational disease, it now encompasses a much broader arena that includes seeking to understand how exogenous and endogenous particles influence development of inflammatory and autoimmune diseases in diverse organs. Interestingly, the mechanisms by which particles trigger autoimmunity align with Polly Matzinger's danger model, which argues that ongoing production and insufficient clearance of danger signals contributes to autoreactivity. Some outstanding knowledge gaps in the field of particle toxicology include understanding how genetics influence the immunotoxic potential of particles, how particles impact other immune cell populations (e.g., innate lymphoid cells, natural killer cells), and how particle toxicology studies can be performed in silico to assess risks associated an individual's environment and lifestyle. Answering these questions will lead to new understanding of the mechanisms by which particles elicit toxicity in the context of the genome and will provide valuable insight into new interventions that can be used to prevent or treat particle-associated inflammatory and autoimmune diseases.

DECLARATIONS

Competing Interests

The authors declare that the research was conducted in the absence of any commercial or financial relationships that could be construed as a potential conflict of interest.

Funding

This work was funded by NIH T32GM142521 (OF), NIH ES027353 (JP), Lupus Foundation of America (JP and MB), the Robert and Carol Deibel Family Endowment (JP), NIH ES024806 (KL), and NSF DMS-1761320 (KL).

Contributions

OF: literature review, manuscript/figure preparation, manuscript submission. JP: manuscript/figure preparation, oversight, project funding. MB: manuscript preparation. KL: manuscript preparation, oversight.

FIGURES

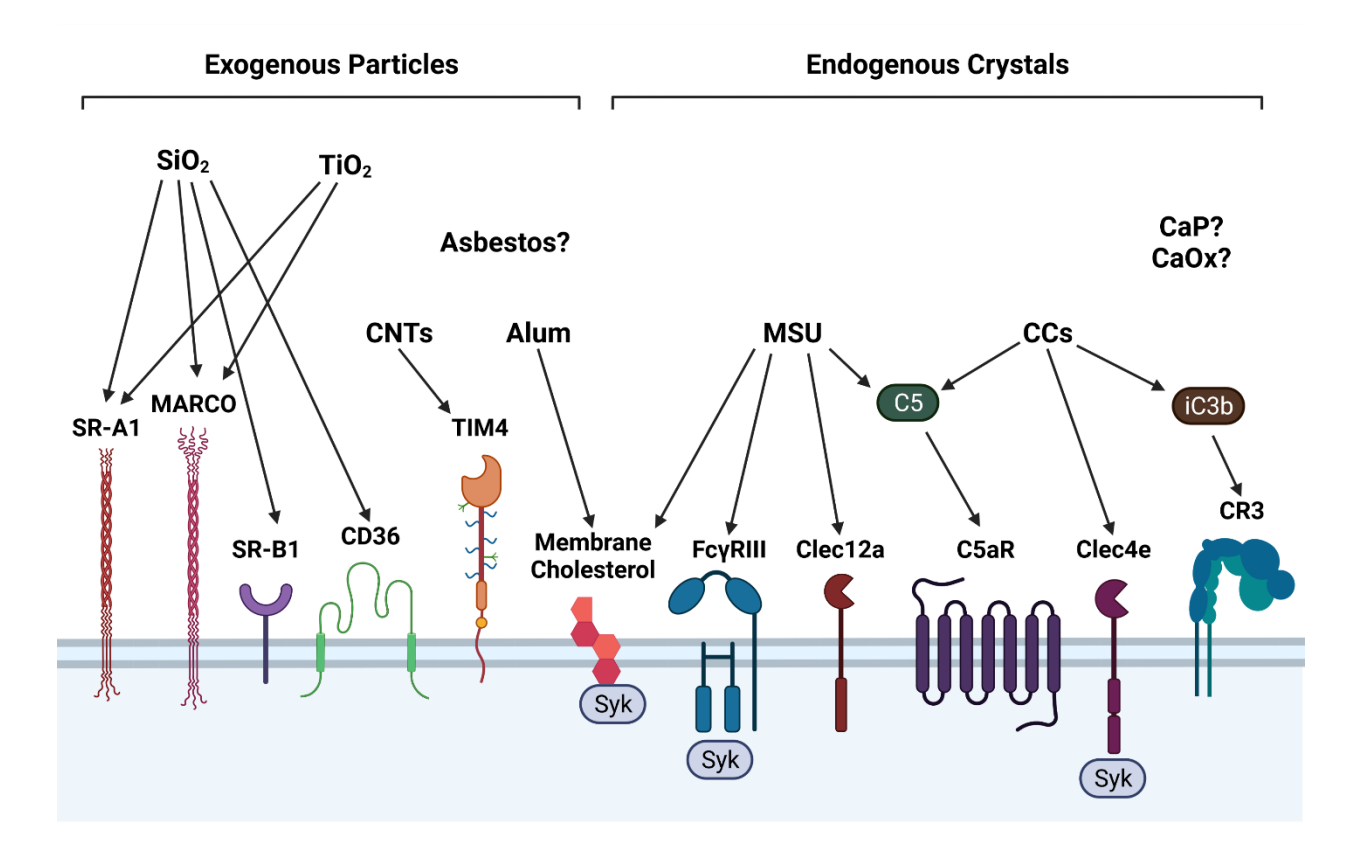


Figure 2.1. Surface receptors involved in detecting exogenous and endogenous particles. Phagocytes employ a diverse assortment of membrane receptors to recognize and ultimately phagocytose particles, some of which are depicted in this illustration. SiO₂ is recognized by scavenger receptors SR-A1, MARCO, SR-B1, CD36. TiO₂ is recognized only by SR-A1 and MARCO. CNTs are recognized by phosphatidylserine receptor Tim4. Alum and MSU interact directly with membrane cholesterol moieties to stimulate Syk signaling. MSU and CCs activate complement components C5 and iC3b, which stimulate C5aR and CR3, respectively. MSU also binds to FcγRIII/CD16 and C-type lectin (Clec)-12a. On human phagocytes only, CCs are recognized by Clec4e. Surface receptors for asbestos fibers and calcium-containing salts (e.g., CaP, CaOx) have not yet been identified. Figure created with BioRender.com.

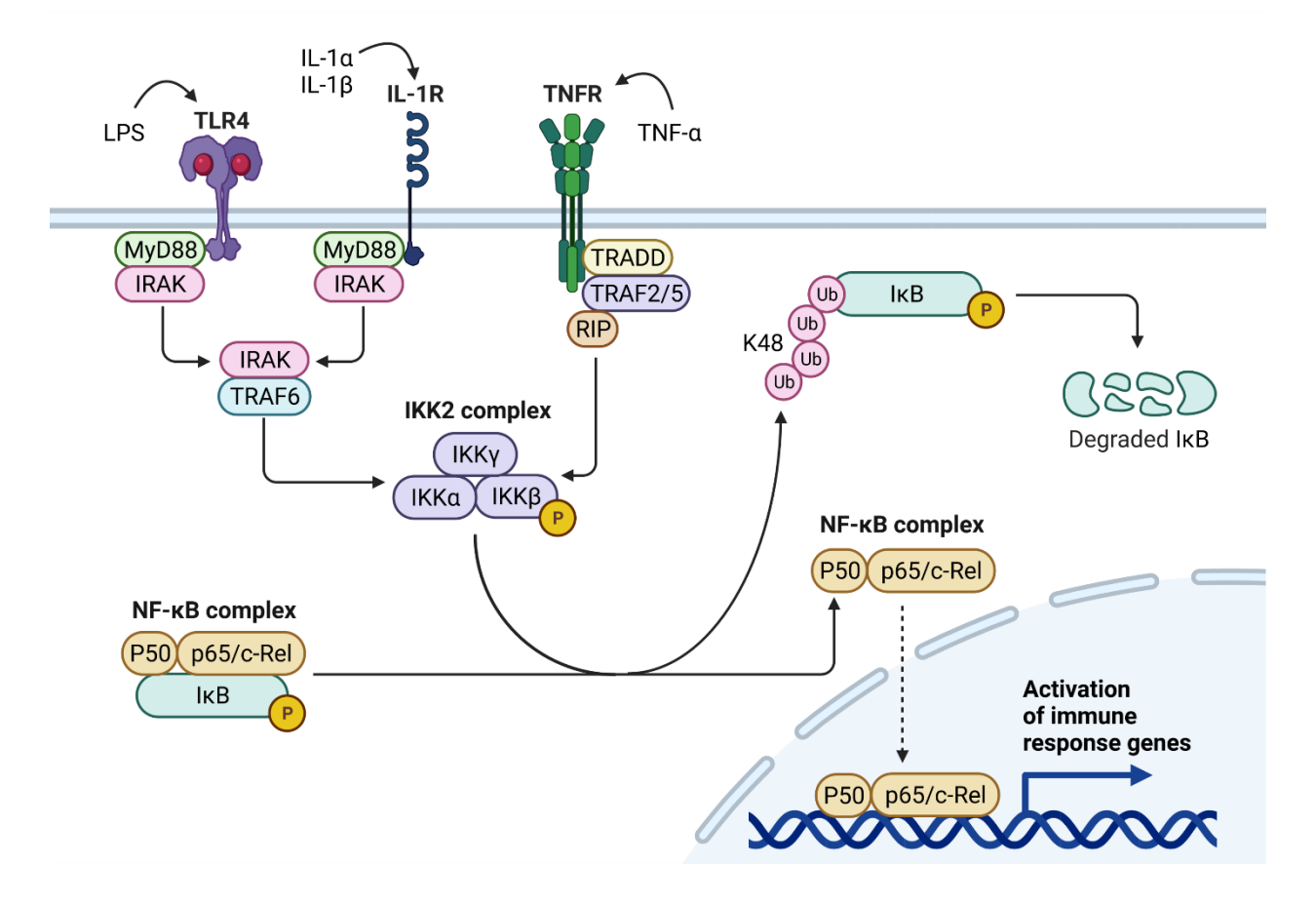


Figure 2.2. Mechanisms of Signal 1 inflammasome priming. Inflammasome priming can be triggered by diverse stimuli including bacterial molecules (e.g., LPS), alarmins (e.g., IL-1α), or proinflammatory cytokines (e.g., IL-1β, TNF-α). LPS binds to TLR4, activates the MyD88-IRAK-TRAF6 pathway, and induces IKKβ activity within the IKK2 complex. Likewise, by binding IL-1R, IL-1α and IL-1β promote IKKβ activity through the MyD88-IRAK-TRAF6 pathway. Conversely, when TNF-α binds TNFR, the TRADD-TRAF2/5-RIP pathway induces IKKβ activity. Once activated, IKKβ phosphorylates IκB within the NF-κB complex, targeting IκB for K48 polyubiquitination and proteasomal degradation. IκB degradation liberates the NF-κB complex (i.e., P50 and p65/c-Rel) and enables its translocation to the nucleus, where it upregulates proinflammatory cytokines, chemokines, and other immune response genes. Figure created with BioRender.com.

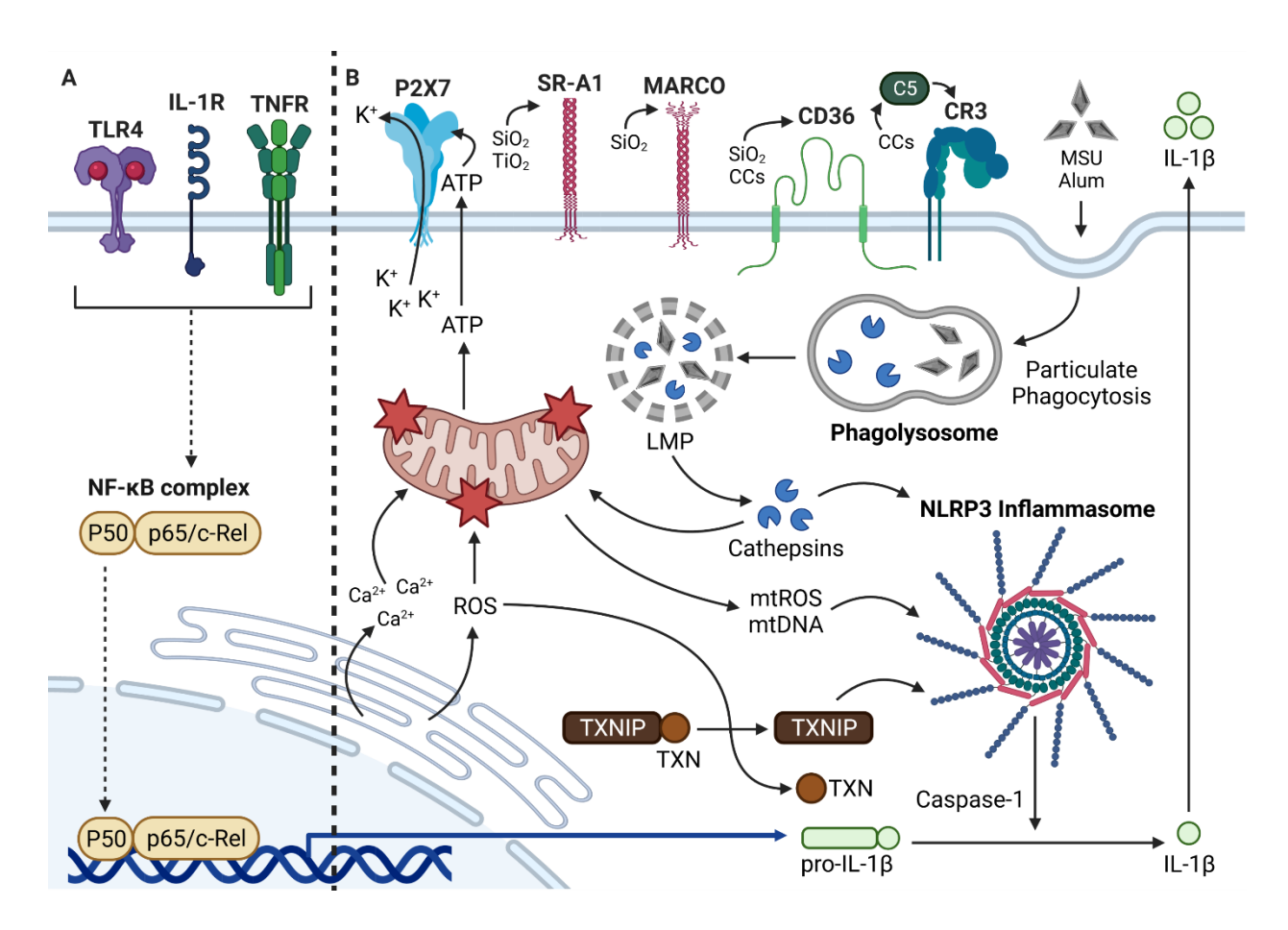


Figure 2.3. Mechanisms of Signal 2 inflammasome activation. (A) Summary of Signal 1 inflammasome priming. Translocation of NF-κB into the nucleus leads to upregulation of proinflammatory cytokines such as pro-IL-1β and inflammasome subunits (i.e., NLRP3, ASC, procaspase-1; not shown). (B) The NLRP3 inflammasome is a cytosolic multiprotein complex that promotes proinflammatory cytokine production in response to extracellular stimuli and intracellular stress. Many extracellular and intracellular components can be involved in particledriven inflammasome oligomerization and activity. Some particles (e.g., SiO₂, TiO₂, CCs) bind transmembrane receptors prior to phagocytosis, whereas other particles (e.g., MSU, alum) interact directly with the plasma membrane. Following phagocytosis, the particle-containing phagosomes fuse with a lysosome to form a phagolysosome. Through undefined mechanisms, the particles aggravate the phagolysosomal membrane and induce lysosomal membrane permeabilization (LMP), which causes release of lysosomal proteases called cathepsins into the cytosol. Some cathepsins such as cathepsin B can directly trigger inflammasome oligomerization. Cathepsins can cause mitochondrial dysfunction and release of mtDAMPs (e.g., ATP, mtROS, mtDNA) into the cytosol. ATP released from dying phagocytes can interact with P2X7 receptors and trigger K⁺ efflux, which can contribute to inflammasome activation, mtROS and mtDNA can also contribute significantly to inflammasome oligomerization. Mitochondrial dysfunction can alternatively be elicited by CHOP-mediated Ca²⁺ release and ROS production from the ER. Cytosolic ROS contributes to dissociation of TXN from TXNIP, the latter of which can promote inflammasome activation. Once the inflammasome is assembled, pro-caspase-1 proteolytically activates adjacent pro-caspase-1 moieties. Activated caspase-1 then proteolytically processes pro-IL-1β to IL-1β,

Figure 2.3 (cont'd)

which is ultimately released from the cell to interact with IL-1R on neighboring phagocytes. Figure created with BioRender.com.

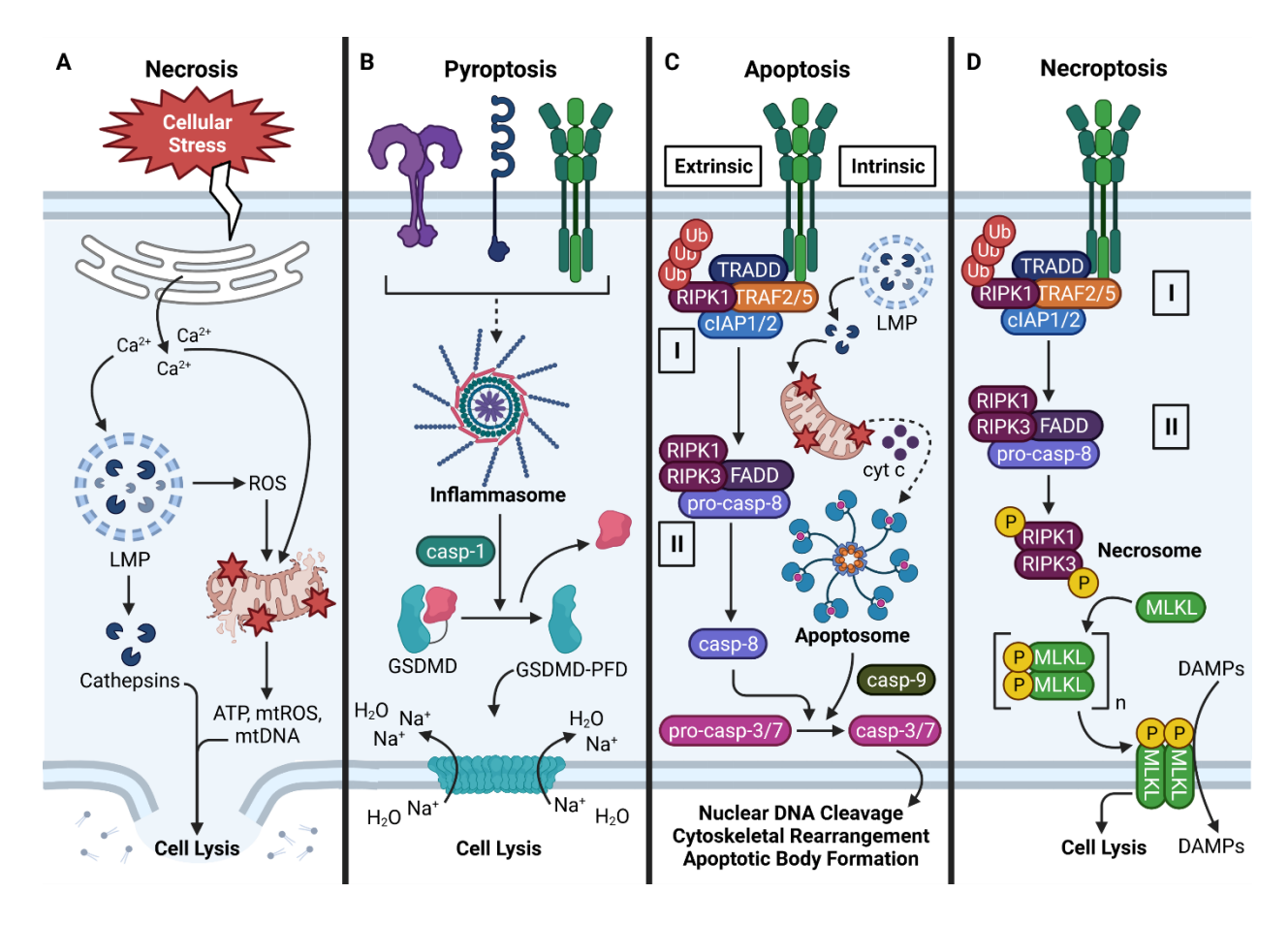


Figure 2.4. Major cell death pathways induced by particles. (A) Overview of necrosis. Necrosis can be triggered by various stimuli that provoke cellular stress. Common hallmarks of necrosis include Ca²⁺ efflux from the ER, Ca²⁺-induced LMP and cathepsin release, ROS-driven mitochondrial dysfunction, cellular swelling, plasma membrane rupture, and DAMP release. (B) Overview of pyroptosis. Following NLRP3 inflammasome oligomerization and activation, caspase-1 proteolytically processes GSDMD to expose its N-terminal pore-forming domain (PFD). GSDMD-PFD polymerizes into a pore in the plasma membrane, which allows Na⁺ to move along its electrochemical gradient into the cell. By osmosis, water enters the cell, causes cellular swelling, and cell lysis. (C) Overview of apoptosis (extrinsic and intrinsic). Extrinsic apoptosis is triggered by activation of a death receptor (e.g., TNFR), which promotes assembly of Complex I. Complex I consists of TRADD, TRAF2/5, cIAP1/2, and ubiquitinated RIPK1. Inhibition of cIAP1/2 and/or deubiquitylation of RIPK1 by CYLD (not shown) induces formation of cytosolic Complex II, which consists of RIPK1, RIPK3, FADD, and pro-caspase-8 oligomers that proteolytically activate themselves. Intrinsic apoptosis is defined by release of cytochrome c (cyt c) from perturbed mitochondria, formation of a multiprotein apoptosome, and activation of caspase-9. In certain cases, LMP-driven cathepsin release may contribute to mitochondrial dysfunction. Caspase-8/9 proteolytically activates caspase-3/7, which promotes nuclear DNA cleavage, cytoskeletal rearrangement, and apoptotic body formation. (**D**) Overview of necroptosis. Necroptosis is characterized by activation of a death receptor (e.g., TNFR), Complex I formation, and Complex II formation as in extrinsic apoptosis. Inhibition of pro-caspase-8 activation allows formation of the RIPK1-RIPK3 necrosome, which phosphorylates MLKL. Phospho-MLKL monomers polymerize into a pore-shaped complex at phosphatidylinositol 3-phosphate sites in the

Figure 2.4 (cont'd)

inner leaflet of the plasma membrane. Consequently, cell lysis occurs, and DAMPs are released from the cell. Some steps in the depicted cell death pathways are omitted for clarity. Figure created with BioRender.com.

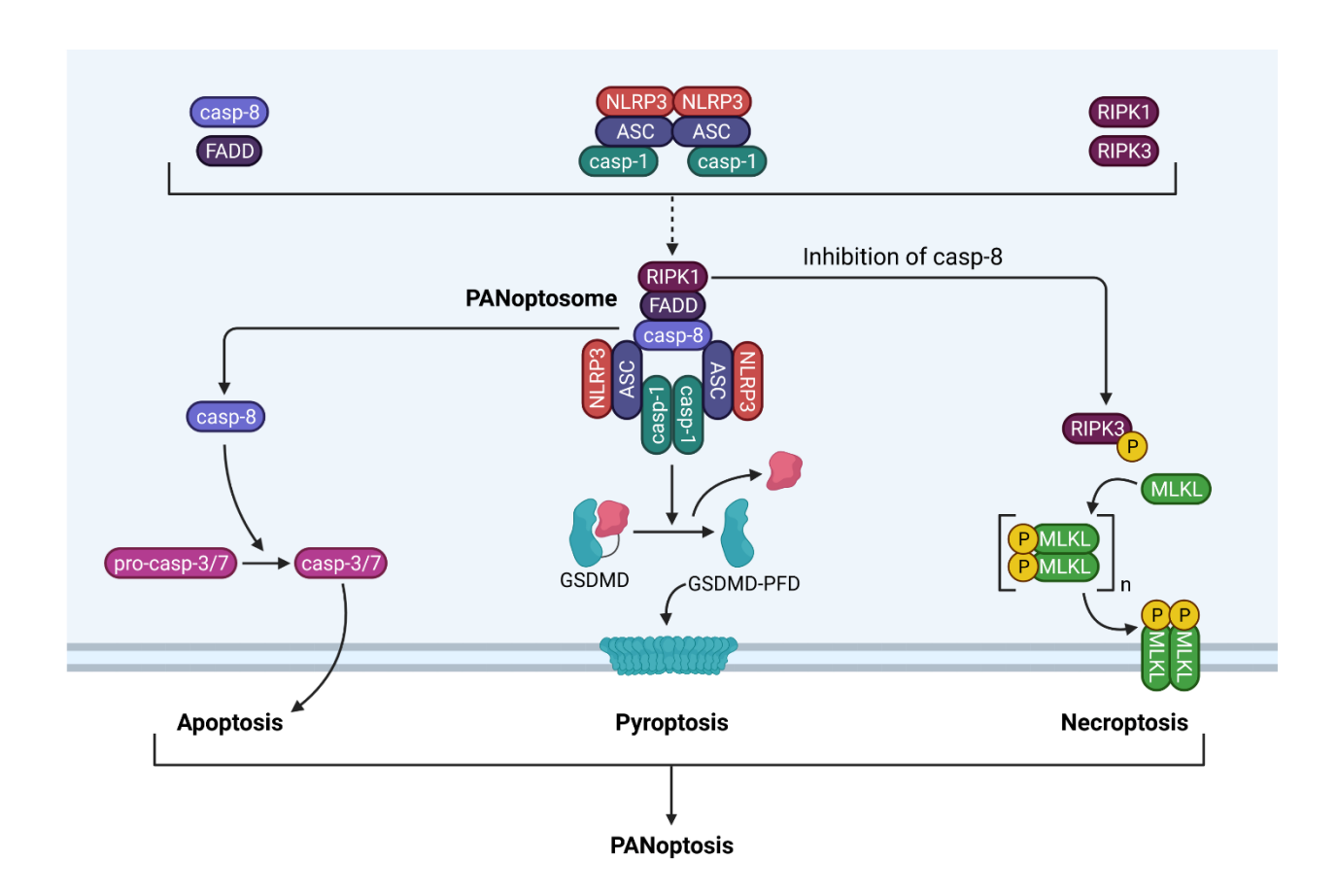


Figure 2.5. PANoptosome components and functionality. The PANoptosome is a multiprotein complex consisting of molecules from the apoptotic, pyroptotic, and necroptotic cell death pathways. Exposure to a proinflammatory stimulus such as LPS causes upregulation and activation of apoptotic proteins (i.e., caspase-8, FADD), pyroptotic proteins (i.e., NLRP3, ASC, caspase-1), and necroptotic proteins (i.e., RIPK1, RIPK3). These proteins associate with one another to form the PANoptosome. Following assembly, the PANoptosome can execute apoptosis, pyroptosis, and necroptosis simultaneously by driving caspase-3/7 activation by caspase-8, GSDMD processing by caspase-1, and MLKL phosphorylation and pore formation by RIPK1 and RIPK3. Cell death by concurrent apoptosis, pyroptosis, and necroptosis is termed PANoptosis. Figure created with BioRender.com.

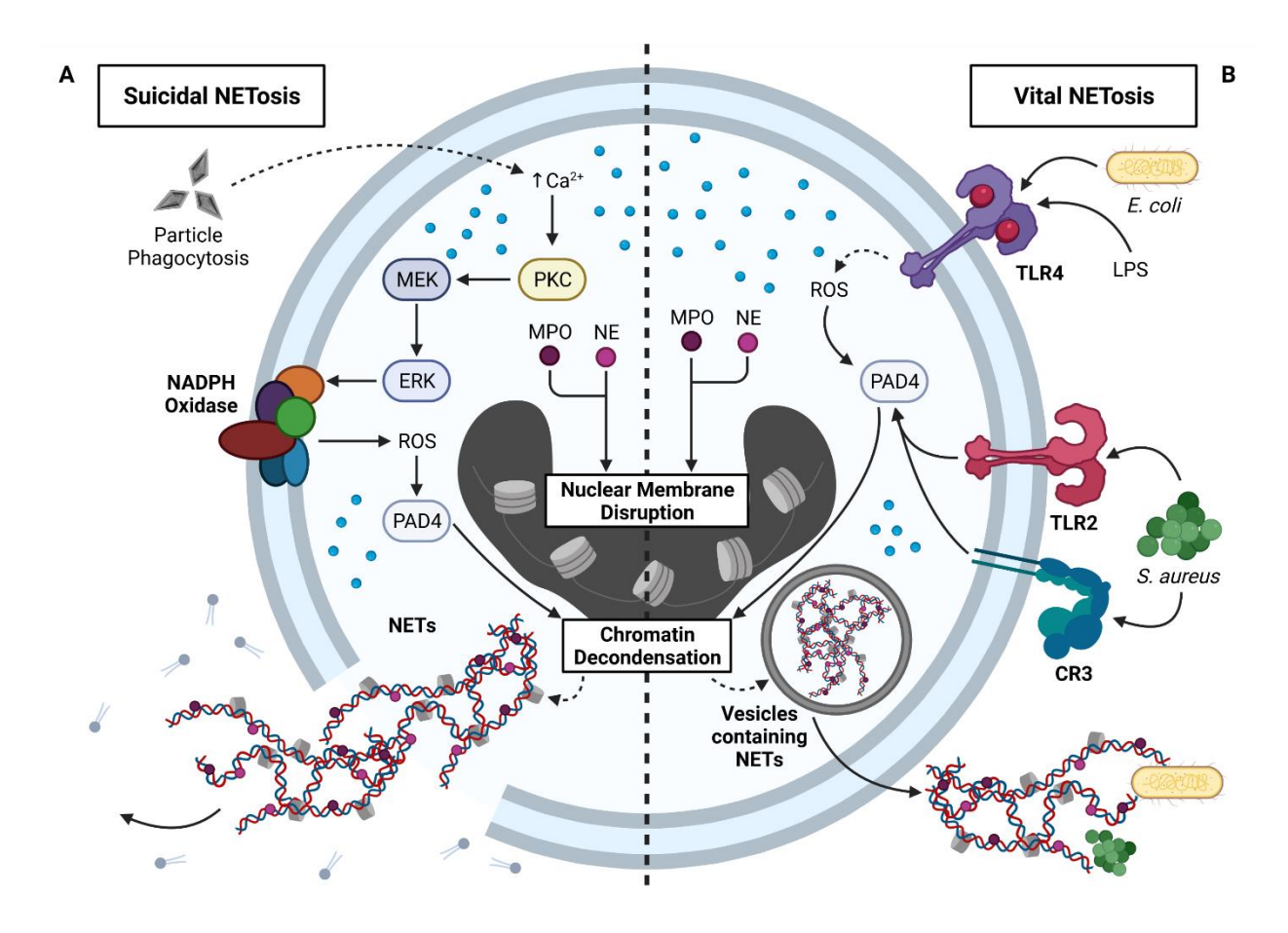


Figure 2.6. Mechanisms that contribute to NETosis. NETosis is the process by which neutrophil extracellular traps (NETs) are formed and released from neutrophils. Two primary forms of NETosis exist: suicidal and vital NETosis. (A) Overview of suicidal NETosis. Neutrophils phagocytose exogenous particles (e.g., SiO₂) and endogenous particles (e.g., CCs), which trigger Ca²⁺ efflux from the ER. Intracellular Ca²⁺ efflux activates protein kinase C (PKC), PKC activates MEK, and MEK activates ERK. ERK stimulates NADPH oxidase via gp91phox phosphorylation, and NADPH oxidase produces ROS. ROS activates peptidyl arginine deiminase 4 (PAD4), which contributes to chromatin decondensation. Translocation of myeloperoxidase (MPO) and neutrophil elastase (NE) into the nucleus leads to nuclear membrane disruption and additional chromatin decondensation. Resultant NETs are directly released into the cytosol, and rupture of the plasma membrane contributes to extracellular NET release and neutrophil death. Suicidal NETosis occurs within a 2-4 h timeframe. (B) Overview of vital NETosis. Activation of TLR4 by LPS or Gramnegative bacteria (e.g., E. coli) contributes to ROS production, which is required for PAD4 activity. Alternatively, activation of TLR2 or CR3 by Gram-positive bacteria (e.g., S. aureus) leads to downstream PAD4 activation. As with suicidal NETosis, PAD4 triggers chromatin decondensation, and nuclear translocation of MPO and NE contributes to disruptions in the nuclear membrane. NETs are encased in nuclear vesicles, and NETs are released from viable neutrophils via exocytosis. Vital NETosis occurs within a 5-60 min timeframe, and released NETs can ensnare bacteria in the extracellular environment. Figure created with BioRender.com.

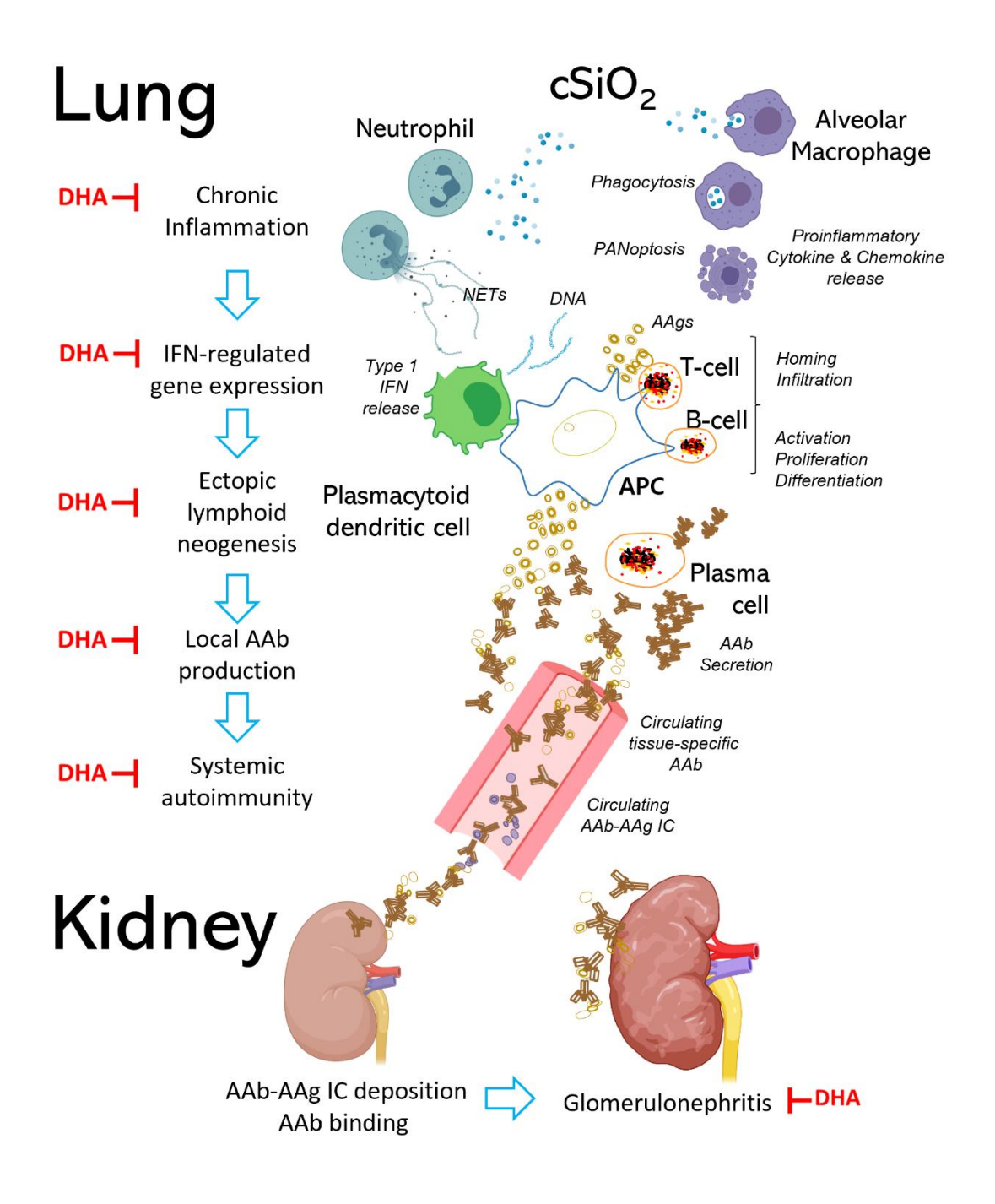


Figure 2.7. Respirable cSiO₂ triggers autoimmune flaring and progression in the SLE-prone female NZBWF1 mouse. Chronic exposure to respirable cSiO₂ particles contributes to irresolvable lung inflammation and systemic autoimmunity, resulting in end-stage glomerulonephritis and shortened lifespan in female NZBWF1 mice. Alveolar macrophages (AMΦs), which serve as one of the first lines of immunological defense in the lung, detect and phagocytose inhaled cSiO₂. Resultantly, cSiO₂ particles engulfed by AMΦs induce immunogenic cell death (i.e., pyroptosis, apoptosis, necrosis), proinflammatory cytokine and chemokine release, and NETosis in neighboring neutrophils. Aberrant accumulation of dead cell corpses,

Figure 2.7 (cont'd)

proinflammatory mediators, and host nucleic acids promotes recruitment of autoreactive T and B cells into the lung and type I interferon (IFN) release from plasmacytoid dendritic cells, leading to formation of ectopic lymphoid tissue (ELT). Type I IFN triggers maturation of B cells into plasma cells, which secrete IgG autoantibodies (AAb) that target local and systemic autoantigens (AAg). Binding of AAbs to their corresponding AAgs can lead to formation of immune complexes (ICs) that circulate in the body via blood vessels and deposit in other organs such as the kidneys. Once deposited, ICs recruit additional proinflammatory cells to the tissue, ultimately resulting in irreversible kidney damage and failure. Steps at which DHA has been shown to interfere with these pathways are indicated by red \bot symbols. Figure created with BioRender.com.

TABLES

Table 2.1. Sources and common exposure routes of exogenous and endogenous particles.

Name	Sources	Route	References
SiO ₂	Construction, mining, ceramic manufacturing, dental mold production, jewelry production	Inhalation	[75] [73] [74]
Asbestos	Construction, mining, pipefitting, shipyard work, insulation manufacturing, textile production	Inhalation	[76] [53] [54]
CNTs	Construction, electronics, biomedicine	Inhalation, Injection	[78] [79] [57] [80]
TiO ₂	Manufacturing, agriculture, food additives, cosmetics, biomedicine	Inhalation, Ingestion	[60] [61] [59]
Alum	Foundry work, vaccine adjuvants	Inhalation, Injection	[82] [63] [81]
MSU	Dietary uric acid, dysregulated purine metabolism, hyperuricemia	N/A	[96] [97]
CCs	Dietary cholesterol, dysregulated cholesterol metabolism, hypercholesterolemia	N/A	[89] [88] [95] [87]
CaP	Dietary calcium and phosphate, hypercalcituria, hyperphosphatemia	N/A	[91] [92] [93]
CaOx	Dietary calcium and oxalate, hypercalcituria, hyperoxaluria	N/A	[91] [92] [93]

Alum, aluminum-containing salts; CaOx, calcium oxalate; CaP, calcium phosphate; CCs, cholesterol crystals; CNTs, carbon nanotubes; SiO_2 , silicon dioxide; TiO_2 , titanium dioxide.

Table 2.2. Examples of studies demonstrating toxic responses of exogenous particles.

Reference	Particle Type(s)	Experimental Model(s)	Dose(s)	Time- point(s)	Results
[130]	SiO ₂ Asbestos	THP-1 cells (human MΦs)	SiO ₂ : 0.2 mg/ml Asbestos: 0.2 mg/ml	6 h	Caspase-1 activation, IL-1β release
[131]	SiO ₂ Alum	Primary murine BMDMΦs, primary human PBMCs	SiO ₂ : 125- 1000 µg/ml Alum: 100-500 µg/ml	3 h	LMP, cathepsin B release, caspase-1 activation, IL-1β release
[354]	Alum	Primary murine peritoneal MΦs	40-240 μg/ml	6 h	Caspase-1 activation, IL-1β maturation
[254]	TiO ₂	Primary murine AMΦs	50-200 μg/ml	1 h, 4 h	LMP, cathepsin B release, ROS production, IL-1β release
[274]	SiO ₂ TiO ₂	Primary murine BMDCs	SiO ₂ : 5-50 µg/cm ² TiO ₂ : 5-50 µg/cm ²	18 h	SiO ₂ : apoptosis, TiO ₂ : ROS production; IL-1β release
[355]	Asbestos CNTs	Primary human MΦs	Asbestos: 100 µg/ml CNTs: 100 µg/ml	6 h	Cathepsin B activity, Syk activity, ROS production, IL-1β release
[356]	Alum	Primary murine peritoneal MΦs, primary murine BMDMΦs	400 μg/ml	2 h, 6 h	LMP, IL-1β synthesis, PGE ₂ synthesis
[183]	SiO ₂	MH-S AMΦs (murine AMΦs)	50 μg/cm ²	30-120 min, 3-6 h	30-120 min: LMP, 3-6 h: caspase-3/9 activation, apoptosis, necrosis
[273]	SiO ₂ Alum	Primary murine BMDCs	SiO ₂ : 62.5-250 μg/ml Alum: 62.5- 250 μg/ml	24 h	Syk activity, IL-2 release, CD4 ⁺ T cell expansion
[234]	SiO ₂ Asbestos	Primary murine neutrophils, primary human neutrophils	SiO ₂ : 0.2 mg/ml Asbestos: 0.2 mg/ml	2 h	NET formation, primary necrosis and necroptosis, NET release

Alum, aluminum-containing salts; AM Φ , alveolar macrophage; BMDC, bone marrow-derived dendritic cell; BMDM Φ , bone marrow-derived macrophage; CNT, carbon nanotube; h, hour(s); LMP, lysosomal membrane permeabilization; min, minute(s); M Φ , macrophage; NET, neutrophil

Table 2.2 (cont'd)

extracellular trap; PBMC, peripheral blood mononuclear cell; PGE $_2$: prostaglandin E $_2$; ROS, reactive oxygen species; SiO $_2$, silicon dioxide; Syk, spleen tyrosine kinase; TiO $_2$, titanium dioxide.

Table 2.3. Examples of studies demonstrating toxic responses of endogenous particles.

Reference	Particle Type(s)	Experimental Model(s)	Dose(s)	Time- point(s)	Results
[133]	MSU CaP	THP-1 cells (human MΦs), primary human monocytes, primary murine peritoneal MΦs	MSU: 1-100 μg/ml CaP: 1-100 μg/ml	6 h	Caspase-1 activation, IL-1β maturation and release
[357]	CCs	Primary human PBMCs	15.6-125 μg/ml	6 h	LMP, caspase-1 activation, IL-1β release
[358]	CCs	THP-1 cells (human MΦs), primary human monocytes, primary human BMDMΦs	0.1-2 mg/ml	4-24 h	LMP, cathepsin B release, K ⁺ efflux, IL-1β release
[271]	MSU	Primary murine BMDCs	250 μg/ml	5 d	Inflammasome activity and Th17- associated cytokine release from BMDCs
[218]	CaP	THP-1 cells (human MΦs), primary human monocytes, primary human MΦs, primary murine BMDMΦs	500 μg/ml	6 h	ROS production, caspase-1 activation, IL-1β release, apoptosis
[359]	CaOx	Primary murine BMDCs	30-1000 μg/ml	6 h	CaOx phagocytosis, K ⁺ efflux, IL-1β maturation and release
[234]	MSU CCs CaP CaOx	Primary murine neutrophils, primary human neutrophils	MSU: 0.2 mg/ml CCs: 0.2 mg/ml CaP: 0.2 mg/ml CaOx: 0.2 mg/ml	2 h	NET formation, primary necrosis and necroptosis, NET release

 $BMDM\Phi, \ bone \ marrow-derived \ macrophage; \ CaOx, \ calcium \ oxalate; \ CaP, \ calcium \ phosphate; \ CC, \ cholesterol \ crystal; \ d, \ day(s); \ h, \ hour(s); \ LMP, \ lysosomal \ membrane \ permeabilization; \ MSU,$

Table 2.3 (cont'd)

monosodium urate; $M\Phi$, macrophage; NET, neutrophil extracellular trap; PBMC, peripheral blood mononuclear cell; ROS, reactive oxygen species; TNF, tumor necrosis factor.

CHAPTER 3: LIPIDOME MODULATION BY DIETARY OMEGA-3 POLYUNSATURATED FATTY ACID SUPPLEMENTATION OR SELECTIVE SOLUBLE EPOXIDE HYDROLASE INHIBITION SUPPRESSES ROUGH LPSACCELERATED GLOMERULONEPHRITIS IN LUPUS-PRONE MICE PUBLICATION NOTICE

The following chapter has been published by Frontiers in Immunology and is available through the Frontiers of Immunology website at "Favor OK*, Chauhan PS*, Pourmand E, Edwards AM, Wagner JG, Lewandowski RP, Heine LK, Harkema JR, Lee KSS, Pestka JJ. Lipidome modulation by dietary omega-3 polyunsaturated fatty acid supplementation or selective soluble epoxide hydrolase inhibition suppresses rough LPS-accelerated glomerulonephritis in lupus-prone mice. Front Immunol. 2023 Feb 16;14:1124910. doi: 10.3389/fimmu.2023.1124910. PMID: 36875087; PMCID: PMC9978350." *Indicates that these authors contributed equally to this work.

ABSTRACT

Introduction: Lipopolysaccharide (LPS)-accelerated autoimmune glomerulonephritis (GN) in NZBWF1 mice is a preclinical model potentially applicable for investigating lipidome-modulating interventions against lupus. LPS can be expressed as one of two chemotypes: smooth LPS (S-LPS) or rough LPS (R-LPS) which is devoid of O-antigen polysaccharide sidechain. Since these chemotypes differentially affect toll-like receptor 4 (TLR4)-mediated immune cell responses, these differences may influence GN induction.

Methods: We initially compared the effects of subchronic intraperitoneal (i.p.) injection for 5 wk with 1) Salmonella S-LPS, 2) Salmonella R-LPS, or 3) saline vehicle (VEH) (Study 1) in female NZBWF1 mice. Based on the efficacy of R-LPS in inducing GN, we next used it to compare the impact of two lipidome-modulating interventions, ω-3 polyunsaturated fatty acid (PUFA) supplementation and soluble epoxide hydrolase (sEH) inhibition, on GN (Study 2). Specifically, effects of consuming w-3 docosahexaenoic acid (DHA) (10 g/kg diet) and/or the sEH inhibitor 1-(4-trifluoro-methoxy-phenyl)-3-(1-propionylpiperidin-4-yl) urea (TPPU) (22.5 mg/kg diet ≈ 3 mg/kg/day) on R-LPS triggering were compared.

Results: In Study 1, R-LPS induced robust elevations in blood urea nitrogen, proteinuria, and hematuria that were not evident in VEH- or S-LPS-treated mice. RLPS-treated mice further exhibited kidney histopathology including robust hypertrophy, hyperplasia, thickened membranes, lymphocytic accumulation containing B and T cells, and glomerular IgG deposition consistent with GN that was not evident in VEH- or SLPS-treated groups. R-LPS but not S-LPS induced spleen enlargement with lymphoid hyperplasia and inflammatory cell recruitment in the liver. In Study 2, resultant blood fatty acid profiles and epoxy fatty acid concentrations reflected the anticipated DHA- and TPPU-mediated lipidome changes, respectively. The relative rank order of

R-LPS-induced GN severity among groups fed experimental diets based on proteinuria, hematuria, histopathologic scoring, and glomerular IgG deposition was: VEH/CON< R-LPS/DHA \approx R-LPS/TPPU<<< R-LPS/TPPU+DHA \approx RLPS/CON. In contrast, these interventions had modest-to-negligible effects on RLPS-induced splenomegaly, plasma antibody responses, liver inflammation, and inflammation-associated kidney gene expression.

Discussion: We show for the first time that absence of O-antigenic polysaccharide in R-LPS is critical to accelerated GN in lupus-prone mice. Furthermore, intervention by lipidome modulation through DHA feeding or sEH inhibition suppressed R-LPS-induced GN; however, these ameliorative effects were greatly diminished upon combining the treatments.

INTRODUCTION

Systemic lupus erythematosus (lupus) is a complex, debilitating autoimmune disease that affects primarily women of childbearing age, attacks multiple organ systems, and features repeated cycles of remission and relapse [360]. Lupus development and progression are associated with chronic inflammation, aberrant accumulation of dead/dying cells, release of autoantigens (AAgs) that promote T and B cell hyperactivation, and aberrant autoantibody (AAb) production [361, 362]. Resultant AAb:AAg immune complex formation and peripheral tissue deposition activate the complement system and trigger infiltration of innate immune cells that subsequently secrete cytokines and chemokines. Collectively, these events promote a perpetual cycle of immune cell infiltration, proinflammatory mediator release, and cell death evoking unresolvable inflammation, further activation of autoreactive lymphocytes, and irreversible tissue damage [363, 364]. Immune complex deposition in the kidneys of patients with lupus can lead to glomerulonephritis (GN) that progresses over time to end-stage kidney disease.

While genetic predilection is a primary contributor to lupus, its onset and progression can be potentiated or attenuated by environmental influences [365, 366]. There is increasing recognition that exposure of individuals with lupus to infectious bacteria can trigger inflammation and activation of autoreactive lymphocytes via pathogen-associated molecular patterns (PAMPs), leading to exacerbation of lupus symptoms [367]. In particular, exposure to Gram-negative bacteria through infection or gut leakage is common and could contribute to lupus flaring [365, 368-370]. Lipopolysaccharide (LPS) is an important structural component of the Gram-negative bacterial cell wall that binds toll-like receptor 4 (TLR4) on innate and adaptive immune cells to promote nuclear translocation of NF-κB, which upregulates expression of genes that contribute to autoimmune disease progression [371-374]. Consistent with this premise, earlier preclinical investigations have reported that repeated LPS exposure elicits autoimmune responses in nonautoimmune BALB/c and C57BL/6 (C57) mice [375-378], and, furthermore, accelerates spontaneous autoimmunity in lupus-prone New Zealand Black/White F1 (NZBWF1), MRL/lpr (MRL) and BXSB mice [379-384]. Key mechanisms that have been proposed for LPS-accelerated autoimmune disease include induction of polyclonal B-cell activation, decreased immune complex uptake by mononuclear phagocytes, delayed clearance of circulating immune complexes, and increased immune complex deposition in the kidney [375-384].

Since there is no cure for lupus, it is managed in the clinic through a variety of prescribed pharmaceuticals, such as glucocorticoids, immunosuppressants, and monoclonal antibodies [385, 386]. Despite the efficacy of these therapeutics against chronic inflammation and autoreactive immunity, patients still incur drug-related adverse side effects and steep financial costs [387]. In addition, these therapeutics might need to be taken indefinitely because lupus symptoms can flare

spontaneously over a lifetime. Therefore, there is a critical need for safer, more cost-effective interventions against lupus onset and progression.

One intervention of potential high relevance to lupus is modulation of the lipidome by dietary supplementation with marine ω -3 polyunsaturated fatty acids (PUFAs). Numerous clinical and preclinical studies have demonstrated that increasing consumption the ω -3 PUFAs docosahexaenoic acid (DHA) and eicosapentaenoic acid (EPA) at the expense of terrestrial ω -6 PUFAs like linoleic acid (LA) and arachidonic acid (ARA) has potential benefits for reducing severity of chronic inflammatory diseases (reviewed in [388]), including autoimmune diseases like lupus [341, 350, 389, 390]. Beneficial effects of ω -3 PUFAs are linked to: 1) reduced production of proinflammatory ω -6 metabolites, 2) generation of specialized pro-resolving mediators, 3) changes in membrane structure/function, and 4) modulation of gene expression by altering G-protein-couple receptor signaling and transcription factor activity [388].

Another possible lipidome-mediated intervention for lupus is to modulate the lipidome by pharmacological inhibition of soluble epoxide hydrolase (sEH). Among the sEH inhibitors employed in preclinical studies, 1-(4-trifluoro-methoxy-phenyl)-3-(1-propionylpiperidin-4-yl) urea (TPPU) is highly preferred because it is safe and exhibits impressive potency, biological activity, and pharmacokinetic distribution [391-393] without evident non-specific binding [394]. TPPU has been shown to be efficacious in preclinical studies at reducing chronic inflammatory diseases [395] and more recently, autoimmune diseases including lupus GN [23], autoimmune encephalitis [396], and rheumatoid arthritis [397]. One mode of action for TPPU and other sEH inhibitors is believed to involve skewing of the cytochrome P450 (CYP) ω-6 metabolite profile to favor anti-inflammatory/pro-resolving epoxy fatty acids (EpFAs) over the proinflammatory or less active dihydroxy fatty acids (DiHFAs; vicinal diols) generated because of sEH activity.

Furthermore, there is intriguing but limited evidence in preclinical models that suggests there is enhanced efficacy in anti-inflammatory effects when ω -3s are combined with pharmacologic inhibition of sEH [21, 398-401].

Preclinical animal models are an integral tool for investigating new therapies for managing lupus progression and resultant GN [402]. Over the past decade, LPS-accelerated severe lupus GN in NZBWF1 mice has been extensively used to explore efficacy of a wide spectrum of novel interventions including Tris dipalladium [32], epigallocatechin-3-gallate [28], traditional Chinese medicinal herbs [403], citral [29], ginsenoside [404], honokial [31], antroquinonol [28], and xenon [30], suggesting that this model might be similarly amenable to for addressing effects of lipidome modulation through dietary supplementation or pharmacotherapy. However, one caveat to the use of the LPS-accelerated GN as a preclinical model is the lack of clarity on how different LPS chemotypes influence the GN response. LPS is comprised of three moieties linked by covalent bonds: i) lipid A, ii) rough core oligosaccharide, and iii) O-antigenic polysaccharide side chain which determines serotype [405]. Importantly, environmental stimuli and genetic mutations can cause Gram-negative bacteria to synthesize LPS with variable polysaccharide lengths via outer membrane remodeling [406]. While smooth LPS (S-LPS) includes the O-antigenic side chain, rough LPS (R-LPS) lacks the side chain completely or, in some cases, contains portions of the rough core oligosaccharide. Clinically relevant Gram-negative bacteria typically express S-LPS; however, some heterogeneously co-express R-LPS of varying lengths [407, 408]. Significantly, the mechanisms by which these two chemotypes activate TLR4 are very different. It has been demonstrated that R-LPS can efficiently activate TLR4 on both CD14⁺ and CD14⁻ cells as compared to S-LPS which acts primarily on CD14⁺ cells [407, 409]. These differences in TLR4 activation between the two chemotypes may influence their capacity to accelerate GN in NZBWF1

mice. However, while some investigations of LPS-accelerated murine GN explicitly specify using R-LPS, typically from *Salmonella* [375-377, 379-384], many others do not report the LPS chemotype used [28-31, 32, 382, 403, 404, 410]. Importantly, there has never been a head-to-head comparison of S-LPS and R-LPS accelerating GN in lupus-prone mice.

To address the research questions described above, we conducted two studies in lupusprone female NZBWF1 mice. In Study 1, we compared the effects of R-LPS and S-LPS on GN
induction to clarify how the presence or absence of O antigen polysaccharide impacts this widely
used preclinical model. The results indicated that repeated injection with R-LPS accelerated severe
GN whereas repeated injection with S-LPS did not. In Study 2, we evaluated how dietary DHA
supplementation and/or pharmacologic inhibition of sEH influence R-LPS-accelerated GN. We
found that DHA consumption and sEH inhibition alone suppressed GN, but the ameliorative
effects of these interventions were lessened upon combining the treatments.

MATERIALS AND METHODS

Animals

The Institutional Animal Care and Use Committee at Michigan State University (MSU) approved all experimental protocols (AUF #201800113) in accordance with guidelines established by the National Institutes of Health. Six-week-old female lupus-prone NZBWF1 mice were procured from the Jackson Laboratory (Bar Harbor, ME) and randomized into experimental groups for each study (**Tables S3.1, S3.2**). Only female NZBWF1 mice were used in this study because female mice of this strain exhibit greater severity and prevalence of lupus-related symptoms (e.g., elevated antinuclear antibody titers, formation of immune complexes, glomerulonephritis) compared to male NZBWF1 mice [339, 411]. Mice were housed two or four per cage in Study 1 and four per cage in Study 2, and all mice were given free access to food and water. Consistent

lighting (12 h light/dark cycle), temperature (21-24 °C), and humidity (40-55%) were maintained in animal housing facilities.

Diets

Four defined diet formulations were prepared as described in **Table S3.3**. All formulations used purified American Institute of Nutrition (AIN)-93G diet (70 g/kg fat) as a base to provide optimal nutrition to experimental rodents [412]. All diets contained 10 g/kg corn oil as a source of essential ω-6 fatty acids. The basal diet for Study 1 and control (CON) diet for Study 2 contained 60 g/kg high-oleic safflower oil (Hain Pure Food, Boulder, CO). For DHA-enriched diets, caloric human equivalent consumption of 5 g DHA per day was achieved by adding 25 g/kg microalgal oil containing 40% DHA (DHASCO; DSM Nutritional Products, Columbia, MD) in place of high-oleic safflower oil, resulting in 10 g DHA/kg diet [19]. For TPPU-amended diets, 22.5 mg TPPU (95% purity based on H-NMR analysis), synthesized and purified as described previously [391], was added to 1 kg of CON or DHA diet, resulting in the TPPU and TPPU+DHA diets. Fatty acid (**Table 3.1**) and TPPU (**Table S3.4**) concentrations in each diet were confirmed as described below.

Dietary fatty acid analyses

Fatty acid composition in each experimental diet was determined by modifying a previously described protocol [413]. Briefly, 400 mg of each diet sample was reconstituted in a 4:1 (v/v) ethanol/methanol solution + 0.1% (v/v) butylated hydroxytoluene (BHT) and heated 15 min at 55 °C in a CEM Mars 6 Xpress microwave digestion system (CEM Corporation, Matthews, NC). Then, 2 mg of extracted fatty acids from each diet sample were converted to fatty acid methyl esters (FAMEs) by treating with 500 μl of toluene and 20 μg of internal standard (methyl-12-tridecenoate), incubating with 2 ml of KOH (0.5 N) at 50 °C for 10 min, then subsequently

incubating with 3 ml of methanolic HCl (5% [v/v] at 80 °C for 10 min to allow base-catalyzed methylation and acid-catalyzed methylation, respectively. Following methylation, 2 ml of HPLC-grade water was added to the samples, and FAMEs were extracted by adding 2 ml of hexane to the samples twice. Extracted FAMEs were dried under nitrogen with an Organomation Multivap Nitrogen Evaporator (Organomation Associates, Berlin, MA). Dried FAMEs were then resuspended in 1 ml of isooctane and kept at -20 °C until further analysis.

FAMEs were analyzed by GC-MS as previously described [413]. Briefly, FAMEs in each sample were separated on a Perkin Elmer 680/600 GC-MS (Waltham, MA) outfitted with a HP-88 capillary column (100 m \times 0.25 mm inner diameter \times 0.2 μ m film thickness; Agilent Technologies, Santa Clara, CA). MassLynx (4.1 SCN 714; Waters Corporation, Milford, MA) was used to compare analyte retention time and electron ionization (EI) mass fragmentation to those in the reference standard, which consisted of Supelco 37 Component FAME Mix (Sigma-Aldrich, St. Louis, MO), mead acid, docosatetraenoic acid, ω -3 docosapentaenoic acid (DPA), ω -6 DPA, and palmitelaidic acid (Cayman Chemical, Ann Arbor, MI). FAME analyte peak areas were converted to individual FAME concentrations using a standard curve based on the reference standard and internal standard. For fatty acids with a detected chain length of 10 to 24 carbon atoms, fatty acid content in the diet is reported as percentage (w/w) of total fatty acids quantified (Table 3.1).

LPS preparation

S-LPS from *Salmonella enterica* serotype minnesota (cat. #L6261) and R-LPS from *Salmonella enterica* serotype minnesota Re 595 (cat. #L9724) were purchased from Sigma Aldrich (St. Louis, MO). Immediately prior to all intraperitoneal (i.p.) injections, stock suspensions of LPS

were prepared in sterile phosphate buffered saline (PBS), sonicated for 15 min, and vortexed for 1 min.

Experimental design

Experimental designs for Study 1 and Study 2 are shown in Figure 3.1A and Figure 3.1B, respectively. In both studies, female lupus-prone mice were administered experimental diets beginning at age 6 wk and maintained on the same diets throughout the entire experiment. To prevent lipid oxidation, all experimental diets were prepared every other week and stored at -20 °C until administered to mice. Mice received fresh diet every day. Starting at age 8 wk, all groups of mice were injected intraperitoneally with S-LPS, S-LPS, or PBS vehicle twice per wk for 5 wk, for 10 total injections. On a weekly basis, body weights were measured and urine sampled for development of proteinuria and hematuria using clinical protein dipsticks (Cortez Diagnostics, Calabasas, CA) and blood dipsticks (Teco Diagnostics, Anaheim, CA), respectively. To compare the inflammatory and autoimmune responses triggered by S-LPS and R-LPS (Study 1), groups of female mice (n = 2-4/gp) were given control (CON) AIN-93G diet and intraperitoneally injected with S-LPS (0.8 µg/g body weight [BW]) or R-LPS (0.8 µg/g BW) in 500 µl of PBS or PBS vehicle as previously described [404]. To assess effects of separate and concurrent DHA and TPPU administration on lupus GN induced by R-LPS (Study 2), female mice (n = 8/gp) were fed one of four experimental diets: 1) CON, 2) DHA, 3) TPPU, or 4) TPPU+DHA. Mice were intraperitoneally injected with R-LPS (0.6 µg/g BW) in 500 µl of PBS or PBS vehicle as previously described [31]. After 5 R-LPS injections, blood samples were collected from the lateral saphenous vein to assess TPPU plasma concentration (Study 2). Mice for both Study 1 and Study 2 were terminated at age 13 wk (5 wk after the first LPS injection). This timepoint was selected for

termination because it corresponds with development of accelerated, severe lupus GN previously reported in female NZBWF1 mice [31, 32, 404].

Necropsy and tissue collection

Primary euthanasia for all mice occurred by intraperitoneal injection of 56 mg/kg BW sodium pentobarbital, followed by abdominal aortic exsanguination as a means of secondary euthanasia. Blood was obtained with heparin-coated syringes and plasma isolated by centrifugation at 3500 x g for 10 min under cold conditions (4 °C). An antioxidant cocktail (0.2 mg/ml butylated hydroxytoluene, 0.2 mg/ml triphenylphosphine, 0.6 mg/ml EDTA) [414] was prepared and added at a 5% (v/v) concentration to all plasma aliquots designated for LC-MS/MS analysis. All plasma samples were stored at -80 °C as single-use aliquots for LC-MS/MS, blood urea nitrogen (BUN) and creatinine quantification, and AAb microarray profiling. The left kidney was removed and fixed in 10% (v/v) neutral-buffered formalin (Fisher Scientific, Pittsburgh, PA) for 24 h. The right kidney was cut longitudinally, with one half immersed in RNAlater (Thermo Fisher Scientific, Waltham, MA) overnight at 4 °C then stored at -80 °C for RNA analysis. The spleen was transversely cut in half, with one half fixed in 10% formalin and the other half immersed in RNAlater as described above. The left lateral lobe of the liver was cut transversely, with one half of the lobe fixed in 10% formalin fixative and the other half immersed in RNAlater as described above. All fixed tissues were transferred to 30% (v/v) ethanol for additional routine processing for light microscopic examination and for long-term storage.

Red blood cell fatty acid analysis

Red blood cell samples were sent to OmegaQuant Inc. for determination of membrane fatty acid concentrations by gas-liquid chromatography (GLC) as previously described [19].

LC-MS/MS quantitation of plasma TPPU and oxylipins

Waters Oasis-HLB cartridges (part #WAT094226, lot #176A30323A) were used for sample preparation and clean-up purposes. Solid-phase extraction (SPE) cartridges were prepared for solid phase extraction by washing once with 2 ml of ethyl acetate, twice with 2 ml of methanol, and twice with 2 ml of 95:5 (v/v) water/methanol + 0.1% (v/v) acetic acid. Plasma was then loaded onto the cartridges, and samples were spiked with 10 µl of deuterated internal standard solution (16 nM BGB2-d4, 10 nM LTB4-d4, 16 nM 8,9-DiHETrE-d11, 16 nM 9-HODE-d4, 20 nM 15(S)-HETE-d8, 40 nM 5(S)-HETE-d8, 40 nM 8,9-EpETrE-d11) and 10 μl of antioxidant cocktail (0.2 mg/ml butylated hydroxytoluene, 0.2 mg/ml triphenylphosphine, 0.6 mg/ml EDTA). After loading samples, cartridges were washed with 1.5 ml of 95:5 (v/v) water/methanol + 0.1% (v/v) acetic acid then dried with a low vacuum for 20 min to remove water and other unwanted residues. For elution, 6 μl of trap solution (30% [v/v] glycerol in methanol) was added to separate 2-ml Eppendorf tubes, then SPE cartridges were washed with 0.5 ml of methanol followed by 1 ml of ethyl acetate. The eluents were then concentrated under a high vacuum, and residues were reconstituted in 100 µl of 75% ethanol (v/v) containing 10 nM 12-[[(cyclohexylamino)carbonyl]amino]-dodecanoic acid (CUDA) as an internal standard. The samples then vortexed for 5 min followed by filtration through a 0.45-µm filter, then the filtrates were transferred to LC-MS/MS vials for analysis.

A XBridge BEH C18 2.1x150 mm, 5 μm, HPLC column, (ser. #01723829118314) was used for ultra-performance liquid chromatography (UPLC). The column was connected to a Waters TQ-XS tandem quadrupole UPLC/MS/MS instrument outfitted with a Waters ACQUITY SDS pump and Waters ACQUITY CM detector (Milford, MA). For UPLC, the chromatographic method was optimized to separate all analytes in 20 min using a sample volume of 10 μl and flow rate of 250 μl/min (**Table S5**). Gradient elution was performed by using 0.1% (v/v) acetic acid in

water for mobile phase A and 84:16 (v/v) acetonitrile/methanol + 0.1% glacial acetic acid for mobile phase B. During sample injection, the Waters ACQUITY FTN autosampler (Milford, MA) was held at a consistent temperature of 10 °C.

The ionization source for multiple reaction monitoring (MRM) modes was electrospray. MRM transitions and source parameters were optimized for each standard compound by individually infusing each compound separately into the mass spectrometer, ultimately to achieve the most optimal selectivity and sensitivity. For each experimental sample, Waters MassLynxTM MS software v4 (Milford, MA) was used to quantify analyte area, internal standard (IS) area, raw concentration (in nM), and signal-to-noise (S/N) ratio based on an 8spots-calibration linear standard curve. Dilution factors were calculated for each sample by dividing the original sample volume (in μl) by 100 μl. Normalized analyte concentrations in each sample were then quantified by dividing raw analyte concentrations by the sample's corresponding dilution factor.

Plasma BUN and creatinine quantification

Plasma levels of BUN and creatinine were quantified using a Urea Nitrogen Colorimetric Detection Kit (Thermo Fisher Scientific, Waltham, MA; cat. #EIABUN) and Creatinine Colorimetric Assay Kit (Cayman Chemical, Ann Arbor, MI; cat. #700460), respectively, according to the manufacturers' instructions.

Histopathology of kidney, spleen, and liver

Formalin-fixed kidneys were embedded in paraffin, sectioned at a thickness of 5 µm, and stained with hematoxylin and eosin (H&E) or Periodic acid-Schiff (PASH). A board-certified veterinary pathologist semi-quantitatively scored sectioned tissues in a blinded manner (i.e., without knowledge of individual animal treatments) using a modification of the International Society of Nephrology/Renal Pathology Society (ISN/RPS) classification system for lupus GN

[415]. Each tissue section was assigned one of the following grades: (0) normal glomeruli and no tubular proteinosis; (1) multifocal segmental proliferative GN with mild tubular proteinosis and occasional early glomerular sclerosis and crescent formation; (2) diffuse segmental proliferative GN with moderate tubular proteinosis, early glomerular sclerosis, and crescent formation; or (3) pervasive global proliferative and sclerosing GN with marked tubular proteinosis.

Fixed spleens and livers were processed and semi-quantitatively scored for histopathological development in a similar manner as the kidneys in this study. Scored liver lesions included (1) hepatocellular small and large vacuoles resembling lipid droplets and (2) periportal cellular inflammation (consisting primarily of inflammatory lymphocytes, plasma cells, and occasional neutrophils). Severity scores for these hepatic lesions were based on the percentage of the liver tissue section affected: (0) no treatment-induced lesions, (1) minimal (<10% affected); (2) mild (11-25% affected), (3) moderate (26-50% affected), (4) marked (51-75% affected), or (5) severe (76-100% affected).

Kidney immunohistochemistry for IgG deposition and accumulation of T and B lymphocytes

Kidney immunohistochemistry was performed as previously described [416]. Briefly, formalin-fixed kidney sections were stained with polyclonal goat anti-mouse IgG antibody (Bethyl Labs, Montgomery, TX; cat. #A-90-100A), polyclonal rabbit anti-mouse CD3 antibody (Abcam, Cambridge, MA; cat. #ab5690), or monoclonal rat anti-mouse CD45R antibody (Becton Dickinson, Franklin Lakes, NJ; cat. #550286) at the MSU Investigative Histopathology Laboratory to detect total IgG, CD3⁺ T lymphocytes, and CD45R⁺ B lymphocytes, respectively. Slides were scanned with a Slideview VS200 research slide scanner (Olympus, Hicksville, NY). Semi-quantitative scores for IgG deposition in kidneys were assigned using the following scale: (0) no

changes compared to VEH/CON mice, (1) minimal (<10% affected), (2) mild (11-25% affected), (3) moderate (26-50% affected), (4) marked (51-75% affected), (5) severe (76-100% affected). <u>High-throughput autoantibody profiling</u>

IgG and IgM AAbs were profiled in plasma (Study 2) by OmicsArrayTM Systemic Autoimmune-associated Antigen Array (Genecopoiea Inc., Rockville, MD; cat. #PA001). All plasma samples within experimental groups were pooled prior to analysis. Briefly plasma samples were incubated on microscope slides with 120 purified antigens adhered to nitrocellulose filters. One identical OmicsArray panel was reserved for a PBS negative sample control. After incubation, all slides were washed and incubated with Cy3-labeled anti-mouse IgG and Cy5-labeled anti-mouse IgM secondary antibodies. Slides were washed and fluorescent signals (532 nm for Cy3/IgG, 635 nm for Cy5/IgM) were detected using a GenePix® 4400B microarray scanner (Molecular Devices, San Jose, CA), and GenePix® 7.0 software (Molecular Devices) was used to determine fluorescent signal intensity values. Antibody scores (Ab-scores) for all AAbs were calculated using normalized signal intensity (NSI) and signal-to-noise ratio (SNR) values using the following formula:

$$Ab$$
- $score = log_2(NSI \times SNR + 1)$

Kidney mRNA expression

Total RNA from kidneys was extracted using TissueLyser II (Qiagen, Germantown, MD) and a RNeasy Mini Kit (Qiagen; cat. #74104) according to the manufacturer's instructions. Isolated RNA was reconstituted in RNase-free water and quantified using a Nanodrop ND-1000 spectrophotometer (Thermo Fisher Scientific, Waltham, MA). cDNA was prepared from isolated RNA at a concentration of 100 ng/µl using a High-Capacity cDNA Reverse Transcriptase Kit (Thermo Fisher Scientific, Waltham, MA). Taqman assays were run with technical triplicates

using a Smart Chip Real-Time PCR System at the MSU Genomics Core to assess interleukin (*Il1a*, *Il1b*, *Il2*, *Il6*, *Il17a*, *Il18*), chemokine (*Ccl2*, *Ccl7*, *Ccl12*, *Cxcl9*, *Cxcl10*, *Cxcl13*), inflammation/autoimmunity (*C1qa*, *C3*, *Casp1*, *Casp4*, *Icam1*, *Ifng*, *Lbp*, *Nfkb1*, *Nlrp3*, *Nos2*, *Pparg*, *Tlr4*, *Tlr9*, *Tnfa*, *Tnfsf13b*), type I interferon (IFN)-related (*Ifi44*, *Irf7*, *Isg15*, *Nlrc5*, *Oas2*), eicosanoid-related (*Alox15*, *Cyp2c44*, *Cyp2j6*, *Cyp2j9*, *Cyp2j11*, *Ephx1*, *Ephx2*, *Pla2g4c*, *Ptgs2*), kidney injury (*Ankrd1*, *Cd14*, *Havcr1*, *Tgfbr1*), oxidative stress-related (*Hmox*, *Ncf1*, *Nqo1*, *Sod2*), and housekeeping (*Actb*, *Gusb*) gene expression. Raw Ct values for each gene were converted to ΔCt values by subtracting the average Ct of the housekeeping genes from the Ct of the specified gene, and ΔΔCt values for each gene were calculated relative to the VEH/CON group by subtracting the average VEH/CON ΔCt value from individual ΔCt values within all experimental groups. The ΔΔCt values for each gene were then converted to relative copy number (RCN) values using the following equation [417]:

$$RCN = 2^{-\Delta \Delta Ct}$$

Data analysis and statistics

All statistical analyses were conducted using GraphPad Prism Version 9 (GraphPad Software, San Diego, CA, www.graphpad.com). Outliers were identified using Grubb's outlier test (Q = 1%), and normality was assessed using the Shapiro-Wilk test $(p \le 0.01)$. Quantitative data that failed to meet the assumption of normality and semi-quantitative data were analyzed by the Kruskal-Wallis nonparametric test followed by Dunn's post-hoc test. The Brown-Forsythe test $(p \le 0.01)$ was used to test the assumption of equal variances across treatment groups. Normal data with unequal variances were analyzed using the Brown-Forsythe/Welch analysis of variance (ANOVA) followed by Dunnett's T3 post-hoc test. Normal data that met the assumption of equal variance were analyzed by standard one-way ANOVA followed by Tukey's post-hoc test. Data

are presented as mean \pm standard error of the mean (SEM), with a p-value < 0.05 considered statistically significant.

RESULTS

<u>Treatment with R-LPS but not S-LPS induces GN</u>

In Study 1 (Figure 3.1A), no significant differences in weight change among experimental groups were observed from 8 to 10 wk of age (Figure 3.2A). Beginning at age 10 wk, mice in the R-LPS group began losing weight while the weights of animals in the VEH and S-LPS groups steadily increased. The average combined kidney weight (sum of left kidney and right kidney) approximated to 0.45 g and 0.40 g within the VEH and S-LPS groups, respectively, at experiment termination (age 13 wk), whereas combined kidney weight the R-LPS group increased to 0.58 g (Figure 3.2B). In line with these findings, mice in the R-LPS group alone began exhibiting proteinuria (Figure 3.2C) and hematuria (Figure 3.2D) after age 10 wk, whereas animals in the VEH and S-LPS groups displayed neither proteinuria nor hematuria at any point during the study. At age 13 wk, trends toward increased blood urea nitrogen (BUN) (Figure 3.2E) and plasma creatinine (Figure 3.2F) were observed in the R-LPS group compared to the VEH and S-LPS groups.

Examination of periodic acid Schiff and hematoxylin (PASH)-stained renal sections and subsequent semi-quantitative scoring revealed minimal to no PAS+ medullary membrane thickening in glomeruli of VEH- and S-LPS- treated mice (**Figures 3.3A, E, G**). In contrast, kidneys of R-LPS- treated mice contained markedly hypertrophic glomeruli with thickened periodic acid fast-stained medullary membranes, hyalinized proteinaceous material in renal tubular lumens, and mild lymphoplasmacytic infiltrate in cortical interstitial tissue, all of which were indicative of GN (**Figures 3.3C, G**). Consistent with these findings, immunohistochemical

staining indicated that R-LPS but not S-LPS induced glomerular deposition of IgG (**Figures 3.3B**, **D**, **F**, **H**). In further congruence with histopathology findings, renal tissue from VEH-injected mice exhibited no significant influx of CD45R⁺ B lymphocytes (**Figure S3.1A**) and minimal influx of CD3⁺ T lymphocytes (**Figure S3.1B**). On the other hand, R-LPS-injected mice demonstrated a moderate increase in renal CD45R⁺ lymphoid cell infiltration (**Figure S3.1C**) and a marked increase in CD3⁺ lymphoid cell infiltration (**Figure S3.1D**), while kidney tissues from S-LPS-injected mice resembled those from VEH-injected mice (**Figures S3.1E, S3.1F**). CD45R⁺ and CD3⁺ lymphocytes did not localize to any specific region in the kidney. Altogether, blood and urine analyses, histopathology, and immunohistochemistry indicated R-LPS but not S-LPS induced robust GN.

R-LPS but not S-LPS elicits lymphoid cell accumulation in spleen and liver

Spleen and liver tissue sections were also histologically evaluated after Study 1 termination (Figures 3.4, 3.5). No histopathology was evident in spleens of VEH-treated control mice (Figures 3.4A, B) that was histologically similar to S-LPS-treated mice (Figures 3.4E, F). Splenic tissue from R-LPS mice (Figures 3.4C, D) had lymphoid cell hyperplasia in white pulp with correspondingly lesser red pulp. Consistent with the expansion of white pulp, the R-LPS group showed a marked average weight increase at 0.30 g compared to the VEH and S-LPS groups at 0.08 g and 0.11g, respectively (Figure 3.4G). Histologic assessment of liver showed periportal large and small hepatocellular vacuoles resembling fatty liver (steatosis) histopathology in VEH-treated control mice (Figure 3.5A). There was marked periportal interstitial lymphoid cell accumulation in R-LPS-treated mice without hepatocellular vacuolization (Figure 3.5B). Histology of liver tissue from S-LPS mice (Figure 3.5C) resembled that of VEH/CON mice. Average liver weights did not significantly change with either R-LPS (1.58 g) or S-LPS (1.41 g)

compared to the VEH group (1.28 g) (**Figure 3.5D**). Accordingly, R-LPS but not S-LPS caused enlargement and lymphoid cell expansion in the spleen as well as modest lymphoid cell recruitment in the liver.

DHA supplementation selectively modulates red blood cell PUFA profile

In Study 2, we compared the effects of i.p. injection of R-LPS on GN and related endpoints in mice fed control CON, DHA, TPPU, and TPPU+DHA diets (Figure 3.1B). When total red blood cell fatty acids including saturated fatty acids (SFAs), monounsaturated fatty acids (MUFAs), ω-6 PUFAs, and ω-3 PUFAs were determined by GLC, the seven most abundant fatty acids were palmitic acid (PA, C16:0), stearic acid (SA, C18:0), oleic acid (OA, C18:1ω9), linoleic acid (LA, C18:2ω6), arachidonic acid (ARA, C20:4ω6), EPA (C20:5ω3), and DHA (C22:6ω3) (Table 3.2, Figure 3.6A). LPS treatment had no effect on fatty acid profiles of CON-fed mice. Consistent with prior findings [19], we found that substituting high-oleic safflower oil with DHArich algal oil in the AIN-93G diet increased incorporation of DHA and EPA into the red blood cell membrane, at the expense of ARA and OA. There was also a slight increase in membrane LA while SA slightly decreased with dietary DHA incorporation. The ω-3 index, or measure of EPA and DHA in relation to total red blood cell fatty acids [418], was elevated in mice that received either DHA or TPPU+DHA diet. TPPU administration alone had no significant effect on total membrane SFAs, MUFA, and PUFAs. Overall, feeding DHA elevated ω-3 PUFAs and decreased total MUFAs and ω -6 PUFAs.

Consumption of DHA- and/or TPPU-amended diets selectively skew plasma CYP450 metabolite profiles

Omega-6 and ω -3 PUFAs act as substrates for CYP450 monooxygenases, which convert the parent PUFA into epoxy-fatty acids (EpFAs). In turn, EpFAs act as substrates for sEH, which

converts EpFAs into their vicinal diols, dihydroxy fatty acids (DiHFAs). Inclusion of TPPU in experimental diets resulted in presence of 5 to 6 µM of the drug in plasma (Figure S3.2) which is consistent with the TPPU blood concentration obtained from efficacious doses (3 mg/kg/day) in other preclinical studies without reported side effects [419-422]. We assessed the impacts of DHA and TPPU on plasma levels of EpFAs, DiHFAs, and other PUFA-derived oxylipins using a comprehensive LC-MS/MS oxylipin panel (Table S3.6). Prominent metabolites included ones derived from LA (i.e., 12,13-EpOME and 12,13-DiHOME) (Figure 3.6B), ARA (i.e., 14,15-EPETrE and 14,15-DiHETrE) (Figure 3.6C), EPA (i.e., 17,18-EPETE and 17,18-DiHETE) (Figure 3.6D), and DHA (i.e., 19,20-EpDPE and 19,20-DiHDPE) (Figure 3.6E). No significant changes were observed between VEH/CON and LPS/CON mice. Consistent with our total red blood cell fatty acid data (Figure 3.6A) and prior reports [423-425], we found that substituting high-oleic safflower oil with DHA-rich algal oil elicited decreases in plasma LA- and ARAderived EpFAs and DiHFAs and corresponding increases in plasma EPA- and DHA-derived EpFAs and DiHFAs (Figure 3.6F). Increases in DHA-derived metabolites were much more pronounced than those of EPA-derived metabolites. In addition, mice in the LPS/TPPU group exhibited modest increases in LA-, ARA-, EPA- and DHA-derived EpFAs compared to the LPS/CON group, whereas LPS/TPPU displayed a modest decrease in 14,15-DiHETrE and but not 17,18-DiHETE and 19,20-DiHDPE. Furthermore, the LPS/TPPU+DHA group displayed modest increases in 14,15-EpETrE and 17,18-EpETE compared to the LPS/TPPU group, although these changes were not statistically significant with the LPS/CON and LPS/DHA groups; 19,20-EpDPE levels were not significantly affected by TPPU. Furthermore, TPPU+DHA co-treatment increased 17,18-DiHETE and 19,20-DiHDPE relative to the TPPU group and caused modest, but not significant, decreases in 14,15-DiHETrE, 17,18-DiHETrE, and 19,20-DiHDPE compared to

CON- or DHA-fed mice. In summary, the LPS/TPPU group exhibited significant increases in epoxide/diol ratios for LA-, ARA-, EPA-, and DHA-derived metabolites compared to the LPS/CON group (**Figure 3.7A**; **Table 3.3**), and the LPS/TPPU+DHA group exhibited significant increases epoxide/diol ratios in EPA- and DHA-derived metabolites compared to the LPS/DHA group (**Figure 3.7B**; **Table 3.3**).

DHA and TPPU treatment alone suppress R-LPS-induced GN

For the duration of the study, mice in all experimental groups gained weight at similar rates, regardless of dietary intervention (Figure S3.3). During the 5 wk of LPS injections, mice were assessed weekly for development of hematuria and proteinuria as indicators of GN (Figures **3.8A, B)**. Individuals in the VEH/CON group did not display proteinuria or hematuria. At 10 wk of age (after 6 injections), mice in the LPS/CON group began developing hematuria (**Figure 3.8A**). At age 11 wk (after 8 injections), mice in the LPS/DHA, LPS/TPPU, and LPS/TPPU+DHA experimental groups began developing hematuria. After the final injection, 75% of animals in the LPS/CON and LPS/TPPU+DHA groups displayed hematuria, 50% of animals in the LPS/TPPU group displayed hematuria, and 38% of animals in the LPS/DHA group displayed hematuria. In similar fashion, mice in the LPS/CON, LPS/DHA, and LPS/TPPU groups began developing proteinuria at age 10 wk (after 6 injections), and mice in the LPS/TPPU+DHA group began developing proteinuria at 11 wk of age (after 8 injections) (**Figure 3.8B**). After the final injection, proteinuria was evident in 87.5% of the LPS/CON group, 75% of the LPS/TPPU+DHA group, 50% of the LPS/TPPU group, and 38% of the LPS/DHA group. Consistent with GN, the average combined kidney weight was significantly elevated in the LPS/CON group compared to the VEH/CON group (Figure 3.8C). The only group that demonstrated a significant decrease in kidney weight compared to the LPS/CON group was the LPS/TPPU group, while no significant differences were observed for the other groups.

Histologic evaluation and scoring of PASH-stained kidney sections showed no evidence GN in VEH/CON-treated mice (**Figures 3.9A, F**). Markedly hypertrophic and hypercellular glomeruli with thickened medullary membranes consistent with GN were observed in kidneys of LPS/CON and LPS/TPPU+DHA mice (**Figures 3.9B, E, F**), while less glomerular histopathology was evident in LPS/DHA and LPS/TPPU mice (**Figures 3.9C,D,F**). Consistent with histopathological findings, immunohistochemical evaluation of kidney sections stained with IgG-specific antibody similarly revealed that DHA alone and TPPU alone suppressed R-LPS-induced IgG deposition in the kidney but are antagonistic when delivered together (**Figures 3.10A-E**).

DHA and TPPU modestly affect R-LPS-induced lymphoid cell accumulation in spleen and liver

All H&E-stained splenic tissues from R-LPS- treated groups were enlarged due to lymphoid hyperplasia (Figures 3.11A-E). Splenic tissue from TPPU-fed mice had slightly less lymphoid hyperplasia than other LPS-treated mice (Figure 3.11D). Mean spleen weights were significantly elevated in the LPS/CON group compared to the VEH/CON group (Figure 3.11F). Mice fed DHA and TPPU diet exhibited trends toward reductions in spleen weight that were not statistically significant. Hematoxylin and eosin-stained liver sections were evaluated for histopathology (Figure 3.12). Periportal hepatocellular vacuolization was prominent in VEH/CON group possibly reflecting steatosis previously reported in NZBWF1 mice (Figure 3.12A). Less hepatocellular vacuolization with marked lymphoid cell infiltration in periportal interstitial tissue in livers of LPS/CON mouse (Figure 3.12B). R-LPS- treated mice fed DHA, TPPU, and TPPU+DHA diet had less periportal inflammatory cells and absence of hepatocellular vacuolization (Figures 3.12C-E, F). Inflammatory severity scores were suppressed in DHA-fed

mice with similar non-significant trends being observed in mice fed TPPU and TPPU+DHA diets (Figure 3.12G).

DHA and/or TPPU do not affect R-LPS-induced autoantibody responses in plasma

Plasma from all mice within each experimental group were pooled and subjected to high-throughput autoantigen array for 120 IgG and IgM AAbs. While R-LPS robustly induced total and group-specific IgG and IgM autoantibodies in CON-fed mice, the magnitude of these responses was unaffected by DHA, TPPU, or TPPU+DHA treatments (**Figure S3.4**).

<u>DHA and/or TPPU have limited impact on R-LPS-induced modulation of inflammatory and fatty</u> acid metabolism gene expression in the kidney

We evaluated the impacts of DHA and TPPU on expression levels of inflammatory/autoimmune (i.e., *Il1b*, *Ccl2*, *Ccl7*, *Cxcl10*, *Cxcl13*, *C1qa*, *C3*, *Casp1*, *Tlr9*, *Tnfa*, *Tnfsf13b*) and fatty acid metabolism genes (i.e., *Alox15*, *Cyp2c44*, *Cyp2j6*, *Cyp2j9*, *Cyp2j11*, *Ephx1*, *Ephx2*, *Pla2g4a*, *Ptgs2*) genes in the kidney (**Figure S3.5A**; **Table S3.7**). R-LPS significantly induced expression of proinflammatory cytokines (i.e., *Il1b*, *Tnfa*), chemokines (i.e., *Ccl2*, *Ccl7*, *Cxcl13*), complement proteins (i.e., *C1qa*, *C3*), and other related (i.e., *Casp1*, *Tlr9*, and *Tnfsf13b*) genes relative to VEH/CON mice. Although *Cxcl10* mRNA was not significantly elevated by R-LPS, it demonstrated a modest increase compared to VEH/CON mice. Intriguingly, none of the selected inflammatory/autoimmune genes were significantly downregulated with DHA or TPPU, though some treatment groups exhibited therapeutic trends. For instance, LPS/DHA mice showed modest decreases in mRNA for *Ccl2*, *Ccl7*, *Cxcl13*, *C1qa*, *Casp1*, *Tlr9*, and *Tnfa* relative to LPS/CON mice. In addition, LPS/TPPU mice exhibited modest reductions in mRNA for *Ccl2*, *Ccl7*, *Casp1*, and *Tnfa*. Upon combining DHA and TPPU, the individual inhibitory

effects of DHA and TPPU were diminished, with an exception to *Tlr9* expression which might be influenced only by DHA.

We found that R-LPS significantly reduced expression of several selected genes involved in lipid metabolite synthesis, including *Cyp2c44*, *Cyp2j6*, *Cyp2j9*, *Cyp2j11*, and *Ephx2*, compared to VEH-injected mice (**Figure S3.5B**; **Table S3.7**). In addition, R-LPS modestly downregulated *Ephx1*, *Pla2g4a*, and *Ptgs2*. In line with our observations for the inflammatory/autoimmune genes, we found that neither DHA nor TPPU significantly restored the expression levels of most fatty acid metabolism genes in our panel except for *Ephx2*, which was significantly upregulated in the LPS/DHA and LPS/TPPU+DHA groups compared to the LPS/CON group.

Other genes measured in our panel are noted in **Table S3.7**. As anticipated, we observed significant upregulation of genes associated with kidney injury (i.e., *Ankrd1*, *Lcn2*) and oxidative stress (i.e., *Hmox*, *Nqo1*, *Sod2*) in LPS/CON mice relative to VEH/CON mice but found no significant expression level changes in DHA- and/or TPPU-treated mice. No significant changes in gene expression were noted for some type I IFN-regulated genes (i.e., *Irf7*, *Isg15*), but *Ifi44* expression was significantly reduced in all DHA-fed mice, regardless of TPPU consumption, relative to VEH/CON and LPS/CON mice.

DISCUSSION

LPS-accelerated autoimmune GN in NZBWF1 mice is increasingly being used as a preclinical model for identifying interventions applicable to preventing end-stage kidney disease associated with lupus [28-31, 404, 410, 426]. We demonstrate here for the first time that the presence or absence of O-antigen polysaccharide profoundly influences the GN response and that R-LPS is required for optimal model performance. Compared to VEH and S-LPS, R-LPS caused significant weight loss associated with proteinuria, hematuria, histopathological scoring,

glomerular IgG deposition, and influx of CD3⁺ and CD45R⁺ lymphocytes that might be associated with classical LPS-induced sickness behavior [427]. When the effects of lipidome modulation by dietary DHA supplementation and/or sEH inhibition on R-LPS-accelerated GN were assessed, several novel findings were made. First, R-LPS treatment of CON-fed mice did not affect the red blood cell fatty acid profile but did reduce plasma concentrations of LA- and ARA-derived EpFAs/DiHFAs. Second, DHA supplementation skewed tissue PUFAs from ω -6 to ω -3 and shifted EpFAs/DiHFAs from primarily LA-/ARA-derived to EPA-/DHA-derived. Third, sEH inhibition with TPPU favored the accumulation of EpFAs over their respective vicinal diols. Fourth, based on proteinuria, hematuria, histopathologic scoring, and glomerular IgG deposition, the relative rank order of R-LPS-induced GN severity among groups fed experimental diets was: VEH/CON < R-LPS/DHA \approx R-LPS/TPPU <<< R-LPS/ TPPU+DHA \approx R-LPS/CON. Fifth, DHA's and TPPU's effects on R-LPS-induced lymphocytic recruitment in spleen and liver were modest to negligible. Lastly, these interventions did not affect LPS-induced plasma AAb responses or kidney gene expression.

This investigation is the first to directly compare the efficacies of R-LPS and S-LPS in accelerating GN in lupus-prone mice. This effort was initiated after several failed preliminary attempts by our laboratory to induce GN with S-LPS. Several mechanisms have been proposed for LPS-accelerated GN including polyclonal B-cell activation, decreased efficiency of the mononuclear phagocyte system to uptake immune complexes, and/or delayed clearance of immune complexes from systemic circulation, all of which can contribute to increased deposits of immune complexes in the kidney [375-384]. Consistent with polyclonal B cell activation, we observed that R-LPS but not S-LPS strongly induced germinal center expansion and splenomegaly, and furthermore, R-LPS elicited a wide array of AAbs of the IgM and IgG isotypes. The mechanisms

by which these two LPS chemotypes activate TLR4 are very different, and these differences may have special relevance to B cell activation. At low doses, S-LPS requires the glycosylphosphatidylinositol (GPI)-anchored co-receptor CD14 to trigger signal transduction through both MyD88-dependent and independent pathways, whereas, at low doses, R-LPS can initiate MyD88-dependent signaling in the absence of CD14 [407, 409]. Thus, R-LPS efficiently activates TLR4 on both CD14⁺ and CD14⁻ cells as compared to S-LPS which acts primarily on CD14⁺ cells. Since B cells express TLR4 but lack CD14, it is tempting to speculate that they preferentially respond to R-LPS and not S-LPS, resulting in polyclonal activation that ultimately perpetuates AAb production and immune complex-driven GN in NZBWF1 mice. However, further studies are needed to test this and alternative hypotheses.

Red blood cells are commonly used as a surrogate to reflect tissue fatty acid profiles [389]. As in our prior studies [19, 428], we found here that substitution of high oleic safflower oil in AIN-93G diets with DHA-containing microalgal oil increased DHA and EPA with nearly equivalent reductions of ARA. While some EPA might have resulted from DHA retroconversion, Metherel and coworkers [429] found that conversion of α-linolenic acid (ALA; C18:3ω3) to docosapentaenoic acid (DPA; C22:5ω3) by elongation/desaturation, mediated via feedback inhibition by DHA, resulted in the majority of EPA found in DHA-fed rats. Importantly, concurrent with elevated tissue concentrations of DHA and EPA, we observed decreases in plasma LA- and ARA-derived EpFAs and DiHFAs and corresponding increases in plasma EPA- and DHA-derived EpFAs and DiHFAs. Thus, consumption of marine ω-3 PUFAs alone can change blood levels of important bioactive CYP450 and sEH metabolites.

Preclinical [345-347] and clinical investigations [341, 348-350] generally support the premise that ω -3 PUFAs attenuate onset and progression of lupus-associated pathologic effects,

including nephritis. Consistent with reported ameliorative actions of marine ω-3 PUFAs for preventing/treating chronic inflammatory and autoimmune diseases, we found here that consumption of DHA alone suppressed R-LPS-accelerated GN. Established mechanisms by which dietary intake of DHA and EPA potentially ameliorate systemic inflammation and downstream tissue damage include 1) modulating the structure and functionality of the plasma membrane and lipid rafts, 2) suppressed expression of proinflammatory cytokines, 3) binding with receptors, transcription factors, and enzymes at the expense of ω-6 PUFA binding, and 4) serving as substrates for highly pro-resolving ω-3 PUFA metabolites (reviewed by [341]). We have previously demonstrated in several macrophage models that ω-3 DHA displaces ω-6 ARA and ω-9 OA from the sn-2 position of membrane phospholipids, suppresses silica-induced expression of proinflammatory genes (e.g., Nlrp3, Il1a, Il1b) and type I IFN-regulated genes (e.g., Irf7, Isg15, Oas2, Ifi44), attenuates cSiO₂-triggered apoptotic and pyroptotic cell death, and enhances efferocytosis of cell corpses [430-432]. Correspondingly, in recent studies using female NZBWF1 mice, we have found that DHA prevents silica-induced development of pulmonary ectopic lymphoid tissue (ELT) and downstream lupus GN, impedes expression of chemokine-related (e.g., Cxcl9, Cxcl10, Ccr5) and type I IFN-related (e.g., Irf7, Isg15, Oas2, Ifi44) genes in lung and kidney, and inhibits secretion of anti-nuclear AAb, proinflammatory cytokines (e.g., IL-1β, TNFα, IL-6), chemokines, (e.g., BLC, MCP-5), enzymes (e.g., MMP-3, granzyme B), adhesion molecules (e.g., E-selectin, VCAM-1), co-stimulatory molecules (e.g., CD40L, CD48), and growth factors (e.g., IGF-1, Epiregulin) in BALF and plasma [20, 351, 352, 433]. Furthermore, Cheng and coworkers have reported in both lupus-prone MRL/lpr mice and lupus patients that resolvin D1, a pro-resolving DHA metabolite, ameliorates disease progression by increasing Treg differentiation and decreasing Th17 differentiation from naïve CD4⁺ T cells [434]. Thus, the proresolving effects of ω-3 PUFAs are multi-pronged and wide-reaching, with therapeutic importance in lupus and other chronic inflammatory/autoimmune pathologies.

Pharmacological effects of TPPU have been previously reported in many preclinical disease models [21, 401, 422, 435-445]. In those studies, TPPU was delivered in drinking water in a polyethylene glycol (PEG) suspension, by oral gavage, or via injection. This investigation is the first to report the delivery of the sEH inhibitor TPPU in experimental rodent diet. Using this approach, we did not face issues associated with the low solubility of TPPU in water (0.06 mg/ml) [394], which was previously reported by Schmelzer and coworkers as a study limitation when administering AUDA, an sEH inhibitor with the same pharmacophore as TPPU, to LPS-challenged C57 mice [446]. We estimate the daily dose of TPPU through diet to be 3 mg/kg/day which was sufficient to achieve plasma concentrations of approximately 5 µM (equivalent to 2000-fold of the Ki of TPPU) 4 wk after initiation of feeding. Our findings indicate that this dose was efficacious at significantly increasing the epoxide/diol ratio for LA. ARA, DHA, and EPA indicating robust inhibition of sEH. Accordingly, TPPU potently inhibits murine sEH and human sEH, with respective IC₅₀ values 2.8 nM and 1.1 nM [391, 447] and respective Ki values of 2.5 nM and 0.64 nM [448]. In addition, Liu and coworkers reported that TPPU exhibits a pharmacokinetic half-life $(t_{1/2})$ of 37 \pm 2.5 h in the blood following administration (3 mg/kg) to mice by oral gavage [449].

In this study, we hypothesized that cotreatment of ω -3 PUFA and sEH inhibitor would stabilize highly potent ω -3 EpFAs and therefore be more efficacious than the treatment of either ω -3 PUFA or sEH inhibitor alone. However, our results suggested that ω -3 PUFAs and the sEH inhibitor antagonize each other's effects. Similar findings have been reported by Harris and coworkers [450] in which co-treatment of sEH inhibitor with DHA diminished the therapeutic effects of TPPU alone in a murine model of liver fibrosis. Although several studies suggest that

ω-3 EpFAs are more potent in specific biological effects including angiotensin-II-dependent hypertension, nociception and autophagy, numerous studies have suggested that EpFAs generated from different PUFAs could play very different roles and the effects from two different subclasses of epoxy fatty acids could oppose each other [451-466]. For example, EpDPE derived from ω-3 DHA is anti-angiogenic [457], but EpETrE derived from ω-6 ARA is proangiogenic [440, 467]. Therefore, our results suggest that EpETrE could be a key lipid mediator for the anti-inflammatory, pro-resolving effects resulting from the treatment of sEH inhibitor TPPU, as it has been suggested by previous studies [453, 454, 459, 468]. Our oxylipin analysis suggested that co-treatment of TPPU with DHA significantly decreases the endogenous level of EpETrE. Thus, DHA could potentially antagonize the effects of TPPU treatment alone.

While the absence of DHA and/or TPPU effects on LPS-induced inflammation-associated gene expression may suggest that these interventions interfere with a downstream event associated with GN development, such as immune complex deposition and associated kidney injury, transcriptomic data is were only collected at termination and may not reflect earlier timepoints. In support of this contention, we have found that DHA suppresses silica-induced inflammatory/autoimmune gene expression in NZBWF1 mice at 1, 5, and 9 wk after silica instillation but not at 13 wk post-instillation [469]. Nevertheless, DHA suppressed silica-induced ELT neogenesis and GN at 13 wk [428]. Thus, it will be important in future mechanistic studies of DHA and/or TPPU effects on R-LPS-induced GN to analyze blood biomarkers and tissues at multiple early timepoints.

One limitation of this study is that we focused primarily on phenotypic effects of DHA and/or TPPU on R-LPS-induced GN rather than underlying mechanisms. As Cavallo and coworkers previously reported in non-autoimmune and lupus-prone mice, R-LPS-induced GN

may be the result of a cascade beginning with polyclonal B cell activation, then progressing to increased systemic AAb secretion, impaired clearance of immune complexes from circulation, and elevated immune complex deposition in the kidney [375-384]. Although we found that R-LPS elicits toxicity in the kidney, spleen, and liver after 5 wk of i.p. injections, future studies should focus on elucidating the temporal mechanistic pathway by which R-LPS induces GN, with particular emphasis on: evaluating toxicokinetic distribution of R-LPS from the peritoneum to downstream tissues, measuring impacts of R-LPS on polyclonal B cell activation, and determining whether R-LPS-induced kidney/spleen/liver toxicity occur dependently or independently of each other. Another constraint of this study is that we measured TPPU plasma concentration only after five R-LPS injections and not at any other timepoint to assess steady-state levels. TPPU has been shown to reach steady-state concentrations in the blood after 1-2 wk of oral administration by drinking water [470]; however, it would be useful to collect plasma at multiple timepoints to confirm these findings in future studies involving dietary TPPU administration. A related limitation is that we focused only on sEH as a pharmacologic target, which is one of many epoxide hydrolases involved with PUFA metabolism (128). However, microsomal epoxide hydrolase is capable of significant EpETrE hydrolysis in sEH-knockout mice, suggesting that pharmacologic sEH inhibition does not completely block EpFA metabolism and therefore could affect experimental endpoints (129).

CONCLUSIONS

Taken together, the results described herein show for the first time that absence of O-antigenic polysaccharide in R-LPS is critical to accelerated GN in lupus-prone mice. While S-LPS elicited minimal toxicity in exposed mice, R-LPS triggered significant renal pathology characterized by proteinuria, hematuria, elevated BUN and plasma creatinine, glomerular damage,

IgG deposition, and influx of CD3⁺/CD45R⁺ lymphocytes. Furthermore, lipidome modulation through DHA supplementation or sEH inhibition suppressed R-LPS-induced GN, but these ameliorative effects were greatly diminished upon combining the treatments. Separately, DHA and sEH inhibition delayed development of proteinuria and hematuria, dampened glomerular damage, and reduced glomerular IgG deposition with no significant effects on plasma autoantibody responses and expression of inflammatory and fatty acid metabolism genes in the kidney. Since it is currently unknown whether the perceived antagonistic relationship between DHA and TPPU is relevant only to our R-LPS mouse model or to other preclinical models for lupus as well, it will be essential in future investigations to evaluate how cotreatment with DHA and TPPU influence disease endpoints in other spontaneously-driven and environmentally-triggered lupus models. Additionally, it will be useful to investigate how direct administration of ω -3/6 EpFAs modulates pathologic biomarkers of R-LPS-induced autoimmunity in female NZBWF1 mice, versus coadministration with ω -3/6 PUFAs and sEH inhibitor. While our approach allowed us to broadly assess the effects of endogenous and DHA-derived EpFAs in R-LPS-induced GN, future investigations involving direct EpFA administration would provide valuable insight on specific EpFAs that may potentiate or prevent disease progression.

DECLARATIONS

Competing Interests

The authors declare that the research was conducted in the absence of any commercial or financial relationships that could be construed as a potential conflict of interest.

Funding

This research was funded by NIH T32GM142521 (OF), NSF DMS1761320 (KSSL), NIH RO3AG075465 (KSSL), MSU DFI Funding (KSSL), NIH RO1ES027353 (JP), Lupus Foundation of America (JP), and Dr. Robert and Carol Deibel Family Endowment (JP).

Contributions

OF: study design, coordination, feeding study, necropsy, data curation. data analysis/interpretation, figure preparation, manuscript preparation and submission. PC: study design, coordination, feeding study, necropsy, data curation, data analysis/interpretation, figure preparation, manuscript writing. EP: LC-MS/MS sample preparation, data analysis, manuscript writing. AE: LC-MS/MS sample preparation. JW: necropsy, lab analysis. RL: necropsy, lab analysis. JH: kidney/spleen/liver histopathology, data analysis, manuscript preparation. LH: AAb data acquisition/analysis, figure preparation. KSSL: study design, oversight, manuscript preparation. JP: study design, oversight, funding acquisition, data analysis/interpretation, manuscript preparation and submission. All authors contributed to the manuscript and approved the submitted version.

<u>Acknowledgments</u>

We would like to thank Amy Porter and the Laboratory of Investigative Histopathology at Michigan State University for their assistance with histotechnology analyses, Leslie Pittsley and Michigan State University's Campus Animal Resources for their assistance with blood collections, the Jennifer Fenton Lab at Michigan State University for their assistance with GC-MS analyses, and the RTSF Mass Spectrometry and Metabolomics Core Facilities at Michigan State University for their assistance with oxylipin and lipidomics analyses.

FIGURES

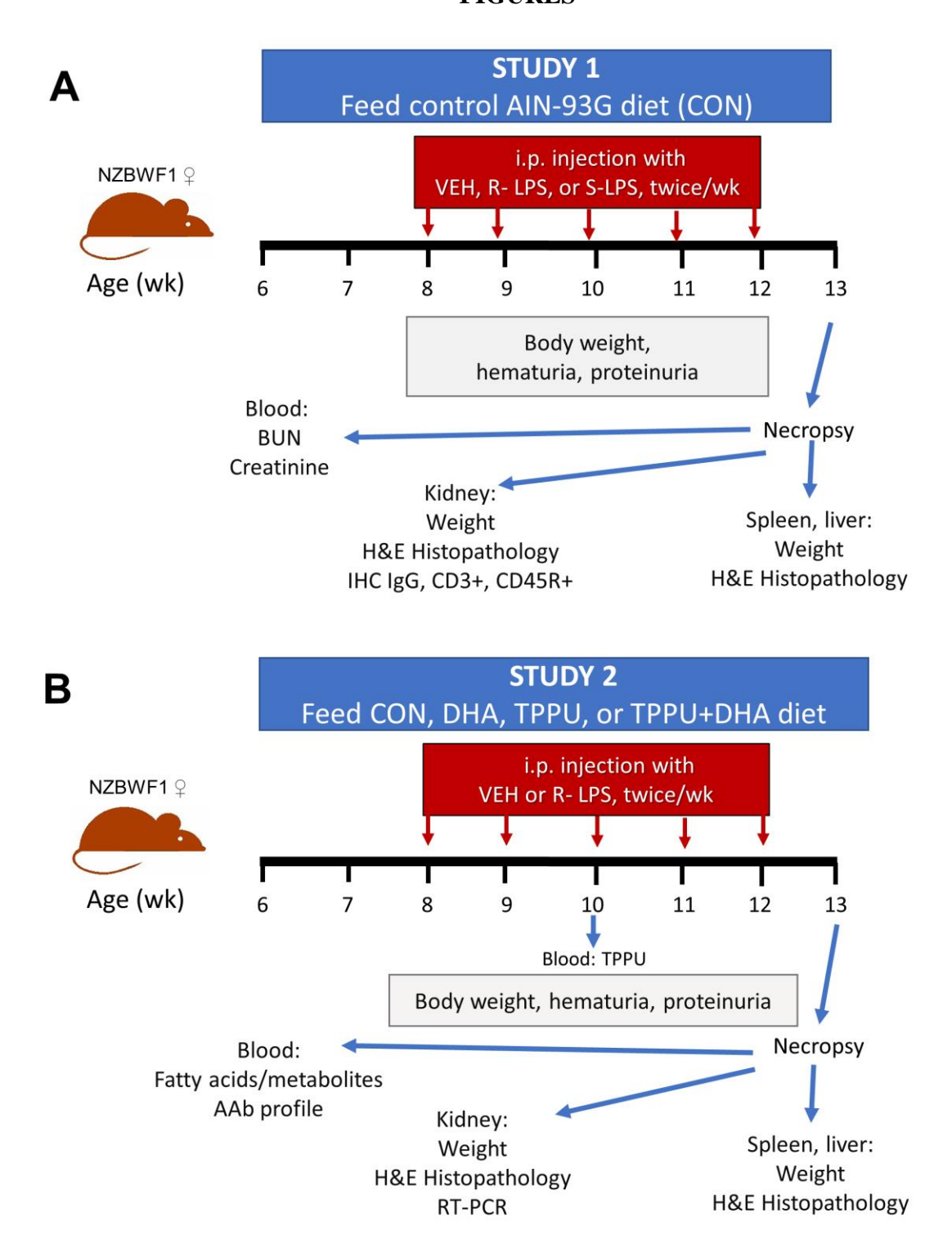


Figure 3.1. Experimental design for Study 1 (A) and Study 2 (B). (A) At 6 wk of age, female NZBWF1 mice (n = 2-4/gp) were placed on CON diet. Beginning at 8 wk of age, mice were

Figure 3.1 (cont'd)

injected interperitoneally twice per wk for 5 wk with 500 μ l of PBS vehicle, 0.8 μ g/g body weight (BW) S-LPS, or 0.8 μ g/g BW R-LPS. Mice were sacrificed at 13 wk of age, or 5 wk after the first LPS injection. (**B**) At 6 wk of age, female NZBWF1 mice (n=8/gp) were placed on CON diet, DHA diet, TPPU diet, or TPPU+DHA diet. Beginning at 8 wk of age, mice were injected interperitoneally twice per wk for 5 wk with 500 μ l of PBS vehicle or 0.6 μ g/g BW R-LPS. Mice were sacrificed at 13 wk of age, or 5 wk after the first LPS injection.

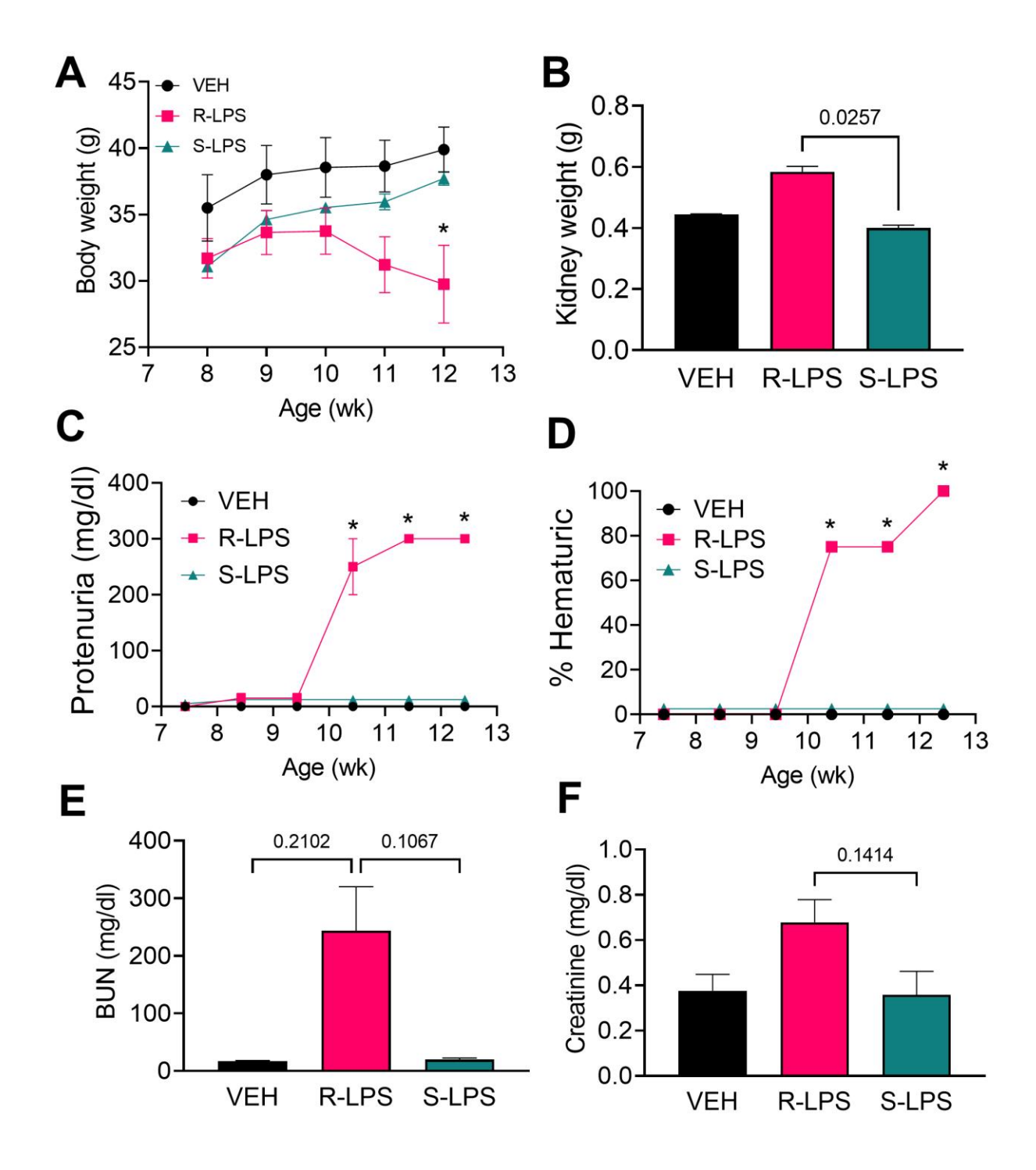


Figure 3.2. R-LPS but not S-LPS suppresses body weight gain, induces kidney enlargement, proteinuria, hematuria, and elevates BUN and creatinine in blood. (A) Mice were weighed weekly, concurrently with the first LPS injection of the wk. Data are presented as mean \pm SEM. (B) Combined weight of left and right kidneys were measured after 5 wk of i.p. LPS injections. Data are presented as mean \pm SEM. R-LPS, but not S-LPS, elicits robust proteinuria (C) and hematuria (D) after 3 wk of intraperitoneal (i.p.) LPS injections. Animals were monitored weekly for development of proteinuria (\geq 300 mg/dl urinary protein) and hematuria (\geq 0 cells/ μ l urine)

Figure 3.2 (cont'd)

using clinical dipsticks. Blood urea nitrogen (**E**) and creatinine (**F**) were measured in plasma after 5 wk of i.p. LPS injections. BUN and creatinine data are presented as mean \pm SEM. For A, C, and D, *p<0.05 indicates statistical significance for R-LPS vs. VEH and R-LPS vs. S-LPS. For B, E, and F, values of p<0.25 are shown, with p<0.05 considered statistically significant.

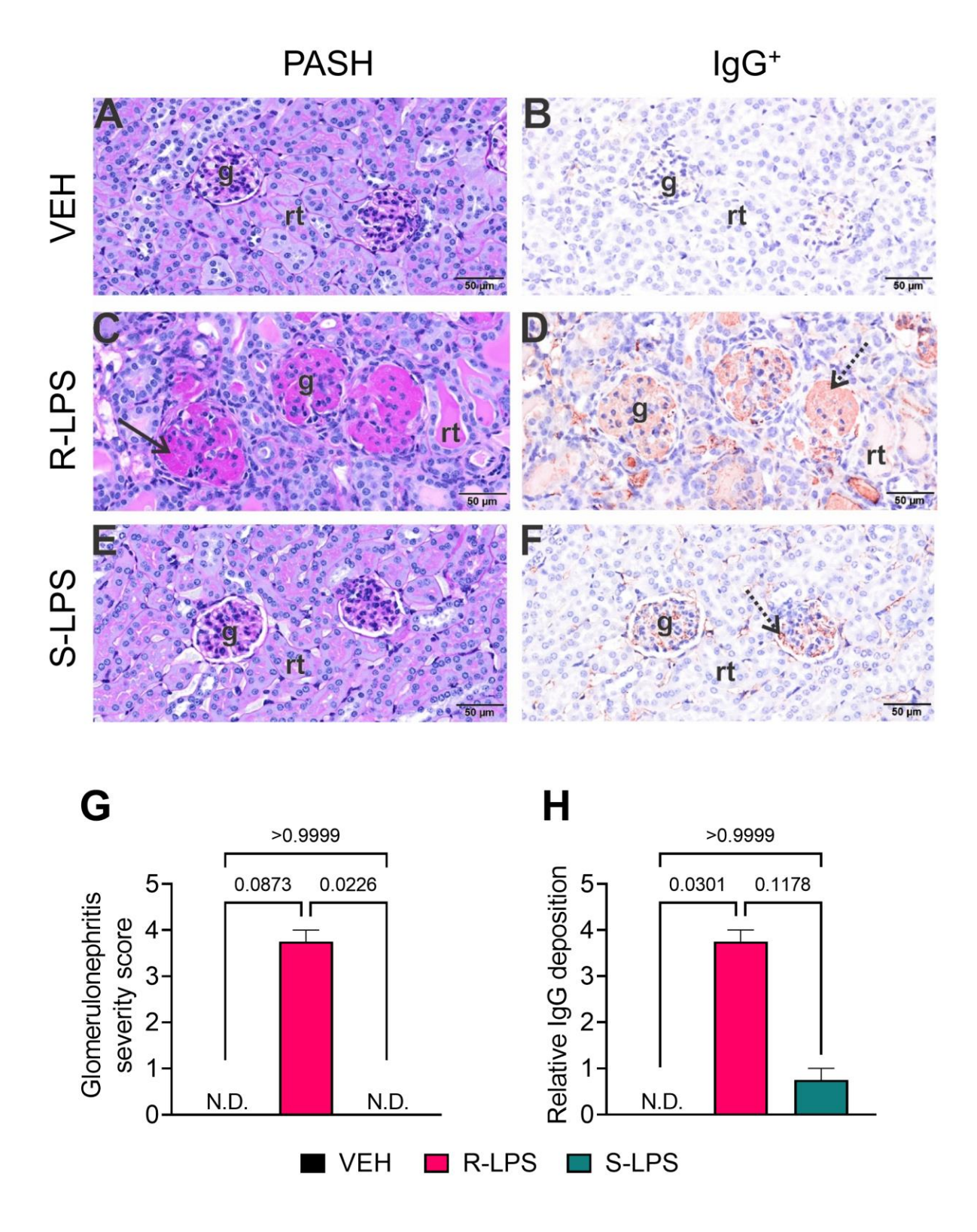


Figure 3.3. R-LPS but not S-LPS induces glomerulonephritis. Light photomicrographs of glomeruli (g) and renal tubules (rt) in the cortex of kidneys from vehicle-treated control mice (A, B), rough (R) LPS-treated mice (C, D), and smooth LPS-treated mice (E, F). Renal tissues were

Figure 3.3 (cont'd)

histochemically stained with periodic acid Schiff and hematoxylin (PASH) (**A**, **C**, **E**) and immunohistochemically stained for IgG protein and counterstained with hematoxylin (**B**, **D**, **F**). Hypertrophic glomeruli with markedly thickened periodic acid fast-stained medullary membranes (solid arrow), hyalinized proteinaceous material in renal tubular lumens, and mild lymphoplasmacytic infiltrate in cortical interstitial tissue of R-LPS-treated mice (**C**). Correspondingly, immunohistochemically stained IgG in glomeruli (stippled arrow), renal tubular lumens and blood vessel lumens (**D**). Minimal to no PAS+ medullary membrane thickening in glomeruli of S-LPS-treated mice (**E**) with minimal IgG+ medullary material (**F**). Semi-quantitative scores for (G) glomerulonephritis severity and (**H**) IgG deposition. Scoring was as follows: 0—no significant finding, 1—minimal, 2—mild, 3—moderate, 4—marked, 5—severe. See text for detailed criteria used in severity scoring. Data are presented as mean \pm SEM (n = 2-4). Values of p<0.1 are shown, with p<0.05 considered statistically significant. g, glomerulus; rt, renal tubule.

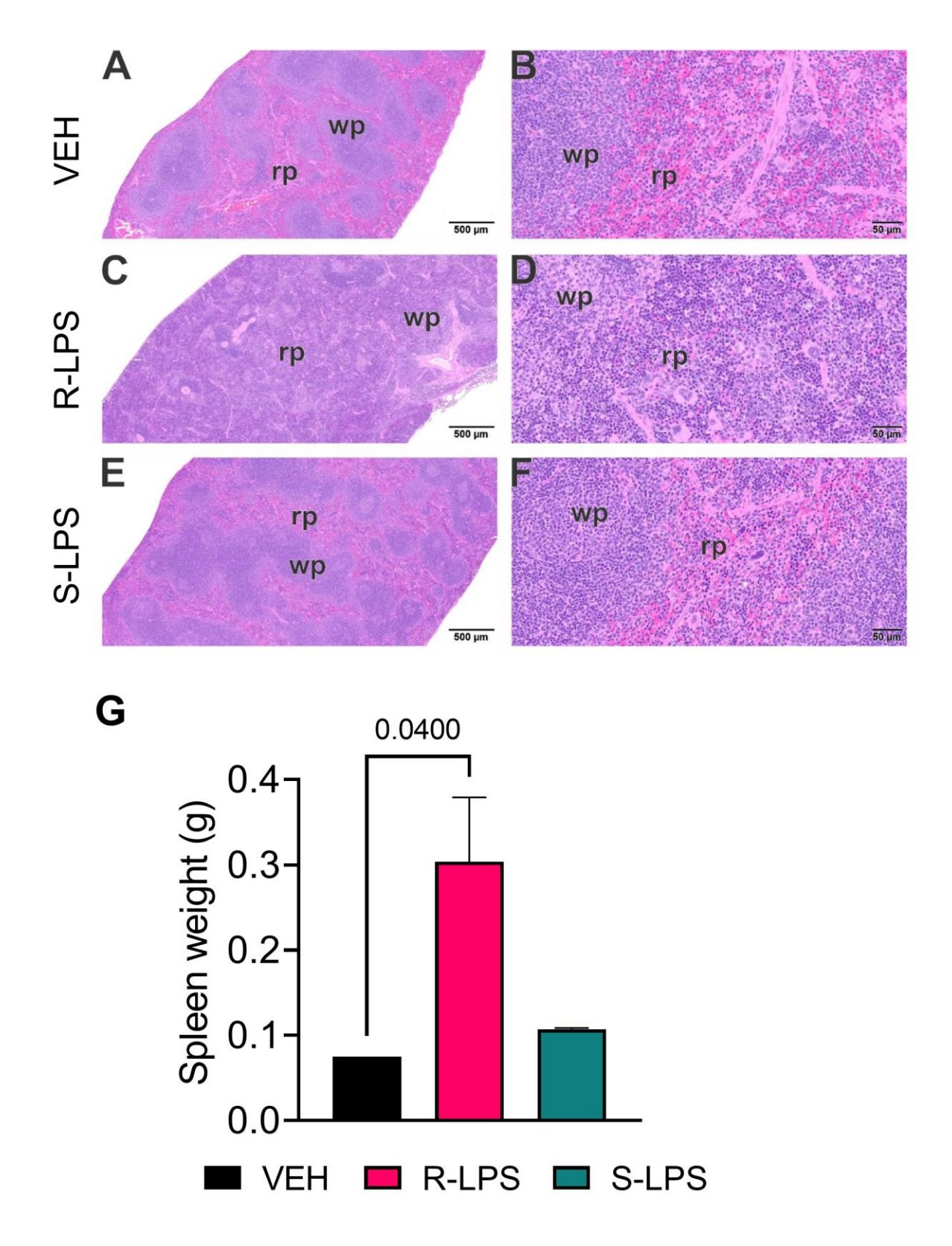


Figure 3.4. R-LPS but not S-LPS induces lymphoid cell hyperplasia and enlargement of spleen. Light photomicrographs of transverse hematoxylin and eosin-stained tissues from the body

Figure 3.4 (cont'd)

of spleens in vehicle (VEH)-treated control mice (A, B), rough (R)-LPS-treated mice (C, D), and smooth-(S) LPS-treated mice (E, F). A, C, and E taken at low magnification and B, D and F taken at higher magnification. Splenic tissue from R-LPS mice (B, D) have lymphoid cell hyperplasia in white pulp (wp) with correspondingly lesser red pulp (rp). No histopathology in spleens of S-LPS-treated mice (E, F) that were histologically similar to vehicle-treated control mice (A, B). R-LPS but not S-LPS contributes to larger spleen weight after 5 wk of i.p. injections (G).

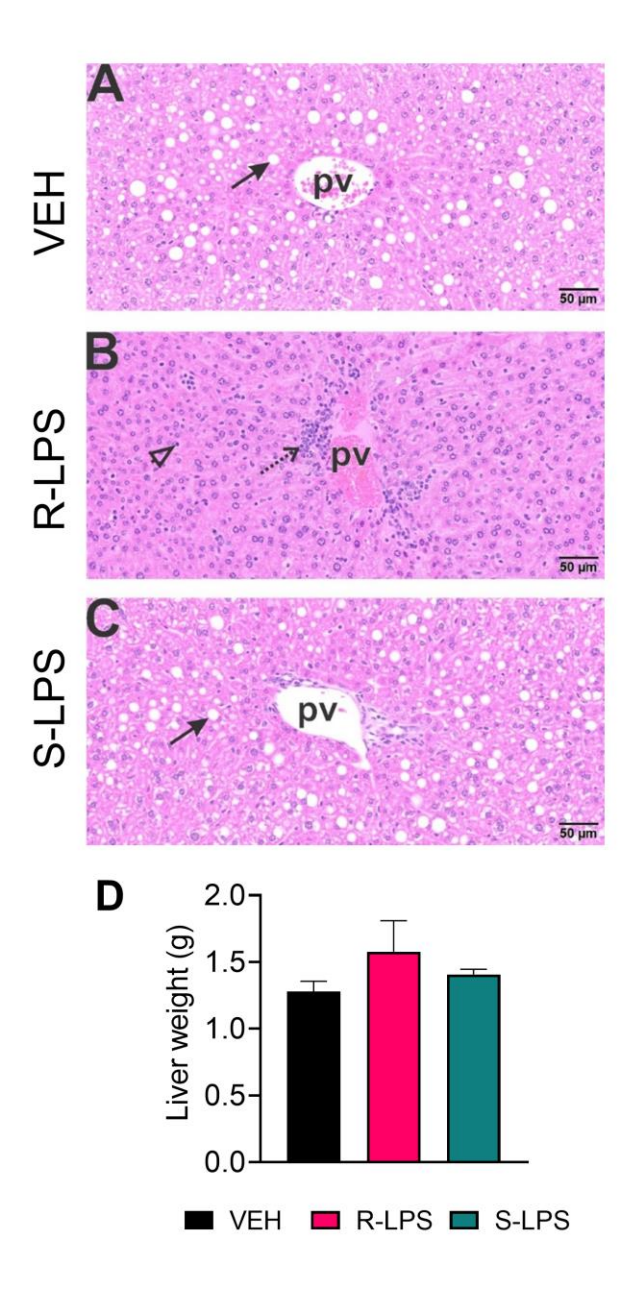


Figure 3.5. R-LPS but not S-LPS induces lymphoid cell accumulation and reduces vacuolization in liver. Light photomicrographs of hematoxylin and eosin-stained hepatic tissue from (**A**) vehicle (VEH)-treated control, (**B**) rough (R)-LPS-treated mice, and (**C**) smooth (S)-LPS-treated mice. Periportal large and small hepatocellular vacuoles resembling fatty liver histopathology (steatosis) in vehicle control mouse (arrow) (**A**). Periportal interstitial lymphoid cell accumulation in rough-LPS-treated mouse (**B**) without hepatocellular vacuolization. Histology of liver tissue from smooth-LPS mouse (**C**) resembles that of vehicle control mouse (**A**). R-LPS and S-LPS effects on liver weight are negligible (**D**). Solid arrow, hepatocellular lipid vacuoles; stippled arrow, periportal cellular inflammation (predominantly mononuclear cells); open arrowhead, mononuclear cells in hepatic sinusoids.

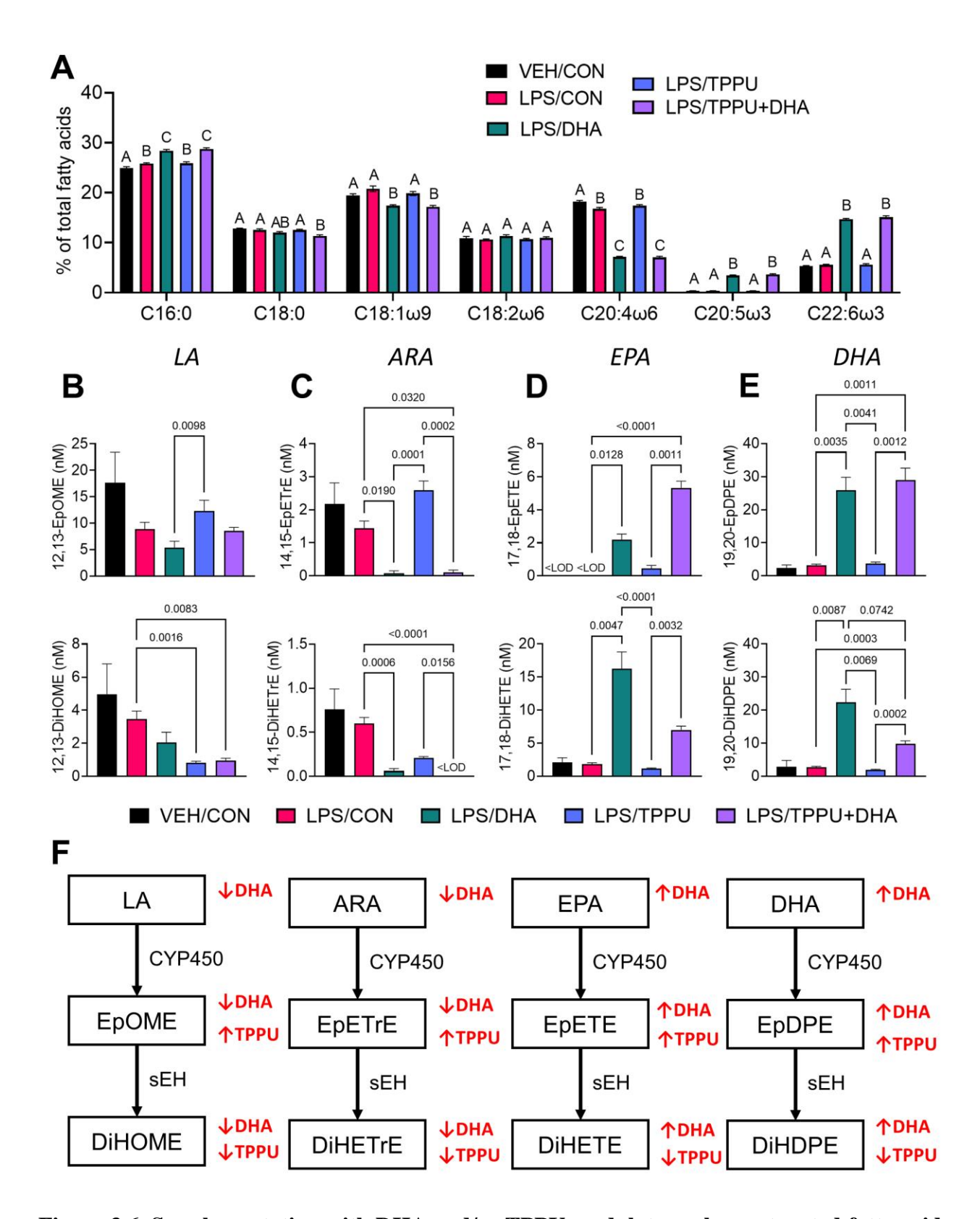


Figure 3.6. Supplementation with DHA and/or TPPU modulates polyunsaturated fatty acid (PUFA) and CYP450 metabolite profiles in red blood cell membranes and plasma. (A) DHA

Figure 3.6 (cont'd)

consumption elevates ω-3 PUFA DHA and EPA in red blood cell membrane at the expense of ω-6 PUFA arachidonic acid and ω-9 PUFA oleic acid. Major red blood cell fatty acids were compared across treatment groups by GLC and expressed as percent of total fatty acids. Different letters indicate statistically significant differences between treatment groups for individual fatty acids (p<0.05). C16:0, palmitic acid; C18:0, stearic acid; C18:1n9, oleic acid; C18:2n6, linoleic acid; C20:4n6, arachidonic acid; C20:5n3, eicosapentaenoic acid (EPA); C22:6n3, docosahexaenoic acid (DHA). (B, C, D) Following sacrifice, plasma was isolated and selected (B) LA metabolites (i.e., 12,13-EpOME, 12,13-DiHOME), (C) ARA metabolites (i.e., 14,15-EpETrE, 14,15-DiHETrE), (D) EPA metabolites (i.e., 17,18-EpETE, 17,18-DiHETE), and (E) DHA metabolites (i.e., 19,20-EpDPE, 19,20-DiHDPE) were measured by LC-MS/MS. Data are presented as mean \pm SEM (n = 6-8). Values of p<0.1 are shown, with p<0.05 considered statistically significant. <LOD = below limit of detection. (F) Depiction of pathways to major epoxy- and dihydroxy fatty acid metabolites derived from ω-6 and ω-3 PUFAs. ω-6 and ω-3 PUFA are substrates of CYP450 monooxygenases, which produce ω-6 and ω-3 epoxy-fatty acids, respectively. The resulting epoxy-fatty acids then are converted to their corresponding ω -6/ ω -3 dihydroxy fatty acids by soluble epoxide hydrolase (sEH). Red arrows indicate how fatty acid and metabolite profiles are affected by LA, linoleic acid; DGLA, dihomo-γ-linolenic acid; ARA, arachidonic acid; EpOME, epoxyoctadecenoic acid; EED, epoxyeicosadienoic acid; DHED, dihydroxyeicosadienoic acid; ARA, arachidonic acid; EpETrE, epoxyeicosatrienoic acid; DiHETrE, dihydroxyeicosatrienoic epoxyoctadecadienoic alpha-linolenic acid; EpODE, acid; dihydroxyoctadecadienoic acid; EPA, eicosapentaenoic acid; EpETE, epoxyeicosatetraenoic acid; dihydroxyeicosatetraenoic DiHETE, acid; DHA, docosahexaenoic acid; EpDPE, epoxydocosapentaenoic acid; DiHDPE, dihydroxydocosapentaenoic acid.

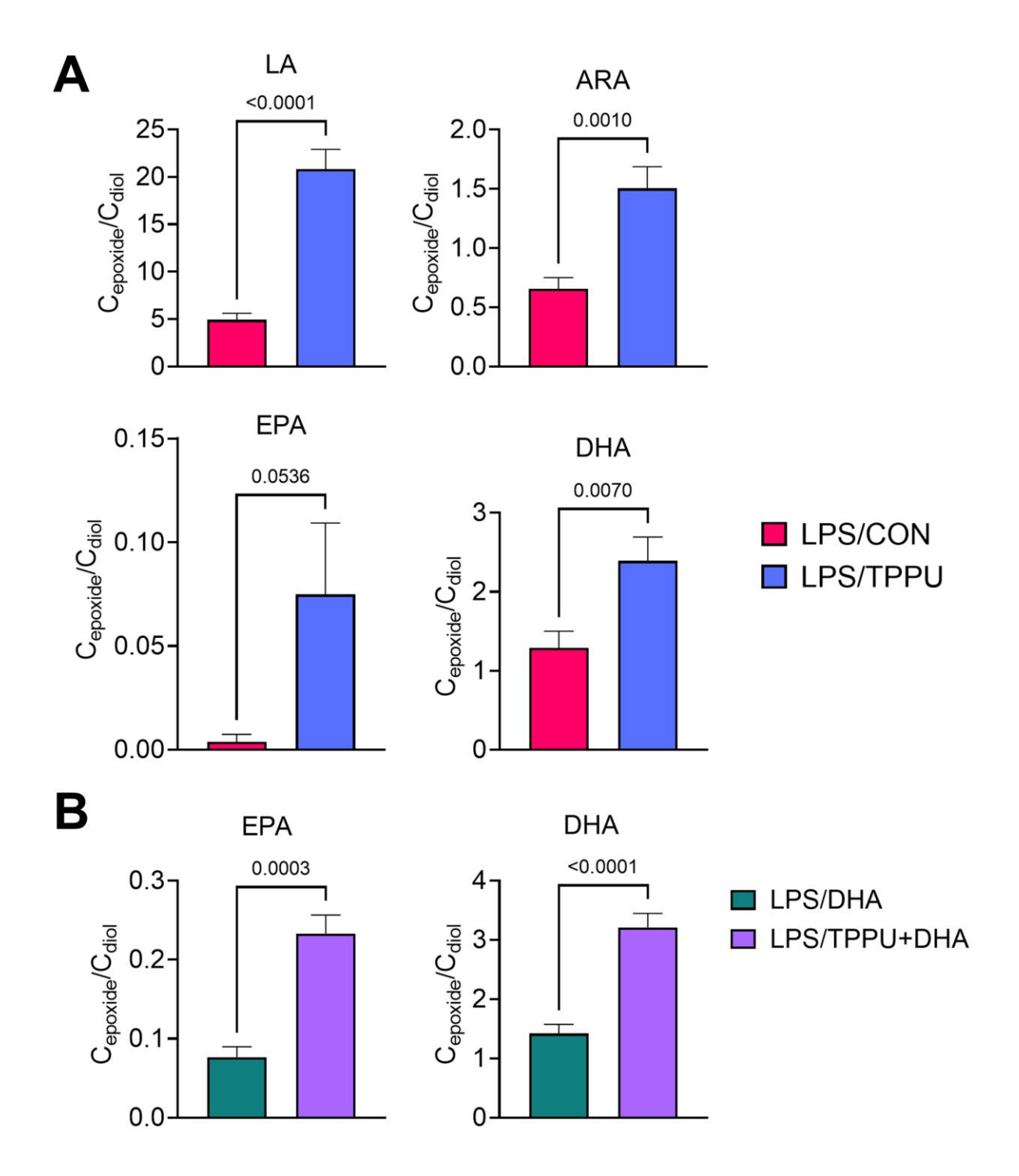


Figure 3.7. Supplementation with DHA and/or TPPU modulates plasma epoxide/diol metabolite ratios in LPS-injected NZBWF1 mice. (A) TPPU consumption significantly shifts epoxide/diol ratios for metabolites derived from LA, ARA, EPA, and DHA. Ratios between sums of all EpFAs and sums of all DiHFAs from each PUFA precursor are shown. (B) DHA supplementation elevates epoxide/diol ratios for EPA-derived metabolites, and combination of DHA+TPPU further shifts epoxide/diol ratios for EPA- and DHA-derived metabolites. Ratios

Figure 3.7 (cont'd)

between sums of all EpFAs and sums of all DiHFAs from each PUFA precursor are shown. Data are presented as mean \pm SEM (n=8). Values of p<0.1 are shown, with p<0.05 considered statistically significant.

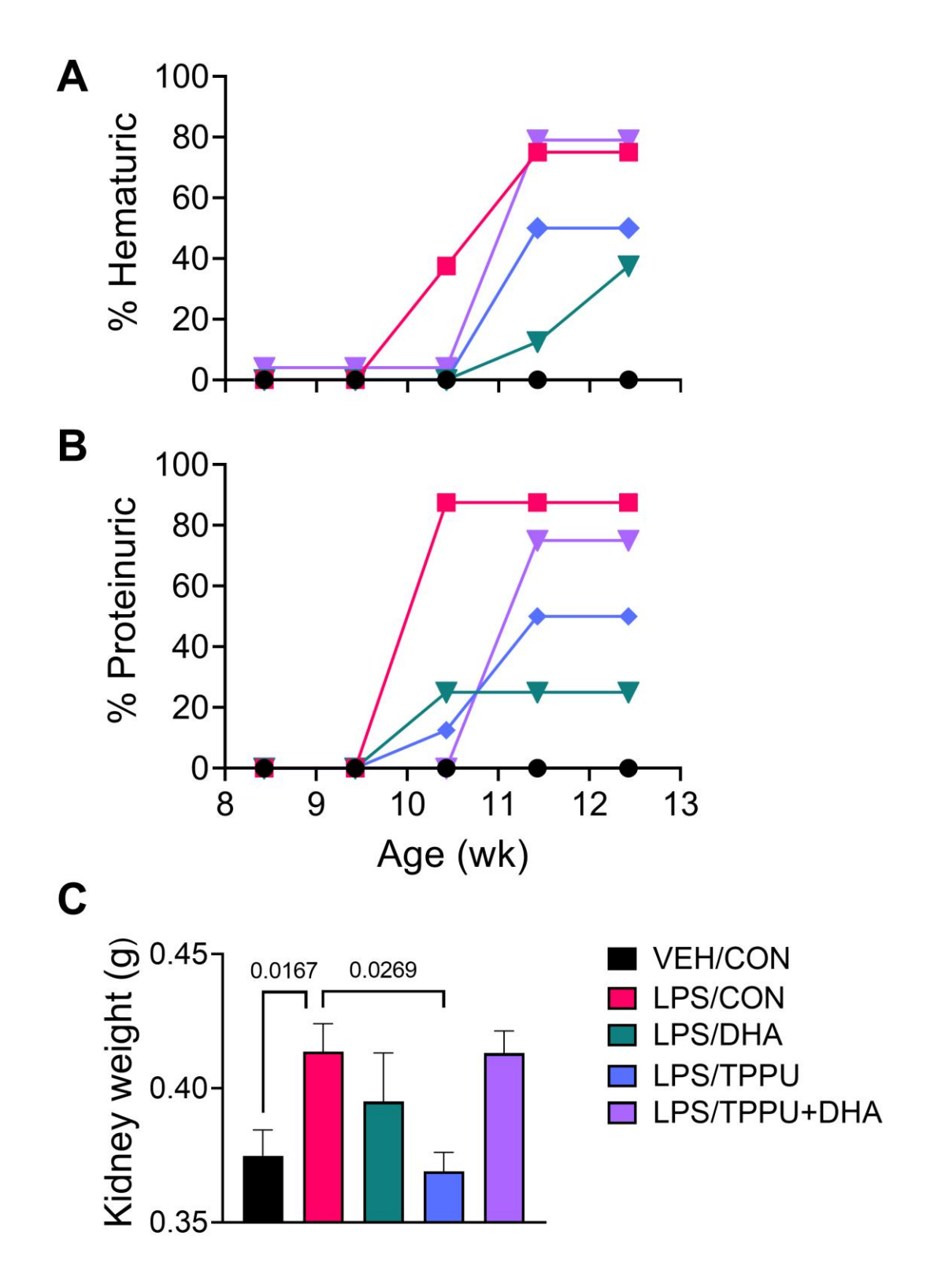


Figure 3.8. DHA alone and TPPU alone delay onset of R-LPS-induced hematuria and proteinuria but are antagonistic when delivered together. Animals were monitored weekly for development of (A) hematuria (>0 cells/µl urine) and (B) proteinuria (≥300 mg/dl urinary protein)

Figure 3.8 (cont'd)

using clinical dipsticks. **(C)** After 5 wk of biweekly i.p. LPS injections, mice were sacrificed, and both left and right kidneys were weighed before additional tissue processing. Data are presented as mean \pm SEM. Statistically significant differences between VEH/CON and LPS/CON were assessed by Student's t-test. LPS/DHA, LPS/TPPU, and LPS/TPPU+DHA were compared to LPS/CON using one-way ANOVA followed by Tukey's *post-hoc* test. Values of p<0.1 are shown, with p<0.05 considered statistically significant.

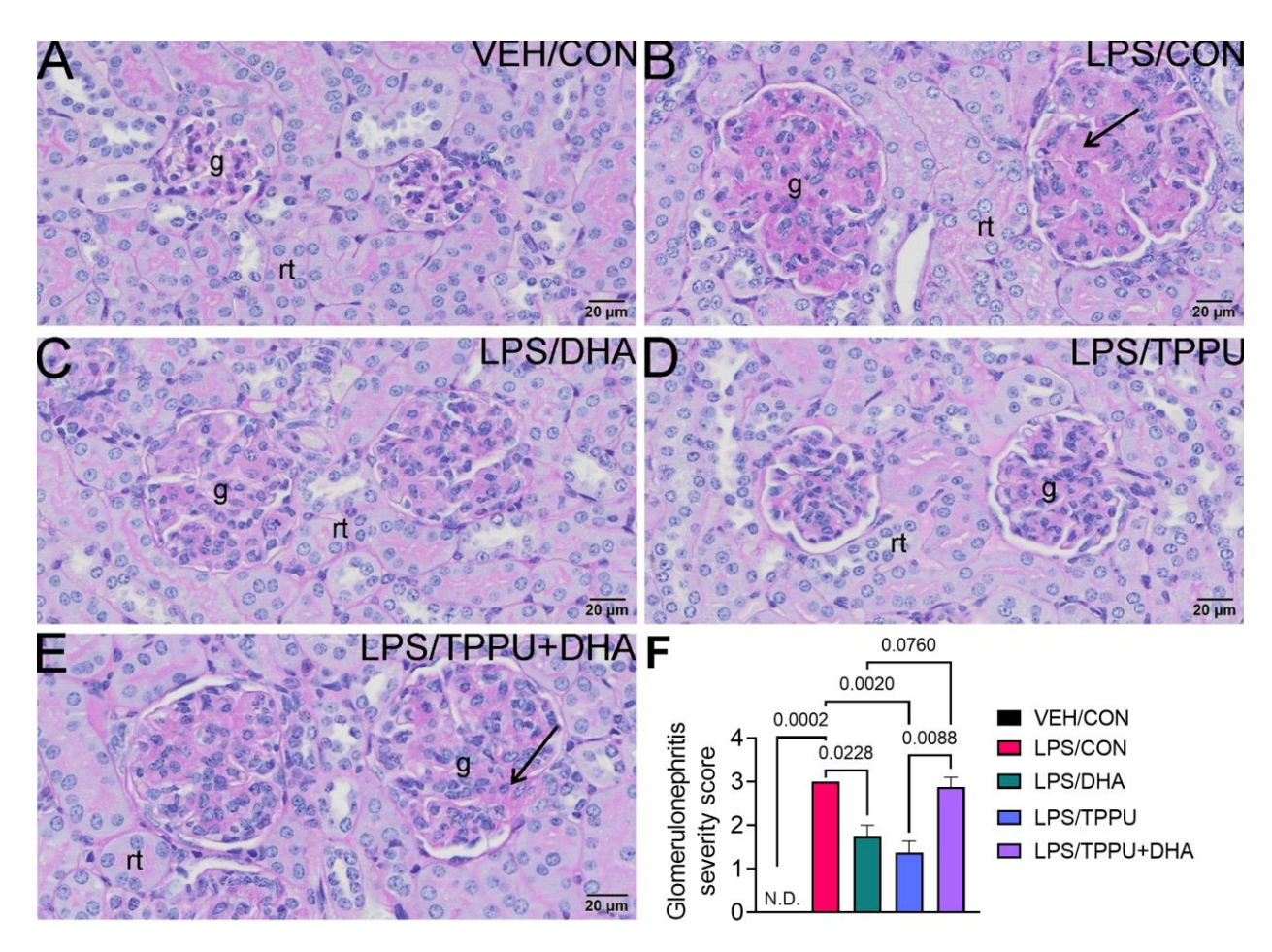


Figure 3.9. DHA alone and TPPU alone suppress R-LPS-induced glomerulonephritis but are antagonistic when delivered together. Light photomicrographs of periodic acid Schiff and hematoxylin (PASH)-stained cortical kidney tissue from (A) vehicle (VEH)-treated/control diet (CON) mouse, (B) rough LPS-treated/CON mouse, (C) LPS/DHA mouse, (D) LPS/TPPU mouse, and (E) LPS/TPPU+DHA mouse. Markedly hypertrophic and hypercellular glomeruli (g) with thickened medullary membranes in kidneys of LPS/CON mice (B) and LPS/TPPU+DHA mice (E). Less glomerular histopathology in kidneys of LPS/DHA mice (C) and LPS/TPPU mice (D). (F) Semi-quantitative scores for glomerulonephritis severity. Scoring was as follows: 0—no significant finding, 1—minimal, 2—mild, 3—moderate, 4—marked, 5—severe. Data are presented as mean \pm SEM (n = 8). Values of p<0.1 are shown, with p<0.05 considered statistically significant. g, glomerulus; rt, renal tubule; N.D., not determined.

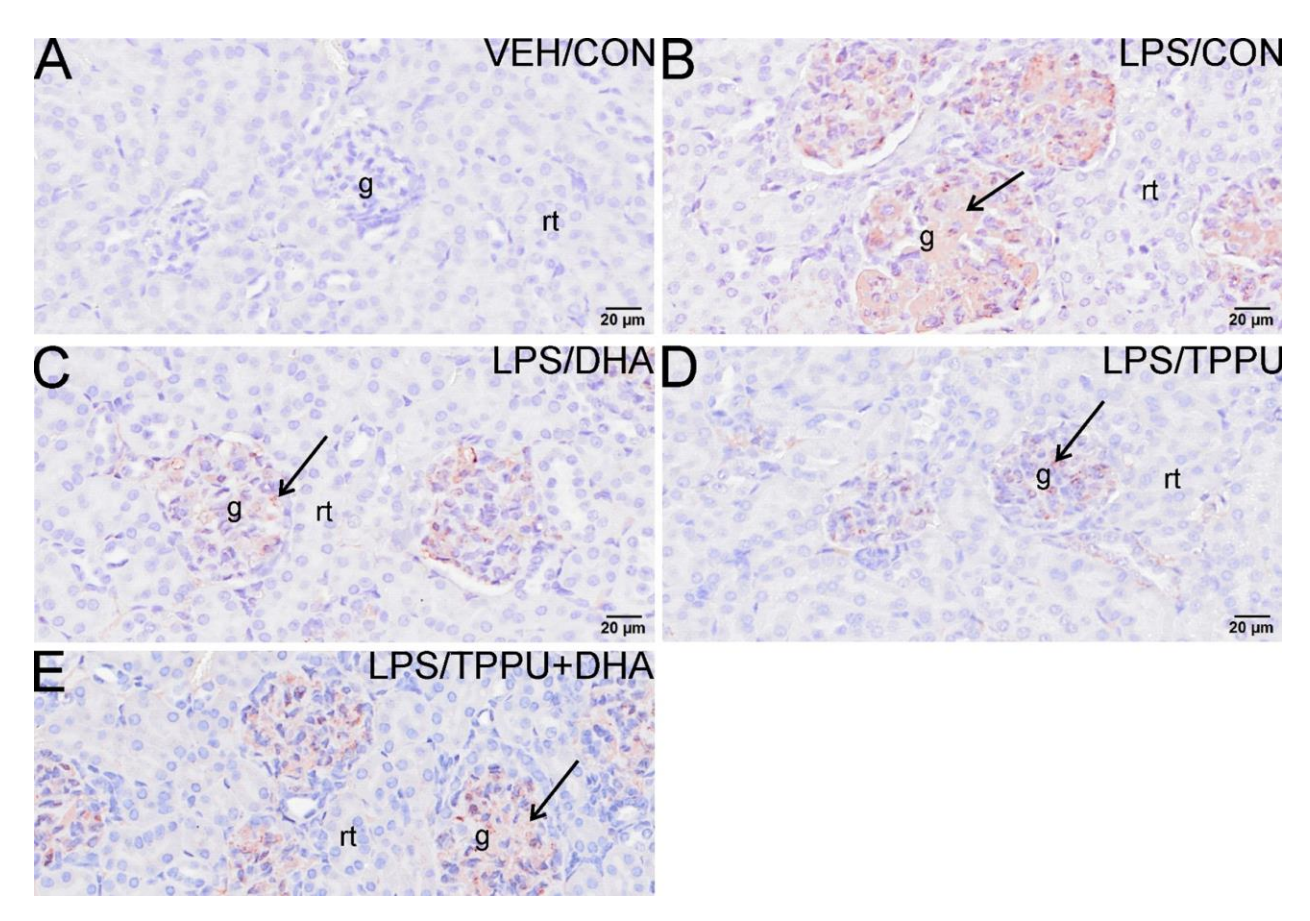


Figure 3.10. DHA alone and TPPU alone suppress R-LPS-induced IgG deposition in the kidney but are antagonistic when delivered together. Light photomicrographs of glomeruli immunohistochemically stained for IgG (arrows; brown chromogen) in kidneys from (**A**) vehicle (VEH)-treated/control diet (CON) mouse, (**B**) rough LPS-treated/CON mouse, (**C**) LPS/DHA mouse, (**D**) LPS/TPPU mouse, and (**E**) LPS/TPPU+DHA. No IgG+ staining in glomeruli of VEH/CON mouse (**A**). Conspicuous IgG+ staining in medullary tissue of markedly enlarged glomeruli in LPS-treated mice (**B**), LPS/DHA mice (**C**), and LPS/TPPU+DHA mice (**E**). Less medullary IgG+ staining in LPS/TPPU mouse (**D**) compared to other LPS-treated mice (**B**, **C**, **E**). g, glomerulus; rt, renal tubule.

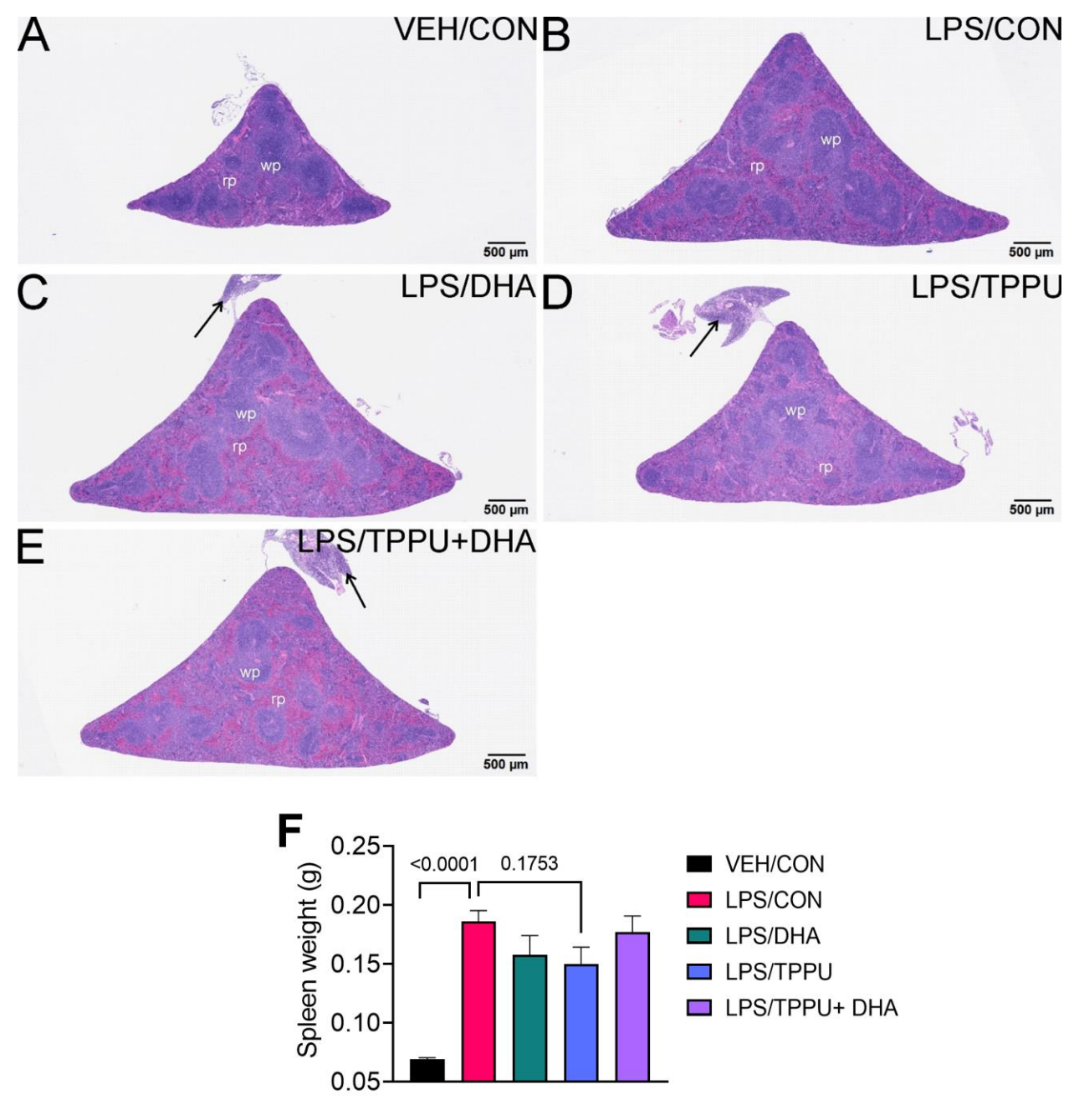


Figure 3.11. TPPU attenuates R-LPS-induced lymphoid hyperplasia in the spleen. Light photomicrographs of hematoxylin and eosin-stained tissue from the spleens of (A) vehicle (VEH)-treated/control diet (CON) mouse, (B) rough LPS-treated/CON mouse, (C) LPS/DHA mouse, (D) LPS/TPPU mouse, and (E) LPS/TPPU+DHA mouse. Spleens from LPS-treated mice (B-E) are enlarged due to lymphoid hyperplasia. Spleen from LPS/TPPU mouse (D) less enlarged than other LPS-treated mice. Mononuclear cell infiltration of peri-splenic fat (arrows) in LPS/DHA mice (C), LPS/TPPU mice (D), and LPS/TPPU+DHA mice (E). (F) After 5 wk of biweekly i.p. LPS injections, mice were sacrificed, and spleens were weighed before additional tissue processing. Data are presented as mean \pm SEM. wp, white pulp; rp, red pulp.

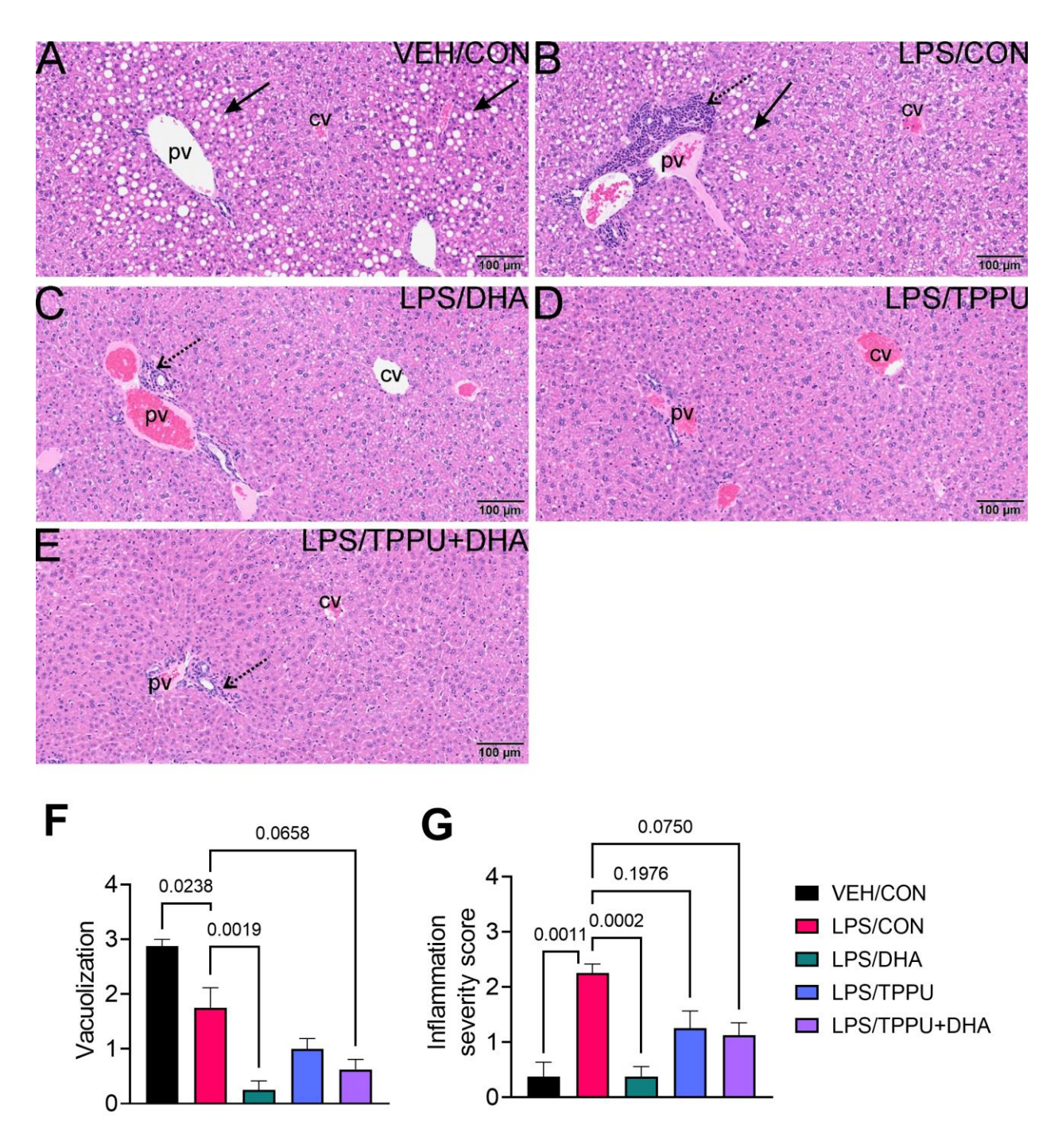


Figure 3.12. DHA suppresses R-LPS-induced liver inflammation and loss of vacuolization. Light photomicrographs of hematoxylin and eosin-stained tissue from the livers of (**A**) vehicle (VEH)-treated/control diet (CON) mouse, (**B**) rough LPS-treated/CON mouse, (**C**) LPS/DHA mouse, (**D**) LPS/TPPU mouse, and (**E**) LPS/TPPU+DHA mouse. Periportal hepatocellular vacuolization (solid arrow; characteristic of steatosis) in VEH/CON mice (**A**) and LPS/CON mice (**B**). Lymphoid cell infiltration in periportal interstitial tissue (stippled arrow) in liver of LPS/CON mouse (**B**) with less hepatocellular vacuolization. Remainder of LPS-treated mice (**C-E**) have less periportal inflammatory cells and absence of hepatocellular vacuolization. Semi-quantitative scores for hepatic vacuolization (**F**) and inflammation severity (**G**). Scoring was as follows: 0—

Figure 3.12 (cont'd)

no significant finding, 1—minimal, 2—mild, 3—moderate, 4—marked, 5—severe. Data are presented as mean \pm SEM (n=8). Values of p<0.1 are shown, with p<0.05 considered statistically significant. pv, periportal vein; cv, central vein; solid arrow, hepatocellular lipid vacuoles; stippled arrow, periportal cellular inflammation (predominantly mononuclear cells).

TABLES

Table 3.1. Experimental diet fatty acid concentrations.

Common Name	Chemical Formula	CON	DHA	TPPU	TPPU+DHA
Capric	C10:0	<lod< td=""><td>0.30 ± 0.07</td><td><lod< td=""><td>0.25 ± 0.06</td></lod<></td></lod<>	0.30 ± 0.07	<lod< td=""><td>0.25 ± 0.06</td></lod<>	0.25 ± 0.06
Lauric	C12:0	0.02 ± 0.00	1.67 ± 0.11	0.01 ± 0.00	1.60 ± 0.06
Myristic	C14:0	0.09 ± 0.00	4.97 ± 0.19	0.10 ± 0.00	4.79 ± 0.02
Myristoleic	C14:1	<lod< td=""><td>0.08 ± 0.00</td><td><lod< td=""><td>0.09 ± 0.01</td></lod<></td></lod<>	0.08 ± 0.00	<lod< td=""><td>0.09 ± 0.01</td></lod<>	0.09 ± 0.01
Pentadecanoic	C15:0	0.02 ± 0.00	0.01 ± 0.00	0.01 ± 0.00	0.01 ± 0.00
Palmitic	C16:0	6.29 ± 0.19	8.63 ± 0.22	6.50 ± 0.02	8.22 ± 0.05
Palmitoleic	C16:1ω7	0.02 ± 0.01	0.02 ± 0.01	0.02 ± 0.00	0.01 ± 0.00
Hygogeic	C16:1ω9	0.08 ± 0.01	0.91 ± 0.08	0.08 ± 0.01	0.99 ± 0.03
Heptadecanoic	C17:0	0.02 ± 0.00	0.02 ± 0.00	0.03 ± 0.00	0.02 ± 0.00
Stearic	C18:0	1.92 ± 0.07	1.55 ± 0.02	1.96 ± 0.07	1.57 ± 0.03
Vaccenic	C18:1ω7	0.81 ± 0.01	0.54 ± 0.01	0.76 ± 0.02	0.53 ± 0.01
Oleic	C18:1ω9	70.38 ± 0.63	50.85 ± 0.86	69.60 ± 0.90	51.98 ± 0.16
Linoleic	C18:2ω6	19.05 ± 0.43	16.16 ± 0.78	19.62 ± 0.93	15.14 ± 0.24
Alpha-Linolenic	C18:3ω3	0.24 ± 0.02	0.20 ± 0.02	0.25 ± 0.02	0.19 ± 0.01
Arachidic	C20:0	0.36 ± 0.02	0.27 ± 0.01	0.35 ± 0.02	0.26 ± 0.01
Eicosenoic	C20:1ω9	0.27 ± 0.01	0.17 ± 0.02	0.27 ± 0.02	0.17 ± 0.02
Arachidonic	C20:4ω6	<lod< td=""><td><lod< td=""><td><lod< td=""><td><lod< td=""></lod<></td></lod<></td></lod<></td></lod<>	<lod< td=""><td><lod< td=""><td><lod< td=""></lod<></td></lod<></td></lod<>	<lod< td=""><td><lod< td=""></lod<></td></lod<>	<lod< td=""></lod<>
Behenic	C22:0	0.24 ± 0.02	0.19 ± 0.02	0.25 ± 0.03	0.20 ± 0.02
Eicosapentaenoic	C20:5ω3	<lod< td=""><td><lod< td=""><td><lod< td=""><td><lod< td=""></lod<></td></lod<></td></lod<></td></lod<>	<lod< td=""><td><lod< td=""><td><lod< td=""></lod<></td></lod<></td></lod<>	<lod< td=""><td><lod< td=""></lod<></td></lod<>	<lod< td=""></lod<>
Docosapentaenoic ω-3	C22:5ω3	<lod< td=""><td>0.22 ± 0.03</td><td><lod< td=""><td>0.24 ± 0.01</td></lod<></td></lod<>	0.22 ± 0.03	<lod< td=""><td>0.24 ± 0.01</td></lod<>	0.24 ± 0.01
Docosahexaenoic	C22:6ω3	<lod< td=""><td>13.12 ± 0.39</td><td><lod< td=""><td>13.61 ± 0.19</td></lod<></td></lod<>	13.12 ± 0.39	<lod< td=""><td>13.61 ± 0.19</td></lod<>	13.61 ± 0.19
Lignoceric	C24:0	0.13 ± 0.01	0.10 ± 0.01	0.14 ± 0.02	0.11 ± 0.01
Nervonic	C24:1ω9	0.08 ± 0.01	0.02 ± 0.01	0.05 ± 0.02	0.03 ± 0.01
Σ SFA		9.08 ± 0.29	17.71 ± 0.52	9.34 ± 0.11	17.02 ± 0.10
Σ MUFA		71.64 ± 0.65	52.59 ± 0.92	70.79 ± 0.88	53.80 ± 0.14
Σ PUFA		19.29 ± 0.42	29.70 ± 0.68	19.87 ± 0.95	29.18 ± 0.08
Σ ω-6 PUFA		19.05 ± 0.43	16.16 ± 0.78	19.62 ± 0.93	15.14 ± 0.24
Σ	0.24 ± 0.02	13.54 ± 0.44	0.25 ± 0.02	14.04 ± 0.19	
ω6/ω3 ratio		82.28 ± 9.13	1.20 ± 0.08	78.73 ± 3.51	1.08 ± 0.03

Data are presented as percent of total fatty acids (mean \pm SEM, n = 8/gp) as measured by GC-MS. LOD, limit of detection.

Table 3.2. Red blood cell fatty acid content as determined by GLC.

Common Name	Chemical Formula	VEH/CON	LPS/CON	LPS/DHA	LPS/TPPU	LPS/TPPU+DHA
Myristic	C14:0	0.18±0.00 ^A	0.16±0.00 ^A	0.36 ± 0.00^{BC}	0.18±0.00 ^A	0.36 ± 0.00^{BC}
Palmitic	C16:0	24.95±0.01 ^A	25.81±0.00 ^A	28.43±0.01 ^C	25.87±0.01 ^A	28.76±0.01 ^C
Palmitolaidic	C16:1ω7t	0.05±0.00 ^A	0.04±0.00 ^A	0.03±0.00 ^B	0.04 ± 0.00^{AB}	0.04 ± 0.00^{AB}
Palmitoleic	C16:1ω7	0.89 ± 0.00^{A}	0.74 ± 0.00^{A}	0.79 ± 0.00^{A}	0.75 ± 0.00^{A}	0.76 ± 0.00^{A}
Stearic	C18:0	12.78±0.00 ^A	12.56±0.01 ^{AB}	11.98±0.01 ^A	12.57±0.00 ^A	11.35±0.00 ^{BC}
Elaidic	C18:1t	0.15 ± 0.00^{AB}	0.15 ± 0.00^{B}	0.12 ± 0.00^{C}	0.15 ± 0.00^{AB}	0.12±0.00 ^C
Oleic	C18:1ω9	19.48±0.01 ^{AB}	20.78±0.02 ^B	17.92±0.00 ^{AC}	19.84±0.01 ^{AB}	17.19±0.01 ^C
Linoelaidic	C18:2ω6t	0.09 ± 0.00^{A}	0.10 ± 0.00^{A}	0.05 ± 0.00^{C}	0.08 ± 0.00^{AB}	0.05 ± 0.00^{C}
Linoleic	C18:2ω6	10.89±0.01 ^{AB}	10.60±0.00 ^A	11.30±0.01 ^{AB}	10.67±0.01 ^{AB}	10.95±0.01 ^{AB}
alpha-Linolenic	C18:3ω3	0.05 ± 0.00^{A}	0.05 ± 0.00^{A}	0.06 ± 0.00^{A}	0.04 ± 0.00^{A}	0.06 ± 0.00^{A}
gamma-Linolenic	C18:3ω6	0.07 ± 0.00^{A}	0.07 ± 0.00^{A}	0.04 ± 0.00^{B}	0.07 ± 0.00^{A}	0.04 ± 0.00^{B}
Arachidic	C20:0	0.18±0.00 ^A	0.15 ± 0.00^{AB}	0.13±0.00 ^B	0.15 ± 0.00^{AB}	0.16±0.00 ^A
Eicosenoic	C20:1ω9	0.38 ± 0.00^{A}	0.39 ± 0.00^{A}	0.25 ± 0.00^{CD}	0.40 ± 0.00^{A}	0.23±0.00 ^D
Eicosadienoic	C20:2ω6	0.31±0.00 ^A	0.32 ± 0.00^{A}	0.24 ± 0.00^{CD}	0.32 ± 0.00^{A}	0.23 ± 0.00^{D}
Dihomo-g- linolenic	C20:3ω6	1.34±0.00 ^A	1.30±0.00 ^A	0.94±0.00 ^{CD}	1.32±0.00 ^A	0.90±0.00 ^D
Arachidonic	C20:4ω6	18.18±0.01 ^A	16.80±0.01 ^{AB}	7.16±0.00 ^C	17.42±0.01 ^{AC}	7.04±0.01 ^D
Behenic	C22:0	0.63±0.00 ^A	0.45 ± 0.00^{AB}	0.23 ± 0.00^{BC}	0.48 ± 0.00^{AB}	0.31 ± 0.00^{BC}
Eicosapentaenoic	C20:5ω3	0.36±0.00 ^A	0.37±0.00 ^A	3.41±0.00 ^B	0.35±0.00 ^A	3.64±0.00 ^B
Docosapentaenoic ω-3	C22:5ω3	0.66±0.00 ^A	0.70±0.00 ^A	1.04±0.00 ^B	0.67±0.00 ^A	1.02±0.00 ^B
Docosapentaenoic ω-6	C22:5ω6	0.74±0.00 ^A	0.69±0.00 ^{AB}	0.20±0.00 ^C	0.72±0.00 ^A	0.24±0.00 ^{BC}
Docosahexaenoic	C22:6ω3	5.33±0.00 ^A	5.55 ± 0.00^{AB}	14.69±0.00 ^C	5.63±0.00 ^{AB}	15.11±0.01 ^C
Lignoceric	C24:0	0.43±0.00 ^A	0.38 ± 0.00^{AB}	0.30 ± 0.00^{BC}	0.40 ± 0.00^{AC}	0.49±0.00 ^A
Nervonic	C24:1ω9	0.41 ± 0.00^{AB}	$0.35 \pm .000^{ABC}$	0.26 ± 0.00^{C}	0.39 ± 0.00^{AB}	0.38 ± 0.00^{A}
	Σ SFA	39.15±0.01 ^A	39.51±0.01 ^A	41.44±0.01 ^B	39.64±0.01 ^{AB}	41.42±0.01 ^B
Σ MUFA		21.35±0.01 ^{AB}	22.46±0.02 ^A	18.87±0.01 ^B	21.55±0.01 ^{AB}	18.72±0.01 ^C
Σ ω-3 PUFA		6.40 ± 0.00^{A}	6.67 ± 0.00^{AB}	19.19±0.01 ^C	6.70 ± 0.01^{AB}	19.83±0.01 ^C
	Σω-6 PUFA	33.10±0.01 ^A	31.37±0.01 ^B	20.50±0.01 ^D	32.11±0.01 ^{AB}	20.02±0.01 ^D
	ω-3 Index	5.69±0.00 ^A	5.92±0.00 ^{AB}	18.10±0.01 ^C	5.98±0.00 ^{AB}	18.75±0.01 ^C

Data are presented as percent of total fatty acids (mean \pm SEM, n = 8/gp) as measured by GLC. Differences between experimental groups were compared by ordinary one-way ANOVA followed by Tukey's *post-hoc* test. Nonparametric versions of these tests were used when applicable. Unique letters indicate significant differences between groups (p<0.05).

Table 3.3. Plasma epoxide/diol metabolite ratios at necropsy as determined by LC-MS/MS.

Fatty acid precursor	VEH/CON	LPS/CON	LPS/DHA	LPS/TPPU	LPS/TPPU+DHA
LA	6.84±0.67	4.92±0.69 ^A	6.29±1.28 ^A	20.83±2.07 ^B	15.37±2.36 ^B
ARA	0.72±0.18	0.66 ± 0.09^{AB}	0.40 ± 0.15^{A}	1.50 ± 0.18^{B}	2.10±1.14 ^{AB}
EPA	0.00 ± 0.00	0.00 ± 0.00^{A}	0.08 ± 0.01^{AB}	0.07 ± 0.03^{A}	0.23±0.02 ^B
DHA	1.69±0.72	1.29±0.21 ^A	1.42±0.15 ^A	2.39 ± 0.30^{AB}	3.21±0.24 ^B
Σω-6 PUFA	1.80±0.37	1.63±0.15 ^A	1.52±0.23 ^A	3.93 ± 0.63^{B}	4.84 ± 0.89^{B}
Σω-3 PUFA	0.13±0.03	0.27±0.04*A	0.54 ± 0.07^{AB}	0.61 ± 0.09^{AB}	1.00±0.10 ^B
Σ PUFA	0.94±0.12	0.95 ± 0.10^{AB}	0.64 ± 0.09^{A}	2.08±0.28 ^C	1.34±0.13 ^{BC}

Data are presented as ratios between plasma epoxide metabolite concentrations (Cepoxide) and plasma diol metabolite concentrations (C_{diol}) (mean ± SEM, n = 8/gp). Epoxides and diols accounted for each fatty acid precursor included: LA) 9,10-EpOME, 9,10-DiHOME, 12,13-EpOME, 12,13-DiHOME; ARA) 5,6-EpETrE, 5,6-DiHETrE, 8,9-EpETrE, 8,9-DiHETrE, 11,12-EpETrE, 11,12-DiHETrE, 14,15-EpETrE, 14,15-DiHETrE; EPA) 5,6-EpETE, 5,6-DiHETE, 8,9-EPETE, 8,9-DiHETE, 11,12-EPETE, 11,12-DiHETE, 14,15-EPETE, 14,15-DiHETE, 17,18-EPETE, 17,18-DiHETE; DHA) 7,8-EpDPE, 7,8-DiHDPE, 10,11-EpDPE, 10,11-DiHDPE, 13,14-EpDPE, 13,14-DiHDPE, 16,17-EpDPE, 16,17-DiHDPE, 19,20-EpDPE, 19,20-DiHDPE. Ratios for total ω-6 PUFA were calculated from the sum of the LA- and ARA-derived epoxides and diols specified above. Ratios for total ω-3 PUFA were calculated from the sum of the EPA- and DHAderived epoxides and diols specified above. Ratios for total PUFA were calculated from the sum of the ω -6- and ω -3-derived epoxides and diols described above. Differences between VEH/CON and LPS/CON groups were compared by Student's t test. LPS/CON, LPS/DHA, LPS/TPPU, and LPS/TPPU+DHA groups were compared by ordinary one-way ANOVA followed by Tukey's post-hoc test. Nonparametric versions of these tests were used when applicable. Asterisks (*) indicate significant differences between VEH/CON and LPS/CON groups (p<0.05). Unique letters indicate significant differences between LPS/CON, LPS/DHA, LPS/TPPU, and LPS/TPPU+DHA groups (p<0.05). LA, linoleic acid; ARA, arachidonic acid; EPA, eicosapentaenoic acid; DHA, docosahexaenoic acid; PUFA, polyunsaturated fatty acid.

CHAPTER 4: OMEGA-3 DOCOSAHEXAENOIC ACID SUPPRESSES SILICAINDUCED PROINFLAMMATORY CYTOKINE RELEASE AND OXYLIPIN PRODUCTION IN NOVEL FETAL LIVER-DERIVED ALVEOLAR-LIKE MACROPHAGES

PUBLICATION NOTICE

The following chapter is currently in preparation to be submitted to *Frontiers in Immunology*. Authors of this work are: Olivia K Favor^{1,2}, Kathryn A Wierenga^{2,3}, Lichchavi D Rajasinghe^{2,4}, Krishna R Maddipati⁵, Kin Sing Stephen Lee^{1,2,7}, Andrew J Olive⁷, and James J Pestka^{2,4,7}. ¹Indicates contributors from the Department of Pharmacology and Toxicology, College of Osteopathic Medicine, Michigan State University. ²Indicates contributors from the Institute for Integrative Toxicology, Michigan State University. ³Indicates contributors from the Department of Biochemistry and Molecular Biology, Michigan State University. ⁴Indicates contributors from the Department of Food Science and Human Nutrition, Michigan State University. ⁵Indicates contributors from the Department of Chemistry, Michigan State University. ⁷Indicates contributors from the Department of Microbiology and Molecular Genetics, Michigan State University.

ABSTRACT

Introduction: Workplace exposure to respirable crystalline silica ($cSiO_2$) is associated with chronic inflammatory and autoimmune diseases. At the mechanistic level, $cSiO_2$ particles are quickly phagocytosed by resident alveolar macrophages (AMs) in the lung, causing a robust cycle of proinflammatory cytokine release, lysosomal rupture, mitochondrial toxicity, and immunogenic cell death if the particle is not efficiently cleared by the lung. We and others have demonstrated in bone marrow-derived and transformed macrophage models that supplementation with the ω -3 polyunsaturated fatty acid (PUFA) docosahexaenoic acid (DHA) contributes to increased membrane phospholipid content of DHA and subsequent suppression of $cSiO_2$ -triggered inflammatory responses. However, mechanistic exploration of ω -3 PUFA effects in AMs is challenging due to reliance on short-lived primary AMs derived from lung lavage fluid.

Methods: To address these limitations, we have employed a recently developed novel self-renewing AM model from C57BL/6 mice, fetal liver-derived alveolar-like macrophages (FLAMs), that is phenotypically representative of primary lung AM populations. We found that incubation of FLAMs with 25 μM DHA as ethanolic suspensions or as complexes with bovine serum albumin were equally effective at increasing ω-3 PUFA content of phospholipids at the expense of the ω-6 PUFA arachidonic acid (ARA) and the ω-9 monounsaturated fatty acid oleic acid. Based on these findings, FLAMs were treated with 25 μM DHA in EtOH or EtOH vehicle (VEH) for 24 h, with or without LPS for 2 h, and with or without cSiO₂ for 1.5 or 4 h then proinflammatory cytokine release, lysosomal membrane permeabilization, and mitochondrial depolarization assessed. In addition, oxylipin metabolites were measured using a targeted LC-MS lipidomics panel of 156 metabolites.

Results: Regardless of whether FLAMs were LPS-primed, cSiO₂-triggered lysosomal permeability, mitochondrial toxicity, and cell death were not impacted by DHA. LPS+cSiO₂ elicited marked IL-1α, IL-1β, and TNF-α release after 1.5 and 4 h of cSiO₂ exposure, which was significantly inhibited by DHA. In VEH-treated cells, cSiO₂ alone and LPS+cSiO₂ induced synthesis of ARA-derived proinflammatory oxylipins including prostaglandins, leukotrienes, and thromboxanes that was suppressed by DHA. In addition, DHA promoted synthesis of proresolving DHA-derived oxylipins at the expense of ARA-derived oxylipins.

Discussion: FLAMs were amenable to lipidome modulation by DHA, which suppressed cSiO₂-triggered proinflammatory cytokine responses and ARA-derived oxylipins that potentially contribute to the particle's toxicity in the lung. FLAMs are a promising *in vitro* alternative to primary AMs for investigating interventions against toxicant-triggered inflammation and autoimmunity in the lung.

INTRODUCTION

Occupational exposure to respirable crystalline silica (cSiO₂) is etiologically linked to silicosis, pulmonary fibrosis, lung cancer, and, in some cases, initiation of autoimmune disease [471-474]. Approximately 2.3 million American workers are commonly exposed to cSiO₂ levels that exceed the Occupational Health and Safety Administration's (OSHA's) Permissible Exposure Limits [475], with the highest exposure levels in construction, manufacturing, sandblasting, farming, ceramics, and dentistry work [328, 476]. In the lung, alveolar macrophages (AMs) serve as a preliminary line of defense against cSiO₂ particles [477]. When inhaled, cSiO₂ travels to the alveoli where AMs readily phagocytose the particles. Following phagocytosis, cSiO₂ induces lysosomal membrane permeabilization (LMP), mitochondrial toxicity, reactive oxygen species (ROS) formation, inflammasome activation, release of proinflammatory proteins and lipid

mediators, and cell death [183, 478]. Resultant proinflammatory cytokines and chemokines can act in a paracrine-like manner to induce expression and secretion of additional proinflammatory mediators by neighboring AMs and other cells. If not properly cleared, cSiO₂ particles released from dead AMs then can be taken up by viable AMs or recruited macrophages, contributing to a perpetual cycle of severe pulmonary inflammation and tissue damage. Accordingly, tissue-resident AMs play a critical role in the initiation of persistent cSiO₂-triggered lung inflammation and development of chronic disease.

Several previous studies have reported that exposing rat, bovine, and human AMs to respirable cSiO₂ drives biosynthesis of oxylipins derived from the ω-6 polyunsaturated fatty acid (PUFA) arachidonic acid (ARA), including prostaglandin E2 (PGE2), leukotriene B4 (LTB4), thromboxane B2 (TXB2), and 5-hydroxyeicosatetraenoic acid (5-HETE) [229, 479-481]. These oxylipins have been associated with increased severity of symptoms in lung-related diseases including asthma, cystic fibrosis, chronic obstructive pulmonary disease (COPD), and extrinsic allergic alveolitis [482-484]. In response to inflammatory stimuli, phospholipase A2 (PLA2) activates and releases ARA, the most abundant PUFA in the sn-2 position of membrane phospholipids, into the cytosol where it is converted into PGE2, LTB4, TXB2, HETEs, and other ω-6 oxylipins that promote further immune cell infiltration and damage to lung tissue [482, 485]. While a few ARA-derived oxylipins have been identified as biomarkers of lung disease and are induced by cSiO₂, it is possible that broad shifts in the cellular lipidome of AMs, rather than changes in individual metabolite levels, are responsible for eliciting ongoing inflammation in the lung. Therefore, it is important to apply a wide-scale omics approach to more fully characterize the impacts that cSiO₂ has on oxylipin production in AMs.

One promising lipidome-modifying agent for preventing cSiO₂-induced inflammatory lung disease is the ω -3 polyunsaturated fatty acid (PUFA) docosahexaenoic acid (C22:6, ω -3, DHA). Mechanistically, ω -3 PUFAs prevent excessive inflammatory responses and promote proresolving immune responses by 1) displacing SFAs and ω -6 PUFAs from the plasma membrane, 2) altering lipid raft structures and attenuating downstream signal transduction, 3) competing with ω -6 PUFAs as substrates for cyclooxygenase (COX), lipoxygenase (LOX) and cytochrome P450 (CYP450) enzymes, 4) preventing NF- κ B-driven expression of proinflammatory mediators, and 5) enhancing efferocytosis of cell corpses by phagocytes [342, 430, 432, 486]. In both mice and humans, DHA consumption leads to elevated tissue and plasma levels of not only DHA but also highly pro-resolving DHA-derived metabolites [487-489]. [490-492]). We have also demonstrated in several macrophage models that DHA displaces ω -6 ARA and ω -9 oleic acid (OA) from membrane phospholipids [430-432]. To mechanistically understand how DHA works, it is imperative to discern how this intervention influences cSiO₂-induced toxicity and production of proinflammatory cytokines and ω -6 oxylipins in AMs.

Several barriers have hindered research efforts into primary AM function. First, only <10⁶ primary cells are typically recovered from one adult mouse by bronchoalveolar lavage, and obtaining sufficient numbers of cells for *in vitro* assays requires sacrificing large numbers of mice [493]. Second, primary AMs undergo rapid phenotypic changes upon being cultured and thus do not accurately reflect AM phenotypes observed in the alveolar milieu. These phenotypic changes also cause primary AMs to be short-lived in culture, unlike their long-living counterparts in the lung [494, 495]. Third, other widely used primary macrophages (e.g., bone marrow-derived macrophages [BMDMs], peritoneal macrophages) and transformed macrophage cell lines (e.g., RAW264.7 cells, THP-1 cells) do not adequately model the tissue-specific phenotype of primary

AMs [496]. Recently, we have overcome these barriers by developing an *ex vivo* fetal liver-derived alveolar macrophage (FLAM) model that is non-transformed and self-replicating in the presence of GM-CSF and TGF-β. Similar to primary AMs, FLAMs are characterized by high surface expression of SiglecF and CD11c, low surface expression of CD14, and stable expression of AMspecific genes such as *Marco*. In addition, the kinetics of cSiO₂ phagocytosis, cell death, and IL-1 cytokine release in FLAMs mirrors that of primary AMs [34]. Accordingly, FLAMs are phenotypically relevant AM surrogates for conducting thorough *in vitro* mechanistic studies involving cSiO₂ exposure.

Herein, we employed FLAMs to understand how DHA incorporation influences cSiO₂-induced toxicity, proinflammatory cytokines, and production of PUFA-derived oxylipins. FLAMs might be a promising *in vitro* alternative to primary AMs for investigating how cSiO₂ and other respirable particles induce inflammation and how these responses can be influenced by modulation of the cellular lipidome.

MATERIALS AND METHODS

Key reagents

All key reagents used in this study and their corresponding catalog numbers are outlined in **Table S4.1**.

Fetal liver-derived alveolar macrophage (FLAM) isolation and cell culture

Experimental protocols were approved by the Institutional Animal Care and Use Committee at Michigan State University (MSU) (Animal Use Form [AUF] #202100252) in accordance with guidelines established by the National Institutes of Health. Six- to 8-wk-old C57BL/6 mice (cat. #000664) were procured from the Jackson Laboratory (Bar Harbor, ME) and were given freely accessible food and water. Animal facilities were maintained with a 12 h

light/dark cycle at consistent temperature (21-24 °C) and humidity (40-55%). Mice were bred for FLAM isolation as previously described [34, 497]. At 14-18 gestational days, pregnant dams (8-10 wk of age) were euthanized by CO₂ asphyxiation for 10 min to ensure death to the neonatal mice (14-18 gestational days), which are resistant to anoxia. As secondary measures of euthanasia, cervical dislocation was performed on the dam and blood supply was cut off to the fetuses. Upon removing the fetuses from the dam, fetal livers were carefully removed and dissociated in ice-cold DPBS. (DPBS without calcium and magnesium) by gentle pipetting. Liver cells were resuspended in complete FLAM medium (RPMI 1640 medium, 10% fetal bovine serum, 1% penicillin-streptomycin [pen-strep], 30 ng/ml recombinant mouse GM-CSF, and 20 ng/ml recombinant human TGF-β1, seeded in 100 mm tissue-culture treated dishes, and incubated at 37 °C and 5% CO₂. Medium was changed every 1-2 d. Cells were lifted with DPBS. containing 10 mM EDTA and gentle scraping upon reaching 70-90% confluency. After 1-2 wk of culture, the adherent cells developed a round morphology resemblant of AMs and were frozen for future use. Cells between passage 5 and 10 were used for this study.

Study 1: Experimental design

For phospholipid fatty acid analyses (Study 1, **Figure 4.1A**), FLAMs were seeded in 6-well plates at a density of 4.50×10⁵ cells/well in complete FLAM medium. Cells were incubated overnight to achieve 70-90% confluency before beginning treatments. The next day, cells washed once with sterile DPBS^{-/-}, fresh complete FLAM medium containing either 1) ethanolic DHA (25 μM) or ethanol (EtOH) VEH, or 2) 25 μM DHA complexed to BSA at a 3:1 ratio (described in [430, 432]) or 8.33 μM BSA VEH, then incubated for 24 h.

Study 1: Measurement of phospholipid fatty acid content in FLAMs treated with ethanolic DHA or DHA-BSA complexes

Comparative phospholipid fatty acid analyses were first conducted on FLAMs incubated for 24 h with DHA as either an ethanolic suspension or as BSA complexes. Following treatments, FLAMs were pelleted and stored in 100% methanol at -80 °C before total fatty acids were measured by OmegaQuant Inc. using gas chromatography (GC) with flame ionization detection as previously described [431]. Pelleted FLAMs were transferred to screw-cap glass vials and dried using a vacuum concentrator. Methanol containing boron trifluoride (14% [v/v]) was added to each vial, and then all vials were vortexed briefly and incubated at 100 °C for 10 min. After allowing the vials to cool, HPLC-grade water and hexane (EMD Chemicals, USA) were sequentially added, and phase separation was expedited by recapping, vortexing, and centrifuging the vials. Fractions from the hexane layer were transferred to separate GC vials for GC analysis using a GC2010 Gas Chromatograph (Shimadzu Corporation, Columbia, MD) outfitted with a SP2560, 100-m fused silica capillary column (0.25 mm internal diameter, 0.2 µm film thickness; Supelco, Bellefonte, PA).

A standard mixture of fatty acids (GLC OQ-A; NuChek Prep, Elysian, MN) was used to generate calibration curves for individual fatty acids and identify fatty acids present in each sample. The following 24 fatty acids were identified (by class): i) saturated (14:0, 16:0, 18:0, 20:0, 22:0, 24:0), ii) cis monounsaturated (16:1, 18:1, 20:1, 24:1), iii) cis ω-6 polyunsaturated (18:2ω6, 18:3ω6, 20:2ω6, 20:3ω6, 20:4ω6, 22:4ω6, 22:5ω6), and iv) cis ω-3 polyunsaturated (18:3ω3, 20:5ω3, 22:5ω3, 22:6ω3). Proportions of individual fatty acids in each sample were expressed as percent of total identified fatty acids. Percent ω-3 PUFAs and highly unsaturated fatty acid (HUFA) score were calculated as previously described [344] using the following equations, with

total fatty acids (FA) equaling the sum of all analyzed FA and total HUFA equaling the sum of 20:3ω6, 20:4ω6, 20:5ω3, 22:5ω6, 22:5ω3, and 22:6ω3:

Percent
$$\omega - 3$$
 PUFAs $= \frac{EPA + DHA}{Total\ FA} \times 100\%$
 $\omega - 3\ HUFA\ score = \frac{EPA + DPA_{\omega-3} + DHA}{Total\ HUFA} \times 100\%$

Study 2: Experimental design

For live-cell microscopic assessment of lysosomal membrane permeabilization, mitochondrial depolarization, and cell death (Study 2, Figure 4.1B), FLAMs were seeded in 48well plates 0.625×10^5 cells/well in complete FLAM medium to achieve 50% confluency after overnight incubation. The next day, cells were washed once with sterile DPBS^{-/-} then treated with either 25 µM ethanolic DHA or EtOH VEH as a control in complete FLAM medium. After 24 h, cells were washed once with sterile DPBS^{-/-} and primed with 20 ng/ml LPS or PBS VEH for 1.5 h. Following LPS priming, cells were washed with sterile DPBS^{+/+} then subsequently incubated for 30 min at 37 °C in the dark with 50 nM LysoTracker Red DND-99 in DPBS+/+ to label lysosomes, 25 nM MitoTracker Red CMXRos to label mitochondria, or 200 nM SYTOX Green to detect cell death. All fluorescent dyes were diluted in DPBS^{+/+} prior to addition to the cells, and 20 ng/ml LPS was simultaneously added to appropriate wells to allow 2 h of total LPS priming prior to cSiO₂ treatment. After 30 min of cell staining, cSiO₂ was added dropwise to a final concentration of 0 or 12.5 $\mu g/cm^2$. LPS and cSiO₂ exposures were done in DPBS^{+/+} to maintain consistent experimental conditions between oxylipin analyses and other analyses conducted in this study.

Study 2: Assessment of lysosomal membrane permeabilization, mitochondrial toxicity, and cell death by fluorescence microscopy

Live-cell fluorescence microscopy began immediately after adding cSiO₂ to the cells. Images of live cells were taken at 2, 3.5, and 6 h using an EVOS FL Auto 2 Cell Imaging System (ThermoFisher Scientific) with an onstage, temperature-controlled incubator (**Figure 4.1B**). For each well, 2-4 images were acquired using fields of view defined before the beginning of the experiment. LysoTracker Red and MitoTracker Red were detected using the Texas Red light cube (Ex: 585/29 nm, Em: 628/32 nm), and SYTOX Green was detected using the GFP light cube (Ex: 482/25 nm, Em: 524/24 nm).

Acquired images were analyzed for lysosomal integrity, mitochondrial integrity, and cell death using CellProfiler 4.2.1 as previously described [34, 498]. Briefly, lysosomal integrity, mitochondrial integrity, and cell death were assessed by quantifying the number of LysoTracker Red⁺, MitoTracker Red⁺, and SYTOX Green⁺ cells, respectively. LysoTracker Red⁺ and MitoTracker Red⁺ puncta were omitted if fluorescent intensity fell below preset minimum thresholds, which were chosen to omit false positives quantified from background fluorescence. Raw counts of LysoTracker Red⁺, MitoTracker Red⁺, and SYTOX Green⁺ cells were exported as .csv files and further analyzed using RStudio 2022.07.1+554 (Posit, Boston, MA).

Study 3: Experimental design

To probe the effects of LPS, cSiO₂, and DHA on release of lysosomal cathepsins, LDH, and proinflammatory cytokines (Study 3, **Figure 4.1C**), FLAMs were seeded in 24-well plates at a density of 1.50×10⁵ cells/well in complete FLAM medium. For lipidomics analyses (Study 3, **Figure 4.1C**), FLAMs were seeded in 6-well plates at a density of 4.50×10⁵ cells/well in complete FLAM medium. Cells were incubated overnight to achieve 70-90% confluency before beginning

treatments. The next day, cells washed once with sterile DPBS^{-/-}, fresh complete FLAM medium containing either 25 μM ethanolic DHA or EtOH VEH added, then cells incubated for 24 h. Following DHA or VEH treatment, cells were washed once with sterile DPBS^{-/-}, treated with either 20 ng/ml LPS in DPBS^{-/-} or DPBS^{-/-} VEH in DPBS^{+/+} (DPBS containing calcium and magnesium) for 2 h, then exposed to 12.5 μg/cm² cSiO₂ or DPBS^{-/-} VEH for 1.5 or 4 h. Cell culture supernatants were collected after cSiO₂ exposure and analyzed for proinflammatory cytokine secretion by ELISA, cathepsin activity by fluorescent assay, and cell death by lactate dehydrogenase (LDH) assay. For lipidomics analyses, cell culture supernatants and cells were pooled together prior to analysis. LPS and cSiO₂ exposures were done in DPBS^{+/+} to minimize interference from fatty acids present in cell culture medium during oxylipin analyses, and to maintain consistent experimental conditions between oxylipin analyses and other analyses conducted in this study.

Study 3: Cathepsin activity assay

Cathepsin B activity was determined as previously described [499]. Briefly, 50 µl of cell culture supernatant and 2 µg Z-LR-AMC were combined in 96-well plates and adjusted to a final volume of 150 µl/well, then all samples were incubated for 1 h at 37 °C. Sample fluorescence was then measured using a FilterMax F3 Multimode plate reader (Molecular Devices, San Jose, CA) set to 380 nm excitation and 460 nm emission. Cathepsin B activity in each well was calculated in units of relative fluorescence units (RFU) by the following equation:

$$RFU_{sample} - RFU_{sample\ blank} = cathepsin\ B\ activity$$

Study 3: Lactate dehydrogenase assay

Lactate dehydrogenase (LDH) activity in the supernatants of treated FLAMs was measured to assess the impacts of DHA, lipid metabolites, and inhibitors on cSiO₂-induced cell death as previously described [430, 432]. Briefly, FLAMs were incubated with 25 µM DHA or EtOH VEH

for 24 h, followed by priming with 0 or 20 ng/ml LPS for 2 h and subsequent exposure to 0 or 12.5 μg/cm² cSiO₂ for 1.5 or 4 h. Separate wells were designated as max-kill (MK) samples and incubated with 0.2% Triton-X (Millipore Sigma) for 5 min. After all treatments, supernatants were collected from all wells and 50 μl was transferred to non-treated, flat-bottom 96-well plates in duplicate. Complete medium (RPMI 1640 containing 10% FBS, 1% pen-strep, 30 ng/ml GM-CSF, 20 ng/ml TGF-β) was used as a sample blank, and complete medium containing 0.2% Triton-X was used as a MK blank. 100 μl of LDH assay reagent (15 μM 1-methoxyphenazine methosulfate [PMS], 2 mM iodonitrotetrazolium [INT], 3.2 mM β-nicotinamide adenine dinucleotide [NAD] sodium salt, and 160 mM lithium lactate in 0.2 M Tris-HCl, pH 8.2) was added to each well, and assay plates were incubated at room temperature for 15 min in the dark. Sample absorbance was then measured using a FilterMax F3 Multimode plate reader (Molecular Devices, San Jose, CA) set to a wavelength of 492 nm. Percent cell death in each well was calculated by the following equation:

$$\frac{Sample_{abs} - Sample \; Blank_{abs}}{Max \; Kill_{abs} - Max \; Kill \; Blank_{abs}} \times 100\% = Percent \; Cell \; Death$$

Study 3: Cytokine ELISAs

Concentrations of proinflammatory cytokines (i.e., IL-1 α , IL-1 β , TNF- α) were quantified by enzyme-linked immunosorbent assay (ELISA) using corresponding mouse DuoSet kits according to the manufacturer's instructions.

Study 3: Measurement of intracellular and extracellular oxylipins

Sample preparation

Following treatments, ice-cold methanol was added to each well, resulting in a final sample volume of 3 ml (1 ml cell culture supernatant + 2 ml methanol). To each sample, 60 µl of antioxidant cocktail (0.2 mg/ml butylated hydroxytoluene, 0.2 mg/ml triphenylphosphine, 0.6

mg/ml EDTA) was added to achieve a total cocktail concentration of 5% (v/v) [414]. Cells and supernatants within each well were pooled together, then samples were frozen at -80 °C until liquid chromatography-mass spectrometry (LC-MS) analysis.

Liquid chromatography-mass spectrometry (LC-MS) analysis

Targeted LC-MS lipidomics for 156 lipid metabolites was conducted at the Lipidomics Core Facility at Wayne State University as previously described [500-502]. Briefly, 100 μl aliquots of cellular samples were thawed and spiked with a cocktail of deuterated internal standards (5 ng each of PGE₁-d₄, RvD2-d₅, LTB₄-d₄, and 15[S]-HETE-d₈; Cayman Chemical, Ann Arbor, MI) for quantification of oxylipins and recovery. Then, fatty acyl lipid metabolites were extracted by using C18 extraction columns that were washed with 15% (v/v) methanol and subsequently hexane, dried in a vacuum, eluted with methanol containing 0.1% (v/v) formic acid, dried under nitrogen gas, and dissolved in a 1:1 mixture of methanol:25 mM aqueous ammonium acetate. Extracted fatty acyl metabolites were subjected to high-performance liquid chromatography (HPLC) using a Luna C18 (3 μm, 2.1×150 mm) column connected to a Prominence XR system (Shimadzu, Somerset, NJ) then analyzed with a QTrap5500 mass spectrometer (AB Sciex, Singapore) set to negative ion mode. Analyst 1.6 software (AB Sciex) and MultiQuant software (AB Sciex) were used to collect and quantify the data in units of ng, respectively. Lipid metabolites classifications are provided in **Table S4.2**.

Data analysis and statistics

Oxylipin data

For oxylipin data, MetaboAnalyst Version 5.0 (Xia Lab, Quebec, Canada, www.metaboanalyst.ca/) [503] was used to conduct statistical analyses. First, raw ng values were converted to corresponding pmol values using Microsoft Excel. Then, in MetaboAnalyst, the one

factor statistical analysis module was chosen, and data were uploaded as a comma separated values (.csv) file with samples in unpaired columns and features (i.e., metabolites) in rows. Features with >70% missing data were removed from the dataset, and remaining missing values were estimated by replacing with the corresponding limits of detection (LODs; 1/5 of the minimum positive value of each variable). After the data was cleaned, the data was normalized by auto scaling only, then the data editor option was used to select experimental groups of interest to compare. For comparisons between experimental groups, one-way analysis of variance (ANOVA) (FDR = 0.05) followed by Tukey's honestly significant difference (HSD) post-hoc test was used, with FDR q <0.05 considered statistically significant.

Other endpoints

For all other endpoints, GraphPad Prism Version 9 (GraphPad Software, San Diego, CA, www.graphpad.com) was used to conduct statistical analyses. The ROUT outlier test (Q = 1%) and the Shapiro-Wilk test (p<0.01) were used to identify outliers and assess normality in the data, respectively. For comparisons between two experimental groups, non-normal and semiquantitative data were analyzed by the Mann-Whitney nonparametric test. The F test was (p<0.05) used to test the assumption of equal variances across both groups. Normal data with unequal variances were analyzed using an unpaired t test with Welch's correction. Normal data that met the assumption of equal variance were analyzed using an unpaired t test. For comparisons between more than two experimental groups, non-normal and semi-quantitative data were analyzed by the Kruskal-Wallis nonparametric test followed by Dunn's post-hoc test. The Brown-Forsythe test (p<0.01) was used to test the assumption of equal variances across treatment groups. Normal data with unequal variances were analyzed using the Brown-Forsythe/Welch analysis of variance (ANOVA) followed by Dunnett's T3 post-hoc test. Normal data that met the assumption of equal variance

were analyzed by standard one-way ANOVA followed by Tukey's post-hoc test. Data are presented as mean \pm standard error of the mean (SEM), with a p-value \leq 0.05 considered statistically significant.

RESULTS

Study 1: DHA displaces the ω -9 monounsaturated fatty acid oleic acid and the ω -6 monounsaturated fatty acid arachidonic acid from membrane phospholipids in FLAMs

Two major methods for introducing ω -3 PUFAs to cell cultures—as ethanolic suspensions and as BSA complexes—were compared for addition in DHA to FLAMs using GLC. Ethanolic DHA-treated FLAMs had significantly greater DHA content (19.3% total fatty acids) compared to EtOH VEH-treated FLAMs (4.4% total fatty acids) (Figure 4.2A). Corresponding with these findings, content of the ω-9 monounsaturated fatty acid (MUFA) oleic acid (OA) and the ω-6 PUFA arachidonic acid (ARA) was significantly decreased in DHA-treated FLAMs (16.5% and 7.2% total fatty acids, respectively) compared to VEH-treated FLAMs (26.5% and 10.6% total fatty acids, respectively) (Figure 4.2A). No notable changes were found for other saturated and unsaturated fatty acids that were analyzed. FLAMs incubated with DHA-BSA complexes or BSA VEH displayed similar DHA membrane incorporation at the expense of OA and ARA (Figure 2B) to that seen for ethanolic DHA (Figures 4.2A, B). Total fatty acid findings were related to percent ω-3 fatty acids, which is the sum of eicosapentaenoic acid (EPA) and DHA as a percentage of all measured FA, and the ω -3 HUFA score, which equals the sum of ω -3 HUFAs (i.e., EPA, ω -3 DPA, and DHA) as a percentage of all measured ω -3/6 HUFAs (i.e., 20:3 ω 6, 20:4 ω 6, 20:5 ω 3, 22:5 ω 6, 22:5ω3, and 22:6ω3). In FLAMs treated with ethanolic DHA, percent ω-3 fatty acids was 22%, while VEH-treated FLAMs exhibited a score of 6% (Figure 4.2C). FLAMs treated with ethanolic DHA also demonstrated a comparatively higher ω-3 HUFA score (74%) compared to VEH-treated

FLAMs (41%) (**Figure 4.2C**). Similarly, FLAMs treated with DHA-BSA complexes exhibited significant increases in percent ω -3 fatty acids (18%) and ω -3 HUFA score (75%) compared to VEH-treated cells (5% and 41%, respectively) (**Figure 4.2D**). Because of its relative simplicity, ethanolic DHA delivery was used for all subsequent experiments.

Study 2: DHA does not suppress cSiO₂-induced lysosomal membrane permeabilization, mitochondrial toxicity, and death in FLAMs

Live-cell imaging using LysoTracker Red (LTR), MitoTracker Red (MTR), and SYTOX Green (SG) was employed to further assess the impacts of DHA on cSiO₂-induced lysosomal membrane permeabilization (LMP), mitochondrial depolarization, and cell death, respectively. In a preliminary experiment, we found that LPS priming slightly expedited cSiO₂-induced loss of LTR⁺ cells (**Figures S4.1A, S4.1D**). LPS did not significantly impact cSiO₂-induced development of SG⁺ cells (**Figures S4.1C**, **S4.1F**). Intriguingly, LPS priming perpetuated cSiO₂-triggered loss of MTR⁺ cells (**Figures S4.1B, S4.1E**). At 2 h, approximately 100% of VEH- and LPS-treated cells were LTR⁺, approximately 100% were MTR⁺, and nearly 0% were SG⁺ (**Figures S4.1D-F**). For simplicity in follow-up assays, we evaluated the impacts of DHA on FLAMs exposed to cSiO₂ alone (Figure 4.3). Similar to our preliminary study, we found that the proportions of LTR⁺ cells (Figures 4.3A, D), MTR⁺ cells (Figures 4.3B, E), and SG⁺ cells (Figures 4.3C, F) at 2 h were nearly 100%, 100%, and 0%, respectively. LMP occurred at very similar rates from 2-6 h in VEHand DHA-treated cells exposed to cSiO₂ (Figures 4.3A, D). Mitochondrial depolarization progressed at approximately the same rate in VEH- and DHA-treated FLAMs from 2-3.5 h, and DHA slightly protected FLAMs from further mitochondrial depolarization from 3.5-6 h (Figures **4.3B, E**). Minimal cell death was observed from 2-3.5 h for both VEH- and DHA-treated cells, and DHA slightly, albeit insignificantly, suppressed cell death from 3.5-6 h (**Figures 4.3C, F**).

Study 3: DHA does not suppress cSiO₂-induced cathepsin and LDH release in FLAMs

To test the potential protective effects of DHA against cSiO₂-induced toxic responses, we pretreated FLAMs with DHA or VEH prior to exposure with cSiO₂ alone or LPS and cSiO₂, then measured lysosomal cathepsin activity and LDH release in collected supernatants (**Figures 4.4A**, **B**). Priming FLAMs with LPS before cSiO₂ exposure increased extracellular lysosomal cathepsin activity (**Figure 4A**) and LDH release (**Figure 4.4B**) at 3.5 h in both VEH- and DHA-treated FLAMs and did not significantly impact lysosomal cathepsin activity or LDH release at 6 h. Cathepsin activity in VEH-treated cells exposed to cSiO₂ alone was higher at 3.5 h (1.1×10⁷ MFI) than at 6 h (5.5×10⁶ MFI). Interestingly, DHA caused a moderate increase in cathepsin activity in FLAMs exposed to cSiO₂ alone or to both LPS and cSiO₂ at 3.5 h but not at 6 h. LDH release in VEH-treated FLAMs treated with cSiO₂ alone was higher at 6 h (9.9%) than at 3.5 h (0.4%). In line with cathepsin activity analyses, DHA caused a slight increase in LDH release in FLAMs exposed to cSiO₂ alone at 3.5 h and did not significantly impact LDH release at 6 h.

Study 3: DHA suppresses cSiO₂-induced release of proinflammatory cytokines from FLAMs

The impacts of DHA on $cSiO_2$ -induced cytokine release from FLAMs were evaluated at 3.5 h and 6 h. At both timepoints, cells treated with either VEH or $cSiO_2$ alone secreted negligible amounts of IL-1 α , IL-1 β , and TNF- α (**Figures 4.5A-C**). FLAMs that were primed with LPS prior to $cSiO_2$ exposure secreted robust amounts of IL-1 α , IL-1 β , and TNF- α both timepoints, with much higher cytokine levels observed at 6 h compared to 3.5 h. In FLAMs that were exposed to both LPS and $cSiO_2$, DHA significantly reduced release of IL-1 α , IL-1 β , and TNF- α release at both timepoints. No notable DHA effects on proinflammatory cytokine release were evident in FLAMs treated with VEH or $cSiO_2$ alone.

Study 3: LPS, $cSiO_2$, and DHA differentially impact production of ω -6 ARA-derived oxylipins and ω -3 DHA-/EPA-derived oxylipins in FLAMs

The combined intracellular and extracellular lipidome was analyzed in VEH- and DHAtreated FLAMs following exposure to LPS and/or cSiO₂. Heat mapping showed that cSiO₂ triggered production of a broad group of ARA-derived oxylipins in VEH-treated FLAMs and DHA-/EPA-derived oxylipins in DHA-treated FLAMs (Figure 4.6A). These broad oxylipin shifts were first observed at 3.5 h with further progression observed at 6 h. The most significantly induced ARA-derived oxylipins included PGE2, TXB2, and several HETE regioisomers, whereas the most significantly induced DHA-/EPA-derived oxylipins included HDoHE and HEPE regioisomers, respectively. DHA supplementation broadly suppressed cSiO₂-induced production of ARA-derived oxylipins at 3.5 h and 6 h and established a higher baseline level of DHA-/EPAderived oxylipins at 2 h. Oxylipins derived from linoleic acid (LA, C18:2ω6) and dihomo-γlinolenic acid (DGLA, C20:3ω6) were also induced by cSiO₂ and suppressed by DHA, while DHA-derived resolvins and maresins were minimally produced during the time-course. In VEHtreated cells, LPS modestly augmented cSiO₂-induced production of ARA-derived oxylipins at 3.5 h and 6 h while slightly dampening cSiO₂-induced production of DHA-/EPA-derived oxylipins. No notable shifts in the lipidome were observed in VEH-treated control FLAMs (i.e., cells not exposed to LPS and/or cSiO₂) for the entirety of the time-course.

Study 3: DHA suppresses levels of total ARA-derived oxylipins and increases levels of total DHAand EPA-derived oxylipins in FLAMs

For follow-up analyses, summarized oxylipin quantities (**Tables 4.1-4.3**) and individual oxylipin quantities (**Tables S4.3-S4.5**) were compared between experimental groups at each designated timepoint. Because oxylipin profile shifts were more pronounced at 3.5 h and 6 h with

cSiO₂ exposure than at 2 h with LPS priming alone (**Figure 4.6A**, **Table 4.1**), we focused our analysis on the 3.5 h and 6 h timepoints. In line with heat mapping, cSiO₂ elevated total levels of ARA-derived oxylipins and DHA-/EPA-derived oxylipins produced from VEH- and DHA-treated FLAMs, respectively (**Figure 4.6B**, **Table 4.2**). In DHA-treated FLAMs, cSiO₂-induced levels of ARA-derived metabolites were significantly decreased, and, correspondingly, cSiO₂-induced levels of DHA-/EPA-derived oxylipins were significantly elevated (**Figure 4.6B**, **Table 4.2**). cSiO₂-induced levels of EPA-derived oxylipins also increased in VEH-treated FLAMs (**Figure 4.6B**, **Table 4.2**). LPS priming elicited a marked increase in cSiO₂-triggered ARA-derived metabolite production in VEH-treated FLAMs and a marked decrease in cSiO₂-triggered EPA-derived metabolite levels in DHA-treated FLAMs (**Figure 4.6B**, **Table 4.2**). Findings at 6 h reflected those found at 3.5 h with higher overall quantities of ARA-, EPA-, and DHA-derived metabolites (**Figure 4.6B**, **Table 4.3**).

<u>Study 3: DHA suppresses cSiO₂-induced production of ARA-derived prostaglandins, leukotrienes,</u> and thromboxanes in FLAMs

At 3.5 h and 6 h, cSiO₂ induced robust increases in total prostaglandins (**Figure 4.7A**), leukotrienes (**Figure 4.8A**), and thromboxanes (**Figure 4.9A**) compared to VEH-treated FLAMs (**Tables 4.2, 4.3**). Levels of PGE2 (**Figure 4.7B**), LTB4 (**Figure 4.8B**), and TXB2 (**Figure 4.9B**), three representative oxylipins from each metabolite class, increased in like manner in the presence of cSiO₂ (**Tables S4.4, S4.5**). Interestingly, LPS priming augmented cSiO₂-triggered production of total prostaglandins, leukotrienes, and thromboxanes, in addition to PGE2, LTB4, and TXB2. DHA significantly reduced cSiO₂-induced prostaglandin, leukotriene, and thromboxane production, yet induction of these metabolites was still significant compared to baseline levels in

DHA-treated FLAMs. LPS priming did not significantly impact cSiO₂-induced levels of prostaglandins, leukotrienes, and thromboxanes in DHA-treated FLAMs.

Study 3: DHA broadly skews $cSiO_2$ -induced hydroxy fatty acids from being ω -6 PUFA-derived to being ω -3 PUFA-derived

Total hydroxy fatty acid (HFA) metabolites were significantly increased by cSiO₂ exposure in both VEH-treated and DHA-treated FLAMs at 3.5 h and 6 h (Figure 4.10; Tables 4.2, 4.3). Additional analyses revealed that DHA supplementation significantly reduced levels of ω-6 HFAs and significantly increased levels of ω -3 HFAs at both timepoints. The suppressive effect of DHA on ω-6 HFA levels was more poignant at 3.5 h than at 6 h, while ω-3 HFA levels steadily increased in DHA-treated FLAMs over time. LPS priming further increased levels of cSiO₂-induced ω-6 HFAs at 3.5 h and decreased levels of cSiO₂-induced ω-3 HFAs at 6 h. Observed changes in ARAderived HFAs reflected those in total ω-6 HFAs: cSiO₂ triggered significant increases in ARAderived HFA levels in both VEH-treated and DHA-treated FLAMs, DHA significantly reduced metabolite levels, and LPS priming further potentiated cSiO₂-induced metabolite production at 3.5 h and 6 h (Figure 4.11A; Tables 4.2, 4.3). Likewise, DHA- and EPA-derived HFA levels reflected total levels of ω-3 HFAs, as DHA- and EPA-derived HFA levels significantly increased in DHAtreated cells exposed to cSiO₂ starting at 3.5 h and continuing at 6 h (Figures 4.12A, 4.13A; Tables 4.2, 4.3). In both VEH-treated FLAMs and DHA-treated FLAMs, quantities of ARA-, EPA-, and DHA-derived HFAs were ranked as follows for both timepoints: ARA > DHA > EPA. Furthermore, ARA-derived HFAs accounted for the majority of total measured ω-6 HFAs, whereas EPA and DHA both accounted for the majority of total measured ω -3 HFAs.

<u>Study 3: DHA suppresses cSiO₂-induced production of ARA-derived HETEs and induces</u> production of EPA-derived HEPEs and DHA-derived HDoHEs

cSiO₂ triggered significant production of ARA-derived 5-HETE, 8-HETE, 9-HETE, 11-HETE, 12-HETE, and 15-HETE in VEH-treated FLAMs at 3.5 h and 6 h (**Figure 4.11B**; **Tables S4.4**, **S4.5**). HETE levels also increased in DHA-treated FLAMs exposed to cSiO₂ but were found to be significant only for 5-HETE, 8-HETE, and 9-HETE at 6 h and 15-HETE at both timepoints. In line with total ARA-derived HFA levels, DHA significantly suppressed 8-HETE at 6 h and 9-HETE at both timepoints. Levels of other cSiO₂-induced HETEs (e.g., 5-HETE, 11-HETE, 12-HETE, 15-HETE) also were reduced in DHA-treated FLAMs, but the findings were not statistically significant. LPS priming elicited a significant increase in cSiO₂-induced 8-HETE and a non-significant increase in 5-HETE in VEH-treated FLAMs at both timepoints.

In DHA-treated FLAMs, cSiO₂ induced significant increases in several DHA-derived HDoHEs (i.e., 4-HDoHE, 7-HDoHE, 8-HDoHE, 10-HDoHE, 11-HDoHE, 14-HDoHE, 16-HDoHE, 17-HDoHE, 20-HDoHE) and in several EPA-derived HEPEs (i.e., 5-HEPE, 8-HEPE, 9-HEPE, 11-HEPE, 12-HEPE, 15[S]-HEPE) at both timepoints (**Figures 4.12B, 4.13B**; **Tables S4.4**, **S4.5**). While cSiO₂ exposure led to significant increases in EPA-derived 5-HEPE, 11-HEPE, and 12-HEPE in VEH-treated cells during the time-course, DHA-derived HDoHEs did not undergo significant increases in VEH-treated cells exposed to cSiO₂. The effects of LPS priming on cSiO₂-induced HEPEs and HDoHEs were minimal, with only marked decreases in 8-HEPE and 12-HEPE at 3.5 h observed.

Quantities of selected cSiO₂-induced HETEs were found to be highest, followed by selected cSiO₂-induced HDoHEs and selected cSiO₂-induced HEPEs. Relative abundance of selected HETEs was: 5-HETE > 11-HETE > 15-HETE > 8-HETE > 12-HETE > 9-HETE. Relative

abundance of selected HEPEs was: $5\text{-HEPE} > 8\text{-HEPE} \approx 11\text{-HEPE} > 15(S)\text{-HEPE} > 12\text{-HEPE} > 9\text{-HEPE}$. Relative abundance of selected HDoHEs was: $4\text{-HDoHE} \approx 20\text{-HDoHE} > 16\text{-HDoHE} > 7\text{-HDoHE} \approx 8\text{-HDoHE} \approx 10\text{-HDoHE} \approx 11\text{-HDoHE} > 14\text{-HDoHE} > 17\text{-HDoHE}$.

Study 3: DHA modestly influences production of the specialized pro-resolving lipid mediators (SPMs) RvD6 (4,17-DiHDoPE) and MaR1_{@-3 DPA} in FLAMs

Specialized pro-resolving mediators (SPMs) are a class of oxylipins comprised of resolvins, maresins, protectins, and lipoxins derived from ARA, EPA, ω-3 DPA, and DHA that limit proinflammatory cytokine release and promote dead cell clearance by macrophages [504]. Most SPMs assessed in our LC-MS oxylipin panel were not detected at any timepoint (**Tables S4.3-S4.5**). On the other hand, DHA supplementation caused a modest increase in RvD6 (4,17-DiHDoPE) and MaR1_{ω-3 DPA} at 3.5 h and 6 h (**Figure 4.14**; **Tables S4.4**, **S4.5**). In DHA-treated FLAMs, cSiO₂ exposure did not significantly influence production of RvD6 at either timepoint (**Figure 4.14A**) but significantly increased MaR1_{ω-3 DPA} at 3.5 h and decreased MaR1_{ω-3 DPA} at 6 h (**Figure 4.14B**). LPS priming significantly suppressed MaR1_{ω-3 DPA} production in DHA-treated FLAMs at 6 h, modestly inhibited MaR1_{ω-3 DPA} at 3.5 h, and modestly decreased RvD6 production at both 3.5 h and 6 h.

Study 3: DHA modestly influences production of EpFAs and DiHFAs in cSiO₂-exposed FLAMs

Total epoxy fatty acids (EpFAs) and CYP450-derived dihydroxy fatty acids (DiHFAs) were quantified from VEH-treated and DHA-treated FLAMs (**Figure 4.15A**; **Tables 4.2, 4.3**). In VEH-treated FLAMs, cSiO₂ modestly induced production of EpFA metabolites at 3.5 h and 6 h and did not significantly impact production of DiHFA metabolites. Conversely, cSiO₂ triggered significant increases in total EpFAs and DiHFAs in DHA-treated FLAMs at both timepoints. Interestingly, LPS priming significantly reduced total DiHFA metabolite levels in the absence of

cSiO₂ in DHA-treated FLAMs. Separate and simultaneous LPS priming and cSiO₂ exposure elicited modest increases in EpFA:DiHFA ratios in both VEH-treated and DHA-treated FLAMs during the time-course.

Effects of cSiO₂ and DHA were also analyzed for selected CYP450 oxylipin products of ARA (i.e., 14,15-EpETrE, 14,15-DiHETrE) and DHA (i.e., 19,20-EpDPE, 19,20-DiHDoPE) (Figure 4.15B; Tables S4.4, S4.5). cSiO₂ evoked production of 14,15-EpETrE and 14,15-DiHETrE starting at 3.5 h and continuing through 6 h in VEH-treated FLAMs and, to a lesser degree, in DHA-treated FLAMs. LPS priming also modestly increased cSiO₂-triggered production of 14,15-EpETrE in VEH-treated FLAMs. Changes in 14,15-EpETrE levels were not significant, and cSiO₂-induced production of 14,15-DiHETrE was significant only at 3.5 h. In contrast, DHA treatment promoted robust production of 19,20-EpDPE and 19,20-DiHDoPE at both timepoints. Exposure to cSiO₂ resulted in a subtle, yet non-significant, increase in 19,20-EpDPE and corresponding decrease in 19,20-DiHDoPE at both timepoints. Intriguingly, LPS priming alone significantly decreased levels of 19,20-EpDPE and 19,20-DiHDoPE during the experiment. Overall, levels of 19,20-EpDPE and 19,20-DiHDoPE were found to be higher than levels of 14,15-EpETrE and 14,15-DiHETrE.

DISCUSSION

AMs comprise the first line of defense against inhaled toxicants, including cSiO₂ [505]. Preclinical studies have demonstrated that cSiO₂ elicits robust inflammatory responses in AMs, serving as a foundation for development of downstream autoimmunity, and DHA suppresses cSiO₂-induced inflammatory and autoimmune responses [19, 430, 506]. However, the effects of cSiO₂ and DHA on bioactive oxylipin production in AMs are not clearly understood. To address this gap in knowledge, we utilized FLAMs, a novel, self-renewing AM model, to test the

hypothesis that DHA dampens $cSiO_2$ -induced toxicity and broadly skews the cellular lipidome from ω -6 PUFA metabolites in favor of ω -3 PUFA metabolites following $cSiO_2$ exposure. We made several notable findings during our investigation. First, administering DHA as either an ethanolic suspension or as BSA complexes were comparable in displacing the ω -9 PUFA OA and ω -6 PUFA ARA from cellular phospholipids in FLAMs, which resulted in increased percent ω -3 PUFAs and ω -3 HUFA score. Second, DHA suppresses $cSiO_2$ -triggered release of IL-1 α , IL-1 β , and TNF- α without impacting $cSiO_2$ -induced LMP, mitochondrial depolarization, or death in FLAMs. Third, $cSiO_2$ exposure elicits time-dependent production of proinflammatory oxylipins derived primarily from ARA, including PGE2, LTB4, TXB2, and HETEs. Fourth, LPS priming on its own does not significantly impact oxylipin production but modestly enhances the effects of $cSiO_2$ on ARA-derived oxylipin production. Fifth, supplementing FLAMs with DHA suppresses $cSiO_2$ -induced production of ARA-derived oxylipins. Finally, pre-incubation of FLAMs with DHA promoted production of DHA- and EPA-derived oxylipins, including HDoHEs and HEPEs, from FLAMs following $cSiO_2$ exposure.

The pro-resolving impacts of the ω -3 PUFA DHA are multifaceted. At the cellular level, DHA 1) modulates membrane fluidity by displacing ω -6 PUFAs from the sn-2 position of membrane phospholipids, 2) suppresses expression and release of proinflammatory cytokines, 3) compete with ω -6 PUFAs as substrates for fatty acid metabolizing enzymes, and 4) undergoes conversion into several classes of highly pro-resolving oxylipins (reviewed in [490-492]). In previously published studies, we have found in several macrophage models that DHA is readily incorporated into membrane phospholipids at the expense of ω -6 ARA and ω -9 OA, suppresses LPS-induced expression of proinflammatory genes and IFN-regulated genes, dampens cSiO₂-induced proinflammatory cytokine release, and stimulates efferocytosis of cSiO₂-killed cell

corpses [430-432]. We report here that DHA suppresses cSiO₂-triggered release of proinflammatory cytokines but does not protect against cSiO₂-induced LMP, mitochondrial toxicity, or cell death in FLAMs. The protective effects of DHA against lysosomal toxicity, mitochondrial toxicity, and cell death might be highly dependent on cellular phenotype [430, 432, 507-512]. DHA's lack of protection against cSiO₂-triggered LMP, mitochondrial depolarization, and cell death in FLAMs suggests that these processes are not involved in DHA-mediated lung protection. Nevertheless, they may be the vehicles by which cSiO₂ drives production of proresolving DHA-derived oxylipins in FLAMs, as DHA-derived HDoHE levels rose at similar rates to ARA-derived HETE levels following cSiO₂ exposure.

In the present study, we report for the first time in FLAMs that supplementation with DHA as an ethanolic suspension and as a BSA complex results in equivalent increases in phospholipid DHA content, displacement of ω -9 OA and ω -6 ARA from phospholipids, and elevation of percent phospholipid ω -3 fatty acids and the HUFA score. Our findings correspond with previously published data from Wiesenfeld and coworkers, who reported that delivery of DHA as ethanolic suspensions and BSA complexes resulted in roughly equal displacement of ARA by DHA in two different macrophage cell lines [513]. From a translational perspective, preclinical and clinical studies suggest that increased ω -3 PUFA intake—and consequently increased ω -3 fatty acid tissue content—are associated with decreased symptom severity in chronic inflammatory conditions such as rheumatoid arthritis [514, 515], lupus [344, 348], and cardiovascular disease [516, 517]. While we used a physiologically relevant DHA dose in the present study [518], the cell culture conditions do not completely reflect other dietary components that could influence AM inflammatory responses. For instance, the ω -6/ ω -3 ratio in the standard Western diet is approximately 20:1 [519], which may increase the risk of inflammatory ARA-derived oxylipin cascades [520]. It will

therefore be informative in future investigations to treat FLAMs with various ratios of ω -6 PUFAs (e.g., LA, ARA) and ω -3 PUFAs (e.g., EPA, DHA) prior to cSiO₂ exposure to more closely model dietary patterns in rodent and human studies.

Our investigation is the first to assess broad impacts of LPS, cSiO₂, and DHA on a comprehensive oxylipin profile consisting of 156 unique metabolites in a novel AM surrogate model. Although our lipid metabolite panel may not account for all oxylipin species present in FLAMs, we found here that cSiO₂ induced production of numerous bioactive oxylipins derived from ARA (e.g., PGE2, LTB4, TXB2, HETEs), EPA (e.g., HEPEs), and DHA (e.g., HDoHEs) in VEH-treated and DHA-treated FLAMs. Oxylipins derived from other less abundant ω-6 PUFAs (e.g., LA, DGLA) were also detected in our analysis, which may play roles in modulating cSiO₂triggered toxicity in FLAMs [521]. These results suggest that cSiO₂ may promote PLA2-mediated release of ω-6 PUFAs and ω-3 PUFAs from the sn-2 position of phospholipids in VEH-treated FLAMs and DHA-treated FLAMs, respectively [522], freeing these PUFAs for subsequent conversion into oxylipins inside the cell. A previously published study by Sager and coworkers suggests that cSiO₂ can induce expression of various PLA2 isozymes in the rat lungs [523], but the impacts of cSiO₂ on PLA2 expression and activity remain unresearched at large. Future studies involving genetic deletion or pharmacological inhibition of different PLA2 isozymes should be conducted to characterize the impacts of cSiO₂ on PLA2 expression and activity and to assess the importance of PLA2 in oxylipin production within FLAMs.

cSiO₂ exposure resulted in production of ARA-derived oxylipins that increased as time progressed, and LPS priming elicited further cSiO₂-induced production of ARA-derived PGE2, LTB4, and TXB2 accompanied by release of the proinflammatory cytokines IL-1α, IL-1β, and TNF-α. Previous studies have shown that priming macrophages with LPS contributes to

upregulation of fatty acid metabolizing enzymes such as COX and LOX isoforms and increased expression of proinflammatory cytokines [431, 524-529]. Accordingly, our observations suggest that LPS priming may upregulate expression of COX and LOX in FLAMs, contributing to heightened production of prostaglandins, leukotrienes, and thromboxanes after cSiO₂ exposure. Meanwhile, HFA levels were not significantly changed when FLAMs were subjected to LPS priming, which suggests that these oxylipins may be produced in our FLAM model as a result of non-enzymatic conversion following exposure to cSiO₂. It remains unclear whether LPS-stimulated proinflammatory cytokines (e.g., IL-1α, IL-1β, TNF-α) interact with their corresponding receptors (e.g., IL-1R, TNFR1) on neighboring FLAMs to stimulate production of ARA-derived oxylipins. Previous studies suggest that certain proinflammatory cytokines, including IL-1β and TNF-α, can induce production of PGE2 and TXB2 in various contexts [530-532]. Therefore, it would be informative in follow-up studies to either genetically knock out or pharmacologically inhibit proinflammatory cytokine receptors of interest to clarify the roles that cytokine-receptor signaling might play in influencing the cellular lipidome.

While numerous HFAs can be produced via the LOX or CYP450 enzymatic pathways (e.g., 5-HETE, 12-HETE, 15-HETE, 20-HETE, 5-HEPE, 12-HEPE, 15(S)-HEPE, 4(S)-HDoHE, 14(S)-HDoHE, 17(S)-HDoHE) [492, 533], HFAs can also be produced via non-enzymatic oxidation by reactive oxygen species (ROS) [534-536]. Here, cSiO₂ caused steady declines in lysosomal integrity and mitochondrial integrity that occurred at similar rates in VEH-treated and DHA-treated FLAMs and also corresponded with increasing HFA production. cSiO₂ uptake by macrophages has been previously demonstrated to increase ROS levels in the cytoplasm and phagolysosome, resulting in LMP [537]. Furthermore, mitochondrial depolarization has been shown to occur after cSiO₂-induced LMP [183], cSiO₂ exposure has been linked to increased

mitochondrial ROS production [538], and increased cytosolic ROS can trigger mitochondrial ROS production in neighboring mitochondria [539]. Although we did not directly measure production of total ROS or mitochondrial ROS in the present study, it is possible that cSiO₂-triggered HFA production in the FLAM is largely caused by non-enzymatic oxidation via ROS released from damaged lysosomes and mitochondria, as no subsets of HFAs were selectively produced in our oxylipin panel. Future follow-up studies should aim to quantify total ROS and mitochondrial ROS produced from cSiO₂-exposed FLAMs and utilize antioxidant agents (e.g., *N*-acetylcyteine, Trolox) to elucidate the impacts of ROS on the production of HFAs and the cellular lipidome as a whole.

It should be noted that we conducted our investigation using FLAMs from non-autoimmune C57BL/6 mice, which limits the translatability of the present study to other studies analyzing respirable cSiO₂ as an autoimmune trigger in genetically susceptible mice and humans. Previously, we have demonstrated in female autoimmune-prone NZBWF1 mice that dietary DHA administered at human caloric equivalents of 2 or 5 g/d dose-dependently reduces perivascular leukocyte infiltration and expression of proinflammatory proteins in the lung [19, 20, 351]. These changes correspond with increased levels of ω-3 PUFAs in erythrocytes and lungs; suppressed levels of cSiO₂-induced inflammatory proteins and autoantibodies in bronchoalveolar lavage fluid (BALF) and plasma; and delayed onset of resultant glomerulonephritis and proteinuria [344, 352, 433]. We chose to focus our investigation on C57BL/6-derived FLAMs first because we recently characterized this model from a functional perspective [34] and found that these cells are amenable to genetic modulation. This prompted us to assess whether this model was also amenable to lipidome modulation. Developing a baseline oxylipin profile for C57BL/6 FLAMs will aid us in future investigations comparing effects of LPS, cSiO₂, and DHA on the lipidome of FLAMs

derived from autoimmune-prone mice (e.g., female NZBWF1 mice). Future investigations should focus on assessing impacts of LPS, cSiO₂, and DHA not only on the lipidome of non-autoimmune FLAMs and autoimmune-prone FLAMs but also on the lipidome of primary AMs and whole lung homogenates from non-autoimmune mice and autoimmune-prone mice. Single-cell lipidomics, analogous to single-cell RNA sequencing [540], would especially be of interest for these follow-up studies.

A limitation of the present study is that although it demonstrated the broad early effects of LPS, cSiO₂, and DHA on the lipidome of a novel AM model, it may not be predictive of early and late changes in the lung lipidome as a whole. Another limitation of our investigation is that intracellular and extracellular oxylipin content was pooled for all LC-MS analyses, making it difficult to discern quantities of secreted oxylipins from quantities of non-secreted oxylipins. By conducting LC-MS on separated cell cultures and supernatants, we would be able to better understand not only how cSiO₂ impacts overall oxylipin production but also how cSiO₂ impacts oxylipin release from FLAMs. Accordingly, prostanoids, leukotrienes, HFAs, and other subclasses of oxylipins elicit biological activity through transmembrane G protein-coupled receptors (GPCRs) and intracellular receptors such as PPARy [541-545]. While receptor-mediated biological effects have been reported—and are still being investigated—for numerous individual oxylipins (Table S4.6), it remains possible that oxylipins also elicit biological activity as mixtures. To this end, it would be of interest to generate conditioned medium containing ARA-derived oxylipins and DHA-derived oxylipins from cSiO₂-exposed VEH-treated FLAMs and cSiO₂exposed DHA-treated FLAMs, respectively, and then measure paracrine effects of the oxylipin mixtures on cSiO₂-induced toxic responses in separate FLAM cultures. Furthermore, the time window should be extended in follow-up analyses to better understand the extent to which cSiO₂ and DHA impact lipid metabolite quantities, as several oxylipin classes (e.g., prostaglandins, leukotrienes, thromboxanes, HFAs) exhibited steady increases during the time-course while other oxylipin classes (e.g., resolvins, maresins) were mostly detected in negligible quantities during the time-course.

CONCLUSIONS

To summarize, the results of the present study suggest that cSiO₂ induces robust biosynthesis of ω-6 ARA-derived oxylipins and DHA supplementation broadly skews the cSiO₂triggered lipidome from ARA-derived oxylipins to ω-3 DHA-/EPA-derived oxylipins. The most upregulated oxylipins included ARA-derived PGE2, LTB4, TXB2, and HETEs; EPA-derived HEPEs; and DHA-derived HDoHEs, with less prominent changes in ω -3/6 EpFAs and DiHFAs. Shifts in the cellular lipidome following cSiO₂ exposure corresponded with release of proinflammatory cytokines (i.e., IL-1α, IL-1β, TNF-α), LMP, mitochondrial depolarization, and cell death. DHA supplementation suppressed release of proinflammatory cytokines but not LMP, mitochondrial toxicity, or cell death. LPS was required for proinflammatory cytokine release and modestly accelerated cSiO₂-induced LMP, mitochondrial depolarization, and ARA-derived oxylipin production (**Figure 4.16**). Together, these findings suggest that dietary ω -3 PUFAs may protect against cSiO₂-triggered lung inflammation by inhibiting biosynthesis of proinflammatory ω-6 oxylipins (e.g., PGE2, LTB4) and promoting biosynthesis of ω-3 oxylipins (e.g., HEPEs, HDoHEs) in lung AMs. Future investigations are necessary in order to characterize the lipidome in AMs and lungs from non-autoimmune and autoimmune-prone mice and relate oxylipin profiles to biomarkers of cSiO₂-induced toxicity.

DECLARATIONS

Competing Interests

The authors declare that the research was conducted in the absence of any commercial or financial relationships that could be construed as a potential conflict of interest.

Funding

This research was funded by NIH RO1ES027353 (JP), Lupus Foundation of America (JP), and Dr. Robert and Carol Deibel Family Endowment (JP).

Contributions

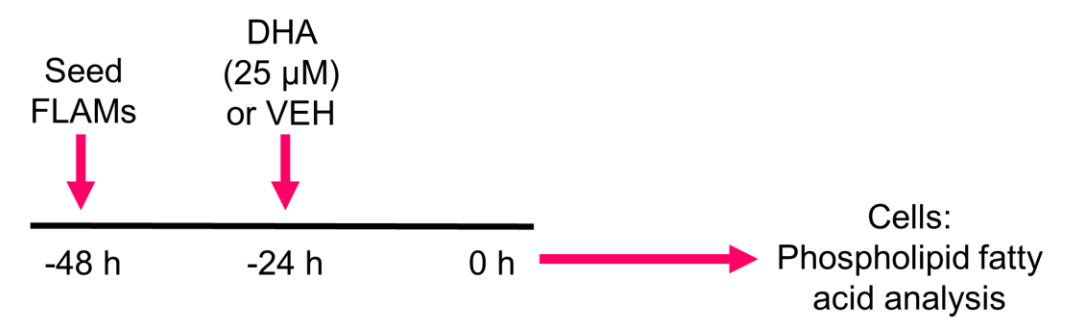
OF, KW, and LR: study design, data analyses/interpretation, figure preparation, and manuscript preparation. KM: LC-MS/MS sample analysis. KSSL: oversight, manuscript preparation. AO: development of experimental model. JP: planning, coordination, oversight, manuscript preparation/submission, and project funding. All authors contributed to the manuscript and approved the submitted version.

<u>Acknowledgments</u>

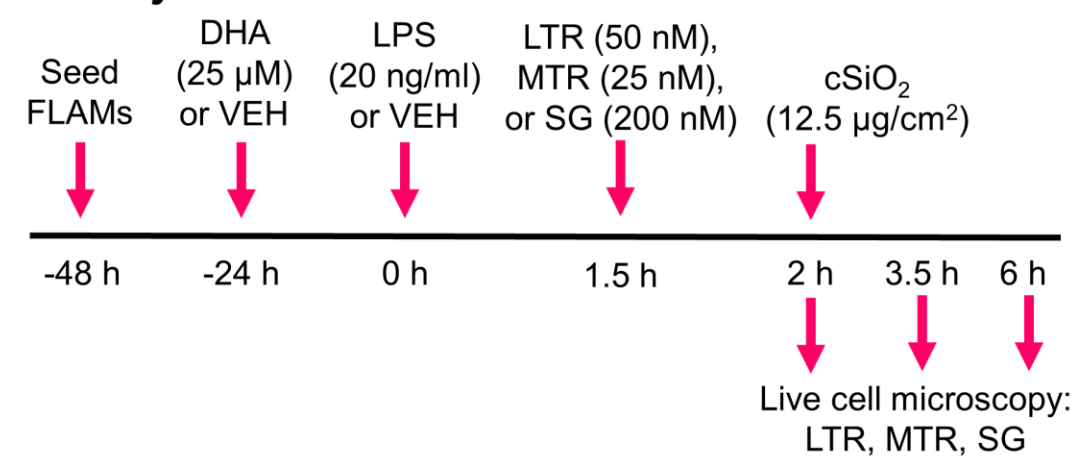
We would like to thank Adrianna Kirby at Michigan State University for her technical assistance with *in vitro* FLAM assays, the Lipidomics Core Facility at Wayne State University for their assistance with oxylipin and lipidomic analyses, and Dr. Charles Serhan at Harvard Medical School for providing experimental expertise on processing cellular samples for lipidomic analyses.

FIGURES

A. Study 1



B. Study 2



C. Study 3

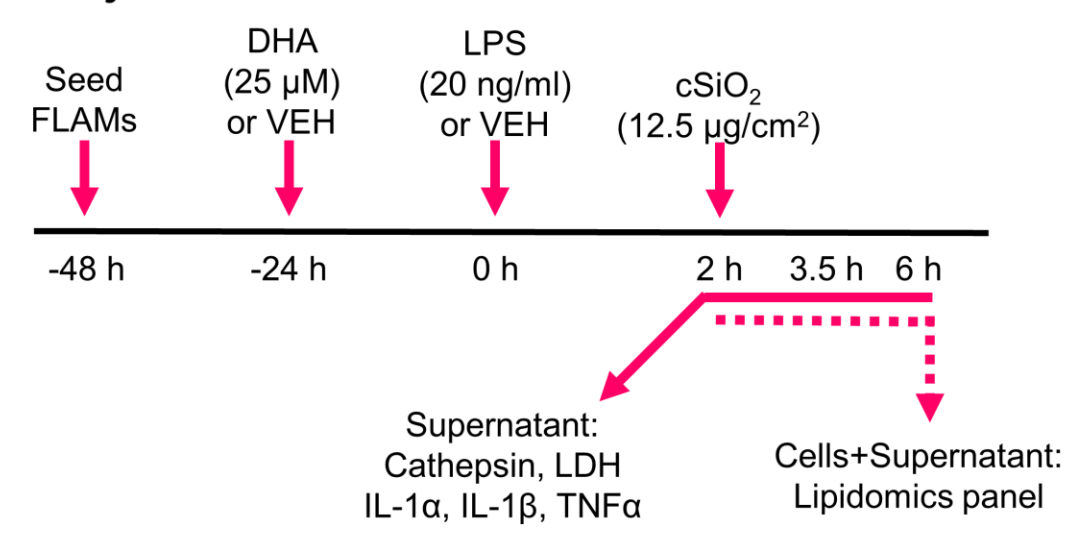


Figure 4.1. Summary of study designs. (A) In Study 1, FLAMs were treated with i) DHA as an ethanolic suspension or ethanol vehicle (VEH) or ii) DHA as a BSA complex or $8.33~\mu M$ BSA

Figure 4.1 (cont'd)

VEH. After 24 h, cells were collected for membrane phospholipid fatty acid analysis by gaschromatography (GC). **(B)** In Study 2, the impacts of DHA, LPS, and cSiO₂ on lysosomal membrane permeabilization, mitochondrial toxicity, and cell death in FLAMs were assessed by live-cell fluorescence microscopy. **(C)** In Study 3, FLAMs were treated with either ethanolic DHA or ethanol VEH, primed with LPS or PBS VEH, then exposed to cSiO₂ or PBS VEH. Lysosomal cathepsin, LDH, and proinflammatory cytokine release were analyzed in supernatants, and total oxylipin production was analyzed in pooled cell and supernatant samples at selected timepoints. Abbreviations: FLAMs, fetal liver-derived alveolar macrophages; VEH, vehicle; DHA, docosahexaenoic acid; LPS, lipopolysaccharide; cSiO₂, crystalline silica; LTR, LysoTracker Red; MTR, MitoTracker Red; SG, SYTOX Green.

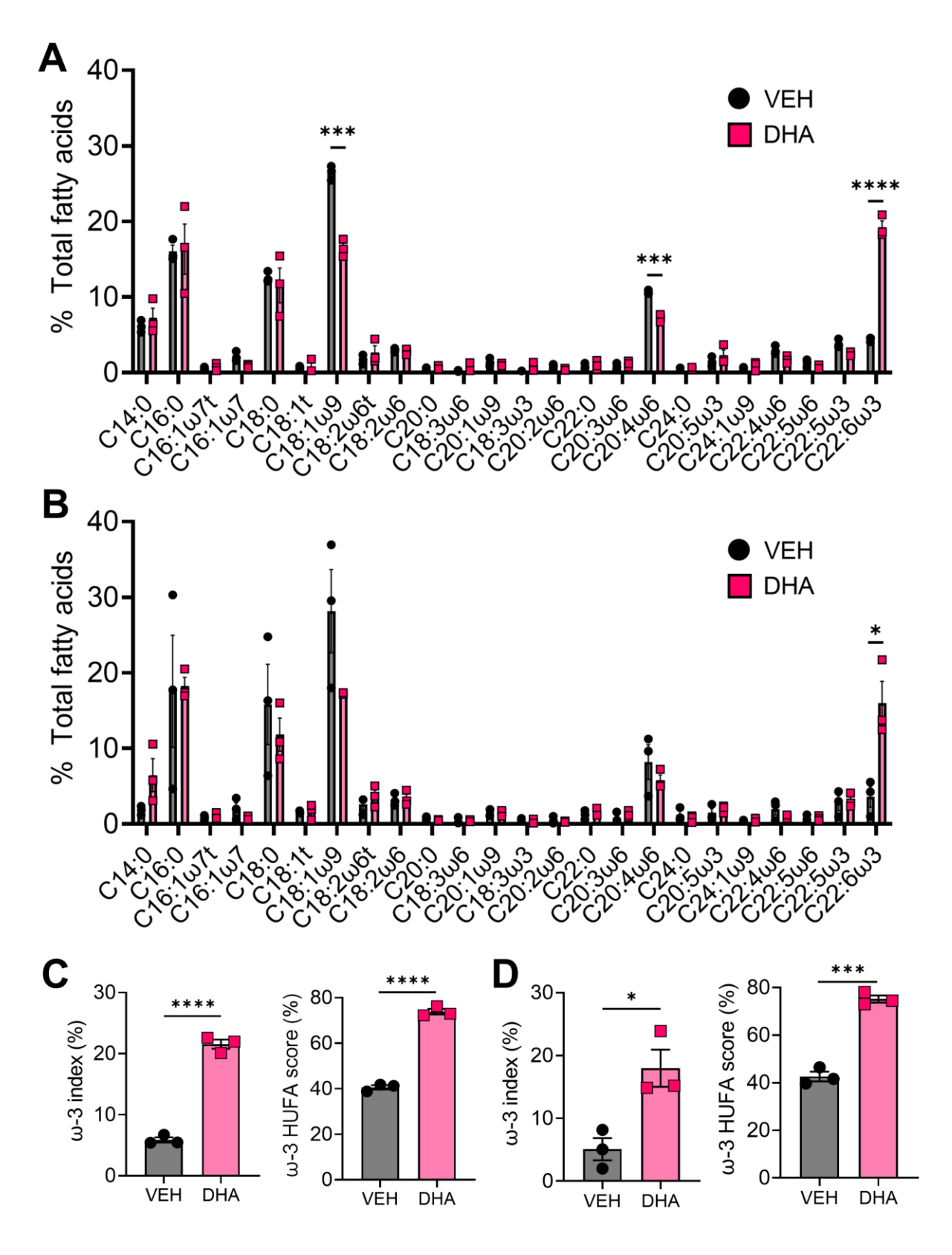


Figure 4.2. Supplementation of FLAMs with DHA significantly decreases arachidonic acid (ARA) and oleic acid (OA) content in FLAMs. (A) FLAMs were treated with DHA (25 μ M) or

Figure 4.2 (cont'd)

EtOH vehicle (VEH) for 24 h and then cell pellets analyzed by gas chromatography (GC). (B) FLAMs were treated with DHA (25 μM) complexed to BSA or BSA VEH (8.33 μM) for 24 h then cell pellets were analyzed by GC. (A-B) Under both treatment conditions, DHA (22:6ω3) displaces ω-9 OA (18:1ω9) and ω-6 ARA (20:4ω6) from FLAMs. (C-D) Percent ω-3 fatty acids (i.e., sum of EPA and DHA as a percentage of total fatty acids) and ω-3 highly unsaturated fatty acid (HUFA) score (i.e., sum of EPA, ω-3 DPA and DHA as a percentage of the sum of 20:3ω6, 20:4ω6, 20:5ω3, 22:5ω6, 22:5ω3, and 22:6ω3) are elevated in FLAMs treated with (C) ethanolic DHA and (D) DHA-BSA complexes. Data are shown as mean ± SEM. *p < 0.05, ***p < 0.001, ****p < 0.0001: Statistically significant differences between VEH-treated FLAMs and DHA-treated FLAMs.

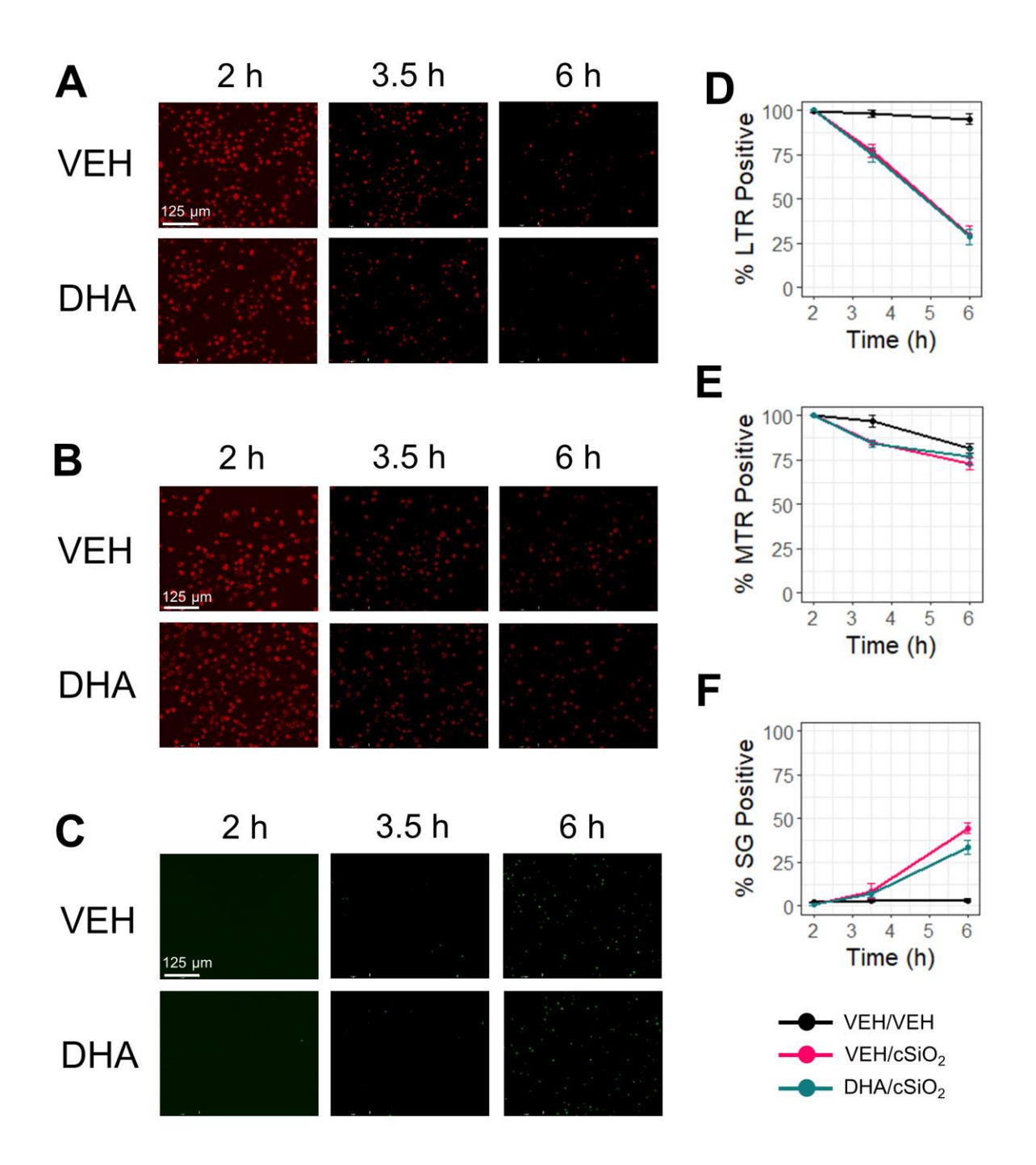


Figure 4.3. DHA does not affect early cSiO₂-induced lysosomal membrane permeabilization, mitochondrial toxicity, and death in FLAMs. FLAMs were treated with DHA (25 μM) or VEH for 24 h, primed with LPS (20 ng/ml), then exposed to cSiO₂ (12.5 μg/cm²). VEH-treated and DHA-treated FLAMs were incubated with DPBS^{+/+} for 1.5 h then stained with (A) LysoTracker Red (LTR; 50 nM), (B) MitoTracker Red (MTR; 25 nM), or (C) SYTOX Green (SG; 200 nM) in DPBS^{+/+} for 30 min. After 30 minutes to allow fluorescent dyes to equilibrate, cSiO₂ was added dropwise at 0 or 12.5 μg/cm². (D) Percent LysoTracker Red⁺, (E) MitoTracker Red⁺, and (F) SYTOX Green⁺ cells from 2 h to 6 h were quantified using CellProfiler 4.2.1 and RStudio Desktop. Data are shown as mean \pm SEM.

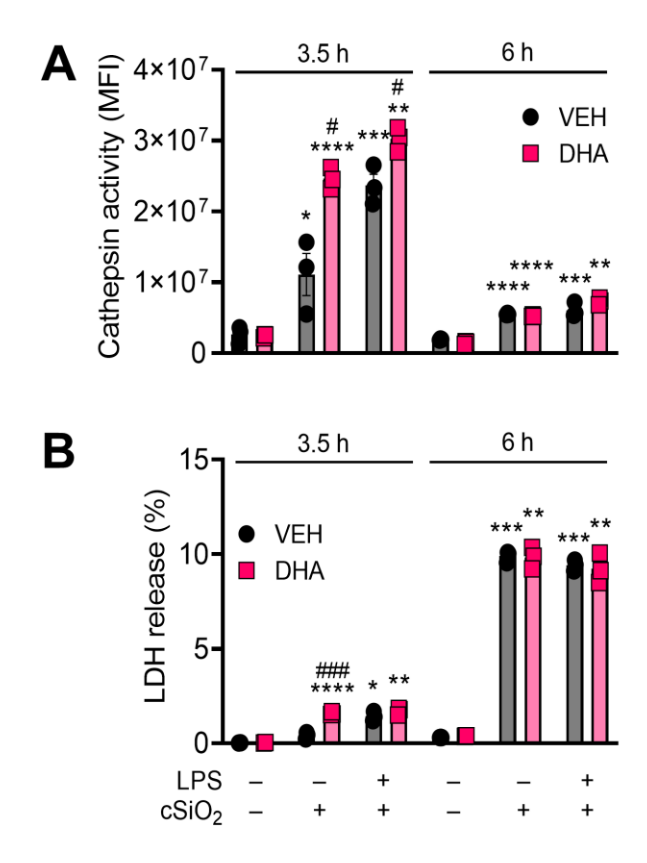


Figure 4.4. DHA does not influence cSiO₂-induced cathepsin and LDH release from FLAMs. FLAMs were treated with DHA (25 μ M) or VEH for 24 hr, primed with LPS (20 ng/ml), then exposed to cSiO₂ (12.5 μ g/cm²). Cell culture supernatants were collected at t = 3.5 h and 6 h, (A) cathepsin activity (expressed in units of mean fluorescence intensity [MFI]) quantified as a metric for lysosomal permeability, and (B) percent LDH release quantified as a metric for cell death. Data are shown as mean \pm SEM. *p < 0.05, **p < 0.01, ***p < 0.001, ****p < 0.0001: Statistically significant differences between cSiO₂ and its corresponding control. *p < 0.05, *#p < 0.01, ***p < 0.001: Statistically significant differences between DHA and its corresponding control. N.D., not determined.

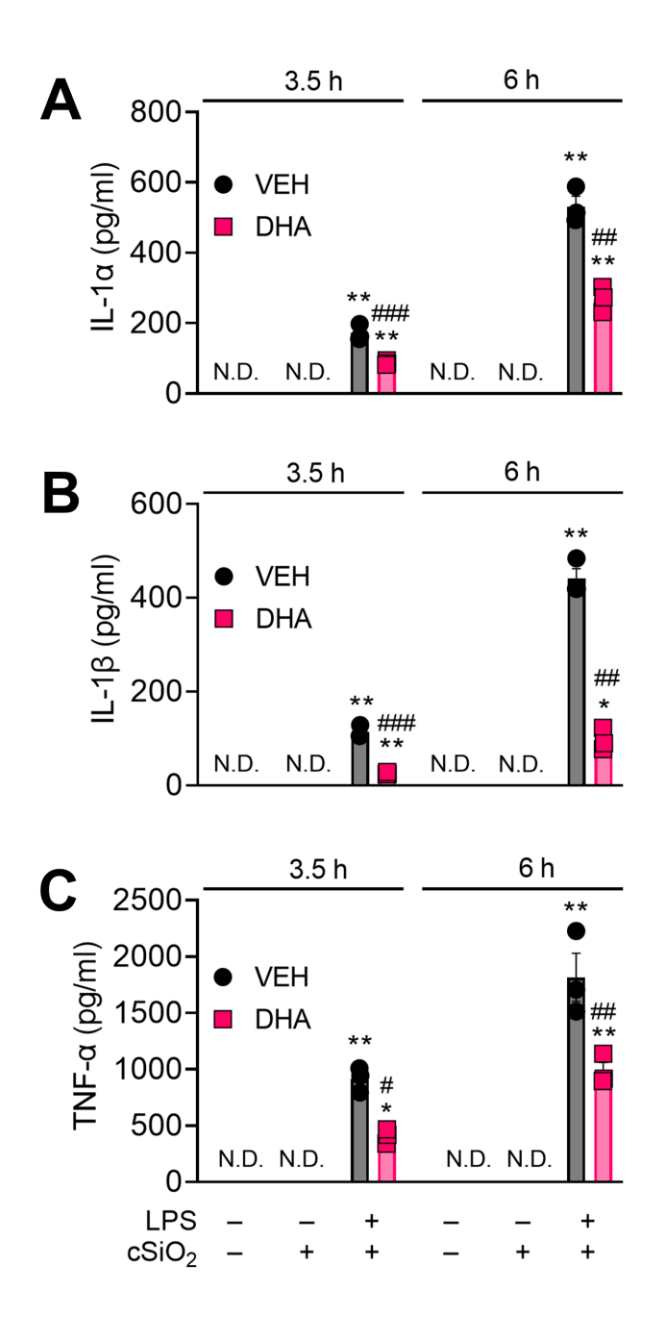


Figure 4.5. DHA suppresses $cSiO_2$ -induced release of proinflammatory cytokines in LPS-stimulated FLAMs. FLAMs were treated with DHA (25 μ M) or VEH for 24 h, primed with LPS (20 ng/ml), then exposed to $cSiO_2$ (12.5 μ g/cm²). Cell culture supernatants were collected at t = 3.5 h and 6 h, and (A) IL-1 α , (B) IL-1 β , (C) TNF- α were quantified by ELISA. *p < 0.05, **p < 0.01: Statistically significant differences between $cSiO_2$ and its corresponding control. *p < 0.05, *#p < 0.01, *##p < 0.001: Statistically significant differences between DHA and its corresponding control. N.D., not determined.

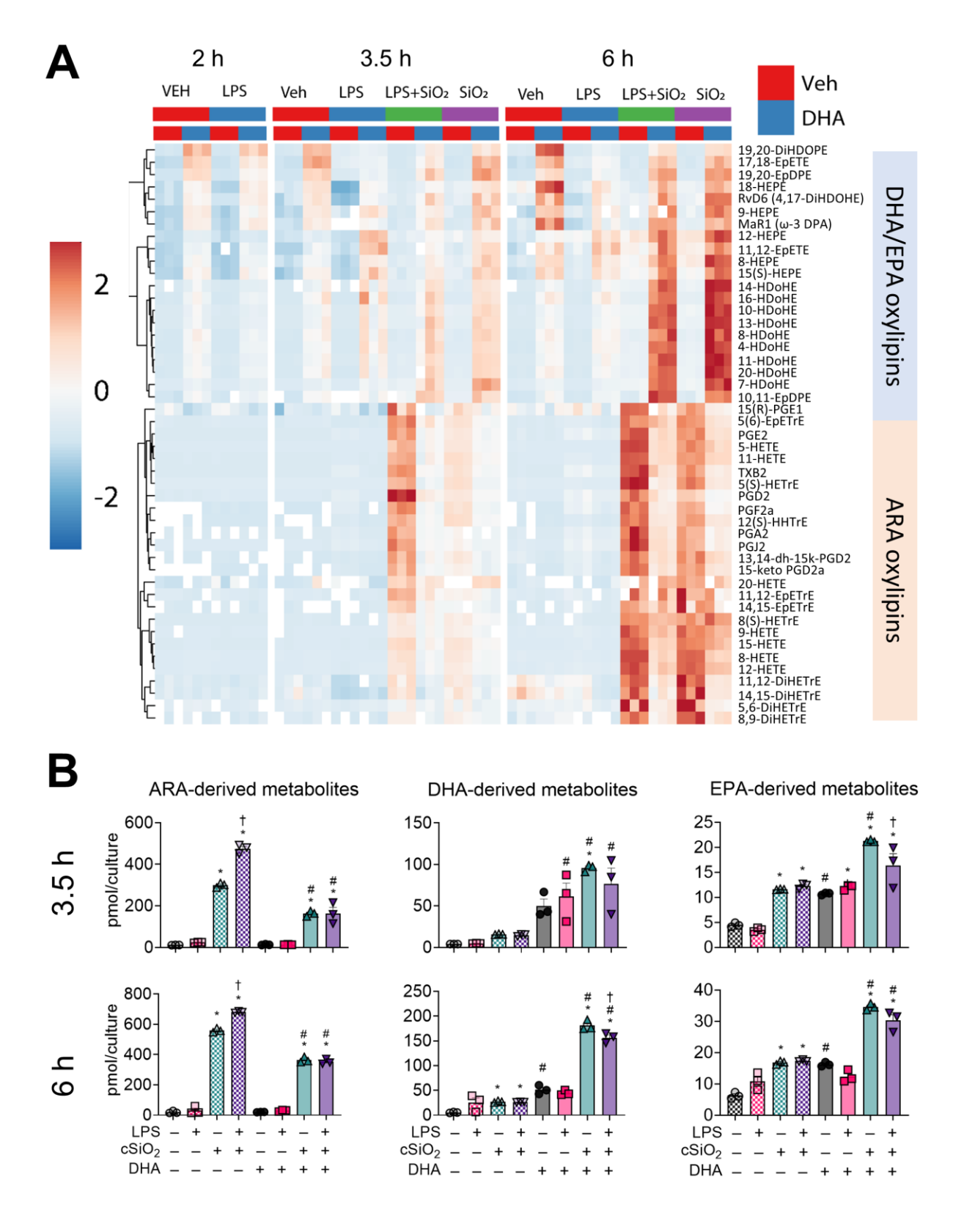


Figure 4.6. LPS, cSiO₂, and DHA differentially impact generation of ARA-, DHA-, and EPA-derived oxylipins from VEH- and LPS-treated FLAMs. FLAMs were treated with DHA (25

Figure 4.6 (cont'd)

μM) or VEH for 24 h, primed with LPS (20 ng/ml), and/or exposed to cSiO₂ (12.5 μg/cm²). Cultured FLAMs and supernatants were pooled at t = 2 h, 3.5 h, and 6 h and 156 oxylipins profiled by LC-MS. (A) Heat maps depicting the concentration of scaled DHA/EPA-derived and ARA-derived oxylipins, using unsupervised clustering with the Euclidean distance method. (B) Total ARA-, DHA-, and EPA-derived metabolites were quantified for all experimental groups at 3.5 h and 6 h. Data are shown as mean \pm SEM. MetaboAnalyst Version 5.0 was used for data normalization and statistical analysis by one-way analysis of variance (ANOVA) (FDR = 0.05) followed by Tukey's honestly significant difference (HSD) *post-hoc* test. Asterisks (*) indicate statistically significant differences (FDR q < 0.05) for cSiO₂-treated groups and their corresponding controls. Hashes (#) indicate statistically significant differences (FDR q < 0.05) for DHA-treated groups and their corresponding controls. Crosses (†) indicate statistically significant differences (FDR q < 0.05) for LPS-treated groups and their corresponding controls.

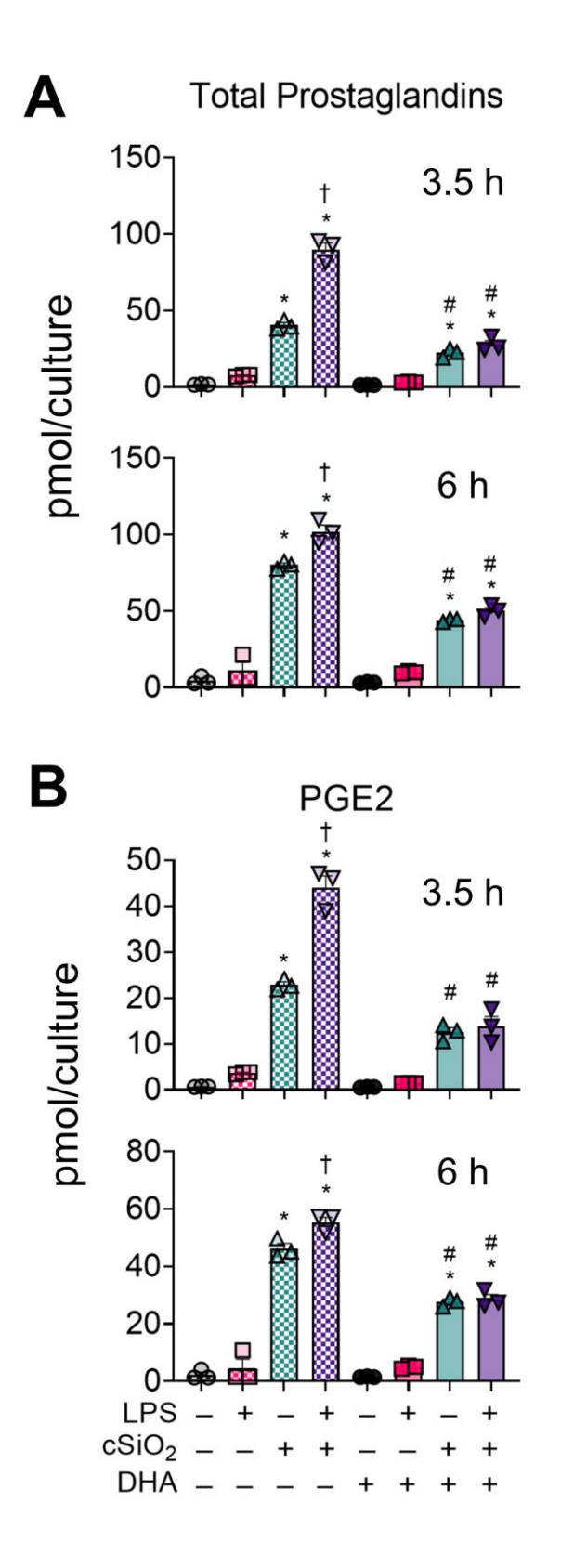


Figure 4.7. DHA dampens cSiO₂-induced production of prostaglandins in FLAMs. (A) Total prostaglandins and (B) PGE2 were quantified for all experimental groups at 3.5 h and 6 h. Data

Figure 4.7 (cont'd)

are shown as mean \pm SEM. MetaboAnalyst Version 5.0 was used for data normalization and statistical analysis by one-way analysis of variance (ANOVA) (FDR = 0.05) followed by Tukey's honestly significant difference (HSD) *post-hoc* test. Asterisks (*) indicate statistically significant differences (FDR q < 0.05) for cSiO₂-treated groups and their corresponding controls. Hashes (#) indicate statistically significant differences (FDR q < 0.05) for DHA-treated groups and their corresponding controls. Crosses (†) indicate statistically significant differences (FDR q < 0.05) for LPS-treated groups and their corresponding controls.

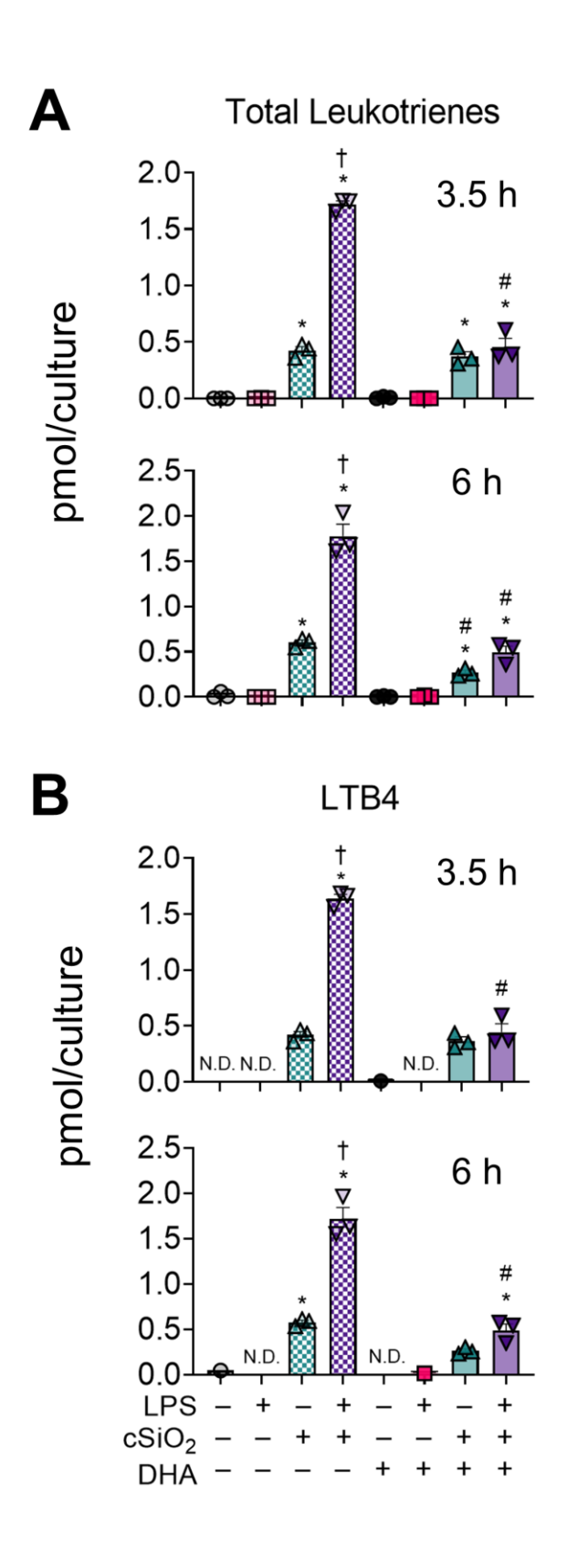


Figure 4.8. DHA inhibits cSiO₂-induced production of leukotrienes in FLAMs. (A) Total leukotrienes and (B) LTB4 were quantified for all experimental groups at 3.5 h and 6 h. Data are

Figure 4.8 (cont'd)

shown as mean \pm SEM. MetaboAnalyst Version 5.0 was used for data normalization and statistical analysis by one-way analysis of variance (ANOVA) (FDR = 0.05) followed by Tukey's honestly significant difference (HSD) *post-hoc* test. Asterisks (*) indicate statistically significant differences (FDR q < 0.05) for cSiO₂-treated groups and their corresponding controls. Hashes (#) indicate statistically significant differences (FDR q < 0.05) for DHA-treated groups and their corresponding controls. Crosses (†) indicate statistically significant differences (FDR q < 0.05) for LPS-treated groups and their corresponding controls. N.D., not determined.

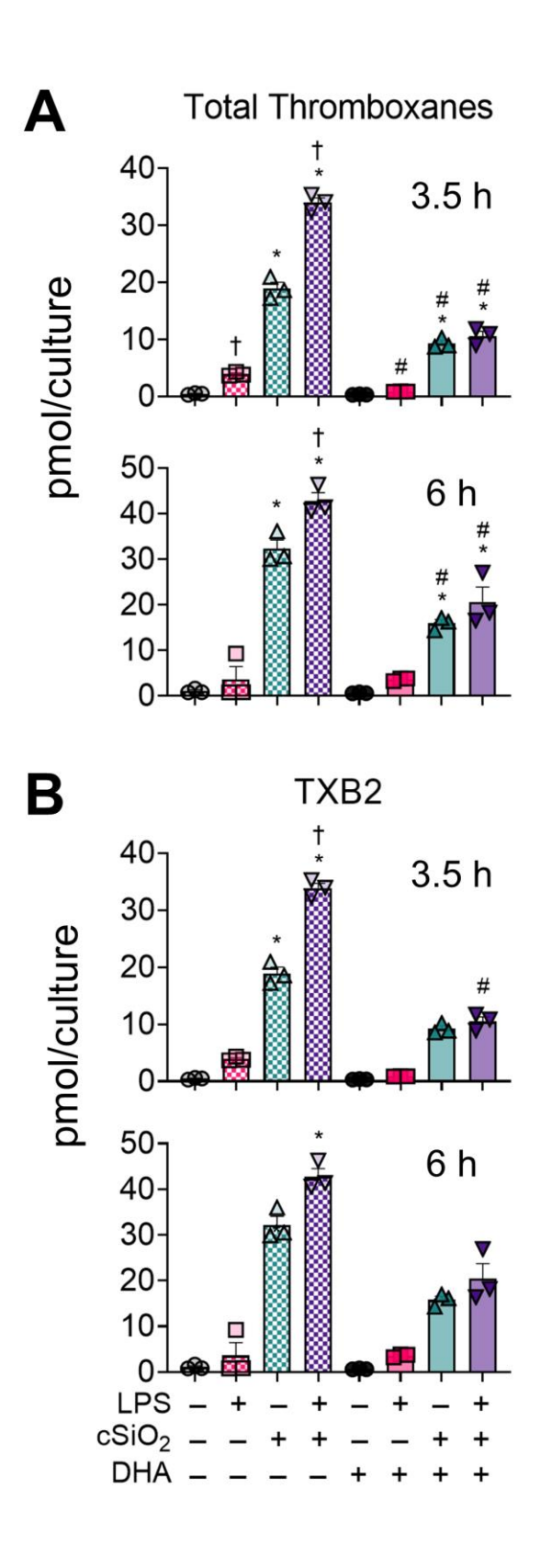


Figure 4.9. DHA suppresses cSiO₂-induced production of thromboxanes in FLAMs. (A) Total thromboxanes and (B) TXB2 were quantified for all experimental groups at 3.5 h and 6 h. Data

Figure 4.9 (cont'd)

are shown as mean \pm SEM. MetaboAnalyst Version 5.0 was used for data normalization and statistical analysis by one-way analysis of variance (ANOVA) (FDR = 0.05) followed by Tukey's honestly significant difference (HSD) *post-hoc* test. Asterisks (*) indicate statistically significant differences (FDR q < 0.05) for cSiO₂-treated groups and their corresponding controls. Hashes (#) indicate statistically significant differences (FDR q < 0.05) for DHA-treated groups and their corresponding controls. Crosses (†) indicate statistically significant differences (FDR q < 0.05) for LPS-treated groups and their corresponding controls. N.D., not determined.

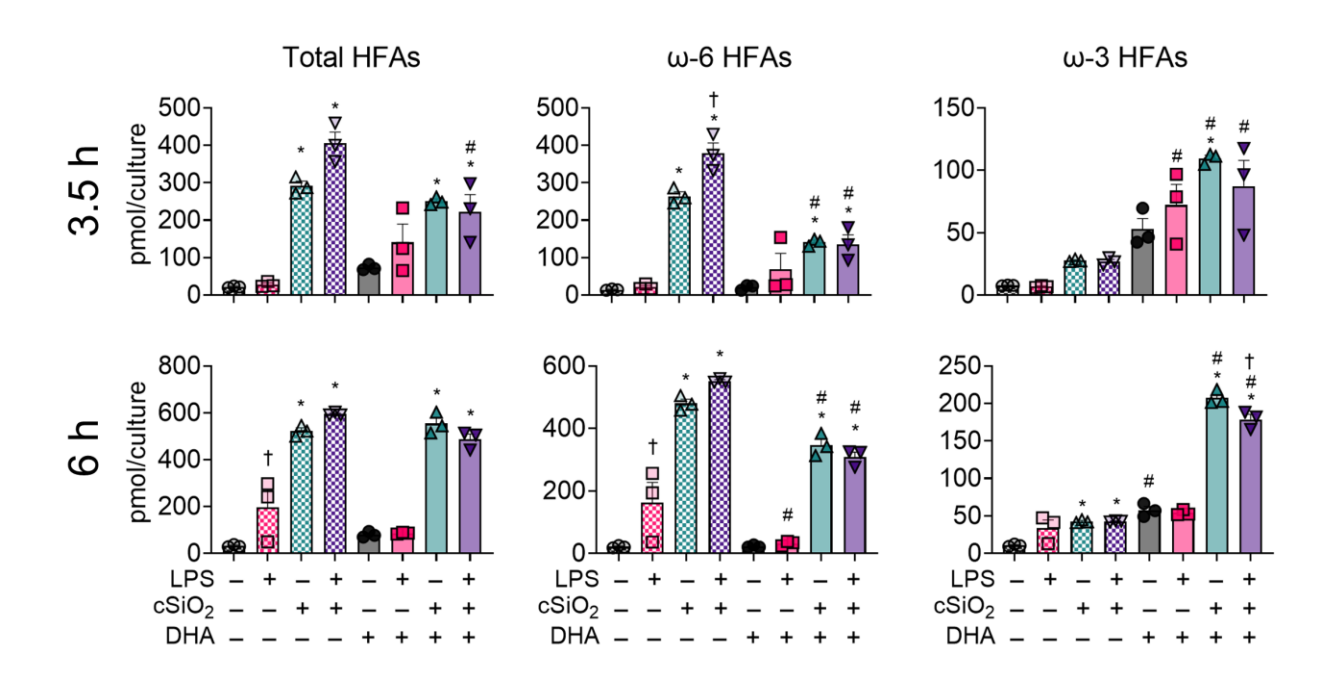


Figure 4.10. DHA skews cSiO₂-induced hydroxy fatty acid (HFA) metabolites from being ω-6 PUFA-derived and toward being ω-3 PUFA-derived. Total hydroxy fatty acids (HFAs), ω-6 HFAs, and ω-3 HFAs were quantified for all experimental groups at 3.5 h and 6 h. Data are shown as mean \pm SEM. MetaboAnalyst Version 5.0 was used for data normalization and statistical analysis by one-way analysis of variance (ANOVA) (FDR = 0.05) followed by Tukey's honestly significant difference (HSD) *post-hoc* test. Asterisks (*) indicate statistically significant differences (FDR q < 0.05) for cSiO₂-treated groups and their corresponding controls. Hashes (#) indicate statistically significant differences (FDR q < 0.05) for DHA-treated groups and their corresponding controls. Crosses (†) indicate statistically significant differences (FDR q < 0.05) for LPS-treated groups and their corresponding controls.

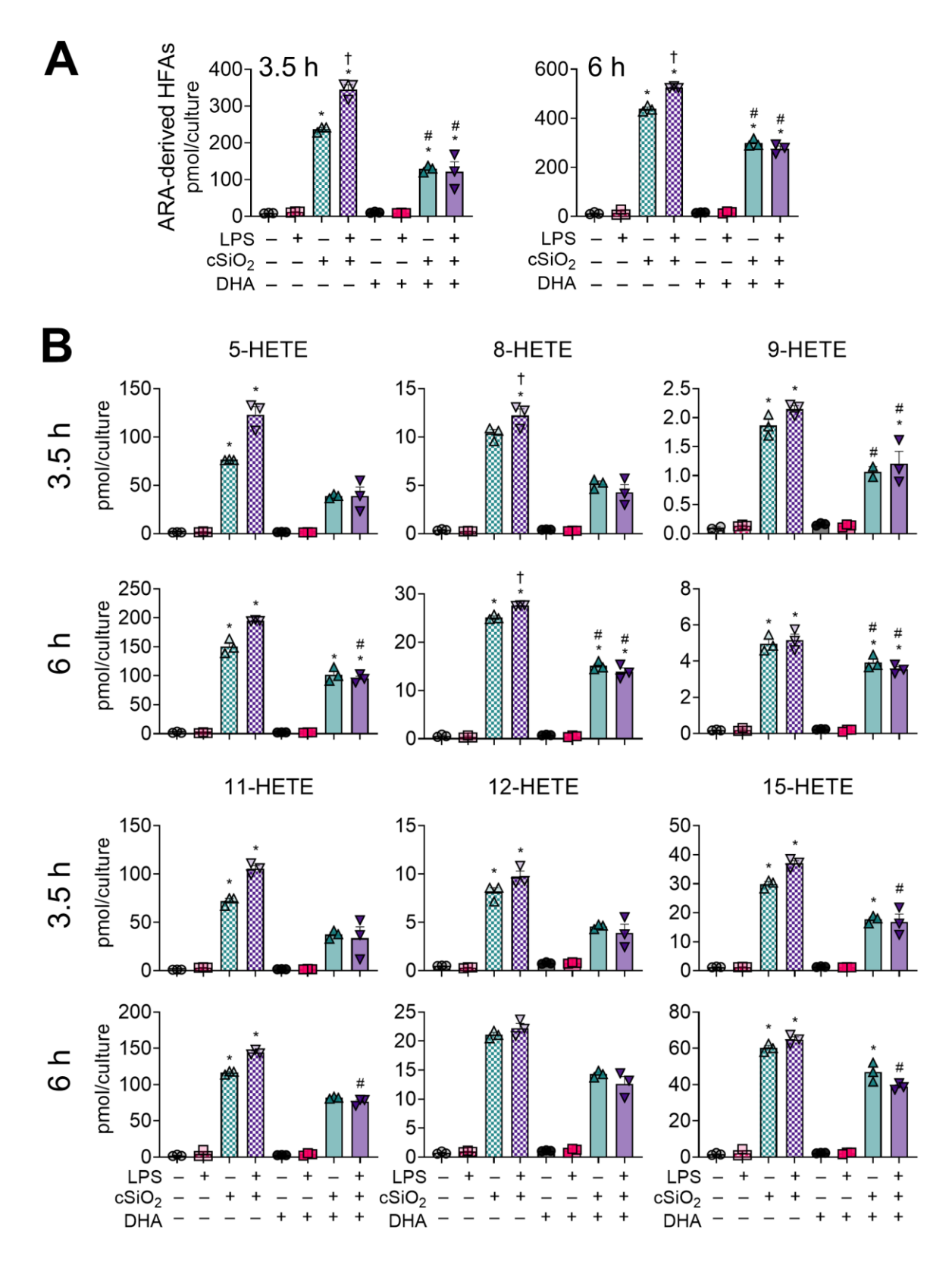


Figure 4.11. cSiO₂-induced production of ARA-derived HFAs is diminished with DHA supplementation. (A) Total ARA-derived HFAs and (B) 5-HETE, 8-HETE, 9-HETE, 11-HETE,

Figure 4.11 (cont'd)

12-HETE, and 15-HETE were quantified for all experimental groups at 3.5 h and 6 h. Data are shown as mean \pm SEM. MetaboAnalyst Version 5.0 was used for data normalization and statistical analysis by one-way analysis of variance (ANOVA) (FDR = 0.05) followed by Tukey's honestly significant difference (HSD) *post-hoc* test. Asterisks (*) indicate statistically significant differences (FDR q < 0.05) for cSiO₂-treated groups and their corresponding controls. Hashes (#) indicate statistically significant differences (FDR q < 0.05) for DHA-treated groups and their corresponding controls. Crosses (†) indicate statistically significant differences (FDR q < 0.05) for LPS-treated groups and their corresponding controls.

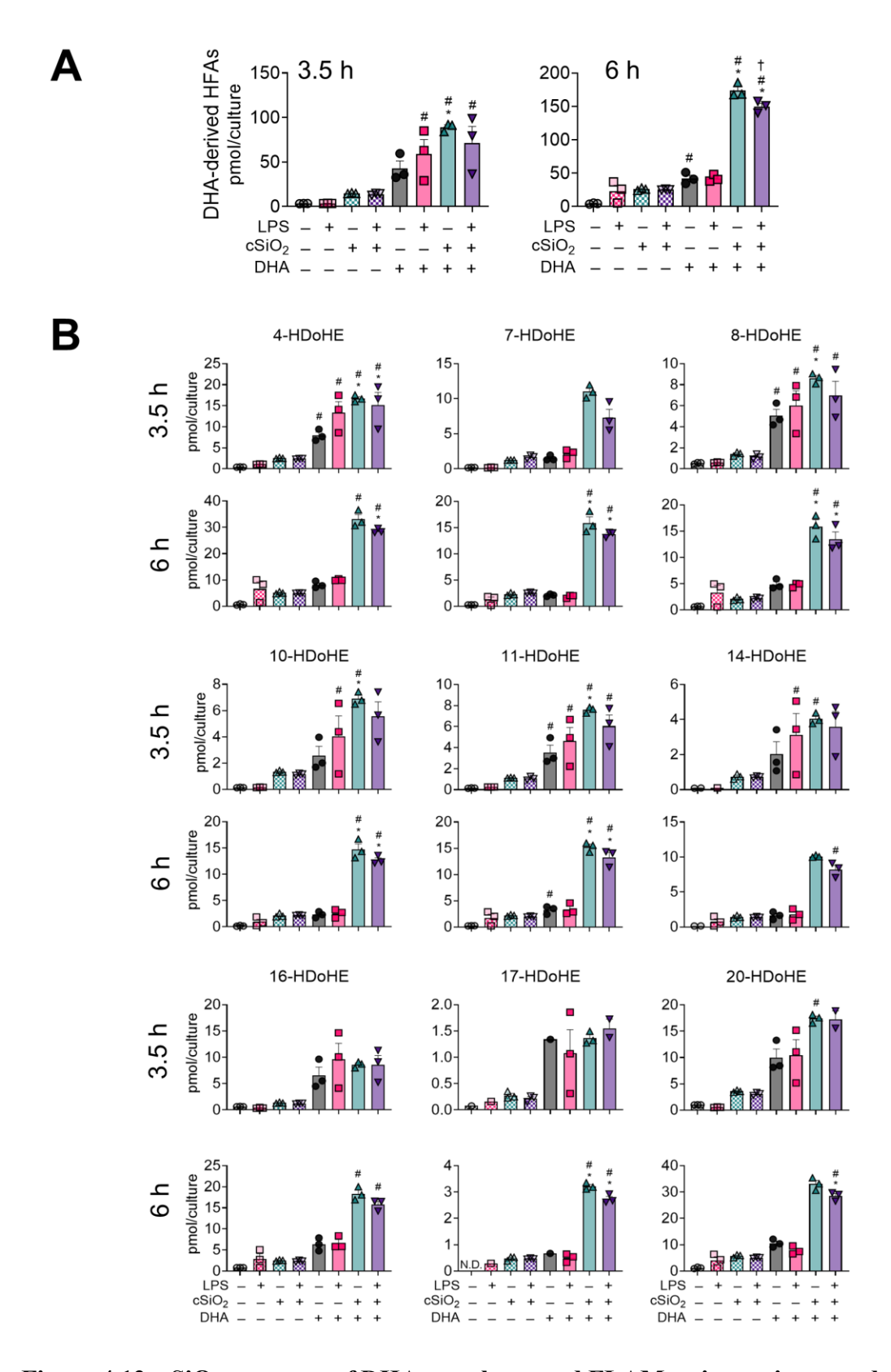


Figure 4.12. cSiO₂ exposure of DHA-supplemented FLAMs triggers increased production of DHA-derived hydroxy fatty acids (HFAs). (A) Total DHA-derived HFAs and (B) 4-HDoHE, 7-

Figure 4.12 (cont'd)

HDoHE, 8-HDoHE, 10-HDoHE, 11-HDoHE, 14-HDoHE, 16-HDoHE, 17-HDoHE, and 20-HDoHE were quantified for all experimental groups at 3.5 h and 6 h. Data are shown as mean \pm SEM. MetaboAnalyst Version 5.0 was used for data normalization and statistical analysis by one-way analysis of variance (ANOVA) (FDR = 0.05) followed by Tukey's honestly significant difference (HSD) *post-hoc* test. Asterisks (*) indicate statistically significant differences (FDR q < 0.05) for cSiO₂-treated groups and their corresponding controls. Hashes (#) indicate statistically significant differences (FDR q < 0.05) for DHA-treated groups and their corresponding controls. Crosses (†) indicate statistically significant differences (FDR q < 0.05) for LPS-treated groups and their corresponding controls.

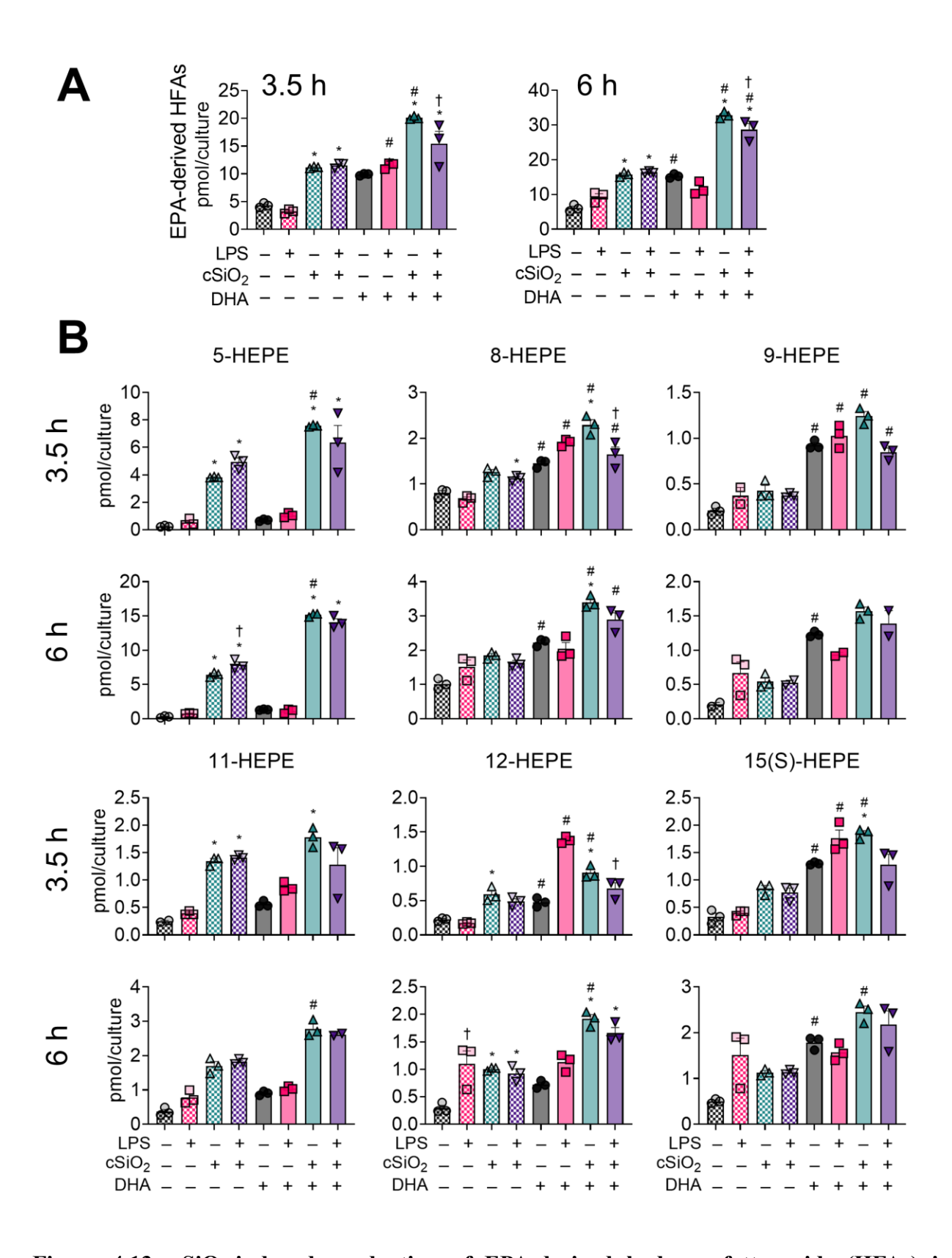


Figure 4.13. cSiO₂-induced production of EPA-derived hydroxy fatty acids (HFAs) is augmented with DHA supplementation. (A) Total EPA-derived HFAs and (B) 5-HEPE, 8-

Figure 4.13 (cont'd)

HEPE, 9-HEPE, 11-HEPE, 12-HEPE, and 15(S)-HEPE were quantified for all experimental groups at 3.5 h and 6 h. Data are shown as mean \pm SEM. MetaboAnalyst Version 5.0 was used for data normalization and statistical analysis by one-way analysis of variance (ANOVA) (FDR = 0.05) followed by Tukey's honestly significant difference (HSD) *post-hoc* test. Asterisks (*) indicate statistically significant differences (FDR q < 0.05) for cSiO₂-treated groups and their corresponding controls. Hashes (#) indicate statistically significant differences (FDR q < 0.05) for DHA-treated groups and their corresponding controls. Crosses (†) indicate statistically significant differences (FDR q < 0.05) for LPS-treated groups and their corresponding controls.

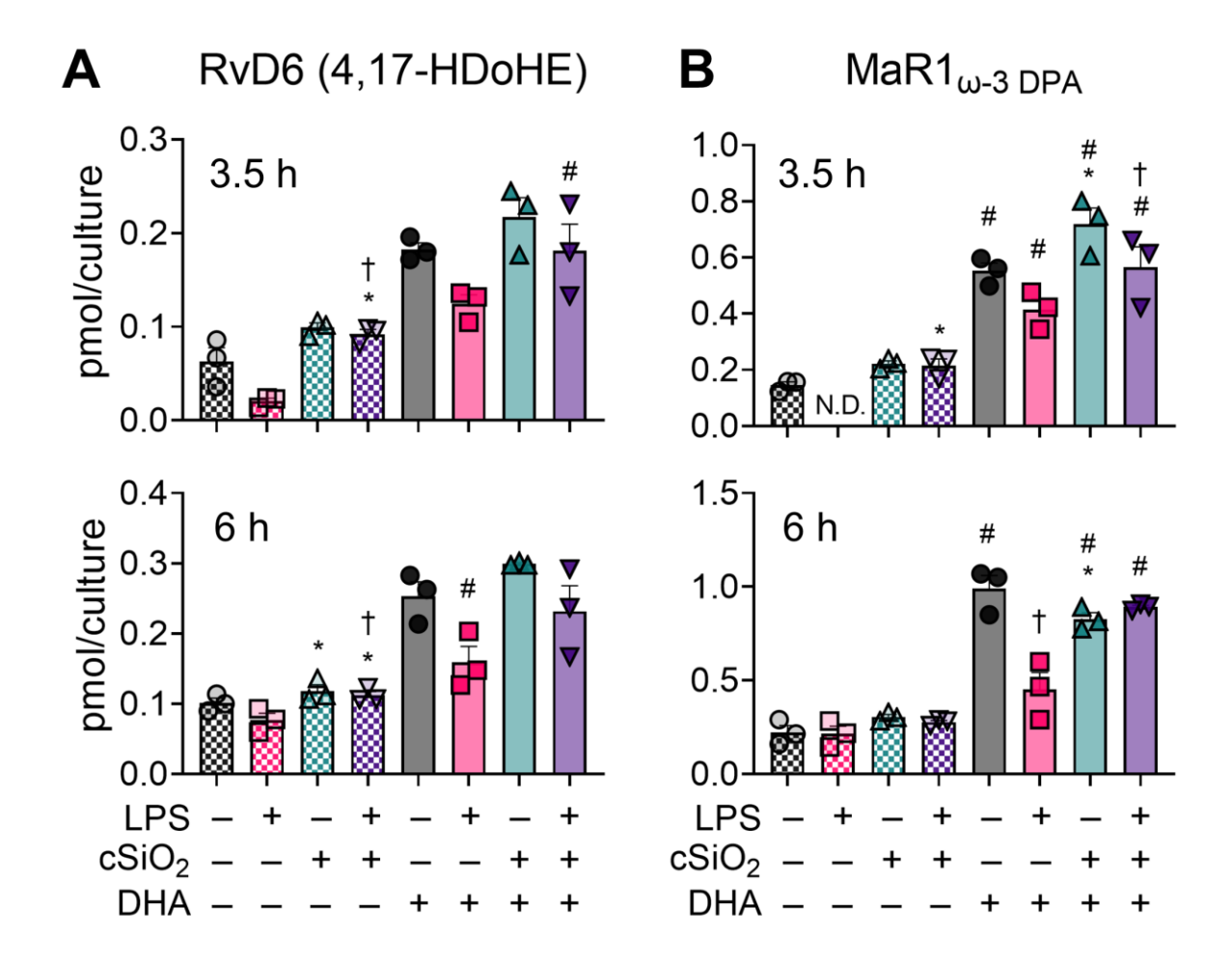


Figure 4.14. DHA supplementation contributes to modest production of specialized proresolving mediators RvD6 (4,17-DiHDoPE) and MaR1 $_{\omega$ -3 DPA in FLAMs. (A) RvD6 (4,17-DiHDoPE) and (B) MaR1 $_{\omega$ -3 DPA were quantified for all experimental groups at 3.5 h and 6 h. Data are shown as mean \pm SEM. MetaboAnalyst Version 5.0 was used for data normalization and statistical analysis by one-way analysis of variance (ANOVA) (FDR = 0.05) followed by Tukey's honestly significant difference (HSD) *post-hoc* test. Asterisks (*) indicate statistically significant differences (FDR q < 0.05) for cSiO₂-treated groups and their corresponding controls. Hashes (#) indicate statistically significant differences (FDR q < 0.05) for DHA-treated groups and their corresponding controls. Crosses (†) indicate statistically significant differences (FDR q < 0.05) for LPS-treated groups and their corresponding controls.

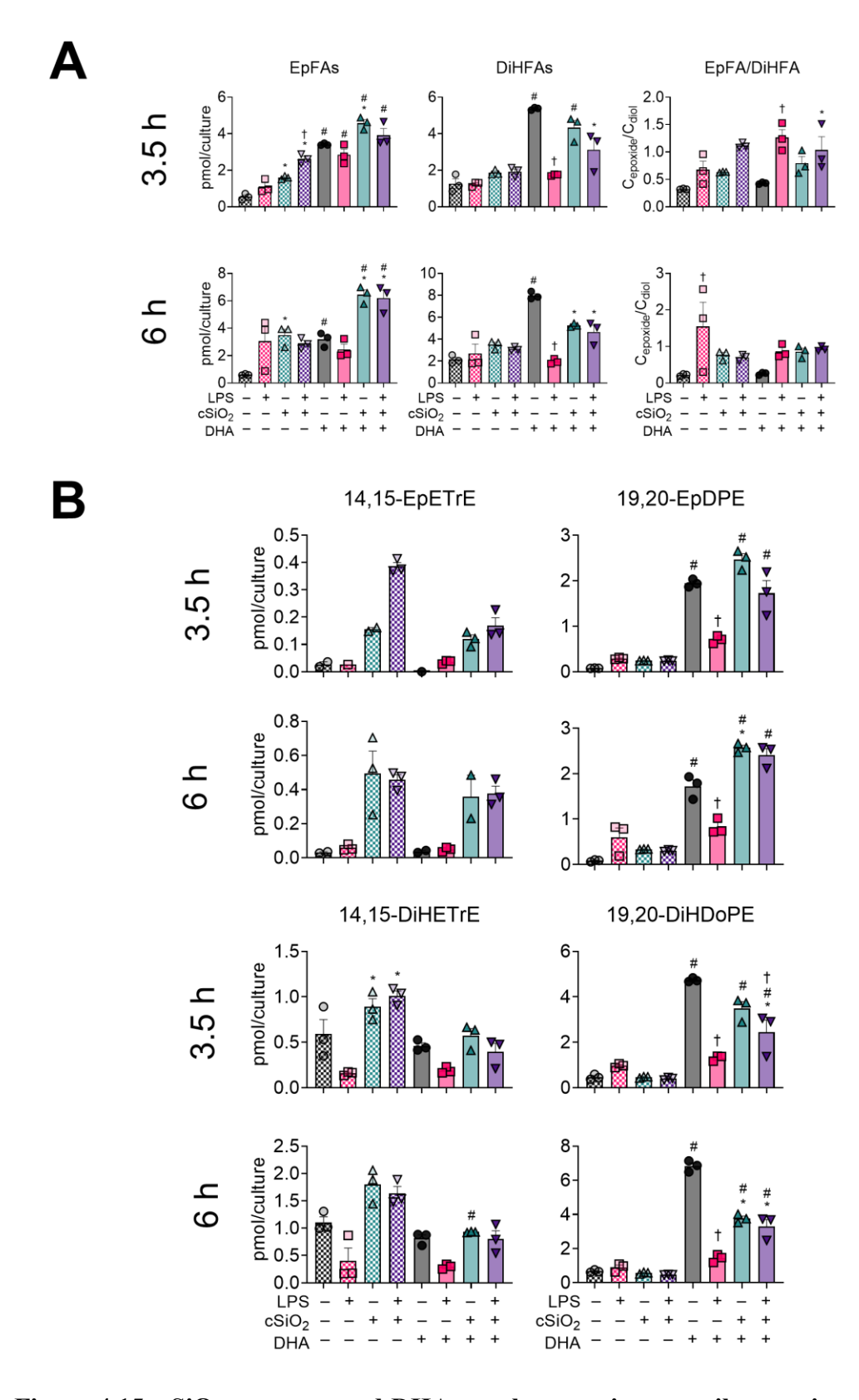


Figure 4.15. cSiO₂ exposure and DHA supplementation contribute to increased production of epoxy fatty acids (EpFAs) and dihydroxy fatty acids (DiHFAs). (A) Total EpFAs, total

Figure 4.15 (cont'd)

DiHFAs, and EpFA:DiHFA ratios ($C_{epoxide}/C_{diol}$) were quantified for all experimental groups at 3.5 h and 6 h. **(B)** 14,15-EpETrE, 14,15-DiHETrE, 19,20-EpDPE, and 19,20-DiHDoPE were quantified for all experimental groups at 3.5 h and 6 h. Data are shown as mean \pm SEM. MetaboAnalyst Version 5.0 was used for data normalization and statistical analysis by one-way analysis of variance (ANOVA) (FDR = 0.05) followed by Tukey's honestly significant difference (HSD) *post-hoc* test. Asterisks (*) indicate statistically significant differences (FDR q < 0.05) for cSiO₂-treated groups and their corresponding controls. Hashes (#) indicate statistically significant differences (FDR q < 0.05) for DHA-treated groups and their corresponding controls. Crosses (†) indicate statistically significant differences (FDR q < 0.05) for LPS-treated groups and their corresponding controls.

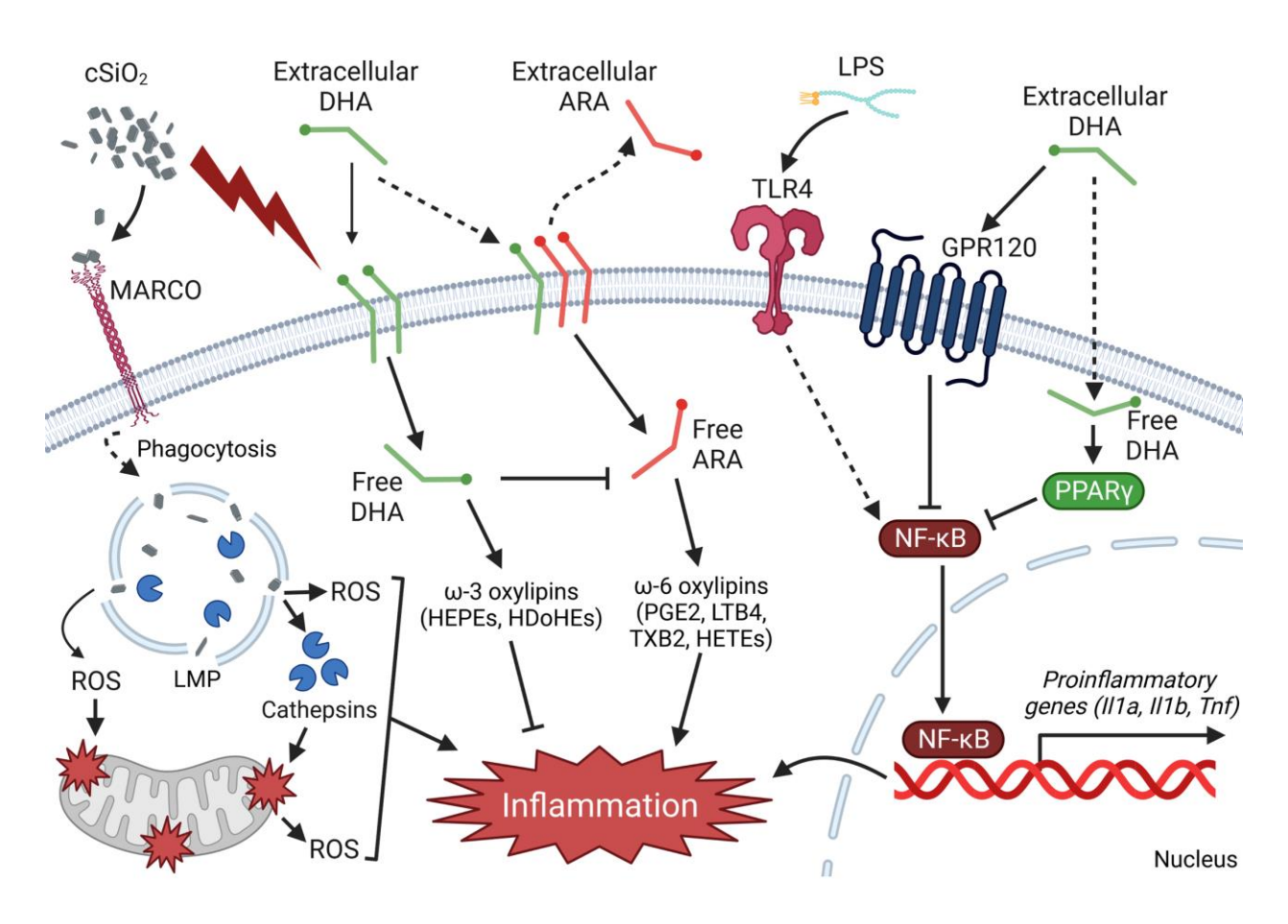


Figure 4.16. Putative model for the effects of DHA on the cSiO₂-triggered lipidome and proinflammatory cytokine release in the FLAM. cSiO₂ binds to MARCO, a cSiO₂ surface receptor, and is phagocytosed by the FLAM. Following phagocytosis, cSiO₂ triggers lysosomal membrane permeabilization (LMP), causing release of lysosomal proteolytical cathepsins and reactive oxygen species (ROS). Lysosomal cathepsin release and ROS elicit mitochondrial membrane depolarization and further ROS release into the cytosol. cSiO2 also triggers phospholipase A2 (PLA2)-mediated release of the ω-6 polyunsaturated fatty acid (PUFA) arachidonic acid (ARA) from the plasma membrane, freeing it for enzymatic and non-enzymatic conversion to various proinflammatory ω-6 oxylipins. Pre-incubation of FLAMs with DHA causes displacement of ARA from the plasma membrane, thereby allowing PLA2-mediated release of DHA into the cytosol following cSiO₂ exposure. Cytosolic DHA competes with ARA as a substrate of enzymatic and non-enzymatic oxylipin production, ultimately leading to generation of various pro-resolving ω-3 oxylipins. When cells are primed with lipopolysaccharide (LPS), toll-like receptor 4 (TLR) stimulates nuclear translocation of NF-κB to upregulate proinflammatory genes. DHA inhibits NF-κB-regulated gene expression through the G protein-coupled receptor GPR120 and the nuclear receptor PPARy. Created with BioRender.com.

TABLES

Table 4.1. Summarized oxylipin data at t = 2 h.

	VEI	H/V	EH	LP	S/VI	EH	DH	IA/V	EH	DHA/LPS				
Σ 18:2ω6	15.25	±	4.37	11.01	±	1.72	10.36	±	2.39	8.64	±	0.36		
Σ 18:3ω3	0.27	±	0.14	0.18	±	0.10	0.43	±	0.23	0.16	±	0.09		
Σ 20:2ω6	0.04	±	0.02	0.04	±	0.03	0.01	±	0.01	0.03	±	0.02		
Σ 20:3ω6	0.59	±	0.05	0.68	±	0.10	0.49	±	0.11	0.53	±	0.08		
Σ 20:4ω6	10.13	±	0.47	13.80	±	1.90	11.99	±	0.63	11.61	±	0.34		
Σ 20:5ω3	3.77	±	0.26	3.56	±	0.27	10.04	±	0.14	9.51	±	0.34		
Σ 22:5ω3	0.09	±	0.01	0.09	±	0.01	0.52	±	0.01	0.54	±	0.03		
Σ 22:6ω3	3.56	±	0.10	3.72	±	0.57	42.78	±	5.23	31.79	±	0.98		
Σ Total ω-6	26.00	±	4.14	25.53	±	2.47	22.84	±	2.36	20.81	±	20.98		
Σ Total ω-3	7.69	±	0.42	7.55	±	0.85	53.77	±	4.93	42.00	±	42.56		
Σ ω-6 ΕρΓΑ	0.41	±	0.06	0.34	±	0.06	0.30	±	0.03	0.29	±	0.01		
Σ ω-3 ΕρΓΑ	0.18	±	0.01	0.22	±	0.03	2.72	±	0.08	1.82	±	0.04		
Σ Total EpFA	0.59	±	0.06	0.55	±	0.07	3.02	±	0.04	2.11	±	0.04		
Σω-6 DiHFA (CYP450 origin)	0.55	±	0.08	0.64	±	0.05	0.69	±	0.05	0.66	±	0.06		
Σω-3 DiHFA (CYP450 origin)	0.34	±	0.06	0.68	±	0.07	0.83	±	0.06	0.77	±	0.04		
Σ Total DiHFA (CYP450 origin)	0.89	±	0.14	0.88	±	0.02	5.49	±	0.35	4.94	±	0.31		
EpFA:DiHFA ratio	0.53	±	0.08	0.48	±	0.08	0.38	±	0.03	0.28	±	0.01		
Σω-6 Prostaglandin	1.33	±	0.15	2.65	±	0.12	1.24	±	0.08	2.05	±	0.09		
Σω-3 Prostaglandin	0.00	±	0.00	0.01	±	0.01	0.00	±	0.00	0.00	±	0.00		
Σ Total Prostaglandin	1.33	±	0.15	2.66	±	0.13	1.24	±	0.08	2.05	±	0.09		
Σω-6 Leukotriene	0.00	±	0.00	0.00	±	0.00	0.00	±	0.00	0.00	±	0.00		
Σω-3 Leukotriene	0.00	±	0.00	0.00	±	0.00	0.00	±	0.00	0.00	±	0.00		
Σ Total Leukotriene	0.00	±	0.00	0.00	±	0.00	0.00	±	0.00	0.00	±	0.00		
Σω-6 Thromboxane	0.31	±	0.03	0.59	±	0.09	0.27	±	0.02	0.41	±	0.03		
Σ ω-3 Thromboxane	0.00	±	0.00	0.00	±	0.00	0.00	±	0.00	0.00	±	0.00		
Σ Total Thromboxane	0.31	±	0.03	0.59	±	0.09	0.27	±	0.02	0.41	±	0.03		
Σω-6 HFA	18.80	±	2.79	17.91	±	2.43	17.35	±	2.15	14.70	±	0.54		
Σω-3 HFA	6.96	±	0.33	6.69	±	0.77	45.35	±	5.16	35.01	±	0.82		
Σ HFA (ARA origin)	8.16	±	0.33	10.31	±	1.80	9.98	±	0.60	8.71	±	0.35		
Σ HFA (EPA origin)	3.63	±	0.24	3.40	±	0.25	9.32	±	0.15	8.94	±	0.32		

Table 4.1 (cont'd)

Σ HFA (DHA origin)	3.05	±	0.07	3.11	±	0.52	35.60	±	5.44	25.91	±	1.03
Σ Total HFA	25.75	±	2.99	24.60	±	3.16	62.71	±	4.19	49.71	±	1.26
Σ Total Oxo-FA	4.59	±	1.24	3.56	±	0.39	3.11	±	0.23	2.81	±	0.22
Σω-6 DiHFA (LOX origin)	0.01	±	0.01	0.01	±	0.01	0.02	±	0.01	0.02	±	0.02
Σω-3 DiHFA (LOX origin)	0.00	±	0.00	0.00	±	0.00	0.00	±	0.00	0.00	±	0.00
Σ Total DiHFA (LOX origin)	0.01	±	0.01	0.01	±	0.01	0.02	±	0.01	0.02	±	0.02
Σ Total Lipoxin	0.00	±	0.00	0.00	±	0.00	0.00	±	0.00	0.00	±	0.00
Σ Resolvin (EPA origin)	0.03	±	0.01	0.04	±	0.01	0.02	±	0.00	0.01	±	0.01
Σ Resolvin (DHA origin)	0.09	±	0.03	0.11	±	0.00	0.20	±	0.03	0.19	±	0.02
Σ Total Resolvin	0.13	±	0.03	0.15	\pm	0.01	0.22	±	0.03	0.20	±	0.02
Σ Maresin (ω-3 DPA origin)	0.09	±	0.01	0.09	±	0.01	0.52	±	0.01	0.54	±	0.03
Σ Maresin (DHA origin)	0.00	±	0.00	0.00	±	0.00	0.00	±	0.00	0.00	±	0.00
Σ Total Maresin	0.09	±	0.01	0.09	±	0.01	0.52	±	0.01	0.54	±	0.03
Σ Protectin (ω-3 DPA origin)	0.00	±	0.00	0.00	±	0.00	0.00	±	0.00	0.00	±	0.00
Σ Protectin (DHA origin)	0.00	±	0.00	0.00	±	0.00	0.01	±	0.01	0.02	±	0.02
Σ Total Protectin	0.00	±	0.00	0.00	±	0.00	0.01	±	0.01	0.02	±	0.02

Data are presented in units of pmol/culture as mean \pm SEM. 18:2 ω 6, linoleic acid; 18:3 ω 3, α -linolenic acid; 20:2 ω 6, eicosadienoic acid; 20:3 ω 6, linoleic acid; dihomo- γ -linolenic acid; 20:4 ω 6, arachidonic acid; 20:5 ω 3, eicosapentaenoic acid; 22:5 ω 3, docosapentaenoic acid; 22:6 ω 3, docosahexaenoic acid; EpFA, epoxy fatty acid; DiHFA, dihydroxy fatty acid; CYP450, cytochrome P450 monooxygenase; HFA, hydroxy fatty acid; oxo-FA, oxo fatty acid; ARA, arachidonic acid; EPA, eicosapentaenoic acid; DPA, docosapentaenoic acid; DHA, docosahexaenoic acid.

Table 4.2. Summarized oxylipin data at t = 3.5 h.

	VEH/VEH	LPS/VEH	VEH/cSiO ₂	LPS/cSiO ₂	DHA- VEH/VEH	DHA- LPS/VEH	DHA- VEH/cSiO ₂	DHA- LPS/cSiO ₂		
Σ 18:2ω6	8.52 ± 1.14	15.87 ± 6.50	27.66 ± 10.16	34.01 ± 20.09	13.82 ± 4.57	79.99 ± 48.52	14.74 ± 1.48	17.80 ± 4.06		
Σ 18:3ω3	0.06 \pm 0.04	0.14 ± 0.09	1.61 ± 0.28	1.48 ± 1.12	0.20 \pm 0.10	1.74 ± 1.71	0.28 \pm 0.22	0.41 \pm 0.21		
Σ 20:2ω6	0.00 \pm 0.00	0.00 ± 0.00	0.34 ± 0.04	0.34 ± 0.03	0.07 ± 0.05	0.25 ± 0.25	0.17 ± 0.02	0.11 ± 0.05		
Σ 20:3ω6	0.38 ± 0.10	0.51 ± 0.06	4.89 ± 0.09	6.69 ± 0.07	0.56 ± 0.07	0.63 ± 0.12	2.45 ± 0.17	2.01 ± 0.53		
Σ 20:4ω6	11.58 ± 0.36	23.81 ± 1.31	299.93 ± 6.36	474.67 ± 11.98	13.47 ± 1.17	13.44 ± 0.55	162.74 ± 7.62	163.41 ± 29.20		
Σ 20:5ω3	4.49 ± 0.25	3.54 ± 0.21	11.62 ± 0.05	12.27 ± 0.32	10.73 ± 0.14	12.04 ± 0.31	21.29 ± 0.15	16.36 ± 2.37		
Σ 22:5ω3	0.15 \pm 0.01	0.00 ± 0.00	0.22 \pm 0.01	0.22 \pm 0.02	0.55 ± 0.03	0.41 \pm 0.04	0.72 ± 0.06	0.56 ± 0.07		
Σ 22:6ω3	4.07 ± 0.01	4.81 ± 0.19	15.97 ± 0.31	14.83 ± 0.74	50.00 ± 8.48	61.29 ± 16.28	95.85 ± 2.43	76.49 ± 19.17		
Σ Total ω-6	$20.47 \hspace{0.2cm} \pm \hspace{0.2cm} 1.30$	40.19 ± 6.86	332.81 ± 12.70	515.71 ± 30.00	27.91 ± 5.20	94.30 ± 48.50	180.10 ± 7.55	183.32 ± 26.56		
Σ Total ω-3	8.76 ± 0.28	8.49 ± 0.48	29.43 ± 0.56	28.79 ± 1.80	61.48 ± 8.52	75.48 ± 16.52	118.13 ± 2.39	93.82 ± 21.49		
Σ ω-6 ΕρΓΑ	0.33 ± 0.09	0.55 ± 0.22	0.93 ± 0.06	1.87 ± 0.12	0.37 ± 0.07	1.49 ± 0.26	0.87 ± 0.08	1.21 \pm 0.22		
Σ ω-3 EpFA	0.22 \pm 0.00	0.56 ± 0.03	0.66 ± 0.03	0.75 ± 0.04	3.04 ± 0.04	1.35 ± 0.08	3.70 ± 0.11	2.71 ± 0.46		
Σ Total EpFA	0.55 \pm 0.09	1.11 ± 0.21	1.59 ± 0.05	2.63 ± 0.14	3.41 ± 0.03	2.85 ± 0.30	4.58 ± 0.19	3.91 ± 0.37		
Σ ω-6 DiHFA (CYP450 origin)	0.94 ± 0.22	0.54 ± 0.13	1.44 ± 0.14	1.57 ± 0.18	0.80 \pm 0.05	1.15 ± 0.20	1.11 ± 0.06	0.93 ± 0.13		
Σω-3 DiHFA (CYP450 origin)	1.00 ± 0.26	0.73 ± 0.21	1.53 ± 0.11	1.72 ± 0.18	1.03 ± 0.06	1.75 ± 0.28	1.35 ± 0.05	1.17 ± 0.11		
Σ Total DiHFA (CYP450 origin)	1.26 ± 0.27	1.24 ± 0.08	1.87 ± 0.08	1.92 ± 0.15	5.37 ± 0.04	1.74 ± 0.03	4.33 ± 0.39	3.12 ± 0.61		
EpFA:DiHFA ratio	0.32 ± 0.01	0.68 ± 0.16	0.63 ± 0.01	1.12 ± 0.03	0.43 ± 0.01	1.26 ± 0.14	0.79 ± 0.12	1.04 ± 0.24		
Σω-6 Prostaglandin	1.75 ± 0.15	7.69 ± 0.39	40.46 ± 1.69	89.94 ± 4.33	1.46 ± 0.03	3.13 ± 0.14	22.29 ± 1.70	27.71 ± 2.65		
Σω-3 Prostaglandin	0.00 \pm 0.00	0.00 ± 0.00	0.06 ± 0.03	0.07 \pm 0.04	0.00 ± 0.00	0.00 ± 0.00	0.15 ± 0.03	0.12 ± 0.01		
Σ Total Prostaglandin	1.75 ± 0.15	7.69 ± 0.39	40.52 ± 1.66	90.01 ± 4.31	1.46 ± 0.03	3.13 ± 0.14	22.44 ± 1.73	27.83 ± 2.66		
Σω-6 Leukotriene	0.00 ± 0.00	0.00 ± 0.00	0.43 \pm 0.03	1.72 ± 0.03	0.00 ± 0.00	0.00 ± 0.00	0.37 ± 0.04	0.46 ± 0.08		
Σω-3 Leukotriene	0.00 \pm 0.00	0.00 ± 0.00	0.00 ± 0.00	0.00 ± 0.00	0.01 ± 0.01	0.00 ± 0.00	0.00 ± 0.00	0.00 \pm 0.00		
Σ Total Leukotriene	0.00 \pm 0.00	0.00 ± 0.00	0.43 ± 0.03	1.72 ± 0.03	0.01 ± 0.00	0.00 ± 0.00	0.37 ± 0.04	0.46 ± 0.08		
$\Sigma \omega$ -6 Thromboxane	0.48 ± 0.09	3.94 ± 0.21	18.92 ± 1.08	33.90 ± 0.80	0.37 ± 0.03	0.89 ± 0.01	9.23 ± 0.50	10.49 ± 0.83		

Table 4.2 (cont'd)

$\Sigma \omega$ -3 Thromboxane	0.00	±	0.00	0.02	±	0.02	0.06	±	0.00	0.14	±	0.02	0.00	±	0.00	0.00	±	0.00	0.11	±	0.02	0.13	±	0.01
Σ Total Thromboxane	0.48	±	0.09	3.95	±	0.20	18.98	±	1.08	34.04	±	0.80	0.37	±	0.03	0.89	±	0.01	9.35	±	0.49	10.61	±	0.84
Σ ω-6 HFA	14.54	±	0.98	21.65	±	4.02	264.09	±	11.95	378.47	±	28.05	21.04	±	3.99	68.88	±	42.49	141.27	±	5.64	135.84	±	25.24
Σ ω-3 HFA	7.75	±	0.17	6.86	±	0.42	27.74	\pm	0.59	26.94	±	1.66	52.88	±	8.50	72.16	±	16.48	109.62	±	2.46	87.35	±	20.55
Σ HFA (ARA origin)	8.72	±	0.48	12.24	±	0.83	237.31	±	4.60	344.44	±	13.61	10.92	±	1.01	9.27	±	0.53	129.16	±	5.38	121.44	±	26.97
Σ HFA (EPA origin)	4.33	±	0.23	3.23	±	0.22	11.16	±	0.10	11.54	±	0.28	9.88	±	0.11	11.51	±	0.33	20.09	±	0.17	15.46	±	2.20
Σ HFA (DHA origin)	3.37	±	0.10	3.48	±	0.13	14.96	±	0.32	13.96	±	0.71	42.80	±	8.45	58.97	±	16.26	89.25	±	2.52	71.52	±	18.43
Σ Total HFA	22.28	±	1.14	28.51	±	3.99	291.83	±	12.54	405.42	±	29.71	73.91	±	4.52	141.05	±	48.85	250.89	±	6.04	223.19	±	45.42
Σ Total Oxo-FA	2.58	±	0.27	6.09	±	2.54	6.53	±	1.17	8.23	±	1.87	3.97	±	1.23	19.53	±	5.90	5.18	±	0.62	6.95	±	1.85
Σω-6 DiHFA (LOX origin)	0.02	±	0.01	0.02	±	0.01	0.05	±	0.01	0.07	±	0.02	0.08	±	0.01	0.02	±	0.00	0.02	±	0.00	0.03	±	0.02
Σω-3 DiHFA (LOX origin)	0.00	±	0.00	0.00	±	0.00	0.00	±	0.00	0.04	±	0.01	0.00	±	0.00	0.00	±	0.00	0.02	±	0.01	0.00	±	0.00
Σ Total DiHFA (LOX origin)	0.02	±	0.01	0.02	±	0.01	0.05	±	0.01	0.10	±	0.02	0.08	±	0.01	0.02	±	0.01	0.04	±	0.01	0.03	±	0.02
Σ Total Lipoxin	0.00	\pm	0.00	0.00	±	0.00	0.01	±	0.01	0.04	±	0.01	0.00	\pm	0.00	0.00	\pm	0.00	0.01	\pm	0.01	0.02	\pm	0.02
Σ Resolvin (EPA origin)	0.03	±	0.01	0.01	±	0.01	0.04	±	0.00	0.04	±	0.00	0.03	±	0.00	0.02	±	0.00	0.05	±	0.02	0.03	±	0.02
Σ Resolvin (DHA origin)	0.11	±	0.06	0.06	±	0.00	0.16	±	0.01	0.11	±	0.02	0.23	±	0.03	0.14	±	0.02	0.26	±	0.05	0.31	±	0.05
Σ Total Resolvin	0.14	±	0.07	0.08	±	0.01	0.20	±	0.01	0.16	±	0.01	0.26	±	0.03	0.17	±	0.03	0.31	±	0.06	0.33	±	0.06
Σ Maresin (ω-3 DPA origin)	0.15	±	0.01	0.00	±	0.00	0.22	±	0.01	0.22	±	0.02	0.55	±	0.03	0.41	±	0.04	0.72	±	0.06	0.56	±	0.07
Σ Maresin (DHA origin)	0.00	±	0.00	0.00	±	0.00	0.01	±	0.01	0.00	±	0.00	0.00	±	0.00	0.00	±	0.00	0.00	±	0.00	0.00	±	0.00
Σ Total Maresin	0.15	±	0.01	0.00	±	0.00	0.24	±	0.02	0.22	±	0.02	0.55	±	0.03	0.41	±	0.04	0.72	±	0.06	0.56	±	0.07
Σ Protectin (ω-3 DPA origin)	0.00	±	0.00	0.00	±	0.00	0.00	±	0.00	0.00	±	0.00	0.00	±	0.00	0.00	±	0.00	0.00	±	0.00	0.00	±	0.00
Σ Protectin (DHA origin)	0.03	±	0.02	0.00	±	0.00	0.00	±	0.00	0.01	±	0.01	0.02	±	0.02	0.00	±	0.00	0.01	±	0.01	0.12	±	0.12
Σ Total Protectin	0.03	±	0.02	0.00	±	0.00	0.00	±	0.00	0.01	±	0.01	0.02	±	0.02	0.00	±	0.00	0.01	±	0.01	0.12	±	0.12

Table 4.2 (cont'd)

Data are presented in units of pmol/culture as mean \pm SEM. 18:2 ω 6, linoleic acid; 18:3 ω 3, α -linolenic acid; 20:2 ω 6, eicosadienoic acid; 20:3 ω 6, linoleic acid; dihomo- γ -linolenic acid; 20:4 ω 6, arachidonic acid; 20:5 ω 3, eicosapentaenoic acid; 22:5 ω 3, docosapentaenoic acid; 22:6 ω 3, docosahexaenoic acid; EpFA, epoxy fatty acid; DiHFA, dihydroxy fatty acid; CYP450, cytochrome P450 monooxygenase; HFA, hydroxy fatty acid; oxo-FA, oxo fatty acid; ARA, arachidonic acid; EPA, eicosapentaenoic acid; DPA, docosapentaenoic acid; DHA, docosahexaenoic acid.

Table 4.3. Summarized oxylipin data at t = 6 h.

	VEH/VEH	LPS/VEH	VEH/cSiO ₂	LPS/cSiO ₂	DHA- VEH/VEH	DHA- LPS/VEH	DHA- VEH/cSiO ₂	DHA- LPS/cSiO ₂
Σ 18:2ω6	11.99 ± 1.87	177.51 ± 85.19	48.76 ± 23.73	21.65 ± 1.83	9.73 ± 2.56	25.77 ± 2.71	59.23 ± 20.61	39.37 ± 11.61
Σ 18:3ω3	0.16 ± 0.11	1.86 ± 1.78	0.97 ± 0.17	0.99 ± 0.12	0.11 ± 0.07	0.29 ± 0.14	1.03 ± 0.36	0.35 \pm 0.30
Σ 20:2ω6	0.00 \pm 0.00	0.00 ± 0.00	0.43 ± 0.04	0.50 ± 0.07	0.02 ± 0.01	0.02 \pm 0.02	0.35 ± 0.03	0.30 ± 0.01
Σ 20:3ω6	0.53 ± 0.13	0.77 ± 0.10	9.04 ± 0.46	10.70 ± 0.06	0.71 ± 0.06	0.80 ± 0.08	6.84 ± 0.32	5.25 ± 0.39
Σ 20:4ω6	19.38 ± 4.42	30.37 ± 14.59	559.57 ± 7.73	680.84 ± 3.00	20.37 ± 0.67	29.77 ± 2.99	364.44 ± 10.83	352.40 ± 9.73
Σ 20:5ω3	6.27 ± 0.58	10.90 ± 1.57	16.83 ± 0.32	17.36 ± 0.20	16.23 ± 0.39	12.36 ± 1.10	34.61 ± 0.61	30.24 ± 1.88
Σ 22:5ω3	0.22 ± 0.04	0.22 ± 0.04	0.31 ± 0.01	0.28 ± 0.01	0.99 ± 0.07	0.45 ± 0.09	0.83 ± 0.03	0.89 ± 0.01
Σ 22:6ω3	5.37 ± 0.51	25.33 ± 9.81	27.20 ± 1.06	26.42 ± 0.34	51.33 ± 5.13	45.04 ± 2.93	181.21 ± 5.82	156.41 ± 5.67
Σ Total ω-6	31.90 ± 3.98	208.64 ± 71.33	617.79 ± 22.68	713.69 ± 1.54	30.83 ± 2.64	56.35 ± 4.94	430.86 ± 29.19	397.33 ± 16.34
Σ Total ω-3	12.02 ± 1.07	38.31 ± 11.79	45.30 ± 1.04	45.05 ± 0.39	68.65 ± 5.26	58.14 ± 2.03	217.68 ± 5.39	187.89 ± 7.58
Σ ω-6 ΕρΓΑ	0.39 ± 0.01	1.86 ± 0.75	2.36 ± 0.41	1.86 ± 0.23	0.34 ± 0.06	0.89 ± 0.22	1.92 ± 0.46	1.89 ± 0.30
Σ ω-3 ΕρΓΑ	0.22 ± 0.03	1.20 ± 0.35	1.12 ± 0.03	1.02 ± 0.01	2.85 ± 0.24	1.56 ± 0.17	4.52 ± 0.11	4.31 ± 0.29
Σ Total EpFA	0.61 ± 0.03	3.05 ± 1.10	3.49 ± 0.44	2.88 ± 0.23	3.18 ± 0.30	2.45 ± 0.39	6.44 ± 0.36	6.20 ± 0.57
Σ ω-6 DiHFA (CYP450 origin)	1.60 ± 0.17	2.62 ± 1.23	2.69 ± 0.25	2.57 ± 0.07	1.31 ± 0.08	1.02 ± 0.13	1.83 ± 0.22	1.66 ± 0.29
Σ ω-3 DiHFA (CYP450 origin)	1.71 ± 0.17	3.31 ± 1.43	3.07 ± 0.48	2.61 ± 0.06	1.40 ± 0.10	1.28 ± 0.27	2.54 ± 0.28	2.01 ± 0.22
Σ Total DiHFA (CYP450 origin)	2.14 ± 0.21	2.69 ± 0.86	3.50 ± 0.22	3.10 ± 0.11	7.97 ± 0.20	1.96 ± 0.13	5.26 ± 0.11	4.64 ± 0.61
EpFA:DiHFA ratio	0.22 ± 0.02	1.55 ± 0.66	0.77 ± 0.08	0.70 ± 0.05	0.26 ± 0.02	0.86 ± 0.10	0.86 ± 0.10	0.94 ± 0.04
Σ ω-6 Prostaglandin	4.43 ± 1.53	11.16 ± 5.08	79.88 ± 1.39	101.69 ± 4.34	3.16 ± 0.24	9.76 ± 0.46	43.81 ± 0.63	49.79 ± 2.11
Σω-3 Prostaglandin	0.00 \pm 0.00	0.03 ± 0.03	0.18 ± 0.02	0.19 ± 0.01	0.00 ± 0.00	0.06 ± 0.01	0.33 ± 0.00	0.28 \pm 0.01
Σ Total Prostaglandin	4.43 ± 1.53	11.19 ± 5.12	80.06 ± 1.41	101.88 ± 4.35	3.16 ± 0.24	9.82 ± 0.47	44.14 ± 0.63	50.07 ± 2.12
Σω-6 Leukotriene	0.02 ± 0.02	0.00 \pm 0.00	0.60 \pm 0.03	1.77 ± 0.14	0.00 \pm 0.00	0.01 \pm 0.01	0.27 \pm 0.02	0.49 \pm 0.07
Σω-3 Leukotriene	0.01 \pm 0.00	0.00 ± 0.00	0.00 \pm 0.00	0.01 \pm 0.01	0.00 ± 0.00	0.00 \pm 0.00	0.00 \pm 0.00	0.00 ± 0.00
Σ Total Leukotriene	0.02 ± 0.02	0.00 ± 0.00	0.60 ± 0.03	1.78 ± 0.13	0.00 ± 0.00	0.01 ± 0.01	0.27 ± 0.02	0.49 ± 0.07
Σω-6 Thromboxane	1.10 ± 0.27	3.63 ± 2.79	32.15 ± 1.95	42.75 ± 1.77	0.69 ± 0.07	3.62 ± 0.19	15.81 ± 0.79	20.50 ± 3.23

Table 4.3 (cont'd)

Σω-3 Thromboxane	0.00	±	0.00	0.03	±	0.03	0.13	±	0.01	0.07	±	0.03	0.00	±	0.00	0.05	±	0.00	0.14	±	0.02	0.15	±	0.02
Σ Total Thromboxane	1.10	±	0.27	3.66	±	2.82	32.28	±	1.94	42.81	±	1.79	0.69	±	0.07	3.66	±	0.19	15.95	±	0.80	20.65	±	3.25
Σ ω-6 HFA	21.14	\pm	2.14	162.03	±	65.44	480.29	±	13.68	552.36	\pm	3.75	22.55	±	2.32	32.16	±	4.16	346.54	±	20.56	308.13	±	16.22
Σ ω-3 HFA	10.70	±	0.96	33.91	±	10.57	42.70	±	1.15	42.76	±	0.40	57.61	±	5.04	54.25	±	2.14	207.63	±	5.55	178.59	±	6.84
Σ HFA (ARA origin)	12.45	±	2.40	14.16	±	6.91	438.46	±	7.15	525.66	±	2.46	15.39	±	0.76	16.30	±	2.38	299.62	±	9.34	275.86	±	11.08
Σ HFA (EPA origin)	6.08	±	0.55	9.34	±	0.88	15.74	±	0.39	16.38	±	0.21	15.31	±	0.34	11.70	±	1.07	32.82	±	0.57	28.69	±	1.72
Σ HFA (DHA origin)	4.46	±	0.47	22.71	±	9.26	25.99	±	1.09	25.38	±	0.38	42.19	±	4.86	42.27	±	3.03	173.78	±	5.95	149.57	±	5.09
Σ Total HFA	31.84	±	2.93	195.93	±	75.11	522.99	±	13.36	595.11	±	4.09	80.16	±	7.16	86.41	±	2.11	554.17	±	25.86	486.72	±	22.94
Σ Total Oxo-FA	3.30	±	0.61	28.18	±	12.24	19.42	±	9.18	10.52	±	0.77	2.88	±	0.57	9.38	±	2.32	20.92	±	8.24	15.12	±	3.81
Σ ω-6 DiHFA (LOX origin)	0.04	±	0.02	1.01	±	1.00	0.09	±	0.02	0.06	±	0.01	0.08	±	0.04	0.02	±	0.01	0.05	±	0.01	0.03	±	0.01
Σω-3 DiHFA (LOX origin)	0.01	±	0.01	0.00	±	0.00	0.03	±	0.01	0.02	±	0.01	0.01	±	0.01	0.00	±	0.00	0.00	±	0.00	0.01	±	0.01
Σ Total DiHFA (LOX origin)	0.05	±	0.03	1.01	±	1.00	0.12	±	0.03	0.08	±	0.02	0.09	±	0.04	0.02	±	0.01	0.05	±	0.01	0.04	±	0.02
Σ Total Lipoxin	0.02	\pm	0.01	0.00	\pm	0.00	0.09	\pm	0.01	0.08	\pm	0.02	0.01	\pm	0.01	0.00	\pm	0.00	0.04	\pm	0.00	0.04	\pm	0.02
Σ Resolvin (EPA origin)	0.06	±	0.00	0.02	±	0.01	0.06	±	0.00	0.05	±	0.00	0.03	±	0.00	0.02	±	0.00	0.11	±	0.01	0.05	±	0.03
Σ Resolvin (DHA origin)	0.13	±	0.02	1.01	±	0.89	0.19	±	0.02	0.17	±	0.04	0.32	±	0.02	0.27	±	0.03	0.34	±	0.02	0.26	±	0.05
Σ Total Resolvin	0.18	\pm	0.02	1.03	±	0.89	0.25	±	0.02	0.22	\pm	0.04	0.35	±	0.02	0.29	±	0.03	0.45	±	0.01	0.31	±	0.07
Σ Maresin (ω-3 DPA origin)	0.22	±	0.04	0.22	±	0.04	0.31	±	0.01	0.28	±	0.01	0.99	±	0.07	0.45	±	0.09	0.83	±	0.03	0.89	±	0.01
Σ Maresin (DHA origin)	0.00	±	0.00	0.00	±	0.00	0.00	±	0.00	0.00	±	0.00	0.00	±	0.00	0.00	±	0.00	0.00	±	0.00	0.00	±	0.00
Σ Total Maresin	0.22	±	0.04	0.22	±	0.04	0.31	±	0.01	0.28	±	0.01	0.99	±	0.07	0.45	±	0.09	0.83	±	0.03	0.89	±	0.01
Σ Protectin (ω-3 DPA origin)	0.00	±	0.00	0.00	±	0.00	0.00	±	0.00	0.00	±	0.00	0.00	±	0.00	0.00	±	0.00	0.00	±	0.00	0.00	±	0.00
Σ Protectin (DHA origin)	0.00	±	0.00	0.00	±	0.00	0.00	±	0.00	0.00	±	0.00	0.01	±	0.01	0.04	±	0.01	0.01	±	0.01	0.03	±	0.02
Σ Total Protectin	0.00	±	0.00	0.00	±	0.00	0.00	±	0.00	0.00	±	0.00	0.01	±	0.01	0.04	±	0.01	0.01	±	0.01	0.03	±	0.02

Table 4.3 (cont'd)

Data are presented in units of pmol/culture as mean \pm SEM. 18:2 ω 6, linoleic acid; 18:3 ω 3, α -linolenic acid; 20:2 ω 6, eicosadienoic acid; 20:3 ω 6, linoleic acid; dihomo- γ -linolenic acid; 20:4 ω 6, arachidonic acid; 20:5 ω 3, eicosapentaenoic acid; 22:5 ω 3, docosapentaenoic acid; 22:6 ω 3, docosahexaenoic acid; EpFA, epoxy fatty acid; DiHFA, dihydroxy fatty acid; CYP450, cytochrome P450 monooxygenase; HFA, hydroxy fatty acid; oxo-FA, oxo fatty acid; ARA, arachidonic acid; EPA, eicosapentaenoic acid; DPA, docosapentaenoic acid; DHA, docosahexaenoic acid.

CHAPTER 5: SOLUBLE EPOXIDE HYDROLASE INHIBITOR TPPU SUPPRESSES PULMONARY INFLAMMATORY CELL INFILTRATION BUT DOES NOT PREVENT LUNG PATHOLOGY OR EARLY AUTOIMMUNITY IN LUPUS-PRONE MICE ACUTELY EXPOSED TO CRYSTALLINE SILICA

PUBLICATION NOTICE

The following chapter is currently in preparation to be submitted to *Scientific Reports*. Authors of this work are: Olivia K Favor^{1,2}, James G Wagner^{2,3}, Ryan P Lewandowski³, Lauren K Heine^{1,2}, Jack R Harkema^{1,2,3}, James J Pestka^{2,4,5}, and Kin Sing Stephen Lee^{1,2,6}. ¹Indicates contributors from the Department of Pharmacology and Toxicology, College of Osteopathic Medicine, Michigan State University. ²Indicates contributors from the Institute for Integrative Toxicology, Michigan State University. ³Indicates contributors from the Department of Pathobiology and Diagnostic Investigation, Michigan State University. ⁴Indicates contributors from the Department of Food Science and Human Nutrition, Michigan State University. ⁵Indicates contributors from the Department of Microbiology and Molecular Genetics, Michigan State University. ⁶Indicates contributors from the Department of Chemistry, Michigan State University.

ABSTRACT

Exposure to respirable crystalline silica (cSiO₂) in the workplace is a trigger of lupus, a debilitating autoimmune disease hallmarked by systemic tissue damage and multiorgan comorbidities. cSiO₂-triggered lupus flaring can be modeled in autoimmune-prone NZBWF1 mice, where the particle induces unresolvable lung inflammation, systemic autoimmunity, and glomerulonephritis. One promising approach for ameliorating environmentally-triggered autoimmunity is employing small-molecule inhibitors of soluble epoxide hydrolase (sEH), which prevent degradative hydrolysis of highly pro-resolving, endogenous epoxy fatty acids. Notably, the sEH inhibitor (sEHI) TPPU has been shown to limit toxicant-triggered pathology and autoimmunity in mice and is currently in human clinical trials for several inflammatory and systemic metabolic diseases. In the present study, we tested the hypothesis that sEH inhibition impedes cSiO₂-triggered inflammation and loss of immunological tolerance in the lungs of female lupus-prone NZBWF1 mice. Mice aged 6 wk were fed control or TPPU-amended diets, intranasally instilled once with 2.5 mg cSiO₂ at age 8 wk, then terminated at 7d post-cSiO₂ instillation (PI) and 28d PI. At 7d PI, cSiO₂ elicited robust infiltration of CD206⁺ monocytes and Ly6B.2⁺ neutrophils into the centriacinar region of the lung, as well as marked centriacinar inflammation and fibrosis. Targeted gene expression and multiplex protein analyses and multiplex analyses revealed that cSiO₂ upregulated proinflammatory cytokines, chemokines, and type I IFN proteins at both timepoints. At 28d PI, cSiO₂ promoted moderate development of centriacinar lymphoid tissue and recruitment of CD3⁺ T lymphocytes and CD45R⁺ B lymphocytes into the lung while monocyte numbers and neutrophil numbers in the BALF and lung tissue approached control levels. In accordance with lymphoid tissue development, antinuclear AAb titers were increased in the BALF and plasma of cSiO₂-exposed mice at 28d PI. Dietary TPPU significantly decreased

infiltration of monocytes (7d PI, 28d PI), neutrophils (7d PI, 28d PI), and lymphocytes (7d PI) in the BALF but did not significantly impact other analyzed biomarkers of cSiO₂-induced lung inflammation and autoimmunity in this preclinical model. Together, our results suggest that while sEH suppressed leukocyte infiltration into the alveolar space, it was insufficient to prevent cSiO₂-triggered inflammation in the lung and autoimmune onset.

INTRODUCTION

Systemic lupus erythematosus (lupus) is a debilitating autoimmune disease that afflicts more than 3 million people worldwide, with the highest prevalence in non-Caucasian women of childbearing age [360]. Common hallmarks of lupus pathogenesis include genetically-driven inflammatory tissue damage, accumulation of cellular corpses, release of autoantigens (AAgs) that hyperactivate T and B lymphocytes, and production of autoantibodies (AAbs) that form circulating immune complexes with their corresponding AAgs [361, 362]. Immune complex deposition in peripheral organs triggers complement activation, innate immune cell recruitment, and secretion of proinflammatory cytokines and chemokines, contributing to a positive feedback loop of cell death, unresolved inflammation, AAb production, and irreparable tissue damage [363, 364]. Over time, deposition of immune complexes in the kidney can cause development of glomerulonephritis and further progression to end-stage kidney disease in lupus patients.

Currently, lupus has no known cure, but a variety of pharmaceuticals including corticosteroids (e.g., prednisone, methylprednisolone), immunosuppressants (e.g., mycophenolate mofetil, azathioprine), and biologicals (e.g., anifrolumab-fnia, belimumab) are used to reduce episodic disease flaring and mortality in individuals with persistent lupus [11, 569-571]. While these mainstay medications have efficacy against lupus flaring, they can further burden individuals with adverse side effects and/or steep financial costs. Long-term use of corticosteroids can lead to

weight gain, osteoporosis, and type 2 diabetes, whereas immunosuppressants and monoclonal antibodies can contribute to insomnia, increased bacterial infections, and heightened risk of shingles [572-575]. In addition, the direct costs of lupus (i.e., disease prevention, diagnosis, treatment) can reach \$70,000 per year per patient while the indirect costs of lupus (i.e., loss of productivity at work and home, decreased quality of life) can exceed \$20,000 per patient per year [15]. Current treatment regimens are further complicated by a high degree of genotypical and phenotypical heterogeneity between lupus-afflicted individuals [576, 577]. There is, therefore, a critical need for safer, less expensive interventions to prevent the initial onset of lupus and ameliorate flaring of lupus symptoms.

Although genetic predispositions play a significant role in the initiation and progression of lupus, environmental factors can hasten or delay the onset of genetically-driven autoimmunity [3, 578]. Occupational exposure to the respirable toxicant crystalline silica (cSiO₂) has been etiologically linked to lupus, other rheumatic autoimmune diseases, silicosis, chronic obstructive pulmonary disease (COPD), pulmonary fibrosis, and lung cancer [331, 471, 474]. The highest levels of cSiO₂ exposure occur in dusty trades including mining, construction, ceramics, and dentistry work [579-581]. In female autoimmune-prone NZBWF1 mice, a preclinical model of lupus, we have demonstrated that 4 weekly intranasal instillations with 1 mg cSiO₂, modeling one half of human lifetime exposure at the exposure limit recommended by NIOSH, potentiates development of ectopic lymphoid tissue (ELT) in the lung, elevated AAb titers and AAgs in the plasma, and hastened onset of glomerulonephritis 12 wk after the final cSiO₂ instillation [20, 318, 352]. In the lung, repeated intranasal doses of cSiO₂ trigger upregulation of proinflammatory mediators (i.e., cytokines, chemokines, interferons, adhesion molecules) and genes involved with innate and adaptive immune cell function in as little as 1 wk post-instillation (PI) with further

upregulation up to 13 wk PI, suggesting that the lung serves as a nexus for cSiO₂-triggered autoimmunity and glomerulonephritis [582].

To better model immediate and short-term effects of cSiO₂ on inflammation and autoimmunity, we recently showed assessed the effects of a singular intranasal dose of 2.5 mg cSiO₂ in female NZBWF1 mice on cellular, histopathological, transcriptomic, and protein biomarkers from 1 to 28 d PI. We found in this acute model of cSiO₂-triggered autoimmune flaring that the particle evokes robust inflammation in the lung by 7 d PI, characterized by i) alveolar infiltration of macrophages, neutrophils, and lymphocytes, ii) cell death and release of cellular dsDNA, iii) upregulation of proinflammatory cytokines, chemokines, and type I interferon (IFN)-regulated genes, and iv) secretion of proinflammatory cytokines and chemokines. Further apparent was the development of T and B lymphocyte-containing ELS in the lung beginning at 21 d PI, indicative of early development of cSiO₂-induced autoimmunity [583]. Taken together, this new model can potentially provide valuable insight into early mechanisms by which cSiO₂ triggers autoimmune flaring in the lung and offers the opportunity for preclinical evaluation of potential interventions against environmentally-driven lupus.

While environmental toxicants such as $cSiO_2$ can potentiate the development of autoimmunity, other environmental factors such as dietary polyunsaturated fatty acids (PUFAs) can also influence disease onset. In the United States, daily intake of ω -6 PUFAs exceeds that of ω -3 PUFAs at a ω -6/ ω -3 ratio of 20:1 and is associated with increased risk of inflammatory and autoimmune diseases [584-586]. When consumed, ω -3/6 PUFAs are incorporated into cell membrane phospholipids and impact membrane fluidly, lipid raft formation, and downstream cellular signaling. In addition, cell membrane PUFAs serve as substrates for potent proinflammatory and pro-resolving lipid mediators. One of the most important cell membrane

PUFAs in inflammatory signaling is arachidonic acid (C20:4, ω-6, ARA), which is metabolized from dietary linoleic acid (C18:2, ω-6, LA) through a series of desaturation and elongation reactions [586]. Phospholipase A2 (PLA2), when activated by an inflammatory stimulus, cleaves ARA from the sn-2 position of phospholipids. Resultant non-esterified ARA can be shunted into one of three major eicosanoid biosynthesis pathways: 1) the cyclooxygenase (COX) pathway which converts ARA into prostaglandins and thromboxanes; 2) the lipoxygenase (LOX) pathway which converts ARA into leukotrienes, hydroxyeicosatetraenoic acids (HETEs), and lipoxins; and 3) the cytochrome P450 (CYP450) pathway which converts ARA into HETEs and epoxyeicosatrienoic acids (EpETrEs). Generally, prostaglandins, thromboxanes, leukotrienes, and HETEs are considered proinflammatory, whereas lipoxins and EpETrEs are considered proresolving [587]. Although little is known about the lipid metabolite profile of lupus patients, it has been previously reported that patients with lupus exhibit elevated erythrocyte/serum ω-6 PUFAs (i.e., LA and ARA), which correlated with plasma antinuclear AAb titers and dsDNA [588, 589]. Accordingly, the proinflammatory lipid metabolite profile that may contribute to lupus disease activity, as is the case with rheumatoid arthritis patients [590].

One possible intervention for delaying the development and progression of environmentally-triggered lupus flaring is pharmacological modification of the endogenous lipidome. Soluble epoxide hydrolase (sEH) is a promising drug target because it converts highly pro-resolving CYP450-derived epoxy fatty acids (EpFAs) (e.g., EpETrEs) to less pro-resolving or more proinflammatory dihydroxy fatty acids (DiHFAs) (e.g., DiHETrEs) [591, 592]. In preclinical rodent studies, the sEH inhibitor (sEHI) 1-(4-trifluoro-methoxy-phenyl)-3-(1-propionylpiperidin-4-yl) urea (TPPU) has been reported to ameliorate ongoing inflammation and fibrosis in multiple organs including the lung and kidney [593, 594], autoimmune encephalitis [396], autoimmune

lupus nephritis [23], and rheumatoid arthritis [397]. TPPU has an excellent pharmacological profile characterized by high systemic distribution, affinity for sEH, and biological potency and minimal non-specific binding and adverse side-effects [391, 393, 394, 470]. Recently, we have demonstrated that oral administration of TPPU in experimental rodent diet shifts the plasma epoxide/diol metabolite ratio toward EpFAs at the expense of DiHFAs, and, furthermore, TPPU ameliorates lipopolysaccharide (LPS)-accelerated glomerulonephritis in female NZBWF1 mice [595] Thus, TPPU may be efficacious in ameliorating lupus symptoms and comorbidities triggered by environmental agents.

The objective of this study was to test the hypothesis that sEH inhibition by TPPU prevents early cSiO₂-induced lung inflammation and autoimmunity in lupus-prone mice. Cohorts of female lupus-prone NZBWF1 mice were fed either control diet or experimental diet supplemented with the sEH inhibitor TPPU (22.5 mg/kg diet) at 6 wk of age, given one intranasal instillation of 2.5 mg cSiO₂ at 8 wk of age, then sacrificed at either 7 d PI or 28 d PI. We found that, while TPPU dampened cSiO₂-induced leukocyte infiltration in the lung, it did not influence pulmonary histopathology, expression and production of proinflammatory proteins in lung tissue, or secretion of autoantibodies in BALF or plasma.

MATERIALS AND METHODS

Key reagents

All key reagents used in this study and their corresponding catalog numbers are summarized in **Table S5.1**.

Animals

All experimental protocols were approved by the Institutional Animal Care and Use Committee (Animal Use Form [AUF] #202100252) at Michigan State University (MSU) in

accordance with guidelines established by the National Institutes of Health. Female lupus-prone NZBWF1 mice (cat. #100008) aged 6 wk were procured from the Jackson Laboratory (Bar Harbor, ME) and randomized into experimental groups (Table 1). Female NZBWF1 mice were used because they express genetic loci that contribute to increased autoreactive T and B cell numbers, elevated B cell hyperactivity, and reduced T cell death [339]. These aberrations ultimately culminate in elevated antinuclear AAb titers, loss of immunological self-tolerance, and spontaneous development of systemic autoimmune disease that is strikingly similar to lupus in humans [339, 596]. Mice were housed 4 per cage and given free access to drinking water and either control (CON) American Institute of Nutrition (AIN)-93G diet (Dyets Inc., Bethlehem, PA) or TPPU-amended AIN-93G diet for the entirety of the study. Animal facilities were maintained under controlled conditions (lighting: 12 h light/dark cycle; temperature: 21-24 °C; humidity: 40-55%). Mice were given 2 wk to acclimate before experiments began (Figure 5.1).

Diets

Two experimental diets were prepared using a modification of AIN-93G diet containing 70 g/kg fat as a base to provide optimal nutrition to experimental rodents [412]. Both CON and TPPU diet contained 60 g/kg high-oleic safflower oil (Hain Pure Food, Boulder, CO) and 10 g/kg corn oil as sources of essential ω -9 and ω -6 fatty acids, respectively. For TPPU diet, 22.5 mg TPPU, synthesized by Dr. Kin Sing Stephen Lee at Michigan State University (East Lansing, MI) [391], was thoroughly mixed into 1 kg of prepared CON diet. To prevent lipid oxidation, experimental diets were prepared biweekly and stored at -20 °C until administered to mice. Fresh diet was given to mice every day. Diet formulations are recorded in **Table 5.2**.

Intranasal cSiO₂ instillation

At 8 wk of age, mice were intranasally instilled once with 2.5 mg cSiO₂ as described previously [583]. Briefly, acid-washed, oven dried cSiO₂ particles (Min-U-Sil® 5, average particle size: 1.5-2.0 µm, Pennsylvania Sand Glass Corporation, Pittsburgh, PA, US) were suspended in sterile phosphate buffered saline (PBS; Millipore Sigma) at a final concentration of 100 mg/ml prior to use. Before intranasal instillation, fresh stock suspensions were sonicated and vortexed vigorously for 1 min. Mice were anesthetized by inhalation with isoflurane (4% in O_2), held in the supine position, and intranasally instilled once with either 2.5 mg cSiO₂ suspended in 25 µl PBS or 25 µl PBS vehicle (VEH). This cSiO₂ dose was chosen because it has been widely used in silicosis studies [597-600], and it allometrically reflects 30 percent of lifetime human occupational exposure to respirable cSiO₂ at the permissible exposure limit (PEL) of 50 μg/m³/d defined by the U.S. Occupational Safety and Health Administration [601]. Mice were held in the same position for a few seconds after instillation to ensure adequate distribution throughout the respiratory tract, then mice were returned to their cages and monitored for signs of distress. No injury or death resulted from the procedure. Cohorts of VEH- and cSiO₂-instilled mice (3 groups, n = 8/group) were terminated at 7d and 28d PI. These endpoints were selected because acute cSiO₂ instillation was previously found to elicit robust pulmonary leukocyte recruitment, chemokine and interferonregulated gene expression, cell death, and AAb secretion at both 7d and 28d PI [583].

Tissue collection and processing

Mice were euthanized by intraperitoneal injection of 56 mg/kg body weight sodium pentobarbital and subsequent abdominal aortic exsanguination. Blood was immediately collected with heparin-coated syringes and centrifuged at 3500 x g for 10 min at 4 °C to isolate plasma. An antioxidant cocktail (0.2 mg/ml butylated hydroxytoluene, 0.2 mg/m triphenylphosphine, 0.6

mg/ml EDTA) [414] was prepared in-house and added at a 5% (v/v) concentration to all plasma aliquots designated for LC-MS/MS analysis. All plasma samples were stored at -80 °C as single-use aliquots for downstream analyses. After blood collection, the trachea was exposed and cannulated, and the lungs and heart were collected *en bloc*. Isolated lungs were flushed twice with 0.8 ml of sterile PBS through the cannulated trachea to recover bronchoalveolar lavage fluid (BALF), and BALF fractions were combined for downstream analyses. The cranial, middle, and accessory lobes were removed, snap-frozen in liquid nitrogen, and stored at -20 °C. The caudal lobe was stored in RNAlater (Thermo Fisher Scientific, Waltham, MA) overnight at 4 °C then stored at -80 °C for RNA analysis. The left lung lobe was then intratracheally fixed with 10% (v/v) neutral-buffered formalin (Fisher Scientific, Pittsburgh, PA) at a constant pressure (30 cm H₂O) for 1 h and subsequently immersed and stored in a large volume of 10% formalin for 24 h. All fixed tissues were transferred to 30% (v/v) ethanol for long-term storage and histological preparation.

BALF inflammatory cell quantitation

Total cells in BALF were determined by counting intact cells with a standard hemocytometer. Cytological slides were prepared by centrifuging 150 µl of BALF from each mouse onto microscopic slides at 600 x g for 10 min using a Shandon Cytospin 3 (Shandon Scientific, PA), drying overnight at 25 °C, and staining with Diff-Quick (Thermo Fisher Scientific, Waltham, MA). Differential counts of monocytes/macrophages, neutrophils, and lymphocytes were determined by assessing morphological criteria of 200 counted cells on each slide.

Lung histopathology, immunofluorescence, and birefringent imaging

Formalin-fixed left lung lobes were cut into 5 μm sections, embedded in paraffin, then deparaffinized and stained with hematoxylin and eosin (H&E) or Masson's trichrome at the MSU

Investigative Histopathology Laboratory. Lung tissues stained with H&E were microscopically imaged and semi-quantitatively graded in a blinded manner by a board-certified veterinary pathologist for the following lung lesions: (a) presence of centriacinar inflammation, (b) presence of centriacinar fibrosis, and (c) presence of perivascular lymphoid cells. Each lung was assigned one of the following semi-quantitative scores for overall histopathology and collagen deposition: (0) no changes compared to control mice, (1) minimal (<10% of total area affected); (2) slight (10-25% of total area affected), (3) moderate (26-50% change affected), (4) severe (51-75% of total area affected), or (5) very severe (>75% of total area affected).

Immunohistochemical identification of neutrophils, monocytes, B lymphocytes, and T lymphocytes in the lung was performed as previously described [318]. Briefly, H&E-stained lung sections were stained with mouse-specific anti-Ly6B.2 monoclonal antibody (BioRad, Hercules, CA) for neutrophil detection, anti-CD206 polyclonal antibody (Abcam, Cambridge, MA) for monocyte detection, anti-CD45R monoclonal antibody (Becton Dickinson, Franklin Lakes, NJ) for B lymphocyte detection, or anti-CD3 polyclonal antibody (Abcam) for T lymphocyte detection. Slides were scanned with an Olympus VS200 virtual slide scanner (Evident Scientific & Olympus VS200, Waltham, MA). Semi-quantitative scores for neutrophil, macrophage, and lymphocyte infiltration in the lung were assigned using the following scale: (0) no changes compared to VEH/CON mice, (1) minimal (<10% affected), (2) mild (11-25% affected), (3) moderate (26-50% affected), (4) marked (51-75% affected), (5) severe (76-100% affected).

Birefringent imaging was conducted to visualize cSiO₂ particle deposition in the lung. H&E-stained lung tissues were scanned with an Olympus Slideview VS200 virtual slide scanner (Olympus) equipped with a UPLXAPO 20X objective lens (Olympus) and a VS-264C RGB camera (IDS Imaging Development Systems Inc., Stoneham, MA). Exposure time was set to 75

ms, and focal points were set to extra high. A randomly selected slide from the VEH/CON group was used to calibrate shading correction and white balance prior to all birefringent imaging, and a randomly selected slide from the cSiO₂/CON group was used to calibrate and re-zero the polarization angle before scanning each experimental group.

Expression of inflammatory cytokine, chemokine, and type I interferon-regulated genes in the lung

Total RNA from the lung was extracted using TissueLyser II (Qiagen, Germantown, MD) and a RNeasy Mini Kit (Qiagen) according to the manufacturer's instructions. Isolated RNA was reconstituted in RNase-free water and quantified using a Nanodrop ND-1000 spectrophotometer (Thermo Fisher Scientific, Waltham, MA). RNA was reverse transcribed at a concentration of 100 ng/μl using a High-Capacity cDNA Reverse Transcriptase Kit (Thermo Fisher Scientific, Waltham, MA). Taqman assays for proinflammatory cytokines (*Il1a, Il1b, Il2, Il6, Tnf*), chemokines (*Ccl2, Ccl7, Ccl8, Cscl1, Cxcl5, Cxcl9, Cxcl10*), type I interferon-related genes (*Mx1, Oas1a, Oas1b, Oas2, Irf7, Isg15, Ifi44, Zbp1, Ifit1, Rsad2, Siglec1, Psmb8*), and endogenous housekeeping genes (*Actb, Gapd, Hprt*) were run with technical triplicates using a Smart Chip Real-Time PCR System at the MSU Genomics Core. Expression levels of selected genes of interest were normalized to the housekeeping genes and reported as fold-change compared to the VEH/CON group using the 2^{-ΔΔCT} method [602].

Profiling of proinflammatory cytokines and chemokines in the lung

Lung tissues were weighed and homogenized in RIPA Lysis and Extraction Buffer (Thermo Fisher Scientific) using TissueLyser II (Qiagen, Germantown, MD) to yield 20% homogenate in buffer (w/v). Total protein in each sample was quantified using a Pierce[™] BCA Protein Assay Kit (Thermo Fisher Scientific) and sample absorbances measured using a FilterMax F3 Multimode plate reader (Molecular Devices, San Jose, CA) set to a wavelength of 562 nm.

Samples were normalized to a total protein concentration of 1000 µg/ml by adding the appropriate volume of RIPA buffer. Then, 100-µl sample aliquots were shipped to Eve Technologies (Calgary, Alberta, Canada) for quantification of homogenate cytokines and chemokines using Mouse Cytokine/Chemokine 44-Plex Discovery Assay® Array. Resultant cytokine and chemokine levels were normalized to the original weight of lung tissue homogenized per animal and reported in units of pg/g lung tissue.

Quantification of IgG AAbs in BALF and plasma

Apoptotic cell (AC)-derived material was generated for solid-phase in an indirect enzyme-linked immunosorbent assay (ELISA) as previously described [603]. Briefly, RAW 264.7 murine macrophage cells were cultured in 100 mm cell culture dishes in RPMI 1640 medium containing 10% fetal bovine serum (FBS) and 1% penicillin-streptomycin (P/S). They were harvested by centrifugation at 500 ×g for 5 min and then resuspended to a final density of 1×10⁷ cells/ml in serum-deprived RPMI 1640 medium containing 1% P/S then treated with 1 μM staurosporine (R&D Systems) to induce apoptosis. Cells were placed in a 37 °C incubator (5% CO₂) for 24 h, then the supernatant was collected, centrifuged at 500 ×g for 10 min, and frozen in 2 ml aliquots at -20 °C.

In addition, cSiO₂-killed cell (SKC)-derived material for ELISA solid-phase was prepared using a previously described protocol [432]. RAW 264.7 cells were seeded in 100 mm cell culture dishes at a density of 3.2×10^5 cells/ml in serum-reduced RPMI 1640 medium containing 0.25% FBS and 1% P/S. Then, cells were treated with $50~\mu$ g/ml cSiO₂ to induce robust cell death. Cells were placed in a 37 °C incubator (5% CO₂) for 20 h, then the supernatant was collected, centrifuged at $500\times g$ for 10 min, and frozen in 2 ml aliquots at -20 °C.

Total dsDNA and protein content in AC-derived material and SKC-derived material were quantitated by using a Quant-iT[™] PicoGreen[®] dsDNA Assay Kit (Thermo Fisher Scientific) and a Pierce[™] BCA Protein Assay Kit (Thermo Fisher Scientific), respectively, according to the manufacturer's instructions. dsDNA was measured using a FilterMax F3 Multimode plate reader (Molecular Devices) set to fluorescence wavelengths of 480/520 nm. Protein was measured using a FilterMax F3 Multimode plate reader (Molecular Devices) set to an absorbance wavelength of 562 nm. Total dsDNA and protein content in AC-derived and SKC-derived material are recorded in **Table S5.2**.

IgG AAbs to dsDNA, nucleosomes, AC-derived material, and SKC-derived material were measured in BALF and plasma of mice from the 28 d PI cohort as described previously [603]. Briefly, 96-well flat-bottom Nunc-ImmunoTM Maxisorp microplates (Thermo Fisher Scientific) were first coated with 20 μg/ml poly-L-lysine in PBS (pH 7.4) and incubated overnight at 4 °C. Plates were washed three times with PBS after all incubation steps. After treating the plates with poly-L-lysine, plates were blocked with 300 µl/well blocking buffer (PBS, 2% [w/v] BSA, 0.05% [v/v] Tween 20) for 2.5 h at room temperature. Then, plates were coated with 50 µl/well of ACderived supernatant, SKC-derived material, 2.5 µg/ml calf thymus dsDNA (Alpha Diagnostic International), or 2.5 µg/ml calf thymus nucleosomes (Arotec Diagnostics) diluted in ELISA dilution buffer (PBS, 0.1% [w/v] BSA, 0.05% [v/v] Tween 20) and incubated for 1 h at room temperature. Following antigen coating, 50 µl of BALF or plasma diluted 1:20 in ELISA dilution buffer was added to the plates and incubated for 1 h at room temperature. Mouse anti-dsDNA antibody (EMD Millipore Corporation, Temecula, CA) was used to establish a standard curve ranging from 2000 arbitrary units (U) to 3.91 U in 2-fold increments. Plates were then incubated with 50 µl/well goat anti-human IgG Fc HRP-conjugated detection antibody (Southern Biotech,

Birmingham, AL) diluted 1:5000 in ELISA dilution buffer for 1 h at room temperature. Finally, plates were incubated with 50 μl/well K-Blue[®] Advanced Plus TMB Substrate (Neogen) for 20 min at room temperature and sample absorbances measured using a FilterMax F3 Multimode plate reader (Molecular Devices, San Jose, CA) set to a wavelength of 650 nm. Using SoftMax Pro Software (Molecular Devices, San Jose, CA), sample absorbances were converted to IgG AAb concentrations (in U/ml) based on the anti-dsDNA antibody standard curve.

Data analysis and statistics

GraphPad Prism Version 9 (GraphPad Software, San Diego, CA, www.graphpad.com) was used to conduct all statistical analyses. The ROUT outlier test (Q = 1%) and the Shapiro-Wilk test (p<0.01) were used to identify outliers and assess normality in the data, respectively. For comparisons between the VEH/CON, cSiO₂/CON, and cSiO₂/TPPU groups in both the 7d PI and 28d PI cohorts, non-normal and semi-quantitative data were analyzed by the Kruskal-Wallis nonparametric test followed by Dunn's post-hoc test. The Brown-Forsythe test (p<0.01) was used to test the assumption of equal variances across treatment groups. Normal data with unequal variances were analyzed using the Brown-Forsythe/Welch analysis of variance (ANOVA) test followed by Dunnett's T3 post-hoc test. Normal data that met the assumption of equal variance were analyzed by standard one-way ANOVA followed by Tukey's post-hoc test. For timepoint comparisons within the VEH/CON, cSiO₂/CON, and cSiO₂/TPPU groups, non-normal and semiquantitative data were analyzed by the Mann-Whitney nonparametric test. The F test (p<0.05) was used to test the assumption of equal variances across the 7d PI and 28d PI groups. Normal data with unequal variances were analyzed using an unpaired t test with Welch's correction. Normal data that met the assumption of equal variance were analyzed using an unpaired t test.

Data are presented as mean \pm standard error of the mean (SEM), with a p-value \leq 0.05 considered statistically significant.

RESULTS

cSiO₂ and TPPU do not affect body or organ weights

Body weights within the 7d PI and 28d PI cohorts were not affected by TPPU or cSiO₂ treatment (**Figure 5.2A**). At 7d PI and 28d PI, no significant changes in kidney, spleen, or liver weights were noted (**Figure 5.2B**); therefore, follow-up analyses focused primarily on pulmonary and systemic endpoints.

<u>Dietary TPPU supplementation suppresses cSiO2-induced inflammatory cell infiltration in the</u>

lung

Total cells, monocytes, and neutrophils in the BALF of cSiO₂/CON mice were significantly elevated compared to VEH/CON mice at both 7d PI and 28d PI (Figure 5.3). cSiO₂/CON mice in the 7d PI cohort demonstrated markedly higher numbers of BALF cells compared to cSiO₂/CON mice in the 28d PI cohort. Lymphocyte accumulation in the alveolar fluid was present in cSiO₂/CON mice at 7d PI but negligible at 28d PI. Dietary TPPU supplementation significantly reduced accumulation of total cells and monocytes in the BALF of cSiO₂-exposed mice at both 7d PI and 28d PI, with the most prominent effects observed in the 7d PI cohort. BALF neutrophils and lymphocytes were significantly decreased in TPPU-fed mice at 7d PI compared to CON-fed mice.

Dietary TPPU supplementation does not influence cSiO₂-triggered lung histopathology

CON-fed mice instilled with VEH had no lung histopathology at either 7d PI or 28d PI. In contrast, cSiO₂-instilled CON-fed mice had multifocal, fibrotic and proliferative lung lesions in centriacinar regions of the lung, primarily in the proximal alveolar ducts (**Figures 5.4, 5.5**). These

focal lesions were composed of intramural interstitial fibrosis, hyperplasia of alveolar epithelial type 2 and transitional cells, and a mixed inflammatory cell infiltration (alveolitis) composed primarily of Ly6B.2⁺ neutrophils and CD206⁺ macrophages/monocytes (**Figure 5.6**). Production of tissue inhibitor of metalloproteinase 1 (TIMP-1), an important cytokine in cSiO₂-induced lung fibrosis [604, 605], increased in cSiO₂-instilled CON-fed mice but did not significantly change with TPPU treatment (**Figure 5.5C**).

Numerous widely scattered birefringent cSiO₂ particles were embedded in the thickened centriacinar interstitial tissue and in associated alveolar airspaces that contained proteinaceous material and cellular debris resulting from degenerating or necrotic phagocytic macrophages (**Figures 5.4D, 5.6A**). Lesser amounts of cSiO₂ particles, inflammatory cells, macrophages/monocytes, and cellular debris were present in airspaces of distal alveolar regions of the lung that were also without the hyperplasia of alveolar type 2 or transitional epithelial cells and septal fibrosis found in the more proximal centriacinar areas.

Centriacinar lung lesions in cSiO₂-instilled mice were less prominent after 28d PI as compared to 7d PI (**Figure 5.4**). Conspicuous accumulation of CD3⁺ and CD45R⁺ lymphoid cells (ectopic lymphoid tissue, ELT) in perivascular and peribronchiolar interstitial tissue were present in the lungs of mice after 28d PI (**Figure 5.7**). Histopathology of cSiO₂-instilled mice fed TPPU-supplemented diet was similar to that of cSiO₂ mice fed CON diet with the exception that TPPU treatment had slightly less neutrophilic inflammation in centriacinar lesions (**Figure 5.6**).

<u>Dietary TPPU supplementation does not significantly affect proinflammatory gene expression and</u> <u>protein production in the lung</u>

At both 7d PI and 28d PI, cSiO₂ significantly upregulated expression of selected proinflammatory cytokines (i.e., *Il1a*, *Il1b*, *Tnf*), chemokines (i.e., *Ccl2*, *Cxcl5*, *Cxcl10*), and type

I IFN-regulated genes (i.e., *Irf7*, *Mx1*, *Oas2*) in the lung (**Figure 5.8**). mRNA transcript levels for most genes were comparable between 7d PI and 28d PI; however, cSiO₂-exposed mice in the 7d PI cohort exhibited higher expression levels of *Ccl2*, *Cxcl10*, and *Oas2* while cSiO₂-exposed mice in the 28d PI cohort displayed higher expression levels of *Il1a*. Dietary TPPU supplementation did not significantly affect expression of proinflammatory cytokines, chemokines, and type I IFN-regulated genes in the lung.

In accordance with observed expression levels of proinflammatory cytokines, chemokines, and type I IFN-regulated genes, cSiO₂ triggered robust production of proinflammatory protein mediators in the lung at both 7d PI and 28d PI (**Table S5.3**). Notably, macrophage-derived cytokines (i.e., IL-6, TNF-α) (**Figure 5.9**), chemokines (i.e., CCL2, CCL3, CCL4, CCL12, CCL17, CCL19, CCL22, CXCL1, CXCL9, CXCL10) (**Figure 5.10**), and growth/inhibitory factors (i.e., GM-CSF, M-CSF, LIF) (**Figure S5.1**) were upregulated by cSiO₂ exposure at both timepoints. The impacts of cSiO₂ on T cell-derived cytokines were more limited, as the particle only elicited significant increases in IL-4 and IL-16 at 28d PI and in IL-17 at both timepoints (**Figure S5.2**). Interestingly, cSiO₂ significantly decreased lung levels of IL-1α at 7d PI (**Figure 5.9**) and VEGF at both timepoints (**Figure S5.1**). Similar to gene expression analyses in the lung, TPPU minimally impacted cSiO₂-induced production of proinflammatory proteins, with an exception to modestly increasing CXCL5, IL-1β, and IL-13 (**Figures 5.9, 5.10**; **Figure S5.2**) and slightly decreasing M-CSF (**Figure S5.1**) at 28d PI.

<u>Dietary TPPU supplementation does not significantly affect cSiO₂-induced secretion of IgG AAbs</u> <u>into BALF and plasma</u>

Mice in the VEH/CON group had higher baseline values for all tested antigens in the plasma compared to the BALF (Figure 5.11). Corresponding with increased numbers of

inflammatory leukocytes in the BALF, mice that received cSiO₂ displayed significant increases in IgG AAb specific to dsDNA, nucleosome antigen, AC-derived material, and SKC-derived material in the BALF. In the plasma, cSiO₂ triggered modest, yet insignificant, increases in IgG specific to dsDNA, nucleosome antigen, and SKC-derived material and a significant increase in IgG specific to AC-derived material (**Figure 11C**). TPPU administration did not significantly change IgG levels in the BALF and plasma of cSiO₂-exposed mice.

DISCUSSION

Acute and subchronic environmental exposure to cSiO₂, an environmental trigger of autoimmune disease in humans, has been etiologically linked to the development of silicosis, restrictive pulmonary disease, and development of systemic autoimmunity in lupus-prone mice [334, 599, 600, 606-610]. This investigation is the first to assess the efficacy of the sEH inhibitor TPPU, a well-established lipidome-modifying agent, against acute cSiO₂-triggered lung inflammation and early autoimmunity in lupus-prone mice. Here, we found that a single intranasal dose of cSiO₂ in the lung induces i) leukocyte accumulation in the BALF, ii) centriacinar inflammation, centriacinar fibrosis, and perivascular ELT development, iii) monocyte and neutrophil recruitment, iv) accumulation of CD3+ T lymphocytes and CD45R+ B lymphocytes in ELT, v) expression of proinflammatory cytokines, chemokines, and type I IFN-regulated mRNAs and proteins, and vi) secretion of AAb targeting dsDNA, nucleosomes, apoptotic cell AAg, and cSiO₂-killed cell AAg in alveolar fluid. Importantly, we found that while TPPU supplementation significantly decreased differential immune cell counts in the BALF and modestly reduced CD206⁺ monocytes and Ly6B.2⁺ neutrophils in the lung, this drug's effects on other measured endpoints were negligible.

In female lupus-prone NZBWF1 mice, we have previously demonstrated that a single intranasal dose of 2.5 mg cSiO₂ triggers i) robust infiltration of neutrophils, monocytes, and lymphocytes into the lung, ii) upregulation of proinflammatory cytokines, chemokines, and type I IFN-regulated genes, and iii) and release of proinflammatory mediators, total cellular protein, and autoantigenic dsDNA in the BALF [583]. In that study, cSiO₂ induced moderate pulmonary centriacinar inflammation at 7d PI that weakened in severity until 28d PI while stimulating infiltration of CD3⁺ T lymphocyte and CD45R⁺ B lymphocytes into the lung starting at 14d PI. Additionally, cSiO₂ promoted vigorous expression of numerous chemokine genes (e.g., Ccl2, Ccl7, Ccl8, Cxcl1, Cxcl5, Cxcl9, Cxcl10) and IFN-regulated genes (e.g., Mx1, Oas2, Irf7) in the lung at 7d PI that persisted until 28d PI. Consistent with the prior study, herein we observed increased numbers of neutrophils and monocytes in the BALF, moderate centriacinar histopathology associated with cSiO₂ particle deposition, and comparable fold changes in proinflammatory chemokine and IFN-regulated mRNA transcripts at 7d PI, accompanied by infiltration of CD3⁺ T lymphocyte and CD45R⁺ B lymphocytes into the lung at 28d PI. In contrast to the previous study [583], cSiO₂-induced centriacinar histopathology persisted in severity from 7d PI to 28d PI, while BALF neutrophil, monocyte, and lymphocyte counts decreased from 7d PI to 28d PI. Nevertheless, it is likely in both cases that insufficient clearance of cSiO₂ from the lung led to a mounting cycle of neutrophilic and monocytic infiltration, cell death, release of proinflammatory chemokines, accumulation of dead cell corpses, further leukocyte chemotaxis, and inflammatory tissue damage.

Lipidome modulation by dietary ω -3 PUFA consumption has been previously associated with suppression of pulmonary leukocyte infiltration, proinflammatory gene expression, and AAb secretion in the lung following subchronic cSiO₂ exposures [19, 351, 352]. In agreement with these

findings, we also found that ω-3 PUFA supplementation suppresses cSiO₂-triggered cell death in the lung at 7d PI, total cell and lymphocyte recruitment in the BALF at 28d PI, autoimmune gene transcription in the lung at 28d PI, and AAb secretion in the lung at 28d PI in our acute model of cSiO₂-induced lupus flaring ([611], data not published). We posited here that sEH inhibition by TPPU would also improve biomarkers of lung inflammation and early autoimmunity following acute cSiO₂ exposure. However, TPPU only suppressed neutrophilic, monocytic, and lymphocytic accumulation in the alveolar fluid and recruitment to centriacinar lung tissue at 7d PI and 28d PI. On the other hand, both ω-3 PUFA consumption and sEH inhibition were effective in ameliorating LPS-accelerated glomerulonephritis in female lupus-prone NZBWF1 mice [595]. One potential explanation for these observations is that the lung tissue concentration of TPPU may differ from concentrations found in other tissues and plasma. Ostermann and coworkers found that continual oral administration of TPPU resulted in the highest tissue concentration in the liver, followed by the heart, kidney, and spleen. TPPU concentration was not reported in lung tissue, however [470]. In addition, we previously found that feeding NZBWF1 mice with TPPU-enriched AIN-93G diet resulted in a drug plasma concentration of approximately 5 µM, which is approximately 2000-fold greater than the Ki of TPPU [595]. Therefore, TPPU's lack of efficacy in the present study may be attributed not to absorption of the drug into the systemic circulation, but rather low distribution of the drug in lung tissue. It will therefore be crucial to quantify TPPU concentration in the lung tissue to further evaluate its pharmacokinetic properties and efficacy in environmentally-triggered lung inflammation.

Pharmacological inhibition of sEH by TPPU and other analogous small-molecule inhibitors has shown to be effective in preventing and limiting toxicant-triggered inflammation in the lung and other organs [593-595]. Herein, we found that prophylactic administration of TPPU

via experimental AIN-93G diet modestly reduced pulmonary infiltration of Ly6B.2⁺ neutrophils and CD206⁺ monocytes 7d following cSiO₂ instillation. However, TPPU did not significantly impact cSiO₂-triggered upregulation of mRNA transcripts for proinflammatory cytokines, chemokines, and type I IFN-regulated genes and minimally impacted production of proinflammatory cytokines, chemokines, and growth factors in the lung at either timepoint. Accordingly, it is plausible in the present study that sEH inhibition suppressed neutrophilic and monocytic recruitment by modulating the plasma lipidome. For instance, sEH inhibition by TPPU was found to increase plasma 14,15-EpETrE levels and resultantly ameliorate neutrophil impairment induced by 14,15-DiHETrE, which downregulated expression of NADPH oxidase subunits, inhibited reactive oxygen species (ROS) production, and suppressed expression of CXCR1 and CXCR2 for chemotaxis [612]. In another study, TPPU treatment significantly increased plasma 14,15-EpETrE levels and decreased BALF neutrophils and macrophages in a murine model of lipopolysaccharide (LPS)-induced acute lung injury [401]. Future investigations are needed to further clarify the impacts of cSiO₂ instillation on the BALF/plasma lipidome and impacts of BALF/plasma oxylipins on cSiO₂-triggered leukocyte recruitment to the lung.

In the present study, we found that sEH inhibition by TPPU did not ameliorate cSiO₂-induced centriacinar fibrosis in the lung, in contrast to several previously published studies. For example, Zhou and coworkers reported that sEH inhibition by TPPU significantly reduced bleomycin-induced collagen deposition in the lung at 14d and 21d PI, levels of TGF-β1, IL-1β, and IL-6 in the serum at 7d and 21d PI, and TGF-β1-induced activation and differentiation of mouse fibroblasts *in vitro* without eliciting notable toxicity [21]. In addition, TPPU pretreatment of primary human lung fibroblasts from idiopathic pulmonary fibrosis patients significantly dampened TGF-β1-mediated fibroblast activation by suppressing expression of α-smooth muscle

actin and type I collagen as well as ROS production [613]. Other studies have reported that TPPU also ameliorates cardiac fibrosis induced by coronary artery ligation [614], hepatic fibrosis induced by carbon tetrachloride exposure [438], and renal interstitial fibrosis induced by unilateral ureteral obstruction [615]. It is possible that the cSiO₂ dose we used in our model evoked fibrosis to a greater degree than the studies described above, which may explain why the therapeutic effects of TPPU were minimal in our model. Therefore, it would be informative to repeat the experiment described here with smaller cSiO₂ doses to verify the effectiveness of sEH inhibition against cSiO₂-triggered lung inflammation and early autoimmunity.

One limitation of our investigation is that we did not analyze the impacts of TPPU on cSiO₂-induced toxicity before 7d PI. While we observed that TPPU did not significantly change expression and production of proinflammatory cytokines and chemokines in the lung at 7d PI, it is possible that TPPU may exhibit notable therapeutic effects on these endpoints within the first week after cSiO₂ exposure. For instance, we previously found that a single intranasal bolus of 2.5 mg cSiO₂ elicited marked upregulation and secretion of IL-6 from the lung at 1d PI but not at 7d PI in female lupus-prone NZBWF1 mice [583], suggesting that some cSiO₂-induced proinflammatory responses are transient. In addition, Bettaieb and coworkers demonstrated in a murine model of cerulein- and arginine-induced acute pancreatitis that sEH inhibition by TPPU significantly downregulated expression of *Il1b*, *Il6*, and *Tnf* in the pancreas up to 48 h after induction of acute pancreatitis, as well as protein levels of IL-1β, IL-6, and TNF-α in the plasma [437]. In future studies, earlier timepoints within the first week post-cSiO₂ exposure (e.g., 1d, 3d, 5d PI) should be considered to better understand the initial events underlying cSiO₂-induced lung toxicity as well as immediate therapeutic effects of sEH inhibition in this model.

Another limitation of our study is that we only analyzed the impacts of cSiO₂ and TPPU on gene expression changes in the lung and not in the immune cell fraction of the BALF. Zhou and coworkers demonstrated in RAW264.7 macrophages that TPPU dose-dependently decreases cellular II1b and Tnf mRNA levels and extracellular IL-1β and TNF-α protein levels following 6 h of LPS exposure [401]. Similar findings have been capitulated by Dong and coworkers in primary murine peritoneal macrophages pretreated with TPPU and exposed to LPS for 6 h [616], which suggests that the primary effects of TPPU in our model may attributed to direct modulation of immune cell functionality. A related constraint of our investigation is that we did not evaluate the effects of TPPU on the cardiovascular system. Both rodents and humans genetically predisposed to lupus are more likely to develop cardiovascular complications compared to healthy controls [617, 618]. In addition, stabilization of epoxyeicosatrienoic acids (EpETrEs) derived from arachidonic acid (ARA; 20:4ω-6) has been associated with decreased NF-κB-driven expression of adhesion molecules on human aortic endothelial cells and corresponding vascular monocyte adhesion [468, 619]. In future studies using our acute model of cSiO₂-triggered toxicity, it will be important to clarify the effects of cSiO₂ and sEH inhibition on expression of adhesion molecules by pulmonary endothelial cells, neutrophils, and monocytes.

CONCLUSIONS

This study is the first to query the impacts of the sEH inhibitor TPPU in a novel acute cSiO₂-triggered lupus model using female NZBWF1 mice. The findings presented herein suggest that the therapeutic benefits of sEH inhibition on cSiO₂-induced lung inflammation and early autoimmunity are questionable. While TPPU suppressed infiltration of proinflammatory neutrophils, monocytes, and lymphocytes to the lung with no perceivable drug-related toxicity, it did not prevent development of centriacinar inflammation and fibrosis, expression and production

of proinflammatory cytokines and chemokines in the lung, or secretion of diverse AAbs in the BALF and plasma. It will be critical in future investigations to clarify 1) the pharmacokinetic distribution of TPPU in lung tissue, 2) the impacts of cSiO₂ on the BALF and plasma lipidome, and 3) the effects of BALF/plasma oxylipins on neutrophilic and monocytic inflammatory responses.

DECLARATIONS

Competing Interests

The authors declare that the research was conducted in the absence of any commercial or financial relationships that could be construed as a potential conflict of interest.

Funding

This research was funded by NIH RO1ES027353 (JP), Lupus Foundation of America (OF and JP), and Dr. Robert and Carol Deibel Family Endowment (JP).

Contributions

OF: study design, coordination, feeding study, necropsy, data curation, data analysis/interpretation, figure preparation, manuscript preparation and submission. JW: necropsy, lab analysis. RL: necropsy, lab analysis. JH: kidney/spleen/liver histopathology, data analysis, manuscript preparation. LH: BALF cell count acquisition/analysis, figure preparation. JP: study design, oversight, funding acquisition, data analysis/interpretation, manuscript preparation and submission. KSSL: study design, oversight, manuscript preparation. All authors contributed to the manuscript and approved the submitted version.

<u>Acknowledgments</u>

We would like to thank Amy Porter and the Laboratory of Investigate Histopathology at Michigan State University for their assistance with histotechnology analyses.

FIGURES

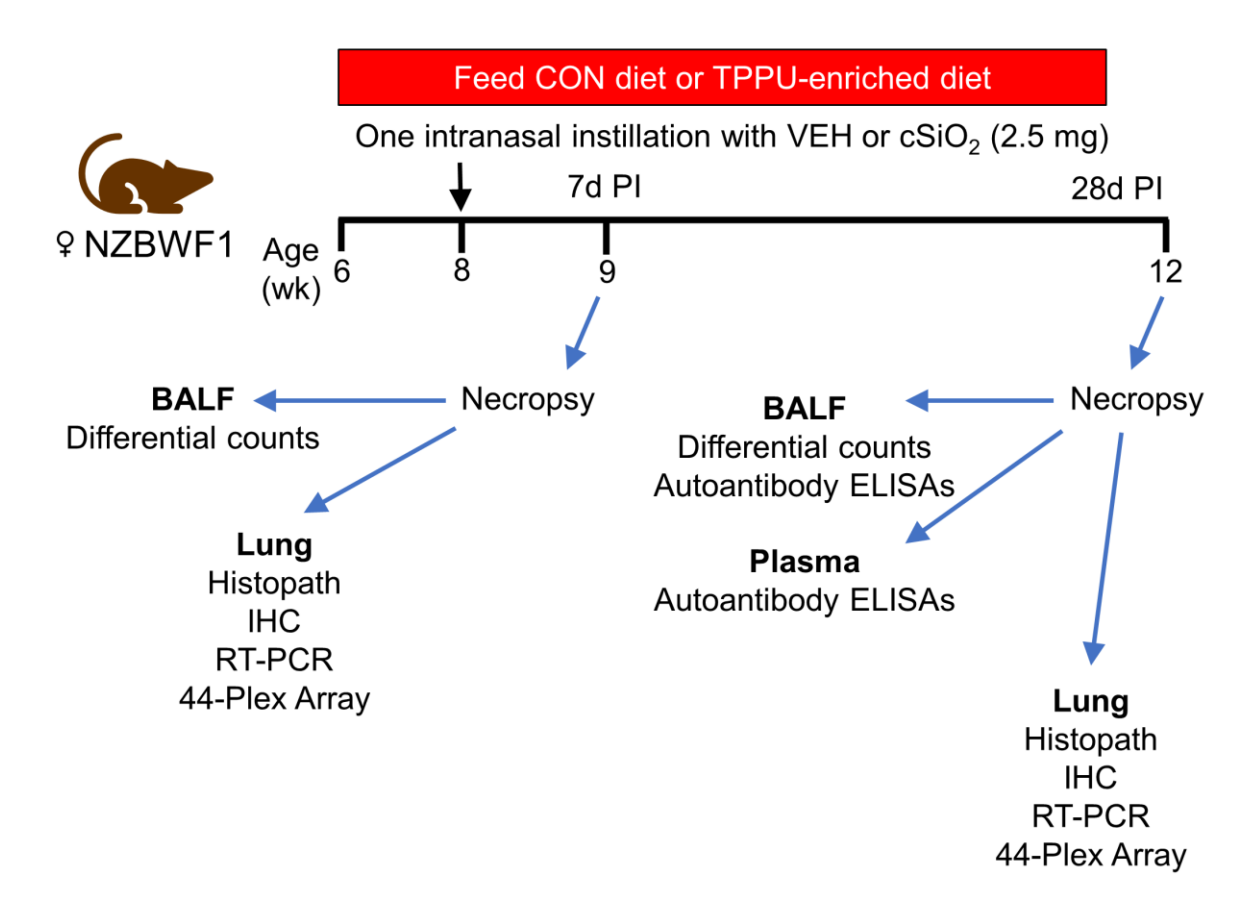


Figure 5.1. Experimental design. At 6 wks of age, female lupus-prone NZBWF1 mice (n=48) were placed on either control (CON) diet or TPPU-enriched diet. Upon reaching 8 wks of age, mice were intranasally instilled with 25 μ l of saline vehicle (VEH) or 2.5 mg of cSiO₂ suspended in 25 μ l of saline. Cohorts of mice were sacrificed at 9 wks of age (7 d post-instillation [PI]) and 12 wks of age (28 d PI). Lung tissue, bronchoalveolar lavage fluid (BALF), and plasma were collected for downstream analyses.

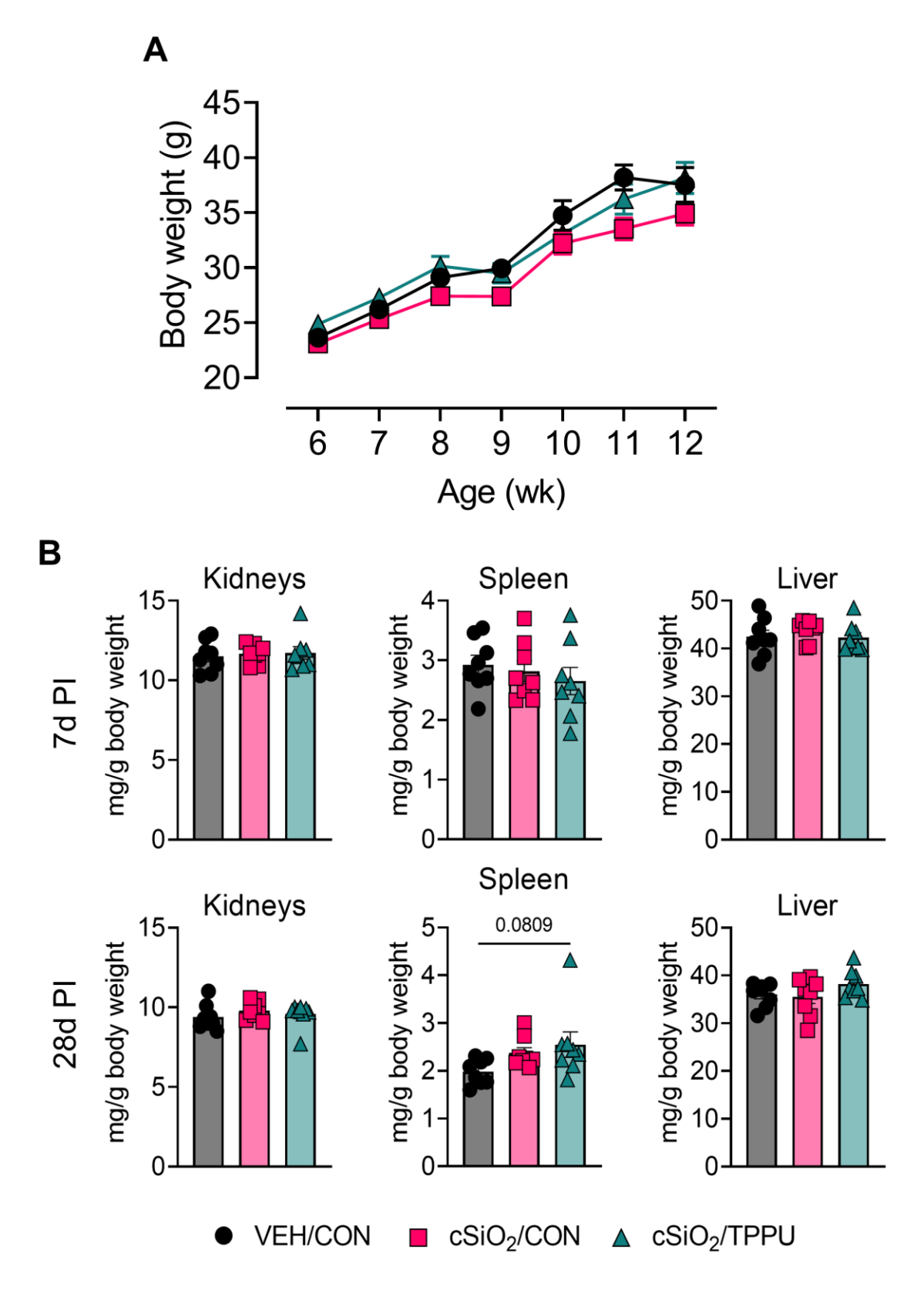


Figure 5.2. Acute cSiO₂ exposure and dietary TPPU supplementation do not significantly impact growth rate and post necropsy kidney, spleen, and liver weights in female lupus-

Figure 5.2 (cont'd)

prone NZBWF1 mice. (A) In both cohorts, body weights were monitored weekly. Data from the 7d PI and 28d PI cohorts were pooled from 6-9 wk of age. $cSiO_2$ and TPPU did not significantly change total body weight during the entire study. (B) At 7d PI and 28d PI, cohorts of NZBWF1 mice were sacrificed, and wet organ weights for both kidneys, spleen, and liver were measured prior to downstream tissue processing. Data are presented as mean \pm SEM. Values of p<0.1 are shown, with p<0.05 considered statistically significant.

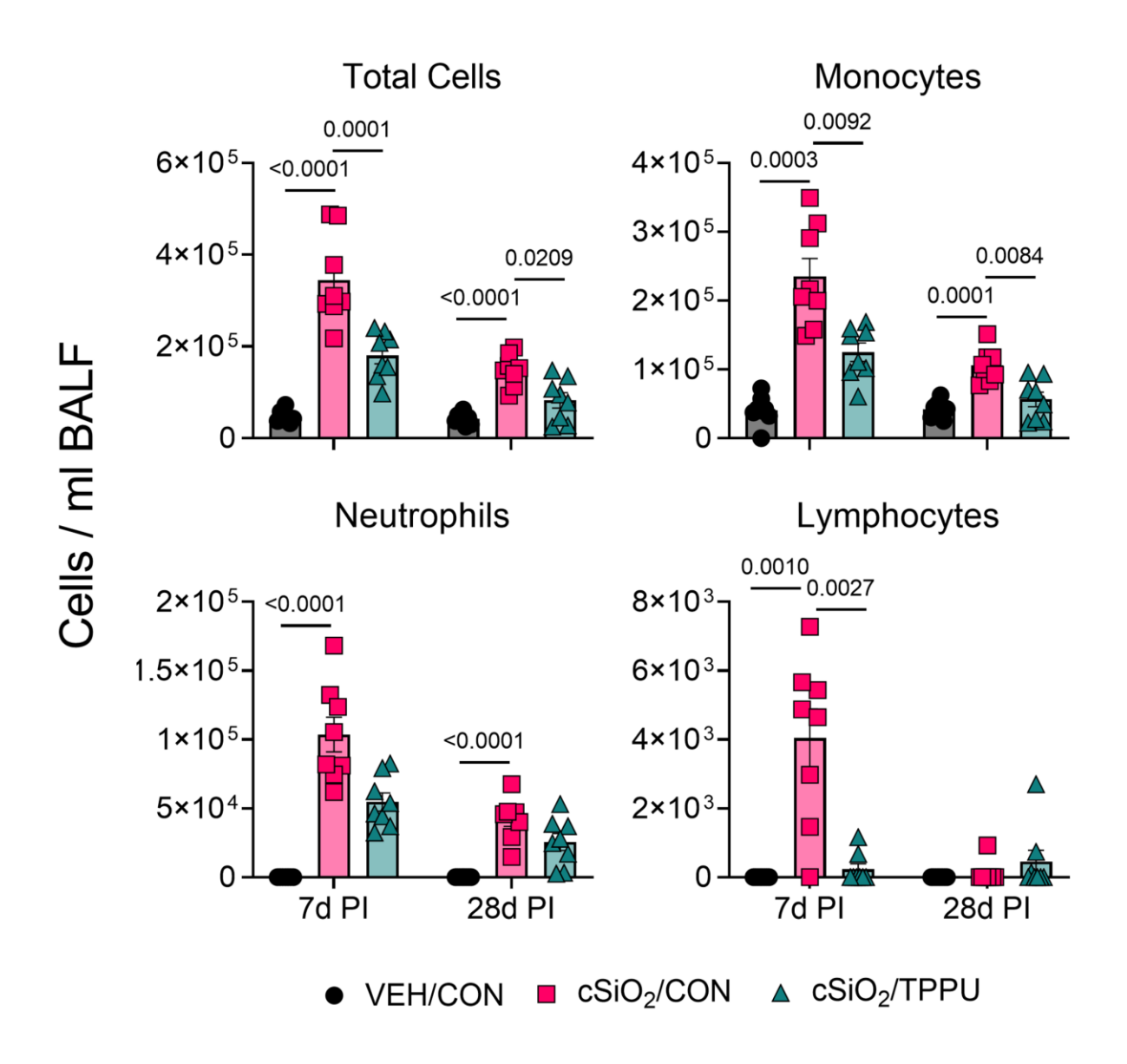


Figure 5.3. Dietary TPPU supplementation suppresses cSiO₂-induced immune cell accumulation in BALF. At necropsy, total cells, monocytes, neutrophils, and lymphocytes were quantified in BALF. Data are presented as mean \pm SEM. Values of p<0.1 are shown, with p<0.05 considered statistically significant.

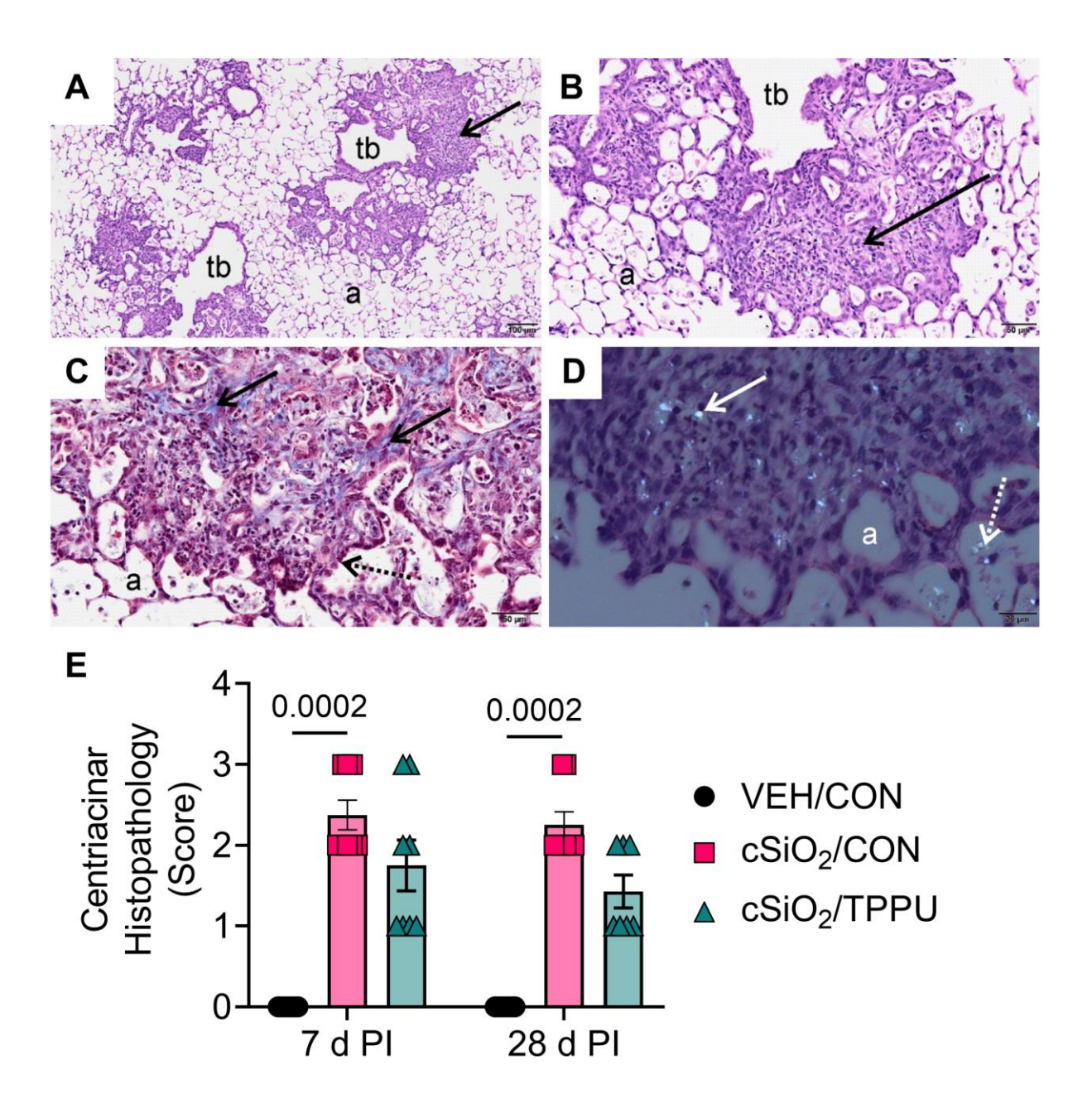


Figure 5.4. Intranasal cSiO₂ instillation induces robust centriacinar histopathology in the lung of NZBWF1 mice. Light Photomicrographs of hematoxylin & eosin (H&E) lungs tissues at (A) low and (B) high magnification illustrating chronic centriacinar lesions (solid black arrows) composed of interstitial fibrosis, mixed inflammatory cell inflammation and alveolar epithelial hyperplasia from cSiO₂/CON mice sacrificed at 7d PI. (C) Centriacinar lung lesion (7d PI) stained with Masson's trichrome illustrating areas of interstitial fibrosis (blue stain; solid black arrows). (D) H&E-stained centriacinar lung lesion taken with polarized light exposing birefringent CSiO₃ particles embedded in the fibrotic lesion (solid white arrow) and associated with degenerating and necrotic phagocytic cells in alveolar airspaces (stippled white arrows). (E) Graphical figure of semi-quantitative severity scores for centriacinar histopathology. Scoring was as follows: 0—no significant finding, 1—minimal, 2—mild, 3—moderate, 4—marked, 5—severe. See text for

Figure 5.4 (cont'd)

detailed criteria used in severity scoring. Data are presented as mean \pm SEM (n=8). Values of p<0.1 are shown, with p<0.05 considered statistically significant. a, alveolar parenchyma; tb, terminal bronchiole.

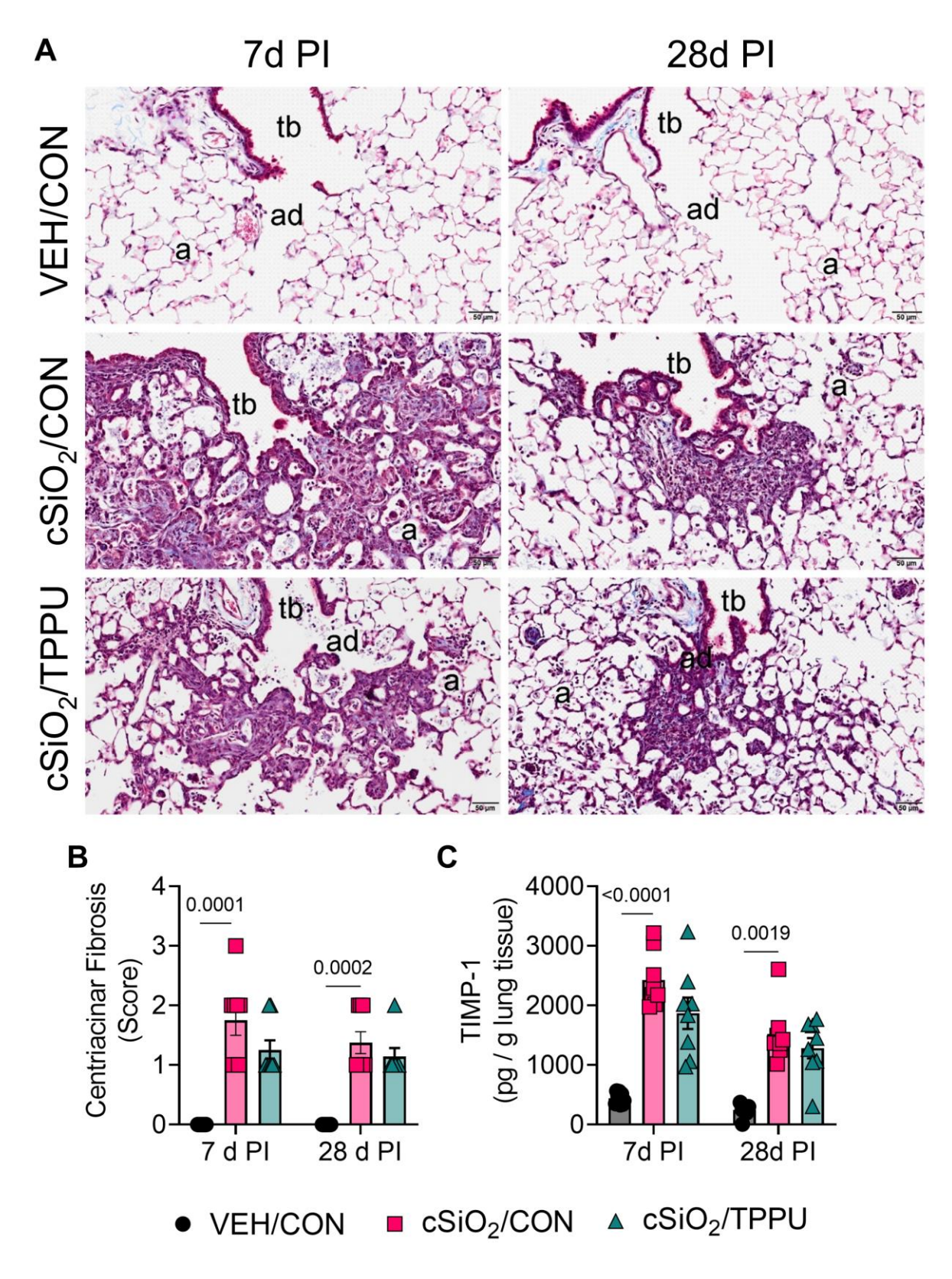


Figure 5.5. Dietary TPPU supplementation does not significantly impact cSiO₂-induced centriacinar fibrosis in the lung. (A) Representative light photomicrographs of Masson's

Figure 5.5 (cont'd)

trichrome-stained lung tissues (centriacinar regions) from VEH/CON, cSiO₂/CON, and cSiO₂/TPPU mice sacrificed at 7d PI and 28d PI. (**B**) Semi-quantitative severity scores for centriacinar interstitial fibrosis. Scoring was as follows: 0—no significant finding, 1—minimal, 2—mild, 3—moderate, 4—marked, 5—severe. See text for detailed criteria used in severity scoring. (**C**) Following sacrifice, middle lung lobes were isolated and homogenates analyzed for production of TIMP-1 using Mouse Cytokine/Chemokine 44-Plex Discovery Assay® Array from Eve Technologies. Protein quantity was normalized to the original weight of lung tissue homogenized for the analysis. For individual data points that fell below the limit of detection, LOD/2 was substituted for statistical analysis. Data are presented as mean \pm SEM (n = 8). Values of p<0.1 are shown, with p<0.05 considered statistically significant. a, alveolar parenchyma; ad, alveolar duct; tb, terminal bronchiole.

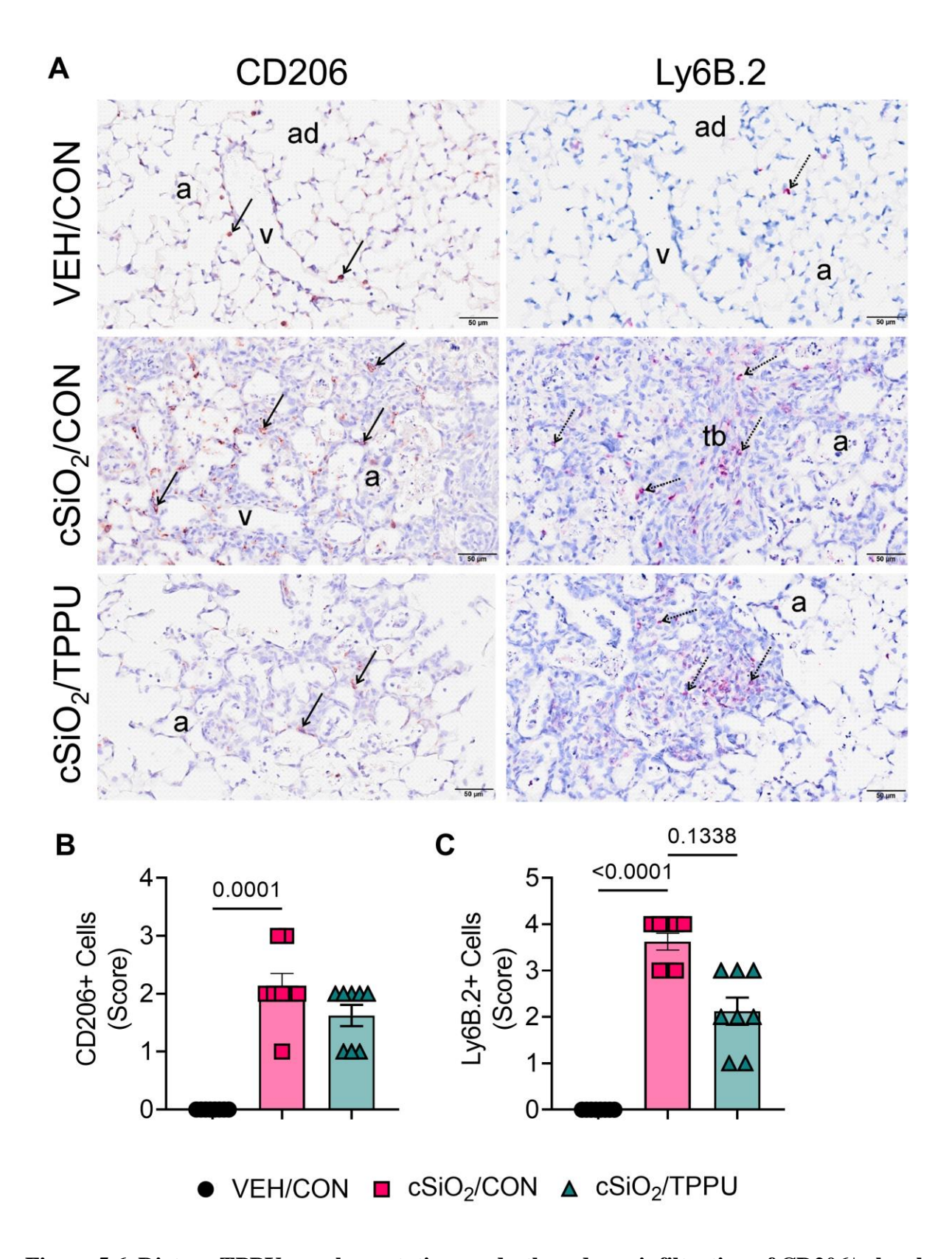


Figure 5.6. Dietary TPPU supplementation modestly reduces infiltration of $CD206^+$ alveolar macrophages/monocytes and $Ly6C^+$ neutrophils in the lung. (A) Representative light

Figure 5.6 (cont'd)

photomicrographs of lung tissues (centriacinar regions) from VEH/CON, cSiO₂/CON, and cSiO₂/TPPU mice sacrificed at 7d PI. Lung tissues were immunohistochemically stained for CD206⁺ alveolar macrophages/monocytes (brown chromagen) and Ly6B.2⁺ neutrophils (red chromagen). Semi-quantitative scores for presence of (**B**) CD206⁺ cells and (**C**) Ly6B.2⁺ cells in the centriacinar regions of the lung. Severity scores were as follows: 0—no significant finding, 1—minimal, 2—mild, 3—moderate, 4—marked, 5—severe. See text for detailed criteria used in severity scoring. Data are presented as mean \pm SEM (n = 8). Values of p<0.25 are shown, with p<0.05 considered statistically significant. a, alveolar parenchyma; ad, alveolar duct; tb, terminal bronchiole; v, pulmonary vein. Solid arrow, CD206⁺ cell; stippled arrow, Ly6B.2⁺ cell.

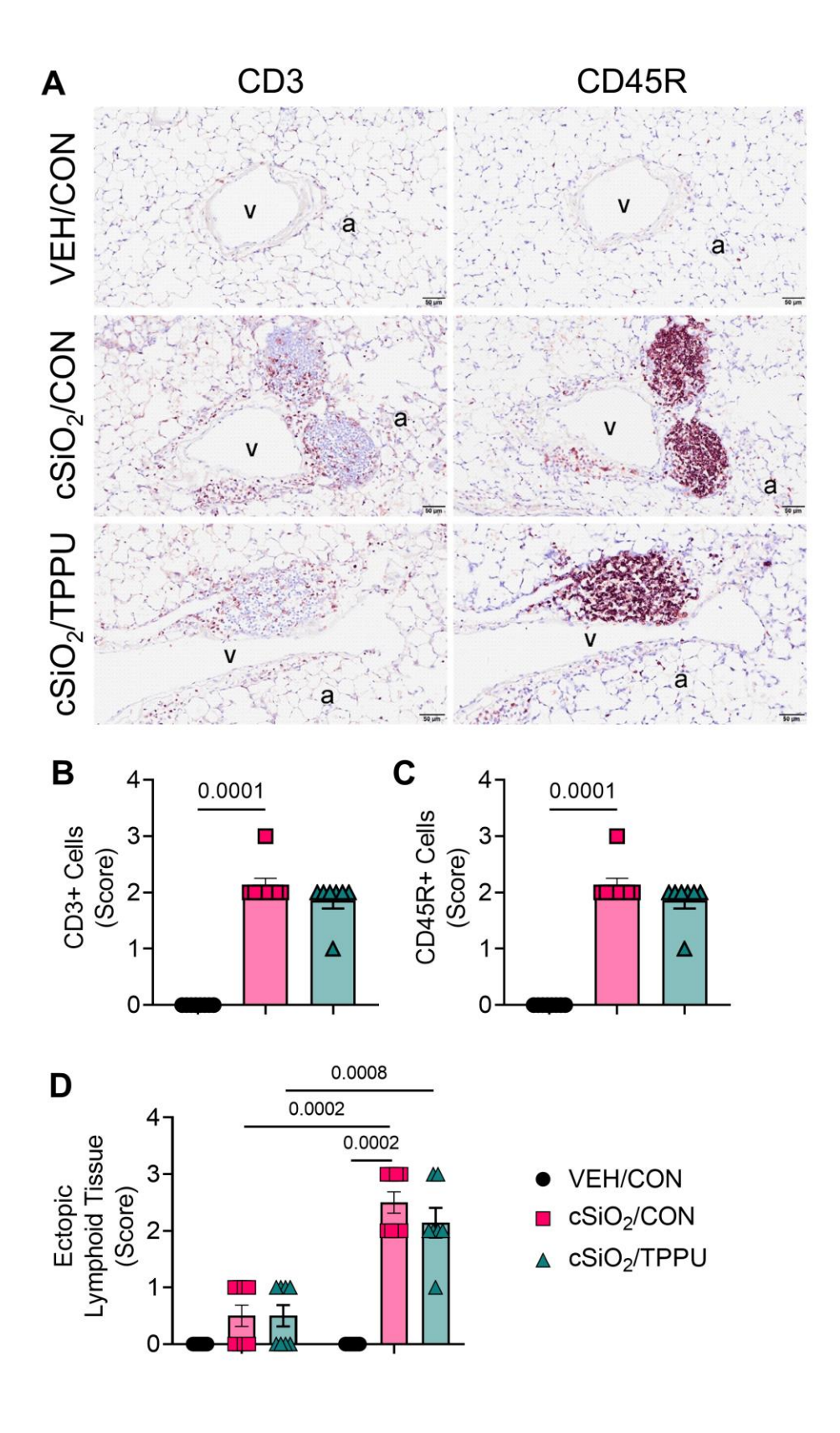


Figure 5.7. Dietary TPPU supplementation does not significantly impact $cSiO_2$ -induced perivascular and – bronchiolar infiltration of $CD3^+$ and $CD45R^+$ lymphocytes in the lung. (A)

Figure 5.7 (cont'd)

Representative light photomicrographs of lung tissues from VEH/CON, cSiO₂/CON, and cSiO₂/TPPU mice sacrificed at 28d PI. Lung tissues were immunohistochemically labeled for CD3⁺ T lymphocytes and CD45R⁺ B lymphocytes (brown chromagen). Semi-quantitative severity scores for presence of (**B**) CD3⁺ cells, (**C**) CD45R⁺ cells, and (**D**) development of ectopic lymphoid tissue in the perivascular and peribronchiolar interstitial tissue. Severity scores for CD3⁺ cells and CD45R⁺ cells were identical. Severity scores were as follows: 0—no significant finding, 1—minimal, 2—mild, 3—moderate, 4—marked, 5—severe. See text for detailed criteria used in severity scoring. Data are presented as mean \pm SEM (n = 8). Values of p<0.1 are shown, with p<0.05 considered statistically significant. a, alveolar parenchyma; v, pulmonary vein.

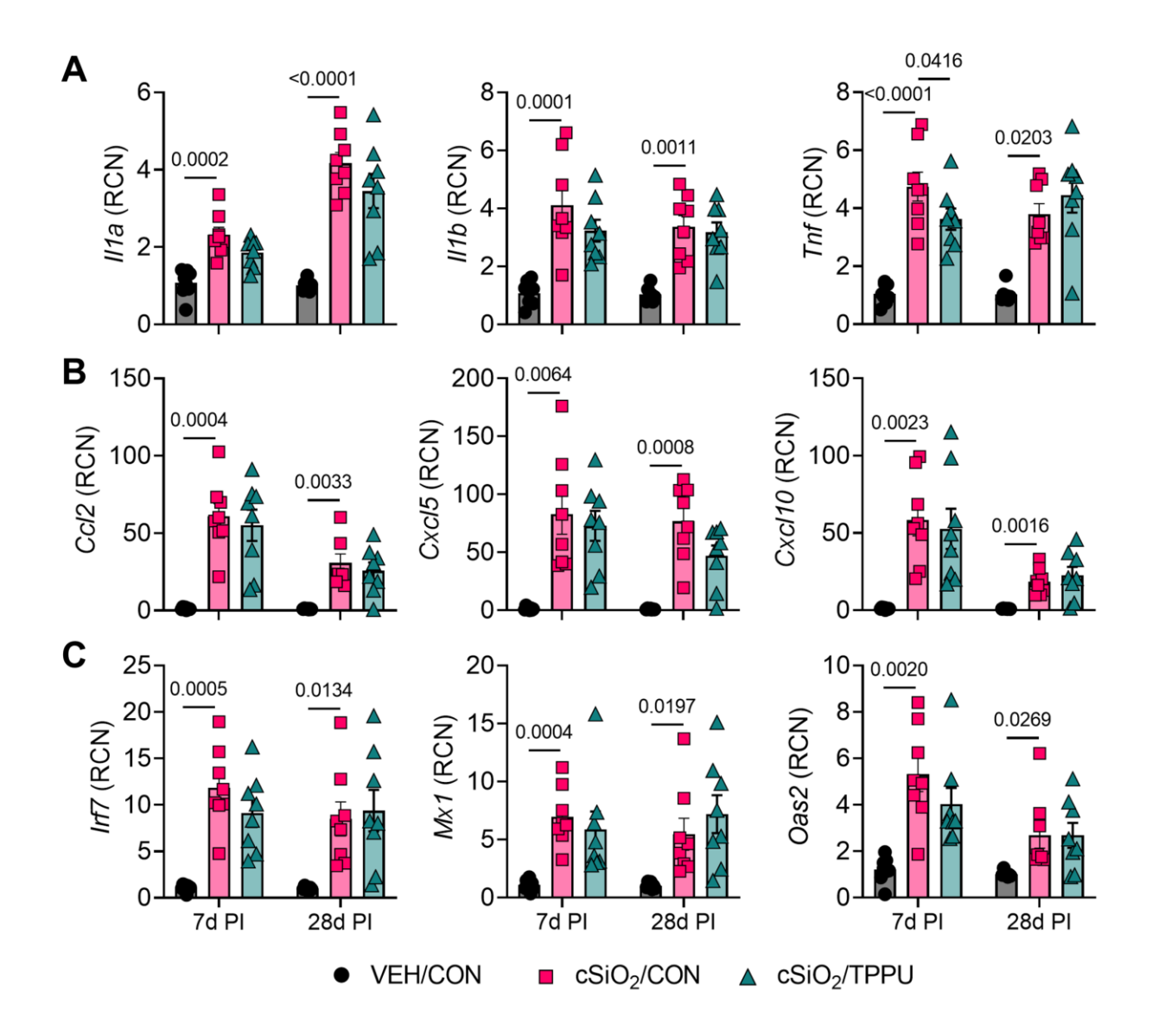


Figure 5.8. Dietary TPPU supplementation does not significantly impact proinflammatory cytokine, chemokine, and IFN-regulated gene expression in the lung. Following sacrifice, caudal lung lobes were isolated and analyzed for RNA expression of selected (A) proinflammatory cytokines (i.e., Il1a, Il1b, Inf), (B) chemokines (i.e., Ccl2, Cxcl5, Cxcl10), and (C) type I interferon-regulated genes (i.e., Irf7, Mx1, Oas2). Data are presented as mean \pm SEM (n = 8). Values of p<0.1 are shown, with p<0.05 considered statistically significant.

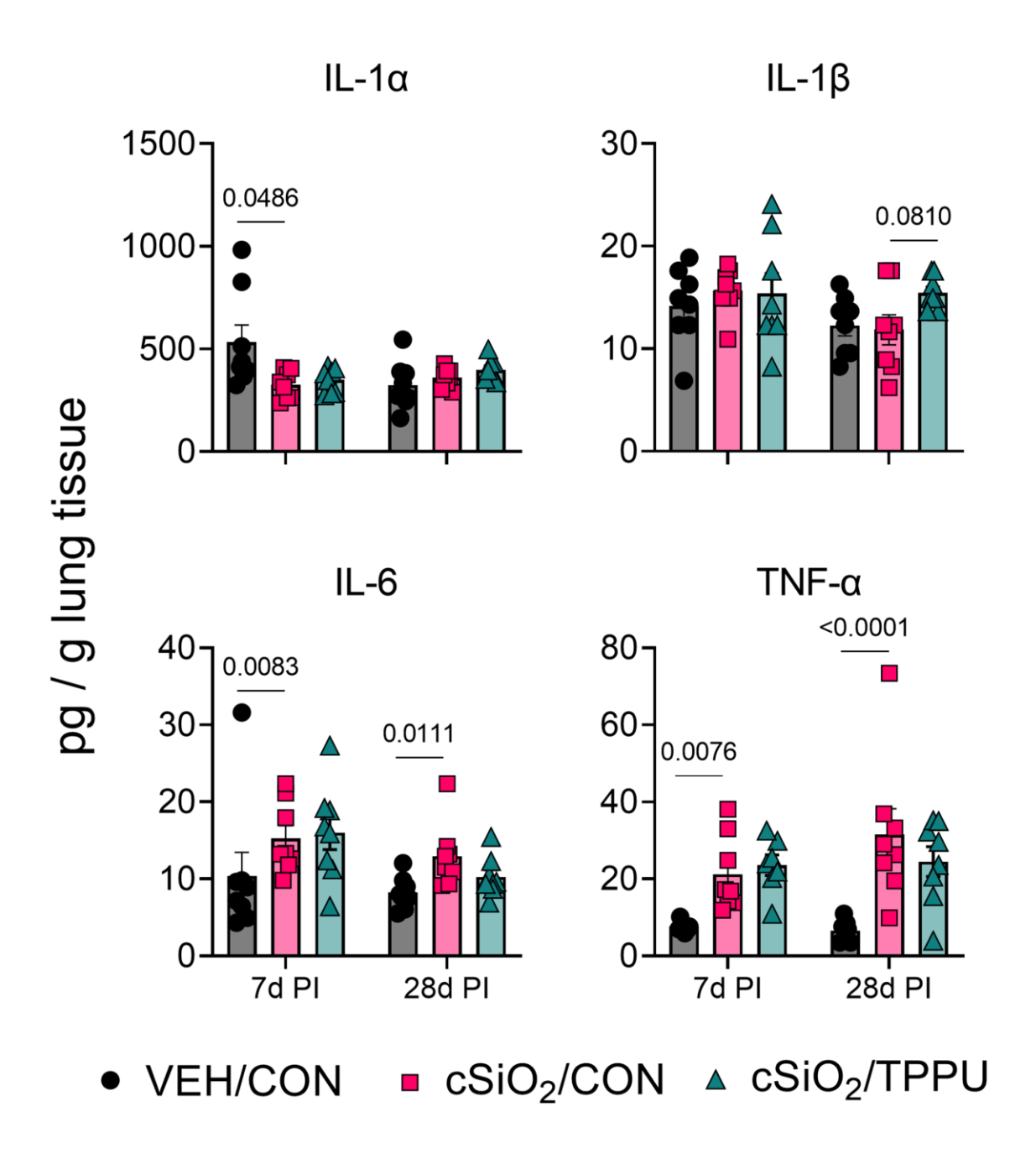


Figure 5.9. Dietary TPPU supplementation has limited effects on cSiO₂-induced production of cytokines from macrophages in the lung. Following sacrifice, middle lung lobes were isolated and homogenates analyzed for production of selected macrophage-derived cytokines (i.e., IL-1α, IL-1β, IL-6, TNF-α) using Mouse Cytokine/Chemokine 44-Plex Discovery Assay® Array from Eve Technologies. Cytokine quantities were normalized to the original weight of lung tissue homogenized for the analysis. For individual data points that fell below the limit of detection, LOD/2 was substituted for statistical analysis. Data are presented as mean \pm SEM (n = 8). Values of p<0.2 are shown, with p<0.05 considered statistically significant.

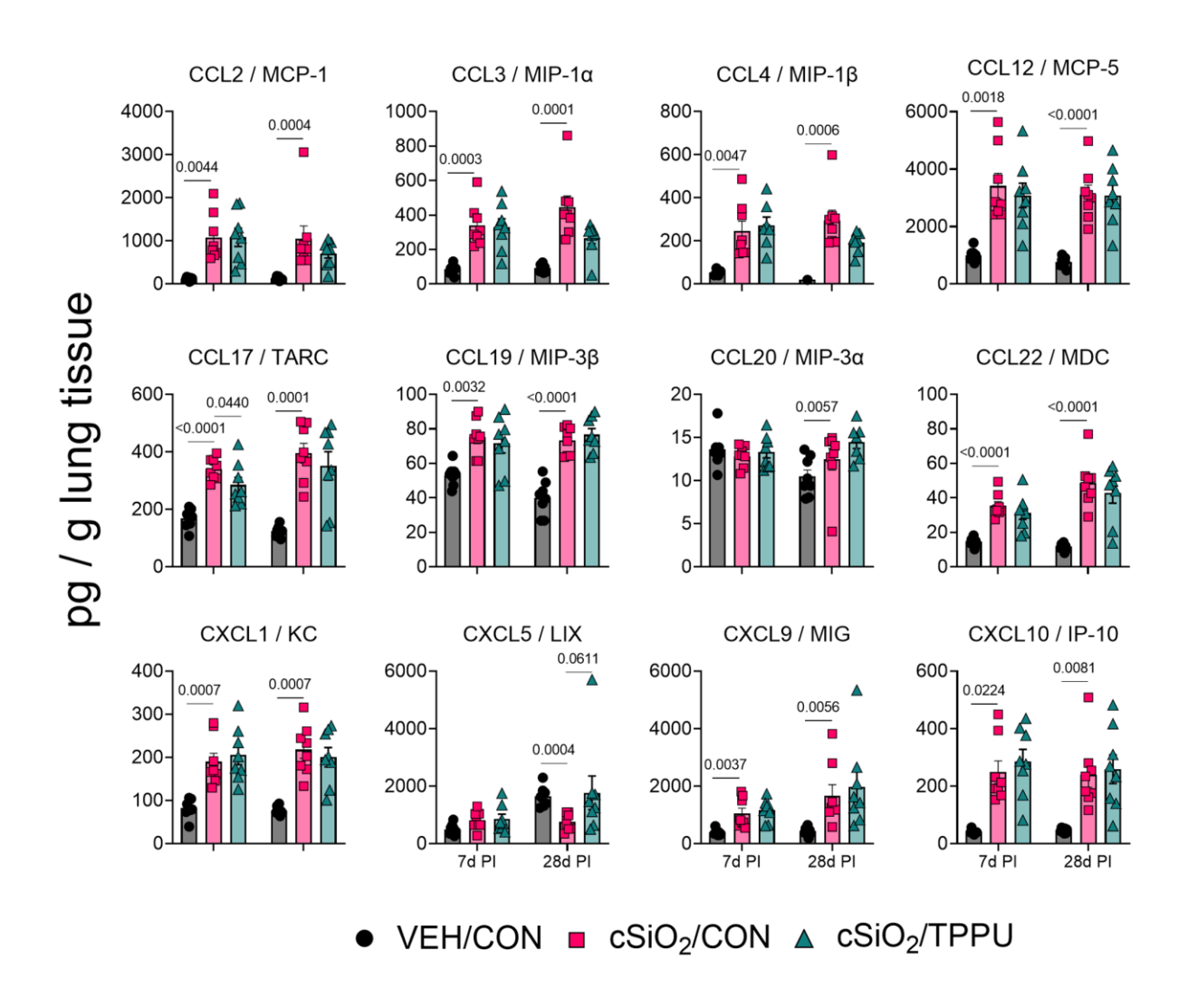


Figure 5.10. Dietary TPPU supplementation has limited effects on cSiO₂-induced chemokine production in the lung. Following sacrifice, middle lung lobes were isolated and homogenates analyzed for production of selected chemokines using Mouse Cytokine/Chemokine 44-Plex Discovery Assay® Array from Eve Technologies. Chemokine quantities were normalized to the original weight of lung tissue homogenized for the analysis. Data are presented as mean \pm SEM (n = 8). Values of p<0.2 are shown, with p<0.05 considered statistically significant.

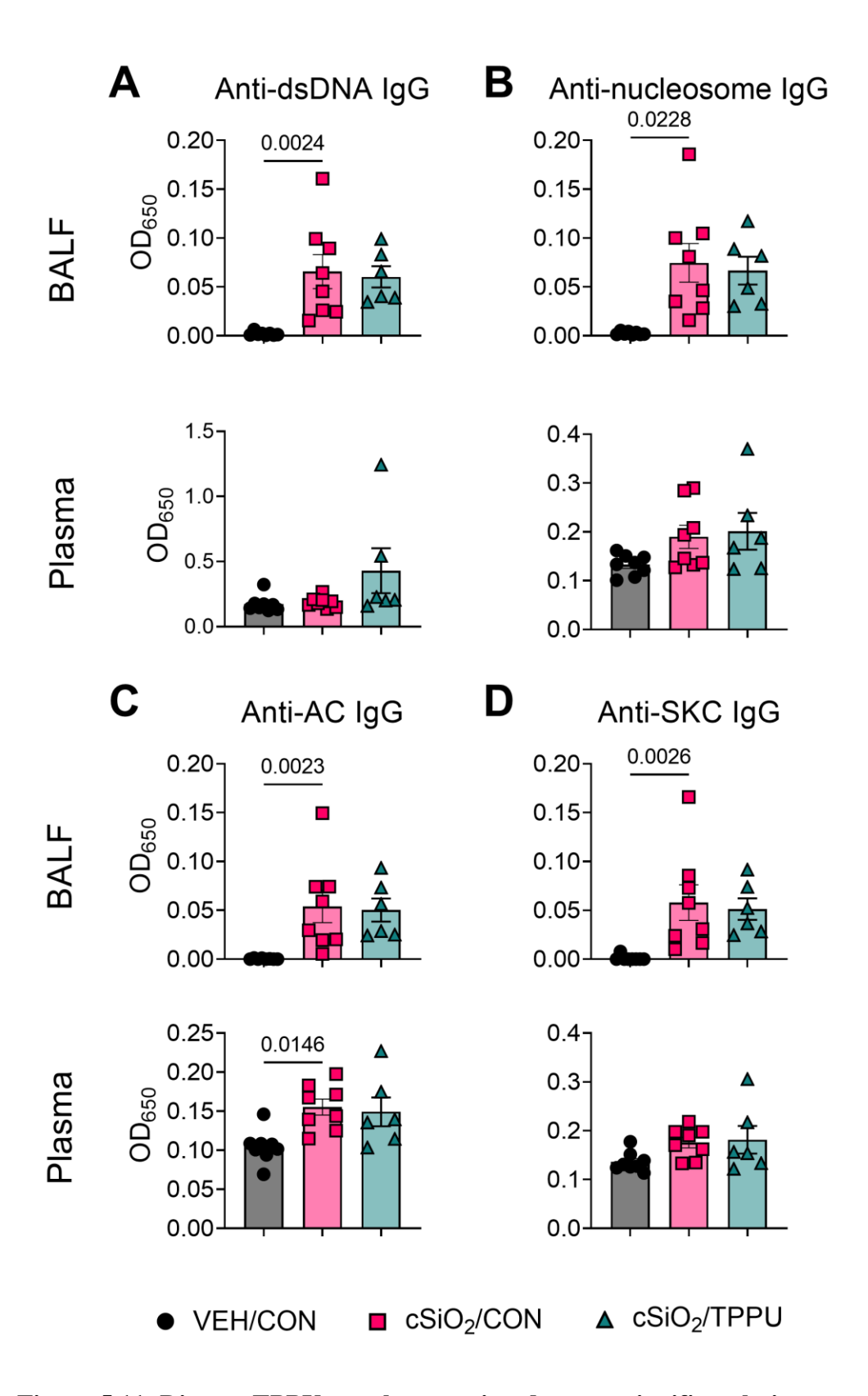


Figure 5.11. Dietary TPPU supplementation does not significantly impact secretion of IgG autoantibodies into BALF and plasma of NZBWF1 mice. Total IgG specific to (A) dsDNA,

Figure 5.11 (cont'd)

(B) nucleosome antigen, **(C)** apoptotic cell (AC)-derived material, and **(D)** cSiO₂-killed cell (SKC)-derived material was measured by ELISA in the BALF and plasma of VEH/CON, cSiO₂/CON, and cSiO₂/TPPU mice sacrificed at 28d PI. Data are presented as mean \pm SEM (n = 8). Values of p<0.1 are shown, with p<0.05 considered statistically significant.

TABLES

Table 5.1. Experimental groups.

Experimental Group	Number of Animals (n)	cSiO ₂ (-/+)	Necropsy Timepoint	Experimental Diet
VEH/CON	8	-	7 d PI	AIN-93G
cSiO ₂ /CON	8	+	7 d PI	AIN-93G
cSiO ₂ /TPPU	8	+	7 d PI	AIN-93G+TPPU
VEH/CON	8	-	28 d PI	AIN-93G
cSiO ₂ /CON	8	+	28 d PI	AIN-93G
cSiO ₂ /TPPU	8	+	28 d PI	AIN-93G+TPPU

VEH, vehicle; CON, control; cSiO₂, crystalline silica; PI, post-cSiO₂ instillation.

Table 5.2. Experimental diet formulations.

Experimental Diet					
-	CON	TPPU			
Macronutrient	(g/kg total diet)				
Carbohydrates					
Corn starch	398	398			
Maltodextrin (Dyetrose)	132	132			
Sucrose	100	100			
Cellulose	50	50			
kcal (% of total)	63.2	63.2			
Proteins					
Casein	200	200			
L-Cysteine	3	3			
kcal (% of total)	19.7	19.7			
Fats ^a					
Corn oil ^b	10	10			
High oleic-safflower oil ^c	60	60			
kcal (% of total)	17.1	17.1			
Other					
AIN-93G mineral mix	35	35			
AIN-93G vitamin mix	10	10			
Choline bitartrate	3	3			
TBHQ antioxidant	0.01	0.01			
TPPU	0	0.0225			

All values are reported as mass (g) per kg of diet. ^a As reported by the manufacturer

b Corn oil contained 612 g/kg linoleic acid and 26 g/kg oleic acid
c High oleic-safflower oil contained 750 g/kg oleic acid and 140 g/kg linoleic acid

CHAPTER 6: CONCLUSIONS AND FUTURE DIRECTIONS

CONCLUSIONS

This research demonstrates that modulating the cellular lipidome by dietary ω -3 polyunsaturated fatty acid (PUFA) administration and by soluble epoxide hydrolase (sEH) inhibition delays the initial onset and development of inflammation and autoimmunity triggered by two environmental toxicants: bacterial lipopolysaccharide (LPS) and respirable crystalline silica (cSiO₂). The results presented in this dissertation provide a strong scientific premise for conducting future investigations to better understand how lipidome modulation via ω -3/6 PUFA administration and pharmacological inhibition impact the progression of toxicant-triggered inflammatory and autoimmune responses in alveolar macrophages (AMs) *in vitro* and in lupusprone NZBWF1 mice *in vivo*.

The findings of the studies discussed herein build upon previously reported research indicating that ω-3 PUFAs and ω-3/6 epoxy fatty acid (EpFA) metabolites preserved by sEH inhibition dampen toxicant-triggered inflammatory responses and autoimmunity. In **Chapter 3**, lipidome modulation via dietary administration of the ω-3 PUFA docosahexaenoic acid (DHA) and pharmacological sEH inhibition with TPPU suppressed rough LPS (R-LPS)-induced glomerulonephritis (GN) separately but not when administered together in lupus-prone NZBFW1 mice. **Chapter 4** utilized a novel *in vitro* surrogate model for AMs—namely, fetal liver-derived alveolar macrophages (FLAMs) [34]—to establish pro-resolving impacts of DHA on cSiO₂-triggered cytokine release and proinflammatory oxylipin production. Finally, the results of **Chapter 5** suggest that sEH inhibition protects against initial cSiO₂-driven lung inflammation by inhibiting elevation total cells, monocytes, neutrophils, and lymphocytes in the bronchoalveolar lavage fluid (BALF) yet, dissimilar to DHA [351, 352], has no significant effect on centriacinar histopathology, recruitment of inflammatory granulocytes and lymphocytes, proinflammatory

gene expression, cytokine and chemokine production, or autoantibody (AAb) release from the lung.

Taken together, these results demonstrate potential roles that lipidome-modulating interventions may have in preventing and treating environmentally-triggered autoimmune diseases, including lupus. Although individuals cannot rid themselves of genetic predispositions to autoimmunity—and exposures to environmental toxicants in some cases—genetically susceptible individuals may be able to alter the exposome by consuming a ω-3 PUFA-rich diet or using pharmacological interventions to modify endogenous lipid metabolites, thereby decreasing their risk of developing autoimmune disease. Current therapeutic interventions for chronic inflammation and autoimmune diseases (e.g., corticosteroids, immunosuppressants, monoclonal antibodies) aim to alleviate disease symptoms by shutting down innate and adaptive immune responses. While effective at alleviating symptoms, these drugs are commonly associated with adverse side effects, development of comorbidities, high financial costs, and reduced quality of life [13-17]. Lipidome-modulating interventions, such as a ω-3 PUFA-rich diet or novel drugs that promote pro-resolving lipid mediator synthesis, may reduce the burden of disease and the costs of mainstay drug use by acting as steroid-sparing agents at minimum or as complete replacements for current mainstay drugs.

In line with the National Institute of Health's (NIH's) ten-year strategic plan for nutrition research, animal and clinical studies suggest that consumption of marine ω -3 PUFAs and inhibition of sEH may prevent development of chronic inflammatory conditions and autoimmune disease [19, 21-23, 390, 397, 491, 515, 620-622]. Both ω -3 PUFA consumption and sEH inhibition have been previously shown to shift fatty acid and oxylipin profiles in the blood, tissues, and immune cells from proinflammatory to pro-resolving in preclinical and clinical contexts [27, 344, 470, 488,

489, 623, 624], and these lipidome shifts have been associated with improved disease outcomes. Future studies will focus on investigating how ω -3 PUFAs, ω -6 PUFAs, and sEH inhibition impact oxylipin profiles in FLAMs, lungs, kidneys, and plasma from lupus-prone mice and relating these findings to resultant environmentally-triggered inflammatory and autoimmune responses *in vitro* and *in vivo*.

FUTURE DIRECTIONS

Compare cSiO₂-induced oxylipin profiles in DHA-, ARA-, and TPPU-treated NZBWF1 FLAM cultures over 24 hours

The membrane phospholipid data presented in Chapter 4 of this dissertation suggest that treating FLAMs derived from non-autoimmune C57BL/6 mice with DHA causes membrane incorporation of DHA at the expense of the ω-9 monounsaturated fatty acid (MUFA) oleic acid (OA; C18:1ω9) and the ω-6 PUFA arachidonic acid (ARA; C20:4ω6). The findings of Chapter 4 also demonstrate that exposing C57BL/6 FLAMs to cSiO₂ triggers biosynthesis of ω-6 ARAderived lipid mediators including prostaglandin E2 (PGE2), leukotriene B4 (LTB4), thromboxane B2 (TXB2), and hydroxyeicosatrienoic acids (HETEs), while DHA pretreatment skews the cSiO₂induced lipidome toward ω-3 PUFA-derived metabolites, such as hydroxyeicosapentaenoic acids (HEPEs) and hydroxydocosahexaenoic acids (HDoHEs). In female lupus-prone NZBWF1 mice, we have previously demonstrated that DHA treatment results in increased ω-3 PUFA content in erythrocytes, lungs, kidneys, spleen, and liver [19, 20, 344, 582, 625]. Correspondingly, the data presented in Chapter 3 of this dissertation further show that dietary DHA administration causes increased levels of ω-3 PUFA-derived lipid mediators in the plasma [595]. Other studies conducted in both mice and humans demonstrate that genome-driven dysregulation of lipid metabolism is linked to accelerated inflammation and tissue damage in lupus [626-630]. Accordingly, it would be informative to compare the impacts of lipidome modulation via ω -3 supplementation with DHA, ω -6 supplementation with ARA, and sEH inhibition with TPPU on the cSiO₂-triggered lipid metabolite profile of autoimmune-prone NZBWF1 FLAMs. Lipidomic profiles should be analyzed over a 24 h window to identify immediate lipid biomarkers associated with cSiO₂ exposure and to track transient changes in proinflammatory and pro-resolving mediators between treatment groups.

Based on our results in C57BL/6 FLAMs (Chapter 4) and data in previously published studies focused on airway exposure to environmental toxicants [631, 632], we expect that cSiO₂ will trigger production of 1) proinflammatory lipid metabolites in ARA-treated NZBWF1 FLAMs, 2) pro-resolving lipid metabolites in DHA-treated FLAMs, and 3) EpFAs derived from endogenous PUFAs at the expense of DiHFAs in TPPU-treated FLAMs. In follow-up studies, NZBWF1 FLAMs could be genetically modified by CRISPR/Cas9 technology or treated with pharmacological inhibitors cyclooxygenase, lipoxygenases, of cytochrome P450 monooxygenases/hydroxylases, and autooxidation to investigate the impacts of these biosynthetic pathways on cSiO₂-triggered lipid metabolite production, proinflammatory cytokine release, and death in ARA-, DHA-, and TPPU-treated cells. If significant effects are observed with NZBWF1 FLAMs, these experiments could be recapitulated in primary AMs isolated from NZBWF1 mice. One challenge associated with the proposed lipidomic studies is that lipid metabolites have relatively low stability compared to their fatty acid precursors. To address this challenge, all samples would be pretreated with an antioxidant cocktail (0.2 mg/ml butylated hydroxytoluene, 0.2 mg/ml triphenylphosphine, 0.6 mg/ml EDTA) [414] prior to mass spectrometry analyses.

Evaluate paracrine effects of DHA-, ARA-, and TPPU-derived oxylipins on cSiO₂-induced proinflammatory cytokine release in NZBWF1 FLAMs

Our lipidomic data in non-autoimmune C57BL/6 FLAMs (Chapter 4) suggest that cSiO₂ induces a variety of proinflammatory and pro-resolving lipid mediators in the absence and presence of DHA, respectively. Many studies have focused on the impacts of individual metabolites on macrophage inflammatory responses have been published [454, 633-640]; however, it is also possible that oxylipins derived from ω-3/6 PUFAs act upon nearby macrophages in a paracrine-like manner as heterogenous mixtures. To address this possibility, FLAMs from autoimmune NZBWF1 mice would be pretreated with ω-3 DHA, ω-6 ARA, or the sEH inhibitor TPPU then exposed to cSiO₂ to generate conditioned medium that contains lipid metabolites released from FLAMs. Separate NZBWF1 FLAM cultures would subsequently be incubated with the oxylipin-containing conditioned medium, exposed to cSiO₂, then analyzed for biomarkers of cSiO₂-induced toxicity (e.g., proinflammatory cytokine expression and released).

I predict that conditioned medium from FLAMs pretreated with DHA and TPPU would more effectively abrogate cSiO₂-triggered toxic responses compared to conditioned medium from ARA-pretreated FLAMs. Non-autoimmune C57BL/6 FLAMs would be used as a positive control for these experiments, and the findings observed in NZBWF1 FLAMs would then be compared against primary NZBWF1 AMs in follow-up studies. Together, these studies would provide deeper mechanistic insight on how lipidome-modulating agents, including dietary PUFAs and pharmacological compounds, impact alveolar macrophage function following toxicant exposure. Treating FLAMs with oxylipin mixtures instead of individual lipid metabolites also would more closely represent the complex changes in mouse and human oxylipin profiles in response to

environmental agents, as many oxylipins are increased and decreased in the plasma, not just one [27, 344, 470, 488, 489, 623, 624].

<u>Identify fatty acid receptors that mediate protective effects of lipid metabolites against cSiO2-induced proinflammatory cytokine release in NZBWF1 FLAMs</u>

Both PUFAs and ω-3/6 PUFA-derived oxylipins mediate their biological effects in part via ligand-receptor interactions. For instance, DHA is believed to activate anti-inflammatory signaling pathways by acting as a ligand for G protein-coupled receptor 120 (GPR120) and PPARy in macrophages [641, 642], whereas there is limited evidence that ARA triggers internalization of GPR120 [643] yet inhibits NF-κB activation through a PPARγ-dependent pathway [644]. Additionally, prostanoids, leukotrienes, HETEs, oxoeicosatrienoic acids (oxo-ETEs), resolvins, maresins, and other oxylipins derived from ω-3/6 PUFAs have been shown to enact proinflammatory and pro-resolving responses through a variety of transmembrane GPRs, which have been thoroughly reviewed [542, 543, 645-648]. Accordingly, it would be of interest to first evaluate the expression levels of these oxylipin receptors (e.g., EP1-4, BLT1-2, ALX4/FPR2, DRV1/GPR32, DRV2/GPR18) in both autoimmune NZBWF1 FLAMs and non-autoimmune C57BL/6 FLAMs. Such an analysis would allow us for the first time to understand how oxylipin receptor expression in AMs is impacted by genetic predisposition to autoimmune disease. After confirming the expression of these receptors, we would genetically inhibit these receptors by producing CRISPR/Cas9 knockout FLAMs and pharmacologically inhibit these receptors by treating unmodified FLAMs with corresponding antagonists, then subsequently evaluate the effects of inhibition on cSiO₂-triggered release of proinflammatory cytokines.

I hypothesize that genetic and/or pharmacological inhibition of receptors for proinflammatory oxylipins (e.g., prostanoids, leukotrienes, HETEs, oxo-ETEs, etc.) will provide

protection against cSiO₂-induced toxicity in vehicle-treated FLAMs, whereas genetic and/or pharmacological inhibition of receptors for pro-resolving oxylipins (e.g., HDoHEs, E- and D-series resolvins, maresins, etc.) would negate the protective effects of DHA in cSiO₂-exposed FLAMs. In follow-up experiments, it would be interesting to instill CRISPR/Cas9-edited knockout FLAMs into the lungs of AM-deficient NZBWF1 mice (methodology described in [494]) to evaluate the roles that different oxylipin receptors play in DHA's ameliorative effects on cSiO₂-triggered toxicity. Such studies could be expanded upon in the future using other inhaled particles (e.g., asbestos [192], carbon nanotubes [265], titanium dioxide [254], agricultural dusts [649]), other types of environmental toxicants (e.g., bacterial LPS [365], ultraviolet light [650]), and other long-chain ω-3/6 PUFAs (e.g., ARA and eicosapentaenoic acid [EPA] [651-653]).

Compare the effects of control, DHA-supplemented, and TPPU-enriched diets on the kinetics of LPS- and cSiO₂-induced changes in pulmonary, renal, and plasma oxylipin profiles

Our *in vivo* findings in lupus-prone NZBWF1 mice (Chapter 3) demonstrate that the ω-3 PUFA DHA and sEH inhibitor TPPU significantly skew the cellular lipidome toward proresolving metabolites. Specifically, dietary DHA supplementation resulted in significant decreases in ARA-derived lipid metabolites and corresponding increases in DHA- and EPA-derived metabolites, and dietary TPPU administration preserved plasma ARA-derived EpFAs in controlfed mice and plasma DHA-/EPA-derived EpFAs in DHA-fed mice. One limitation of this study is that we only focused on profiling plasma lipid metabolites at one timepoint and did not perform lipidomic profiling of other organs, such as the lung and kidney. While previous studies have demonstrated that LPS and cSiO₂ increases cellular ARA availability and ARA-derived lipid metabolite production in the lung [480, 654-659], comprehensive lipidomic studies have not yet been conducted in animal models of environmentally-triggered autoimmunity. In the LPS-

accelerated GN model [595] and the cSiO₂-induced lupus models that we have developed [318, 583], investigating changes in plasma, lung, and kidney oxylipin profiles over time in NZBWF1 mice fed control, DHA-enriched, or TPPU-enriched diet would allow us to address this knowledge gap by identifying lipid biomarkers associated with LPS- and cSiO₂-triggered pathology and elucidating the kinetic rates at which DHA and TPPU skew the lipidome in the plasma, lung, and kidney in the context of environmental toxicant exposure.

I expect that LPS and cSiO₂ would cause a steady increase in proinflammatory ARA-derived lipid metabolites (i.e., prostanoids, leukotrienes, HETEs) in control-fed mice, while these environmental toxicants would provoke a steady increase in pro-resolving DHA-/EPA-derived lipid mediators (i.e., resolvins, maresins, protectins, EpFAs, HFAs) in DHA- and TPPU-fed mice. Based on our previous findings in our LPS-accelerated GN model and cSiO₂-induced lupus models, we anticipate that oxylipin levels would remain elevated within the first 4 wk of toxicant exposure due to inefficient toxicant clearance and corresponding unresolved inflammation. However, it would also be informative to profile the plasma, lung, and kidney at later timepoints (e.g., 3 mo, 6 mo, etc.) to discern whether oxylipins remain stable, diminish, or increase over longer periods of time. The findings from these profiling studies would then be correlated with biomarkers of LPS- and cSiO₂-induced autoimmunity (e.g., proinflammatory gene expression, proinflammatory cytokine release, AAb production, lung/kidney histopathology) in mice, which could provide valuable insight on how the lipidome may impact the initiation and progression of autoimmunity in genetically predisposed individuals.

<u>Investigate impacts of direct lipid metabolite administration on LPS- and cSiO₂-triggered</u> <u>autoimmunity in female lupus-prone NZBWF1 mice</u>

Previous studies have demonstrated that direct administration of pro-resolving lipid metabolites in lieu of dietary PUFAs and sEH inhibitors has ameliorated inflammatory responses in rodent and human studies [660-664]. This approach may more reliably impart amelioration against toxicant-triggered inflammation compared to coadministration of ω -3 PUFAs with pharmacological enzyme inhibitors, such as sEH inhibitors. While some researchers have reported that ω -3 PUFA and sEH inhibitor cotreatment more effectively reduces inflammatory biomarkers in several rodent models [450, 621, 665], these findings are limited and have been contradicted by others, including us [595, 666]. Accordingly, it is possible that simultaneous ω -3 PUFA administration and pharmacological inhibition skews the lipidome such that certain pro-resolving metabolites are decreased (e.g., EpETrEs) and both proinflammatory metabolites (e.g., HETEs) and pro-resolving DHA-derived metabolites (e.g., EpDPEs) are increased.

By directly administering individual pro-resolving oxylipins to LPS- and cSiO₂-exposed NZBWF1 mice, we would be able to evaluate the impacts of individual metabolites on the plasma, lung, and kidney lipidome and biomarkers of toxicity (e.g., proinflammatory gene expression, proinflammatory cytokine release, AAb production, lung/kidney histopathology), then compare with results generated from mice administered ω-3 PUFAs and/or pharmacological inhibitors. If successful, these studies also would provide compelling preclinical rationale for developing proresolving oxylipin analogs for individuals at risk of developing environmentally-triggered autoimmunity. To this end, a stable analog of EpETrE previously has been reported to delay development of GN in lupus-prone NZBWF1 mice [667], which suggests similar pro-resolving oxylipin analogs may prove efficacious in both rodents and humans.

REFERENCES

- 1. Vojdani, A., K.M. Pollard, and A.W. Campbell, *Environmental triggers and autoimmunity*. Autoimmune Dis, 2014. **2014**: p. 798029.
- 2. Pestka, J.J., K.M. Pollard, and A.J. Rosenspire, *Editorial: The Role of the Environment in Autoimmunity*. Front Immunol, 2021. **12**: p. 641171.
- 3. Leffers, H.C.B., et al., *The study of interactions between genome and exposome in the development of systemic lupus erythematosus.* Autoimmun Rev, 2019. **18**(4): p. 382-392.
- 4. Wang, L., F.S. Wang, and M.E. Gershwin, *Human autoimmune diseases: a comprehensive update*. J Intern Med, 2015. **278**(4): p. 369-95.
- 5. Vojdani, A. and E. Vojdani, *The Role of Exposomes in the Pathophysiology of Autoimmune Diseases I: Toxic Chemicals and Food.* Pathophysiology, 2021. **28**(4): p. 513-543.
- 6. Association, A.A.R.D. *What is autoimmune disease?* 2019 [cited 2023 2/24/2023]; Available from: https://autoimmune.org/wp-content/uploads/2019/12/1-in-5-Brochure.pdf.
- 7. Sloan, M., et al., Medically explained symptoms: a mixed methods study of diagnostic, symptom and support experiences of patients with lupus and related systemic autoimmune diseases. Rheumatol Adv Pract, 2020. 4(1): p. rkaa006.
- 8. Cho, J.H. and M. Feldman, *Heterogeneity of autoimmune diseases: pathophysiologic insights from genetics and implications for new therapies.* Nat Med, 2015. **21**(7): p. 730-8.
- 9. Richard-Eaglin, A. and B.A. Smallheer, *Immunosuppressive/Autoimmune Disorders*. Nurs Clin North Am, 2018. **53**(3): p. 319-334.
- 10. Jung, S.M. and W.U. Kim, *Targeted Immunotherapy for Autoimmune Disease*. Immune Netw, 2022. **22**(1): p. e9.
- 11. Thong, B. and N.J. Olsen, *Systemic lupus erythematosus diagnosis and management*. Rheumatology (Oxford), 2017. **56**(suppl_1): p. i3-i13.
- 12. Singh, J.A., *Treatment Guidelines in Rheumatoid Arthritis*. Rheum Dis Clin North Am, 2022. **48**(3): p. 679-689.
- 13. Li, P., Y. Zheng, and X. Chen, *Drugs for Autoimmune Inflammatory Diseases: From Small Molecule Compounds to Anti-TNF Biologics.* Front Pharmacol, 2017. **8**: p. 460.
- 14. Rice, J.B., et al., *Healthcare resource use and cost associated with varying dosages of extended corticosteroid exposure in a US population*. J Med Econ, 2018. **21**(9): p. 846-852.

- 15. Carter, E.E., S.G. Barr, and A.E. Clarke, *The global burden of SLE: prevalence, health disparities and socioeconomic impact.* Nat Rev Rheumatol, 2016. **12**(10): p. 605-20.
- 16. McCormick, N., C.A. Marra, and J.A. Avina-Zubieta, *Productivity Losses and Costs in the Less-Common Systemic Autoimmune Rheumatic Diseases*. Curr Rheumatol Rep, 2017. **19**(11): p. 72.
- 17. Kawalec, P.P. and K.P. Malinowski, *The indirect costs of systemic autoimmune diseases, systemic lupus erythematosus, systemic sclerosis and sarcoidosis: a summary of 2012 reallife data from the Social Insurance Institution in Poland.* Expert Rev Pharmacoecon Outcomes Res, 2015. **15**(4): p. 667-73.
- 18. Health, N.I.o. 2020–2030 Strategic Plan for NIH Nutrition Research. 2020 [cited 2023 2/25/2023]; Available from: https://dpcpsi.nih.gov/sites/default/files/2020NutritionStrategicPlan_508.pdf.
- 19. Bates, M.A., et al., Silica-Triggered Autoimmunity in Lupus-Prone Mice Blocked by Docosahexaenoic Acid Consumption. PLoS One, 2016. 11(8): p. e0160622.
- 20. Bates, M.A., et al., Dietary Docosahexaenoic Acid Prevents Silica-Induced Development of Pulmonary Ectopic Germinal Centers and Glomerulonephritis in the Lupus-Prone NZBWF1 Mouse. Front Immunol, 2018. 9(September): p. 2002.
- 21. Zhou, Y., et al., *Soluble epoxide hydrolase inhibitor 1-trifluoromethoxyphenyl-3- (1-propionylpiperidin-4-yl) urea attenuates bleomycin-induced pulmonary fibrosis in mice.* Cell Tissue Res, 2016. **363**(2): p. 399-409.
- 22. Biliktu, M., et al., *Pharmacological inhibition of soluble epoxide hydrolase attenuates chronic experimental autoimmune encephalomyelitis by modulating inflammatory and anti-inflammatory pathways in an inflammasome-dependent and -independent manner.* Inflammopharmacology, 2020. **28**(6): p. 1509-1524.
- 23. Klocke, J., et al., *Prophylactic inhibition of soluble epoxide hydrolase delays onset of nephritis and ameliorates kidney damage in NZB/W F1 mice*. Sci Rep, 2019. **9**(1): p. 8993.
- 24. Charoenwoodhipong, P., et al., *Dietary omega polyunsaturated fatty acid intake and patient-reported outcomes in systemic lupus erythematosus: The Michigan Lupus Epidemiology & Surveillance (MILES) Program.* Arthritis Care Res (Hoboken), 2019.
- 25. Kostoglou-Athanassiou, I., L. Athanassiou, and P. Athanassiou, *The Effect of Omega-3 Fatty Acids on Rheumatoid Arthritis*. Mediterr J Rheumatol, 2020. **31**(2): p. 190-194.
- 26. Lee, K.S.S., et al., *Preparation and evaluation of soluble epoxide hydrolase inhibitors with improved physical properties and potencies for treating diabetic neuropathic pain.* Bioorg Med Chem, 2020. **28**(22): p. 115735.

- 27. Martini, R.P., et al., A Double-Blind, Randomized, Placebo-Controlled Trial of Soluble Epoxide Hydrolase Inhibition in Patients with Aneurysmal Subarachnoid Hemorrhage. Neurocrit Care, 2022. **36**(3): p. 905-915.
- 28. Tsai, P.Y., et al., Epigallocatechin-3-gallate prevents lupus nephritis development in mice via enhancing the Nrf2 antioxidant pathway and inhibiting NLRP3 inflammasome activation. Free Radic Biol Med, 2011. **51**(3): p. 744-54.
- 29. Ka, S.M., et al., Citral alleviates an accelerated and severe lupus nephritis model by inhibiting the activation signal of NLRP3 inflammasome and enhancing Nrf2 activation. Arthritis Res Ther, 2015. 17: p. 331.
- 30. Yang, S.R., et al., *Xenon blunts NF-kappaB/NLRP3 inflammasome activation and improves acute onset of accelerated and severe lupus nephritis in mice.* Kidney Int, 2020. **98**(2): p. 378-390.
- 31. Yang, S.R., et al., *Accelerated, severe lupus nephritis benefits from treatment with honokiol by immunoregulation and differentially regulating NF-kappaB/NLRP3 inflammasome and sirtuin 1/autophagy axis.* FASEB J, 2020. **34**(10): p. 13284-13299.
- 32. Wu, C.Y., et al., *Tris DBA Ameliorates Accelerated and Severe Lupus Nephritis in Mice by Activating Regulatory T Cells and Autophagy and Inhibiting the NLRP3 Inflammasome.* J Immunol, 2020. **204**(6): p. 1448-1461.
- 33. Chang, Y.P., et al., Resveratrol inhibits NLRP3 inflammasome activation by preserving mitochondrial integrity and augmenting autophagy. J Cell Physiol, 2015. **230**(7): p. 1567-79.
- 34. Thomas, S.T., et al., Fetal Liver-Derived Alveolar-like Macrophages: A Self-Replicating Ex Vivo Model of Alveolar Macrophages for Functional Genetic Studies. Immunohorizons, 2022. **6**(2): p. 156-169.
- 35. Donaldson, K. and A. Seaton, *A short history of the toxicology of inhaled particles*. Part Fibre Toxicol, 2012. **9**(1): p. 13.
- 36. Perlman, D.M. and L.A. Maier, *Occupational Lung Disease*. Med Clin North Am, 2019. **103**(3): p. 535-548.
- 37. Beheshti, S.O., et al., Worldwide Prevalence of Familial Hypercholesterolemia: Meta-Analyses of 11 Million Subjects. J Am Coll Cardiol, 2020. **75**(20): p. 2553-2566.
- 38. Butler, F., A. Alghubayshi, and Y. Roman, *The Epidemiology and Genetics of Hyperuricemia and Gout across Major Racial Groups: A Literature Review and Population Genetics Secondary Database Analysis.* J Pers Med, 2021. **11**(3).
- 39. Rock, K.L., H. Kataoka, and J.J. Lai, *Uric acid as a danger signal in gout and its comorbidities*. Nat Rev Rheumatol, 2013. **9**(1): p. 13-23.

- 40. Jin, M., et al., *Uric acid, hyperuricemia and vascular diseases*. Front Biosci (Landmark Ed), 2012. **17**(2): p. 656-69.
- 41. Goldstein, J.L. and M.S. Brown, *A century of cholesterol and coronaries: from plaques to genes to statins*. Cell, 2015. **161**(1): p. 161-172.
- 42. Nidorf, S.M., A. Fiolet, and G.S. Abela, *Viewing atherosclerosis through a crystal lens:* How the evolving structure of cholesterol crystals in atherosclerotic plaque alters its stability. J Clin Lipidol, 2020. **14**(5): p. 619-630.
- 43. Ioannou, G.N., *The Role of Cholesterol in the Pathogenesis of NASH*. Trends Endocrinol Metab, 2016. **27**(2): p. 84-95.
- 44. Di Ciaula, A., D.Q. Wang, and P. Portincasa, *An update on the pathogenesis of cholesterol gallstone disease*. Curr Opin Gastroenterol, 2018. **34**(2): p. 71-80.
- 45. Matzinger, P., *Tolerance*, *danger*, *and the extended family*. Annu Rev Immunol, 1994. **12**: p. 991-1045.
- 46. Matzinger, P., *The danger model: a renewed sense of self.* Science, 2002. **296**(5566): p. 301-5.
- 47. Gallucci, S. and P. Matzinger, *Danger signals: SOS to the immune system*. Curr Opin Immunol, 2001. **13**(1): p. 114-9.
- 48. Tveita, A.A., *The danger model in deciphering autoimmunity*. Rheumatology (Oxford), 2010. **49**(4): p. 632-9.
- 49. Doria, A., et al., *Autoinflammation and autoimmunity: bridging the divide*. Autoimmun Rev, 2012. **12**(1): p. 22-30.
- 50. Boraschi, D., et al., *Nanoparticles and innate immunity: new perspectives on host defence.* Semin Immunol, 2017. **34**: p. 33-51.
- 51. Mossman, B.T. and R.E. Glenn, *Bioreactivity of the crystalline silica polymorphs, quartz and cristobalite, and implications for occupational exposure limits (OELs)*. Crit Rev Toxicol, 2013. **43**(8): p. 632-60.
- 52. Mulay, S.R. and H.J. Anders, *Crystallopathies*. N Engl J Med, 2016. **374**(25): p. 2465-76.
- 53. Kusiorowski, R., et al., *Thermal decomposition of different types of asbestos*. Journal of Thermal Analysis and Calorimetry, 2012. **109**(2): p. 693-704.
- 54. Goswami, E., et al., *Domestic asbestos exposure: a review of epidemiologic and exposure data.* Int J Environ Res Public Health, 2013. **10**(11): p. 5629-70.
- 55. Iijima, S., Helical microtubules of graphitic carbon. Nature, 1991. **354**(6348): p. 56-58.

- Venkataraman, A., et al., *Carbon Nanotube Assembly and Integration for Applications*. Nanoscale Res Lett, 2019. **14**(1): p. 220.
- 57. Zhang, A. and C.M. Lieber, *Nano-Bioelectronics*. Chem Rev, 2016. **116**(1): p. 215-57.
- 58. Porter, D.W., et al., *Differential mouse pulmonary dose and time course responses to titanium dioxide nanospheres and nanobelts.* Toxicol Sci, 2013. **131**(1): p. 179-93.
- 59. Musial, J., et al., *Titanium Dioxide Nanoparticles in Food and Personal Care Products-What Do We Know about Their Safety?* Nanomaterials (Basel), 2020. **10**(6).
- 60. Mohajerani, A., et al., *Nanoparticles in Construction Materials and Other Applications, and Implications of Nanoparticle Use.* Materials (Basel), 2019. **12**(19): p. 3052.
- 61. Baranowska-Wojcik, E., et al., *Effects of Titanium Dioxide Nanoparticles Exposure on Human Health-a Review.* Biol Trace Elem Res, 2020. **193**(1): p. 118-129.
- 62. Glenny, A.T., et al., *Immunological notes*. *XVII-XXIV*. The Journal of Pathology and Bacteriology, 1926. **29**(1): p. 31-40.
- 63. Tomljenovic, L. and C.A. Shaw, *Aluminum vaccine adjuvants: are they safe?* Curr Med Chem, 2011. **18**(17): p. 2630-7.
- 64. Dominici, F., et al., Chemical Composition of Fine Particulate Matter and Life Expectancy: In 95 US Counties Between 2002 and 2007. Epidemiology, 2015. **26**(4): p. 556-64.
- 65. Adams, K., et al., *Particulate matter components, sources, and health: Systematic approaches to testing effects.* J Air Waste Manag Assoc, 2015. **65**(5): p. 544-58.
- 66. Kelly, F.J. and J.C. Fussell, *Toxicity of airborne particles-established evidence, knowledge gaps and emerging areas of importance*. Philos Trans A Math Phys Eng Sci, 2020. **378**(2183): p. 20190322.
- 67. Park, M., et al., *Differential toxicities of fine particulate matters from various sources*. Sci Rep, 2018. **8**(1): p. 17007.
- 68. Peixoto, M.S., M.F. de Oliveira Galvao, and S.R. Batistuzzo de Medeiros, *Cell death pathways of particulate matter toxicity*. Chemosphere, 2017. **188**: p. 32-48.
- 69. Zhao, C.N., et al., *Emerging role of air pollution in autoimmune diseases*. Autoimmun Rev, 2019. **18**(6): p. 607-614.
- 70. Curtis, L., *PM*(2.5), *NO*(2), wildfires, and other environmental exposures are linked to higher Covid 19 incidence, severity, and death rates. Environ Sci Pollut Res Int, 2021. **28**(39): p. 54429-54447.

- 71. Elliott, J.H., *Silicosis in Ontario Gold Miners*. Trans Am Climatol Clin Assoc, 1923. **39**: p. 24-43.
- 72. Heffernan, P., *Some Notes on the Biophysics of Silica and the Etiology of Silicosis*. Br Med J, 1929. **2**(3584): p. 489-92.
- 73. Russ, K.A., et al., *Biological effects of inhaled hydraulic fracturing sand dust. IV. Pulmonary effects.* Toxicol Appl Pharmacol, 2020. **409**: p. 115284.
- 74. Hall, N.B., et al., Assessment of pneumoconiosis in surface coal miners after implementation of a national radiographic surveillance program, United States, 2014-2019. Am J Ind Med, 2020. **63**(12): p. 1104-1108.
- 75. Fazen, L.E., B. Linde, and C.A. Redlich, *Occupational lung diseases in the 21st century:* the changing landscape and future challenges. Curr Opin Pulm Med, 2020. **26**(2): p. 142-148.
- 76. Mossman, B.T., et al., *Pulmonary endpoints (lung carcinomas and asbestosis) following inhalation exposure to asbestos.* J Toxicol Environ Health B Crit Rev, 2011. **14**(1-4): p. 76-121.
- 77. Pira, E., et al., *Exposure to asbestos: past, present and future*. J Thorac Dis, 2018. **10**(Suppl 2): p. S237-S245.
- 78. Donaldson, K., et al., Asbestos, carbon nanotubes and the pleural mesothelium: a review of the hypothesis regarding the role of long fibre retention in the parietal pleura, inflammation and mesothelioma. Part Fibre Toxicol, 2010. **7**(1): p. 5.
- 79. Beg, S., et al., Advancement in carbon nanotubes: basics, biomedical applications and toxicity. J Pharm Pharmacol, 2011. **63**(2): p. 141-63.
- 80. Negri, V., et al., *Carbon Nanotubes in Biomedicine*. Top Curr Chem (Cham), 2020. **378**(1): p. 15.
- 81. Gherardi, R.K. and F.J. Authier, *Macrophagic myofasciitis: characterization and pathophysiology*. Lupus, 2012. **21**(2): p. 184-9.
- 82. Polizzi, S., et al., *Neurotoxic effects of aluminium among foundry workers and Alzheimer's disease.* Neurotoxicology, 2002. **23**(6): p. 761-74.
- 83. Rifat, S.L., et al., *Effect of exposure of miners to aluminium powder*. Lancet, 1990. **336**(8724): p. 1162-5.
- 84. NIOSH. *Silica*, *amorphous*. 2019 10/30/2019 [cited 2021 8/2/2021]; Available from: https://www.cdc.gov/niosh/npg/npgd0552.html.
- 85. Fukakusa, J., et al., Factors influencing respirator use at work in respiratory patients. Occup Med (Lond), 2011. **61**(8): p. 576-82.

- 86. Gallo, P.M. and S. Gallucci, *The dendritic cell response to classic, emerging, and homeostatic danger signals. Implications for autoimmunity.* Front Immunol, 2013. **4**: p. 138.
- 87. Pownall, H.J. and A.M. Gotto, Jr., *Cholesterol: Can't Live With It, Can't Live Without It.* Methodist Debakey Cardiovasc J, 2019. **15**(1): p. 9-15.
- 88. Defesche, J.C., et al., *Familial hypercholesterolaemia*. Nat Rev Dis Primers, 2017. **3**: p. 17093.
- 89. Schaftenaar, F., et al., *Atherosclerosis: the interplay between lipids and immune cells.* Curr Opin Lipidol, 2016. **27**(3): p. 209-15.
- 90. Varsano, N., et al., *Two polymorphic cholesterol monohydrate crystal structures form in macrophage culture models of atherosclerosis.* Proc Natl Acad Sci U S A, 2018. **115**(30): p. 7662-7669.
- 91. Khan, S.R., et al., *Kidney stones*. Nat Rev Dis Primers, 2016. **2**: p. 16008.
- 92. Karasawa, T. and M. Takahashi, *Role of NLRP3 Inflammasomes in Atherosclerosis*. J Atheroscler Thromb, 2017. **24**(5): p. 443-451.
- 93. Sayer, J.A., *Progress in Understanding the Genetics of Calcium-Containing Nephrolithiasis*. J Am Soc Nephrol, 2017. **28**(3): p. 748-759.
- 94. Holdt, L.M. and D. Teupser, *From genotype to phenotype in human atherosclerosis--recent findings*. Curr Opin Lipidol, 2013. **24**(5): p. 410-8.
- 95. Dron, J.S. and R.A. Hegele, *Genetics of Triglycerides and the Risk of Atherosclerosis*. Curr Atheroscler Rep, 2017. **19**(7): p. 31.
- 96. Tai, V., T.R. Merriman, and N. Dalbeth, *Genetic advances in gout: potential applications in clinical practice.* Curr Opin Rheumatol, 2019. **31**(2): p. 144-151.
- 97. Kawamura, Y., et al., *Genome-wide association study revealed novel loci which aggravate asymptomatic hyperuricaemia into gout.* Ann Rheum Dis, 2019. **78**(10): p. 1430-1437.
- 98. Nishijima, N., et al., *Human Scavenger Receptor A1-Mediated Inflammatory Response to Silica Particle Exposure Is Size Specific.* Front Immunol, 2017. **8**: p. 379.
- 99. Tsugita, M., et al., SR-B1 Is a Silica Receptor that Mediates Canonical Inflammasome Activation. Cell Rep, 2017. **18**(5): p. 1298-1311.
- 100. Thakur, S.A., et al., *Critical role of MARCO in crystalline silica-induced pulmonary inflammation*. Toxicol Sci, 2009. **108**(2): p. 462-71.
- 101. Zani, I.A., et al., *Scavenger receptor structure and function in health and disease*. Cells, 2015. **4**(2): p. 178-201.

- 102. Omori, S., et al., *Tim4 recognizes carbon nanotubes and mediates phagocytosis leading to granuloma formation*. Cell Rep, 2021. **34**(6): p. 108734.
- 103. Neumann, K., et al., *Clec12a is an inhibitory receptor for uric acid crystals that regulates inflammation in response to cell death.* Immunity, 2014. **40**(3): p. 389-99.
- 104. Li, K., et al., *The uric acid crystal receptor Clec12A potentiates type I interferon responses*. Proc Natl Acad Sci U S A, 2019. **116**(37): p. 18544-18549.
- 105. Barabe, F., et al., Crystal-induced neutrophil activation VI. Involvment of FcgammaRIIIB (CD16) and CD11b in response to inflammatory microcrystals. FASEB J, 1998. 12(2): p. 209-20.
- 106. Nimmerjahn, F. and J.V. Ravetch, *Fcgamma receptors as regulators of immune responses*. Nat Rev Immunol, 2008. **8**(1): p. 34-47.
- 107. Kiyotake, R., et al., *Human Mincle Binds to Cholesterol Crystals and Triggers Innate Immune Responses*. J Biol Chem, 2015. **290**(42): p. 25322-32.
- 108. Desaulniers, P., et al., *Crystal-induced neutrophil activation. VII. Involvement of Syk in the responses to monosodium urate crystals.* J Leukoc Biol, 2001. **70**(4): p. 659-68.
- 109. Clement, M., et al., Necrotic Cell Sensor Clec4e Promotes a Proatherogenic Macrophage Phenotype Through Activation of the Unfolded Protein Response. Circulation, 2016. **134**(14): p. 1039-1051.
- 110. Ng, G., et al., Receptor-independent, direct membrane binding leads to cell-surface lipid sorting and Syk kinase activation in dendritic cells. Immunity, 2008. **29**(5): p. 807-18.
- 111. Flach, T.L., et al., *Alum interaction with dendritic cell membrane lipids is essential for its adjuvanticity.* Nat Med, 2011. **17**(4): p. 479-87.
- 112. An, L.L., et al., Complement C5a potentiates uric acid crystal-induced IL-1beta production. Eur J Immunol, 2014. **44**(12): p. 3669-79.
- 113. Niyonzima, N., et al., *Complement activation by cholesterol crystals triggers a subsequent cytokine response.* Mol Immunol, 2017. **84**: p. 43-50.
- 114. Ingersoll, M.A., et al., *Comparison of gene expression profiles between human and mouse monocyte subsets.* Blood, 2010. **115**(3): p. e10-9.
- 115. Stephen, S.L., et al., Scavenger receptors and their potential as therapeutic targets in the treatment of cardiovascular disease. Int J Hypertens, 2010. **2010**: p. 646929.
- 116. Prabhudas, M., et al., *Standardizing scavenger receptor nomenclature*. J Immunol, 2014. **192**(5): p. 1997-2006.

- 117. Li, Y., et al., Dioscin attenuates oxLDL uptake and the inflammatory reaction of dendritic cells under high glucose conditions by blocking p38 MAPK. Mol Med Rep, 2020. **21**(1): p. 304-310.
- 118. Wong, K., et al., *Phosphatidylserine receptor Tim-4 is essential for the maintenance of the homeostatic state of resident peritoneal macrophages*. Proc Natl Acad Sci U S A, 2010. **107**(19): p. 8712-7.
- 119. Caronni, N., et al., *TIM4 expression by dendritic cells mediates uptake of tumor-associated antigens and anti-tumor responses.* Nat Commun, 2021. **12**(1): p. 2237.
- 120. Vaillancourt, M., et al., Expression of the myeloid inhibitory receptor CLEC12A correlates with disease activity and cytokines in early rheumatoid arthritis. Sci Rep, 2021. **11**(1): p. 11248.
- 121. Ley, K., et al., *How Mouse Macrophages Sense What Is Going On.* Front Immunol, 2016. **7**(204): p. 204.
- 122. Beattie, L., et al., Bone marrow-derived and resident liver macrophages display unique transcriptomic signatures but similar biological functions. J Hepatol, 2016. **65**(4): p. 758-768.
- 123. N, A.G., et al., *Phagocytosis imprints heterogeneity in tissue-resident macrophages*. J Exp Med, 2017. **214**(5): p. 1281-1296.
- 124. Lv, L.L., et al., *The pattern recognition receptor, Mincle, is essential for maintaining the M1 macrophage phenotype in acute renal inflammation.* Kidney Int, 2017. **91**(3): p. 587-602.
- 125. Tanaka, M., et al., *C-type lectin Mincle mediates cell death-triggered inflammation in acute kidney injury.* J Exp Med, 2020. **217**(11).
- 126. Gren, S.T., et al., A Single-Cell Gene-Expression Profile Reveals Inter-Cellular Heterogeneity within Human Monocyte Subsets. PLoS One, 2015. **10**(12): p. e0144351.
- 127. Kerntke, C., F. Nimmerjahn, and M. Biburger, *There Is (Scientific) Strength in Numbers:* A Comprehensive Quantitation of Fc Gamma Receptor Numbers on Human and Murine Peripheral Blood Leukocytes. Front Immunol, 2020. **11**(118): p. 118.
- 128. Lobato-Pascual, A., et al., *Rat macrophage C-type lectin is an activating receptor expressed by phagocytic cells.* PLoS One, 2013. **8**(2): p. e57406.
- 129. Huh, H.Y., et al., Regulated expression of CD36 during monocyte-to-macrophage differentiation: potential role of CD36 in foam cell formation. Blood, 1996. **87**(5): p. 2020-8
- 130. Dostert, C., et al., *Innate immune activation through Nalp3 inflammasome sensing of asbestos and silica*. Science, 2008. **320**(5876): p. 674-7.

- 131. Hornung, V., et al., Silica crystals and aluminum salts activate the NALP3 inflammasome through phagosomal destabilization. Nat Immunol, 2008. **9**(8): p. 847-56.
- 132. Tsugita, M., N. Morimoto, and M. Nakayama, SiO(2) and TiO(2) nanoparticles synergistically trigger macrophage inflammatory responses. Part Fibre Toxicol, 2017. **14**(1): p. 11.
- 133. Martinon, F., et al., *Gout-associated uric acid crystals activate the NALP3 inflammasome*. Nature, 2006. **440**(7081): p. 237-41.
- 134. Dominguez-Gutierrez, P.R., et al., *Calcium Oxalate Differentiates Human Monocytes Into Inflammatory M1 Macrophages*. Front Immunol, 2018. **9**: p. 1863.
- 135. Karasawa, T. and M. Takahashi, *Saturated fatty acid-crystals activate NLRP3 inflammasome*. Aging (Albany NY), 2019. **11**(6): p. 1613-1614.
- 136. Luz, H.L., et al., *P2X7 Receptor Stimulation Is Not Required for Oxalate Crystal-Induced Kidney Injury.* Sci Rep, 2019. **9**(1): p. 20086.
- 137. Strowig, T., et al., *Inflammasomes in health and disease*. Nature, 2012. **481**(7381): p. 278-86.
- 138. Sayan, M. and B.T. Mossman, *The NLRP3 inflammasome in pathogenic particle and fibre-associated lung inflammation and diseases.* Part Fibre Toxicol, 2016. **13**(1): p. 51.
- 139. Gasteiger, G., et al., *Cellular Innate Immunity: An Old Game with New Players*. J Innate Immun, 2017. **9**(2): p. 111-125.
- 140. Mitchell, P.S., A. Sandstrom, and R.E. Vance, *The NLRP1 inflammasome: new mechanistic insights and unresolved mysteries.* Curr Opin Immunol, 2019. **60**: p. 37-45.
- 141. Haneklaus, M. and L.A. O'Neill, *NLRP3 at the interface of metabolism and inflammation*. Immunol Rev, 2015. **265**(1): p. 53-62.
- 142. Duncan, J.A. and S.W. Canna, *The NLRC4 Inflammasome*. Immunol Rev, 2018. **281**(1): p. 115-123.
- 143. Lugrin, J. and F. Martinon, *The AIM2 inflammasome: Sensor of pathogens and cellular perturbations.* Immunol Rev, 2018. **281**(1): p. 99-114.
- 144. Heilig, R. and P. Broz, Function and mechanism of the pyrin inflammasome. Eur J Immunol, 2018. **48**(2): p. 230-238.
- 145. Matsuoka, Y., et al., *NLRP2 inflammasome in dorsal root ganglion as a novel molecular platform that produces inflammatory pain hypersensitivity.* Pain, 2019. **160**(9): p. 2149-2160.

- 146. Elinav, E., et al., *NLRP6 inflammasome regulates colonic microbial ecology and risk for colitis.* Cell, 2011. **145**(5): p. 745-57.
- 147. Khare, S., et al., An NLRP7-containing inflammasome mediates recognition of microbial lipopeptides in human macrophages. Immunity, 2012. **36**(3): p. 464-76.
- 148. Vladimer, G.I., et al., *The NLRP12 inflammasome recognizes Yersinia pestis*. Immunity, 2012. **37**(1): p. 96-107.
- 149. Janowski, A.M. and F.S. Sutterwala, *Atypical Inflammasomes*. Methods Mol Biol, 2016. **1417**: p. 45-62.
- 150. So, A., et al., *Targeting inflammasomes in rheumatic diseases*. Nat Rev Rheumatol, 2013. **9**(7): p. 391-9.
- 151. Heneka, M.T., R.M. McManus, and E. Latz, *Inflammasome signalling in brain function and neurodegenerative disease*. Nat Rev Neurosci, 2018. **19**(10): p. 610-621.
- 152. Toldo, S. and A. Abbate, *The NLRP3 inflammasome in acute myocardial infarction*. Nat Rev Cardiol, 2018. **15**(4): p. 203-214.
- 153. Komada, T. and D.A. Muruve, *The role of inflammasomes in kidney disease*. Nat Rev Nephrol, 2019. **15**(8): p. 501-520.
- 154. Wada, J. and H. Makino, *Innate immunity in diabetes and diabetic nephropathy*. Nat Rev Nephrol, 2016. **12**(1): p. 13-26.
- 155. Rheinheimer, J., et al., Current role of the NLRP3 inflammasome on obesity and insulin resistance: A systematic review. Metabolism, 2017. **74**: p. 1-9.
- 156. Moossavi, M., et al., *Role of the NLRP3 inflammasome in cancer*. Mol Cancer, 2018. **17**(1): p. 158.
- 157. Freeman, T.L. and T.H. Swartz, *Targeting the NLRP3 Inflammasome in Severe COVID-19*. Front Immunol, 2020. **11**: p. 1518.
- 158. Kelley, N., et al., *The NLRP3 Inflammasome: An Overview of Mechanisms of Activation and Regulation*. Int J Mol Sci, 2019. **20**(13): p. 3328.
- 159. He, Y., H. Hara, and G. Nunez, *Mechanism and Regulation of NLRP3 Inflammasome Activation*. Trends Biochem Sci, 2016. **41**(12): p. 1012-1021.
- 160. Gaidt, M.M. and V. Hornung, *Alternative inflammasome activation enables IL-1beta release from living cells*. Curr Opin Immunol, 2017. **44**: p. 7-13.
- 161. Yi, Y.S., Caspase-11 non-canonical inflammasome: a critical sensor of intracellular lipopolysaccharide in macrophage-mediated inflammatory responses. Immunology, 2017. **152**(2): p. 207-217.

- 162. Zheng, D., T. Liwinski, and E. Elinav, *Inflammasome activation and regulation: toward a better understanding of complex mechanisms*. Cell Discov, 2020. **6**(1): p. 36.
- 163. McKee, C.M. and R.C. Coll, *NLRP3 inflammasome priming: A riddle wrapped in a mystery inside an enigma*. J Leukoc Biol, 2020. **108**(3): p. 937-952.
- 164. Rai, V. and D.K. Agrawal, *The role of damage- and pathogen-associated molecular patterns in inflammation-mediated vulnerability of atherosclerotic plaques*. Can J Physiol Pharmacol, 2017. **95**(10): p. 1245-1253.
- Wang, S. and Y. Zhang, *HMGB1 in inflammation and cancer*. J Hematol Oncol, 2020. **13**(1): p. 116.
- 166. Dorrington, M.G. and I.D.C. Fraser, *NF-kappaB Signaling in Macrophages: Dynamics, Crosstalk, and Signal Integration.* Front Immunol, 2019. **10**(705): p. 705.
- 167. Zitvogel, L., O. Kepp, and G. Kroemer, *Decoding cell death signals in inflammation and immunity*. Cell, 2010. **140**(6): p. 798-804.
- 168. Rabolli, V., D. Lison, and F. Huaux, *The complex cascade of cellular events governing inflammasome activation and IL-1beta processing in response to inhaled particles.* Part Fibre Toxicol, 2016. **13**(1): p. 40.
- 169. Di Virgilio, F., et al., *The P2X7 Receptor in Infection and Inflammation*. Immunity, 2017. **47**(1): p. 15-31.
- 170. Zhou, R., et al., *A role for mitochondria in NLRP3 inflammasome activation*. Nature, 2011. **469**(7329): p. 221-5.
- 171. Shimada, K., et al., Oxidized mitochondrial DNA activates the NLRP3 inflammasome during apoptosis. Immunity, 2012. **36**(3): p. 401-14.
- 172. Scheiblich, H., et al., *Activation of the NLRP3 inflammasome in microglia: the role of ceramide.* J Neurochem, 2017. **143**(5): p. 534-550.
- 173. Munoz-Planillo, R., et al., K(+) efflux is the common trigger of NLRP3 inflammasome activation by bacterial toxins and particulate matter. Immunity, 2013. **38**(6): p. 1142-53.
- 174. Lawlor, K.E. and J.E. Vince, *Ambiguities in NLRP3 inflammasome regulation: is there a role for mitochondria?* Biochim Biophys Acta, 2014. **1840**(4): p. 1433-40.
- 175. Rosales, C. and E. Uribe-Querol, *Phagocytosis: A Fundamental Process in Immunity*. Biomed Res Int, 2017. **2017**: p. 9042851.
- 176. Campden, R.I. and Y. Zhang, *The role of lysosomal cysteine cathepsins in NLRP3 inflammasome activation*. Arch Biochem Biophys, 2019. **670**: p. 32-42.

- 177. Boya, P. and G. Kroemer, *Lysosomal membrane permeabilization in cell death.* Oncogene, 2008. **27**(50): p. 6434-51.
- 178. Pavan, C., et al., Nearly free surface silanols are the critical molecular moieties that initiate the toxicity of silica particles. Proc Natl Acad Sci U S A, 2020. **117**(45): p. 27836-27846.
- 179. Chevriaux, A., et al., *Cathepsin B Is Required for NLRP3 Inflammasome Activation in Macrophages, Through NLRP3 Interaction.* Front Cell Dev Biol, 2020. **8**: p. 167.
- 180. Orlowski, G.M., et al., *Multiple Cathepsins Promote Pro-IL-1beta Synthesis and NLRP3-Mediated IL-1beta Activation*. J Immunol, 2015. **195**(4): p. 1685-97.
- 181. Niemi, K., et al., Serum amyloid A activates the NLRP3 inflammasome via P2X7 receptor and a cathepsin B-sensitive pathway. J Immunol, 2011. **186**(11): p. 6119-28.
- 182. Thibodeau, M.S., et al., *Silica-induced apoptosis in mouse alveolar macrophages is initiated by lysosomal enzyme activity.* Toxicol Sci, 2004. **80**(1): p. 34-48.
- 183. Joshi, G.N. and D.A. Knecht, *Silica phagocytosis causes apoptosis and necrosis by different temporal and molecular pathways in alveolar macrophages.* Apoptosis, 2013. **18**(3): p. 271-85.
- 184. Mills, E.L., B. Kelly, and L.A.J. O'Neill, *Mitochondria are the powerhouses of immunity*. Nat Immunol, 2017. **18**(5): p. 488-498.
- 185. Luna-Gomes, T., P.T. Santana, and R. Coutinho-Silva, *Silica-induced inflammasome activation in macrophages: role of ATP and P2X7 receptor*. Immunobiology, 2015. **220**(9): p. 1101-6.
- 186. Martinez-Garcia, J.J., et al., *P2X7 receptor induces mitochondrial failure in monocytes and compromises NLRP3 inflammasome activation during sepsis.* Nat Commun, 2019. **10**(1): p. 2711.
- 187. Thibodeau, M., C. Giardina, and A.K. Hubbard, *Silica-induced caspase activation in mouse alveolar macrophages is dependent upon mitochondrial integrity and aspartic proteolysis*. Toxicol Sci, 2003. **76**(1): p. 91-101.
- 188. Hu, S., et al., Silica-induced apoptosis in alveolar macrophages: evidence of in vivo thiol depletion and the activation of mitochondrial pathway. J Toxicol Environ Health A, 2006. **69**(13): p. 1261-84.
- 189. Lim, Y., et al., *Silica-induced apoptosis in vitro and in vivo*. Toxicol Lett, 1999. **108**(2-3): p. 335-9.
- 190. Iyer, R., et al., *Silica-induced apoptosis mediated via scavenger receptor in human alveolar macrophages*. Toxicol Appl Pharmacol, 1996. **141**(1): p. 84-92.

- 191. Hirano, S., et al., *Differential Regulation of IL-1beta and IL-6 Release in Murine Macrophages*. Inflammation, 2017. **40**(6): p. 1933-1943.
- 192. Hamilton, R.F., L.L. Iyer, and A. Holian, *Asbestos induces apoptosis in human alveolar macrophages*. Am J Physiol, 1996. **271**(5 Pt 1): p. L813-9.
- 193. Zhong, Z., et al., New mitochondrial DNA synthesis enables NLRP3 inflammasome activation. Nature, 2018. **560**(7717): p. 198-203.
- 194. Gross, C.J., et al., K(+) Efflux-Independent NLRP3 Inflammasome Activation by Small Molecules Targeting Mitochondria. Immunity, 2016. **45**(4): p. 761-773.
- 195. Harijith, A., D.L. Ebenezer, and V. Natarajan, *Reactive oxygen species at the crossroads of inflammasome and inflammation*. Front Physiol, 2014. **5**: p. 352.
- 196. Hennig, P., et al., *The Crosstalk between Nrf2 and Inflammasomes*. Int J Mol Sci, 2018. **19**(2): p. 562.
- 197. Brieger, K., et al., *Reactive oxygen species: from health to disease*. Swiss Med Wkly, 2012. **142**: p. w13659.
- 198. Heid, M.E., et al., *Mitochondrial reactive oxygen species induces NLRP3-dependent lysosomal damage and inflammasome activation.* J Immunol, 2013. **191**(10): p. 5230-8.
- 199. Murakami, T., et al., *Critical role for calcium mobilization in activation of the NLRP3 inflammasome*. Proc Natl Acad Sci U S A, 2012. **109**(28): p. 11282-7.
- 200. Kim, S., et al., Endoplasmic reticulum stress is sufficient for the induction of IL-1beta production via activation of the NF-kappaB and inflammasome pathways. Innate Immun, 2014. **20**(8): p. 799-815.
- 201. Zhou, Y., et al., *The Roles of Endoplasmic Reticulum in NLRP3 Inflammasome Activation*. Cells, 2020. **9**(5): p. 1219.
- 202. Chen, F., et al., Endoplasmic Reticulum Stress Cooperates in Silica Nanoparticles-Induced Macrophage Apoptosis via Activation of CHOP-Mediated Apoptotic Signaling Pathway. Int J Mol Sci, 2019. **20**(23).
- 203. Ryan, A.J., et al., Asbestos-induced disruption of calcium homeostasis induces endoplasmic reticulum stress in macrophages. J Biol Chem, 2014. **289**(48): p. 33391-403.
- 204. Long, J., et al., Multi-walled carbon nanotubes (MWCNTs) promoted lipid accumulation in THP-1 macrophages through modulation of endoplasmic reticulum (ER) stress. Nanotoxicology, 2019. 13(7): p. 938-951.
- 205. Rello, S., et al., *Morphological criteria to distinguish cell death induced by apoptotic and necrotic treatments.* Apoptosis, 2005. **10**(1): p. 201-8.

- 206. Niemann, B. and S. Rohrbach, *Metabolically Relevant Cell Biology Role of Intracellular Organelles for Cardiac Metabolism*, in *The Scientist's Guide to Cardiac Metabolism*, M. Schwarzer and T. Doenst, Editors. 2016, Academic Press: Boston. p. 19-38.
- 207. Green, D.R. and F. Llambi, *Cell Death Signaling*. Cold Spring Harb Perspect Biol, 2015. **7**(12).
- 208. Davidovich, P., C.J. Kearney, and S.J. Martin, *Inflammatory outcomes of apoptosis*, *necrosis and necroptosis*. Biol Chem, 2014. **395**(10): p. 1163-71.
- 209. Ito, F., et al., Asbestos conceives Fe(II)-dependent mutagenic stromal milieu through ceaseless macrophage ferroptosis and beta-catenin induction in mesothelium. Redox Biol, 2020. **36**: p. 101616.
- 210. Mulay, S.R., et al., *Mitochondria Permeability Transition versus Necroptosis in Oxalate-Induced AKI*. J Am Soc Nephrol, 2019. **30**(10): p. 1857-1869.
- 211. Reus, T.L., et al., *Dose-dependent cell necrosis induced by silica nanoparticles*. Toxicol In Vitro, 2020. **63**: p. 104723.
- 212. Nirmala, J.G. and M. Lopus, *Cell death mechanisms in eukaryotes*. Cell Biol Toxicol, 2020. **36**(2): p. 145-164.
- 213. Lamkanfi, M. and V.M. Dixit, *Mechanisms and functions of inflammasomes*. Cell, 2014. **157**(5): p. 1013-22.
- 214. Abe, J. and C. Morrell, *Pyroptosis as a Regulated Form of Necrosis: PI+/Annexin V-/High Caspase 1/Low Caspase 9 Activity in Cells = Pyroptosis?* Circ Res, 2016. **118**(10): p. 1457-60.
- 215. Ros, U., L. Pedrera, and A.J. Garcia-Saez, *Partners in Crime: The Interplay of Proteins and Membranes in Regulated Necrosis.* Int J Mol Sci, 2020. **21**(7).
- 216. Geng, Y.J., et al., Cholesterol crystallization and macrophage apoptosis: implication for atherosclerotic plaque instability and rupture. Biochem Pharmacol, 2003. **66**(8): p. 1485-92.
- 217. Kim, S.K., J.Y. Choe, and K.Y. Park, Enhanced p62 Is Responsible for Mitochondrial Pathway-Dependent Apoptosis and Interleukin-Ibeta Production at the Early Phase by Monosodium Urate Crystals in Murine Macrophage. Inflammation, 2016. **39**(5): p. 1603-16.
- 218. Pazar, B., et al., *Basic calcium phosphate crystals induce monocyte/macrophage IL-1beta secretion through the NLRP3 inflammasome in vitro*. J Immunol, 2011. **186**(4): p. 2495-502.

- 219. Santavanond, J.P., et al., *Apoptotic bodies: mechanism of formation, isolation and functional relevance*, in *New Frontiers: Extracellular Vesicles*, S. Mathivanan, et al., Editors. 2021, Springer International Publishing: Cham. p. 61-88.
- 220. Nagata, S., *Apoptosis and Clearance of Apoptotic Cells*. Annu Rev Immunol, 2018. **36**(1): p. 489-517.
- 221. Elmore, S., *Apoptosis: a review of programmed cell death.* Toxicol Pathol, 2007. **35**(4): p. 495-516.
- 222. Trapani, J.A. and M.J. Smyth, *Functional significance of the perforin/granzyme cell death pathway*. Nat Rev Immunol, 2002. **2**(10): p. 735-47.
- 223. Voskoboinik, I., et al., *Perforin: structure, function, and role in human immunopathology*. Immunol Rev, 2010. **235**(1): p. 35-54.
- 224. Voskoboinik, I., J.C. Whisstock, and J.A. Trapani, *Perforin and granzymes: function, dysfunction and human pathology*. Nat Rev Immunol, 2015. **15**(6): p. 388-400.
- 225. Chen, Q., et al., TiO(2) nanoparticles cause mitochondrial dysfunction, activate inflammatory responses, and attenuate phagocytosis in macrophages: A proteomic and metabolomic insight. Redox Biol, 2018. **15**: p. 266-276.
- 226. Brown, D.M., et al., An in vitro study of the potential of carbon nanotubes and nanofibres to induce inflammatory mediators and frustrated phagocytosis. Carbon, 2007. **45**(9): p. 1743-1756.
- 227. Perkins, R.C., et al., *Human alveolar macrophage cytokine release in response to in vitro and in vivo asbestos exposure*. Exp Lung Res, 1993. **19**(1): p. 55-65.
- 228. Gozal, E., et al., Silica-induced apoptosis in murine macrophage: involvement of tumor necrosis factor-alpha and nuclear factor-kappaB activation. Am J Respir Cell Mol Biol, 2002. **27**(1): p. 91-8.
- 229. Dubois, C.M., E. Bissonnette, and M. Rola-Pleszczynski, *Asbestos fibers and silica* particles stimulate rat alveolar macrophages to release tumor necrosis factor. *Autoregulatory role of leukotriene B4*. Am Rev Respir Dis, 1989. **139**(5): p. 1257-64.
- 230. Tummers, B. and D.R. Green, *Caspase-8: regulating life and death*. Immunol Rev, 2017. **277**(1): p. 76-89.
- 231. Walsh, J.G., et al., *Executioner caspase-3 and caspase-7 are functionally distinct proteases.* Proc Natl Acad Sci U S A, 2008. **105**(35): p. 12815-9.
- 232. Segawa, K. and S. Nagata, *An Apoptotic 'Eat Me' Signal: Phosphatidylserine Exposure*. Trends Cell Biol, 2015. **25**(11): p. 639-650.

- 233. D'Arcy, M.S., Cell death: a review of the major forms of apoptosis, necrosis and autophagy. Cell Biol Int, 2019. **43**(6): p. 582-592.
- 234. Desai, J., et al., Particles of different sizes and shapes induce neutrophil necroptosis followed by the release of neutrophil extracellular trap-like chromatin. Sci Rep, 2017. **7**(1): p. 15003.
- 235. Honarpisheh, M., et al., *Phagocytosis of environmental or metabolic crystalline particles induces cytotoxicity by triggering necroptosis across a broad range of particle size and shape.* Sci Rep, 2017. **7**(1): p. 15523.
- 236. Frank, D. and J.E. Vince, *Pyroptosis versus necroptosis: similarities, differences, and crosstalk.* Cell Death Differ, 2019. **26**(1): p. 99-114.
- 237. Newton, K. and G. Manning, *Necroptosis and Inflammation*. Annu Rev Biochem, 2016. **85**(1): p. 743-63.
- 238. Su, Z., et al., *Cancer therapy in the necroptosis era*. Cell Death Differ, 2016. **23**(5): p. 748-56.
- 239. Galluzzi, L., et al., *Necroptosis: Mechanisms and Relevance to Disease*. Annu Rev Pathol, 2017. **12**: p. 103-130.
- 240. Malireddi, R.K.S., S. Kesavardhana, and T.D. Kanneganti, *ZBP1 and TAK1: Master Regulators of NLRP3 Inflammasome/Pyroptosis*, *Apoptosis*, *and Necroptosis (PANoptosis)*. Front Cell Infect Microbiol, 2019. **9**: p. 406.
- 241. Samir, P., R.K.S. Malireddi, and T.D. Kanneganti, *The PANoptosome: A Deadly Protein Complex Driving Pyroptosis*, *Apoptosis*, *and Necroptosis* (*PANoptosis*). Front Cell Infect Microbiol, 2020. **10**: p. 238.
- 242. Malireddi, R.K.S., et al., Innate immune priming in the absence of TAK1 drives RIPK1 kinase activity-independent pyroptosis, apoptosis, necroptosis, and inflammatory disease. J Exp Med, 2020. 217(3).
- 243. Mulay, S.R., et al., *Editorial: Nano- and Microparticle-Induced Cell Death, Inflammation and Immune Responses.* Front Immunol, 2019. **10**(844): p. 844.
- 244. Schwarzer, R., L. Laurien, and M. Pasparakis, New insights into the regulation of apoptosis, necroptosis, and pyroptosis by receptor interacting protein kinase 1 and caspase-8. Curr Opin Cell Biol, 2020. **63**: p. 186-193.
- 245. Rada, B., *Neutrophil Extracellular Traps and Microcrystals*. J Immunol Res, 2017. **2017**: p. 2896380.
- 246. Li, Y., et al., Neutrophil Extracellular Traps Formation and Aggregation Orchestrate Induction and Resolution of Sterile Crystal-Mediated Inflammation. Front Immunol, 2018. 9: p. 1559.

- 247. Sollberger, G., D.O. Tilley, and A. Zychlinsky, *Neutrophil Extracellular Traps: The Biology of Chromatin Externalization*. Dev Cell, 2018. **44**(5): p. 542-553.
- 248. Papayannopoulos, V., *Neutrophil extracellular traps in immunity and disease*. Nat Rev Immunol, 2018. **18**(2): p. 134-147.
- 249. Yipp, B.G. and P. Kubes, *NETosis: how vital is it?* Blood, 2013. **122**(16): p. 2784-94.
- 250. Delgado-Rizo, V., et al., Neutrophil Extracellular Traps and Its Implications in Inflammation: An Overview. Front Immunol, 2017. **8**(81): p. 81.
- 251. Jorch, S.K. and P. Kubes, *An emerging role for neutrophil extracellular traps in noninfectious disease*. Nat Med, 2017. **23**(3): p. 279-287.
- 252. Murphy, F.A., et al., Length-dependent retention of carbon nanotubes in the pleural space of mice initiates sustained inflammation and progressive fibrosis on the parietal pleura. Am J Pathol, 2011. **178**(6): p. 2587-600.
- 253. Boyles, M.S., et al., Multi-walled carbon nanotube induced frustrated phagocytosis, cytotoxicity and pro-inflammatory conditions in macrophages are length dependent and greater than that of asbestos. Toxicol In Vitro, 2015. **29**(7): p. 1513-28.
- 254. Hamilton, R.F., et al., *Particle length-dependent titanium dioxide nanomaterials toxicity and bioactivity*. Part Fibre Toxicol, 2009. **6**(1): p. 35.
- 255. Mischler, S.E., et al., *Differential activation of RAW 264.7 macrophages by size-segregated crystalline silica.* J Occup Med Toxicol, 2016. **11**: p. 57.
- 256. Kusaka, T., et al., *Effect of silica particle size on macrophage inflammatory responses*. PLoS One, 2014. **9**(3): p. e92634.
- 257. Fenoglio, I., et al., *Thickness of multiwalled carbon nanotubes affects their lung toxicity*. Chem Res Toxicol, 2012. **25**(1): p. 74-82.
- 258. Cohignac, V., et al., Carbon nanotubes, but not spherical nanoparticles, block autophagy by a shape-related targeting of lysosomes in murine macrophages. Autophagy, 2018. **14**(8): p. 1323-1334.
- 259. Turci, F., et al., Revisiting the paradigm of silica pathogenicity with synthetic quartz crystals: the role of crystallinity and surface disorder. Part Fibre Toxicol, 2016. **13**(1): p. 32.
- 260. Nahle, S., et al., Single wall and multiwall carbon nanotubes induce different toxicological responses in rat alveolar macrophages. J Appl Toxicol, 2019. **39**(5): p. 764-772.
- 261. Sager, T.M. and V. Castranova, Surface area of particle administered versus mass in determining the pulmonary toxicity of ultrafine and fine carbon black: comparison to ultrafine titanium dioxide. Part Fibre Toxicol, 2009. **6**(1): p. 15.

- 262. Rabolli, V., et al., *Influence of size, surface area and microporosity on the in vitro cytotoxic activity of amorphous silica nanoparticles in different cell types.* Nanotoxicology, 2010. **4**(3): p. 307-18.
- 263. Morishige, T., et al., *The effect of surface modification of amorphous silica particles on NLRP3 inflammasome mediated IL-1beta production, ROS production and endosomal rupture.* Biomaterials, 2010. **31**(26): p. 6833-42.
- 264. Hamilton, R.F., Jr., et al., *NLRP3 inflammasome activation in murine alveolar macrophages and related lung pathology is associated with MWCNT nickel contamination*. Inhal Toxicol, 2012. **24**(14): p. 995-1008.
- 265. Hamilton, R.F., et al., *The Effects of Varying Degree of MWCNT Carboxylation on Bioactivity in Various In Vivo and In Vitro Exposure Models*. Int J Mol Sci, 2018. **19**(2).
- 266. Baranov, M.V., et al., *Modulation of Immune Responses by Particle Size and Shape*. Front Immunol, 2020. **11**(3854): p. 607945.
- 267. Aust, A.E., P.M. Cook, and R.F. Dodson, *Morphological and chemical mechanisms of elongated mineral particle toxicities*. J Toxicol Environ Health B Crit Rev, 2011. **14**(1-4): p. 40-75.
- 268. Sukhanova, A., et al., *Dependence of Nanoparticle Toxicity on Their Physical and Chemical Properties.* Nanoscale Res Lett, 2018. **13**(1): p. 44.
- 269. Grazioli, S. and J. Pugin, *Mitochondrial Damage-Associated Molecular Patterns: From Inflammatory Signaling to Human Diseases*. Front Immunol, 2018. **9**: p. 832.
- 270. Balan, S., M. Saxena, and N. Bhardwaj, *Dendritic cell subsets and locations*. Int Rev Cell Mol Biol, 2019. **348**: p. 1-68.
- 271. Conforti-Andreoni, C., et al., *Uric acid-driven Th17 differentiation requires inflammasome-derived IL-1 and IL-18.* J Immunol, 2011. **187**(11): p. 5842-50.
- 272. Westerterp, M., et al., *Cholesterol Accumulation in Dendritic Cells Links the Inflammasome to Acquired Immunity*. Cell Metab, 2017. **25**(6): p. 1294-1304 e6.
- 273. Khameneh, H.J., et al., *The Syk-NFAT-IL-2 Pathway in Dendritic Cells Is Required for Optimal Sterile Immunity Elicited by Alum Adjuvants*. J Immunol, 2017. **198**(1): p. 196-204.
- 274. Winter, M., et al., Activation of the inflammasome by amorphous silica and TiO2 nanoparticles in murine dendritic cells. Nanotoxicology, 2011. **5**(3): p. 326-40.
- 275. Sutton, C., et al., A crucial role for interleukin (IL)-1 in the induction of IL-17-producing T cells that mediate autoimmune encephalomyelitis. J Exp Med, 2006. **203**(7): p. 1685-91.

- 276. Yang, D., et al., *High mobility group box-1 protein induces the migration and activation of human dendritic cells and acts as an alarmin.* J Leukoc Biol, 2007. **81**(1): p. 59-66.
- 277. Schnurr, M., et al., Extracellular ATP and TNF-alpha synergize in the activation and maturation of human dendritic cells. J Immunol, 2000. **165**(8): p. 4704-9.
- 278. Parackova, Z., et al., Neutrophil Extracellular Trap Induced Dendritic Cell Activation Leads to Th1 Polarization in Type 1 Diabetes. Front Immunol, 2020. 11: p. 661.
- 279. Jego, G., et al., *Dendritic cells control B cell growth and differentiation*. Curr Dir Autoimmun, 2005. **8**: p. 124-39.
- 280. Hilpert, C., et al., *Dendritic Cells Control Regulatory T Cell Function Required for Maintenance of Intestinal Tissue Homeostasis*. J Immunol, 2019. **203**(11): p. 3068-3077.
- 281. Raker, V.K., M.P. Domogalla, and K. Steinbrink, *Tolerogenic Dendritic Cells for Regulatory T Cell Induction in Man.* Front Immunol, 2015. **6**(569): p. 569.
- 282. Sakaguchi, S., et al., *Regulatory T cells and immune tolerance*. Cell, 2008. **133**(5): p. 775-87.
- 283. Ma, Q., *Polarization of Immune Cells in the Pathologic Response to Inhaled Particulates.* Front Immunol, 2020. **11**: p. 1060.
- 284. Dai, W., et al., Blockade of Wnt/beta-Catenin Pathway Aggravated Silica-Induced Lung Inflammation through Tregs Regulation on Th Immune Responses. Mediators Inflamm, 2016. **2016**: p. 6235614.
- 285. Dai, X.J., et al., Changes of Treg/Th17 Ratio in Spleen of Acute Gouty Arthritis Rat Induced by MSU Crystals. Inflammation, 2018. **41**(5): p. 1955-1964.
- 286. Liu, F., et al., CD4+CD25+Foxp3+ regulatory T cells depletion may attenuate the development of silica-induced lung fibrosis in mice. PLoS One, 2010. 5(11): p. e15404.
- 287. Lo Re, S., et al., *Platelet-derived growth factor-producing CD4+ Foxp3+ regulatory T lymphocytes promote lung fibrosis*. Am J Respir Crit Care Med, 2011. **184**(11): p. 1270-81.
- 288. Maeda, M., et al., *Induction of IL-17 production from human peripheral blood CD4+ cells by asbestos exposure*. Int J Oncol, 2017. **50**(6): p. 2024-2032.
- 289. Burbelo, P.D., et al., *Autoantibodies Targeting Intracellular and Extracellular Proteins in Autoimmunity*. Front Immunol, 2021. **12**(5): p. 548469.
- 290. Stranges, P.B., et al., *Elimination of antigen-presenting cells and autoreactive T cells by Fas contributes to prevention of autoimmunity*. Immunity, 2007. **26**(5): p. 629-41.

- 291. Riedhammer, C. and R. Weissert, *Antigen Presentation, Autoantigens, and Immune Regulation in Multiple Sclerosis and Other Autoimmune Diseases*. Front Immunol, 2015. **6**: p. 322.
- 292. Rosen, A. and L. Casciola-Rosen, *Autoantigens as Partners in Initiation and Propagation of Autoimmune Rheumatic Diseases*. Annu Rev Immunol, 2016. **34**: p. 395-420.
- 293. Doyle, H.A., et al., *Autoantigens: novel forms and presentation to the immune system.* Autoimmunity, 2014. **47**(4): p. 220-33.
- 294. Terzoglou, A.G., et al., *Post-translational modifications of the major linear epitope 169-190aa of Ro60 kDa autoantigen alter the autoantibody binding*. Clin Exp Immunol, 2006. **146**(1): p. 60-5.
- 295. Nagai, K., et al., Altered posttranslational modification on U1 small nuclear ribonucleoprotein 68k in systemic autoimmune diseases detected by 2D Western blot. Electrophoresis, 2012. **33**(13): p. 2028-35.
- 296. Brahms, H., et al., The C-terminal RG dipeptide repeats of the spliceosomal Sm proteins D1 and D3 contain symmetrical dimethylarginines, which form a major B-cell epitope for anti-Sm autoantibodies. J Biol Chem, 2000. **275**(22): p. 17122-9.
- 297. van Bavel, C.C., et al., *Apoptosis-associated acetylation on histone H2B is an epitope for lupus autoantibodies*. Mol Immunol, 2009. **47**(2-3): p. 511-6.
- 298. Lande, R., et al., Complementary Effects of Carbamylated and Citrullinated LL37 in Autoimmunity and Inflammation in Systemic Lupus Erythematosus. Int J Mol Sci, 2021. 22(4).
- 299. Chang, M.K., et al., *Apoptotic cells with oxidation-specific epitopes are immunogenic and proinflammatory*. J Exp Med, 2004. **200**(11): p. 1359-70.
- 300. Doyle, H.A., D.W. Aswad, and M.J. Mamula, *Autoimmunity to isomerized histone H2B in systemic lupus erythematosus*. Autoimmunity, 2013. **46**(1): p. 6-13.
- 301. Yang, C.A. and B.L. Chiang, *Inflammasomes and human autoimmunity: A comprehensive review.* J Autoimmun, 2015. **61**: p. 1-8.
- 302. Cho, J.H. and P.K. Gregersen, *Genomics and the multifactorial nature of human autoimmune disease*. N Engl J Med, 2011. **365**(17): p. 1612-23.
- 303. Lemke, G., *Biology of the TAM receptors*. Cold Spring Harb Perspect Biol, 2013. **5**(11): p. a009076.
- 304. Caso, F., et al., From autoinflammation to autoimmunity: old and recent findings. Clin Rheumatol, 2018. **37**(9): p. 2305-2321.

- 305. Gough, S.C. and M.J. Simmonds, *The HLA Region and Autoimmune Disease: Associations and Mechanisms of Action*. Curr Genomics, 2007. **8**(7): p. 453-65.
- 306. Pollard, K.M., *Perspective: The Lung, Particles, Fibers, Nanomaterials, and Autoimmunity.* Front Immunol, 2020. **11**: p. 587136.
- 307. Westerfield, B.T., Asbestos-related lung disease. South Med J, 1992. **85**(6): p. 616-20.
- 308. Brody, A.R., *Asbestos-induced lung disease*. Environ Health Perspect, 1993. **100**: p. 21-30.
- 309. Bartrip, P.W., *History of asbestos related disease*. Postgrad Med J, 2004. **80**(940): p. 72-6.
- 310. Dong, J. and Q. Ma, Macrophage polarization and activation at the interface of multi-walled carbon nanotube-induced pulmonary inflammation and fibrosis. Nanotoxicology, 2018. **12**(2): p. 153-168.
- 311. Kobayashi, N., H. Izumi, and Y. Morimoto, *Review of toxicity studies of carbon nanotubes*. J Occup Health, 2017. **59**(5): p. 394-407.
- 312. Czajka, M., et al., *Toxicity of titanium dioxide nanoparticles in central nervous system.* Toxicol In Vitro, 2015. **29**(5): p. 1042-52.
- 313. Zhao, L., et al., Cardiopulmonary effects induced by occupational exposure to titanium dioxide nanoparticles. Nanotoxicology, 2018. **12**(2): p. 169-184.
- 314. Rosenthal, A.K. and L.M. Ryan, *Calcium Pyrophosphate Deposition Disease*. N Engl J Med, 2016. **374**(26): p. 2575-84.
- 315. Lorenz, E.C., et al., *Update on oxalate crystal disease*. Curr Rheumatol Rep, 2013. **15**(7): p. 340.
- 316. Kalampogias, A., et al., *Basic Mechanisms in Atherosclerosis: The Role of Calcium.* Med Chem, 2016. **12**(2): p. 103-13.
- 317. Lison, D., G. Vietti, and S. van den Brule, *Paracelsus in nanotoxicology*. Part Fibre Toxicol, 2014. **11**(1): p. 35.
- 318. Bates, M.A., et al., Silica Triggers Inflammation and Ectopic Lymphoid Neogenesis in the Lungs in Parallel with Accelerated Onset of Systemic Autoimmunity and Glomerulonephritis in the Lupus-Prone NZBWF1 Mouse. PLoS One, 2015. **10**(5): p. e0125481.
- 319. Mayeux, J.M., et al., *Silicosis and Silica-Induced Autoimmunity in the Diversity Outbred Mouse.* Front Immunol, 2018. **9**: p. 874.

- 320. De Klerk, N.H., G.L. Ambrosini, and A.W. Musk, *Crystalline Silica Exposure and Major Health Effects in Western Australian Gold Miners*. The Annals of Occupational Hygiene, 2002. **46**(suppl_1): p. 1-3.
- 321. Boudigaard, S.H., et al., *Occupational exposure to respirable crystalline silica and risk of autoimmune rheumatic diseases: a nationwide cohort study.* International Journal of Epidemiology, 2021. **50**(4): p. 1213-1226.
- 322. Vadasz, Z., et al., Age-related autoimmunity. BMC Med, 2013. 11: p. 94.
- 323. Watad, A., et al., *Autoimmunity in the Elderly: Insights from Basic Science and Clinics A Mini-Review.* Gerontology, 2017. **63**(6): p. 515-523.
- 324. Amador-Patarroyo, M.J., A. Rodriguez-Rodriguez, and G. Montoya-Ortiz, *How does age at onset influence the outcome of autoimmune diseases?* Autoimmune Dis, 2012. **2012**: p. 251730.
- 325. Ngo, S.T., F.J. Steyn, and P.A. McCombe, *Gender differences in autoimmune disease*. Front Neuroendocrinol, 2014. **35**(3): p. 347-69.
- 326. Angum, F., et al., *The Prevalence of Autoimmune Disorders in Women: A Narrative Review.* Cureus, 2020. **12**(5): p. e8094.
- 327. Pollard, K.M., Gender differences in autoimmunity associated with exposure to environmental factors. J Autoimmun, 2012. **38**(2-3): p. J177-86.
- 328. Finckh, A., et al., Occupational silica and solvent exposures and risk of systemic lupus erythematosus in urban women. Arthritis Rheum, 2006. **54**(11): p. 3648-54.
- 329. Krainer, J., S. Siebenhandl, and A. Weinhausel, *Systemic autoinflammatory diseases*. J Autoimmun, 2020. **109**: p. 102421.
- 330. Parks, C.G., et al., Occupational exposure to crystalline silica and risk of systemic lupus erythematosus: a population-based, case-control study in the southeastern United States. Arthritis Rheum, 2002. **46**(7): p. 1840-50.
- 331. Pollard, K.M., Silica, Silicosis, and Autoimmunity. Front Immunol, 2016. 7: p. 97.
- 332. Morotti, A., et al., Systematic review and meta-analysis of epidemiological studies on the association of occupational exposure to free crystalline silica and systemic lupus erythematosus. Rheumatology (Oxford), 2021. **60**(1): p. 81-91.
- 333. Moulton, V.R., et al., *Pathogenesis of Human Systemic Lupus Erythematosus: A Cellular Perspective.* Trends Mol Med, 2017. **23**(7): p. 615-635.
- 334. Brown, J.M., et al., *Silica accelerated systemic autoimmune disease in lupus-prone New Zealand mixed mice*. Clin Exp Immunol, 2003. **131**(3): p. 415-21.

- 335. Brown, J.M., J.C. Pfau, and A. Holian, *Immunoglobulin and lymphocyte responses following silica exposure in New Zealand mixed mice*. Inhal Toxicol, 2004. **16**(3): p. 133-9.
- 336. Brown, J.M., et al., *Silica, apoptosis, and autoimmunity*. J Immunotoxicol, 2005. **1**(3): p. 177-87.
- 337. Clark, A., et al., *Inhaled silica induces autoimmunity in a strain-dependent manner*. Journal of Immunology, 2017. **198**(1): p. 58.13.
- 338. Foster, M.H., et al., Silica Exposure Differentially Modulates Autoimmunity in Lupus Strains and Autoantibody Transgenic Mice. Front Immunol, 2019. **10**: p. 2336.
- 339. Borchers, A., et al., *The pathogenesis of autoimmunity in New Zealand mice*. Semin Arthritis Rheum, 2000. **29**(6): p. 385-99.
- 340. Wierenga, K.A., J.R. Harkema, and J.J. Pestka, *Lupus, Silica, and Dietary Omega-3 Fatty Acid Interventions*. Toxicol Pathol, 2019. **47**(8): p. 1004-1011.
- 341. Akbar, U., et al., *Omega-3 Fatty Acids in Rheumatic Diseases: A Critical Review.* J Clin Rheumatol, 2017. **23**(6): p. 330-339.
- 342. Calder, P.C., *Omega-3 fatty acids and inflammatory processes: from molecules to man.* Biochem Soc Trans, 2017. **45**(5): p. 1105-1115.
- 343. Ferreira, H.B., et al., *Lipidomics in autoimmune diseases with main focus on systemic lupus erythematosus.* J Pharm Biomed Anal, 2019. **174**: p. 386-395.
- 344. Wierenga, K.A., et al., Requisite Omega-3 HUFA Biomarker Thresholds for Preventing Murine Lupus Flaring. Front Immunol, 2020. 11(1796): p. 1796.
- 345. Halade, G.V., et al., *Docosahexaenoic acid-enriched fish oil attenuates kidney disease and prolongs median and maximal life span of autoimmune lupus-prone mice.* J Immunol, 2010. **184**(9): p. 5280-6.
- 346. Halade, G.V., et al., Concentrated fish oil (Lovaza(R)) extends lifespan and attenuates kidney disease in lupus-prone short-lived (NZBxNZW)F1 mice. Exp Biol Med (Maywood), 2013. **238**(6): p. 610-22.
- 347. Pestka, J.J., et al., Comparative effects of n-3, n-6 and n-9 unsaturated fatty acid-rich diet consumption on lupus nephritis, autoantibody production and CD4+ T cell-related gene responses in the autoimmune NZBWF1 mouse. PLoS One, 2014. **9**(6): p. e100255.
- 348. Charoenwoodhipong, P., et al., *Dietary Omega Polyunsaturated Fatty Acid Intake and Patient-Reported Outcomes in Systemic Lupus Erythematosus: The Michigan Lupus Epidemiology and Surveillance Program.* Arthritis Care Res (Hoboken), 2020. **72**(7): p. 874-881.

- 349. Li, X., et al., Therapeutic Potential of omega-3 Polyunsaturated Fatty Acids in Human Autoimmune Diseases. Front Immunol, 2019. **10**: p. 2241.
- 350. Duarte-Garcia, A., et al., *Effect of omega-3 fatty acids on systemic lupus erythematosus disease activity: A systematic review and meta-analysis.* Autoimmun Rev, 2020. **19**(12): p. 102688.
- 351. Benninghoff, A.D., et al., *Docosahexaenoic Acid Consumption Impedes Early Interferon*and Chemokine-Related Gene Expression While Suppressing Silica-Triggered Flaring of Murine Lupus. Front Immunol, 2019. **10**(2851): p. 2851.
- 352. Rajasinghe, L.D., et al., *Omega-3 fatty acid intake suppresses induction of diverse autoantibody repertoire by crystalline silica in lupus-prone mice*. Autoimmunity, 2020. **53**(7): p. 415-433.
- 353. Pestka, J.J., et al., *Omega-3 Polyunsaturated Fatty Acid Intervention Against Established Autoimmunity in a Murine Model of Toxicant-Triggered Lupus*. Front Immunol, 2021. **12**: p. 653464.
- 354. Kool, M., et al., Cutting edge: alum adjuvant stimulates inflammatory dendritic cells through activation of the NALP3 inflammasome. J Immunol, 2008. **181**(6): p. 3755-9.
- 355. Palomaki, J., et al., Long, needle-like carbon nanotubes and asbestos activate the NLRP3 inflammasome through a similar mechanism. ACS Nano, 2011. 5(9): p. 6861-70.
- 356. Kuroda, E., et al., Silica crystals and aluminum salts regulate the production of prostaglandin in macrophages via NALP3 inflammasome-independent mechanisms. Immunity, 2011. **34**(4): p. 514-26.
- 357. Duewell, P., et al., *NLRP3 inflammasomes are required for atherogenesis and activated by cholesterol crystals.* Nature, 2010. **464**(7293): p. 1357-61.
- 358. Rajamaki, K., et al., Cholesterol crystals activate the NLRP3 inflammasome in human macrophages: a novel link between cholesterol metabolism and inflammation. PLoS One, 2010. 5(7): p. e11765.
- 359. Mulay, S.R., et al., Calcium oxalate crystals induce renal inflammation by NLRP3-mediated IL-1beta secretion. J Clin Invest, 2013. **123**(1): p. 236-46.
- 360. Fanouriakis, A., et al., *Update omicronn the diagnosis and management of systemic lupus erythematosus*. Ann Rheum Dis, 2021. **80**(1): p. 14-25.
- 361. Tsokos, G.C., et al., New insights into the immunopathogenesis of systemic lupus erythematosus. Nat Rev Rheumatol, 2016. **12**(12): p. 716-730.
- 362. Catalina, M.D., et al., *The pathogenesis of systemic lupus erythematosus: Harnessing big data to understand the molecular basis of lupus.* J Autoimmun, 2020. **110**: p. 102359.

- 363. Qiu, W., T. Yu, and G.M. Deng, *The role of organ-deposited IgG in the pathogenesis of multi-organ and tissue damage in systemic lupus erythematosus.* Front Immunol, 2022. **13**: p. 924766.
- 364. Flores-Mendoza, G., et al., *Mechanisms of Tissue Injury in Lupus Nephritis*. Trends Mol Med, 2018. **24**(4): p. 364-378.
- 365. Mu, Q., H. Zhang, and X.M. Luo, *SLE: Another Autoimmune Disorder Influenced by Microbes and Diet?* Front Immunol, 2015. **6**: p. 608.
- 366. Parks, C.G., et al., Expert panel workshop consensus statement on the role of the environment in the development of autoimmune disease. Int J Mol Sci, 2014. **15**(8): p. 14269-97.
- 367. Battaglia, M. and L.A. Garrett-Sinha, *Bacterial infections in lupus: Roles in promoting immune activation and in pathogenesis of the disease*. J Transl Autoimmun, 2021. **4**: p. 100078.
- 368. Qiu, C.C., R. Caricchio, and S. Gallucci, *Triggers of Autoimmunity: The Role of Bacterial Infections in the Extracellular Exposure of Lupus Nuclear Autoantigens.* Front Immunol, 2019. **10**: p. 2608.
- 369. Kronbichler, A., J. Kerschbaum, and G. Mayer, *The Influence and Role of Microbial Factors in Autoimmune Kidney Diseases: A Systematic Review.* J Immunol Res, 2015. **2015**: p. 858027.
- 370. Zhang, H., et al., *Dynamics of gut microbiota in autoimmune lupus*. Appl Environ Microbiol, 2014. **80**(24): p. 7551-60.
- 371. Ma, K., et al., *Roles of B cell-intrinsic TLR signals in systemic lupus erythematosus.* Int J Mol Sci, 2015. **16**(6): p. 13084-105.
- 372. Liu, Y., et al., *TLR2 and TLR4 in autoimmune diseases: a comprehensive review*. Clin Rev Allergy Immunol, 2014. **47**(2): p. 136-47.
- 373. Jiang, W. and G. Gilkeson, Sex differences in monocytes and TLR4 associated immune responses; implications for systemic lupus erythematosus (SLE). J Immunother Appl, 2014. 1: p. 1.
- 374. Lee, T.P., et al., Transgenic overexpression of anti-double-stranded DNA autoantibody and activation of Toll-like receptor 4 in mice induce severe systemic lupus erythematosus syndromes. J Autoimmun, 2010. **35**(4): p. 358-67.
- 375. Cavallo, T., et al., *Altered glomerular permeability in the early phase of immune complex nephritis.* Kidney Int, 1983. **24**(5): p. 632-7.

- 376. Cavallo, T., M. Goldman, and P.H. Lambert, *Animal model of human disease. Proliferative glomerulonephritis associated with polyclonal B-cell activation.* Am J Pathol, 1984. **114**(2): p. 346-8.
- 377. Cavallo, T. and N.A. Granholm, Repeated exposure to bacterial lipopolysaccharide interferes with disposal of pathogenic immune complexes in mice. Clin Exp Immunol, 1990. **79**(2): p. 253-9.
- 378. Ramos-Niembro, F., G. Fournie, and P.H. Lambert, *INDUCTION OF CIRCULATING IMMUNE-COMPLEXES AND THEIR RENAL LOCALIZATION AFTER ACUTE OR CHRONIC POLYCLONAL B-CELL ACTIVATION IN MICE.* Kidney International, 1982. **21**: p. S29-S38.
- 379. Cavallo, T. and N.A. Granholm, *Lipopolysaccharide from gram-negative bacteria enhances polyclonal B cell activation and exacerbates nephritis in MRL/lpr mice*. Clin Exp Immunol, 1990. **82**(3): p. 515-21.
- 380. Cavallo, T. and N.A. Granholm, *BACTERIAL LIPOPOLYSACCHARIDE TRANSFORMS MESANGIAL INTO PROLIFERATIVE LUPUS NEPHRITIS WITHOUT INTERFERING WITH PROCESSING OF PATHOGENIC IMMUNE-COMPLEXES IN NZB/W MICE.* AMERICAN JOURNAL OF PATHOLOGY, 1990. **137**(4): p. 971-978.
- 381. Cavallo, T. and N.A. Granholm, *Accelerated (proliferative) lupus nephritis*. Am J Pathol, 1990. **137**(6): p. 1549-51.
- 382. Fournie, G.J., et al., Acceleration of glomerulonephritis in NZB x NZW mice by early immunization with DNA and injection of bacterial lipopolysaccharide. Experimental approach to the treatment of lupus nephritis by use of the accelerated model of NZB x NZW mouse disease. J Clin Lab Immunol, 1980. **4**(2): p. 103-6.
- 383. Granholm, N.A. and T. Cavallo, *Bacterial lipopolysaccharide enhances deposition of immune complexes and exacerbates nephritis in BXSB lupus-prone mice*. Clin Exp Immunol, 1991. **85**(2): p. 270-7.
- 384. Granholm, N.A. and T. Cavallo, *Bacterial lipopolysaccharide causes variable deposits of diverse immunoglobulin isotypes in kidneys of lupus-prone mice*. Lupus, 1992. **1**(4): p. 255-61.
- 385. Basta, F., et al., *Systemic Lupus Erythematosus (SLE) Therapy: The Old and the New.* Rheumatol Ther, 2020. **7**(3): p. 433-446.
- 386. Gatto, M., et al., *New therapeutic strategies in systemic lupus erythematosus management.* Nat Rev Rheumatol, 2019. **15**(1): p. 30-48.
- 387. Hobeika, L., L. Ng, and I.J. Lee, *Moving Forward With Biologics in Lupus Nephritis*. Adv Chronic Kidney Dis, 2019. **26**(5): p. 338-350.

- 388. Calder, P.C., et al., *Lipids in Parenteral Nutrition: Biological Aspects*. JPEN J Parenter Enteral Nutr, 2020. **44 Suppl 1**: p. S21-S27.
- 389. Wierenga, K.A., et al., Requisite Omega-3 HUFA Biomarker Thresholds for Preventing Murine Lupus Flaring. Front Immunol, 2020. 11: p. 1796.
- 390. Ramessar, N., A. Borad, and N. Schlesinger, *The effect of Omega-3 fatty acid supplementation in systemic lupus erythematosus patients: A systematic review.* Lupus, 2022. **31**(3): p. 287-296.
- 391. Rose, T.E., et al., *1-Aryl-3-(1-acylpiperidin-4-yl)urea inhibitors of human and murine soluble epoxide hydrolase: structure-activity relationships, pharmacokinetics, and reduction of inflammatory pain.* J Med Chem, 2010. **53**(19): p. 7067-75.
- 392. Ulu, A., et al., *Pharmacokinetics and in vivo potency of soluble epoxide hydrolase inhibitors in cynomolgus monkeys.* Br J Pharmacol, 2012. **165**(5): p. 1401-12.
- 393. Liu, J.Y., et al., Substituted phenyl groups improve the pharmacokinetic profile and anti-inflammatory effect of urea-based soluble epoxide hydrolase inhibitors in murine models. Eur J Pharm Sci, 2013. **48**(4-5): p. 619-27.
- 394. Lee, K.S., et al., *Optimized inhibitors of soluble epoxide hydrolase improve in vitro target residence time and in vivo efficacy.* J Med Chem, 2014. **57**(16): p. 7016-30.
- 395. Shi, Z., Z. He, and D.W. Wang, *CYP450 Epoxygenase Metabolites, Epoxyeicosatrienoic Acids, as Novel Anti-Inflammatory Mediators.* Molecules, 2022. **27**(12).
- 396. Jonnalagadda, D., et al., *A Soluble Epoxide Hydrolase Inhibitor, 1-TrifluoromethoxyPhenyl-3-(1-Propionylpiperidin-4-yl) Urea, Ameliorates Experimental Autoimmune Encephalomyelitis.* Int J Mol Sci, 2021. **22**(9).
- 397. Trindade-da-Silva, C.A., et al., *Soluble epoxide hydrolase inhibitor, TPPU, increases regulatory T cells pathway in an arthritis model.* FASEB J, 2020. **34**(7): p. 9074-9086.
- 398. Lopez-Vicario, C., et al., *Inhibition of soluble epoxide hydrolase modulates inflammation and autophagy in obese adipose tissue and liver: role for omega-3 epoxides.* Proc Natl Acad Sci U S A, 2015. **112**(2): p. 536-41.
- 399. Wang, L., et al., *Use of a soluble epoxide hydrolase inhibitor in smoke-induced chronic obstructive pulmonary disease.* Am J Respir Cell Mol Biol, 2012. **46**(5): p. 614-22.
- 400. Yang, J., et al., Soluble epoxide hydrolase inhibitor attenuates inflammation and airway hyperresponsiveness in mice. Am J Respir Cell Mol Biol, 2015. **52**(1): p. 46-55.
- 401. Zhou, Y., et al., Soluble Epoxide Hydrolase Inhibitor Attenuates Lipopolysaccharide-Induced Acute Lung Injury and Improves Survival in Mice. Shock, 2017. **47**(5): p. 638-645.

- 402. Moore, E. and C. Putterman, *Are lupus animal models useful for understanding and developing new therapies for human SLE?* J Autoimmun, 2020. **112**: p. 102490.
- 403. Tsai, P.Y., et al., *Therapeutic potential of DCB-SLE1*, an extract of a mixture of Chinese medicinal herbs, for severe lupus nephritis. Am J Physiol Renal Physiol, 2011. **301**(4): p. F751-64.
- 404. Lin, T.J., et al., Accelerated and Severe Lupus Nephritis Benefits From M1, an Active Metabolite of Ginsenoside, by Regulating NLRP3 Inflammasome and T Cell Functions in Mice. Front Immunol, 2019. **10**: p. 1951.
- 405. Alexander, C. and E.T. Rietschel, *Bacterial lipopolysaccharides and innate immunity*. J Endotoxin Res, 2001. **7**(3): p. 167-202.
- 406. Dias, R.P., et al., Outer Membrane Remodeling: The Structural Dynamics and Electrostatics of Rough Lipopolysaccharide Chemotypes. J Chem Theory Comput, 2014. **10**(6): p. 2488-97.
- 407. Huber, M., et al., *R-form LPS*, the master key to the activation of TLR4/MD-2-positive cells. Eur J Immunol, 2006. **36**(3): p. 701-11.
- 408. Pupo, E., et al., Intact rough- and smooth-form lipopolysaccharides from Escherichia coli separated by preparative gel electrophoresis exhibit differential biologic activity in human macrophages. FEBS J, 2013. **280**(4): p. 1095-111.
- 409. Jiang, Z., et al., *CD14 is required for MyD88-independent LPS signaling*. Nat Immunol, 2005. **6**(6): p. 565-70.
- 410. Tsai, P.Y., et al., Antroquinonol differentially modulates T cell activity and reduces interleukin-18 production, but enhances Nrf2 activation, in murine accelerated severe lupus nephritis. Arthritis Rheum, 2012. **64**(1): p. 232-42.
- 411. Dubois, E.L., et al., *NZB/NZW mice as a model of systemic lupus erythematosus*. JAMA, 1966. **195**(4): p. 285-9.
- 412. Reeves, P.G., F.H. Nielsen, and G.C. Fahey, Jr., AIN-93 purified diets for laboratory rodents: final report of the American Institute of Nutrition ad hoc writing committee on the reformulation of the AIN-76A rodent diet. J Nutr, 1993. **123**(11): p. 1939-51.
- 413. Sergin, S., et al. Fatty Acid and Antioxidant Profile of Eggs from Pasture-Raised Hens Fed a Corn- and Soy-Free Diet and Supplemented with Grass-Fed Beef Suet and Liver. Foods, 2022. 11, DOI: 10.3390/foods11213404.
- 414. Rand, A.A., et al., *LC-MS/MS Analysis of the Epoxides and Diols Derived from the Endocannabinoid Arachidonoyl Ethanolamide*. Methods Mol Biol, 2018. **1730**: p. 123-133.

- 415. Yu, F., et al., Redefining lupus nephritis: clinical implications of pathophysiologic subtypes. Nat Rev Nephrol, 2017. **13**(8): p. 483-495.
- 416. Pestka, J.J., et al., Omega-3 polyunsaturated fatty acid intervention against established autoimmunity in a murine model of toxicant-triggered lupus. Frontiers in immunology, 2021. **12**: p. 653464.
- 417. Livak, K.J. and T.D. Schmittgen, *Analysis of relative gene expression data using real-time quantitative PCR and the 2(-Delta Delta C(T)) Method.* Methods, 2001. **25**(4): p. 402-8.
- 418. McBurney, M.I., N.L. Tintle, and W.S. Harris, *The omega-3 index is inversely associated with the neutrophil-lymphocyte ratio in adults'*. Prostaglandins Leukot Essent Fatty Acids, 2022. **177**: p. 102397.
- 419. Wan, X., et al., *Lack of rewarding effects of a soluble epoxide hydrolase inhibitor TPPU in mice: Comparison with morphine.* Neuropsychopharmacology Reports, 2020. **40**(4): p. 412-416.
- 420. Cui, Z., et al., *Inhibition of Soluble Epoxide Hydrolase Attenuates Bosutinib-Induced Blood Pressure Elevation*. Hypertension, 2021. **78**(5): p. 1527-1540.
- 421. Trindade-da-Silva, C.A., et al., Soluble epoxide hydrolase inhibitor, TPPU, increases regulatory T cells pathway in an arthritis model. The FASEB Journal, 2020. **34**(7): p. 9074-9086.
- 422. Ren, Q., et al., Gene deficiency and pharmacological inhibition of soluble epoxide hydrolase confers resilience to repeated social defeat stress. Proc Natl Acad Sci U S A, 2016. **113**(13): p. E1944-52.
- 423. Ostermann, A.I. and N.H. Schebb, *Effects of omega-3 fatty acid supplementation on the pattern of oxylipins: a short review about the modulation of hydroxy-, dihydroxy-, and epoxy-fatty acids.* Food & Function, 2017. **8**(7): p. 2355-2367.
- 424. Schmöcker, C., et al., *Effect of Omega-3 Fatty Acid Supplementation on Oxylipins in a Routine Clinical Setting.* International Journal of Molecular Sciences, 2018. **19**(1): p. 180.
- 425. Ulu, A., et al., Anti-inflammatory Effects of ω-3 Polyunsaturated Fatty Acids and Soluble Epoxide Hydrolase Inhibitors in Angiotensin-II–Dependent Hypertension. Journal of Cardiovascular Pharmacology, 2013. **62**(3): p. 285-297.
- 426. Shui, H.A., et al., *LPS-evoked IL-18 expression in mesangial cells plays a role in accelerating lupus nephritis.* Rheumatology (Oxford), 2007. **46**(8): p. 1277-84.
- 427. Lasselin, J., et al., Comparison of bacterial lipopolysaccharide-induced sickness behavior in rodents and humans: Relevance for symptoms of anxiety and depression. Neurosci Biobehav Rev, 2020. **115**: p. 15-24.

- 428. Bates, M.A., et al., *Dietary docosahexaenoic acid prevents silica-induced development of pulmonary ectopic germinal centers and glomerulonephritis in the lupus-prone NZBWF1 mouse.* Front Immunol, 2018. **9**: p. 2002.
- 429. Metherel, A.H., et al., Retroconversion is a minor contributor to increases in eicosapentaenoic acid following docosahexaenoic acid feeding as determined by compound specific isotope analysis in rat liver. Nutr Metab (Lond), 2017. 14: p. 75.
- 430. Wierenga, K.A., et al., *Docosahexaenoic Acid Suppresses Silica-Induced Inflammasome Activation and IL-1 Cytokine Release by Interfering With Priming Signal.* Front Immunol, 2019. **10**: p. 2130.
- 431. Wierenga, K.A., et al., Single cell analysis of docosahexaenoic acid suppression of sequential LPS-induced proinflammatory and interferon-regulated gene expression in the macrophage. Front Immunol, 2022. 13: p. 993614.
- 432. Rajasinghe, L.D., et al., Omega-3 Docosahexaenoic Acid (DHA) Impedes Silica-Induced Macrophage Corpse Accumulation by Attenuating Cell Death and Potentiating Efferocytosis. Front Immunol, 2020. 11: p. 2179.
- 433. Rajasinghe, L.D., et al., Silica Induction of Diverse Inflammatory Proteome in Lungs of Lupus-Prone Mice Quelled by Dietary Docosahexaenoic Acid Supplementation. Front Immunol, 2021. 12: p. 781446.
- 434. Cheng, T., et al., Resolvin D1 Improves the Treg/Th17 Imbalance in Systemic Lupus Erythematosus Through miR-30e-5p. Front Immunol, 2021. 12: p. 668760.
- 435. Qiu, H., et al., *Soluble epoxide hydrolase inhibitors and heart failure*. Cardiovasc Ther, 2011. **29**(2): p. 99-111.
- 436. Shen, H.C. and B.D. Hammock, *Discovery of inhibitors of soluble epoxide hydrolase: a target with multiple potential therapeutic indications.* J Med Chem, 2012. **55**(5): p. 1789-808.
- 437. Bettaieb, A., et al., Soluble Epoxide Hydrolase Pharmacological Inhibition Ameliorates Experimental Acute Pancreatitis in Mice. Mol Pharmacol, 2015. **88**(2): p. 281-90.
- 438. Harris, T.R., et al., *Inhibition of soluble epoxide hydrolase attenuates hepatic fibrosis and endoplasmic reticulum stress induced by carbon tetrachloride in mice*. Toxicol Appl Pharmacol, 2015. **286**(2): p. 102-11.
- 439. Goswami, S.K., et al., *Anti-Ulcer Efficacy of Soluble Epoxide Hydrolase Inhibitor TPPU on Diclofenac-Induced Intestinal Ulcers.* J Pharmacol Exp Ther, 2016. **357**(3): p. 529-36.
- 440. Supp, D.M., et al., Soluble Epoxide Hydrolase Inhibition and Epoxyeicosatrienoic Acid Treatment Improve Vascularization of Engineered Skin Substitutes. Plast Reconstr Surg Glob Open, 2016. **4**(12): p. e1151.

- 441. Chen, Y., et al., Soluble epoxide hydrolase inhibition Promotes White Matter Integrity and Long-Term Functional Recovery after chronic hypoperfusion in mice. Sci Rep, 2017. **7**(1): p. 7758.
- 442. Wu, Q., et al., *The effects of sEH inhibitor on depression-like behavior and neurogenesis in male mice.* J Neurosci Res, 2017. **95**(12): p. 2483-2492.
- 443. Huang, H.J., et al., Soluble Epoxide Hydrolase Inhibition Attenuates MPTP-Induced Neurotoxicity in the Nigrostriatal Dopaminergic System: Involvement of α-Synuclein Aggregation and ER Stress. Mol Neurobiol, 2018. 55(1): p. 138-144.
- 444. Napimoga, M.H., et al., *Soluble epoxide hydrolase inhibitor promotes immunomodulation to inhibit bone resorption.* J Periodontal Res, 2018. **53**(5): p. 743-749.
- 445. Tu, R., et al., Soluble epoxide hydrolase inhibition decreases reperfusion injury after focal cerebral ischemia. Sci Rep, 2018. **8**(1): p. 5279.
- 446. Schmelzer, K.R., et al., *Soluble epoxide hydrolase is a therapeutic target for acute inflammation.* Proc Natl Acad Sci U S A, 2005. **102**(28): p. 9772-7.
- 447. Wan, D., et al., *In vitro and in vivo Metabolism of a Potent Inhibitor of Soluble Epoxide Hydrolase*, *1-(1-Propionylpiperidin-4-yl)-3-(4-(trifluoromethoxy)phenyl)urea*. Front Pharmacol, 2019. **10**: p. 464.
- 448. Lee, K.S.S., et al., *Optimized Inhibitors of Soluble Epoxide Hydrolase Improve in Vitro Target Residence Time and in Vivo Efficacy*. Journal of Medicinal Chemistry, 2014. **57**(16): p. 7016-7030.
- 449. Liu, J.-Y., et al., Substituted phenyl groups improve the pharmacokinetic profile and antiinflammatory effect of urea-based soluble epoxide hydrolase inhibitors in murine models. European Journal of Pharmaceutical Sciences, 2013. **48**(4): p. 619-627.
- 450. Harris, T.R., et al., *An omega-3-enriched diet alone does not attenuate CCl(4)-induced hepatic fibrosis*. J Nutr Biochem, 2016. **38**: p. 93-101.
- 451. Spector, A.A., *Arachidonic acid cytochrome P450 epoxygenase pathway*. J Lipid Res, 2009. **50 Suppl**(Suppl): p. S52-6.
- 452. Sarparast, M., et al., Cytochrome P450 Metabolism of Polyunsaturated Fatty Acids and Neurodegeneration. Nutrients, 2020. **12**(11).
- 453. Morin, C., et al., *EET displays anti-inflammatory effects in TNF-alpha stimulated human bronchi: putative role of CPI-17.* Am J Respir Cell Mol Biol, 2008. **38**(2): p. 192-201.
- 454. Node, K., et al., *Anti-inflammatory properties of cytochrome P450 epoxygenase-derived eicosanoids.* Science, 1999. **285**(5431): p. 1276-9.

- 455. Kundu, S., et al., *Metabolic products of soluble epoxide hydrolase are essential for monocyte chemotaxis to MCP-1 in vitro and in vivo.* J Lipid Res, 2013. **54**(2): p. 436-47.
- 456. Wang, W., et al., Targeted Metabolomics Identifies the Cytochrome P450 Monooxygenase Eicosanoid Pathway as a Novel Therapeutic Target of Colon Tumorigenesis. Cancer Res, 2019. **79**(8): p. 1822-1830.
- 457. Zhang, G., et al., *Epoxy metabolites of docosahexaenoic acid (DHA) inhibit angiogenesis, tumor growth, and metastasis.* Proc Natl Acad Sci U S A, 2013. **110**(16): p. 6530-5.
- 458. Panigrahy, D., et al., *Epoxyeicosanoids stimulate multiorgan metastasis and tumor dormancy escape in mice.* J Clin Invest, 2012. **122**(1): p. 178-91.
- 459. Gilroy, D.W., et al., *CYP450-derived oxylipins mediate inflammatory resolution*. Proc Natl Acad Sci U S A, 2016. **113**(23): p. E3240-9.
- 460. Campbell, W.B. and I. Fleming, *Epoxyeicosatrienoic acids and endothelium-dependent responses*. Pflugers Arch, 2010. **459**(6): p. 881-95.
- 461. Campbell, W.B. and D.R. Harder, *Endothelium-derived hyperpolarizing factors and vascular cytochrome P450 metabolites of arachidonic acid in the regulation of tone*. Circ Res, 1999. **84**(4): p. 484-8.
- 462. Roman, R.J. and F. Fan, 20-HETE: hypertension and beyond. Hypertension, 2018. **72**(1): p. 12-18.
- 463. Wu, C.C., et al., 20-HETE and blood pressure regulation: clinical implications. Cardiol Rev, 2014. **22**(1): p. 1-12.
- 464. Kodani, S.D. and C. Morisseau, *Role of epoxy-fatty acids and epoxide hydrolases in the pathology of neuro-inflammation*. Biochimie, 2019. **159**: p. 59-65.
- 465. Chen, Z., et al., sEH Inhibitor Tppu Ameliorates Cecal Ligation and Puncture-Induced Sepsis by Regulating Macrophage Functions. Shock, 2020. **53**(6): p. 761-771.
- 466. Deng, B.Q., et al., *Epoxide metabolites of arachidonate and docosahexaenoate function conversely in acute kidney injury involved in GSK3beta signaling*. Proc Natl Acad Sci U S A, 2017. **114**(47): p. 12608-12613.
- 467. Panigrahy, D., et al., *Epoxyeicosanoids promote organ and tissue regeneration*. Proc Natl Acad Sci U S A, 2013. **110**(33): p. 13528-33.
- 468. Falck, J.R., et al., 11,12-epoxyeicosatrienoic acid (11,12-EET): structural determinants for inhibition of TNF-alpha-induced VCAM-1 expression. Bioorg Med Chem Lett, 2003. 13(22): p. 4011-4.

- 469. Benninghoff, A.D., et al., *Docosahexaenoic Acid Consumption Impedes Early Interferonand Chemokine-Related Gene Expression While Suppressing Silica-Triggered Flaring of Murine Lupus.* Front Immunol, 2019. **10**: p. 2851.
- 470. Ostermann, A.I., et al., *Oral treatment of rodents with soluble epoxide hydrolase inhibitor* 1-(1-propanoylpiperidin-4-yl)-3-[4-(trifluoromethoxy)phenyl]urea (TPPU): Resulting drug levels and modulation of oxylipin pattern. Prostaglandins Other Lipid Mediat, 2015. **121**(Pt A): p. 131-7.
- 471. Hoy, R.F. and D.C. Chambers, *Silica-related diseases in the modern world*. Allergy, 2020. **75**(11): p. 2805-2817.
- 472. OSHA. *Silica, Crystalline*. 2016 2016 [cited 2020 6/1/2020]; Available from: https://www.osha.gov/dsg/topics/silicacrystalline/index.html.
- 473. Farhat, S.C., et al., *Air pollution in autoimmune rheumatic diseases: a review*. Autoimmun Rev, 2011. **11**(1): p. 14-21.
- 474. Boudigaard, S.H., et al., *Occupational exposure to respirable crystalline silica and risk of autoimmune rheumatic diseases: a nationwide cohort study.* Int J Epidemiol, 2021. **50**(4): p. 1213-1226.
- 475. OSHA. Workers' Exposure to Respirable Crystalline Silica: Final Rule Overview. 2016 3/2016 [cited 2020 6/2/2020]; Available from: https://www.osha.gov/Publications/OSHA3683.pdf.
- 476. Parks, C.G. and A.J. De Roos, *Pesticides, chemical and industrial exposures in relation to systemic lupus erythematosus.* Lupus, 2014. **23**(6): p. 527-36.
- 477. Joshi, N., J.M. Walter, and A.V. Misharin, *Alveolar Macrophages*. Cell Immunol, 2018. **330**: p. 86-90.
- 478. Hindman, B. and Q. Ma, Carbon nanotubes and crystalline silica stimulate robust ROS production, inflammasome activation, and IL-1beta secretion in macrophages to induce myofibroblast transformation. Arch Toxicol, 2019. **93**(4): p. 887-907.
- 479. Garcia, J.G., et al., Alveolar macrophages from patients with asbestos exposure release increased levels of leukotriene B4. Am Rev Respir Dis, 1989. **139**(6): p. 1494-501.
- 480. Mohr, C., et al., Enhanced release of prostaglandin E2 from macrophages of rats with silicosis. Am J Respir Cell Mol Biol, 1992. **6**(4): p. 390-6.
- 481. Koren, H.S., et al., *Modulation of eicosanoid production by human alveolar macrophages exposed to silica in vitro*. Environ Health Perspect, 1992. **97**: p. 77-83.
- 482. Lundstrom, S.L., et al., *Lipid mediator profiling in pulmonary disease*. Curr Pharm Biotechnol, 2011. **12**(7): p. 1026-52.

- 483. Claar, D., T.V. Hartert, and R.S. Peebles, Jr., *The role of prostaglandins in allergic lung inflammation and asthma*. Expert Rev Respir Med, 2015. **9**(1): p. 55-72.
- 484. Teopompi, E., et al., Arachidonic Acid and Docosahexaenoic Acid Metabolites in the Airways of Adults With Cystic Fibrosis: Effect of Docosahexaenoic Acid Supplementation. Front Pharmacol, 2019. **10**: p. 938.
- 485. Wang, B., et al., *Metabolism pathways of arachidonic acids: mechanisms and potential therapeutic targets.* Signal Transduct Target Ther, 2021. **6**(1): p. 94.
- 486. Gutierrez, S., S.L. Svahn, and M.E. Johansson, *Effects of Omega-3 Fatty Acids on Immune Cells*. Int J Mol Sci, 2019. **20**(20).
- 487. Hartling, I., et al., Quantitative profiling of inflammatory and pro-resolving lipid mediators in human adolescents and mouse plasma using UHPLC-MS/MS. Clin Chem Lab Med, 2021. **59**(11): p. 1811-1823.
- 488. Schuchardt, J.P., et al., *Effect of DHA supplementation on oxylipin levels in plasma and immune cell stimulated blood.* Prostaglandins Leukot Essent Fatty Acids, 2017. **121**: p. 76-87.
- 489. Ostermann, A.I., et al., *Plasma oxylipins respond in a linear dose-response manner with increased intake of EPA and DHA: results from a randomized controlled trial in healthy humans.* Am J Clin Nutr, 2019. **109**(5): p. 1251-1263.
- 490. Favor, O.K., et al., Centrality of Myeloid-Lineage Phagocytes in Particle-Triggered Inflammation and Autoimmunity. Front Toxicol, 2021. **3**(51): p. 777768.
- 491. Calder, P.C., *n-3 PUFA and inflammation: from membrane to nucleus and from bench to bedside.* Proc Nutr Soc, 2020: p. 1-13.
- 492. Kuda, O., *Bioactive metabolites of docosahexaenoic acid.* Biochimie, 2017. **136**: p. 12-20.
- 493. Busch, C.J., et al., *Isolation and Long-term Cultivation of Mouse Alveolar Macrophages*. Bio Protoc, 2019. **9**(14).
- 494. Gorki, A.D., et al., Murine Ex Vivo Cultured Alveolar Macrophages Provide a Novel Tool to Study Tissue-Resident Macrophage Behavior and Function. Am J Respir Cell Mol Biol, 2022. **66**(1): p. 64-75.
- 495. McQuattie-Pimentel, A.C., et al., *The lung microenvironment shapes a dysfunctional response of alveolar macrophages in aging.* J Clin Invest, 2021. **131**(4).
- 496. Murray, P.J. and T.A. Wynn, *Obstacles and opportunities for understanding macrophage polarization*. J Leukoc Biol, 2011. **89**(4): p. 557-63.

- 497. Fejer, G., et al., Nontransformed, GM-CSF-dependent macrophage lines are a unique model to study tissue macrophage functions. Proc Natl Acad Sci U S A, 2013. **110**(24): p. E2191-8.
- 498. Stirling, D.R., et al., *CellProfiler 4: improvements in speed, utility and usability.* BMC Bioinformatics, 2021. **22**(1): p. 433.
- 499. Sager, T.M., et al., Role of engineered metal oxide nanoparticle agglomeration in reactive oxygen species generation and cathepsin B release in NLRP3 inflammasome activation and pulmonary toxicity. Inhal Toxicol, 2016. **28**(14): p. 686-697.
- 500. So, J., et al., EPA and DHA differentially modulate monocyte inflammatory response in subjects with chronic inflammation in part via plasma specialized pro-resolving lipid mediators: A randomized, double-blind, crossover study. Atherosclerosis, 2021. **316**: p. 90-98.
- 501. Lamon-Fava, S., et al., *Dose- and time-dependent increase in circulating anti-inflammatory and pro-resolving lipid mediators following eicosapentaenoic acid supplementation in patients with major depressive disorder and chronic inflammation.* Prostaglandins Leukot Essent Fatty Acids, 2021. **164**: p. 102219.
- 502. Markworth, J.F., et al., *Divergent shifts in lipid mediator profile following supplementation with n-3 docosapentaenoic acid and eicosapentaenoic acid.* FASEB J, 2016. **30**(11): p. 3714-3725.
- 503. Pang, Z., et al., Using MetaboAnalyst 5.0 for LC-HRMS spectra processing, multi-omics integration and covariate adjustment of global metabolomics data. Nat Protoc, 2022. 17(8): p. 1735-1761.
- 504. Basil, M.C. and B.D. Levy, *Specialized pro-resolving mediators: endogenous regulators of infection and inflammation.* Nat Rev Immunol, 2016. **16**(1): p. 51-67.
- 505. Woo, Y.D., D. Jeong, and D.H. Chung, *Development and Functions of Alveolar Macrophages*. Mol Cells, 2021. **44**(5): p. 292-300.
- 506. Hamilton, R.F., Jr., S.A. Thakur, and A. Holian, *Silica binding and toxicity in alveolar macrophages*. Free Radic Biol Med, 2008. **44**(7): p. 1246-58.
- 507. Pacheco, F.J., et al., *Docosahexanoic acid antagonizes TNF-alpha-induced necroptosis by attenuating oxidative stress, ceramide production, lysosomal dysfunction, and autophagic features.* Inflamm Res, 2014. **63**(10): p. 859-71.
- 508. Chen, C.Y., et al., *Omega-3 polyunsaturated fatty acids reduce preterm labor by inhibiting trophoblast cathepsin S and inflammasome activation*. Clin Sci (Lond), 2018. **132**(20): p. 2221-2239.

- 509. Fletcher, P., et al., *Docosahexaenoic acid impacts macrophage phenotype subsets and phagolysosomal membrane permeability with particle exposure.* J Toxicol Environ Health A, 2021. **84**(4): p. 152-172.
- 510. Stillwell, W., et al., Effect of docosahexaenoic acid on mouse mitochondrial membrane properties. Lipids, 1997. **32**(5): p. 497-506.
- 511. Ng, Y., et al., *The role of docosahexaenoic acid in mediating mitochondrial membrane lipid oxidation and apoptosis in colonocytes.* Carcinogenesis, 2005. **26**(11): p. 1914-21.
- 512. Li, G., et al., Antioxidant Activity of Docosahexaenoic Acid (DHA) and Its Regulatory Roles in Mitochondria. J Agric Food Chem, 2021. **69**(5): p. 1647-1655.
- 513. Wiesenfeld, P.W., U.S. Babu, and M.W. O'Donnell, *Effect of long-chain fatty acids in the culture medium on fatty acid composition of WEHI-3 and J774A.1 cells.* Comp Biochem Physiol B Biochem Mol Biol, 2001. **128**(1): p. 123-34.
- 514. Morin, C., P.U. Blier, and S. Fortin, *Eicosapentaenoic acid and docosapentaenoic acid monoglycerides are more potent than docosahexaenoic acid monoglyceride to resolve inflammation in a rheumatoid arthritis model.* Arthritis Res Ther, 2015. **17**(1): p. 142.
- 515. Dawczynski, C., et al., *Docosahexaenoic acid in the treatment of rheumatoid arthritis: A double-blind, placebo-controlled, randomized cross-over study with microalgae vs. sunflower oil.* Clin Nutr, 2018. **37**(2): p. 494-504.
- 516. Khan, R.S., et al., Fish oil selectively improves heart function in a mouse model of lipid-induced cardiomyopathy. J Cardiovasc Pharmacol, 2013. **61**(4): p. 345-54.
- 517. Kris-Etherton, P.M., et al., Recent Clinical Trials Shed New Light on the Cardiovascular Benefits of Omega-3 Fatty Acids. Methodist Debakey Cardiovasc J, 2019. **15**(3): p. 171-178.
- 518. Fritsche, K., Important differences exist in the dose-response relationship between diet and immune cell fatty acids in humans and rodents. Lipids, 2007. **42**(11): p. 961-79.
- 519. Simopoulos, A.P., An Increase in the Omega-6/Omega-3 Fatty Acid Ratio Increases the Risk for Obesity. Nutrients, 2016. **8**(3): p. 128.
- 520. Lands, B., *Omega-3 PUFAs Lower the Propensity for Arachidonic Acid Cascade Overreactions*. Biomed Res Int, 2015. **2015**: p. 285135.
- 521. Sarparast, M., et al., *Dihydroxy-Metabolites of Dihomo-gamma-linolenic Acid Drive Ferroptosis-Mediated Neurodegeneration*. bioRxiv, 2023.
- 522. Mouchlis, V.D. and E.A. Dennis, *Phospholipase A(2) catalysis and lipid mediator lipidomics*. Biochim Biophys Acta Mol Cell Biol Lipids, 2019. **1864**(6): p. 766-771.

- 523. Sager, T.M., et al., *Tobacco Smoke Exposure Exacerbated Crystalline Silica-Induced Lung Toxicity in Rats.* Toxicol Sci, 2020. **178**(2): p. 375-390.
- 524. Wilborn, J., D.L. DeWitt, and M. Peters-Golden, *Expression and role of cyclooxygenase isoforms in alveolar and peritoneal macrophages*. Am J Physiol, 1995. **268**(2 Pt 1): p. L294-301.
- 525. Vijayan, V., et al., A New Immunomodulatory Role for Peroxisomes in Macrophages Activated by the TLR4 Ligand Lipopolysaccharide. J Immunol, 2017. **198**(6): p. 2414-2425.
- 526. Wuest, S.J., et al., *Expression and regulation of 12/15-lipoxygenases in human primary macrophages*. Atherosclerosis, 2012. **225**(1): p. 121-7.
- 527. Lee, S.J., K.W. Seo, and C.D. Kim, *LPS Increases 5-LO Expression on Monocytes via an Activation of Akt-Sp1/NF-kappaB Pathways*. Korean J Physiol Pharmacol, 2015. **19**(3): p. 263-8.
- 528. Abrial, C., et al., 15-Lipoxygenases regulate the production of chemokines in human lung macrophages. Br J Pharmacol, 2015. **172**(17): p. 4319-30.
- 529. Rossol, M., et al., *LPS-induced cytokine production in human monocytes and macrophages*. Crit Rev Immunol, 2011. **31**(5): p. 379-446.
- 530. Smith, G.S., et al., *The effect of an interleukin receptor antagonist (IL-1ra) on colonocyte eicosanoid release.* Mediators Inflamm, 1996. **5**(6): p. 449-52.
- 531. Molina-Holgado, E., et al., *Induction of COX-2 and PGE(2) biosynthesis by IL-1beta is mediated by PKC and mitogen-activated protein kinases in murine astrocytes.* Br J Pharmacol, 2000. **131**(1): p. 152-9.
- 532. Conti, P., et al., In vitro enhanced thromboxane B2 release by polymorphonuclear leukocytes and macrophages after treatment with human recombinant interleukin 1. Prostaglandins, 1986. **32**(1): p. 111-5.
- 533. Massey, K.A. and A. Nicolaou, *Lipidomics of oxidized polyunsaturated fatty acids*. Free Radic Biol Med, 2013. **59**(100): p. 45-55.
- 534. Mattmiller, S.A., et al., *Reduced macrophage selenoprotein expression alters oxidized lipid metabolite biosynthesis from arachidonic and linoleic acid.* J Nutr Biochem, 2014. **25**(6): p. 647-54.
- 535. Fischer, R., et al., *Dietary omega-3 fatty acids modulate the eicosanoid profile in man primarily via the CYP-epoxygenase pathway*. J Lipid Res, 2014. **55**(6): p. 1150-64.
- 536. Derogis, P.B., et al., *The development of a specific and sensitive LC-MS-based method for the detection and quantification of hydroperoxy- and hydroxydocosahexaenoic acids as a tool for lipidomic analysis.* PLoS One, 2013. **8**(10): p. e77561.

- 537. Joshi, G.N., A.M. Goetjen, and D.A. Knecht, *Silica particles cause NADPH oxidase-independent ROS generation and transient phagolysosomal leakage*. Mol Biol Cell, 2015. **26**(18): p. 3150-64.
- 538. Fazzi, F., et al., *TNFR1/phox interaction and TNFR1 mitochondrial translocation Thwart silica-induced pulmonary fibrosis.* J Immunol, 2014. **192**(8): p. 3837-46.
- 539. Zorov, D.B., M. Juhaszova, and S.J. Sollott, *Mitochondrial ROS-induced ROS release: an update and review.* Biochim Biophys Acta, 2006. **1757**(5-6): p. 509-17.
- 540. Li, Z., et al., Single-cell lipidomics with high structural specificity by mass spectrometry. Nat Commun, 2021. **12**(1): p. 2869.
- 541. Biringer, R.G., A Review of Prostanoid Receptors: Expression, Characterization, Regulation, and Mechanism of Action. J Cell Commun Signal, 2021. **15**(2): p. 155-184.
- 542. Biringer, R.G., A review of non-prostanoid, eicosanoid receptors: expression, characterization, regulation, and mechanism of action. J Cell Commun Signal, 2022. **16**(1): p. 5-46.
- 543. Powell, W.S. and J. Rokach, *Biosynthesis*, *biological effects*, *and receptors of hydroxyeicosatetraenoic acids (HETEs) and oxoeicosatetraenoic acids (oxo-ETEs) derived from arachidonic acid*. Biochim Biophys Acta, 2015. **1851**(4): p. 340-55.
- 544. Milligan, G., et al., *Complex Pharmacology of Free Fatty Acid Receptors*. Chem Rev, 2017. **117**(1): p. 67-110.
- 545. Liu, J., et al., *The omega-3 hydroxy fatty acid 7(S)-HDHA is a high-affinity PPARalpha ligand that regulates brain neuronal morphology.* Sci Signal, 2022. **15**(741): p. eabo1857.
- 546. Canning, B.J., et al., *Ozone reduces murine alveolar and peritoneal macrophage phagocytosis: the role of prostanoids.* Am J Physiol, 1991. **261**(4 Pt 1): p. L277-82.
- 547. Birrell, M.A., et al., *Anti-inflammatory effects of PGE2 in the lung: role of the EP4 receptor subtype.* Thorax, 2015. **70**(8): p. 740-7.
- 548. Speth, J.M., et al., Alveolar Epithelial Cell-Derived Prostaglandin E2 Serves as a Request Signal for Macrophage Secretion of Suppressor of Cytokine Signaling 3 during Innate Inflammation. J Immunol, 2016. **196**(12): p. 5112-20.
- 549. Tang, T., et al., *Macrophage responses to lipopolysaccharide are modulated by a feedback loop involving prostaglandin E*(2), dual specificity phosphatase 1 and tristetraprolin. Sci Rep, 2017. **7**(1): p. 4350.
- 550. Penke, L.R., et al., *PGE*(2) accounts for bidirectional changes in alveolar macrophage self-renewal with aging and smoking. Life Sci Alliance, 2020. **3**(11).

- 551. Ford-Hutchinson, A.W., et al., *Leukotriene B, a potent chemokinetic and aggregating substance released from polymorphonuclear leukocytes.* Nature, 1980. **286**(5770): p. 264-5.
- 552. Hafstrom, I., et al., Leukotriene B4--a stereospecific stimulator for release of lysosomal enzymes from neutrophils. FEBS Lett, 1981. **130**(1): p. 146-8.
- 553. Wasserman, M.A. and R.L. Griffin, *Thromboxane B2--comparative bronchoactivity in experimental systems*. Eur J Pharmacol, 1977. **46**(4): p. 303-13.
- 554. Kitchen, E.A., J.R. Boot, and W. Dawson, *Chemotactic activity of thromboxane B2, prostaglandins and their metabolites for polymorphonuclear leucocytes.* Prostaglandins, 1978. **16**(2): p. 239-44.
- 555. Burhop, K.E., W.M. Selig, and A.B. Malik, *Monohydroxyeicosatetraenoic acids* (5-HETE and 15-HETE) induce pulmonary vasoconstriction and edema. Circ Res, 1988. **62**(4): p. 687-98.
- 556. Goetzl, E.J., et al., *Modulation of human neutrophil function by monohydroxy-eicosatetraenoic acids*. Immunology, 1980. **39**(4): p. 491-501.
- 557. Chang, J., et al., Modulation by hydroxyeicosatetraenoic acids (HETEs) of arachidonic acid metabolism in mouse resident peritoneal macrophages. Eur J Pharmacol, 1985. 107(2): p. 215-22.
- 558. Chavis, C., et al., Formation of lipoxins and leukotrienes by human alveolar macrophages incubated with 15(S)-HETE: a model for cellular cooperation between macrophages and airway epithelial cells. Eicosanoids, 1992. **5**(3-4): p. 203-11.
- 559. Onodera, T., et al., *Eicosapentaenoic acid and 5-HEPE enhance macrophage-mediated Treg induction in mice.* Sci Rep, 2017. **7**(1): p. 4560.
- 560. Heidel, J.R., et al., *In vivo chemotaxis of bovine neutrophils induced by 5-lipoxygenase metabolites of arachidonic and eicosapentaenoic acid.* Am J Pathol, 1989. **134**(3): p. 671-6.
- 561. Yamada, H., A. Uemura, and R. Miyasaka, 8(R)-Hydroxyeicosapentaenoic acid (8R-HEPE) induces transcription of cholesterol efflux receptors via activation of liver X receptor in macrophages. Biosci Biotechnol Biochem, 2023. 87(6): p. 584-591.
- 562. Miller, C., R.Y. Yamaguchi, and V.A. Ziboh, Guinea pig epidermis generates putative anti-inflammatory metabolites from fish oil polyunsaturated fatty acids. Lipids, 1989. **24**(12): p. 998-1003.
- 563. Sapieha, P., et al., 5-Lipoxygenase metabolite 4-HDHA is a mediator of the antiangiogenic effect of omega-3 polyunsaturated fatty acids. Sci Transl Med, 2011. **3**(69): p. 69ra12.

- 564. Borsini, A., et al., Omega-3 polyunsaturated fatty acids protect against inflammation through production of LOX and CYP450 lipid mediators: relevance for major depression and for human hippocampal neurogenesis. Mol Psychiatry, 2021. **26**(11): p. 6773-6788.
- 565. Croset, M., et al., *Inhibition by lipoxygenase products of TXA2-like responses of platelets and vascular smooth muscle. 14-Hydroxy from 22:6n-3 is more potent than 12-HETE.* Biochem Pharmacol, 1988. **37**(7): p. 1275-80.
- 566. Gonzalez-Periz, A., et al., *Docosahexaenoic acid (DHA) blunts liver injury by conversion to protective lipid mediators: protectin D1 and 17S-hydroxy-DHA*. FASEB J, 2006. **20**(14): p. 2537-9.
- 567. Weylandt, K.H., et al., Suppressed liver tumorigenesis in fat-1 mice with elevated omega-3 fatty acids is associated with increased omega-3 derived lipid mediators and reduced TNF-alpha. Carcinogenesis, 2011. **32**(6): p. 897-903.
- 568. Bento, A.F., et al., Omega-3 fatty acid-derived mediators 17(R)-hydroxy docosahexaenoic acid, aspirin-triggered resolvin D1 and resolvin D2 prevent experimental colitis in mice. J Immunol, 2011. **187**(4): p. 1957-69.
- 569. Ruiz-Irastorza, G. and G. Bertsias, *Treating systemic lupus erythematosus in the 21st century: new drugs and new perspectives on old drugs.* Rheumatology (Oxford), 2020. **59**(Suppl5): p. v69-v81.
- 570. Morand, E.F., et al., *Trial of Anifrolumab in Active Systemic Lupus Erythematosus*. N Engl J Med, 2020. **382**(3): p. 211-221.
- 571. Navarra, S.V., et al., Efficacy and safety of belimumab in patients with active systemic lupus erythematosus: a randomised, placebo-controlled, phase 3 trial. Lancet, 2011. 377(9767): p. 721-31.
- 572. Ericson-Neilsen, W. and A.D. Kaye, *Steroids: pharmacology, complications, and practice delivery issues*. Ochsner J, 2014. **14**(2): p. 203-7.
- 573. Wiseman, A.C., *Immunosuppressive Medications*. Clin J Am Soc Nephrol, 2016. **11**(2): p. 332-43.
- 574. Srivastava, A., *Belimumab in Systemic Lupus Erythematosus*. Indian J Dermatol, 2016. **61**(5): p. 550-3.
- 575. Tummala, R., et al., Safety profile of anifrolumab in patients with active SLE: an integrated analysis of phase II and III trials. Lupus Sci Med, 2021. **8**(1): p. e000464.
- 576. Puri, P., et al., *Understand SLE heterogeneity in the era of omics, big data, and artificial intelligence.* Rheumatology & Autoimmunity, 2021. **1**(1): p. 40-51.
- 577. Allen, M.E., V. Rus, and G.L. Szeto, *Leveraging Heterogeneity in Systemic Lupus Erythematosus for New Therapies*. Trends Mol Med, 2021. **27**(2): p. 152-171.

- 578. Woo, J.M.P., et al., *The role of environmental exposures and gene-environment interactions in the etiology of systemic lupus erythematous.* J Intern Med, 2022. **291**(6): p. 755-778.
- 579. Salamon, F., et al., Occupational exposure to crystalline silica in artificial stone processing. J Occup Environ Hyg, 2021. **18**(12): p. 547-554.
- 580. Wiebert, P., et al., Occupational exposure to respirable crystalline silica and acute myocardial infarction among men and women in Sweden. Occup Environ Med, 2022. **80**(1): p. 21-6.
- 581. Misra, S., et al., Occupational exposure to respirable crystalline silica among US metal and nonmetal miners, 2000-2019. Am J Ind Med, 2023. **66**(3): p. 199-212.
- 582. Bates, M.A., et al., Mapping of Dynamic Transcriptome Changes Associated With Silica-Triggered Autoimmune Pathogenesis in the Lupus-Prone NZBWF1 Mouse. Front Immunol, 2019. **10**: p. 632.
- 583. Chauhan, P.S., et al., Rapid Induction of Pulmonary Inflammation, Autoimmune Gene Expression, and Ectopic Lymphoid Neogenesis Following Acute Silica Exposure in Lupus-Prone Mice. Front Immunol, 2021. **12**(275): p. 635138.
- 584. DiNicolantonio, J.J. and J. O'Keefe, *The Importance of Maintaining a Low Omega-6/Omega-3 Ratio for Reducing the Risk of Autoimmune Diseases, Asthma, and Allergies.* Mo Med, 2021. **118**(5): p. 453-459.
- 585. Forsyth, S., S. Gautier, and N. Salem, Jr., Global Estimates of Dietary Intake of Docosahexaenoic Acid and Arachidonic Acid in Developing and Developed Countries. Ann Nutr Metab, 2016. **68**(4): p. 258-67.
- 586. Innes, J.K. and P.C. Calder, *Omega-6 fatty acids and inflammation*. Prostaglandins Leukot Essent Fatty Acids, 2018. **132**: p. 41-48.
- 587. Calder, P.C., *Eicosanoids*. Essays Biochem, 2020. **64**(3): p. 423-441.
- 588. Aghdassi, E., et al., *Alterations in circulating fatty acid composition in patients with systemic lupus erythematosus: a pilot study.* JPEN J Parenter Enteral Nutr, 2011. **35**(2): p. 198-208.
- 589. Gorczyca, D., et al., Serum levels of n-3 and n-6 polyunsaturated fatty acids in patients with systemic lupus erythematosus and their association with disease activity: a pilot study. Scand J Rheumatol, 2022. **51**(3): p. 230-236.
- 590. Bartikoski, B.J., et al., A Review of Metabolomic Profiling in Rheumatoid Arthritis: Bringing New Insights in Disease Pathogenesis, Treatment and Comorbidities. Metabolites, 2022. 12(5).

- 591. Wagner, K.M., et al., Soluble epoxide hydrolase as a therapeutic target for pain, inflammatory and neurodegenerative diseases. Pharmacol Ther, 2017. **180**: p. 62-76.
- 592. Iyer, M.R., B. Kundu, and C.M. Wood, *Soluble epoxide hydrolase inhibitors: an overview and patent review from the last decade*. Expert Opin Ther Pat, 2022. **32**(6): p. 629-647.
- 593. Guan, X.X., et al., *Epoxyeicosatrienoic Acids and Fibrosis: Recent Insights for the Novel Therapeutic Strategies*. Int J Mol Sci, 2021. **22**(19): p. 10714.
- 594. Shi, Z., Z. He, and D.W. Wang, *CYP450 Epoxygenase Metabolites, Epoxyeicosatrienoic Acids, as Novel Anti-Inflammatory Mediators.* Molecules, 2022. **27**(12): p. 3873.
- 595. Favor, O.K., et al., Lipidome modulation by dietary omega-3 polyunsaturated fatty acid supplementation or selective soluble epoxide hydrolase inhibition suppresses rough LPS-accelerated glomerulonephritis in lupus-prone mice. Front Immunol, 2023. **14**: p. 1124910.
- 596. Raveche, E.S., J.H. Tjio, and A.D. Steinberg, *Genetic studies in NZB mice. IV. The effect of sex hormones on the spontaneous production of anti-T cell autoantibodies.* Arthritis Rheum, 1980. **23**(1): p. 48-56.
- 597. Kumari, S. and R. Singh, *Protective effects of intranasal curcumin on silica-induced lung damage*. Cytokine, 2022. **157**: p. 155949.
- 598. Nakashima, K., et al., *Regulatory role of heme oxygenase-1 in silica-induced lung injury*. Respir Res, 2018. **19**(1): p. 144.
- 599. Zhao, Y., et al., *Silica particles disorganize the polarization of pulmonary macrophages in mice*. Ecotoxicol Environ Saf, 2020. **193**: p. 110364.
- 600. Re, S.L., et al., Uncoupling between inflammatory and fibrotic responses to silica: evidence from MyD88 knockout mice. PLoS One, 2014. **9**(7): p. e99383.
- 601. OSHA, Occupational Exposure to Respirable Crystalline Silica. 2019.
- 602. Vandesompele, J., et al., *Accurate normalization of real-time quantitative RT-PCR data by geometric averaging of multiple internal control genes*. Genome Biol, 2002. **3**(7): p. RESEARCH0034.
- 603. Stearns, N.A., et al., *The Use of Poly-L-Lysine as a Capture Agent to Enhance the Detection of Antinuclear Antibodies by ELISA*. PLoS One, 2016. **11**(9): p. e0161818.
- 604. Zelko, I.N., et al., *Pulmonary hypertension and vascular remodeling in mice exposed to crystalline silica*. Respiratory Research, 2016. **17**(1): p. 160.
- 605. Isabelle, M., et al., *Effect of nintedanib on silica-induced lung inflammation and fibrosis in mice*. European Respiratory Journal, 2012. **40**(Suppl 56): p. 4531.

- 606. Davis, G.S., K.O. Leslie, and D.R. Hemenway, *Silicosis in mice: effects of dose, time, and genetic strain.* J Environ Pathol Toxicol Oncol, 1998. **17**(2): p. 81-97.
- 607. Li, C., et al., Blocking the 4-1BB Pathway Ameliorates Crystalline Silica-induced Lung Inflammation and Fibrosis in Mice. Theranostics, 2016. **6**(12): p. 2052-2067.
- 608. Guo, J.L., et al., [The role of interleukin-1β on the pulmonary fibrosis in mice exposed to crystalline silica]. Zhonghua Lao Dong Wei Sheng Zhi Ye Bing Za Zhi, 2013. **31**(7): p. 481-6.
- 609. van den Brûle, S., et al., *Overexpression of cathepsin K during silica-induced lung fibrosis and control by TGF-beta*. Respir Res, 2005. **6**(1): p. 84.
- 610. Wollin, L., et al., *Antifibrotic and anti-inflammatory activity of the tyrosine kinase inhibitor nintedanib in experimental models of lung fibrosis*. J Pharmacol Exp Ther, 2014. **349**(2): p. 209-20.
- 611. Chauhan, P.S., et al., *Identification of early mechanisms for omega-3 fatty acid suppression of acute silica-triggered pulmonary inflammation and autoimmunity in lupus-prone NZBWF1 mice.* Front Immunol (in preparation), 2023.
- 612. Bergmann, C.B., et al., *TPPU treatment of burned mice dampens inflammation and generation of bioactive DHET which impairs neutrophil function.* Sci Rep, 2021. **11**(1): p. 16555.
- 613. Kim, H.S., et al., *The arachidonic acid metabolite 11,12-epoxyeicosatrienoic acid alleviates pulmonary fibrosis.* Exp Mol Med, 2021. **53**(5): p. 864-874.
- 614. Sirish, P., et al., Suppression of inflammation and fibrosis using soluble epoxide hydrolase inhibitors enhances cardiac stem cell-based therapy. STEM CELLS Translational Medicine, 2020. **9**(12): p. 1570-1584.
- 615. Kim, J., et al., *Inhibition of soluble epoxide hydrolase prevents renal interstitial fibrosis and inflammation.* Am J Physiol Renal Physiol, 2014. **307**(8): p. F971-80.
- 616. Dong, L., et al., Soluble Epoxide Hydrolase Inhibitor Suppresses the Expression of Triggering Receptor Expressed on Myeloid Cells-1 by Inhibiting NF-kB Activation in Murine Macrophage. Inflammation, 2017. **40**(1): p. 13-20.
- 617. Ryan, H., L. Morel, and E. Moore, *Vascular Inflammation in Mouse Models of Systemic Lupus Erythematosus*. Front Cardiovasc Med, 2022. **9**: p. 767450.
- 618. Liu, Y. and M.J. Kaplan, *Cardiovascular disease in systemic lupus erythematosus: an update*. Curr Opin Rheumatol, 2018. **30**(5): p. 441-448.
- 619. Sun, C., et al., 11,12-Epoxyecosatrienoic acids mitigate endothelial dysfunction associated with estrogen loss and aging: Role of membrane depolarization. J Mol Cell Cardiol, 2016. **94**: p. 180-188.

- 620. Lozovoy, M.A., et al., Fish oil N-3 fatty acids increase adiponectin and decrease leptin levels in patients with systemic lupus erythematosus. Mar Drugs, 2015. **13**(2): p. 1071-83.
- 621. Ulu, A., et al., Anti-inflammatory effects of omega-3 polyunsaturated fatty acids and soluble epoxide hydrolase inhibitors in angiotensin-II-dependent hypertension. J Cardiovasc Pharmacol, 2013. **62**(3): p. 285-97.
- 622. Hammock, B.D., et al., Movement to the Clinic of Soluble Epoxide Hydrolase Inhibitor EC5026 as an Analgesic for Neuropathic Pain and for Use as a Nonaddictive Opioid Alternative. J Med Chem, 2021. **64**(4): p. 1856-1872.
- 623. Lindqvist, H.M., et al., *Influence of Dietary n-3 Long Chain Polyunsaturated Fatty Acid Intake on Oxylipins in Erythrocytes of Women with Rheumatoid Arthritis.* Molecules, 2023. **28**(2).
- 624. Abdalla, H.B., et al., Soluble epoxide hydrolase inhibition enhances production of specialized pro-resolving lipid mediator and promotes macrophage plasticity. Br J Pharmacol, 2022.
- 625. Gilley, K.N., et al., *Influence of total western diet on docosahexaenoic acid suppression of silica-triggered lupus flaring in NZBWF1 mice.* PLoS One, 2020. **15**(5): p. e0233183.
- 626. Ozaki, T., et al., Comprehensive lipidomics of lupus-prone mice using LC-MS/MS identifies the reduction of palmitoylethanolamide that suppresses TLR9-mediated inflammation. Genes Cells, 2022. **27**(7): p. 493-504.
- 627. Zhang, J., et al., Lipidomics Revealed Aberrant Lipid Metabolism Caused by Inflammation in Cardiac Tissue in the Early Stage of Systemic Lupus Erythematosus in a Murine Model. Metabolites, 2022. 12(5).
- 628. Wang, Y., H. Yu, and J. He, *Role of dyslipidemia in accelerating inflammation, autoimmunity, and atherosclerosis in systemic lupus erythematosus and other autoimmune diseases.* Discov Med, 2020. **30**(159): p. 49-56.
- 629. Szabo, M.Z., P. Szodoray, and E. Kiss, *Dyslipidemia in systemic lupus erythematosus*. Immunol Res, 2017. **65**(2): p. 543-550.
- 630. Kurien, B.T. and R.H. Scofield, *Lipid peroxidation in systemic lupus erythematosus*. Indian J Exp Biol, 2006. **44**(5): p. 349-56.
- 631. Kilburg-Basnyat, B., et al., Specialized Pro-Resolving Lipid Mediators Regulate Ozone-Induced Pulmonary and Systemic Inflammation. Toxicol Sci, 2018. **163**(2): p. 466-477.
- 632. Gouveia-Figueira, S., et al., Mass spectrometry profiling of oxylipins, endocannabinoids, and N-acylethanolamines in human lung lavage fluids reveals responsiveness of prostaglandin E2 and associated lipid metabolites to biodiesel exhaust exposure. Anal Bioanal Chem, 2017. **409**(11): p. 2967-2980.

- 633. Ricciotti, E. and G.A. FitzGerald, *Prostaglandins and inflammation*. Arterioscler Thromb Vasc Biol, 2011. **31**(5): p. 986-1000.
- 634. Peters-Golden, M. and W.R. Henderson, Jr., *Leukotrienes*. N Engl J Med, 2007. **357**(18): p. 1841-54.
- 635. Croasdell, A., et al., *Resolvins attenuate inflammation and promote resolution in cigarette smoke-exposed human macrophages*. Am J Physiol Lung Cell Mol Physiol, 2015. **309**(8): p. L888-901.
- 636. Ruiz, A., et al., Resolvin D1 (RvD1) and maresin 1 (Mar1) contribute to human macrophage control of M. tuberculosis infection while resolving inflammation. Int Immunopharmacol, 2019. **74**: p. 105694.
- 637. Schwab, J.M., et al., Resolvin E1 and protectin D1 activate inflammation-resolution programmes. Nature, 2007. **447**(7146): p. 869-74.
- 638. Wang, W., et al., MAR1 suppresses inflammatory response in LPS-induced RAW 264.7 macrophages and human primary peripheral blood mononuclear cells via the SIRT1/PGC-1alpha/PPAR-gamma pathway. J Inflamm (Lond), 2021. **18**(1): p. 8.
- 639. Deng, B., et al., Maresin biosynthesis and identification of maresin 2, a new antiinflammatory and pro-resolving mediator from human macrophages. PLoS One, 2014. 9(7): p. e102362.
- 640. Dai, M., et al., *Epoxyeicosatrienoic acids regulate macrophage polarization and prevent LPS-induced cardiac dysfunction*. J Cell Physiol, 2015. **230**(9): p. 2108-19.
- 641. Oh, D.Y., et al., *GPR120 is an omega-3 fatty acid receptor mediating potent anti-inflammatory and insulin-sensitizing effects.* Cell, 2010. **142**(5): p. 687-98.
- 642. Chang, H.Y., et al., *Docosahexaenoic acid induces M2 macrophage polarization through peroxisome proliferator-activated receptor gamma activation.* Life Sci, 2015. **120**: p. 39-47.
- 643. Villegas-Comonfort, S., et al., *Effects of arachidonic acid on FFA4 receptor: Signaling, phosphorylation and internalization.* Prostaglandins Leukot Essent Fatty Acids, 2017. **117**: p. 1-10.
- 644. Alaoui-El-Azher, M., et al., Arachidonic acid differentially affects basal and lipopolysaccharide-induced sPLA(2)-IIA expression in alveolar macrophages through NF-kappaB and PPAR-gamma-dependent pathways. Mol Pharmacol, 2002. **61**(4): p. 786-94.
- 645. Hirata, T. and S. Narumiya, *Prostanoid receptors*. Chem Rev, 2011. **111**(10): p. 6209-30.
- 646. Nakamura, M. and T. Shimizu, *Leukotriene receptors*. Chem Rev, 2011. **111**(10): p. 6231-98.

- 647. Chiang, N. and C.N. Serhan, *Structural elucidation and physiologic functions of specialized pro-resolving mediators and their receptors.* Mol Aspects Med, 2017. **58**: p. 114-129.
- 648. Dalli, J. and C.N. Serhan, *Pro-Resolving Mediators in Regulating and Conferring Macrophage Function*. Front Immunol, 2017. **8**: p. 1400.
- 649. Heires, A.J., et al., Agricultural dust derived bacterial extracellular vesicle mediated inflammation is attenuated by DHA. Sci Rep, 2023. **13**(1): p. 2767.
- 650. Mak, A. and S.H. Tay, *Environmental factors, toxicants and systemic lupus erythematosus.* Int J Mol Sci, 2014. **15**(9): p. 16043-56.
- 651. Molchanova, A.Y., et al., *Deuterated Arachidonic Acid Ameliorates Lipopolysaccharide-Induced Lung Damage in Mice.* Antioxidants (Basel), 2022. **11**(4).
- 652. Brigham, E.P., et al., *Omega-3 and Omega-6 Intake Modifies Asthma Severity and Response to Indoor Air Pollution in Children*. Am J Respir Crit Care Med, 2019. **199**(12): p. 1478-1486.
- 653. Tong, H., et al., Lung Function and Short-Term Ambient Air Pollution Exposure: Differential Impacts of Omega-3 and Omega-6 Fatty Acids. Ann Am Thorac Soc, 2022. 19(4): p. 583-593.
- 654. Surette, M.E., et al., *Lipopolysaccharides prime whole human blood and isolated neutrophils for the increased synthesis of 5-lipoxygenase products by enhancing arachidonic acid availability: involvement of the CD14 antigen.* J Exp Med, 1993. **178**(4): p. 1347-55.
- 655. Brown, G.P., M.M. Monick, and G.W. Hunninghake, *Human alveolar macrophage arachidonic acid metabolism*. Am J Physiol, 1988. **254**(6 Pt 1): p. C809-15.
- 656. Demers, L.M. and D.C. Kuhn, *Influence of mineral dusts on metabolism of arachidonic acid by alveolar macrophage*. Environ Health Perspect, 1994. **102 Suppl 10**(Suppl 10): p. 97-100.
- 657. O'Reilly, K.M., et al., Crystalline and amorphous silica differentially regulate the cyclooxygenase-prostaglandin pathway in pulmonary fibroblasts: implications for pulmonary fibrosis. Am J Physiol Lung Cell Mol Physiol, 2005. **288**(6): p. L1010-6.
- 658. Fukui, H., et al., The induction of lipid peroxidation during the acute oxidative stress response induced by intratracheal instillation of fine crystalline silica particles in rats. Toxicol Ind Health, 2016. **32**(8): p. 1430-1437.
- 659. Pang, J., et al., *Multi-omics study of silicosis reveals the potential therapeutic targets PGD*(2) *and TXA*(2). Theranostics, 2021. **11**(5): p. 2381-2394.

- 660. Walker, J., et al., *Lipoxin a4 increases survival by decreasing systemic inflammation and bacterial load in sepsis.* Shock, 2011. **36**(4): p. 410-6.
- 661. Hsiao, H.M., et al., *Resolvin D1 Reduces Emphysema and Chronic Inflammation*. Am J Pathol, 2015. **185**(12): p. 3189-201.
- 662. Chiang, N., et al., *Novel Resolvin D2 Receptor Axis in Infectious Inflammation*. J Immunol, 2017. **198**(2): p. 842-851.
- 663. Morisseau, C., et al., Naturally occurring monoepoxides of eicosapentaenoic acid and docosahexaenoic acid are bioactive antihyperalgesic lipids. J Lipid Res, 2010. **51**(12): p. 3481-90.
- 664. Fattori, V., et al., *The specialised pro-resolving lipid mediator maresin 1 reduces inflammatory pain with a long-lasting analgesic effect.* Br J Pharmacol, 2019. **176**(11): p. 1728-1744.
- 665. Pardeshi, R., et al., Docosahexaenoic Acid Increases the Potency of Soluble Epoxide Hydrolase Inhibitor in Alleviating Streptozotocin-Induced Alzheimer's Disease-Like Complications of Diabetes. Front Pharmacol, 2019. **10**(288): p. 288.
- 666. Rehman, S.F., et al., Soluble epoxide hydrolase inhibition alleviates inflammation in cigarette smoke-induced experimental COPD irrespective of dietary fat content. European Respiratory Journal, 2022. **60**(suppl 66): p. 3378.
- 667. Hye Khan, M.A., et al., *Epoxyeicosatrienoic Acid Analog EET-A Blunts Development of Lupus Nephritis in Mice.* Front Pharmacol, 2019. **10**: p. 512.

APPENDIX A: CHAPTER 3 SUPPORTING FIGURES AND TABLES

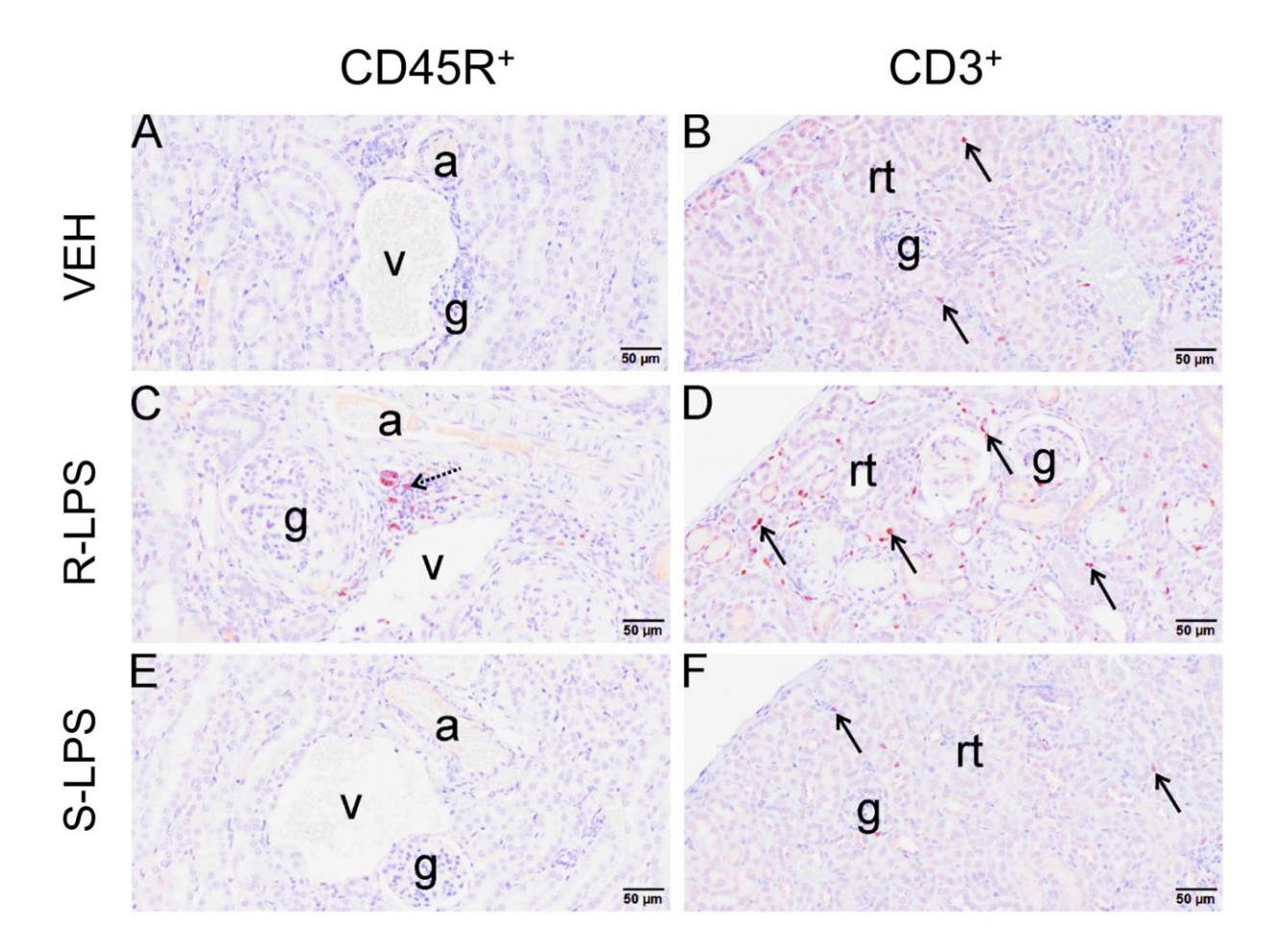


Figure S3.1. R-LPS but **not S-LPS induces B and T cell accumulation in kidney.** Light photomicrographs of cortical tissues from kidneys of mice that received i.p. injections of saline vehicle (VEH) alone (**A**, **B**), rough (R)-LPS (**C**, **D**), and smooth (S)-LPS (**E**, **F**). Tissues were immunohistochemically stained for CD45R+ lymphoid B cells (stippled arrows) (**A**, **C**, **E**) or CD3+ lymphoid T cells (solid arrows) (**B**, **D**, **F**), and counter stained with hematoxylin. a, cortical artery; v, cortical vein; g, glomerulus; rt, renal tubule.

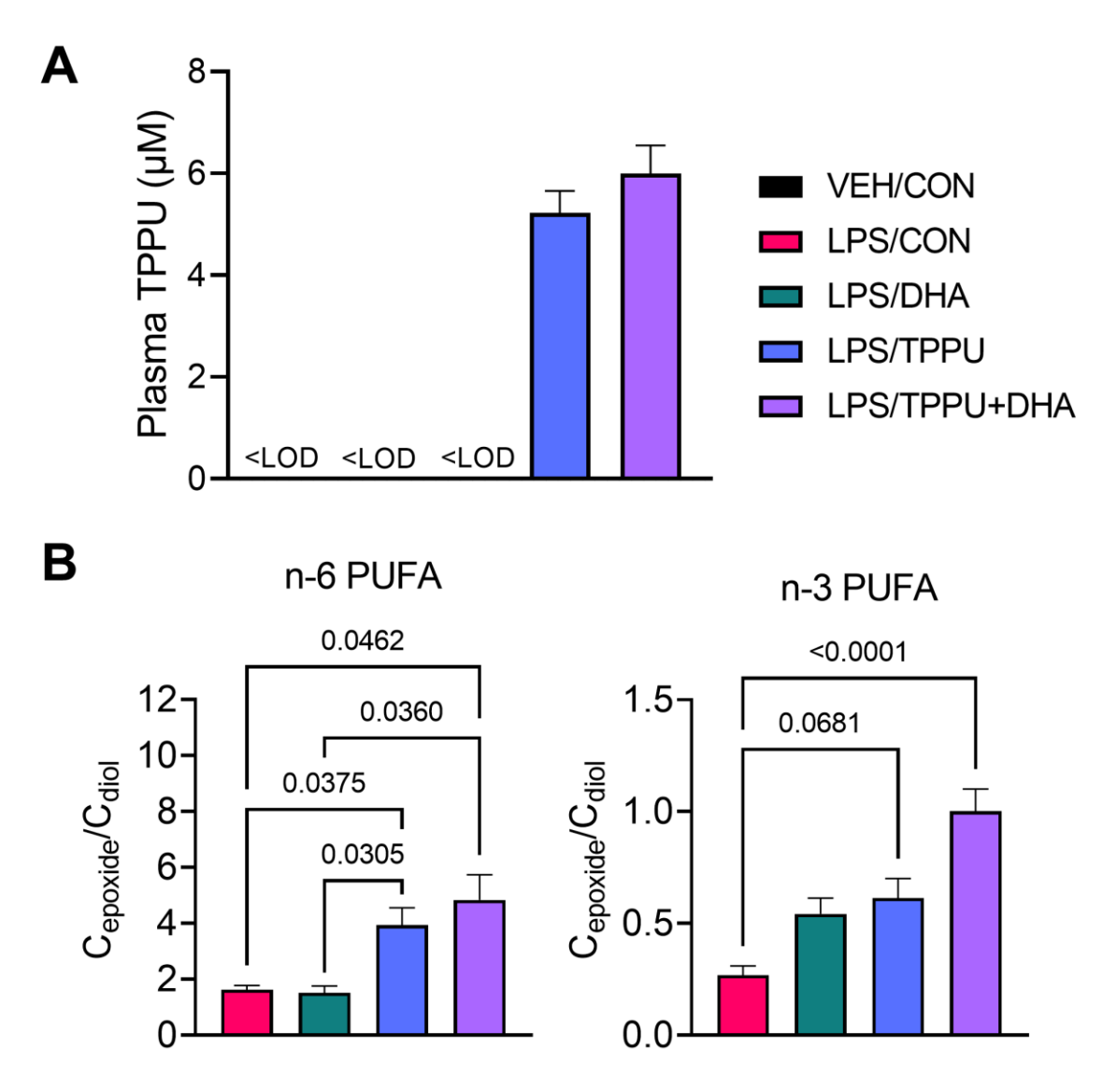


Figure S3.2. TPPU delivery via diet increases the drug in plasma and inhibits sEH. (A) TPPU delivered by dietary supplementation is efficiently transferred to plasma. Plasma concentration of TPPU was measured at 10 wk of age by LC-MS/MS. Data are presented as mean \pm SEM. <LOD = below limit of detection. (B) Supplementation with DHA and/or TPPU modulates plasma omega-6 and omega-3 epoxide/diol metabolite ratios in LPS-injected NZBWF1 mice. Administration of TPPU separately and with DHA significantly increases epoxide/diol ratios of pooled omega-6 metabolites (i.e., LA, ARA) and pooled omega-3 metabolites (i.e., EPA, DHA). Data are presented as mean \pm SEM (n = 8). Values of p<0.1 are shown, with p<0.05 considered statistically significant.

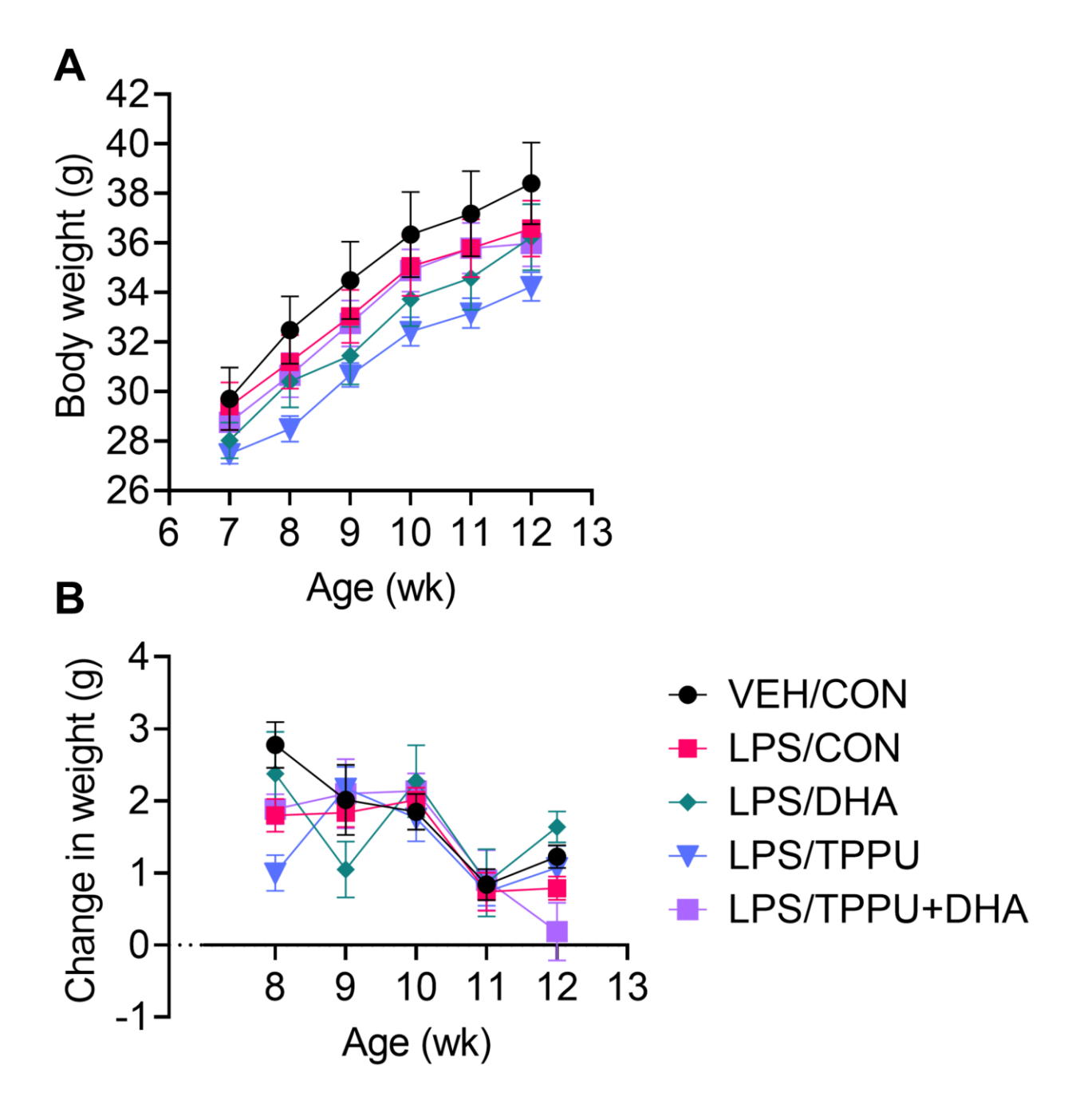


Figure S3.3. Dietary DHA and/or TPPU supplementation does not significantly affect body weight and weight gain over time. (A) Mice were weighed weekly, concurrently with the first LPS injection of the wk. Data are presented as mean \pm SEM. (B) Weekly changes in body weight were calculated by taking the difference between body weight one wk and body weight the subsequent wk. Data are presented as mean \pm SEM.

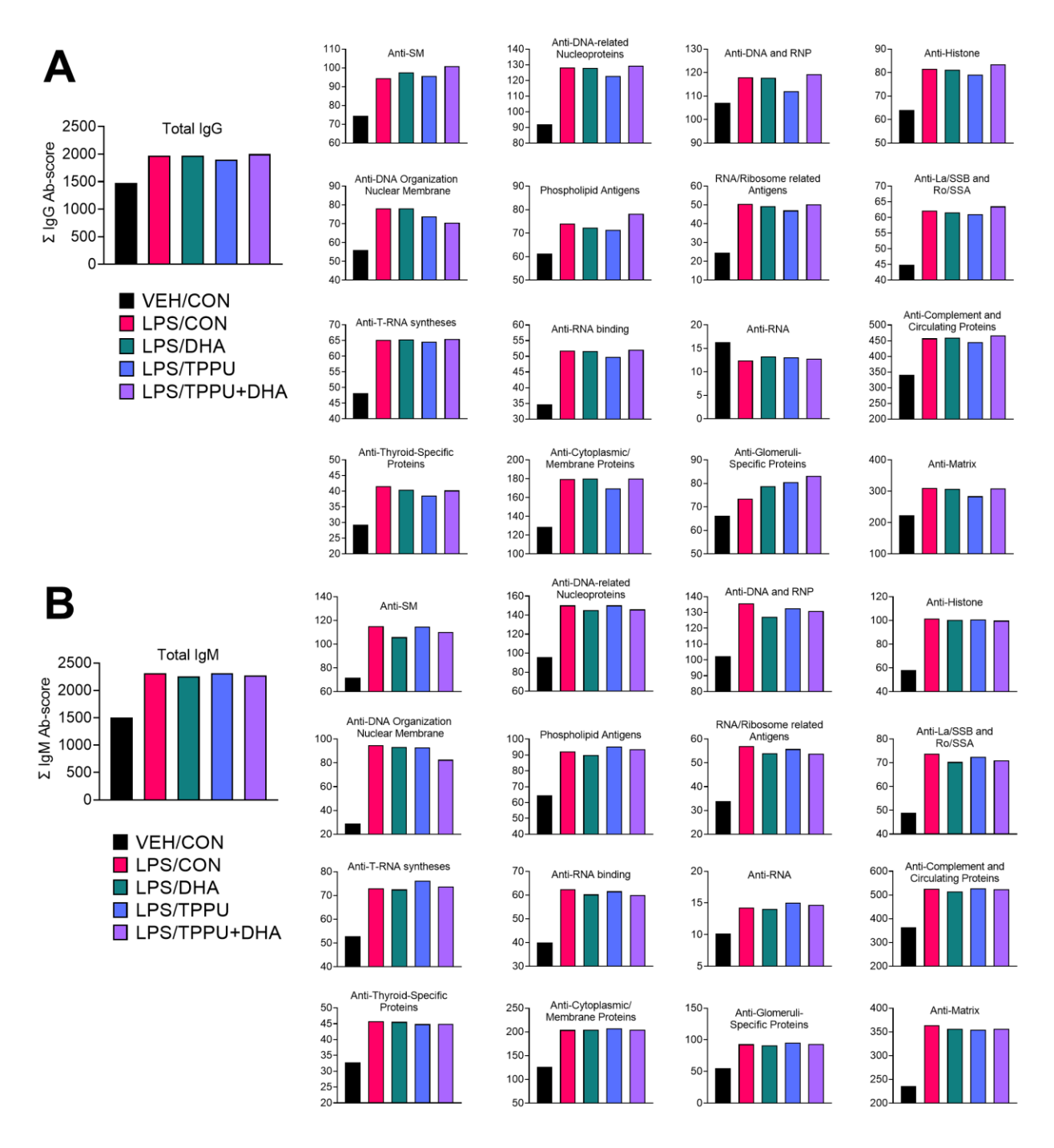


Figure S3.4. Broad spectrum of IgG and IgM autoantibodies (AAbs) induced by R-LPS are largely unaffected by DHA and/or TPPU. Plasma from all individuals within each experimental group (n=8/gp) were pooled and 122 IgG and IgM AAbs measured by high-throughput AAb array. Antibody scores (Ab-scores) were calculated for total and specified (A) IgG and (B) IgM AAbs. Data for total AAbs depicted as Σ IgG Ab-score and Σ IgM Ab-score, respectively. Data for specified AAbs depicted as individual IgM and IgM Ab-scores, respectively.

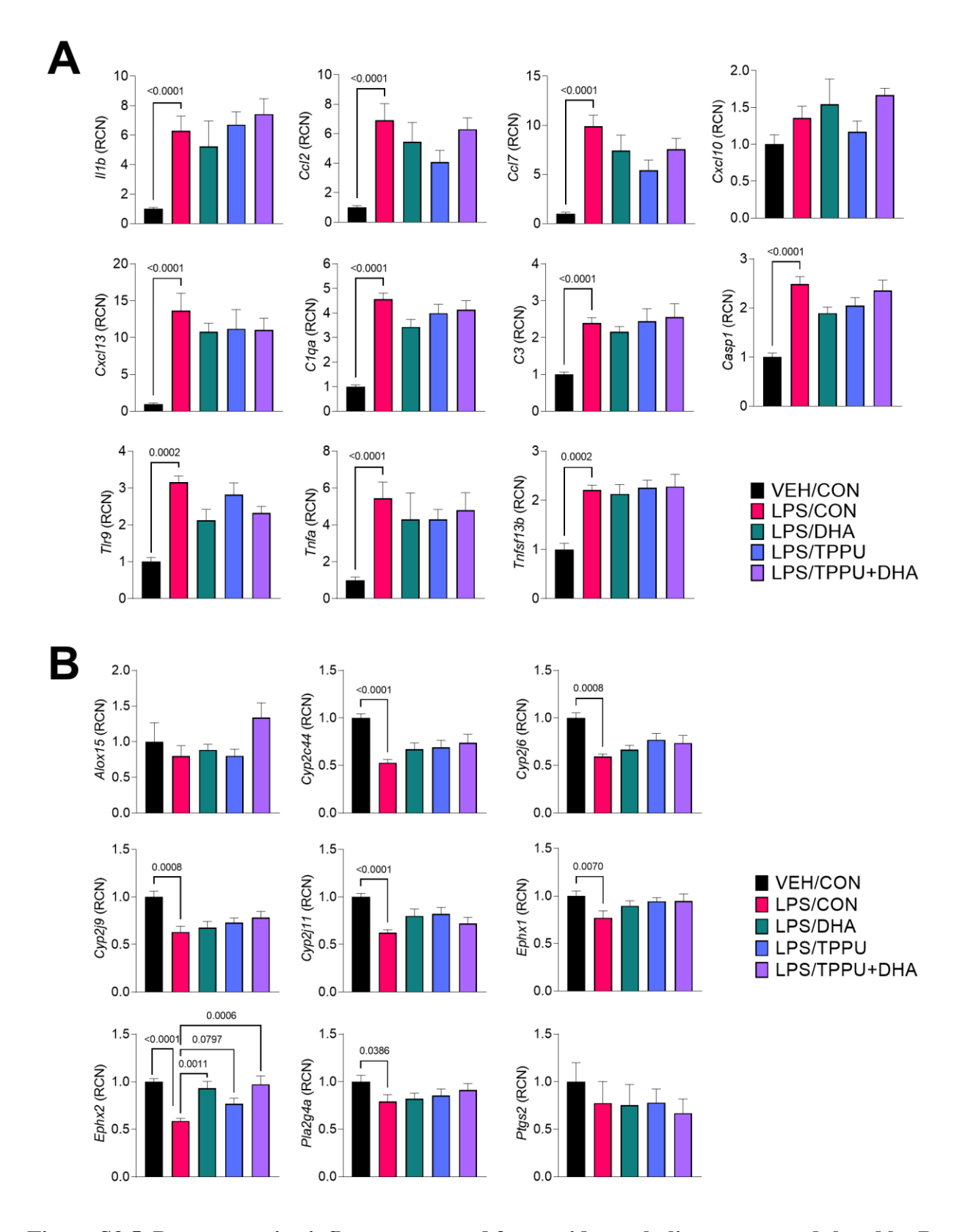


Figure S3.5. Representative inflammatory and fatty acid metabolism genes modulated by R-LPS in kidney are largely unaffected by DHA and/or TPPU. Following sacrifice, kidneys were

Figure S3.5 (cont'd)

isolated and analyzed for RNA expression of selected (**A**) inflammatory/autoimmune genes (i.e., *Il1b*, *Ccl2*, *Ccl7*, *Cxcl10*, *Cxcl13*, *C1qa*, *C3*, *Casp1*, *Tlr9*, *Tnfa*, *Tnfsf13b*) and (**B**) fatty acid metabolism genes (i.e., *Alox15*, *Cyp2c44*, *Cyp2j6*, *Cyp2j9*, *Cyp2j11*, *Ephx1*, *Ephx2*, *Pla2g4a*, *Ptgs2*). Data are presented as mean \pm SEM (n = 6-8). Values of p<0.1 are shown, with p<0.05 considered statistically significant.

Table S3.1. Study 1 experimental groups.

Experimental Group	Number of Animals (n)	LPS (-/+)	Experimental Diet
VEH/CON	2	-	AIN-93G
R-LPS/CON	4	+	AIN-93G
S-LPS/CON	4	+	AIN-93G

VEH, vehicle; CON, control; R-LPS, rough lipopolysaccharide; S-LPS, smooth lipopolysaccharide.

Table S3.2. Study 2 experimental groups.

Experimental Group	Number of Animals (n)	LPS (-/+)	Experimental Diet
VEH/CON	8	-	CON (AIN-93G)
LPS/CON	8	+	CON (AIN-93G)
LPS/DHA	8	+	DHA (10 g/kg CON diet)
LPS/TPPU	8	+	TPPU (22.5 mg/kg CON diet)
LPS/TPPU+DHA	8	+	TPPU (22.5 mg/kg CON diet) + DHA (10 g/kg CON diet)

VEH, vehicle; CON, control; LPS, lipopolysaccharide; DHA, docosahexaenoic acid; TPPU, 1-(4-trifluoro-methoxy-phenyl)-3-(1-propionylpiperidin-4-yl) urea.

Table S3.3. Study 2 experimental diet formulations.

	(g/kg total diet)				
	CON	DHA	TPPU	TPPU+DHA	
Carbohydrates					
Corn starch	398	398	398	398	
Maltodextrin (Dyetrose)	132	132	132	132	
Sucrose	100	100	100	100	
Cellulose	50	50	50	50	
kcal (% of total)	63.2	63.2	63.2	63.2	
Proteins					
Casein	200	200	200	200	
L-Cysteine	3	3	3	3	
kcal (% of total)	19.7	19.7	19.7	19.7	
Fats ^a					
Corn oil ^b	10	10	10	10	
High oleic-safflower oil ^c	60	35	60	35	
DHA-enriched algal oil ^d	0	25 ^e	0	25 ^e	
kcal (% of total)	17.1	17.1	17.1	17.1	
Other					
AIN-93G mineral mix	35	35	35	35	
AIN-93G vitamin mix	10	10	10	10	
Choline bitartrate	3	3	3	3	
TBHQ antioxidant	0.01	0.01	0.01	0.01	
TPPU	0	0	0.0225	0.0225	

All values are reported as mass (g) per kg of diet.

Table S3.4. Study 2 experimental diet TPPU mass per kilogram of diet.

	$(mg TPPU / kg diet, mean \pm SEM)$		
	TPPU TPPU+DH		
Expected Mass (mg/kg diet)	22.50	22.50	
Measured Mass (mg/kg diet)	27.68 ± 3.85	32.80 ± 3.21	

Data are presented as mg TPPU per kg experimental diet (mean \pm SEM, n = 3) as measured by LC-MS/MS. TPPU was not measured in CON or DHA diets, as the expected mass was 0 mg/kg diet.

^a As reported by the manufacturer

^b Corn oil contained 612 g/kg linoleic acid and 26 g/kg oleic acid

^c High oleic-safflower oil contained 750 g/kg oleic acid and 140 g/kg linoleic acid

^d Algal oil contained 395 g/kg DHA and 215 g/kg oleic acid

^e 10 g DHA/kg diet; calorically equivalent to human DHA consumption of 5 g/d

 $\label{thm:constraint} Table~S3.5.~Waters~TQ-XS~tandem~quadrupole~UPLC/MS/MS~linear~gradient~chromatographic~method~for~analyte~separation.$

Mobile phase	A: 0.1% acetic acid in water	B: 84:16 acetonitrile/methanol + 0.1% acetic acid
Gradient (minutes)	Percentage	Percentage
Initial	65.0	35.0
1.00	60.0	40.0
3.00	45.0	55.0
8.50	35.0	65.0
12.50	28.0	72.0
15.00	18.0	82.0
16.00	0.0	100.0
18.10	65.0	35.0

Injection Volume: 10 µl Flow Rate: 0.25 ml/min

Table S3.6. Plasma oxylipin levels at necropsy as determined by LC-MS/MS.

		(concentration in nM, mean ± SEM)						
PUFA Precursor	Metabolite	VEH/CON	LPS/CON	LPS/DHA	LPS/TPPU	LPS/ TPPU+DHA	LOQ	LOD
LA	9,10- EpOME	12.96±4.06	6.99±1.03 ^A	4.50±0.88 ^A	5.75±1.47 ^A	3.92±0.67 ^A	0.312	0.0468
LA	12,13- EpOME	17.62±5.81	8.85±1.31 ^{AB}	5.37±1.23 ^A	12.29±2.06 ^B	8.55±0.64 ^{AB}	0.312	0.0468
LA	9,10- DiHOME	11.82±6.15	5.87±0.61 ^A	2.91±0.61 ^B	4.94±0.66 ^A	2.79±0.30 ^B	0.630	0.0945
LA	12,13- DiHOME	4.97±1.83	3.47±0.48 ^A	2.04±0.63 ^{AB}	0.82±0.09 ^B	0.82±0.09 ^B	0.630	0.0945
LA	9-HODE	31.16±9.16	15.09±1.49 ^A	9.63±1.44 ^B	12.38±1.95 ^A	9.15±0.66 ^B	0.250	0.0375
LA	13-HODE	104.90±33.75	44.05±3.75 ^A	28.38±4.26 ^B	34.16±5.16 ^A	24.74±1.70 ^B	0.500	0.075
LA	9-oxo-ODE	8.48±4.07	2.52±0.53 ^A	0.50±0.35 ^B	1.21±0.53 ^{AB}	1.23±0.22 ^{AB}	0.500	0.075
LA	13-oxo- ODE	7.18±2.27	3.02±0.33*A	1.74±0.32 ^{AB}	1.02±0.19 ^B	1.67±0.27 ^{AB}	0.312	0.0468
LA	EKODE	7.81±2.54	3.41±0.37 ^A	2.01±0.24 ^{AB}	1.47±0.28 ^B	1.81±0.16 ^{AB}	0.500	0.075
DGLA	15(S)- HETrE	1.24±0.59	0.13±0.13 ^A	<lod<sup>A</lod<sup>	0.48±0.14 ^B	<lod<sup>A</lod<sup>	0.125	0.0187
ARA	LTB4	1.74±0.92	0.16±0.3 ^A	0.11±0.07 ^A	0.06±0.06 ^A	0.52±0.04 ^B	0.250	0.0375
ARA	5,6- EpETrE	2.35±0.67	1.50±0.16 ^A	0.44±0.07 ^B	1.96±0.28 ^A	0.39±0.02 ^B	1.25	0.1875
ARA	8,9- EpETrE	7.35±2.02	2.99±0.96 ^A	2.06±1.06 ^A	3.09±0.43 ^A	6.91±4.14 ^A	1.25	0.1875
ARA	11,12- EpETrE	1.04±0.54	0.79±0.08 ^A	0.17±0.01 ^B	1.39±0.16 ^A	0.02±0.02 ^B	0.625	0.0937
ARA	14,15- EpETrE	2.17±0.65	1.44±0.22 ^A	0.08±0.08 ^B	2.59±0.27 ^A	0.11±0.07 ^B	0.625	0.0937
ARA	5,6- DiHETrE	1.06±0.11	1.24±0.12 ^A	0.20±0.05 ^B	0.48±0.02 ^C	0.15±0.03 ^B	0.250	0.0375
ARA	8,9- DiHETrE	16.26±1.91	8.18±0.50*A	5.57±0.36 ^B	5.23±0.47 ^B	2.99±0.26 ^C	0.250	0.0375
ARA	11,12- DiHETrE	0.20±0.06	0.36±0.06*A	<lod<sup>B</lod<sup>	0.22±0.04 ^{AB}	<lodb< td=""><td>0.250</td><td>0.0375</td></lodb<>	0.250	0.0375
ARA	14,15- DiHETrE	0.76±0.23	0.60±0.07 ^A	0.06±0.03 ^{BC}	0.21±0.01 ^{AB}	<lod<sup>C</lod<sup>	0.630	0.0945
ARA	5-НЕТЕ	3.68±1.19	2.05±0.21 ^A	0.05±0.05 ^B	2.03±0.18 ^A	0.09±0.06 ^B	0.500	0.075
ARA	11-НЕТЕ	4.34±1.56	1.37±0.49 ^A	0.19±0.10 ^B	2.01±0.70 ^A	0.15±0.03 ^B	0.125	0.0187
ARA	12-НЕТЕ	306.30±102.3	77.58±49.40 ^A	25.94±16.94 ^A B	175.60±82.19 ^A B	9.05±4.12 ^B	0.500	0.075
ARA	15-HETE	7.08±3.06	1.67±0.73 ^A	0.12±0.12 ^B	3.11±1.16 ^A	<lodb< td=""><td>0.312</td><td>0.0468</td></lodb<>	0.312	0.0468
ARA	19-НЕТЕ	<lod< td=""><td>1.66±1.66^A</td><td>0.81±0.81^A</td><td><lod<sup>A</lod<sup></td><td><lod<sup>A</lod<sup></td><td>0.625</td><td>0.0937</td></lod<>	1.66±1.66 ^A	0.81±0.81 ^A	<lod<sup>A</lod<sup>	<lod<sup>A</lod<sup>	0.625	0.0937
ARA	5-oxo-ETE	1.46±0.99	0.10±0.10 ^A	0.05±0.05 ^A	0.29±0.15 ^A	<lod<sup>A</lod<sup>	1.25	0.1875

Table S3.6 (cont'd)

ARA	12-oxo-ETE	5.28±2.97	0.41±0.41 ^A	<lod<sup>A</lod<sup>	0.43±0.28 ^A	<lod<sup>A</lod<sup>	1.25	0.1875
ARA	15-oxo-ETE	1.58±0.63	0.46±0.08 ^A	<lod<sup>B</lod<sup>	0.18±0.06 ^{AB}	<lod<sup>B</lod<sup>	0.250	0.0375
ALA	9,10-EpODE	0.24±0.11	0.21±0.08 ^A	<lod<sup>B</lod<sup>	0.15±0.07 ^{AB}	0.02±0.02 ^B	0.312	0.0468
ALA	15,16- EpODE	1.13±0.31	0.81±0.10 ^A	0.27±0.12 ^A	1.01±0.27 ^A	0.75±0.10 ^A	0.250	0.0375
ALA	9,10- DiHODE	0.01±0.01	0.07±0.02 ^{AB}	<lod<sup>A</lod<sup>	0.13±0.02 ^B	0.06±0.01 ^{AB}	0.630	0.0945
ALA	12,13- DiHODE	0.31±0.06	0.17±0.07 ^A	0.18±0.08 ^A	0.17±0.06 ^A	0.17±0.07 ^A	1.25	0.1875
ALA	15,16- DiHODE	<lod< th=""><th>0.36±0.04^A</th><th>0.25±0.07^{AB}</th><th>0.01±0.01^C</th><th>0.05±0.02^{BC}</th><th>0.630</th><th>0.0945</th></lod<>	0.36±0.04 ^A	0.25±0.07 ^{AB}	0.01±0.01 ^C	0.05±0.02 ^{BC}	0.630	0.0945
ALA	9-HOTrE	1.23±0.22	0.69±0.07 ^A	0.42±0.07 ^B	0.37±0.08 ^B	0.43±0.03 ^{AB}	0.312	0.0468
ALA	13-HOTrE	1.30±0.45	0.26±0.13 ^A	0.11±0.01 ^A	0.12±0.08 ^A	<lod<sup>A</lod<sup>	0.625	0.0937
EPA	11,12- EpETE	<lod< th=""><th><lod<sup>A</lod<sup></th><th>0.94±0.25^B</th><th>0.01±0.01^A</th><th>1.03±0.26^B</th><th>0.250</th><th>0.0375</th></lod<>	<lod<sup>A</lod<sup>	0.94±0.25 ^B	0.01±0.01 ^A	1.03±0.26 ^B	0.250	0.0375
EPA	14,15- EpETE	<lod< th=""><th><lod<sup>A</lod<sup></th><th>0.36±0.17^{AB}</th><th><lod<sup>A</lod<sup></th><th>0.79±0.07^B</th><th>0.500</th><th>0.075</th></lod<>	<lod<sup>A</lod<sup>	0.36±0.17 ^{AB}	<lod<sup>A</lod<sup>	0.79±0.07 ^B	0.500	0.075
EPA	17,18- EpETE	<lod< th=""><th><lod<sup>A</lod<sup></th><th>2.20±0.33^{BC}</th><th>0.45±0.19^{AB}</th><th>5.33±0.41^C</th><th>1.25</th><th>0.1875</th></lod<>	<lod<sup>A</lod<sup>	2.20±0.33 ^{BC}	0.45±0.19 ^{AB}	5.33±0.41 ^C	1.25	0.1875
EPA	5,6-DiHETE	20.61±8.55	8.90±0.76 ^A	28.37±2.94 ^B	5.12±0.36 ^C	23.59±2.00 ^B	2.50	0.375
EPA	8,9-DiHETE	0.21±0.13	0.19±0.08 ^A	0.55±0.09 ^B	0.02±0.01 ^A	0.72±0.14 ^B	0.630	0.0945
EPA	11,12- DiHETE	<lod< th=""><th><lod<sup>A</lod<sup></th><th>0.37±0.07^B</th><th><lod<sup>A</lod<sup></th><th>0.33±0.03^B</th><th>0.630</th><th>0.0945</th></lod<>	<lod<sup>A</lod<sup>	0.37±0.07 ^B	<lod<sup>A</lod<sup>	0.33±0.03 ^B	0.630	0.0945
EPA	14,15- DiHETE	<lod< th=""><th><lod<sup>A</lod<sup></th><th>0.46±0.07^B</th><th>0.02±0.01^A</th><th>0.25±0.03^A</th><th>0.630</th><th>0.0945</th></lod<>	<lod<sup>A</lod<sup>	0.46±0.07 ^B	0.02±0.01 ^A	0.25±0.03 ^A	0.630	0.0945
EPA	17,18- DiHETE	2.10±0.68	1.83±0.20 ^{AB}	16.25±2.52 ^C	1.17±0.07 ^B	6.98±0.58 ^{AC}	1.25	0.1875
EPA	5-НЕРЕ	<lod< th=""><th><lod<sup>A</lod<sup></th><th>1.39±0.17^B</th><th><lod<sup>A</lod<sup></th><th>1.60±0.10^B</th><th>0.625</th><th>0.0937</th></lod<>	<lod<sup>A</lod<sup>	1.39±0.17 ^B	<lod<sup>A</lod<sup>	1.60±0.10 ^B	0.625	0.0937
EPA	8-НЕРЕ	0.10±0.10	<lod<sup>A</lod<sup>	0.89±0.18 ^B	<lod<sup>A</lod<sup>	0.54±0.13 ^{AB}	0.625	0.0937
EPA	12-НЕРЕ	2.67±1.23	0.65±0.35 ^A	26.59±12.75 ^B	0.96±0.52 ^A	12.75±3.80 ^B	0.312	0.0468
EPA	15-НЕРЕ	<lod< th=""><th>0.02±0.02^A</th><th>0.73±0.37^A</th><th><lod<sup>A</lod<sup></th><th>0.28±0.11^A</th><th>0.312</th><th>0.0468</th></lod<>	0.02±0.02 ^A	0.73±0.37 ^A	<lod<sup>A</lod<sup>	0.28±0.11 ^A	0.312	0.0468
EPA	18-НЕРЕ	0.03±0.03	0.004±0.003 ^A	0.73±0.22 ^B	<lod<sup>A</lod<sup>	0.74±0.04 ^A	0.625	0.0937
EPA	20-НЕРЕ	<lod< th=""><th><lod<sup>A</lod<sup></th><th>1.56±0.13^B</th><th><lod<sup>A</lod<sup></th><th>1.32±0.26^B</th><th>0.625</th><th>0.0937</th></lod<>	<lod<sup>A</lod<sup>	1.56±0.13 ^B	<lod<sup>A</lod<sup>	1.32±0.26 ^B	0.625	0.0937
DHA	7,8-EpDPE	0.43±0.30	0.10±0.07 ^A	3.59±1.17 ^B	0.33±0.17 ^A	2.18±0.45 ^B	1.25	0.1875
DHA	10,11- EpDPE	0.05±0.05	0.13±0.07 ^A	1.17±0.23 ^B	0.16±0.08 ^A	0.89±0.10 ^B	0.250	0.0375
DHA	13,14- EpDPE	0.25±0.17	0.11±0.07 ^A	1.93±0.48 ^B	0.29±0.12 ^{AC}	1.12±0.23 ^{BC}	0.625	0.0937
DHA	16,17- EpDPE	0.22±0.15	<lod<sup>A</lod<sup>	2.49±0.85 ^B	0.21±0.09 ^A	2.04±0.35 ^B	1.25	0.1875

Table S3.6 (cont'd)

DHA	19,20- EpDPE	2.44±0.88	3.21±0.37 ^A	25.91±3.91 ^A	3.73±0.46 ^A	28.93±3.63 ^A	0.625	0.0937
DHA	7,8-DiHDPE	0.13±0.13	0.17±0.09 ^A	1.11±0.34 ^A	<lod<sup>A</lod<sup>	<lod<sup>A</lod<sup>	0.625	0.0937
DHA	10,11- DiHDPE	<lod< th=""><th><lod<sup>A</lod<sup></th><th>0.52±0.09^B</th><th><lod<sup>A</lod<sup></th><th>0.19±0.04^{AB}</th><th>0.250</th><th>0.0375</th></lod<>	<lod<sup>A</lod<sup>	0.52±0.09 ^B	<lod<sup>A</lod<sup>	0.19±0.04 ^{AB}	0.250	0.0375
DHA	13,14- DiHDPE	<lod< th=""><th><lod<sup>A</lod<sup></th><th>0.73±0.10^B</th><th>0.004±0.002^A</th><th>0.52±0.06^B</th><th>0.250</th><th>0.0375</th></lod<>	<lod<sup>A</lod<sup>	0.73±0.10 ^B	0.004±0.002 ^A	0.52±0.06 ^B	0.250	0.0375
DHA	16,17- DiHDPE	<lod< th=""><th><lod<sup>A</lod<sup></th><th>1.15±0.15^B</th><th>0.03±0.02^{AC}</th><th>0.46±0.03^{BC}</th><th>0.125</th><th>0.0187</th></lod<>	<lod<sup>A</lod<sup>	1.15±0.15 ^B	0.03±0.02 ^{AC}	0.46±0.03 ^{BC}	0.125	0.0187
DHA	19,20- DiHDPE	2.79±1.96	2.69±0.32 ^A	22.32±3.97 ^B	1.88±0.20 ^A	9.74±0.94 ^B	0.250	0.0375
DHA	20-HDHA	1.43±0.82	0.45±0.23 ^A	4.93±1.56 ^B	1.01±0.25 ^A	3.92±0.62 ^B	1.25	0.1875
DHA	22-HDHA	<lod< th=""><th><lod<sup>A</lod<sup></th><th>5.99±0.71^B</th><th><lod<sup>A</lod<sup></th><th>4.28±0.65^B</th><th>0.625</th><th>0.0937</th></lod<>	<lod<sup>A</lod<sup>	5.99±0.71 ^B	<lod<sup>A</lod<sup>	4.28±0.65 ^B	0.625	0.0937

Data are presented as percent of total fatty acids (mean ± SEM, n = 8/gp) as measured by LC-MS/MS. Differences between VEH/CON and LPS/CON groups were compared by Student's t test. LPS/CON, LPS/DHA, LPS/TPPU, and LPS/TPPU+DHA groups were compared by ordinary one-way ANOVA followed by Tukey's *post-hoc* test. Nonparametric versions of these tests were used when applicable. Asterisks (*) indicate significant differences between VEH/CON and LPS/CON groups (p<0.05). Unique letters indicate significant differences between LPS/CON, LPS/DHA, LPS/TPPU, and LPS/TPPU+DHA groups (p<0.05). PUFA, polyunsaturated fatty acid; LOQ, limit of quantitation; LOD, limit of detection; LA, linoleic acid; DGLA, dihomo-γ-linolenic acid; ARA, arachidonic acid; ALA, alpha-linolenic acid; EPA, eicosapentaenoic acid; DHA, docosahexaenoic acid.

Table S3.7. Study 2 renal mRNA expression as determined by RT-PCR.

		(Relative copy number, mean ± SEM)							
Gene	VEH/CON	LPS/CON	LPS/DHA	LPS/TPPU	LPS/TPPU+DHA				
Interleuki		•							
Il1a	1.00±0.07	1.52±0.33 ^A	2.91±0.76 ^A	1.43±0.27 ^A	2.53±0.55 ^A				
Il1b	1.00±0.10	6.31±0.99*A	5.24±1.73 ^A	6.71±0.87 ^A	7.44±1.04 ^A				
Il6	1.00±0.48	1.32±0.25 ^A	2.08±0.37 ^A	1.82±0.35 ^A	2.00±0.20 ^A				
Il18	1.00±0.07	0.95±0.09 ^A	0.99±0.08 ^A	0.92±0.07 ^A	1.03±0.06 ^A				
Chemokir	nes								
Ccl2	1.00±0.12	6.91±1.13*A	5.44±1.32 ^A	4.09±0.78 ^A	6.31±0.77 ^A				
Ccl7	1.00±0.17	9.92±1.12* ^A	7.45±1.56 ^A	5.42±1.04 ^A	7.57±1.11 ^A				
Ccl12	1.00±0.18	2.52±0.31*A	1.81±0.39 ^A	1.52±0.33 ^A	2.20±0.24 ^A				
Cxcl9	1.00±0.15	1.19±0.17 ^A	0.96±0.28 ^A	0.72±0.11 ^A	0.97±0.14 ^A				
Cxcl10	1.00±0.13	1.36±0.16 ^A	1.54±0.34 ^A	1.17±0.15 ^A	1.67±0.09 ^A				
Cxcl13	1.00±0.14	13.68±2.35*A	10.77±1.17 ^A	11.19±2.60 ^A	11.06±1.57 ^A				
Inflamma	tion and Auto	immunity							
C1qa	1.00±0.08	4.56±0.25*A	3.44±0.30 ^A	3.99±0.36 ^A	4.13±0.37 ^A				
СЗ	1.00±0.06	2.40±0.14* ^A	2.16±0.14 ^A	2.45±0.34 ^A	2.56±0.36 ^A				
Casp1	1.00±0.08	2.49±0.15*A	1.89±0.12 ^A	2.05±0.16 ^A	2.36±0.21 ^A				
Casp4	1.00±0.14	2.53±0.18*A	1.90±0.23 ^A	2.23±0.20 ^A	2.63±0.21 ^A				
Icam1	1.00±0.04	1.66±0.08*A	1.57±0.12 ^A	2.05±0.15 ^A	1.86±0.11 ^A				
Ifng	1.00±0.10	1.29±0.25 ^A	1.05±0.16 ^A	1.21±0.21 ^A	1.39±0.24 ^A				
Lbp	1.00±0.06	1.12±0.03 ^{AB}	1.06±0.07 ^A	1.40±0.10 ^B	1.24±0.11 ^{AB}				
Nfkb1	1.00±0.04	0.89±0.04 ^A	0.91±0.03 ^A	1.00±0.06 ^A	0.91±0.03 ^A				
Nlrp3	1.00±0.21	1.59±0.18* ^A	1.12±0.20 ^A	1.20±0.12 ^A	1.27±0.24 ^A				
Nos2	1.00±0.15	1.36±0.10*A	0.78±0.17 ^B	1.08±0.14 ^{AB}	1.19±0.19 ^{AB}				
Pparg	1.00±0.20	1.02±0.15 ^A	0.71±0.07 ^{AB}	0.68±0.08 ^{AB}	0.60±0.03 ^B				
Tlr4	1.00±0.03	1.40±0.11*A	1.27±0.08 ^A	1.37±0.11 ^A	1.38±0.10 ^A				
Tlr9	1.00±0.12	3.16±0.17*A	2.13±0.29 ^A	2.81±0.32 ^A	2.32±0.18 ^A				
Tnfa	1.00±0.17	5.45±0.88* ^A	4.29±1.45 ^A	4.29±0.54 ^A	4.79±0.96 ^A				
Tnfsf13b	1.00±0.12	2.21±0.10*A	2.13±0.19 ^A	2.26±0.15 ^A	2.28±0.25 ^A				
Type I int	erferon-regula	ited genes							
Ifi44	1.00±0.08	0.81±0.07 ^{AB}	0.67±0.04 ^B	1.01±0.08 ^A	0.71±0.07 ^B				
Irf7	1.00±0.09	0.80±0.06 ^A	0.76±0.09 ^A	0.92±0.08 ^A	0.85±0.10 ^A				
Isg15	1.00±0.12	0.89±0.07 ^A	0.95±0.14 ^A	1.10±0.09 ^A	1.16±0.07 ^A				

Table S3.7 (cont'd)

Nlrc5	1.00±0.21	1.99±0.20*A	1.33±0.17 ^A	1.80±0.19 ^A	1.41 ± 0.15^{A}			
Oas2	1.00±0.12	0.89 ± 0.11^{A}	1.12±0.27 ^A	1.38±0.23 ^A	1.24±0.19 ^A			
Fatty Acid	Fatty Acid Metabolism							
Alox15	1.00±0.27	0.80 ± 0.15^{A}	0.89 ± 0.08^{A}	0.80±0.23 ^A	1.34±0.21 ^A			
Cyp2c44	1.00±0.04	0.53±0.03* ^A	0.67±0.07 ^A	0.69±0.07 ^A	0.74 ± 0.09^{A}			
Cyp2j6	1.00±0.05	0.59±0.03*A	0.67±0.04 ^A	0.77±0.07 ^A	0.74 ± 0.08^{A}			
Cyp2j9	1.00±0.06	0.63±0.06*A	0.68±0.07 ^A	0.73±0.05 ^A	0.78 ± 0.06^{A}			
Cyp2j11	1.00±0.04	0.63±0.03*A	0.80±0.07 ^A	0.82±0.07 ^A	0.72±0.07 ^A			
Ephx1	1.00±0.05	0.77±0.07* ^A	0.90±0.05 ^A	0.94±0.04 ^A	0.95±0.07 ^A			
Ephx2	1.00±0.03	0.59±0.03*A	0.93±0.07 ^B	0.77±0.06 ^{AB}	0.97±0.09 ^B			
Pla2g4a	1.00±0.07	0.79±0.07* ^A	0.82±0.06 ^A	0.85±0.07 ^A	0.91±0.07 ^A			
Ptgs2	1.00±0.20	0.77±0.23 ^A	0.75±0.22 ^A	0.78±0.14 ^A	0.67±0.15 ^A			
Kidney In	jury							
Ankrd1	1.00±0.08	2.96±0.26*A	2.77±0.36 ^A	2.48±0.25 ^A	3.43±0.49 ^A			
Haver1	1.00±0.07	1.00±0.13 ^A	1.11±0.23 ^A	2.00±0.35 ^A	1.11±0.21 ^A			
Lcn2	1.00±0.13	2.78±0.48*A	2.27±0.34 ^A	2.52±0.61 ^A	4.68±0.95 ^A			
Tgfb1	1.00±0.06	1.66±0.10*A	1.34±0.08 ^A	1.58±0.18 ^A	1.58±0.12 ^A			
Oxidative	Oxidative Stress							
Нтох	1.00±0.06	1.79±0.07* ^A	1.76±0.13 ^A	1.52±0.07 ^A	2.60±0.77 ^A			
Ncf1	1.00±0.10	4.71±0.18* ^A	3.47±0.29 ^A	3.67±0.30 ^A	4.23±0.56 ^A			
Nqo1	1.00±0.05	0.55±0.03*A	0.75±0.04 ^A	0.63±0.05 ^A	0.79±0.09 ^A			
Sod2	1.00±0.04	0.58±0.02*A	0.76±0.06 ^A	0.76±0.08 ^A	0.77±0.07 ^A			

Gene expression data are presented as relative copy numbers (mean \pm SEM, n = 8/gp) in relation to housekeeping genes. Differences between VEH/CON and LPS/CON groups were compared by Student's t test. LPS/CON, LPS/DHA, LPS/TPPU, and LPS/TPPU+DHA groups were compared by ordinary one-way ANOVA followed by Tukey's post-hoc test. Nonparametric versions of these tests were used when applicable. Asterisks (*) indicate significant differences between VEH/CON and LPS/CON groups (p<0.05). Unique letters indicate significant differences between LPS/CON, LPS/DHA, LPS/TPPU, and LPS/TPPU+DHA groups (p<0.05).

Table S3.8. List of Key Reagents, Chemicals, and Kits.

Reagent	Vendor	Catalog Number
AIN-93G Purified Rodent Diet without	Dyets Inc.	110700
Vitamin Mix	Dyets IIIc.	110700
AIN-93G VX Vitamin Mix	Dyets Inc.	310025
LouAna Safflower Oil	LouAna Oils	
Mazola Corn Oil	Mazola	
Microalgal Oil Containing 40% DHA	DHASCO	
TPPU	Synthesized in-house	
S-LPS from <i>Salmonella enterica</i> serotype minnesota	Sigma Aldrich	L6261
R-LPS from <i>Salmonella enterica</i> serotype minnesota Re 595	Sigma Aldrich	L9724
Urine Reagent Strip (Glucose-Protein) Rapid Test Kit	Cortez Diagnostics	URS-2P
Urine Reagent Strip-1B (URS-1B) Blood	Teco Diagnostics	URS-1B
Urea Nitrogen (BUN) Colorimetric Detection Kit	Thermo Fisher Scientific	EIABUN
Creatinine (serum) Colorimetric Assay Kit	Cayman Chemical	700460
Polyclonal Goat Anti-IgG Antibody	Bethyl Labs	A-90-100A
Polyclonal Rabbit Anti-Mouse CD3 Antibody	Abcam	ab5690
Monoclonal Rat Anti-Mouse CD45R Antibody	Becton Dickinson	550286
RNeasy Mini Kit	Qiagen	74104

APPENDIX B: CHAPTER 4 SUPPORTING FIGURES AND TABLES

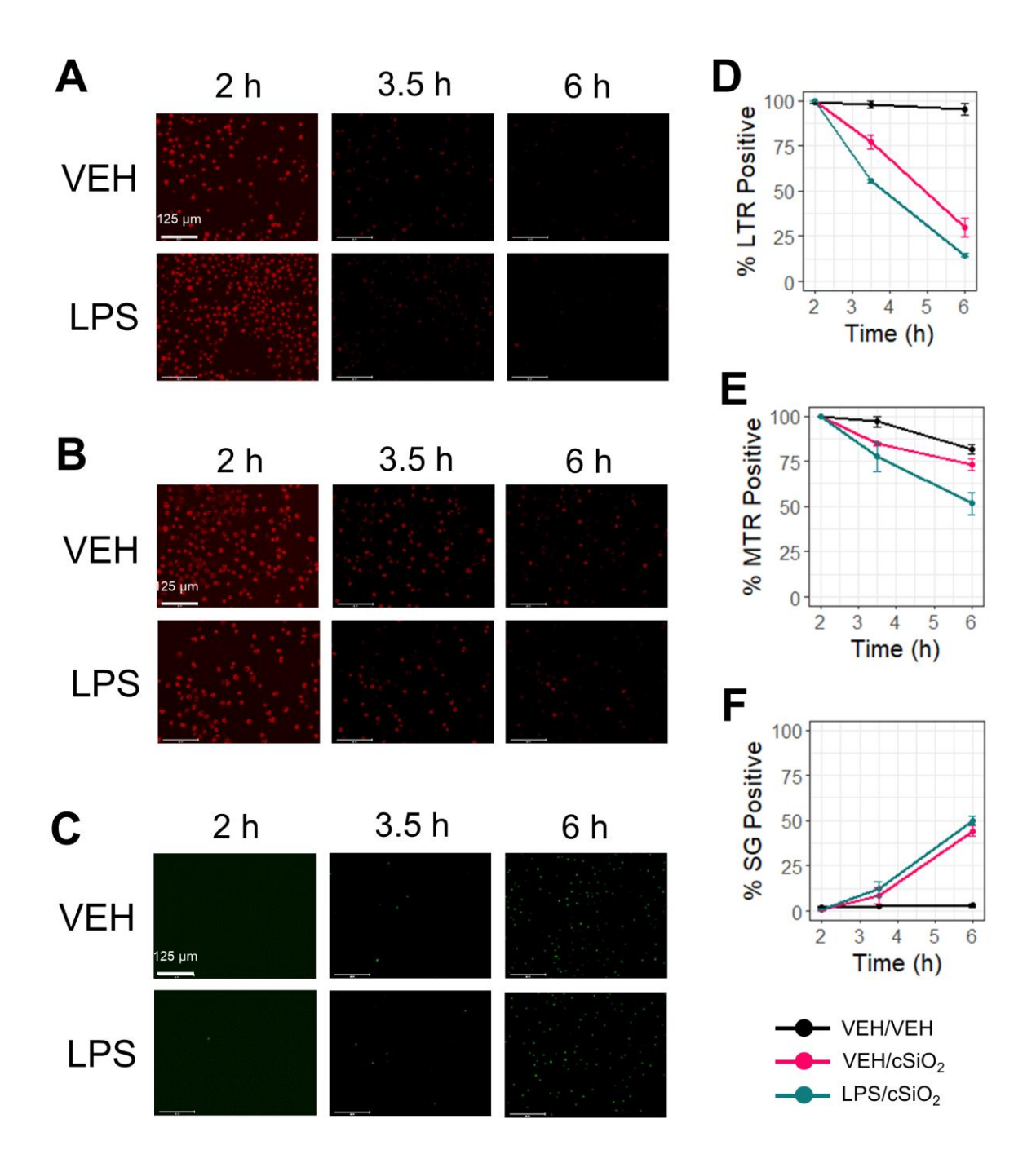


Figure S4.1. LPS priming has modest effects on rates of cSiO₂-induced lysosomal membrane permeabilization and mitochondrial toxicity and minimal effects on cSiO₂-induced death in FLAMs. VEH-treated and DHA-treated FLAMs were incubated with either with LPS (20 ng/ml) in DPBS^{+/+} or DPBS^{+/+} for 1.5 h then stained with (A) LysoTracker Red (LTR; 50 nM), (B) MitoTracker Red (MTR; 25 nM), or (C) SYTOX Green (SG; 200 nM) in DPBS^{+/+} for 30 min. After 30 minutes to allow fluorescent dyes to equilibrate, cSiO₂ was added dropwise at 12.5

Figure S4.1 (cont'd)

 $\mu g/cm^2$. Representative images from samples, taken at 20x magnification. (**D**) Percent LysoTracker Red⁺, (**E**) MitoTracker Red⁺, and (**F**) SYTOX Green⁺ cells from 2 h to 6 h were quantified using CellProfiler 4.2.1 and RStudio Desktop. Data are shown as mean \pm SEM.

Table S4.1. List of Key Reagents, Chemicals, and Kits.

Reagent	Manufacturer	Catalog Number
Costar® 6-Well Cell Culture Plate	Corning	3516
Costar® 24-Well Cell Culture Plate	Corning	3524
Falcon® 48-Well Cell Culture Plate	Corning	353078
RPMI 1640	Gibco	21875034
Fetal Bovine Serum	R&D Systems	S11150H
Penicillin-Streptomycin	Invitrogen	15140122
mGM-CSF	Peprotech	315-03
h-TGFβ	Peprotech	100-21
0.5 M EDTA	Invitrogen	15575-038
DPBS, no calcium, no magnesium	Gibco	14190144
DPBS, calcium, magnesium	Gibco	14040133
Lipopolysaccharide from Salmonella enterica	Millipore Sigma	L6143
Crystalline Silica	U.S. Silica	Min-U-Sil-5
Docosahexaenoic Acid	NU-Chek Prep	U-84-A
Triton X-100	Millipore Sigma	T8787
CulturPlate-96, White Opaque 96-well Microplate	PerkinElmer	6005680
Z-L-R-AMC Fluorogenic Peptide Substrate VII	R&D Systems	ES008
Polystyrene Microplates	R&D Systems	DY990
Bovine Serum Albumin	Millipore Sigma	A3912
Mouse IL-1 alpha/IL-1F1 DuoSet ELISA	R&D Systems	DY400
Mouse IL-1 beta/IL-1F2 DuoSet ELISA	R&D Systems	DY401
Mouse TNF-alpha DuoSet ELISA	R&D Systems	DY410
K-Blue® Advanced Plus TMB Substrate	Neogen	319175
LysoTracker TM Red DND-99	Thermo Fisher Scientific	L7528
MitoTracker TM Red CM-H2Xros	Thermo Fisher Scientific	M7513
SYTOX TM Green Nucleic Acid Stain	Thermo Fisher Scientific	S7020

Table S4.2. Classification of oxylipins analyzed by the Wayne State University Lipidomics Core Facility.

Oxylipin	Fatty Acid Substrate	Classification
9,10-DiHOME	18:2ω6	DiHFA (CYP450)
12,13-DiHOME	18:2ω6	DiHFA (CYP450)
9(10)-EpOME	18:2ω6	EpFA
12(13)-EpOME	18:2ω6	EpFA
9-HODE	18:2ω6	HFA
13-HODE	18:2ω6	HFA
9-OxoODE	18:2ω6	Oxo-FA
13-OxoODE	18:2ω6	Oxo-FA
13(S)-HOTrE	18:3ω3	HFA
13(S)-HOTrE(g)	18:3ω3	HFA
9(S)-HOTrE	18:3ω3	HFA
9-OxoOTrE	18:3ω3	Oxo-FA
11(R)-HEDE	20:2ω6	HFA
15(S)-HEDE	20:2ω6	HFA
15-OxoEDE	20:2ω6	Oxo-FA
8(S)-HETrE	20:3ω6	HFA
5(S)-HETrE	20:3ω6	HFA
13,14dhPGE1	20:3ω6	Prostaglandin
13,14dh-15k-PGE1	20:3ω6	Prostaglandin
D17-PGE1	20:3ω6	Prostaglandin
PGE1	20:3ω6	Prostaglandin
15(R)-PGE1	20:3ω6	Prostaglandin
15-keto PGE1	20:3ω6	Prostaglandin
Bicyclo PGE1	20:3ω6	Prostaglandin
19(R)-hydroxy PGE1	20:3ω6	Prostaglandin
2,3-dinor PGE1	20:3ω6	Prostaglandin
PGF1α	20:3ω6	Prostaglandin
6-keto PGE1	20:3ω6	Prostaglandin
5,6-DiHETrE	20:4ω6	DiHFA (CYP450)
8,9-DiHETrE	20:4ω6	DiHFA (CYP450)
11,12-DiHETrE	20:4ω6	DiHFA (CYP450)
14,15-DiHETrE	20:4ω6	DiHFA (CYP450)
5(S),12(S)-DiHETE	20:4ω6	DiHFA (LOX)
5(S),15(S)-DiHETE	20:4ω6	DiHFA (LOX)
8(S),15(S)-DiHETE	20:4ω6	DiHFA (LOX)
5(S),6(S)-DiHETE	20:4ω6	DiHFA (LOX)
5(6)-EpETrE	20:4ω6	EpFA
8(9)-EpETrE	20:4ω6	EpFA

Table S4.2 (cont'd)

11(12)-EpETrE	20:4ω6	EpFA
14(15)-EpETrE	20:4ω6	EpFA
12-HETE	20:4ω6	HFA
tetranor 12-HETE	20:4ω6	HFA
15-HETE	20:4ω6	HFA
5-HETE	20:4ω6	HFA
8-HETE	20:4ω6	HFA
12(S)-HHTrE	20:4ω6	HFA
20-HETE	20:4ω6	HFA
9-HETE	20:4ω6	HFA
11-HETE	20:4ω6	HFA
LTB4	20:4ω6	Leukotriene
12-OxoLTB4	20:4ω6	Leukotriene
20-hydroxy LTB4	20:4ω6	Leukotriene
20-COOH LTB4	20:4ω6	Leukotriene
18-carboxy dinor LTB4	20:4ω6	Leukotriene
LXA4	20:4ω6	Lipoxin
15-epi LXA4	20:4ω6	Lipoxin
15-oxo LXA4	20:4ω6	Lipoxin
LXA5	20:4ω6	Lipoxin
LXB4	20:4ω6	Lipoxin
12-OxoETE	20:4ω6	Oxo-FA
15-OxoETE	20:4ω6	Oxo-FA
5-oxoETE	20:4ω6	Oxo-FA
PGE2	20:4ω6	Prostaglandin
15-keto PGE2	20:4ω6	Prostaglandin
13,14dh-15k-PGE2	20:4ω6	Prostaglandin
Bicyclo PGE2	20:4ω6	Prostaglandin
PGA2	20:4ω6	Prostaglandin
19(R)-OH PGE2 & 20-OH PGE2	20:4ω6	Prostaglandin
tetranor PGEM	20:4ω6	Prostaglandin
PGD2	20:4ω6	Prostaglandin
PGJ2	20:4ω6	Prostaglandin
Δ12-PGJ2	20:4ω6	Prostaglandin
15d-Δ12,14-PGJ2	20:4ω6	Prostaglandin
13,14dh-15k-PGD2	20:4ω6	Prostaglandin
PGF2α	20:4ω6	Prostaglandin
15-keto PGF2α	20:4ω6	Prostaglandin
13,14dh-15k-PGF2α	20:4ω6	Prostaglandin
19(R)-OH PGF2α & 20-OH PGF2α	20:4ω6	Prostaglandin

Table S4.2 (cont'd)

8-isoPGF2α & 11bPGF2α	20:4ω6	Prostaglandin
iPF-VI	20:4ω6	Prostaglandin
6kPGF1α	20:4ω6	Prostaglandin
6,15-diketo PGFα	20:4ω6	Prostaglandin
TXB2	20:4ω6	Thromboxane
11dh-TXB2	20:4ω6	Thromboxane
2,3-dinor TXB2	20:4ω6	Thromboxane
11dh-2,3-dinor TXB2	20:4ω6	Thromboxane
5,6-DiHETE(EPA)	20:5ω3	DiHFA (CYP450)
5(S),15(S)-DiHEPE	20:5ω3	DiHFA (LOX)
8(9)-EpETE	20:5ω3	EpFA
11(12)-EpETE	20:5ω3	EpFA
14(15)-EpETE	20:5ω3	EpFA
17(18)-EpETE	20:5ω3	EpFA
12-HEPE	20:5ω3	HFA
15(S)-HEPE	20:5ω3	HFA
5-HEPE	20:5ω3	HFA
8-HEPE	20:5ω3	HFA
18-HEPE	20:5ω3	HFA
9-HEPE	20:5ω3	HFA
11-HEPE	20:5ω3	HFA
LTB5	20:5ω3	Leukotriene
PGE3	20:5ω3	Prostaglandin
PGD3	20:5ω3	Prostaglandin
15d-D12,14-PGJ3	20:5ω3	Prostaglandin
PGF3α	20:5ω3	Prostaglandin
RvE1	20:5ω3	Resolvin
RvE2	20:5ω3	Resolvin
RvE3	20:5ω3	Resolvin
TXB3	20:5ω3	Thromboxane
11dh TXB3	20:5ω3	Thromboxane
MaR1(n-3DPA)	22:5ω3	Maresin
PD1(n-3, DPA)	22:5ω3	Protectin
RvD5(n-3DPA) (7,17-DiHDoPE)	22:5ω3	Resolvin
19,20-DiHDoPE	22:6ω3	DiHFA (CYP450)
7(8)-EpDPE	22:6ω3	EpFA
10(11)-EpDPE	22:6ω3	EpFA
13(14)-EpDPE	22:6ω3	EpFA
16(17)-EpDPE	22:6ω3	EpFA
19(20)-EpDPE	22:6ω3	EpFA
14-HDoHE	22:6ω3	HFA

Table S4.2 (cont'd)

17-HDoHE	22:6ω3	HFA
4-HDoHE	22:6ω3	HFA
7-HDoHE	22:6ω3	HFA
8-HDoHE	22:6ω3	HFA
10-HDoHE	22:6ω3	HFA
11-HDoHE	22:6ω3	HFA
13-HDoHE	22:6ω3	HFA
16-HDoHE	22:6ω3	HFA
20-HDoHE	22:6ω3	HFA
Maresin1	22:6ω3	Maresin
7(S)-Maresin1	22:6ω3	Maresin
PD1	22:6ω3	Protectin
AT-PD1	22:6ω3	Protectin
10S,17S-DiHDoHE	22:6ω3	Protectin
22-OH-PD1	22:6ω3	Protectin
RvD1 & AT-RvD1	22:6ω3	Resolvin
RvD2	22:6ω3	Resolvin
RvD3	22:6ω3	Resolvin
AT-RvD3	22:6ω3	Resolvin
RvD4	22:6ω3	Resolvin
RvD5	22:6ω3	Resolvin
RvD6 (4,17-DiHDoHE)	22:6ω3	Resolvin
8-oxoRvD1	22:6ω3	Resolvin
17-oxoRvD1	22:6ω3	Resolvin

18:2ω6, linoleic acid; 18:3ω3, α-linolenic acid; 20:2ω6, eicosadienoic acid; 20:3ω6, linoleic acid; dihomo-γ-linolenic acid; 20:4ω6, arachidonic acid; 20:5ω3, eicosapentaenoic acid; 22:5ω3, docosapentaenoic acid; 22:6ω3, docosahexaenoic acid; DiHFA, dihydroxy fatty acid; EpFA, epoxy fatty acid; HFA, hydroxy fatty acid; oxo-FA, oxo fatty acid; CYP450, cytochrome P450 monooxygenase; LOX, lipoxygenase.

Table S4.3. Combined intracellular and extracellular oxylipin content at $t=2\ h$.

12,13-Dihome 0.02 ± 0.01 0.00 ± 0.00 0.02 ± 0.01 0.00 ± 0.00 9(10)-Epome 0.19 ± 0.04 0.17 ± 0.02 0.15 ± 0.02 0.11 ± 0.01 12(13)-Epome 0.08 ± 0.02 0.03 ± 0.03 0.08 ± 0.01 0.05 ± 0.03 9Hode 2.10 ± 0.84 1.51 ± 0.35 1.22 ± 0.39 1.17 ± 0.09 13-Hode 8.38 ± 2.36 5.90 ± 1.08 6.01 ± 1.91 4.67 ± 0.21 9-OxoOde 1.97 ± 0.49 1.46 ± 0.18 1.31 ± 0.11 1.30 ± 0.10 13-OxoOde 2.48 ± 0.75 1.91 ± 0.29 1.55 ± 0.14 1.32 ± 0.13 13(S)-Hotre 0.06 ± 0.06 0.07 ± 0.04 0.12 ± 0.06 0.10 ± 0.05 13(S)-Hotre(g) 0.12 ± 0.12 0.00 ± 0.00 0.02 ± 0.20 0.00 ± 0.00 9(S)-Hotre 0.09 ± 0.06 0.10 ± 0.06 0.11 ± 0.11 0.05 ± 0.05 9-OxoOtre 0.00 ± 0.00 0.00 ± 0.00 0.00 ± 0.00 0.00 ± 0.00 11(R)-Hede 0.03 ± 0.02 0.03 ± 0.02 0.00 ± 0.00 0.00 ± 0.00 15(S)-Hede 0.01 ± 0.01 0.01 ± 0.01 0.01 ± 0.01 0.01 ± 0.01 15-OxoEde 0.00 ± 0.00 0.00 ± 0.00 0.00 ± 0.00 0.00 ± 0.00 8(S)-Hetre 0.07 ± 0.01 0.11 ± 0.01 0.11 ± 0.00 0.09 ± 0.00 5(S)-Hetre 0.00 ± 0.00 0.00 ± 0.00 0.00 ± 0.00 0.00 ± 0.00 13,14dh-15k-PGE1 0.00 ± 0.00 0.00 ± 0.00 0.00 ± 0.00 0.00 ± 0.00 15(R)-PGE1 0.00 ± 0.00 0.00 ± 0.00 0.00 ± 0.00 0.00 ± 0.00 15(R)-PGE1 0.00 ± 0.00 0.00 ± 0.00 0.00 ± 0.00 0.00 ± 0.00 15(R)-PGE1 0.00 ± 0.00 0.00 ± 0.00 0.00 ± 0.00 0.00 ± 0.00 15(R)-PGE1 0.00 ± 0.00 0.00 ± 0.00 0.00 ± 0.00 0.00 ± 0.00 15(R)-PGE1 0.00 ± 0.00 0.00 ± 0.00 0.00 ± 0.00 0.00 ± 0.00 15(R)-PGE1 0.00 ± 0.00 0.00 ± 0.00 0.00 ± 0.00 0.00 ± 0.00 15(R)-PGE1 0.00 ± 0.00 0.00 ± 0.00 0.00 ± 0.00 0.00 ± 0.00 15(R)-PGE1 0.00 ± 0.00 0.00 ± 0.00 0.00 ± 0.00 0.00 ± 0.00 15(R)-PGE1 0.00 ± 0.00 0.00 ± 0.00 0.00 ± 0.00 0.00 ± 0.00 15(R)-PGE1 0.00 ± 0.00 0.00 ± 0.00 0.00 ± 0.00 0.00 ± 0.00 15(R)-PGE1 0.00 ± 0.00 0.00 ± 0.00 0.00 ± 0.00 0.00 ± 0.00 15(R)-PGE1 0.00 ± 0.00 0.00 ± 0.00 0.00 ± 0.00	Oxylipin	VEH/VEH	LPS/VEH	DHA/VEH	DHA/LPS
9(10)-EpOME	9,10-DiHOME				
12(13)-Epome	12,13-DiHOME	0.02 ± 0.01	0.00 ± 0.00	0.02 ± 0.01	0.00 ± 0.00
9-HODE 2.10 ± 0.84 1.51 ± 0.35 1.22 ± 0.39 1.17 ± 0.09 13-HODE 8.38 ± 2.36 5.90 ± 1.08 6.01 ± 1.91 4.67 ± 0.21 9-OxoODE 1.97 ± 0.49 1.46 ± 0.18 1.31 ± 0.11 1.30 ± 0.10 13-OxoODE 2.48 ± 0.75 1.91 ± 0.29 1.55 ± 0.14 1.32 ± 0.13 13(S)-HOTrE 0.06 ± 0.06 0.07 ± 0.04 0.12 ± 0.06 0.10 ± 0.05 13(S)-HOTrE 0.09 ± 0.06 0.10 ± 0.00 0.20 ± 0.20 0.00 ± 0.00 9(S)-HOTrE 0.09 ± 0.06 0.10 ± 0.00 0.0	9(10)-EpOME	0.19 ± 0.04	0.17 ± 0.02	0.15 ± 0.02	0.11 ± 0.01
13-HODE	12(13)-EpOME	0.08 ± 0.02	0.03 ± 0.03	0.08 ± 0.01	0.05 ± 0.03
9-OxoODE	9-HODE	2.10 ± 0.84	1.51 ± 0.35	1.22 ± 0.39	1.17 ± 0.09
13-Oxoode	13-HODE	8.38 ± 2.36	5.90 ± 1.08	6.01 ± 1.91	4.67 ± 0.21
13(S)-HOTrE	9-OxoODE	$1.97 \hspace{0.2cm} \pm \hspace{0.2cm} 0.49$	1.46 ± 0.18	1.31 ± 0.11	1.30 ± 0.10
13(S)-HOTrE(g)	13-OxoODE	$2.48 \hspace{0.1cm} \pm \hspace{0.1cm} 0.75$	1.91 ± 0.29	1.55 ± 0.14	1.32 ± 0.13
9(S)-HOTrE	13(S)-HOTrE	$0.06 \hspace{0.2cm} \pm \hspace{0.2cm} 0.06$	0.07 ± 0.04	0.12 ± 0.06	0.10 ± 0.05
9-OxoOTrE	13(S)-HOTrE(g)	$0.12 \hspace{0.2cm} \pm \hspace{0.2cm} 0.12$	0.00 \pm 0.00	0.20 ± 0.20	0.00 ± 0.00
11(R)-HEDE	9(S)-HOTrE	$0.09 \hspace{0.2cm} \pm \hspace{0.2cm} 0.06$	0.10 \pm 0.06	0.11 ± 0.11	0.05 ± 0.05
15(S)-HEDE	9-OxoOTrE	$0.00 \hspace{0.1cm} \pm \hspace{0.1cm} 0.00$	0.00 \pm 0.00	0.00 \pm 0.00	0.00 ± 0.00
15-OxoEDE	11(R)-HEDE	$0.03 \hspace{0.2cm} \pm \hspace{0.2cm} 0.02$	0.03 ± 0.02	0.00 \pm 0.00	0.02 ± 0.01
8(S)-HETrE 0.07 ± 0.01 0.11 ± 0.01 0.11 ± 0.00 0.00 ± 0.00 0.09 ± 0.00 5(S)-HETrE 0.04 ± 0.01 0.04 ± 0.00 0.03 ± 0.00 0.03 ± 0.00 0.03 ± 0.00 13,14dhPGE1 0.00 ± 0.00 <td>15(S)-HEDE</td> <td>$0.01 \hspace{0.2cm} \pm \hspace{0.2cm} 0.01$</td> <td>$0.01$ \pm 0.01</td> <td>0.01 ± 0.01</td> <td>0.01 ± 0.01</td>	15(S)-HEDE	$0.01 \hspace{0.2cm} \pm \hspace{0.2cm} 0.01$	0.01 \pm 0.01	0.01 ± 0.01	0.01 ± 0.01
5(S)-HETrE 0.04 ± 0.01 0.04 ± 0.00 0.03 ± 0.00 0.03 ± 0.00 0.03 ± 0.00 13,14dhPGE1 0.00 ± 0.00 0.00 ± 0.00 0.00 ± 0.00 0.00 ± 0.00 0.00 ± 0.00 0.00 ± 0.00 13,14dh-15k-PGE1 0.00 ± 0.00 0.00 ± 0.	15-OxoEDE	$0.00 \hspace{0.1cm} \pm \hspace{0.1cm} 0.00$	0.00 \pm 0.00	0.00 ± 0.00	0.00 ± 0.00
13,14dhPGE1	8(S)-HETrE	$0.07 \hspace{0.2cm} \pm \hspace{0.2cm} 0.01$	0.11 ± 0.01	0.11 ± 0.00	0.09 ± 0.00
13,14dh-15k-PGE1	5(S)-HETrE	0.04 ± 0.01	0.04 ± 0.00	0.03 ± 0.00	0.03 ± 0.00
D17-PGE1	13,14dhPGE1	0.00 ± 0.00	0.00 \pm 0.00	0.00 ± 0.00	0.00 ± 0.00
PGE1 0.00 ± 0.00 0.00 ± 0.00 ± 0.00 0.00 ± 0.00 ± 0.00 0.00 ± 0.00 ± 0.00 15(R)-PGE1 0.32 ± 0.03 0.34 ± 0.03 0.18 ± 0.02 0.21 ± 0.02 15-keto PGE1 0.00 ± 0.00 0.00 ± 0.00 0.00 ± 0.00 0.00 ± 0.00 0.00 ± 0.00 0.00 ± 0.00 Bicyclo PGE1 0.16 ± 0.08 0.19 ± 0.09 0.17 ± 0.09 0.19 ± 0.07 19(R)-hydroxy PGE1 0.00 ± 0.00 0.01 ± 0.01 0.01 ± 0.01 0.01 ± 0.01 0.01 ± 0.01 0.01 ± 0.01 0.01 ± 0.01 0.01 ± 0.01 0.01 ± 0.01 0.01 ± 0.01 0.01 ± 0.01	13,14dh-15k-PGE1	$0.00 \hspace{0.1cm} \pm \hspace{0.1cm} 0.00$	0.00 \pm 0.00	0.00 \pm 0.00	0.00 ± 0.00
15(R)-PGE1 0.32 ± 0.03 0.34 ± 0.03 0.18 ± 0.02 0.21 ± 0.02 15-keto PGE1 0.00 ± 0.00 0.00 ± 0.00 0.00 ± 0.00 0.00 ± 0.00 0.00 ± 0.00 Bicyclo PGE1 0.16 ± 0.08 0.19 ± 0.09 0.17 ± 0.09 0.19 ± 0.07 19(R)-hydroxy PGE1 0.00 ± 0.00 0.00 ± 0.00 0.00 ± 0.00 0.00 ± 0.00 0.00 ± 0.00 2,3-dinor PGE1 0.00 ± 0.00 0.01 ± 0.01 0.00 ± 0.00 0.02 ± 0.01 PGF1a 0.00 ± 0.00 0.00 ± 0.00 0.00 ± 0.00 0.00 ± 0.00 0.00 ± 0.00 6-keto PGE1 0.00 ± 0.00 0.01 ± 0.00 0.00 ± 0.00 0.00 ± 0.00 0.00 ± 0.00 8,9-DiHETrE 0.00 ± 0.00 0.01 ± 0.00 0.01 ± 0.01 0.01 ± 0.01 0.01 ± 0.01 11,12-DiHETrE 0.11 ± 0.02 0.08 ± 0.01 0.10 ± 0.01 0.10 ± 0.01 0.10 ± 0.01 45(S),12(S)-DiHETE 0.00 ± 0.00 0.00 ± 0.00 0.00 ± 0.00 0.00 ± 0.00 0.00 ± 0.00 5(S),15(S)-DiHETE 0.01 ± 0.01 0.01 ± 0.01 0.02 ± 0.01 0.02 ± 0.00 5(S),6(S)-DiHETE 0.00 ± 0.00 0.00 ± 0.00 0.00 ± 0.00 <td< td=""><td>D17-PGE1</td><td>$0.00 \hspace{0.1cm} \pm \hspace{0.1cm} 0.00$</td><td>$0.00$ \pm 0.00</td><td>0.00 \pm 0.00</td><td>0.00 ± 0.00</td></td<>	D17-PGE1	$0.00 \hspace{0.1cm} \pm \hspace{0.1cm} 0.00$	0.00 \pm 0.00	0.00 \pm 0.00	0.00 ± 0.00
15-keto PGE1	PGE1	$0.00 \hspace{0.1cm} \pm \hspace{0.1cm} 0.00$	0.00 \pm 0.00	0.00 \pm 0.00	0.00 ± 0.00
Bicyclo PGE1 0.16 ± 0.08 0.19 ± 0.09 0.17 ± 0.09 0.19 ± 0.07 $19(R)$ -hydroxy PGE1 0.00 ± 0.00 0.01 ± 0.01 0.01 ± 0	15(R)-PGE1	$0.32 \hspace{0.1cm} \pm \hspace{0.1cm} 0.03$	0.34 ± 0.03	$0.18 \hspace{0.1cm} \pm \hspace{0.1cm} 0.02$	0.21 ± 0.02
$\begin{array}{c ccccccccccccccccccccccccccccccccccc$	15-keto PGE1	$0.00 \hspace{0.1cm} \pm \hspace{0.1cm} 0.00$	0.00 \pm 0.00	0.00 \pm 0.00	0.00 ± 0.00
PGE1 $0.00 \pm 0.00 \pm 0.00$ 0.00 ± 0.00 0.01 ± 0.00 0.00 ± 0	Bicyclo PGE1	$0.16 \hspace{0.2cm} \pm \hspace{0.2cm} 0.08$	0.19 ± 0.09	$0.17 \hspace{0.2cm} \pm \hspace{0.2cm} 0.09$	$0.19 \hspace{0.2cm} \pm \hspace{0.2cm} 0.07$
PGF1a	19(R)-hydroxy PGE1	0.00 ± 0.00	0.00 \pm 0.00	0.00 \pm 0.00	0.00 ± 0.00
6-keto PGE1 0.00 ± 0.00 0.01 ± 0.00 0.01 ± 0.00 0.01 ± 0.01 0.02 ± 0.01 0.02 ± 0.02 0.01 ± 0.01 $0.$	2,3-dinor PGE1	$0.00 \hspace{0.1cm} \pm \hspace{0.1cm} 0.00$	0.01 \pm 0.01	0.00 \pm 0.00	0.02 ± 0.01
5,6-DiHETrE 0.00 ± 0.00 ± 0.00 0.01 ± 0.00 ± 0.00 0.03 ± 0.00 ± 0.01 ± 0	PGF1a	$0.00 \hspace{0.1cm} \pm \hspace{0.1cm} 0.00$	0.00 \pm 0.00	0.00 \pm 0.00	0.00 ± 0.00
8,9-DiHETrE $0.00 \pm 0.00 \pm 0.00$ 0.01 ± 0.00 0.01 ± 0.00 0.01 ± 0.01 0.01 ± 0.01 0.01 ± 0.00 $11,12$ -DiHETrE 0.11 ± 0.02 0.08 ± 0.01 0.10 ± 0.01 0.10 ± 0.01 0.10 ± 0.01 $14,15$ -DiHETrE 0.39 ± 0.05 0.37 ± 0.04 0.37 ± 0.04 0.39 ± 0.04 $5(S),12(S)$ -DiHETE 0.00 ± 0.00 $5(S),15(S)$ -DiHETE 0.01 ± 0.01 0.01 ± 0.01 0.02 ± 0.01 0.02 ± 0.01 $8(S),15(S)$ -DiHETE 0.00 ± 0.00 0.00 ± 0.00 0.00 ± 0.00 0.00 ± 0.00 $5(S),6(S)$ -DiHETE 0.00 ± 0.00 0.00 ± 0.00 0.00 ± 0.00 0.00 ± 0.00 $5(S)$ -EpETrE 0.03 ± 0.01 0.04 ± 0.01 0.03 ± 0.00 0.03 ± 0.00	6-keto PGE1	$0.00 \hspace{0.1cm} \pm \hspace{0.1cm} 0.00$	0.00 \pm 0.00	0.00 \pm 0.00	0.00 ± 0.00
11,12-DiHETrE 0.11 ± 0.02 0.08 ± 0.01 0.10 ± 0.01 0.10 ± 0.01 0.10 ± 0.01 14,15-DiHETrE 0.39 ± 0.05 0.37 ± 0.04 0.37 ± 0.04 0.39 ± 0.04 5(S),12(S)-DiHETE 0.00 ± 0.00 5(S),15(S)-DiHETE 0.01 ± 0.01 0.01 ± 0.01 0.02 ± 0.01 0.02 ± 0.01 0.02 ± 0.00 8(S),15(S)-DiHETE 0.00 ± 0.00 5(S),6(S)-DiHETE 0.00 ± 0.00 0.00 ± 0.00 0.00 ± 0.00 0.00 ± 0.00 5(G)-EpETrE 0.03 ± 0.01 0.04 ± 0.01 0.03 ± 0.00 0.03 ± 0.00	5,6-DiHETrE	$0.00 \hspace{0.1cm} \pm \hspace{0.1cm} 0.00$	0.01 \pm 0.00	0.03 ± 0.00	0.01 ± 0.01
14,15-DiHETrE 0.39 ± 0.05 0.37 ± 0.04 0.37 ± 0.04 0.39 ± 0.04 5(S),12(S)-DiHETE 0.00 ± 0.00 5(S),15(S)-DiHETE 0.01 ± 0.01 0.01 ± 0.01 0.02 ± 0.01 0.02 ± 0.01 0.02 ± 0.00 8(S),15(S)-DiHETE 0.00 ± 0.00 5(S),6(S)-DiHETE 0.00 ± 0.00 0.00 ± 0.00 0.00 ± 0.00 0.00 ± 0.00 5(6)-EpETrE 0.03 ± 0.01 0.04 ± 0.01 0.03 ± 0.00 0.03 ± 0.00	8,9-DiHETrE	$0.00 \hspace{0.1cm} \pm \hspace{0.1cm} 0.00$	0.01 \pm 0.00	0.01 ± 0.01	0.01 ± 0.00
$5(S),12(S)$ -DiHETE 0.00 ± 0.00	11,12-DiHETrE	$0.11 \hspace{0.2cm} \pm \hspace{0.2cm} 0.02$	0.08 ± 0.01	0.10 ± 0.01	0.10 ± 0.01
$5(S),15(S)$ -DiHETE 0.01 ± 0.01 0.01 ± 0.01 0.02 ± 0.01 0.02 ± 0.02 $8(S),15(S)$ -DiHETE 0.00 ± 0.00	14,15-DiHETrE	$0.39 \hspace{0.1cm} \pm \hspace{0.1cm} 0.05$	0.37 ± 0.04	$0.37 \hspace{0.2cm} \pm \hspace{0.2cm} 0.04$	0.39 ± 0.04
8(S),15(S)-DiHETE 0.00 ± 0.00 0.00 ± 0	5(S),12(S)-DiHETE	0.00 ± 0.00	0.00 ± 0.00	0.00 ± 0.00	0.00 ± 0.00
5(S),6(S)-DiHETE 0.00 ± 0.00 0.00 ± 0.00 0.00 ± 0.00 0.00 ± 0.00 5(6)-EpETrE 0.03 ± 0.01 0.04 ± 0.01 0.03 ± 0.00 0.03 ± 0.00	5(S),15(S)-DiHETE	0.01 ± 0.01	0.01 ± 0.01	0.02 ± 0.01	0.02 ± 0.02
5(6)-EpETrE 0.03 ± 0.01 0.04 ± 0.01 0.03 ± 0.00 0.03 ± 0.00	8(S),15(S)-DiHETE	0.00 ± 0.00	0.00 ± 0.00	0.00 ± 0.00	0.00 ± 0.00
	5(S),6(S)-DiHETE	0.00 ± 0.00	0.00 ± 0.00	0.00 ± 0.00	0.00 ± 0.00
8(9)-EpETrE $0.00 \pm 0.00 \mid 0.00 \pm 0.00 \mid 0.00 \pm 0.00 \mid 0.00 \pm 0.00$	5(6)-EpETrE	0.03 ± 0.01	0.04 ± 0.01	0.03 ± 0.00	0.03 ± 0.00
	8(9)-EpETrE	0.00 ± 0.00	0.00 ± 0.00	0.00 ± 0.00	0.00 ± 0.00

Table S4.3 (cont'd)

11(12)-EpETrE	0.09 ± 0.00	0.09 ± 0.01	0.02 ± 0.01	0.06 ± 0.01
14(15)-EpETrE	0.02 ± 0.01	0.01 ± 0.01	0.02 ± 0.01	0.04 ± 0.01
12-HETE	0.51 ± 0.02	0.51 ± 0.08	0.75 ± 0.06	0.60 ± 0.03
tetranor 12-HETE	3.09 ± 0.09	2.99 ± 0.38	2.94 ± 0.18	2.96 ± 0.14
15-HETE	1.05 ± 0.05	0.95 ± 0.10	1.53 ± 0.06	1.12 ± 0.05
5-HETE	1.42 ± 0.11	1.81 ± 0.12	1.58 ± 0.08	1.36 ± 0.02
8-НЕТЕ	0.33 ± 0.02	0.39 ± 0.08	0.42 ± 0.03	0.35 ± 0.01
12(S)-HHTrE	0.00 ± 0.00	0.23 ± 0.05	0.29 ± 0.16	0.19 ± 0.03
20-НЕТЕ	$0.74 \hspace{0.1cm} \pm \hspace{0.1cm} 0.04$	1.88 ± 0.70	0.76 ± 0.39	0.64 ± 0.33
9-НЕТЕ	0.07 ± 0.04	0.12 ± 0.02	0.16 ± 0.01	0.13 ± 0.01
11-HETE	0.96 ± 0.08	1.43 ± 0.29	1.55 ± 0.10	1.37 ± 0.11
LTB4	0.00 ± 0.00	0.00 ± 0.00	0.00 ± 0.00	0.00 ± 0.00
12-OxoLTB4	0.00 ± 0.00	0.00 ± 0.00	0.00 ± 0.00	0.00 ± 0.00
20-hydroxy LTB4	0.00 ± 0.00	0.00 ± 0.00	0.00 ± 0.00	0.00 ± 0.00
20-COOH LTB4	0.00 ± 0.00	0.00 ± 0.00	0.00 ± 0.00	0.00 ± 0.00
18-carboxy dinor LTB4	0.00 ± 0.00	0.00 ± 0.00	0.00 ± 0.00	0.00 ± 0.00
LXA4	$0.00 \hspace{0.1cm} \pm \hspace{0.1cm} 0.00$	0.00 \pm 0.00	0.00 ± 0.00	0.00 ± 0.00
15-epi LXA4	0.00 ± 0.00	0.00 \pm 0.00	0.00 ± 0.00	0.00 ± 0.00
15-oxo LXA4	0.00 ± 0.00	0.00 \pm 0.00	0.00 ± 0.00	0.00 ± 0.00
LXA5	0.00 ± 0.00	0.00 \pm 0.00	0.00 ± 0.00	0.00 ± 0.00
LXB4	$0.00 \hspace{0.1cm} \pm \hspace{0.1cm} 0.00$	0.00 \pm 0.00	0.00 ± 0.00	0.00 ± 0.00
12-OxoETE	$0.00 \hspace{0.1cm} \pm \hspace{0.1cm} 0.00$	0.00 \pm 0.00	0.00 ± 0.00	0.00 ± 0.00
15-OxoETE	$0.14 \hspace{0.1cm} \pm \hspace{0.1cm} 0.01$	0.11 ± 0.06	0.22 ± 0.03	0.17 ± 0.02
5-oxoETE	0.00 ± 0.00	0.07 ± 0.03	0.03 ± 0.03	0.02 ± 0.02
PGE2	$0.49 \hspace{0.2cm} \pm \hspace{0.2cm} 0.06$	1.04 ± 0.13	$0.49 \hspace{0.2cm} \pm \hspace{0.2cm} 0.02$	$0.86 \hspace{0.2cm} \pm \hspace{0.2cm} 0.02$
15-keto PGE2	$0.01 \hspace{0.2cm} \pm \hspace{0.2cm} 0.01$	0.00 \pm 0.00	0.00 ± 0.00	0.00 ± 0.00
13,14dh-15k-PGE2	0.00 ± 0.00	0.00 \pm 0.00	0.00 ± 0.00	0.00 ± 0.00
Bicyclo PGE2	$0.00 \hspace{0.1cm} \pm \hspace{0.1cm} 0.00$	0.00 \pm 0.00	0.00 ± 0.00	0.00 ± 0.00
PGA2	$0.04 \hspace{0.2cm} \pm \hspace{0.2cm} 0.04$	0.06 ± 0.06	0.04 ± 0.02	0.06 ± 0.03
19(R)-OH PGE2 & 20-OH PGE2	0.00 ± 0.00	0.00 \pm 0.00	0.00 ± 0.00	0.00 ± 0.00
tetranor PGEM	0.01 ± 0.00	0.00 \pm 0.00	0.00 ± 0.00	0.00 ± 0.00
PGD2	$0.21 \hspace{0.1cm} \pm \hspace{0.1cm} 0.04$	0.59 ± 0.07	0.22 ± 0.02	0.47 ± 0.02
PGJ2	$0.04 \hspace{0.1cm} \pm \hspace{0.1cm} 0.02$	0.10 \pm 0.01	0.06 ± 0.01	0.08 ± 0.00
D12-PGJ2	0.00 ± 0.00	0.01 \pm 0.01	0.00 ± 0.00	0.00 ± 0.00
15d-D12,14-PGJ2	0.00 ± 0.00	0.00 \pm 0.00	0.00 ± 0.00	0.00 ± 0.00
13,14dh-15k-PGD2	0.05 ± 0.05	0.11 ± 0.01	0.04 ± 0.02	0.03 ± 0.03
PGF2a	0.00 ± 0.00	0.14 ± 0.03	0.02 ± 0.02	0.08 ± 0.01

Table S4.3 (cont'd)

15-keto PGF2a	0.00 ± 0.00	0.04 ± 0.00	0.00 ± 0.00	0.03 ± 0.01
13,14dh-15k- PGF2a	0.00 ± 0.00	0.00 ± 0.00	0.00 ± 0.00	0.00 ± 0.00
19(R)-OH PGF2a & 20-OH PGF2a	0.01 ± 0.01	0.01 ± 0.01	0.00 ± 0.00	0.01 ± 0.01
8-isoPGF2a & 11bPGF2a	0.00 ± 0.00	0.00 \pm 0.00	0.00 ± 0.00	0.00 ± 0.00
iPF-VI	$0.02 \hspace{0.2cm} \pm \hspace{0.2cm} 0.01$	0.02 ± 0.01	0.01 ± 0.01	$0.01 \hspace{0.2cm} \pm \hspace{0.2cm} 0.01$
6kPGF1a	$0.00 \hspace{0.1cm} \pm \hspace{0.1cm} 0.00$	0.00 \pm 0.00	0.00 \pm 0.00	0.00 ± 0.00
6,15-diketo PGFa	0.00 ± 0.00	0.00 \pm 0.00	0.00 ± 0.00	0.00 ± 0.00
TXB2	0.31 ± 0.03	0.59 ± 0.09	0.27 ± 0.02	0.41 ± 0.03
11dh-TXB2	$0.00 \hspace{0.1cm} \pm \hspace{0.1cm} 0.00$	0.00 \pm 0.00	0.00 \pm 0.00	0.00 ± 0.00
2,3-dinor TXB2	0.00 ± 0.00	0.00 \pm 0.00	0.00 \pm 0.00	0.00 ± 0.00
11dh-2,3-dinor TXB2	0.00 ± 0.00	0.00 \pm 0.00	0.00 ± 0.00	0.00 ± 0.00
5,6-DiHETE(EPA)	0.00 ± 0.00	0.00 ± 0.00	0.00 ± 0.00	0.00 ± 0.00
5(S),15(S)-DiHEPE	0.00 ± 0.00	0.00 \pm 0.00	0.00 ± 0.00	0.00 \pm 0.00
8(9)-EpETE	0.00 ± 0.00	0.00 \pm 0.00	0.00 ± 0.00	0.00 ± 0.00
11(12)-EpETE	0.05 ± 0.00	0.03 ± 0.01	0.12 ± 0.00	$0.11 \hspace{0.2cm} \pm \hspace{0.2cm} 0.01$
14(15)-EpETE	0.00 ± 0.00	0.00 ± 0.00	0.00 ± 0.00	0.00 ± 0.00
17(18)-EpETE	0.06 ± 0.00	0.09 ± 0.01	0.58 ± 0.01	0.44 ± 0.03
12-НЕРЕ	0.10 ± 0.05	0.18 ± 0.04	0.48 ± 0.01	0.37 ± 0.02
15(S)-HEPE	0.36 ± 0.01	0.33 ± 0.03	1.30 ± 0.06	1.23 ± 0.10
5-НЕРЕ	0.23 ± 0.02	0.31 ± 0.07	0.76 ± 0.02	0.60 ± 0.03
8-НЕРЕ	0.66 ± 0.03	0.59 ± 0.03	1.53 ± 0.07	1.41 ± 0.01
18-НЕРЕ	1.87 ± 0.15	1.59 ± 0.03	3.77 ± 0.13	4.05 ± 0.14
9-НЕРЕ	0.19 ± 0.01	0.19 ± 0.04	0.89 ± 0.02	0.76 ± 0.06
11-НЕРЕ	0.23 ± 0.04	0.22 ± 0.05	0.57 ± 0.00	0.53 ± 0.02
LTB5	0.00 ± 0.00	0.00 ± 0.00	0.00 ± 0.00	0.00 ± 0.00
PGE3	0.00 ± 0.00	0.00 ± 0.00	0.00 ± 0.00	0.00 ± 0.00
PGD3	0.00 ± 0.00	0.01 ± 0.01	0.00 ± 0.00	0.00 ± 0.00
15d-D12,14-PGJ3	0.00 ± 0.00	0.00 ± 0.00	0.00 ± 0.00	0.00 ± 0.00
PGF3a	0.00 ± 0.00	0.00 ± 0.00	0.00 ± 0.00	0.00 ± 0.00
RvE1	0.00 ± 0.00	0.00 ± 0.00	0.00 ± 0.00	0.00 ± 0.00
RvE2	0.03 ± 0.01	0.02 ± 0.01	0.02 ± 0.00	0.01 ± 0.01
RvE3	0.00 ± 0.00	0.02 ± 0.01	0.00 ± 0.00	0.00 ± 0.00
TXB3	0.00 ± 0.00	0.00 ± 0.00	0.00 ± 0.00	0.00 ± 0.00
11dh TXB3	0.00 ± 0.00	0.00 ± 0.00	0.00 ± 0.00	0.00 ± 0.00
MaR1(ω-3DPA)	0.09 ± 0.01	0.09 ± 0.01	0.52 ± 0.01	0.54 ± 0.03
PD1(ω-3, DPA)	0.00 ± 0.00	0.00 ± 0.00	0.00 ± 0.00	0.00 ± 0.00
RvD5(ω-3DPA) (7,17-DiHDoPE)	0.00 ± 0.00	0.00 \pm 0.00	0.00 ± 0.00	0.00 ± 0.00

Table S4.3 (cont'd)

19,20-DiHDoPE	0.34 ± 0.06	0.40 ± 0.04	4.95 ± 0.30	4.41 ± 0.26
7(8)-EpDPE	0.00 ± 0.00	0.00 ± 0.00	0.05 ± 0.02	0.03 ± 0.00
10(11)-EpDPE	0.02 ± 0.00	0.02 ± 0.01	0.10 ± 0.01	0.09 ± 0.01
13(14)-EpDPE	0.00 ± 0.00	0.00 ± 0.00	0.06 ± 0.03	0.03 ± 0.03
16(17)-EpDPE	0.00 ± 0.00	0.00 ± 0.00	0.03 ± 0.03	0.02 ± 0.02
19(20)-EpDPE	0.05 ± 0.00	0.08 ± 0.01	1.78 ± 0.04	1.10 ± 0.03
14-HDoHE	0.07 ± 0.04	0.11 ± 0.02	1.35 ± 0.44	0.88 ± 0.05
17-HDoHE	0.03 ± 0.03	0.00 ± 0.00	0.19 ± 0.19	0.00 ± 0.00
4-HDoHE	$0.39 \hspace{0.2cm} \pm \hspace{0.2cm} 0.02$	0.47 ± 0.05	8.01 ± 0.85	6.13 ± 0.28
7-HDoHE	$0.14 \hspace{0.2cm} \pm \hspace{0.2cm} 0.01$	0.13 ± 0.02	1.61 ± 0.21	1.19 ± 0.04
8-HDoHE	$0.51 \hspace{0.1cm} \pm \hspace{0.1cm} 0.02$	0.35 ± 0.05	4.63 ± 0.64	2.89 ± 0.27
10-HDoHE	$0.16 \hspace{0.2cm} \pm \hspace{0.2cm} 0.01$	0.20 \pm 0.05	2.07 ± 0.67	1.34 ± 0.12
11-HDoHE	$0.17 \hspace{0.2cm} \pm \hspace{0.2cm} 0.03$	0.20 ± 0.05	2.87 ± 0.56	1.97 ± 0.07
13-HDoHE	$0.14 \hspace{0.1cm} \pm \hspace{0.1cm} 0.01$	0.17 ± 0.04	2.15 ± 0.51	1.47 ± 0.09
16-HDoHE	$0.57 \hspace{0.2cm} \pm \hspace{0.2cm} 0.02$	0.54 ± 0.11	4.64 ± 0.81	3.60 ± 0.22
20-HDoHE	$0.87 \hspace{0.2cm} \pm \hspace{0.2cm} 0.04$	0.94 ± 0.19	8.09 ± 0.62	6.44 ± 0.19
Maresin1	$0.00 \hspace{0.1cm} \pm \hspace{0.1cm} 0.00$	0.00 \pm 0.00	0.00 ± 0.00	0.00 ± 0.00
7(S)-Maresin1	$0.00 \hspace{0.1cm} \pm \hspace{0.1cm} 0.00$	0.00 \pm 0.00	0.00 ± 0.00	0.00 ± 0.00
PD1	$0.00 \hspace{0.1cm} \pm \hspace{0.1cm} 0.00$	0.00 \pm 0.00	0.01 ± 0.01	0.02 ± 0.02
AT-PD1	$0.00 \hspace{0.1cm} \pm \hspace{0.1cm} 0.00$	0.00 \pm 0.00	0.00 ± 0.00	0.00 ± 0.00
10S,17S-DiHDoHE	$0.00 \hspace{0.1cm} \pm \hspace{0.1cm} 0.00$	0.00 \pm 0.00	0.00 ± 0.00	0.00 ± 0.00
22-OH-PD1	$0.00 \hspace{0.1cm} \pm \hspace{0.1cm} 0.00$	0.00 \pm 0.00	0.00 ± 0.00	0.00 ± 0.00
RvD1 & AT-RvD1	$0.00 \hspace{0.1cm} \pm \hspace{0.1cm} 0.00$	0.00 \pm 0.00	0.00 ± 0.00	0.00 ± 0.00
RvD2	$0.00 \hspace{0.1cm} \pm \hspace{0.1cm} 0.00$	0.00 \pm 0.00	0.00 ± 0.00	0.00 ± 0.00
RvD3	$0.00 \hspace{0.1cm} \pm \hspace{0.1cm} 0.00$	0.00 \pm 0.00	$0.02 \hspace{0.2cm} \pm \hspace{0.2cm} 0.02$	0.03 ± 0.03
AT-RvD3	$0.04 \hspace{0.2cm} \pm \hspace{0.2cm} 0.02$	0.05 ± 0.00	0.03 ± 0.03	0.00 \pm 0.00
RvD4	$0.00 \hspace{0.1cm} \pm \hspace{0.1cm} 0.00$	0.00 \pm 0.00	0.00 ± 0.00	0.00 ± 0.00
RvD5	$0.00 \hspace{0.1cm} \pm \hspace{0.1cm} 0.00$	0.00 \pm 0.00	0.00 ± 0.00	0.00 \pm 0.00
RvD6 (4,17- DiHDoHE)	$0.06 \hspace{0.2cm} \pm \hspace{0.2cm} 0.01$	0.06 \pm 0.00	0.15 ± 0.01	0.16 ± 0.01
8-oxoRvD1	$0.00 \hspace{0.1cm} \pm \hspace{0.1cm} 0.00$	0.00 \pm 0.00	0.00 ± 0.00	0.00 \pm 0.00
17-oxoRvD1	0.00 ± 0.00	0.00 \pm 0.00	0.00 ± 0.00	0.00 ± 0.00

Data are presented in units of pmol/culture as mean \pm SEM.

Table S4.4. Combined intracellular and extracellular oxylipin content at $t=3.5\ h.$

Oxylipin	VEH/VEH	LPS/VEH	VEH/cSiO ₂	LPS/cSiO ₂	DHA- VEH/VEH	DHA- LPS/VEH	DHA- VEH/cSiO ₂	DHA- LPS/cSiO ₂
9,10-DiHOME	0.02 ± 0.01	0.04 ± 0.03	$0.05 ~\pm~ 0.00$	$0.04 \pm \ 0.00$	0.02 ± 0.01	0.09 ± 0.06	0.03 ± 0.01	0.06 ± 0.03
12,13-DiHOME	$0.00 ~\pm~ 0.00$	$0.02~\pm~0.01$	0.03 ± 0.01	$0.02 \pm \ 0.0s1$	0.01 ± 0.01	0.06 ± 0.02	$0.03 ~\pm~ 0.00$	$0.02 \hspace{0.1cm} \pm \hspace{0.1cm} 0.01$
9(10)-EpOME	0.17 ± 0.03	0.33 ± 0.12	0.12 ± 0.06	0.09 ± 0.09	0.18 ± 0.05	0.80 ± 0.16	$0.24 ~\pm~ 0.04$	0.33 ± 0.24
12(13)-EpOME	$0.06 ~\pm~ 0.04$	$0.19~\pm~0.10$	$0.09 ~\pm~ 0.02$	0.15 ± 0.11	0.09 ± 0.02	0.58 ± 0.11	0.14 ± 0.03	$0.06 \hspace{0.1cm} \pm \hspace{0.1cm} 0.03$
9-HODE	1.28 ± 0.16	$1.88~\pm~0.69$	4.68 ± 2.35	4.46 ± 2.71	1.67 ± 0.46	12.17 ± 8.76	1.78 ± 0.15	$2.72 \hspace{0.1cm} \pm \hspace{0.1cm} 0.68$
13-HODE	$4.47 \hspace{0.1cm} \pm \hspace{0.1cm} 0.72$	$7.47 ~\pm~ 3.04$	17.7 ± 6.63	23.99 ± 15.4	$8.22~\pm~~2.83$	47.11 ± 33.71	8.33 ± 0.86	9.87 ± 1.83
9-OxoODE	1.10 ± 0.15	$2.21~\pm~0.77$	$2.25 ~\pm~ 0.53$	1.88 ± 0.34	$1.66~\pm~0.54$	4.90 ± 0.36	1.54 ± 0.46	$2.13 \ \pm \ 0.64$
13-OxoODE	1.41 ± 0.22	3.73 ± 1.77	2.71 ± 0.69	3.37 ± 1.59	$1.98~\pm~0.73$	14.3 ± 5.45	$2.66 ~\pm~ 0.28$	$2.61 \ \pm \ 0.70$
13(S)-HOTrE	$0.03 \hspace{0.1cm} \pm \hspace{0.1cm} 0.03$	$0.02~\pm~0.02$	0.21 ± 0.15	0.49 ± 0.49	0.10 ± 0.06	0.74 ± 0.74	$0.00 ~\pm~ 0.00$	$0.06 ~\pm~ 0.06$
13(S)-HOTrE(g)	$0.00 ~\pm~ 0.00$	$0.00~\pm~0.00$	$0.97 ~\pm~ 0.17$	$0.45 \pm \ 0.22$	$0.00~\pm~0.00$	0.00 ± 0.00	$0.22 ~\pm~ 0.22$	$0.19 ~\pm~ 0.19$
9(S)-HOTrE	$0.02 \hspace{0.1cm} \pm \hspace{0.1cm} 0.02$	$0.12~\pm~0.10$	$0.43 ~\pm~ 0.26$	$0.51 \pm \ 0.46$	$0.09~\pm~0.06$	0.94 ± 0.91	$0.06 ~\pm~ 0.03$	$0.12 \hspace{0.1cm} \pm \hspace{0.1cm} 0.07$
9-OxoOTrE	$0.01 \hspace{0.1cm} \pm \hspace{0.1cm} 0.01$	$0.00~\pm~0.00$	$0.00 ~\pm~ 0.00$	$0.04 \pm \ 0.04$	$0.00~\pm~0.00$	0.06 ± 0.06	$0.00 ~\pm~ 0.00$	$0.03 \hspace{0.1cm} \pm \hspace{0.1cm} 0.03$
11(R)-HEDE	$0.00 ~\pm~ 0.00$	$0.00~\pm~0.00$	$0.28 ~\pm~ 0.02$	$0.24 \pm \ 0.02$	$0.05~\pm~0.03$	0.16 ± 0.16	$0.09 ~\pm~ 0.01$	$0.06 ~\pm~ 0.03$
15(S)-HEDE	$0.00 \hspace{0.1cm} \pm \hspace{0.1cm} 0.00$	$0.00~\pm~0.00$	$0.06 ~\pm~ 0.06$	$0.10 \pm \ 0.03$	$0.02~\pm~0.02$	0.06 ± 0.06	$0.07 \hspace{0.1cm} \pm \hspace{0.1cm} 0.01$	$0.05 \hspace{0.1cm} \pm \hspace{0.1cm} 0.02$
15-OxoEDE	$0.00 \hspace{0.1cm} \pm \hspace{0.1cm} 0.00$	$0.00~\pm~0.00$	$0.00 ~\pm~ 0.00$	$0.00 \pm \ 0.00$	$0.00~\pm~0.00$	0.02 ± 0.02	$0.00 ~\pm~ 0.00$	$0.00 ~\pm~ 0.00$
8(S)-HETrE	$0.04 \hspace{0.1cm} \pm \hspace{0.1cm} 0.02$	$0.02~\pm~0.01$	1.72 ± 0.08	1.85 ± 0.11	$0.12~\pm~0.01$	0.08 ± 0.06	1.14 ± 0.06	1.11 ± 0.20
5(S)-HETrE	$0.03 \hspace{0.1cm} \pm \hspace{0.1cm} 0.00$	0.03 ± 0.01	$2.31 \ \pm \ 0.06$	$3.39 \pm \ 0.16$	$0.04~\pm~0.00$	0.04 ± 0.01	$0.70 ~\pm~ 0.02$	$0.59 ~\pm~ 0.21$
13,14dhPGE1	$0.00 \hspace{0.1cm} \pm \hspace{0.1cm} 0.00$	$0.00~\pm~0.00$	$0.00 ~\pm~ 0.00$	$0.00 \pm \ 0.00$	$0.00~\pm~0.00$	0.00 ± 0.00	$0.00 ~\pm~ 0.00$	$0.00 ~\pm~ 0.00$
13,14dh-15k- PGE1	0.00 ± 0.00	$0.00~\pm~0.00$	$0.03 ~\pm~ 0.00$	$0.05 \pm \ 0.00$	$0.00~\pm~0.00$	0.00 ± 0.00	$0.00 ~\pm~ 0.00$	$0.00 ~\pm~ 0.00$
D17-PGE1	0.00 ± 0.00	$0.00~\pm~0.00$	$0.00 ~\pm~ 0.00$	$0.00 \pm \ 0.00$	$0.00~\pm~0.00$	0.00 ± 0.00	$0.00 ~\pm~ 0.00$	$0.00 ~\pm~ 0.00$
PGE1	$0.00 ~\pm~ 0.00$	$0.02~\pm~0.02$	$0.07 ~\pm~ 0.07$	$0.47 \pm \ 0.02$	$0.00~\pm~0.00$	0.00 ± 0.00	$0.05 ~\pm~ 0.05$	$0.10 \ \pm \ 0.05$
15(R)-PGE1	$0.20 ~\pm~ 0.06$	$0.29~\pm~0.03$	$0.50 ~\pm~ 0.05$	0.67 ± 0.10	$0.23~\pm~0.02$	0.17 ± 0.03	$0.39 ~\pm~ 0.05$	$0.17 \hspace{0.1cm} \pm \hspace{0.1cm} 0.09$
15-keto PGE1	$0.00 \hspace{0.1cm} \pm \hspace{0.1cm} 0.00$	$0.00~\pm~0.00$	$0.00~\pm~0.00$	0.00 ± 0.00	$0.00~\pm~0.00$	0.00 ± 0.00	$0.00 ~\pm~ 0.00$	$0.00 ~\pm~ 0.00$
Bicyclo PGE1	0.12 ± 0.06	$0.11 ~\pm~ 0.06$	$0.22 ~\pm~ 0.01$	$0.22 \pm \ 0.02$	$0.17 ~\pm~ 0.05$	0.21 ± 0.03	0.13 ± 0.07	$0.02 \ \pm \ 0.02$
19(R)-hydroxy PGE1	0.00 ± 0.00	$0.00~\pm~0.00$	0.00 ± 0.00	$0.00 \pm \ 0.00$	$0.00~\pm~0.00$	0.00 ± 0.00	0.00 ± 0.00	$0.00 ~\pm~ 0.00$

Table S4.4 (cont'd)

2,3-dinor PGE1	0.00 ± 0.00	0.03 ± 0.01	0.00 ± 0.00	0.00 ± 0.00	$0.00~\pm~0.00$	0.13 ± 0.09	$0.02 ~\pm~ 0.02$	$0.00 ~\pm~ 0.00$
PGF1a	0.00 ± 0.00	0.00 ± 0.00	0.03 ± 0.01	0.04 ± 0.02	0.00 ± 0.00	0.00 ± 0.00	0.03 ± 0.02	0.01 ± 0.01
6-keto PGE1	0.00 ± 0.00	0.00 ± 0.00	0.00 ± 0.00	0.00 ± 0.00	0.00 ± 0.00	0.00 ± 0.00	0.00 ± 0.00	0.00 ± 0.00
5,6-DiHETrE	$0.02 \hspace{0.1cm} \pm \hspace{0.1cm} 0.00$	0.01 ± 0.00	$0.07 ~\pm~ 0.02$	0.06 ± 0.01	$0.02~\pm~0.00$	0.02 ± 0.00	$0.04 ~\pm~ 0.01$	$0.04 \hspace{0.1cm} \pm \hspace{0.1cm} 0.01$
8,9-DiHETrE	$0.01 \hspace{0.1cm} \pm \hspace{0.1cm} 0.00$	$0.01~\pm~0.00$	$0.04 ~\pm~ 0.00$	$0.04 \pm \ 0.00$	$0.01~\pm~0.00$	0.01 ± 0.00	$0.03 ~\pm~ 0.00$	$0.02 \hspace{0.1cm} \pm \hspace{0.1cm} 0.01$
11,12-DiHETrE	$0.15 \hspace{0.1cm} \pm \hspace{0.1cm} 0.03$	$0.03~\pm~0.00$	$0.30 ~\pm~ 0.01$	$0.33 \pm \ 0.04$	0.11 ± 0.02	0.05 ± 0.03	0.16 ± 0.01	$0.14 \hspace{0.1cm} \pm \hspace{0.1cm} 0.02$
14,15-DiHETrE	$0.59 \hspace{0.1cm} \pm \hspace{0.1cm} 0.16$	$0.16~\pm~0.01$	$0.89 ~\pm~ 0.09$	$1.01 \pm \ 0.05$	$0.46~\pm~0.03$	$0.19 \hspace{0.2cm} \pm \hspace{0.2cm} 0.02$	0.57 ± 0.08	$0.40 \ \pm \ 0.09$
5(S),12(S)- DiHETE	$0.01 \hspace{0.1cm} \pm \hspace{0.1cm} 0.01$	$0.00~\pm~0.00$	$0.01 ~\pm~ 0.00$	$0.01 \pm \ 0.01$	$0.00~\pm~0.00$	0.00 \pm 0.00	$0.00 ~\pm~ 0.00$	$0.01 ~\pm~ 0.00$
5(S),15(S)- DiHETE	$0.00 ~\pm~ 0.00$	$0.02 ~\pm~ 0.01$	0.03 ± 0.00	$0.06 \pm \ 0.02$	$0.06~\pm~0.00$	0.01 \pm 0.00	0.02 ± 0.01	$0.01 ~\pm~ 0.01$
8(S),15(S)- DiHETE	$0.00 ~\pm~ 0.00$	$0.00~\pm~0.00$	$0.00 ~\pm~ 0.00$	0.00 \pm 0.00	$0.01 ~\pm~ 0.01$	0.00 \pm 0.00	$0.00 ~\pm~ 0.00$	$0.02 ~\pm~ 0.02$
5(S),6(S)-DiHETE	$0.01 \hspace{0.1cm} \pm \hspace{0.1cm} 0.01$	$0.00~\pm~0.00$	$0.00 ~\pm~ 0.00$	0.00 ± 0.00	$0.00~\pm~0.00$	0.00 \pm 0.00	$0.00 ~\pm~ 0.00$	$0.00 ~\pm~ 0.00$
5(6)-EpETrE	$0.03 \hspace{0.1cm} \pm \hspace{0.1cm} 0.01$	$0.01~\pm~0.00$	$0.28 ~\pm~ 0.01$	0.50 ± 0.03	$0.03~\pm~0.00$	0.02 ± 0.00	0.15 ± 0.01	$0.22 \ \pm \ 0.04$
8(9)-EpETrE	$0.00 \hspace{0.1cm} \pm \hspace{0.1cm} 0.00$	$0.00~\pm~0.00$	0.00 ± 0.00	0.00 ± 0.00	$0.00~\pm~0.00$	0.00 ± 0.00	$0.00 ~\pm~ 0.00$	$0.04 \hspace{0.1cm} \pm \hspace{0.1cm} 0.04$
11(12)-EpETrE	$0.05 \hspace{0.1cm} \pm \hspace{0.1cm} 0.03$	$0.01 ~\pm~ 0.01$	0.35 ± 0.01	$0.74 \pm \ 0.02$	$0.07~\pm~0.01$	0.06 ± 0.00	0.23 ± 0.05	$0.39 ~\pm~ 0.07$
14(15)-EpETrE	$0.02 \ \pm \ 0.01$	$0.01 ~\pm~ 0.01$	0.10 ± 0.05	0.39 ± 0.01	$0.00~\pm~0.00$	0.04 ± 0.00	0.12 ± 0.02	$0.17 \hspace{0.1cm} \pm \hspace{0.1cm} 0.03$
12-HETE	$0.51 \hspace{0.1cm} \pm \hspace{0.1cm} 0.01$	$0.32~\pm~0.03$	8.12 ± 0.48	9.77 ± 0.55	$0.79~\pm~0.05$	$0.80 \hspace{0.2cm} \pm \hspace{0.2cm} 0.04$	4.58 ± 0.14	$3.91 \ \pm \ 0.90$
tetranor 12-HETE	3.01 ± 0.19	$1.44~\pm~0.09$	3.40 ± 0.12	$2.94 \pm \ 0.04$	$3.13~\pm~0.23$	1.84 ± 0.02	3.84 ± 0.06	2.81 ± 0.21
15-HETE	$1.28 \ \pm \ 0.07$	$1.29~\pm~0.06$	29.96 ± 0.83	37.04 ± 0.94	$1.39~\pm~0.07$	1.19 ± 0.04	17.75 ± 0.76	$16.82 \ \pm \ 2.74$
5-HETE	$1.27 \hspace{0.1cm} \pm \hspace{0.1cm} 0.09$	$1.83~\pm~0.33$	76.41 ± 0.29	123.05 ± 8.30	$1.63~\pm~0.06$	1.31 ± 0.11	38.77 ± 1.25	39.02 ± 9.14
8-НЕТЕ	$0.38 \ \pm \ 0.04$	$0.25~\pm~0.02$	10.37 ± 0.41	12.22 ± 0.70	$0.41~\pm~0.01$	$0.28 \hspace{0.2cm} \pm \hspace{0.2cm} 0.01$	5.16 ± 0.28	$4.27 \ \pm \ 0.79$
12(S)-HHTrE	$0.17 \hspace{0.1cm} \pm \hspace{0.1cm} 0.17$	$2.87~\pm~0.23$	34.88 ± 0.56	46.78 ± 1.25	$0.15~\pm~0.15$	0.95 ± 0.08	16.34 ± 0.50	16.07 ± 1.29
20-HETE	$0.86 \hspace{0.1cm} \pm \hspace{0.1cm} 0.03$	$0.81 ~\pm~ 0.81$	$0.00 ~\pm~ 0.00$	4.81 ± 0.19	1.67 ± 1.15	1.11 ± 0.52	4.53 ± 0.11	3.65 ± 0.30
9-НЕТЕ	$0.07 \hspace{0.1cm} \pm \hspace{0.1cm} 0.04$	$0.14~\pm~0.01$	1.86 ± 0.11	$2.15 \pm \ 0.06$	$0.16~\pm~0.01$	0.14 ± 0.02	0.71 ± 0.36	1.21 ± 0.21
11-HETE	$1.16 ~\pm~ 0.06$	$3.30~\pm~0.19$	72.31 ± 2.58	105.68 ± 3.27	$1.59~\pm~0.04$	1.65 ± 0.12	37.47 ± 2.45	33.68 ± 11.8
LTB4	$0.00 ~\pm~ 0.00$	$0.00~\pm~0.00$	$0.42 \ \pm \ 0.03$	1.64 ± 0.04	$0.00~\pm~0.00$	0.00 \pm 0.00	$0.36 ~\pm~ 0.04$	$0.44 ~\pm~ 0.08$
12-OxoLTB4	$0.00 ~\pm~ 0.00$	$0.00~\pm~0.00$	$0.00 ~\pm~ 0.00$	$0.02 \pm \ 0.00$	$0.00~\pm~0.00$	$0.00 \hspace{0.1cm} \pm \hspace{0.1cm} 0.00$	$0.00 ~\pm~ 0.00$	$0.01 ~\pm~ 0.01$

Table S4.4 (cont'd)

20-hydroxy LTB4	$0.00 \hspace{0.1cm} \pm \hspace{0.1cm} 0.00$	$0.00~\pm~0.00$	$0.00 ~\pm~ 0.00$	0.05 ± 0.01	$0.00~\pm~0.00$	0.00 ± 0.00	$0.00 ~\pm~ 0.00$	$0.00 ~\pm~ 0.00$
20-COOH LTB4	$0.00 \hspace{0.1cm} \pm \hspace{0.1cm} 0.00$	$0.00~\pm~0.00$	$0.00 ~\pm~ 0.00$	0.00 ± 0.00	$0.00~\pm~0.00$	0.00 ± 0.00	$0.00 ~\pm~ 0.00$	$0.00 ~\pm~ 0.00$
18-carboxy dinor LTB4	0.00 ± 0.00	0.00 ± 0.00	0.00 ± 0.00	0.00 ± 0.00	0.00 ± 0.00	0.00 ± 0.00	$0.00 ~\pm~ 0.00$	$0.00 ~\pm~ 0.00$
LXA4	$0.00 \hspace{0.1cm} \pm \hspace{0.1cm} 0.00$	$0.00~\pm~0.00$	$0.01 \hspace{0.1cm} \pm \hspace{0.1cm} 0.01$	0.04 ± 0.01	$0.00~\pm~0.00$	0.00 ± 0.00	$0.01 \hspace{0.1cm} \pm \hspace{0.1cm} 0.01$	$0.02 ~\pm~ 0.02$
15-epi LXA4	$0.00 \hspace{0.1cm} \pm \hspace{0.1cm} 0.00$	$0.00~\pm~0.00$	$0.00 ~\pm~ 0.00$	0.00 ± 0.00	$0.00~\pm~0.00$	0.00 ± 0.00	$0.00 ~\pm~ 0.00$	$0.00 ~\pm~ 0.00$
15-oxo LXA4	$0.00 \hspace{0.1cm} \pm \hspace{0.1cm} 0.00$	0.00 ± 0.00	$0.00 ~\pm~ 0.00$	0.00 ± 0.00	0.00 ± 0.00	0.00 ± 0.00	0.00 ± 0.00	$0.00 ~\pm~ 0.00$
LXA5	0.00 ± 0.00	0.00 ± 0.00	0.00 ± 0.00	0.00 ± 0.00	0.00 ± 0.00	0.00 ± 0.00	0.00 ± 0.00	0.00 ± 0.00
LXB4	0.00 ± 0.00	0.00 ± 0.00	0.00 ± 0.00	0.00 ± 0.00	0.00 ± 0.00	0.00 ± 0.00	0.00 ± 0.00	0.00 ± 0.00
12-OxoETE	$0.00 \hspace{0.1cm} \pm \hspace{0.1cm} 0.00$	0.00 ± 0.00	$0.00 ~\pm~ 0.00$	0.19 ± 0.19	0.00 ± 0.00	0.00 ± 0.00	0.00 ± 0.00	$0.00 ~\pm~ 0.00$
15-OxoETE	0.03 ± 0.03	0.15 ± 0.01	$0.27 ~\pm~ 0.04$	0.47 ± 0.01	0.27 ± 0.00	0.22 ± 0.03	0.21 ± 0.03	1.06 ± 0.73
5-oxoETE	0.03 ± 0.03	0.00 ± 0.00	1.30 ± 0.05	2.28 ± 0.07	0.07 ± 0.04	0.05 ± 0.02	0.77 ± 0.08	1.11 ± 0.43
PGE2	$0.68 ~\pm~ 0.04$	3.68 ± 0.17	22.90 ± 0.66	44.06 ± 2.57	0.58 ± 0.05	1.48 ± 0.01	12.52 ± 1.04	13.89 ± 2.09
15-keto PGE2	0.01 ± 0.01	0.00 ± 0.00	0.16 ± 0.00	0.35 ± 0.03	0.01 ± 0.01	0.00 ± 0.00	0.11 ± 0.02	0.11 ± 0.06
13,14dh-15k- PGE2	$0.05 ~\pm~ 0.05$	0.00 ± 0.00	0.91 ± 0.02	1.76 ± 0.09	0.00 ± 0.00	0.00 ± 0.00	0.50 ± 0.03	0.53 ± 0.10
Bicyclo PGE2	$0.00 \hspace{0.1cm} \pm \hspace{0.1cm} 0.00$	$0.02~\pm~0.01$	$0.24 ~\pm~ 0.01$	0.46 ± 0.02	$0.00~\pm~0.00$	0.00 ± 0.00	0.11 ± 0.02	0.14 ± 0.01
PGA2	0.11 ± 0.03	0.60 ± 0.05	1.66 ± 0.85	6.50 ± 0.45	0.05 ± 0.03	0.18 ± 0.02	0.97 ± 0.48	1.87 ± 0.11
19(R)-OH PGE2 & 20-OH PGE2	0.00 ± 0.00	0.00 ± 0.00	0.00 ± 0.00	0.00 ± 0.00	0.00 ± 0.00	0.00 ± 0.00	$0.00 ~\pm~ 0.00$	0.00 ± 0.00
tetranor PGEM	$0.00 \hspace{0.1cm} \pm \hspace{0.1cm} 0.00$	$0.01 ~\pm~ 0.00$	$0.00 ~\pm~ 0.00$	0.01 ± 0.00	$0.00~\pm~0.00$	0.01 ± 0.00	$0.01 \hspace{0.1cm} \pm \hspace{0.1cm} 0.00$	$0.00 ~\pm~ 0.00$
PGD2	$0.32 \ \pm \ 0.04$	1.61 ± 0.10	7.42 ± 0.14	21.64 ± 0.98	$0.22~\pm~0.01$	0.48 ± 0.00	4.14 ± 0.03	6.73 ± 0.84
PGJ2	$0.04 \hspace{0.1cm} \pm \hspace{0.1cm} 0.02$	0.43 ± 0.04	1.61 ± 0.13	4.79 ± 0.34	0.05 ± 0.01	0.14 ± 0.02	0.96 ± 0.02	1.29 ± 0.08
D12-PGJ2	0.00 ± 0.00	0.10 ± 0.00	0.49 ± 0.03	1.32 ± 0.02	0.01 ± 0.01	0.01 ± 0.01	0.28 ± 0.01	$0.42 ~\pm~ 0.07$
15d-D12,14-PGJ2	0.00 ± 0.00	0.00 ± 0.00	0.01 ± 0.01	0.09 ± 0.01	0.00 ± 0.00	0.01 ± 0.01	0.01 ± 0.01	0.02 ± 0.01
13,14dh-15k- PGD2	$0.08 ~\pm~ 0.04$	0.19 ± 0.03	1.45 ± 0.09	2.59 ± 0.20	0.06 ± 0.03	0.11 ± 0.01	0.69 ± 0.11	0.84 ± 0.18
PGF2a	$0.05 \hspace{0.1cm} \pm \hspace{0.1cm} 0.02$	$0.39~\pm~0.01$	$1.67 ~\pm~ 0.06$	$2.77 \pm \ 0.14$	$0.04~\pm~0.02$	0.08 ± 0.04	$0.76 ~\pm~ 0.05$	0.83 ± 0.11
15-keto PGF2a	$0.01 \hspace{0.1cm} \pm \hspace{0.1cm} 0.01$	$0.17~\pm~0.02$	$0.99 ~\pm~ 0.04$	1.99 ± 0.14	$0.01 ~\pm~ 0.01$	0.06 ± 0.01	$0.57 ~\pm~ 0.07$	$0.69 ~\pm~ 0.05$

Table S4.4 (cont'd)

$0.03 \hspace{0.1cm} \pm \hspace{0.1cm} 0.01$	$0.00~\pm~0.00$	0.01 ± 0.01	$0.00 \pm \ 0.00$	$0.00~\pm~0.00$	0.00 ± 0.00	$0.00 ~\pm~ 0.00$	$0.00 ~\pm~ 0.00$
$0.02 ~\pm~ 0.01$	$0.02 ~\pm~ 0.00$	$0.00 ~\pm~ 0.00$	0.02 ± 0.01	$0.00~\pm~0.00$	0.03 ± 0.00	$0.04 ~\pm~ 0.02$	$0.00 ~\pm~ 0.00$
$0.00 ~\pm~ 0.00$	0.00 ± 0.00	$0.04 ~\pm~ 0.02$	0.09 ± 0.01	0.00 ± 0.00	0.00 ± 0.00	0.01 ± 0.01	0.00 ± 0.00
$0.04 \hspace{0.1cm} \pm \hspace{0.1cm} 0.02$	$0.00~\pm~0.00$	$0.05 ~\pm~ 0.01$	0.05 ± 0.00	$0.03~\pm~0.00$	0.01 ± 0.01	$0.00 ~\pm~ 0.00$	$0.02 \ \pm \ 0.01$
$0.00 ~\pm~ 0.00$	$0.00~\pm~0.00$	$0.00 ~\pm~ 0.00$	0.00 ± 0.00	$0.00~\pm~0.00$	0.00 ± 0.00	$0.00 ~\pm~ 0.00$	$0.00 ~\pm~ 0.00$
$0.00 \hspace{0.1cm} \pm \hspace{0.1cm} 0.00$	$0.00~\pm~0.00$	$0.00~\pm~0.00$	0.00 ± 0.00	$0.00~\pm~0.00$	$0.00 \hspace{0.1cm} \pm \hspace{0.1cm} 0.00$	$0.00 ~\pm~ 0.00$	$0.00 ~\pm~ 0.00$
$0.48 \hspace{0.1cm} \pm \hspace{0.1cm} 0.09$	3.94 ± 0.21	$18.92 ~\pm~ 1.08$	$33.89 \hspace{0.2cm} \pm \hspace{0.2cm} 0.82$	$0.37~\pm~0.03$	0.89 ± 0.01	$9.23 ~\pm~ 0.50$	$10.49~\pm~0.83$
$0.00 ~\pm~ 0.00$	$0.00~\pm~0.00$	$0.00 ~\pm~ 0.00$	$0.02 \pm \ 0.02$	$0.00~\pm~0.00$	0.00 ± 0.00	$0.00 ~\pm~ 0.00$	$0.00 ~\pm~ 0.00$
$0.00 \hspace{0.1cm} \pm \hspace{0.1cm} 0.00$	$0.00~\pm~0.00$	$0.00 ~\pm~ 0.00$	$0.00 \pm \ 0.00$	$0.00~\pm~0.00$	$0.00 \hspace{0.1cm} \pm \hspace{0.1cm} 0.00$	$0.00 ~\pm~ 0.00$	$0.00 ~\pm~ 0.00$
$0.00 ~\pm~ 0.00$	$0.00~\pm~0.00$	$0.00 ~\pm~ 0.00$	0.00 \pm 0.00	$0.00~\pm~0.00$	0.00 ± 0.00	$0.00 ~\pm~ 0.00$	$0.00 ~\pm~ 0.00$
0.00 ± 0.00	$0.00~\pm~0.00$	0.01 ± 0.01	0.02 ± 0.00	0.00 ± 0.00	0.01 ± 0.01	0.00 ± 0.00	0.01 ± 0.01
$0.00 ~\pm~ 0.00$	$0.00~\pm~0.00$	$0.00~\pm~0.00$	$0.04 \pm \ 0.01$	0.00 ± 0.00	0.00 ± 0.00	$0.02 ~\pm~ 0.01$	$0.00 ~\pm~ 0.00$
$0.00 ~\pm~ 0.00$	$0.00~\pm~0.00$	$0.00 ~\pm~ 0.00$	$0.00 \pm \ 0.00$	$0.00~\pm~0.00$	$0.00 \hspace{0.2cm} \pm \hspace{0.2cm} 0.00$	$0.00 ~\pm~ 0.00$	$0.00 ~\pm~ 0.00$
$0.05 \hspace{0.1cm} \pm \hspace{0.1cm} 0.00$	$0.06~\pm~0.01$	0.10 ± 0.01	$0.09 \pm \ 0.00$	$0.12~\pm~0.01$	0.24 ± 0.01	$0.21 ~\pm~ 0.01$	$0.10 ~\pm~ 0.05$
$0.00 \hspace{0.1cm} \pm \hspace{0.1cm} 0.00$	$0.00~\pm~0.00$	0.09 ± 0.01	$0.19 \pm \ 0.02$	$0.00~\pm~0.00$	$0.00 \hspace{0.1cm} \pm \hspace{0.1cm} 0.00$	$0.00 ~\pm~ 0.00$	0.11 ± 0.06
$0.08 \hspace{0.1cm} \pm \hspace{0.1cm} 0.00$	$0.21~\pm~0.01$	0.11 ± 0.01	$0.13 \pm \ 0.01$	$0.70~\pm~0.02$	$0.26 \hspace{0.2cm} \pm \hspace{0.2cm} 0.01$	$0.65 ~\pm~ 0.03$	$0.40 ~\pm~ 0.05$
$0.23 \hspace{0.1cm} \pm \hspace{0.1cm} 0.01$	0.17 ± 0.01	0.59 ± 0.06	$0.49 \pm \ 0.04$	$0.48~\pm~0.04$	1.38 ± 0.03	$0.91 ~\pm~ 0.05$	$0.68 ~\pm~ 0.08$
$0.33 \hspace{0.1cm} \pm \hspace{0.1cm} 0.07$	$0.41~\pm~0.03$	$0.84 ~\pm~ 0.06$	$0.77 \pm \ 0.08$	$1.30~\pm~0.01$	1.76 ± 0.15	1.85 ± 0.05	1.28 ± 0.19
$0.25 \hspace{0.1cm} \pm \hspace{0.1cm} 0.03$	$0.53~\pm~0.15$	3.83 ± 0.02	4.94 ± 0.30	$0.70~\pm~0.04$	1.06 ± 0.10	7.57 ± 0.05	6.35 ± 1.25
$0.80 ~\pm~ 0.06$	$0.67~\pm~0.05$	$1.26 ~\pm~ 0.06$	$1.13 \pm \ 0.04$	$1.45~\pm~0.05$	1.91 ± 0.05	$2.29 ~\pm~ 0.12$	1.64 ± 0.17
$2.34 ~\pm~ 0.20$	$0.80~\pm~0.10$	2.86 ± 0.12	$2.43 \pm \ 0.05$	$4.47~\pm~0.09$	3.50 ± 0.12	$4.46 \ \pm \ 0.18$	3.38 ± 0.23
0.21 ± 0.03	$0.25~\pm~0.13$	$0.43 ~\pm~ 0.06$	0.38 ± 0.01	0.93 ± 0.03	1.03 ± 0.07	1.24 ± 0.05	0.85 ± 0.05
$0.17 \hspace{0.1cm} \pm \hspace{0.1cm} 0.08$	$0.40~\pm~0.02$	$1.35 ~\pm~ 0.05$	$1.41 \pm \ 0.02$	0.56 ± 0.03	0.87 ± 0.05	1.78 ± 0.10	1.28 ± 0.31
$0.00 ~\pm~ 0.00$	$0.00~\pm~0.00$	$0.00 ~\pm~ 0.00$	$0.00 \pm \ 0.00$	$0.01 ~\pm~ 0.01$	$0.00 \hspace{0.1cm} \pm \hspace{0.1cm} 0.00$	$0.00 ~\pm~ 0.00$	$0.00 ~\pm~ 0.00$
$0.00 \hspace{0.1cm} \pm \hspace{0.1cm} 0.00$	$0.00~\pm~0.00$	$0.06 ~\pm~ 0.03$	$0.07 \pm \ 0.04$	$0.00~\pm~0.00$	0.00 ± 0.00	0.14 ± 0.02	$0.09 ~\pm~ 0.04$
	0.02 ± 0.01 0.00 ± 0.00 0.04 ± 0.02 0.00 ± 0.00 0.48 ± 0.09 0.00 ± 0.00 0.05 ± 0.00 0.08 ± 0.00 0.08 ± 0.00 0.23 ± 0.01 0.33 ± 0.07 0.25 ± 0.03 0.80 ± 0.06 2.34 ± 0.20 0.21 ± 0.03 0.17 ± 0.08 0.00 ± 0.00	0.02 ± 0.01 0.02 ± 0.00 0.00 ± 0.00 0.04 ± 0.00 0.00 ± 0.00 0.48 ± 0.09 0.00 ± 0.00 0.00	$\begin{array}{cccccccccccccccccccccccccccccccccccc$	$\begin{array}{cccccccccccccccccccccccccccccccccccc$	$\begin{array}{cccccccccccccccccccccccccccccccccccc$	$\begin{array}{cccccccccccccccccccccccccccccccccccc$	$\begin{array}{cccccccccccccccccccccccccccccccccccc$

Table S4.4 (cont'd)

PGD3	0.00 ± 0.00	0.00 ± 0.00	0.00 ± 0.00	0.00 ± 0.00	0.00 ± 0.00	0.00 ± 0.00	0.00 ± 0.00	0.00 ± 0.00
15d-D12,14-PGJ3	0.00 ± 0.00	0.00 ± 0.00	0.00 ± 0.00	0.00 ± 0.00	0.00 ± 0.00	0.00 ± 0.00	0.00 ± 0.00	0.00 ± 0.00
PGF3a	0.00 ± 0.00	0.00 ± 0.00	0.00 ± 0.00	0.00 ± 0.00	0.00 ± 0.00	0.00 ± 0.00	0.01 ± 0.01	0.04 ± 0.04
RvE1	0.00 ± 0.00	0.00 ± 0.00	0.00 ± 0.00	0.00 ± 0.00	$0.00~\pm~0.00$	0.00 ± 0.00	0.00 ± 0.00	0.00 ± 0.00
RvE2	0.03 ± 0.01	0.01 ± 0.01	0.04 ± 0.00	0.04 ± 0.00	0.03 ± 0.00	0.02 ± 0.00	0.03 ± 0.01	0.02 ± 0.01
RvE3	$0.00 \hspace{0.1cm} \pm \hspace{0.1cm} 0.00$	$0.00~\pm~0.00$	$0.00 ~\pm~ 0.00$	0.00 ± 0.00	$0.00~\pm~0.00$	0.00 ± 0.00	$0.02 \ \pm \ 0.02$	$0.01 \hspace{0.1cm} \pm \hspace{0.1cm} 0.01$
TXB3	$0.00 \hspace{0.1cm} \pm \hspace{0.1cm} 0.00$	$0.02~\pm~0.02$	$0.06 ~\pm~ 0.00$	0.14 ± 0.02	$0.00~\pm~0.00$	0.00 ± 0.00	0.11 ± 0.02	$0.12 \hspace{0.1cm} \pm \hspace{0.1cm} 0.01$
11dh TXB3	$0.00 \hspace{0.1cm} \pm \hspace{0.1cm} 0.00$	$0.00~\pm~0.00$	$0.00 ~\pm~ 0.00$	0.00 ± 0.00	$0.00~\pm~0.00$	0.00 ± 0.00	$0.00 ~\pm~ 0.00$	$0.00 ~\pm~ 0.00$
MaR1(ω-3DPA)	$0.15 \hspace{0.1cm} \pm \hspace{0.1cm} 0.01$	$0.00~\pm~0.00$	$0.22 \ \pm \ 0.01$	$0.22 \pm \ 0.02$	$0.55~\pm~0.03$	0.41 ± 0.04	$0.72 \ \pm \ 0.06$	$0.56 ~\pm~ 0.07$
PD1(ω-3, DPA)	$0.00 \hspace{0.1cm} \pm \hspace{0.1cm} 0.00$	$0.00~\pm~0.00$	$0.00 ~\pm~ 0.00$	0.00 ± 0.00	$0.00~\pm~0.00$	0.00 ± 0.00	$0.00 ~\pm~ 0.00$	$0.00 ~\pm~ 0.00$
RvD5(ω-3DPA) (7,17-DiHDoPE)	0.00 ± 0.00	$0.00~\pm~0.00$	$0.00 ~\pm~ 0.00$	0.00 \pm 0.00	$0.00~\pm~0.00$	0.00 \pm 0.00	$0.00 ~\pm~ 0.00$	$0.00 ~\pm~ 0.00$
19,20-DiHDoPE	$0.47 \hspace{0.1cm} \pm \hspace{0.1cm} 0.07$	$0.97~\pm~0.05$	$0.47 ~\pm~ 0.02$	0.40 ± 0.03	$4.74~\pm~0.05$	1.31 ± 0.07	3.49 ± 0.30	$2.44 \ \pm \ 0.54$
7(8)-EpDPE	$0.00 \hspace{0.1cm} \pm \hspace{0.1cm} 0.00$	$0.00~\pm~0.00$	$0.04 ~\pm~ 0.00$	0.03 ± 0.00	$0.03~\pm~0.00$	0.04 ± 0.00	$0.06 ~\pm~ 0.00$	$0.02 \ \pm \ 0.02$
10(11)-EpDPE	$0.01 \hspace{0.1cm} \pm \hspace{0.1cm} 0.01$	$0.00~\pm~0.00$	$0.08 ~\pm~ 0.00$	0.07 ± 0.03	$0.12~\pm~0.01$	0.11 ± 0.02	$0.22 \ \pm \ 0.02$	$0.24 \ \pm \ 0.01$
13(14)-EpDPE	$0.00 \hspace{0.1cm} \pm \hspace{0.1cm} 0.00$	$0.00~\pm~0.00$	$0.00 ~\pm~ 0.00$	0.00 ± 0.00	$0.02~\pm~0.02$	0.00 ± 0.00	$0.05 ~\pm~ 0.05$	$0.00 ~\pm~ 0.00$
16(17)-EpDPE	$0.00 \hspace{0.1cm} \pm \hspace{0.1cm} 0.00$	$0.00~\pm~0.00$	$0.00 ~\pm~ 0.00$	0.00 ± 0.00	$0.10~\pm~0.01$	0.00 ± 0.00	$0.04 \hspace{0.1cm} \pm \hspace{0.1cm} 0.04$	$0.11 \hspace{0.1cm} \pm \hspace{0.1cm} 0.06$
19(20)-EpDPE	$0.08 \hspace{0.1cm} \pm \hspace{0.1cm} 0.00$	$0.29~\pm~0.01$	$0.24 ~\pm~ 0.00$	$0.24 \pm \ 0.01$	$1.95~\pm~0.05$	0.71 ± 0.05	2.47 ± 0.12	$1.73 \hspace{0.1cm} \pm \hspace{0.1cm} 0.28$
14-HDoHE	$0.06 \hspace{0.1cm} \pm \hspace{0.1cm} 0.03$	$0.03~\pm~0.03$	$0.75 ~\pm~ 0.08$	$0.73 \pm \ 0.03$	$2.02~\pm~0.71$	3.12 ± 1.22	$4.04 \hspace{0.1cm} \pm \hspace{0.1cm} 0.18$	3.59 ± 0.87
17-HDoHE	$0.03 \hspace{0.1cm} \pm \hspace{0.1cm} 0.03$	$0.05~\pm~0.05$	$0.28 ~\pm~ 0.04$	0.22 ± 0.03	$0.45~\pm~0.45$	1.08 ± 0.45	1.36 ± 0.07	$1.04 \hspace{0.1cm} \pm \hspace{0.1cm} 0.53$
4-HDoHE	$0.44 \hspace{0.1cm} \pm \hspace{0.1cm} 0.02$	1.10 ± 0.03	$2.56 ~\pm~ 0.08$	2.42 ± 0.05	$7.96~\pm~0.78$	13.39 ± 2.59	16.71 ± 0.45	15.18 ± 2.99
7-HDoHE	$0.20 \hspace{0.1cm} \pm \hspace{0.1cm} 0.01$	$0.20~\pm~0.02$	$1.26 ~\pm~ 0.01$	1.69 ± 0.16	$1.53~\pm~0.22$	2.18 ± 0.36	11.01 ± 0.53	$7.30 ~\pm~ 1.20$
8-HDoHE	$0.54 \hspace{0.1cm} \pm \hspace{0.1cm} 0.05$	0.61 ± 0.03	1.42 ± 0.11	1.15 ± 0.14	$5.04~\pm~0.62$	6.03 ± 1.38	8.61 ± 0.28	$6.99 \hspace{0.1cm} \pm \hspace{0.1cm} 1.33$
10-HDoHE	$0.15 \hspace{0.1cm} \pm \hspace{0.1cm} 0.01$	0.16 ± 0.01	$1.36 ~\pm~ 0.05$	1.16 ± 0.05	2.57 ± 0.71	4.04 ± 1.56	6.91 ± 0.27	5.57 ± 1.10
11-HDoHE	0.16 ± 0.01	0.26 ± 0.01	1.14 ± 0.02	1.07 ± 0.10	3.55 ± 0.70	4.61 ± 1.30	7.60 ± 0.16	6.05 ± 1.06
13-НДоНЕ	0.13 ± 0.01	0.12 ± 0.01	1.27 ± 0.04	1.20 ± 0.04	3.14 ± 1.08	4.41 ± 1.50	6.96 ± 0.35	5.74 ± 2.07
16-НДоНЕ	0.64 ± 0.02	$0.39~\pm~0.05$	1.35 ± 0.06	1.23 ± 0.04	6.57 ± 1.58	9.63 ± 3.05	8.62 ± 0.32	8.58 ± 1.78
20-НДоНЕ	1.01 ± 0.02	$0.55~\pm~0.04$	3.59 ± 0.12	3.08 ± 0.17	9.96 ± 1.67	10.5 ± 2.90	17.43 ± 0.46	11.48 ± 5.82

Table S4.4 (cont'd)

Maresin1	$0.00 \hspace{0.1cm} \pm \hspace{0.1cm} 0.00$	$0.00~\pm~0.00$	$0.01 ~\pm~ 0.01$	0.00 ± 0.00	$0.00~\pm~0.00$	0.00 ± 0.00	$0.00~\pm~0.00$	$0.00 ~\pm~ 0.00$
7(S)-Maresin1	$0.00 \hspace{0.1cm} \pm \hspace{0.1cm} 0.00$	$0.00~\pm~0.00$	$0.00 ~\pm~ 0.00$	0.00 ± 0.00	$0.00~\pm~0.00$	0.00 ± 0.00	$0.00 ~\pm~ 0.00$	$0.00 ~\pm~ 0.00$
PD1	$0.03 \hspace{0.1cm} \pm \hspace{0.1cm} 0.02$	$0.00~\pm~0.00$	$0.00 ~\pm~ 0.00$	0.00 ± 0.00	$0.02~\pm~0.02$	0.00 ± 0.00	$0.01 \hspace{0.1cm} \pm \hspace{0.1cm} 0.01$	$0.02 \ \pm \ 0.02$
AT-PD1	$0.00 \hspace{0.1cm} \pm \hspace{0.1cm} 0.00$	$0.00~\pm~0.00$	$0.00 ~\pm~ 0.00$	0.01 ± 0.01	$0.00~\pm~0.00$	0.00 ± 0.00	$0.00 ~\pm~ 0.00$	$0.00 ~\pm~ 0.00$
10S,17S- DiHDoHE	0.00 ± 0.00	0.00 ± 0.00	0.00 ± 0.00	0.00 ± 0.00	0.00 ± 0.00	0.00 ± 0.00	0.00 ± 0.00	0.10 ± 0.10
22-OH-PD1	$0.00 \hspace{0.1cm} \pm \hspace{0.1cm} 0.00$	$0.00~\pm~0.00$	$0.00 ~\pm~ 0.00$	0.00 \pm 0.00	$0.00~\pm~0.00$	0.00 ± 0.00	$0.00 ~\pm~ 0.00$	$0.00 ~\pm~ 0.00$
RvD1 & AT-RvD1	$0.00 \hspace{0.1cm} \pm \hspace{0.1cm} 0.00$	$0.00~\pm~0.00$	$0.00 ~\pm~ 0.00$	0.00 \pm 0.00	$0.00~\pm~0.00$	0.00 ± 0.00	$0.00 ~\pm~ 0.00$	$0.00 ~\pm~ 0.00$
RvD2	$0.00 \hspace{0.1cm} \pm \hspace{0.1cm} 0.00$	$0.00~\pm~0.00$	$0.00 ~\pm~ 0.00$	0.00 \pm 0.00	$0.00~\pm~0.00$	0.00 ± 0.00	$0.00 ~\pm~ 0.00$	$0.03 \hspace{0.1cm} \pm \hspace{0.1cm} 0.03$
RvD3	$0.01 \hspace{0.1cm} \pm \hspace{0.1cm} 0.01$	0.00 ± 0.00	$0.00 ~\pm~ 0.00$	0.00 \pm 0.00	$0.05~\pm~0.02$	0.00 ± 0.00	$0.00 ~\pm~ 0.00$	$0.00 ~\pm~ 0.00$
AT-RvD3	$0.03 \hspace{0.1cm} \pm \hspace{0.1cm} 0.03$	$0.04~\pm~0.00$	$0.06 ~\pm~ 0.01$	$0.02 \pm \ 0.02$	$0.00~\pm~0.00$	0.02 ± 0.02	$0.03 \ \pm \ 0.03$	$0.08 ~\pm~ 0.05$
RvD4	$0.00 \hspace{0.1cm} \pm \hspace{0.1cm} 0.00$	$0.00~\pm~0.00$	$0.00 ~\pm~ 0.00$	0.00 \pm 0.00	$0.00~\pm~0.00$	0.00 ± 0.00	$0.01 \hspace{0.1cm} \pm \hspace{0.1cm} 0.01$	$0.01 \hspace{0.1cm} \pm \hspace{0.1cm} 0.01$
RvD5	$0.00 \hspace{0.1cm} \pm \hspace{0.1cm} 0.00$	0.00 ± 0.00	$0.00 ~\pm~ 0.00$	0.00 \pm 0.00	$0.00~\pm~0.00$	0.00 ± 0.00	$0.00 ~\pm~ 0.00$	$0.00 ~\pm~ 0.00$
RvD6 (4,17- DiHDoHE)	$0.06 ~\pm~ 0.01$	$0.02~\pm~0.00$	$0.10 ~\pm~ 0.00$	0.09 ± 0.01	0.18 ± 0.01	0.12 ± 0.01	$0.22 ~\pm~ 0.02$	0.18 ± 0.03
8-oxoRvD1	$0.00 \hspace{0.1cm} \pm \hspace{0.1cm} 0.00$	$0.00~\pm~0.00$	$0.00 ~\pm~ 0.00$	0.00 ± 0.00	$0.00~\pm~0.00$	0.00 ± 0.00	$0.00 ~\pm~ 0.00$	$0.00 ~\pm~ 0.00$
17-oxoRvD1	$0.00 ~\pm~ 0.00$	$0.00~\pm~0.00$	$0.00 ~\pm~ 0.00$	$0.00 \pm \ 0.00$	$0.00~\pm~0.00$	$0.00 \hspace{0.1cm} \pm \hspace{0.1cm} 0.00$	$0.00 ~\pm~ 0.00$	$0.00 ~\pm~ 0.00$

Data are presented in units of pmol/culture as mean \pm SEM.

Table S4.5. Combined intracellular and extracellular oxylipin content at t = 6 h.

Oxylipin	VEH/VEH	LPS/VEH	VEH/cSiO ₂	LPS/cSiO ₂	DHA- VEH/VEH	DHA- LPS/VEH	DHA- VEH/cSiO ₂	DHA- LPS/cSiO ₂
9,10-DiHOME	$0.01 \hspace{0.1cm} \pm \hspace{0.1cm} 0.01$	0.14 ± 0.12	0.06 ± 0.02	$0.04 \pm \ 0.00$	$0.03 \hspace{0.1cm} \pm \hspace{0.1cm} 0.01$	$0.07 \hspace{0.1cm} \pm \hspace{0.1cm} 0.03$	0.07 ± 0.03	$0.06 ~\pm~ 0.00$
12,13-DiHOME	0.01 ± 0.01	0.10 ± 0.05	$0.05 \hspace{0.2cm} \pm \hspace{0.2cm} 0.02$	0.02 ± 0.01	$0.02 \hspace{0.1cm} \pm \hspace{0.1cm} 0.00$	$0.04 ~\pm~ 0.02$	0.05 ± 0.01	$0.03 \hspace{0.1cm} \pm \hspace{0.1cm} 0.02$
9(10)-EpOME	$0.17 \hspace{0.1cm} \pm \hspace{0.1cm} 0.02$	$0.98 \hspace{0.2in} \pm \hspace{0.2in} 0.50$	$0.00 \hspace{0.2cm} \pm \hspace{0.2cm} 0.00$	0.18 ± 0.09	$0.16 \hspace{0.1cm} \pm \hspace{0.1cm} 0.02$	0.55 ± 0.11	0.37 ± 0.24	0.31 ± 0.16
12(13)-EpOME	0.09 ± 0.01	0.72 ± 0.29	0.49 ± 0.30	0.09 ± 0.04	$0.06 \hspace{0.1cm} \pm \hspace{0.1cm} 0.03$	0.22 ± 0.15	0.54 ± 0.23	0.19 ± 0.19
9-HODE	$1.86 ~\pm~ 0.28$	29.94 ± 14.65	7.10 ± 3.07	3.45 ± 0.50	$1.42 \hspace{0.1cm} \pm \hspace{0.1cm} 0.49$	3.46 ± 0.82	8.58 ± 2.84	6.22 ± 2.24
13-HODE	6.70 ± 1.02	117.71 ± 57.50	26.58 ± 11.06	13.24 ± 1.00	5.54 ± 1.46	$12.24~\pm~0.94$	32.24 ± 9.90	21.04 ± 5.37
9-OxoODE	$1.26 ~\pm~ 0.23$	4.19 ± 1.49	4.82 ± 3.13	2.01 ± 0.14	$0.97 \hspace{0.1cm} \pm \hspace{0.1cm} 0.23$	3.35 ± 0.89	5.73 ± 2.19	4.30 ± 1.16
13-OxoODE	1.88 ± 0.39	23.73 ± 10.74	9.67 ± 6.20	2.63 ± 0.28	1.53 ± 0.35	5.83 ± 1.51	11.65 ± 5.69	7.22 ± 2.91
13(S)-HOTrE	$0.09 ~\pm~ 0.05$	0.03 ± 0.03	$0.06 \hspace{0.2cm} \pm \hspace{0.2cm} 0.06$	0.07 ± 0.04	$0.05 \hspace{0.1cm} \pm \hspace{0.1cm} 0.05$	$0.07 \hspace{0.1cm} \pm \hspace{0.1cm} 0.03$	0.17 ± 0.10	$0.00 ~\pm~ 0.00$
13(S)-HOTrE(g)	$0.00 ~\pm~ 0.00$	$0.00 \hspace{0.2cm} \pm \hspace{0.2cm} 0.00$	0.89 ± 0.13	0.88 ± 0.05	$0.00 \hspace{0.1cm} \pm \hspace{0.1cm} 0.00$	0.13 ± 0.13	0.76 ± 0.39	$0.28 ~\pm~ 0.28$
9(S)-HOTrE	$0.07 ~\pm~ 0.07$	1.83 ± 1.80	0.02 ± 0.02	$0.04 \pm \ 0.04$	$0.06 \hspace{0.1cm} \pm \hspace{0.1cm} 0.03$	$0.09 ~\pm~ 0.05$	0.09 ± 0.06	0.06 ± 0.03
9-OxoOTrE	$0.00 ~\pm~ 0.00$	0.01 ± 0.01	$0.00 \hspace{0.2cm} \pm \hspace{0.2cm} 0.00$	0.00 ± 0.00	$0.00 \hspace{0.1cm} \pm \hspace{0.1cm} 0.00$	$0.00 ~\pm~ 0.00$	0.00 \pm 0.00	0.01 ± 0.01
11(R)-HEDE	$0.00 ~\pm~ 0.00$	$0.00 \hspace{0.2cm} \pm \hspace{0.2cm} 0.00$	0.43 ± 0.04	0.40 ± 0.03	$0.02 \hspace{0.1cm} \pm \hspace{0.1cm} 0.01$	$0.01 \hspace{0.1cm} \pm \hspace{0.1cm} 0.01$	0.26 ± 0.02	$0.22 ~\pm~ 0.02$
15(S)-HEDE	$0.00 ~\pm~ 0.00$	$0.00 \hspace{0.2cm} \pm \hspace{0.2cm} 0.00$	$0.00 \hspace{0.2cm} \pm \hspace{0.2cm} 0.00$	0.09 ± 0.04	$0.00 \hspace{0.1cm} \pm \hspace{0.1cm} 0.00$	$0.01 \hspace{0.1cm} \pm \hspace{0.1cm} 0.01$	0.10 ± 0.01	$0.09 ~\pm~ 0.02$
15-OxoEDE	$0.00 ~\pm~ 0.00$	$0.00 \hspace{0.2cm} \pm \hspace{0.2cm} 0.00$	$0.00 \hspace{0.2cm} \pm \hspace{0.2cm} 0.00$	0.01 ± 0.01	$0.00 \hspace{0.1cm} \pm \hspace{0.1cm} 0.00$	$0.00 ~\pm~ 0.00$	0.00 \pm 0.00	$0.00 ~\pm~ 0.00$
8(S)-HETrE	$0.07 \hspace{0.1cm} \pm \hspace{0.1cm} 0.04$	0.15 ± 0.11	3.57 ± 0.19	$3.89 \pm \ 0.04$	$0.14 \hspace{0.1cm} \pm \hspace{0.1cm} 0.02$	$0.10 \hspace{0.1cm} \pm \hspace{0.1cm} 0.02$	3.91 ± 0.33	3.10 ± 0.06
5(S)-HETrE	$0.06 ~\pm~ 0.03$	0.07 ± 0.01	4.16 ± 0.22	5.64 ± 0.16	$0.04 \hspace{0.1cm} \pm \hspace{0.1cm} 0.00$	$0.03 ~\pm~ 0.00$	1.84 ± 0.05	1.60 ± 0.15
13,14dhPGE1	0.00 ± 0.00	0.00 ± 0.00	0.00 ± 0.00	0.00 ± 0.00	0.00 ± 0.00	0.00 ± 0.00	0.00 ± 0.00	0.00 ± 0.00
13,14dh-15k- PGE1	0.00 ± 0.00	0.00 \pm 0.00	0.04 ± 0.00	0.05 ± 0.01	0.00 ± 0.00	$0.00 ~\pm~ 0.00$	0.01 ± 0.01	$0.02 ~\pm~ 0.01$
D17-PGE1	0.00 ± 0.00	0.00 ± 0.00	0.00 ± 0.00	$0.00 \pm \ 0.00$	$0.00 \hspace{0.1cm} \pm \hspace{0.1cm} 0.00$	$0.00 ~\pm~ 0.00$	$0.00 \pm \ 0.00$	$0.00 ~\pm~ 0.00$
PGE1	$0.00 ~\pm~ 0.00$	0.00 ± 0.00	0.21 ± 0.10	$0.13 \pm \ 0.13$	$0.00 \hspace{0.1cm} \pm \hspace{0.1cm} 0.00$	$0.02 \hspace{0.2cm} \pm \hspace{0.2cm} 0.02$	0.12 ± 0.06	$0.00 ~\pm~ 0.00$
15(R)-PGE1	$0.33 ~\pm~ 0.04$	0.21 ± 0.06	0.68 ± 0.03	$0.80 \pm \ 0.00$	$0.33 \hspace{0.1cm} \pm \hspace{0.1cm} 0.07$	0.34 ± 0.07	0.44 ± 0.02	0.33 ± 0.17
15-keto PGE1	$0.00 ~\pm~ 0.00$	$0.00 \hspace{0.2cm} \pm \hspace{0.2cm} 0.00$	$0.00 \hspace{0.2cm} \pm \hspace{0.2cm} 0.00$	0.00 ± 0.00	$0.00 \hspace{0.1cm} \pm \hspace{0.1cm} 0.00$	$0.00 ~\pm~ 0.00$	0.00 ± 0.00	$0.00 ~\pm~ 0.00$
Bicyclo PGE1	$0.08 ~\pm~ 0.08$	0.23 ± 0.01	0.25 ± 0.02	0.14 ± 0.07	0.21 ± 0.06	0.17 ± 0.03	0.42 ± 0.01	0.14 ± 0.14
19(R)-hydroxy PGE1	0.00 ± 0.00	0.00 ± 0.00	0.00 ± 0.00	0.00 ± 0.00	0.00 ± 0.00	$0.00 ~\pm~ 0.00$	0.00 ± 0.00	$0.00 ~\pm~ 0.00$

Table S4.5 (cont'd)

2,3-dinor PGE1	$0.00 \hspace{0.1cm} \pm \hspace{0.1cm} 0.00$	0.11 ± 0.04	0.10 ± 0.03	0.00 ± 0.00	$0.00 \hspace{0.1cm} \pm \hspace{0.1cm} 0.00$	$0.14 \hspace{0.1cm} \pm \hspace{0.1cm} 0.07$	0.10 ± 0.03	$0.05 ~\pm~ 0.03$
PGF1a	$0.00 ~\pm~ 0.00$	0.00 ± 0.00	0.03 ± 0.02	0.06 ± 0.01	$0.00 \hspace{0.1cm} \pm \hspace{0.1cm} 0.00$	$0.00 ~\pm~ 0.00$	0.01 ± 0.01	$0.00 ~\pm~ 0.00$
6-keto PGE1	$0.00 \hspace{0.1cm} \pm \hspace{0.1cm} 0.00$	0.00 ± 0.00	$0.00 \hspace{0.2cm} \pm \hspace{0.2cm} 0.00$	0.00 ± 0.00	$0.00 \hspace{0.1cm} \pm \hspace{0.1cm} 0.00$	$0.00 ~\pm~ 0.00$	0.00 ± 0.00	$0.00 ~\pm~ 0.00$
5,6-DiHETrE	$0.03 \hspace{0.1cm} \pm \hspace{0.1cm} 0.01$	0.03 ± 0.02	0.25 ± 0.05	$0.24 \pm \ 0.05$	$0.04 \hspace{0.1cm} \pm \hspace{0.1cm} 0.00$	$0.02 \hspace{0.2cm} \pm \hspace{0.2cm} 0.01$	0.08 ± 0.01	$0.09 ~\pm~ 0.01$
8,9-DiHETrE	$0.02 \hspace{0.1cm} \pm \hspace{0.1cm} 0.01$	0.01 ± 0.01	0.11 ± 0.01	0.09 ± 0.00	$0.03 \hspace{0.1cm} \pm \hspace{0.1cm} 0.00$	$0.00 ~\pm~ 0.00$	0.06 ± 0.01	$0.05 ~\pm~ 0.00$
11,12-DiHETrE	$0.28 ~\pm~ 0.04$	0.11 ± 0.07	0.64 ± 0.05	0.59 ± 0.02	$0.20 \hspace{0.1cm} \pm \hspace{0.1cm} 0.02$	$0.09 \hspace{0.1cm} \pm \hspace{0.1cm} 0.01$	0.31 ± 0.01	$0.31 \ \pm \ 0.04$
14,15-DiHETrE	1.11 ± 0.10	0.41 ± 0.23	1.80 ± 0.18	1.63 ± 0.13	$0.82 \hspace{0.1cm} \pm \hspace{0.1cm} 0.07$	$0.30 ~\pm~ 0.03$	0.93 ± 0.01	0.80 ± 0.15
5(S),12(S)- DiHETE	$0.00 ~\pm~ 0.00$	0.99 ± 0.99	0.03 ± 0.00	0.00 ± 0.00	0.00 ± 0.00	$0.00 ~\pm~ 0.00$	0.01 ± 0.01	$0.02 ~\pm~ 0.00$
5(S),15(S)- DiHETE	$0.04 ~\pm~ 0.02$	0.01 ± 0.01	0.06 ± 0.02	0.06 ± 0.01	$0.08 ~\pm~ 0.04$	$0.02 ~\pm~ 0.01$	0.03 ± 0.00	$0.02 ~\pm~ 0.01$
8(S),15(S)- DiHETE	$0.00 ~\pm~ 0.00$	0.00 \pm 0.00	0.00 ± 0.00	0.00 ± 0.00	0.00 ± 0.00	$0.00 ~\pm~ 0.00$	0.00 \pm 0.00	$0.00 ~\pm~ 0.00$
5(S),6(S)-DiHETE	$0.00 ~\pm~ 0.00$	0.00 ± 0.00	$0.00 \hspace{0.2cm} \pm \hspace{0.2cm} 0.00$	0.00 ± 0.00	$0.00 \hspace{0.1cm} \pm \hspace{0.1cm} 0.00$	$0.00 ~\pm~ 0.00$	0.00 ± 0.00	0.00 ± 0.00
5(6)-EpETrE	$0.03 \hspace{0.1cm} \pm \hspace{0.1cm} 0.00$	0.03 ± 0.01	0.49 ± 0.01	$0.51 \pm \ 0.03$	$0.03 \hspace{0.1cm} \pm \hspace{0.1cm} 0.00$	$0.02 \hspace{0.2cm} \pm \hspace{0.2cm} 0.01$	$0.27 \pm \ 0.02$	$0.36 ~\pm~ 0.04$
8(9)-EpETrE	$0.00 \hspace{0.1cm} \pm \hspace{0.1cm} 0.00$	0.00 ± 0.00	$0.00 \hspace{0.2cm} \pm \hspace{0.2cm} 0.00$	0.05 ± 0.05	$0.00 \hspace{0.1cm} \pm \hspace{0.1cm} 0.00$	$0.00 ~\pm~ 0.00$	0.00 ± 0.00	$0.15 ~\pm~ 0.04$
11(12)-EpETrE	$0.08 \hspace{0.1cm} \pm \hspace{0.1cm} 0.01$	0.06 ± 0.01	0.89 ± 0.20	0.58 ± 0.30	$0.07 \hspace{0.1cm} \pm \hspace{0.1cm} 0.01$	$0.05 ~\pm~ 0.03$	0.50 ± 0.17	0.51 ± 0.27
14(15)-EpETrE	$0.02 \hspace{0.1cm} \pm \hspace{0.1cm} 0.01$	0.06 ± 0.01	0.49 ± 0.13	$0.46 \pm \ 0.03$	$0.02 \hspace{0.1cm} \pm \hspace{0.1cm} 0.01$	$0.05 \hspace{0.1cm} \pm \hspace{0.1cm} 0.01$	0.24 ± 0.14	$0.38 ~\pm~ 0.04$
12-HETE	0.73 ± 0.12	0.96 ± 0.07	21.09 ± 0.37	22.23 ± 0.82	$1.10 \hspace{0.1cm} \pm \hspace{0.1cm} 0.04$	1.15 ± 0.21	14.30 ± 0.33	12.62 ± 1.26
tetranor 12-HETE	3.22 ± 0.25	2.02 ± 0.09	3.40 ± 0.09	$3.18 \pm \ 0.08$	$4.62 \hspace{0.1cm} \pm \hspace{0.1cm} 0.18$	2.33 ± 0.15	3.75 ± 0.05	3.68 ± 0.20
15-HETE	1.68 ± 0.31	2.16 ± 1.12	60.21 ± 1.33	64.87 ± 1.47	$2.28 \hspace{0.1cm} \pm \hspace{0.1cm} 0.08$	2.21 ± 0.27	46.87 ± 3.02	38.84 ± 1.03
5-HETE	2.24 ± 0.71	1.54 ± 0.53	150.52 ± 7.16	194.93 ± 0.72	$2.35 ~\pm~ 0.06$	$2.13 ~\pm~ 0.30$	101.94 ± 6.89	95.16 ± 4.11
8-НЕТЕ	0.61 ± 0.14	0.42 ± 0.15	25.16 ± 0.28	27.59 ± 0.04	$0.77 \hspace{0.1cm} \pm \hspace{0.1cm} 0.05$	0.52 ± 0.11	15.10 ± 0.51	13.86 ± 0.82
12(S)-HHTrE	$0.23 ~\pm~ 0.23$	3.08 ± 1.83	50.65 ± 1.81	60.63 ± 1.82	$0.67 \hspace{0.1cm} \pm \hspace{0.1cm} 0.20$	2.59 ± 0.32	$28.47 \hspace{0.2cm} \pm \hspace{0.2cm} 0.36$	28.23 ± 0.64
20-НЕТЕ	1.33 ± 0.18	-0.57 ± 0.36	5.81 ± 0.19	2.84 ± 1.59	$0.49 \hspace{0.1cm} \pm \hspace{0.1cm} 0.49$	1.31 ± 0.41	3.24 ± 1.63	3.70 ± 1.85
9-НЕТЕ	$0.19 ~\pm~ 0.02$	0.21 ± 0.05	4.97 ± 0.26	5.16 ± 0.33	$0.23 \hspace{0.1cm} \pm \hspace{0.1cm} 0.01$	$0.17 \hspace{0.1cm} \pm \hspace{0.1cm} 0.04$	3.93 ± 0.21	3.55 ± 0.14
11-HETE	$2.23 ~\pm~ 0.57$	4.34 ± 2.78	116.64 ± 1.46	144.23 ± 1.98	$2.87 \hspace{0.1cm} \pm \hspace{0.1cm} 0.14$	3.87 ± 0.96	82.02 ± 0.81	76.23 ± 2.70
LTB4	$0.02 \ \pm \ 0.02$	0.00 ± 0.00	0.58 ± 0.02	1.72 ± 0.13	$0.00 \hspace{0.1cm} \pm \hspace{0.1cm} 0.00$	$0.01 \hspace{0.1cm} \pm \hspace{0.1cm} 0.01$	$0.27 \pm \ 0.02$	$0.49 ~\pm~ 0.07$
12-OxoLTB4	$0.00 ~\pm~ 0.00$	0.00 ± 0.00	$0.00 \hspace{0.2cm} \pm \hspace{0.2cm} 0.00$	0.01 ± 0.01	0.00 ± 0.00	$0.00 ~\pm~ 0.00$	0.00 ± 0.00	$0.00 ~\pm~ 0.00$

Table S4.5 (cont'd)

± 0.00 ± 0.00 ± 0.00 ± 0.02
± 0.00
+ 0.02
⊥ 0.02
$\pm~0.00$
$\pm~0.00$
± 0.00
± 0.00
± 0.32
± 0.02
± 0.14
± 1.68
± 0.01
± 0.06
± 0.02
\pm 0.36
± 0.00
$\pm~0.00$
\pm 1.42
± 0.24
\pm 0.01
\pm 0.02
± 0.10
\pm 0.04
± 0.11

Table S4.5 (cont'd)

13,14dh-15k- PGF2a	0.03 ± 0.01	0.00 ± 0.00	0.03 ± 0.03	0.02 ± 0.02	0.00 ± 0.00	0.00 ± 0.00	0.00 ± 0.00	$0.00 ~\pm~ 0.00$
19(R)-OH PGF2a & 20-OH PGF2a	$0.01 ~\pm~ 0.01$	0.02 ± 0.00	0.03 ± 0.00	0.01 ± 0.01	$0.01 \hspace{0.1cm} \pm \hspace{0.1cm} 0.01$	0.04 ± 0.01	0.02 ± 0.01	$0.01 ~\pm~ 0.01$
8-isoPGF2a & 11bPGF2a	0.00 ± 0.00	0.00 ± 0.00	0.05 ± 0.03	0.10 ± 0.01	0.00 ± 0.00	$0.00 ~\pm~ 0.00$	0.00 \pm 0.00	$0.02 ~\pm~ 0.02$
iPF-VI	$0.06 ~\pm~ 0.01$	0.00 ± 0.00	0.08 ± 0.01	0.09 ± 0.01	$0.02 \hspace{0.1cm} \pm \hspace{0.1cm} 0.01$	$0.00 ~\pm~ 0.00$	0.09 ± 0.01	$0.10 ~\pm~ 0.02$
6kPGF1a	0.00 ± 0.00	0.00 ± 0.00	0.00 ± 0.00	0.00 \pm 0.00	$0.00 \hspace{0.1cm} \pm \hspace{0.1cm} 0.00$	$0.00 ~\pm~ 0.00$	$0.00 \pm \ 0.00$	$0.00 ~\pm~ 0.00$
6,15-diketo PGFa	0.00 ± 0.00	0.00 ± 0.00	$0.00 \hspace{0.2cm} \pm \hspace{0.2cm} 0.00$	0.00 \pm 0.00	$0.00 \hspace{0.1cm} \pm \hspace{0.1cm} 0.00$	$0.00 ~\pm~ 0.00$	0.00 ± 0.00	$0.00 ~\pm~ 0.00$
TXB2	$1.10 ~\pm~ 0.27$	3.63 ± 2.79	32.15 ± 1.95	42.75 ± 1.77	$0.69 \hspace{0.1cm} \pm \hspace{0.1cm} 0.07$	3.62 ± 0.19	15.81 ± 0.79	20.50 ± 3.23
11dh-TXB2	$0.00 ~\pm~ 0.00$	0.00 ± 0.00	$0.00 \hspace{0.2cm} \pm \hspace{0.2cm} 0.00$	0.00 \pm 0.00	$0.00 \hspace{0.1cm} \pm \hspace{0.1cm} 0.00$	$0.00 ~\pm~ 0.00$	0.00 ± 0.00	$0.00 ~\pm~ 0.00$
2,3-dinor TXB2	$0.00 ~\pm~ 0.00$	0.00 ± 0.00	$0.00 \hspace{0.2cm} \pm \hspace{0.2cm} 0.00$	0.00 ± 0.00	$0.00 \hspace{0.1cm} \pm \hspace{0.1cm} 0.00$	$0.00 ~\pm~ 0.00$	0.00 ± 0.00	$0.00 ~\pm~ 0.00$
11dh-2,3-dinor TXB2	0.00 ± 0.00	0.00 \pm 0.00	0.00 \pm 0.00	0.00 \pm 0.00	0.00 ± 0.00	$0.00 ~\pm~ 0.00$	0.00 \pm 0.00	$0.00 ~\pm~ 0.00$
5,6- DiHETE(EPA)	$0.01 \hspace{0.1cm} \pm \hspace{0.1cm} 0.01$	1.00 ± 1.00	0.02 ± 0.01	$0.02 \pm \ 0.01$	0.00 ± 0.00	$0.00 ~\pm~ 0.00$	0.00 \pm 0.00	$0.01 ~\pm~ 0.01$
5(S),15(S)- DiHEPE	$0.01 \hspace{0.1cm} \pm \hspace{0.1cm} 0.01$	0.00 \pm 0.00	0.03 ± 0.01	0.02 ± 0.01	$0.01 \hspace{0.1cm} \pm \hspace{0.1cm} 0.01$	$0.00 ~\pm~ 0.00$	0.00 \pm 0.00	$0.01 ~\pm~ 0.01$
8(9)-EpETE	$0.00 ~\pm~ 0.00$	0.00 ± 0.00	$0.00 \hspace{0.2cm} \pm \hspace{0.2cm} 0.00$	0.00 ± 0.00	$0.00 \hspace{0.1cm} \pm \hspace{0.1cm} 0.00$	$0.00 ~\pm~ 0.00$	$0.01 \pm \ 0.00$	$0.00 ~\pm~ 0.00$
11(12)-EpETE	$0.04 ~\pm~ 0.02$	0.22 ± 0.06	0.17 ± 0.01	0.15 ± 0.01	$0.20 \hspace{0.1cm} \pm \hspace{0.1cm} 0.02$	$0.22 \ \pm \ 0.02$	0.27 ± 0.01	$0.26 ~\pm~ 0.03$
14(15)-EpETE	0.00 ± 0.00	0.00 ± 0.00	0.36 ± 0.01	$0.33 \pm \ 0.04$	$0.00 \hspace{0.1cm} \pm \hspace{0.1cm} 0.00$	$0.00 ~\pm~ 0.00$	$0.29 \pm \ 0.02$	$0.19 ~\pm~ 0.09$
17(18)-EpETE	$0.08 ~\pm~ 0.01$	0.26 ± 0.03	0.14 ± 0.02	$0.14 \pm \ 0.01$	$0.66 \hspace{0.1cm} \pm \hspace{0.1cm} 0.04$	0.31 ± 0.02	0.64 ± 0.03	$0.61 \hspace{0.1cm} \pm \hspace{0.1cm} 0.02$
12-HEPE	$0.29 ~\pm~ 0.05$	1.10 ± 0.23	1.01 ± 0.02	$0.92 \pm \ 0.08$	$0.72 \hspace{0.1cm} \pm \hspace{0.1cm} 0.04$	1.13 ± 0.09	$1.92 \pm \ 0.08$	1.66 ± 0.10
15(S)-HEPE	$0.50 ~\pm~ 0.03$	1.51 ± 0.37	1.13 ± 0.04	1.14 ± 0.03	1.79 ± 0.08	1.57 ± 0.11	2.45 ± 0.13	2.18 ± 0.30
5-НЕРЕ	$0.29 ~\pm~ 0.08$	0.78 ± 0.04	6.44 ± 0.19	7.88 ± 0.41	$1.33 ~\pm~ 0.04$	1.14 ± 0.18	15.15 ± 0.16	$14.10~\pm~0.50$
8-НЕРЕ	1.02 ± 0.09	1.51 ± 0.20	1.85 ± 0.06	$1.63 \pm \ 0.07$	$2.23 ~\pm~ 0.06$	2.04 ± 0.18	3.40 ± 0.10	$2.90 ~\pm~ 0.19$
18-НЕРЕ	3.47 ± 0.20	2.99 ± 0.06	3.07 ± 0.09	2.64 ± 0.15	7.11 ± 0.26	4.15 ± 0.50	5.55 ± 0.19	5.18 ± 0.35
9-НЕРЕ	$0.14 \hspace{0.1cm} \pm \hspace{0.1cm} 0.07$	0.67 ± 0.16	0.54 ± 0.06	0.35 ± 0.18	$1.23 ~\pm~ 0.02$	0.63 ± 0.31	1.57 ± 0.06	$0.93 \hspace{0.1cm} \pm \hspace{0.1cm} 0.48$
11-НЕРЕ	$0.36 ~\pm~ 0.07$	0.78 ± 0.11	1.70 ± 0.13	1.82 ± 0.05	$0.90 \hspace{0.1cm} \pm \hspace{0.1cm} 0.03$	$1.03 ~\pm~ 0.04$	2.78 ± 0.14	1.74 ± 0.87
LTB5	$0.01 \hspace{0.1cm} \pm \hspace{0.1cm} 0.00$	0.00 ± 0.00	0.00 ± 0.00	0.01 ± 0.01	$0.00 \hspace{0.1cm} \pm \hspace{0.1cm} 0.00$	$0.00 ~\pm~ 0.00$	0.00 ± 0.00	$0.00 ~\pm~ 0.00$
PGE3	$0.00 ~\pm~ 0.00$	0.03 ± 0.03	0.18 ± 0.02	0.19 ± 0.01	$0.00 ~\pm~ 0.00$	$0.06 \hspace{0.1cm} \pm \hspace{0.1cm} 0.01$	$0.33 \pm \ 0.00$	$0.28 ~\pm~ 0.01$

Table S4.5 (cont'd)

PGD3	$0.00 ~\pm~ 0.00$	0.00 ± 0.00	$0.00 \hspace{0.1cm} \pm \hspace{0.1cm} 0.00$	0.00 ± 0.00	0.00 ± 0.00	0.00 ± 0.00	0.00 ± 0.00	$0.00 ~\pm~ 0.00$
15d-D12,14-PGJ3	$0.00 ~\pm~ 0.00$	$0.00 \hspace{0.2cm} \pm \hspace{0.2cm} 0.00$	$0.00 \hspace{0.2cm} \pm \hspace{0.2cm} 0.00$	0.00 ± 0.00	$0.00 \hspace{0.1cm} \pm \hspace{0.1cm} 0.00$	$0.00 ~\pm~ 0.00$	0.00 ± 0.00	$0.00 ~\pm~ 0.00$
PGF3a	$0.00 ~\pm~ 0.00$	0.00 ± 0.00	$0.00 \hspace{0.2cm} \pm \hspace{0.2cm} 0.00$	0.00 ± 0.00	$0.00 \hspace{0.1cm} \pm \hspace{0.1cm} 0.00$	$0.00 ~\pm~ 0.00$	0.00 ± 0.00	$0.00 ~\pm~ 0.00$
RvE1	$0.00 ~\pm~ 0.00$	0.00 ± 0.00	$0.00 \hspace{0.2cm} \pm \hspace{0.2cm} 0.00$	0.00 ± 0.00	$0.00 \hspace{0.1cm} \pm \hspace{0.1cm} 0.00$	$0.00 ~\pm~ 0.00$	0.00 ± 0.00	$0.00 ~\pm~ 0.00$
RvE2	$0.06 ~\pm~ 0.00$	0.02 ± 0.01	0.06 ± 0.00	$0.05 \pm \ 0.00$	$0.03 \hspace{0.1cm} \pm \hspace{0.1cm} 0.00$	$0.02 \hspace{0.1cm} \pm \hspace{0.1cm} 0.00$	0.10 ± 0.01	$0.05 ~\pm~ 0.03$
RvE3	$0.00 ~\pm~ 0.00$	0.00 ± 0.00	0.00 \pm 0.00	$0.00 \pm \ 0.00$	$0.00 \hspace{0.1cm} \pm \hspace{0.1cm} 0.00$	$0.00 ~\pm~ 0.00$	$0.01 \pm \ 0.01$	$0.00 ~\pm~ 0.00$
TXB3	$0.00 ~\pm~ 0.00$	0.03 ± 0.03	0.13 ± 0.01	$0.07 \pm \ 0.03$	$0.00 \hspace{0.1cm} \pm \hspace{0.1cm} 0.00$	$0.05 \hspace{0.1cm} \pm \hspace{0.1cm} 0.00$	$0.14 \pm \ 0.02$	$0.15 ~\pm~ 0.02$
11dh TXB3	$0.00 ~\pm~ 0.00$	0.00 ± 0.00	0.00 \pm 0.00	$0.00 \pm \ 0.00$	$0.00 \hspace{0.1cm} \pm \hspace{0.1cm} 0.00$	$0.00 ~\pm~ 0.00$	$0.00 \pm \ 0.00$	$0.00 ~\pm~ 0.00$
MaR1(ω-3DPA)	$0.22 \ \pm \ 0.04$	0.22 ± 0.04	0.31 ± 0.01	$0.28 \pm \ 0.01$	$0.99 \hspace{0.1cm} \pm \hspace{0.1cm} 0.07$	$0.45 \hspace{0.1cm} \pm \hspace{0.1cm} 0.09$	$0.83 \pm \ 0.03$	0.89 ± 0.01
PD1(ω -3, DPA)	$0.00 ~\pm~ 0.00$	0.00 ± 0.00	$0.00 \hspace{0.2cm} \pm \hspace{0.2cm} 0.00$	$0.00 \pm \ 0.00$	$0.00 \hspace{0.1cm} \pm \hspace{0.1cm} 0.00$	$0.00 ~\pm~ 0.00$	0.00 ± 0.00	$0.00 ~\pm~ 0.00$
RvD5(ω-3DPA) (7,17-DiHDoPE)	0.00 ± 0.00	0.00 \pm 0.00	0.00 \pm 0.00	0.00 \pm 0.00	$0.00 ~\pm~ 0.00$	$0.00 ~\pm~ 0.00$	0.00 \pm 0.00	$0.00 ~\pm~ 0.00$
19,20-DiHDoPE	$0.67 \hspace{0.1cm} \pm \hspace{0.1cm} 0.04$	0.90 ± 0.14	0.57 ± 0.03	$0.47 \pm \ 0.01$	$6.83 \hspace{0.1cm} \pm \hspace{0.1cm} 0.19$	1.43 ± 0.13	3.76 ± 0.14	3.30 ± 0.41
7(8)-EpDPE	$0.00 ~\pm~ 0.00$	0.03 ± 0.01	0.04 ± 0.01	$0.03 \pm \ 0.01$	$0.08 \hspace{0.1cm} \pm \hspace{0.1cm} 0.02$	$0.03 \hspace{0.1cm} \pm \hspace{0.1cm} 0.00$	$0.10 \pm \ 0.00$	0.14 ± 0.03
10(11)-EpDPE	$0.02 \ \pm \ 0.00$	0.09 ± 0.03	0.06 ± 0.01	$0.06 \pm \ 0.02$	$0.10 \hspace{0.1cm} \pm \hspace{0.1cm} 0.02$	$0.10 \hspace{0.1cm} \pm \hspace{0.1cm} 0.00$	$0.33 \pm \ 0.01$	0.38 ± 0.01
13(14)-EpDPE	$0.00 ~\pm~ 0.00$	0.00 ± 0.00	0.00 \pm 0.00	$0.00 \pm \ 0.00$	$0.02 \hspace{0.1cm} \pm \hspace{0.1cm} 0.02$	$0.04 \hspace{0.1cm} \pm \hspace{0.1cm} 0.02$	0.08 ± 0.08	0.17 ± 0.09
16(17)-EpDPE	0.00 ± 0.00	0.00 ± 0.00	0.01 ± 0.01	$0.00 \pm \ 0.00$	$0.06 \hspace{0.1cm} \pm \hspace{0.1cm} 0.03$	$0.03 \hspace{0.1cm} \pm \hspace{0.1cm} 0.03$	$0.23 \pm \ 0.01$	0.16 ± 0.08
19(20)-EpDPE	0.08 ± 0.01	0.60 ± 0.21	0.34 ± 0.00	$0.31 \pm \ 0.01$	1.72 ± 0.15	$0.83 \hspace{0.1cm} \pm \hspace{0.1cm} 0.10$	2.57 ± 0.06	2.41 ± 0.15
14-HDoHE	0.11 ± 0.05	0.80 ± 0.39	1.45 ± 0.11	1.41 ± 0.05	1.64 ± 0.32	$1.80 ~\pm~ 0.46$	$10.10 \hspace{1.5em} \pm \hspace{1.5em} 0.09$	8.21 ± 0.60
17-HDoHE	0.00 ± 0.00	0.06 ± 0.12	0.48 ± 0.05	$0.47 \pm \ 0.01$	$0.22 \hspace{0.1cm} \pm \hspace{0.1cm} 0.22$	0.51 ± 0.09	$3.22 \pm \ 0.07$	2.74 ± 0.10
4-HDoHE	0.64 ± 0.13	6.60 ± 2.65	5.11 ± 0.22	4.98 ± 0.04	$8.16 \hspace{0.1cm} \pm \hspace{0.1cm} 0.72$	10.03 ± 0.21	33.12 ± 1.80	28.67 ± 0.50
7-HDoHE	$0.31 \ \pm \ 0.01$	1.26 ± 0.52	2.32 ± 0.14	$2.58 \pm \ 0.07$	$2.14 \hspace{0.1cm} \pm \hspace{0.1cm} 0.14$	1.88 ± 0.17	15.90 ± 1.15	13.73 ± 0.32
8-HDoHE	0.68 ± 0.05	3.30 ± 1.38	2.10 ± 0.18	2.19 ± 0.14	$4.86 \hspace{0.1cm} \pm \hspace{0.1cm} 0.54$	4.75 ± 0.26	15.87 ± 1.28	13.42 ± 1.42
10-HDoHE	0.18 ± 0.05	0.98 ± 0.48	2.18 ± 0.20	$2.21 \pm \ 0.04$	$2.32 \ \pm \ 0.34$	2.57 ± 0.46	$14.75 \hspace{0.2cm} \pm \hspace{0.2cm} 1.04$	12.70 ± 0.45
11-HDoHE	$0.25 ~\pm~ 0.01$	1.72 ± 0.78	2.21 ± 0.09	2.00 ± 0.05	$3.28 \ \pm \ 0.44$	3.35 ± 0.63	15.27 ± 0.52	13.27 ± 0.94
13-HDoHE	$0.25 ~\pm~ 0.02$	1.14 ± 0.48	1.89 ± 0.08	$2.12 \pm \ 0.03$	$2.68 ~\pm~ 0.50$	2.87 ± 0.38	14.16 ± 0.12	12.61 ± 0.28
16-HDoHE	0.83 ± 0.01	2.88 ± 1.22	2.51 ± 0.09	$2.37 \pm \ 0.12$	$6.35 \hspace{0.1cm} \pm \hspace{0.1cm} 0.89$	6.67 ± 0.84	18.33 ± 0.90	15.77 ± 0.77
20-HDoHE	1.21 ± 0.16	3.97 ± 1.49	5.73 ± 0.31	5.04 ± 0.13	$10.55~\pm~0.87$	7.84 ± 0.89	33.07 ± 1.38	28.45 ± 0.96

Table S4.5 (cont'd)

Maresin1	$0.00 ~\pm~ 0.00$	$0.00 \hspace{0.2cm} \pm \hspace{0.2cm} 0.00$	0.00 ± 0.00	0.00 ± 0.00	$0.00 \hspace{0.1cm} \pm \hspace{0.1cm} 0.00$	$0.00 ~\pm~ 0.00$	0.00 ± 0.00	$0.00 ~\pm~ 0.00$
7(S)-Maresin1	$0.00 \hspace{0.1cm} \pm \hspace{0.1cm} 0.00$	$0.00 \hspace{0.2cm} \pm \hspace{0.2cm} 0.00$	$0.00 \hspace{0.2cm} \pm \hspace{0.2cm} 0.00$	0.00 ± 0.00	$0.00 \hspace{0.1cm} \pm \hspace{0.1cm} 0.00$	$0.00 ~\pm~ 0.00$	0.00 ± 0.00	$0.00 ~\pm~ 0.00$
PD1	$0.00 \hspace{0.1cm} \pm \hspace{0.1cm} 0.00$	$0.00 \hspace{0.2cm} \pm \hspace{0.2cm} 0.00$	$0.00 \hspace{0.2cm} \pm \hspace{0.2cm} 0.00$	0.00 ± 0.00	$0.01 \hspace{0.2cm} \pm \hspace{0.2cm} 0.01$	$0.04 \hspace{0.1cm} \pm \hspace{0.1cm} 0.01$	0.01 ± 0.01	$0.03 \hspace{0.1cm} \pm \hspace{0.1cm} 0.02$
AT-PD1	$0.00 ~\pm~ 0.00$	$0.00 \hspace{0.2cm} \pm \hspace{0.2cm} 0.00$	$0.00 \hspace{0.2cm} \pm \hspace{0.2cm} 0.00$	0.00 ± 0.00	$0.00 \hspace{0.1cm} \pm \hspace{0.1cm} 0.00$	$0.00 ~\pm~ 0.00$	0.00 \pm 0.00	$0.00 ~\pm~ 0.00$
10S,17S- DiHDoHE	$0.00 ~\pm~ 0.00$	0.00 \pm 0.00	0.00 ± 0.00	0.00 ± 0.00	0.00 ± 0.00	$0.00 ~\pm~ 0.00$	0.00 ± 0.00	$0.00 ~\pm~ 0.00$
22-OH-PD1	$0.00 ~\pm~ 0.00$	$0.00 \hspace{0.2cm} \pm \hspace{0.2cm} 0.00$	$0.00 \hspace{0.2cm} \pm \hspace{0.2cm} 0.00$	0.00 ± 0.00	$0.00 \hspace{0.1cm} \pm \hspace{0.1cm} 0.00$	$0.00 ~\pm~ 0.00$	0.00 \pm 0.00	$0.00 ~\pm~ 0.00$
RvD1 & AT-RvD1	$0.00 ~\pm~ 0.00$	$0.00 \hspace{0.2cm} \pm \hspace{0.2cm} 0.00$	0.00 ± 0.00	0.00 ± 0.00	$0.00 \hspace{0.1cm} \pm \hspace{0.1cm} 0.00$	$0.00 ~\pm~ 0.00$	0.00 \pm 0.00	$0.00 ~\pm~ 0.00$
RvD2	$0.00 ~\pm~ 0.00$	$0.00 \hspace{0.2cm} \pm \hspace{0.2cm} 0.00$	0.00 ± 0.00	0.00 ± 0.00	$0.00 \hspace{0.1cm} \pm \hspace{0.1cm} 0.00$	$0.00 ~\pm~ 0.00$	0.00 \pm 0.00	$0.00 ~\pm~ 0.00$
RvD3	0.01 ± 0.01	$0.00 \hspace{0.2cm} \pm \hspace{0.2cm} 0.00$	0.00 ± 0.00	0.00 ± 0.00	$0.04 \hspace{0.1cm} \pm \hspace{0.1cm} 0.02$	$0.02 ~\pm~ 0.02$	0.00 \pm 0.00	$0.03 \hspace{0.1cm} \pm \hspace{0.1cm} 0.03$
AT-RvD3	$0.01 \hspace{0.1cm} \pm \hspace{0.1cm} 0.01$	0.93 ± 0.89	$0.07 \hspace{0.2cm} \pm \hspace{0.2cm} 0.02$	$0.04 \pm \ 0.02$	$0.03 \hspace{0.1cm} \pm \hspace{0.1cm} 0.03$	$0.07 \hspace{0.1cm} \pm \hspace{0.1cm} 0.04$	0.00 \pm 0.00	$0.00 ~\pm~ 0.00$
RvD4	$0.00 ~\pm~ 0.00$	$0.00 \hspace{0.2cm} \pm \hspace{0.2cm} 0.00$	0.00 ± 0.00	0.01 ± 0.01	$0.00 \hspace{0.1cm} \pm \hspace{0.1cm} 0.00$	$0.02 ~\pm~ 0.02$	0.04 ± 0.02	$0.00 ~\pm~ 0.00$
RvD5	0.00 ± 0.00	$0.00 \hspace{0.2cm} \pm \hspace{0.2cm} 0.00$	0.00 ± 0.00	0.00 ± 0.00	0.00 ± 0.00	0.00 ± 0.00	0.00 ± 0.00	$0.00 ~\pm~ 0.00$
RvD6 (4,17- DiHDoHE)	0.10 ± 0.01	0.08 ± 0.01	0.12 ± 0.01	0.11 ± 0.01	$0.25 ~\pm~ 0.02$	0.16 ± 0.02	0.30 ± 0.00	0.23 ± 0.04
8-oxoRvD1	$0.00 ~\pm~ 0.00$	0.00 ± 0.00	0.00 ± 0.00	0.00 ± 0.00	$0.00 \hspace{0.1cm} \pm \hspace{0.1cm} 0.00$	$0.00 ~\pm~ 0.00$	0.01 ± 0.01	$0.00 ~\pm~ 0.00$
17-oxoRvD1	$0.00 ~\pm~ 0.00$	0.00 ± 0.00	0.00 ± 0.00	$0.00 \pm \ 0.00$	$0.00 ~\pm~ 0.00$	$0.00 ~\pm~ 0.00$	0.00 \pm 0.00	$0.00~\pm~0.00$

Data are presented in units of pmol/culture as mean \pm SEM.

 $\label{thm:constraing} \textbf{Table S4.6. Examples of studies demonstrating biological functions of selected PUFA-derived oxylipins.}$

	Fatty			
Oxylipin Acid		Functions	References	
	Substrate			
		Suppresses phagocytic capacity in AMs	[546]	
		Inhibits LPS-induced cytokine release from	[547]	
		murine and human monocytes via EP4 receptor	[317]	
		Promotes secretion of SOCS3 from AMs, which		
PGE2	20:4ω6	suppresses JAK-STAT signaling in alveolar	[548]	
		epithelial cells		
		Inhibits COX-2 expression from BMDMs	[549]	
		Suppresses TNF-α release BMDMs		
		Inhibits AM proliferation via EP2 receptor	[550]	
		Promotes chemotaxis of PMNs	[551]	
		Promotes release of lysosomal enzymes from	[552]	
LTB4	20:4ω6	PMNs	[332]	
		Promotes secretion of TNF-α from cSiO ₂ - and	[229]	
		asbestos-exposed AMs		
	20:4ω6	Decreases pulmonary airflow rate, tidal volume,		
TXB2		and dynamic lung compliance in guinea pigs and	[553]	
17102		dogs		
		Promotes chemotaxis of PMNs	[554]	
	20:4ω6	Induces pulmonary vasoconstriction and edema	[555]	
		Increases lung vascular permeability	[888]	
5-НЕТЕ		Promotes chemotaxis of neutrophils more potently	[556]	
		than 5-HEPE	[330]	
		Suppresses biosynthesis of PGE2, LTC4, and	[557]	
		TXB2 in murine peritoneal macrophages		
11-HETE	20:4ω6	Promotes chemotaxis of neutrophils	[556]	
		Induces pulmonary vasoconstriction and edema	[555]	
		Increases lung vascular permeability	[333]	
	20:4ω6	Suppresses biosynthesis of LTB4 and 5-HETE	[558]	
15-HETE		from AMs		
	201100	Promotes chemotaxis of neutrophils	[556]	
		Suppresses biosynthesis of PGE2, LTC4, and		
		TXB2 in murine peritoneal macrophages more	[557]	
		potently than 5-HETE		
		Promotes macrophage-mediated Treg induction in	[559]	
5-HEPE	22:5ω3	C57BL/6 mice	[227]	
		Promotes chemotaxis of neutrophils less potently	[560]	
		than 5-HETE	[500]	
		8(R)-HEPE but not 8(S)-HEPE promotes		
8-HEPE	22:5ω3	expression of cholesterol efflux receptors in	[561]	
		macrophages		

Table S4.6 (cont'd)

15-HEPE	22:5ω3	Inhibits activity of 5-LOX	[562]
4-HDoHE	22:6ω3	Prevents endothelial cell infiltration and angiogenesis via PPARγ	[563]
4-пропе		Prevents apoptotic cell death of hippocampal progenitor cells	[564]
14- HDoHE	22:6ω3	Inhibits human platelet aggregation and smooth muscle contraction	[565]
	22:6ω3	Inhibits activity of 5-LOX	[562]
		Suppresses 5-LOX expression and TNF-α in macrophages	[566]
17- HDoHE		Suppresses LPS-induced TNF-α release from macrophage-like RAW 264.7 cells	[567]
		Decreases adhesion molecule expression and secretion of proinflammatory cytokines in murine colitis model	[568]

PGE2, prostaglandin E2; LTB4, leukotriene B4; LTC4, leukotriene C4; TXB2, thromboxane B2; HETE, hydroxyeicosatrienoic acid; HEPE, hydroxyeicosapentaenoic acid; HDoHE, hydroxydocosahexaenoic acid; 20:4ω6, arachidonic acid; 22:5ω3, eicosapentaenoic acid; 22:6ω3, docosahexaenoic acid; COX, cyclooxygenase; AM, alveolar macrophage; EP, prostaglandin E2 receptor; BMDM, bone marrow-derived macrophage; PMN, polymorphonuclear leukocyte.

APPENDIX C: CHAPTER 5 SUPPORTING FIGURES AND TABLES

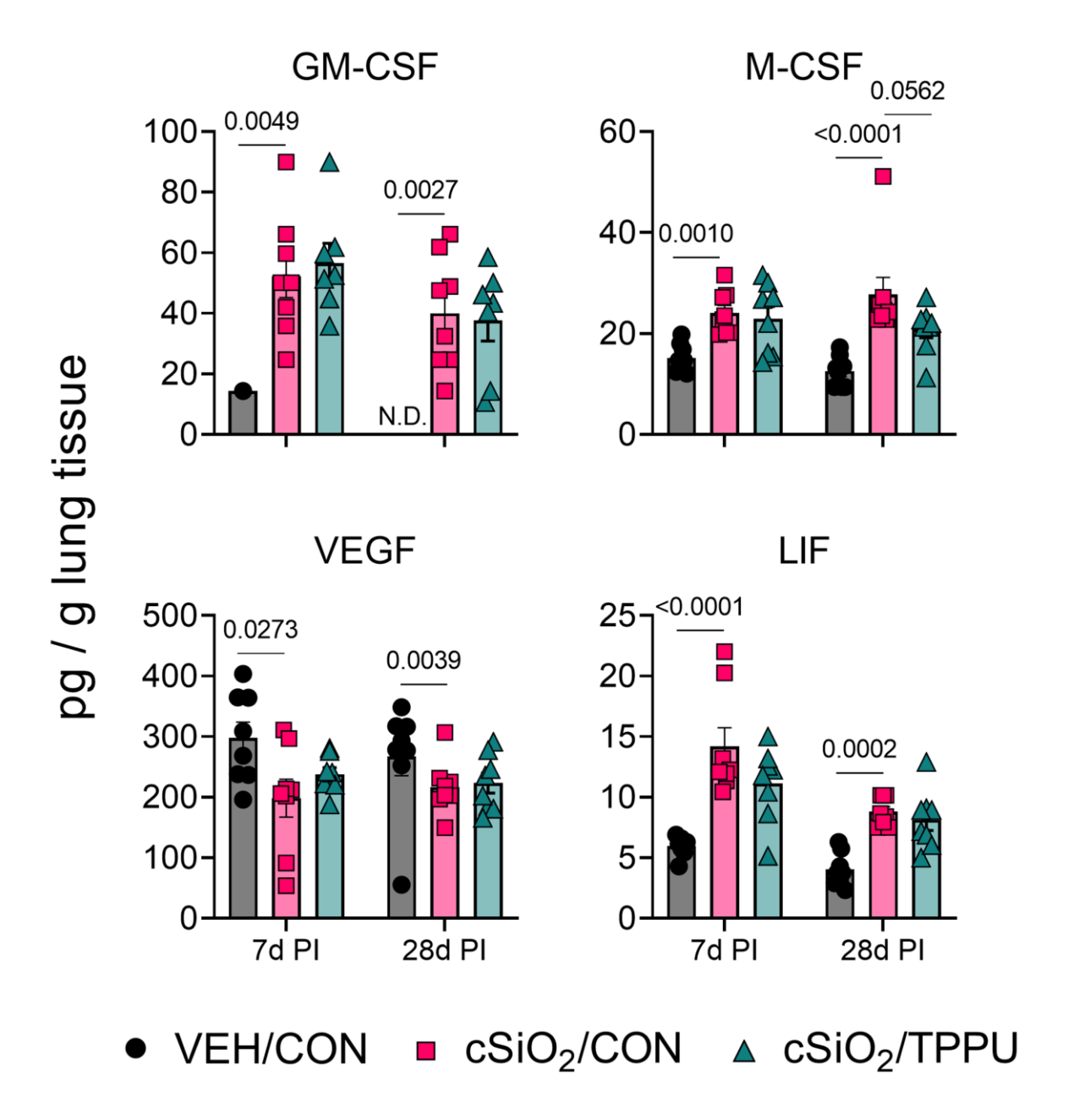


Figure S5.1. Dietary TPPU supplementation has limited effects on cSiO₂-induced changes in growth factor and inhibitory factor levels in the lung. Following sacrifice, middle lung lobes were isolated and homogenates analyzed for production of selected growth factors (i.e., GM-CSF, M-CSF, VEGF) and the inhibitory factor LIF using Mouse Cytokine/Chemokine 44-Plex Discovery Assay® Array from Eve Technologies. Protein quantities were normalized to the original weight of lung tissue homogenized for the analysis. For individual data points that fell below the limit of detection, LOD/2 was substituted for statistical analysis. Data are presented as mean \pm SEM (n = 8). Values of p<0.2 are shown, with p<0.05 considered statistically significant.

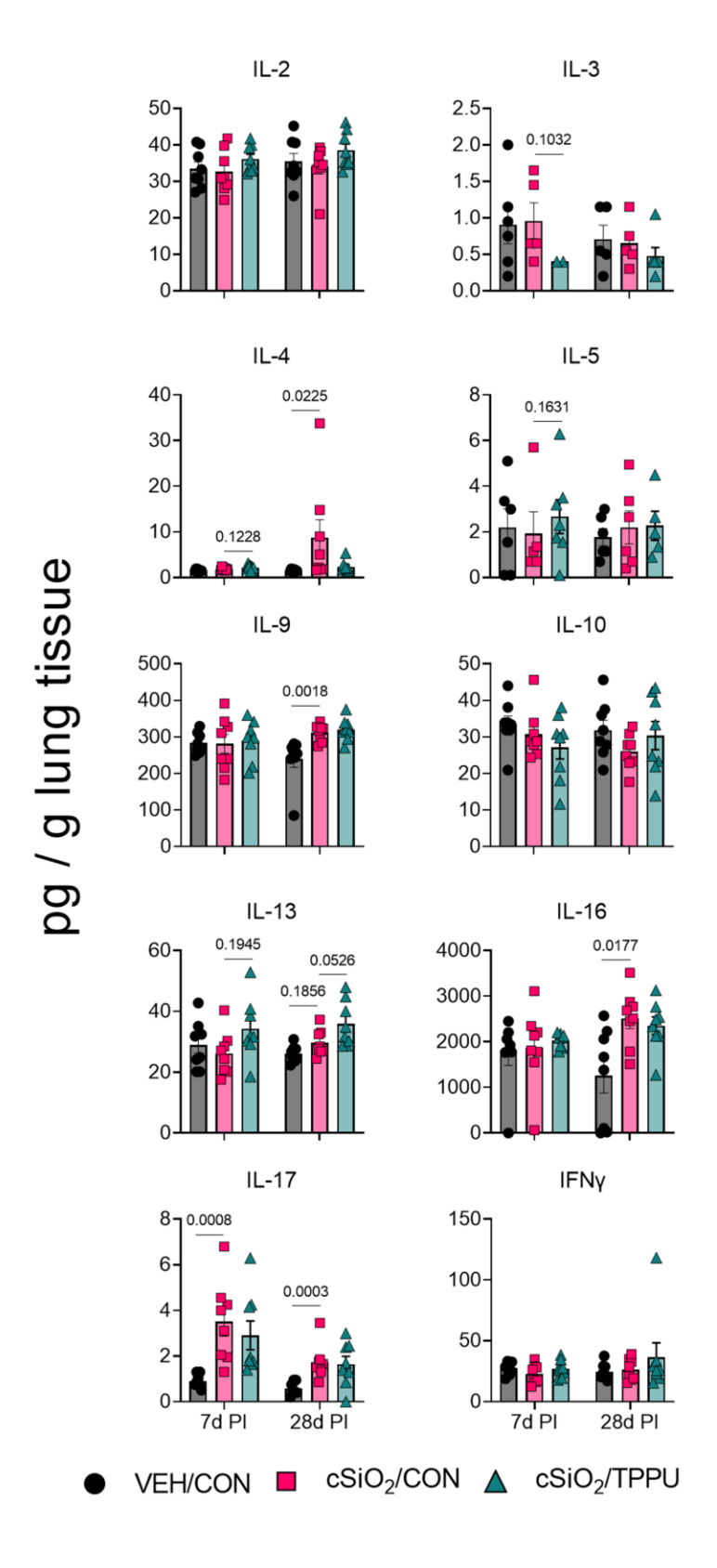


Figure S5.2. cSiO₂ instillation and dietary TPPU supplementation have limited effects on production of cytokines from T cells in the lung. Following sacrifice, middle lung lobes were

Figure S5.2 (cont'd)

isolated and homogenates analyzed for production of selected T cell-derived cytokines (i.e., IL-2, IL-3, IL-4, IL-5, IL-10, IL-13, IL-15, IL-17, IFN γ) using Mouse Cytokine/Chemokine 44-Plex Discovery Assay® Array from Eve Technologies. Cytokine quantities were normalized to the original weight of lung tissue homogenized for the analysis. For individual data points that fell below the limit of detection, LOD/2 was substituted for statistical analysis. IL-3 was detected in only two samples within the cSiO₂/TPPU group in the 7d PI cohort. Data are presented as mean \pm SEM (n=8). Values of p<0.2 are shown, with p<0.05 considered statistically significant.

Table S5.1. List of Key Reagents, Chemicals, and Kits.

Reagent	Vendor	Catalog Number
AIN-93G Purified Rodent Diet	Dyets Inc.	110700
without Vitamin Mix	·	
AIN-93G VX Vitamin Mix	Dyets Inc.	310025
LouAna Safflower Oil	LouAna Oils	
Mazola Corn Oil	Mazola	
Microalgal Oil Containing	DHASCO	
40% DHA		
TPPU	Synthesized in-house) () () () ()
Crystalline Silica	U.S. Silica	Min-U-Sil-5
Monoclonal Rat Anti-Mouse Ly6B.2 Alloantigen Antibody	BioRad	MCA771G
Polyclonal Rabbit Anti-Mouse CD206 Antibody	Abcam	ab64693
Polyclonal Rabbit Anti-Mouse CD3 Antibody	Abcam	ab5690
Monoclonal Rat Anti-Mouse CD45R Antibody	Becton Dickinson	550286
RNeasy Mini Kit	Qiagen	74104
Mouse Cytokine/Chemokine 44-Plex Discovery Assay®	Eve Technologies	MD44
Array Nunc 96-Well Flat Bottom May: Sam Immuna Plates	Thermo Fisher Scientific	442404
MaxiSorp Immuno Plates Poly-L-Lysine Solution, 0.1% (w/v)	Sigma Aldrich	P8920
Purified Native dsDNA, Calf Thymus	Alpha Diagnostic International	DNAD25-N-1
Purified Nucleosome Antigen, Bovine Thymus	Arotec Diagnostics	ATN02
Anti-DNA Antibody, double stranded, clone BV16-13	Millipore Sigma	MAB030
Staurosporine	R&D Systems	1285
Goat Anti-Mouse IgG (heavy-chain sp.)-HRP conjugate	Alpha Diagnostic International	40120
Quant-iT [™] PicoGreen [®] dsDNA Assay Kit	Thermo Fisher Scientific	P7589
Pierce TM BCA Protein Assay Kit	Thermo Fisher Scientific	23225
RNeasy Mini Kit	Qiagen	74104
RIPA Lysis and Extraction Buffer	Thermo Fisher Scientific	89901

 $\begin{tabular}{ll} Table S5.2. Total dsDNA and protein content in AC-derived material and SKC-derived material generated for AAb ELISAs. \end{tabular}$

	AC-derived material	SKC-derived material
Total dsDNA (ng/ml)	2390	375
Total protein (µg/ml)	1381	737
ng dsDNA/mg protein	1731	508
dsDNA used in ELISAs (ng/ml)	10	10
Protein used in ELISAs (µg/ml)	20	6

Table S5.3. Lung homogenate cytokine levels as determined by Eve Technologies Mouse Cytokine/Chemokine 44-Plex Discovery Assay® Array.

	VEH/CON 7d PI	cSiO ₂ /CON 7d PI	cSiO ₂ /TPPU 7d PI	VEH/CON 28d PI	cSiO ₂ /CON 28d PI	cSiO ₂ /TPPU 28d PI
Cytokine	7411			$e, mean \pm SEM$		20011
CCL2/MCP-1	121.3±13.3 ^A	1080±191.4 ^B	$1084\pm210.6^{\text{B}}$	124.3 ± 14.3^{a}	1054±293.9b	710.6±106.5 ^b
CCL3/MIP-1α	85.38±9.58 ^A	339.8±48.9 ^B	331.0±48.1 ^B	92.99±7.79 ^a	446.2±65.2 ^b	267.1±32.7 ^b
CCL4/MIP-1β	53.85±7.99 ^A	247.0±44.5 ^B	271.1±39.6 ^B	19.85±0.00*a	295.3±47.0 ^b	192.3±18.3 ^{ab}
CCL5/RANTES	11.93±0.68 ^A	12.18±0.92 ^A	12.93±0.65 ^A	10.17±0.81 ^a	9.76±0.60*a	11.09±0.85 ^a
CCL11/Eotaxin	866.9±81.5 ^A	749.0±43.8 ^A	774.2±27.6 ^A	910.6±100.8*a	885.0±49.0*a	965.9±62.9 ^a
CCL12/MCP-5	991.5±77.6 ^A	3415±442.8 ^B	3083±427.3 ^B	778.5±61.2*a	3122±327.2 ^b	3086±365.9b
CCL17/TARC	168.9±11.7 ^A	340.5±13.5 ^B	285.2±26.1 ^C	123.7±6.62*a	395.5±34.1 ^b	351.5±49.5 ^b
CCL19/MIP-3β	53.23±2.14 ^A	75.18±3.68 ^B	71.67±5.66 ^B	40.02±3.52*a	73.21±2.86 ^b	76.74±3.48 ^b
CCL20/MIP-3α	13.60±0.71 ^A	12.63±0.42 ^A	13.31±0.67 ^A	10.47±0.78 ^a	12.49±1.25 ^b	14.59±0.67 ^b
CCL21/6Ckine	8212±7850	22399±0	106.3±0	11937±5508	N.D.	15019±0
CCL21/OCKINE CCL22/MDC	14.51±0.83 ^A	35.45±2.44 ^B	31.23±3.71 ^B	11.63±0.69*a	48.83±4.88*b	42.78±5.84 ^b
CXCL1/KC	82.23±7.40 ^A	189.7±19.9 ^B	205.5±22.4 ^B	76.90±3.25°	218.0±20.3 ^b	200.5±22.5 ^b
CXCL2/MIP-2	122.3±7.40	128.2±8.3 ^A	123.8±11.4 ^A	145.2±29.0 ^a	130.1±10.0 ^a	127.0±6.5 ^a
CXCL5/LIX	502.4±64.3 ^A	807.1±111.6 ^A	862.6±162.7 ^A	143.2±29.0 1642±120.5*a	757.7±101.0 ^b	127.0±0.5** 1773±584.7 ^{ab}
CXCL9/MIG	391.3±35.8 ^A	1056±182.3 ^B	1167±133.8 ^B	442.5±47.65 ^a	1672±380.6 ^b	1773±384.7 th 1983±532.2 ^b
CXCL10/IP-10			285.7±42.4 ^B		239.3±42.9b	
	41.20±2.52 ^A	249.1±39.0 ^B 1226±67.9 ^B		47.37±2.78*a 1532±120.1a	239.3±42.9° 1757±159.4*a	259.3±50.2 ^b 1663±128.7*a
CX3CL1/Fractalkine	1810±162.6 ^A		1132±107.5 ^B			
EPO	N.D. 1.82±0.53 ^A	N.D.	N.D.	N.D.	N.D.	N.D.
G-CSF		3.96±1.02 ^A	4.98±1.14 ^A	2.24±0.84 ^a	1.02±0.38*a	1.83±0.71 ^a
GM-CSF	14.35±0.00 ^A	52.33±7.09 ^B	56.61±6.48 ^B	N.D.*a	40.08±6.66 ^b	37.71±6.86 ^b
IFNβ-1	173.8±4.6 ^A	158.2±4.9 ^A	147.5±15.4 ^A	118.6±9.3*a	159.6±11.9 ^b	156.7±13.1 ^{ab}
IFNγ	27.27±1.83 ^A	22.76±2.78 ^A	27.01±2.47 ^A	24.79±2.35°	26.16±3.15 ^a	36.46±11.85 ^a
IL-1α	532.7±84.7 ^A	325.2±23.8 ^B	348.9±20.5 ^B	324.4±41.2ª	359.7±16.9 ^a	398.0±19.1ª
IL-1β	14.19±1.33 ^A	15.70±0.80 ^A	15.41±1.92 ^A	12.29±1.01 ^a	11.86±1.46*a	15.46±0.55 ^a
IL-2	33.47±1.86 ^A	32.66±2.07 ^A	36.21±1.29 ^A	35.44±2.20°	34.03±2.01 ^a	38.52±1.75 ^a
IL-3	0.91±0.26 ^A	0.96±0.25 ^{AB}	0.40±0.00 ^B	142.0±37.9*a	130.0±28.8*a	95.0±23.9*a
IL-4	1.57±0.07 ^A	1.86±0.11 ^A	2.23±0.19 ^B	1.59±0.06 ^a	8.76±3.94 ^b	2.36±0.46 ^{ab}
IL-5	2.20±0.81 ^A	1.92±0.95 ^A	2.67±0.74 ^A	1.77±0.38 ^a	2.20±0.72 ^a	2.27±0.63 ^a
IL-6	10.34±3.12 ^A	15.27±1.63 ^B	16.03±2.21 ^B	8.21±0.74 ^a	12.95±1.49 ^b	10.26±0.92*ab
IL-7	13.48±1.48 ^A	12.38±1.16 ^A	13.91±2.17 ^A	10.98±1.37 ^a	10.28±1.41 ^a	14.59±1.09 ^a
IL-9	283.2±10.1 ^A	281.2±25.4 ^A	289.9±19.6 ^A	239.7±22.7 ^a	311.4±8.25 ^b	320.3±11.0 ^b
IL-10	33.49±2.29 ^A	30.68±2.39 ^A	27.16±3.22 ^A	31.80±2.74 ^a	25.99±1.72 ^a	30.37±3.86 ^a
IL-11	16.99±1.07 ^A	23.97±2.44 ^A	18.91±2.25 ^A	11.28±0.57*a	15.53±0.97*b	16.98±0.97 ^b
IL-12p40	55.26±6.85 ^A	46.92±3.82 ^A	49.83±6.36 ^A	55.75±3.54 ^a	37.93±4.08 ^b	50.16±3.43 ^{ab}
IL-12p70	9.95±2.83 ^A	12.21±3.37 ^A	4.17±1.96 ^A	11.28±10.43*a	6.53±4.76 ^a	8.42±3.77 ^a
IL-13	28.97±2.81 ^A	26.14±2.55 ^A	34.26±3.55 ^A	26.08±0.98a	29.66±1.49ab	35.89±2.66 ^b
IL-15	86.33±7.13 ^A	80.44±8.44 ^A	74.50±5.66 ^A	79.20±9.38 ^a	67.25±4.50 ^a	70.23±6.77 ^a
IL-16	1746±263.3 ^A	1922±351.7 ^A	2033±55.2 ^A	1256±376.6a	2514±222.0b	2259±247.8ab
IL-17	0.91±0.10 ^A	3.50±0.63 ^B	2.91±0.63 ^B	0.59±0.11*a	1.72±0.27*b	1.64±0.34 ^b
IL-20	34.75±3.74 ^A	31.65±3.44 ^A	45.84±5.58 ^A	24.83±2.43*a	34.37±2.20 ^a	24.87±5.47*a
LIF	5.97±0.29 ^A	14.19±1.55 ^B	11.14±1.08 ^B	4.27±0.49*a	8.81±0.42*b	8.13±0.86*b
M-CSF	15.15±1.00 ^A	24.09±1.51 ^B	22.94±2.45 ^B	12.56±1.06 ^a	27.73±3.39 ^b	20.83±1.65 ^b
TIMP-1	443.1±34.6 ^A	2427±164.8 ^B	1868±263.2 ^B	243.6±38.5*a	1518±167.4*b	1281±170.1 ^b
TNF-α	7.62±0.43 ^A	21.24±3.44 ^B	21.08±3.41 ^B	7.46±1.00a	33.26±6.06 ^b	24.78±3.85 ^b
VEGF	297.6±26.3 ^A	198.5±31.4 ^B	238.3±10.7 ^{AB}	267.5±32.0a	216.9±15.6b	223.3±16.5 ^b

Table S5.3 (cont'd)

Data are presented as pg cytokine per g of lung tissue (mean ± SEM, n = 8/gp). Differences between VEH/CON, cSiO₂/CON, and cSiO₂/TPPU groups within the 7d PI and 28d PI cohorts were compared by one-way ANOVA. Differences between the 7d PI and 28d PI VEH/CON, cSiO₂/CON, and cSiO₂/TPPU groups were also compared by Student's t test. Alternative versions of these tests were used when data did not meet the assumption of normality and/or equal variances. Asterisks indicate significant differences between the VEH/CON 7d PI and VEH/CON 28d PI groups, cSiO₂/CON 7d PI and cSiO₂/CON 28d PI groups, or cSiO₂/TPPU 7d PI and cSiO₂/TPPU 28d PI groups (p<0.05). Unique uppercase letters indicate significant differences between the VEH/CON 28d PI, cSiO₂/CON 28d PI, and cSiO₂/TPPU 28d PI groups (p<0.05).